Procoagulant signalling in lung injury and fibrosis

By Natalia Smoktunowicz

A thesis submitted to University College London
for the degree of Doctor of Philosophy

Centre for Inflammation and Tissue Repair,
Rayne Institute, University College London
5 University Street, London, WCE1 6JJ

Acknowledgments

I would like to thank many people that I have met during my time at the Centre for Respiratory Research, and more recently Centre for Inflammation and Tissue Repair, who generously shared their knowledge with me, offered support as well as friendship and laughter.

I would like to express my special thanks to my primary supervisor, Professor Rachel Chambers, for nurturing my passion for science, her immense knowledge, guidance and advice through the world of scientific thinking and writing, and critical appraisal of this thesis.

Dr Paul Mercer, my secondary supervisor, for igniting my curiosity and passion for science and for guiding my first steps as a scientist.

Dr Chris Scotton for his invaluable expertise, advice and enthusiasm while discussing endless possible answers to my numerous scientific questions.

Mr Robert Alexander for his help, support and most importantly friendship for life.

Dr Gabor Jarai for his scientific advice and support during my work at Novartis.

Medical Research Council and Novartis for funding this study.

My family in Poland and England for their love, support and encouragement in the course of my studies.

Finally, thank you to my partner, David, who has embarked on this journey with me and has been source of love, understanding and motivation to keep going, and to whom I dedicate this thesis.

Declaration

I confirm that the work contained in this thesis is entirely my own.

To David

Abstract

Coagulation proteinases, such as thrombin, exert a plethora of cellular effects via activation of proteinase-activated receptors (PARs). Abnormal activation of the coagulation cascade has been widely implicated in the pathology of fibroproliferative lung disease, including the most common form idiopathic pulmonary fibrosis (IPF). The high-affinity thrombin receptor PAR-1 is over-expressed in the lungs of IPF patients, particularly by the hyperplastic epithelium and fibroblasts within fibrotic foci. Moreover, viral infections are implicated in aberrant coagulation activation and accumulating evidence points to viruses as contributory factors to acute exacerbations that lead to deterioration of lung function in IPF patients.

This thesis focuses on investigating and extending our current understanding of the role of PAR-1 in driving lung injury and fibrosis. Data show that primary human lung fibroblasts and microvascular endothelial cells express abundant PAR-1 and elicit robust calcium signalling responses following thrombin stimulation. In contrast, normal human alveolar and bronchial epithelial cells express low levels of PAR-1 but high levels of PAR-2. Exposure of the alveolar epithelial cell line, A549, to TGFβ increases PAR-1 expression and functional responses but this was not seen in freshly isolated primary human alveolar and bronchial epithelial cells.

The role of TGFβ and pro-coagulant signalling responses was also investigated in an in vivo model of viral infection on a background of pulmonary fibrosis. Herpesvirus infection in the fibrotic lung promoted robust inflammatory responses characterized by extensive pulmonary consolidation but did not lead to an increase in lung collagen deposition. Importantly, viral infection was associated with the local upregulation of key components of the extrinsic coagulation pathway. Although PAR-1 is known to contribute to lung injury and fibrosis in a single hit experimental model of pulmonary fibrosis by promoting the activation of latent TGFβ, systemic targeting of TGFβ and the coagulation cascade does not impact on inflammation induced by viral infection in the fibrotic lung.

List of Figures

List of Tables

List of Abbreviations

6MWT	6 minute walk test
ACM	alveolar-capillary membrane
AE	acute exacerbation
AEC	alveolar epithelial cell
ALI	acute lung injury
ALK	activin receptor-like kinase
APC	activated protein C
ARDS	acute respiratory distress syndrome
AP	anionic phospholipids
AT	antithrombin
BALF	bronchoalveolar lavage fluid
BLM	bleomycin
BM	basement membrane
BSA	bovine serum albumin
CCL	chemokine (C-C motif) ligand
CCR	C-C chemokine receptor
CMV	cytomegalovirus
COX	cyclooxygenase
CTGF	connective tissue growth factor
CXCL	C-X-C chemokine ligand
CXCR	C-X-C chemokine receptor
DAPI	4',6-diamidino-2-phenylindole
DLCO	diffusing capacity of lung for carbon monoxide
DMEM	Dulbecco's modified eagle's medium
DMSO	dimethyl sulfoxide
DNA	deoxyribonucleic acid
DPLD	diffuse parenchymal lung disease
EBV	Epstein Barr virus
ECM	extracellular matrix
EDTA	ethylenediaminetetracetic acid
ELISA	enzyme-linked immunoassay
EMT	epithelial-mesenchymal transition
EPCR	endothelial protein C receptor
ERK	extracellular signal-regulated

	kinase
ET	Endothelin
FGF	fibroblast growth factor
FLIPR	fluorescent image plate reader
FVC	forced vital capacity
FBS	foetal bovine serum
γHV	gamma herpesvirus
HBEC	human bronchial epithelial cell
HHV	human herpesvirus
HLMEC	human lung microvascular endothelial cell
HLF	human lung fibroblast
HPLC	high pressure liquid chromatography
HRCT	high resolution computed tomography
HUVEC	human umbilical vein endothelial cell
GPCR	G-protein coupled receptor
ICAM	intercellular adhesion molecule
IFN	interferon
IIP	idiopathic interstitial pneumonia
IKK	IκB kinase
ILD	interstitial lung disease
IPF	idiopathic pulmonary fibrosis
JAK	janus kinase
JNK	c-Jun amino-terminal kinase
kDa	kilodalton
KGF	keratinocyte growth factor
LAP	latency-associated peptide
LPA	lysophosphatidic acid
LPS	lipopolysaccharide
LTBP	latent TGFβ binding protein
μCT	micro computed tomography
MAPK	mitogen activated protein kinase
MEK	mitogen activated protein kinase kinase
MHC	major histocompatibility complex
MLF	murine lung fibroblast
NAC	N-acetylcysteine

NK	natural killer
NSIP	non-specific interstitial pneumonia
PAI	plasminogen activator inhibitor
PAR	proteinase activated receptor
PBS	phosphate buffered saline
PDGF	platelet derived growth factor
PECAM	platelet endothelial cell adhesion molecule
PF	pulmonary fibrosis
PFA	paraformaldehyde
PGE2	prostaglandin E2
PS	phosphatidylserine
qRT-PCR	real time quantitative reverse transcription polymerase chain reaction
RNA	ribonucleic acid
RT-PCR	reverse transcription polymerase chain reaction
SDS-PAGE	sodium dodecyl sulfate polyacrylamide gel electrophoresis
SEM	standard error of mean
SMA	smooth muscle actin
TGF-β	transforming growth factor-β
TF	tissue factor
TFPI	tissue factor pathway inhibitor
Th	T-helper
TM	thrombomodulin
UIP	usual interstitial pneumonia
VEGF	vascular endothelial growth factor

Table of Contents

Chapter 1: Introduction

1.1 Pulmonary fibrosis

Pulmonary fibrosis (PF) is an end stage of a heterogeneous group of fibroproliferative lung diseases categorised as interstitial lung diseases (ILD). The hallmark of ILDs is the deposition of extracellular matrix (ECM) proteins in the interstitium suggestive of extensive and abnormal tissue repair responses. Large areas of disorganised fibrotic tissue composed of proliferating mesenchymal cells and accumulated collagen replace alveolar spaces and thereby prevent efficient gas exchange. The disease is progressive and inevitably leads to respiratory failure and premature death.

ILDs, also termed diffuse parenchymal lung diseases (DPLD) include a range of disorders that frequently share features of clinical presentation but aetiologically and pathologically are independent entities. A number of ILDs have well-characterised causes that include radiation, drug toxicity and environmental exposures (e.g. asbestos in the case of asbestosis). Systemic fibrotic conditions, for example systemic sclerosis, collagen vascular disease or rheumatoid arthritis can also lead to the development of ILD. However, the largest group of ILDs are of unknown aetiology and are termed idiopathic interstitial pneumonias (IIPs).

Although there are different molecular mechanisms underlying IIPs, many exhibit similar clinical presentations and radiological and pathological features. This makes diagnosis, associated treatment and prognosis problematic and in 2002 the American Thoracic Society (ATS) in collaboration with the European Respiratory Society (ERS) introduced criteria for the characterisation and diagnosis of IIPs (**Table 1.1**).

Histological pattern	Diagnosis based on clinical, radiological and histological findings
Usual interstitial pneumonia (UIP)	Idiopathic pulmonary fibrosis (IPF)
Non-specific interstitial pneumonia (NSIP)	Non-specific interstitial pneumonia (NSIP)
Organizing pneumonia	Cryptogenic organizing pneumonia
Diffuse alveolar damage	Acute interstitial pneumonia
Respiratory bronchiolitis	Respiratory bronchiolitis-associated interstitial lung disease
Desquamative interstitial pneumonia	Desquamative interstitial pneumonia
Lymphoid interstitial pneumonia	Lymphoid interstitial pneumonia

Table 1.1. Classification of the Idiopathic Interstitial Pneumonias (ATS, ERS 2002).

1.2 Idiopathic pulmonary fibrosis

IPF is a progressive lung disease with an estimated incidence in the UK of 4.6 per 100,000 people and 1,500 deaths registered every year. Furthermore, between 1991 and 2003 the incidence of IPF increased by 11% and the overall trend is rising (Gribbin et al. 2006; Hubbard et al. 1996). The disease affects largely middle-aged people with around two-thirds being over 60 at the time of diagnosis. The median survival rate of IPF patients is approximately three years from the time of diagnosis, which is the worst prognosis of all IIPs. The prevalence is higher in men and there is an emerging pattern of differences in IPF occurrence and progression between ethnic/racial populations (Swigris et al., 2012).

Clinical presentation of IPF includes long-lasting, progressive dyspnoea and significant gas exchange abnormalities confirmed by respiratory tests. Non-productive cough and systemic symptoms, such as fever and weight loss, are also reported (ATS, ERS 2002). Radiology and high-resolution computer tomography scans (HRCT) show basal reticular opacities, subpleural honeycombing and traction

bronchiectasis. Histological analysis of lung biopsies classically reveals the pattern of Usual Interstitial Pneumonia (UIP) with heterogeneous appearance of a healthy lung interspersed with well-defined areas of dense interstitial fibrosis, predominantly found in peripheral subpleural parenchyma. The hallmark histological features of fibrotic areas are honeycomb changes resulting from enlarged and distorted air spaces lined with bronchial epithelium and filled with mucin, and prominent fibrotic foci composed of aggregates of hyperproliferative and hypersynthetic fibroblasts and myofibroblasts enclosed in extracellular matrix and overlaid by hyperplastic and injured alveolar epithelium (**Figure 1.1**) (Chambers, 2008; Katzenstein et al., 2002; 2002). As the disease progresses, the fibrotic tissue obliterates alveolar spaces leading to irreversible architectural distortion of the lung that results in respiratory failure. The UIP pattern is distinctively different from other lung diseases, however non-specific interstitial pneumonia (NSIP)-like areas, characterised by thickening of alveolar septae and varying degrees of inflammatory infiltrates, have been observed in the background of otherwise typical UIP (Katzenstein et al., 2002). These findings can lead to discordant diagnosis of the condition when the biopsies are taken from different lobes of the lung (Flaherty et al., 2001) but can also provide an explanation for a heterogeneous clinical outcome in IPF patients.

The median survival of IPF is less than three years (Kim et al., 2006a) and clinical progression is highly variable between patients. IPF is usually diagnosed when the disease is advanced and the fibrotic changes in the lung begin to have a significant restrictive effect on respiratory physiology. Nonetheless, recent studies in familial IPF identified patients in the asymptomatic phase of disease with fibrotic and architectural changes in the lung detected by HRCT scans (Rosas et al., 2007; Steele et al., 2005) confirming the temporal separation between the onset of disease and the symptoms becoming apparent.

Following diagnosis, IPF patients can experience steady or rapid progression of the disease with a subpopulation of patients experiencing periods of acute exacerbation that greatly increase morbidity and mortality. The acute exacerbation of IPF will be discussed in detail in the next section. Accelerated progression of IPF and

premature death correlate with decline in lung function as clinically assessed by physiological tests, the most predictive being lung forced vital capacity (FVC), diffusing capacity of lung for carbon monoxide (DLCO) and the 6 minute walk test (6MWT). Other risk factors also predictive of a worse outcome include high dyspnoea score, old age, male sex, smoking status and comorbidities with pulmonary hypertension being the most severe (Ley et al., 2011).

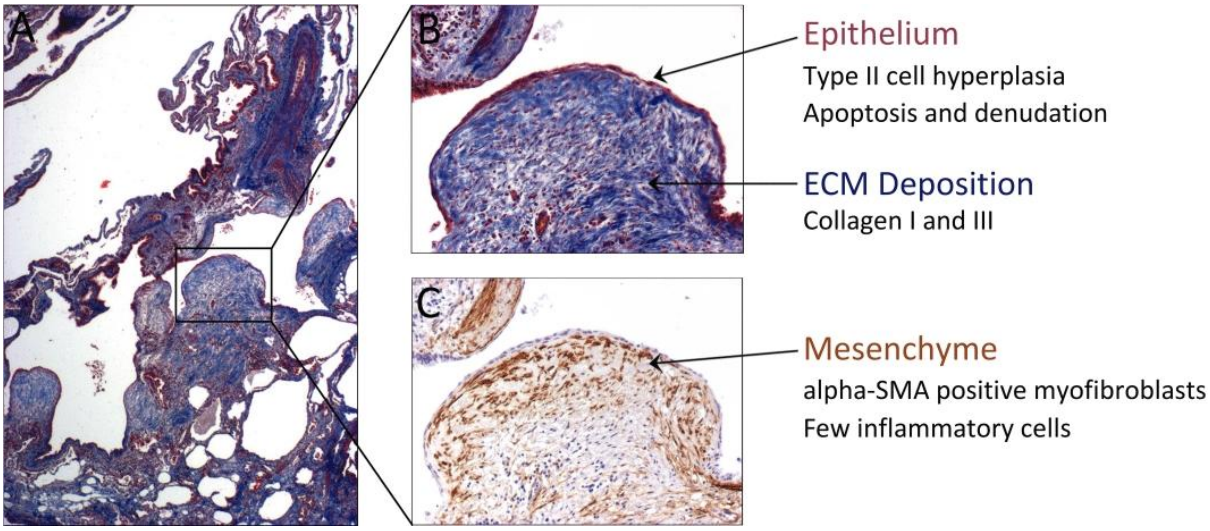

Figure 1.1 Fibrotic foci– a histological hallmark of IPF.

Histological analysis of human IPF tissue reveals the presence of dense collagen deposition within the interstitium (Martius Scarlet Blue staining; original magnification ×10). Fibroblastic foci are revealed as accumulations of fibroblasts and alpha-SMA positive myofibroblasts, which are highly synthetic for collagen and have a contractile phenotype (B: Martius Scarlet Blue staining; C: immunohistochemistry for alpha-SMA. Original magnification ×20). The overlying epithelium is often hyperplastic, with frequent apoptosis and areas of denudation. The presence and distribution of fibrotic foci, together with the spatial and temporal heterogeneity of the pathology is crucial to defining a UIP pattern. [reproduced from (Datta et al., 2011)]

1.2.1 Acute exacerbation of IPF

The progressive course of IPF can be further accelerated by incidents of rapid deterioration termed acute exacerbations (AE). Clinical presentation includes the development of severe dyspnoea within 30 days and often additional flu-like symptoms. Hospitalization is often necessary due to severe hypoxia and the need for mechanical ventilation.

Acute exacerbation of IPF (AE IPF) can have well-determined causes, such as infection, left heart failure and pulmonary embolism or can be triggered by unknown factors. Collard and colleagues performed a retrospective analysis of patients with rapid deterioration of unknown aetiology and estimated that the incidence of AE IPF is 9.6% and mortality as high as 78% (Collard et al., 2007). This study also proposed diagnostic criteria for AE IPF that include previous or concurrent diagnosis of IPF, unexplained worsening or development of dyspnoea within 30 days, new pulmonary changes and abnormalities visible on the HRCT scans, and lack of evidence for common pulmonary infection.

Prominent progressive changes identified on radiological and HRCT scans are central features of AE IPF. The images of exacerbated lungs reveal the presence of new bilateral ground-glass abnormalities and consolidation superimposed on a background of UIP pattern typical of IPF (**Figure 1.2**). Histological evaluation of AE IPF reveals interstitial oedema, hyaline membrane formation and extensive diffuse alveolar damage and haemorrhage (Collard et al., 2007). These features are hallmark findings of acute lung injury (ALI) suggesting that AE IPF and ALI have similar clinical and pathological features.

Although radiological and histological findings imply that AEs are caused by ALI in the setting of fibrotic lung disease, these conditions have significantly different plasma biomarker profiles indicating distinct underlying pathologies. Plasma biomarkers are useful tools for defining the biological phenotype of the disease and are frequently adequate predictors of survival. ALI has a well-characterised plasma biomarker profile that includes increase in markers of type I and type II alveolar epithelial cell (AEC I and II) injury and/or proliferation and endothelial cell injury,

elevated pro-inflammatory cytokines and changes in markers of coagulation. Protein C is significantly reduced and plasminogen activator inhibitor (PAI) levels are increased (Ware et al. 2007), which indicates an altered balance between coagulation and fibrinolysis and propagation of a procoagulant state and fibrin generation. Indeed, fibrin deposition in the lung, evident as hyaline membranes, is a hallmark feature of ALI (Chambers, 2008). In AE IPF, biomarkers of AEC II damage and death are also elevated but there is no difference in markers of AEC I injury or inflammatory mediators. Total protein C levels are significantly increased and thrombomodulin concentration is reduced (Collard et al., 2010). This biomarker profile suggests that AEs are driven by damage to the type II alveolar epithelium, which is central to the pathogenesis of IPF and will be described in detail later in this thesis. Furthermore, there is a clear indication that major anticoagulant pathways are dysregulated in AE IPF suggesting that coagulation abnormalities may also contribute to the progression of disease.

Taken together, current evidence suggest that the pathology of AE IPF is distinct from the pathology of ALI, which is further corroborated by data obtained from genetic profiling of lung tissue from patients with these respiratory conditions (Konishi et al., 2009). Gene expression in AE IPF is similar to stable IPF and there is no dramatic shift or upregulation of pro-inflammatory genes that is evident in ALI. The cell cycle regulator cyclin A2 encoding gene- CCNA2 was one of a few significantly upregulated genes and was found to be localised to epithelial cells, but not mesenchymal cells (Konishi et al., 2009). These results support the emerging hypothesis that AE IPF is driven by acute injury to AEC II leading to severe deterioration of the underlying fibroproliferative condition (Collard et al., 2007).

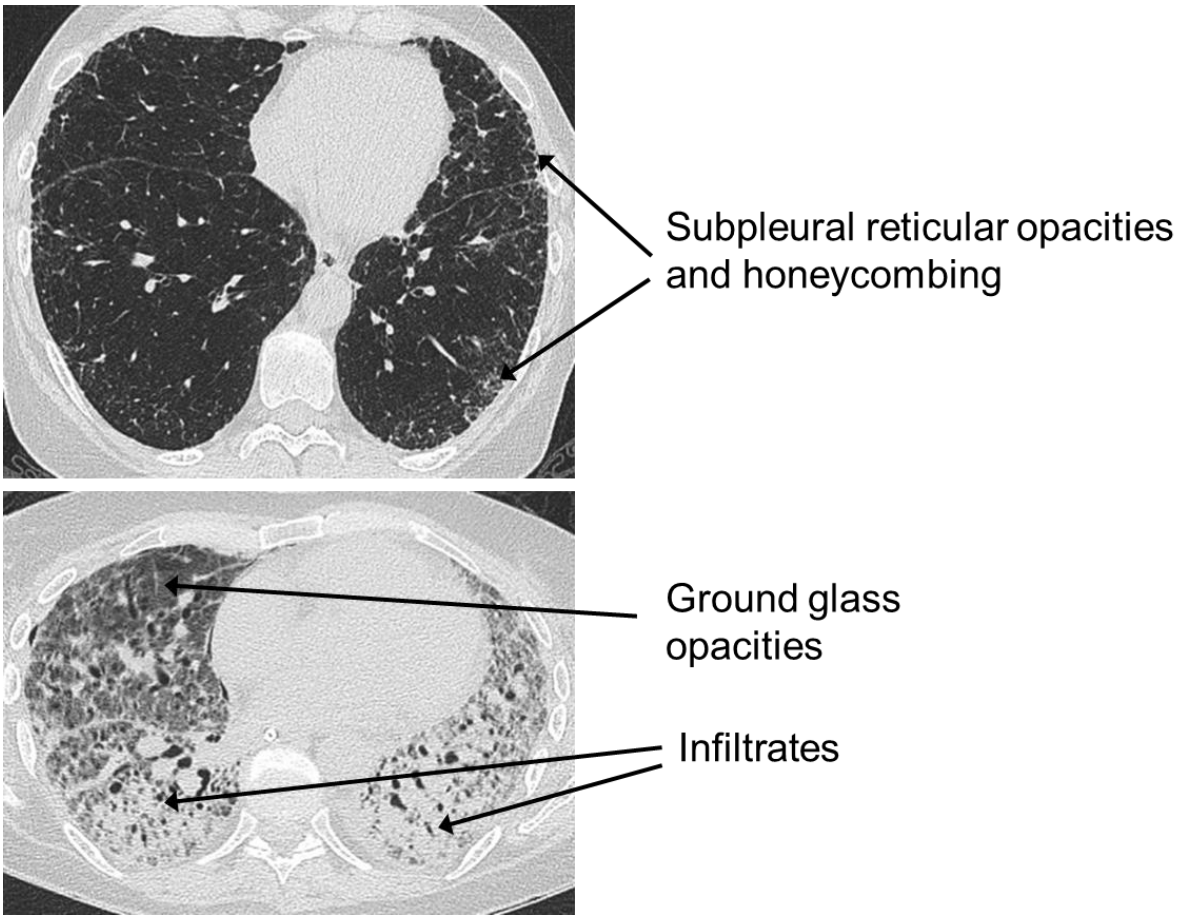

Figure 1.2 Acute exacerbation of IPF.

Case study of IPF patient at baseline- upper panel and with acute exacerbation- lower panel. The patient initially presented with mild disease, distinct subpleural reticular opacities and honeycombing as identified on the upper HRCT. Within 4 weeks the patient developed an acute exacerbation with HRCT scan revealing extensive bilateral ground glass opacities and infiltrations (courtesy of Dr Toby Maher, Royal Brompton Hospital).

1.3 Pathogenesis of IPF

Although the aetiology of IPF is unknown, the current consensus is that persistent and repetitive damage to the epithelium leads to dysregulation of repair mechanisms, irreversible destruction of the basement membrane and altered interactions between epithelial and mesenchymal cells. The following risk factors have been implicated in the development of IPF: cigarette smoking (Baumgartner et al., 1997), gastro-oesophageal reflux (Kottmann et al., 2009), drug toxicity, prolonged environmental exposure (wood or metal dust), viral infections (Tang et al. 2003) and genetic predisposition (Lawson et al., 2011). The incomplete understanding of the pathogenesis of IPF is reflected by the lack of effective treatment for this disease.

Initial investigations into the mechanism of the disease led to the belief that IPF is a chronic inflammatory disorder and immunomodulatory agents have been used extensively in IPF. Their limited efficacy suggests that the role of inflammation in pulmonary fibrosis is of lesser relevance than predicted and the pathogenesis of the disease is more complex. Nevertheless, low doses of steroids and other immunosuppressive drugs such as azathioprine, lately supplemented with antioxidant N-acetylcysteine (NAC) remained the main line of treatment for IPF (Raghu et al., 2012). Recently a combination therapy of prednisone, azathioprine and NAC was tested in the PANTHER double-blinded, randomised and placebo-controlled clinical trial, which was stopped at interim analysis due to increased mortality, hospitalisations and the adverse effects in the treatment arm when compared with placebo (Raghu et al., 2012). The NAC-only arm of this study is still ongoing as the evidence from previous IFIGENIA trail showed that high dose of NAC significantly ameliorates progression of the disease in IPF patients (Behr et al., 2009; Demedts et al., 2005).

The latest treatment for IPF involves the recently approved drug- pirfenidone, which has been shown to prevent the deterioration of lung function in IPF patients (Noble et al., 2011). Although the exact mechanism of action is not known, pirfenidone has broad anti-inflammatory and anti-fibrotic effects and has been

shown to inhibit fibroblast proliferation and collagen production *in vitro* (Hisatomi et al., 2012).

Despite numerous studies and clinical trials there is currently a dramatic lack of efficacious treatments for IPF. The conventionally used therapies appear to accelerate the disease while new agents are being evaluated in a slow and opportunistic manner. There is a pressing need to improve the understanding of IPF pathogenesis and respond with better-suited and targeted treatments.

1.3.1 Bleomycin model of acute lung injury and fibrosis

A great deal of insight into the molecular and cellular mechanisms of pulmonary fibrosis comes from animal models. The most common model of pulmonary fibrosis involves administration of bleomycin to mice via multiple routes including: subcutaneous, intravenous and intraperitoneal. A direct and most widely used route of administration to induce localised lung injury and fibrosis involves intratracheal instillation of bleomycin that produces fibrosis with bronchiocentric distribution. Oropharyngeal instillation (Lakatos et al., 2006) is also a direct route of bleomycin administration that is currently used in our laboratory and causes a more homogenous injury with peripheral and subpleural fibrosis, and hence is considered to be a more representative model of human disease (Scotton et al., 2013).

Bleomycin is an antibiotic glycopeptide with antineoplastic properties produced by bacterium *Streptomyces verticillus,* which is used as a chemotherapy agent to treat many types of cancer including testicular cancer, lymphomas, head and neck cancers (Bokemeyer, 2008). Bleomycin causes extensive DNA damage and has been strongly associated with pulmonary toxicity in cancer patients and the development of interstitial and alveolar fibrosis in animal models (Bokemeyer, 2008; Chaudhary et al., 2006; Sikic et al., 1978). Administration of bleomycin causes acute lung injury that is characterised by extensive epithelial damage and vascular leak, upregulation of inflammatory cytokines and subsequent infiltration of neutrophils, macrophages and lymphocytes into the lung (Janick-Buckner et al., 1989). This early inflammatory phase of the model peaks during the first week following the injury. Fibrotic lesions

develop subsequently and fibrosis establishes at 2-3 weeks post-injury (Scotton et al., 2009). Typical histological features include hyperplasia of alveolar epithelial cells, basement membrane damage and interstitial and intraalveolar fibrosis (Usuki and Fukuda, 1995). Marked expansion of fibroblasts and myofibroblasts and extensive deposition of extracellular matrix are evident in the areas of the repairing lung (Chaudhary et al., 2006).

The major drawback of this model is the lack of restrictive physiology and progression of fibrosis. Furthermore, the question of resolution of bleomycin-induced pulmonary fibrosis has been controversial with some research groups showing complete resolution within three months (Degryse et al., 2010) while others report persistent and lasting fibrotic lesions (Hodges et al., 2004; Scotton et al., 2013). Nonetheless, the bleomycin model of pulmonary fibrosis has contributed immensely to our understanding of mechanisms leading to fibrosis and proven invaluable in the identification of many key pathways and cytokines involved in the development of pulmonary fibrosis *in vivo*.

1.3.2 Lung injury in pulmonary fibrosis

On average 11,000 litres of air enters the respiratory system on a daily basis carrying the oxygen essential for eukaryotic life but also noxious agents such as dust, pollutants and microbial agents that contribute a constant source of potential microinjury to the lung epithelium. The lungs therefore are maintained in a state of subtle equilibrium between swift responses to injury and wound healing processes to minimise the alterations to delicate lung architecture. The haemostatic balance in the normal lung is generally antithrombotic and pro-fibrinolytic (Chambers, 2008). The loss of this balance combined with extensive and persistent damage to the alveolar spaces and over-exuberant activation of tissue repair mechanisms can result in a number of detrimental fibroproliferative conditions. Indeed, pulmonary fibrosis is a potential complication of ALI and its most severe form- acute respiratory distress syndrome (ARDS). ALI and ARDS are most commonly caused by infection, such as sepsis or pneumonia, or trauma to the lung caused by aspiration

of gastric contents or drowning. It is estimated that 40% of ARDS patients develop terminal pulmonary fibrosis (Marshall et al. 1998).

The initial stages of lung injury involve diffuse alveolar damage that is characterised by disruption to epithelial and endothelial barrier and cell death. Subsequent loss of basement membrane integrity leads to increased vascular permeability and leak, inflammatory cell influx into the lung and proliferation of interstitial mesenchymal cells with the deposition of provisional ECM. The newly deposited ECM is utilised as a scaffold for wound closure mediated by fibroblasts and myofibroblasts. The central features of a normal wound healing response in the lung are re-epithelialisation and re-endothelisation with subsequent ECM remodelling and reabsorption. During the resolution phase fibroblasts and myofibroblasts undergo apoptosis and homeostasis is restored with minimal alteration to the lung architecture (reviewed in Chambers 2008). In contrast, in a fibrotic lung these tissue repair mechanisms are dysregulated and lead to major alteration in the architecture of the organ eventually leading to its dysfunction and failure. The persistent and/or repetitive injuries to the alveolar epithelial cells followed by the denudation and loss of integrity of basement membrane have been proposed as the tipping point between the healthy response and the fibrotic phenotype (Strieter and Mehrad, 2009).

1.3.3 Dysregulated epithelial-mesenchymal crosstalk in IPF

Current hypothesis states that IPF is the consequence of an aberrant wound healing response. Persistent or repetitive injury to the alveolar epithelium and over-exuberant mesenchymal cell response leads to denudation of alveolar spaces, extensive deposition of extracellular matrix and fibroblasts expansion that eventually obliterates the normal architecture of the lung. The paradox evident in fibrosis revolves around increased apoptosis of the injured epithelium and increased survival of the mesenchymal cells (Maher et al., 2010).

1.3.3.1 The epithelium in IPF

Recurrent and non-resolving injury to the alveolar epithelium is a major factor driving the pathogenesis of pulmonary fibrosis and extensive apoptosis of AECII is a hallmark of IPF lung (Kuwano et al. 2012; Plataki et al. 2005; Uhal et al. 1998). Mutations in the structure of surfactant C protein are a proposed genetic factor leading to an increased death of AECII in fibrosis. The resultant abnormal protein fails to fold correctly and cannot be secreted from cells, which subsequently leads to the protein retention in the endoplasmic reticulum and causes cellular stress and apoptosis of AECII (Thomas et al., 2002; Wang et al., 2009). Endoplasmic reticulum stress has been described as a pathologic feature of IPF (Lawson et al., 2008). Moreover, IPF has been primarily associated with the damage to the alveolar epithelium but emerging evidence points to the airway epithelium also being affected by the pathogenesis of the disease. A genetic variant in mucin (MUC5B) is significantly associated with familial and sporadic IPF (Seibold et al., 2011).

Extensive apoptosis of lung epithelial cells negatively impacts on the re-epithelisation process and results in alterations in the phenotype of surviving AECII. These changes include regenerative hyperplasia and bronchiolarization. Furthermore, excessive epithelial apoptosis leads to the disruption of the integrity of the alveolar basement membrane, which in turn facilitates the continuous influx of fibroblasts and further perpetuates the destruction of alveoli (Strieter and Mehrad, 2009). Pockets of hyperproliferative and hypersynthetic fibroblasts and myofibroblasts overlaid by hyperplastic alveolar epithelium protrude from the alveolar septae and form characteristic fibrotic foci that are considered to be the leading edge of the fibroproliferative processes in IPF (Uhal et al. 1998) (**Figure 1.1**). Furthermore, i*n vitro* co-culture experiments demonstrated that interstitial fibroblasts can induce apoptosis in injured epithelial cells through secretion of angiotensin II (ANGII) (Uhal et al., 1998; Wang et al., 1999). In addition, injured epithelium is a prominent source of major profibrotic mediators, including TGFβ (Kapanci et al., 1995), TNFα (Kapanci et al. 1995; Nash et al. 1993), CCL2 (Mercer et al., 2009) and CTGF (Pan et al., 2001), all of which will be described in detail in

Section 1.3.4 of this thesis. Furthermore, injured alveolar epithelium has increased capacity to activate TGFβ via αvβ6 integrin-mediated mechanism (Jenkins et al., 2006). The expression of αvβ6 integrin is considered to be restricted to the alveolar epithelium in the lung and becomes upregulated in lung injury and fibrosis (Munger et al. 1999; Breuss et al. 1995; Zambruno et al. 1995; Breuss et al. 1993). TGFβ has also been shown to induce expression of β6 integrin subunit in epithelial cells (Wang et al., 1996) and targeting αvβ6 in experimental pulmonary fibrosis attenuates the fibrosis (Horan et al., 2008; Puthawala et al., 2008).

Targeted injury to alveolar AECII directly causes the development of pulmonary fibrosis. Transgenic mice with AECII susceptible to diphtheria toxin injury were generated by conjoining the murine surfactant protein C promoter with the diphtheria toxin receptor. Diphtheria toxin interferes with protein synthesis in eukaryotic cells and leads to apoptosis and increased regenerative proliferation. A causal relationship was established between AECII injury and weight loss, collagen accumulation and eventually development of pulmonary fibrosis in these mice (Sisson et al. 2010). Epithelial cell apoptosis in response to TGFβ overexpression also inevitably triggers fibroproliferative disease *in vivo* that can be attenuated by targeting the apoptotic pathways and TGFβ signalling (Lee et al., 2004).

Furthermore, following exposure to fibrotic mediators, primarily TGFβ, epithelial cells have been shown to undergo epithelial to mesenchymal transition (EMT). This process is characterised by the loss of cell polarity, loss of epithelial markers including tight junctions Zona Occludens 1 (ZO-1) and E-cadherin, reorganisation of the cytoskeleton and acquisition of mesenchymal cell markers including αSMA (Kalluri and Neilson, 2003). EMT has been observed *in vitro* (Willis et al., 2005) and TGFβ readily induced EMT in epithelial cells cultured on fibronectin, which is representative of provisional matrix deposited in an early wound healing response. However, when cells were grown on mature matrix mimicked by collagen and matrigel, exposure to TGFβ caused epithelial cell apoptosis (Kim et al., 2006b). A similar behaviour was reported in bronchial epithelial cells cultured on fibronectin that acquired mesenchymal phenotype when exposed to TGFβ (Câmara and Jarai,

2010). EMT has also been demonstrated to occur *in vivo* in a model of renal fibrosis where a third of fibroblasts in fibrotic tissue was shown to be of epithelial origin using cell-specific genetic tagging technology (Iwano, 2002). Using a similar approach in the model of lung injury and fibrosis, AECII were selectively tagged with β-galactosidase (β-gal) and following overexpression of TGFβ in the lung it was noted that majority of cells expressing fibroblast marker N-vimentin were also β-gal positive (Kim et al., 2006b). In contrast, another study using cell lineage tracing technology to investigate the origin of myofibroblasts in bleomycin-induced pulmonary fibrosis failed to detect fibroblast or myofibroblasts of epithelial origin (Rock et al., 2011). EMT in the human lung is difficult to investigate and many *in vitro* studies with alveolar epithelium have been performed in cancer cell lines, where EMT is an established process in tumour invasiveness and metastasis. Therefore, the relevance of EMT process in the progression of fibrosis has been recently closely scrutinised, particularly in the light of contradictory experimental data. However, there are suggestions that EMT may be a part of response to injury and a potential mechanism to escape apoptosis in epithelial cells and does not necessarily involve a full conversion to mesenchymal phenotype (Kage and Borok, 2012).

1.3.3.2 Fibroblasts and myofibroblasts in IPF

Fibroblasts and myofibroblasts are cells of mesenchymal origin, which are crucial for wound healing. However, in fibroproliferative lung disease these cell types acquire a proliferative, synthetic and contractile phenotype and drive fibrosis. Human fibrotic fibroblasts have the potential to induce pulmonary fibrosis demonstrated by a study with transgenic mice that lack innate and adaptive immunity (Pierce et al. 2007). Adoptive transfer of fibrotic lung fibroblasts into these mice resulted in the development of pulmonary fibrosis. Transfer of normal lung fibroblasts did not cause any pathologies providing evidence that the fibrotic fibroblasts have a distinct and aggressive phenotype (Pierce et al. 2007) .

Myofibroblast is a mesenchymal cell characterised by an intermediate phenotype between a fibroblast and a smooth muscle cell. It lacks desmin, heavy chain myosin

chains and smoothelin expressed by smooth muscle cells but expresses stress fibres composed of α-SMA that account for its contractility and make it a key cell responsible for a wound closure in the physiological healing processes. Mesenchymal cells orchestrating wound closure are a heterogeneous population and include fibroblasts, fully-differentiated myofibroblasts and also cells that express stress fibres but are αSMA-negative. These cells have intermediate properties between fibroblast and myofibroblast and are termed proto-myofibroblast (reviewed in Hinz 2010). Myofibroblast is central to the pathogenesis of fibroproliferative disorders due to its increased contractile potential (Miki et al., 2000) and greater capacity for ECM protein synthesis in response to profibrotic mediator stimulation (Hetzel et al., 2005). In IPF, three main possible cellular sources of myofibroblasts have been described: fibroblast to myofibroblast differentiation, epithelial-mesenchymal transition (EMT) and recruitment of bone-marrow derived fibrocytes (Datta et al., 2011; Scotton and Chambers, 2007). TGFβ, mechanical stress and matrix remodelling are recognized contributory factors for myofibroblast differentiation and proliferation.

Myofibroblasts and fibroblasts isolated from IPF patients display increased migratory potential (Suganuma et al., 1995) and greater capacity for profibrotic mediators production in comparison to fibroblasts derived from healthy lungs (Moodley et al., 2003). Furthermore, in healthy lungs a prostaglandin-based anti-fibrotic mechanism regulates the activation of fibroblasts in an autocrine negative feedback loop. Stimulated fibroblasts secrete prostaglandins, primarily PGE_2, which in turn inhibit their proliferation, differentiation, chemotaxis and collagen synthesis (Bauman et al. 2010; Hodges et al. 2004; Jenkins et al. 2002; McAnulty et al. 1995). In the fibrotic phenotype this auto-regulatory pathway is disrupted and IPF fibroblasts have diminished potential to upregulate cyclooxygenase-2 (COX-2) expression necessary to generate and release prostaglandins (Keerthisingam et al. 2001). This failure to produce PGE_2 by the fibrotic fibroblasts promotes cell survival and addition of exogenous PGE_2 to the cell culture leads to fibroblast apoptosis. Moreover, inhibition of PGE_2 production in the normal fibroblasts produces an apoptosis-resistant phenotype (Maher et al., 2010).

Fibroblasts are robust producers of ECM and have mechanosensory and mechanotransducing properties. Tissue fibroblasts attach to and communicate with ECM through assembly of focal adhesions (FAs) and reorganisation of FAs occurs in the process of differentiation to myofibroblasts. FAs formation is mediated by integrins, which link actin cytoskeleton on the intracellular interface with the ECM. Fibronectin ectodomain splice variant ED-A is an ECM protein which contains RGD-integrin binding sequence and enhances formation of FAs (Dugina et al., 2001). Fibronectin, fibrin and intracellular actin stress fibres align alongside the cell membrane and converge at the FAs, which sets in place all the components of the feedback mechanism that allows cells to continuously sense changes in the environment and rearrange the cytoskeleton accordingly. FAs communicate changes in the matrix stiffness to the cell, which responds by adjusting FAs size and the ability to contract in a linear fashion (Hinz and Gabbiani, 2003). This process, known as maturation of FAs, usually occurs in the wound healing scenario and also involves expression of FA-specific proteins including vinculin, paxilin, tensin and focal adhesion kinase (FAK). Differentiation to myofibroblasts is associated with supermaturation of FAs, which involves increased expression of ED-A fibronectin and other FAs proteins. Furthermore, FAs increase in size and assemble into organised networks in myofibroblasts, which in turn increase the formation of αSMA-positive stress fibres (Dugina et al., 2001). Therefore, increasing matrix stiffness stimulates myofibroblast contractility, collagen synthesis and ECM deposition. As measured by Young's elastic modulus the stiffness of a normal lung is between 1-5 kPa, which in fibrotic lung can increase to 20-100 kPa (Hinz, 2012). Studies subjecting fibroblasts to stretch forces *in vitro* have determined a range in which fibroblast acquire stress fibres to be between 3-5 kPa, while the pressure needs to increase to 16-20 kPa for αSMA to be incorporated into these stress fibres (Hinz, 2010). However, intermediate matrix stiffness of 5-9 kPa is required for cells to be sufficiently contractile to cause putative conformational change in TGFβ latency complex and release active cytokine, which subsequently induces the expression of proteins of contractility apparatus and stimulates ECM production in fibroblasts and myofibroblasts (Hinz, 2010).

Although fibroblasts have been shown to express αSMA de novo when cultured on a stiff matrix, TGFβ is required for uniform and global differentiation into myofibroblasts. TGFβ is a potent inducer of fibroblast to myofibroblast differentiation (Desmoulière et al., 1993) and can engage multiple cellular pathways in the process, which will be described further in this thesis (**Section 1.3.4.2**).

1.3.4 Inflammatory and profibrotic mediators in pulmonary fibrosis

IPF is a complex disease and a number of highly profibrotic mediators have been shown to be upregulated in IPF patients as well as in the experimental models of fibrosis. Key mediators with the strongest causative relationship in pulmonary fibrosis will be described in this section and are summarised in **Table 1.2**.

1.3.4.1 Overview of fibrotic mediators

The role of inflammation in IPF has been questioned primarily due to immunosuppressive therapies being ineffective in the treatment of the disease. However, aggregates of lymphoid tissue with reactivated B and T cells are prominent in the IPF lung (Marchal-Sommé et al., 2007) and microarray studies have revealed that several inflammatory genes are upregulated in IPF (Zuo et al., 2002). Furthermore, in the fibrotic lung the immune responses are largely influenced by the type 2 T-helper lymphocytes (Th2) (Wynn, 2004) and their signature cytokines IL-4 and IL-13 (Wilson and Wynn, 2009). IL-4 has been shown to promote the production of extracellular matrix proteins in fibroblasts (Sempowski et al., 1994) while IL-13 increases the production of TGFβ (Lee et al., 2001) and monocyte chemoattractant proteins (MCP) including CCL2 (Zhu et al., 2002). Furthermore, overexpression of IL-13 in mice leads to the development of allergic airway disease and airway fibrosis that subsequently progresses to the parenchyma (Zhu et al., 2001). Interestingly, in experimental pulmonary fibrosis IL-13 deficient mice, but not IL-4 deficient mice, develop less fibrosis due to diminished collagen production by fibroblasts (Kolodsick et al., 2004). These findings were corroborated by a recent study showing that IL-13 induces collagen production in airway

fibroblasts and subsequent airway remodelling in an MMP-2- and TGFβ-dependent manner (Firszt et al., 2013).

The Th1 and Th2 imbalance in the lungs of IPF patients also leads to decreased levels of IFNγ, which is an important component of antiviral immunity but also has anti-fibrotic effects. IFNγ inhibits fibroblast proliferation (Rosenbloom et al., 1984), collagen production (Narayanan et al., 1992) and disrupts TGFβ expression and signalling (Ulloa et al., 1999; Varga et al., 1990). Administration of IFNγ in the bleomycin model of pulmonary fibrosis reduced expression of TGFβ and collagen and consequently attenuated fibrosis (Gurujeyalakshmi and Giri, 1995). In a small clinical study, combined IFNγ and prednisolone therapy showed beneficial effect on improving the lung function of IPF patients resistant to glucocorticoids treatment (Ziesche et al., 1999). Following from this encouraging result, a large randomised and placebo-controlled clinical trial of IFNγ treatment in IPF was performed but failed to demonstrate a significant health benefit to IPF patients (Raghu et al., 2004). However, a trend toward clinical improvement with long-term IFNγ treatment was identified (Raghu et al., 2004) and supported by another study showing that IFNγ treatment over two year period offered a significant improvement in the clinical outcome in mild to moderate IPF (Antoniou et al., 2006). In contrast, another large phase III clinical trial INSPIRE has been terminated early after having shown no survival benefit in patients receiving IFNγ (King et al., 2009). Despite these contradictory results, IFNγ is still being tested in IPF patients in inhaled aerosol form with a view to localise the administration to the lung and reduce systemic side effects (Diaz et al., 2012). Furthermore, the scientific rationale for beneficial effect of IFNγ therapy in IPF patients has been reinforced by analysis of IPF lung biopsies, plasma and bronchoalveolar lavage fluids (BALF) that showed reduction in profibrotic and proliferative mediators (including procollagen I and III, elastin, platelet derived growth factor PDGF) with IFNγ treatment (Strieter et al., 2004).

IL-1β and TNFα are potent cytokines highly expressed in the acute and chronic inflammation of the lung and have been shown to be elevated in BALF from IPF and

asbestosis patients (Zhang et al., 1993). Furthermore, stimulation of fibroblasts with IL-1β and TNFα increased the gene expression of extracellular matrix proteins including collagen and fibronectin (Zhang et al., 1993). Overexpression of IL-1β *in vivo* leads to acute alveolar and parenchymal inflammation that progresses into interstitial fibrosis with accumulation of fibroblasts and myofibroblasts in the lung (Kolb et al., 2001). Moreover, IL-1β-mediated fibrosis depends on activation and signalling via TGFβ/Smad3 pathway. This causative relationship was confirmed in a study where IL-1β was overexpressed in a Smad3-null rats, which developed inflammatory response but showed attenuated fibrosis (Bonniaud et al., 2005a).

TNFα has been shown to upregulate TGFβ gene expression (Sullivan et al., 2009) and overexpression of TNFα in rat lungs leads to acute inflammation that progresses into mild but persistent fibrosis (Sime et al., 1998). The fibrotic phase is marked by increased levels of TGFβ in the BALFs and accumulation of αSMA positive myofibroblasts in the lung. Furthermore, TNFα receptor knockout mice are protected from fibroproliferative lung disease induced by bleomycin and silica (Ortiz et al., 1999) but develop fibrosis following overexpression of TGFβ (Liu et al., 2001). Taken together, these data suggest that the main profibrotic effect mediated by IL-1β and TNFα occurs via stimulation of TGFβ expression.

Platelet derived growth factor (PDGF) is a potent mitogen and chemoattractant for mesenchymal cells and mediator of extracellular matrix production (Bonner, 2004). PDGF is secreted from alveolar macrophages, fibroblasts and myofibroblasts in the pulmonary fibrosis creating paracrine and autocrine feedback loops that stimulate production of extracellular matrix (Scotton and Chambers, 2007). Alveolar macrophages isolated from bronchoalveolar lavage fluid of IPF patients secrete four times more PDGF than macrophages from healthy controls (Martinet et al., 1987). Moreover, dual inhibition of TGFβ and PDGF signalling pathways by imatinib mesylate, a receptor tyrosine kinase inhibitor that blocks PDGF receptor, has been shown to have an anti-fibrotic effect in the bleomycin model of dermal fibrosis (Distler et al., 2007), asbestos-induced pulmonary fibrosis (Vuorinen et al., 2007) and radiation-induced pulmonary fibrosis (Li et al., 2009). Furthermore, imatinib

mesylate attenuates bleomycin-induced pulmonary fibrosis when administered prophylactically (Daniels et al., 2004). Despite promising *in vitro* and *in vivo* data and some clinical evidence that imatinib mesylate can improve outcome of interstitial lung disease (Distler et al., 2008), a large randomised and placebo-controlled trial failed to show improvement in the clinical outcome of IPF patients (Daniels et al., 2010). Nonetheless, PDGF continues to be targeted in IPF by a multiple receptor tyrosine kinase inhibitor nintedanib (BIBF1120) that also inhibits fibroblasts growth factor 2 (FGF2) and vascular endothelial growth factors (VEGF). FGF2 is a potent mitogen of smooth muscle cells, fibroblasts and myofibroblasts and is strongly expressed in IPF (Inoue et al., 2002). VEGF is potent promoter of endothelial cells proliferation and neovascularisation. Loss of microvasculature, redistribution of blood vessels and thickening of small vessel walls is well characterised in IPF (Renzoni et al., 2003). Reduced level of VEGF was reported in the model of pulmonary fibrosis mediated by TGFβ overexpression, which was reflected in excessive endothelial cells apoptosis and loss of microvasculature (Farkas et al., 2009). In turn, loss of small blood vessels inversely correlated with the pulmonary arterial pressure and increased the risk of development of pulmonary hypertension, which is a major comorbidity in IPF. This abnormal phenotype was rescued by restoring VEGF but interestingly was associated with worse fibrosis (Farkas et al., 2009). In contrast, early administration of decoy VEGF receptor in murine model of bleomycin-induced pulmonary fibrosis attenuated inflammation and vascular leak and resulted in attenuated fibrosis (Hamada et al., 2005). Although there is a controversy regarding the role of VEGF in IPF and development of associated pulmonary hypertension, aberrant neovascularisation contributes to pathogenesis of pulmonary fibrosis. Moreover, PDGF and FGF2 have been shown to act synergistically to promote angiogenesis independently of VEGF (Nissen et al., 2007). Preliminary clinical testing of nintedanib in IPF has shown that this compound has a potential to prevent decline in lung function, reduce incidence of acute exacerbations and preserve the quality of life in IPF patients (Richeldi et al., 2011).

Endothelin (ET-1) is a potent vasoconstrictor and is mainly secreted by endothelial cells. In the lung, ET-1 regulates the tone of airways and blood vessels (Kedzierski and Yanagisawa, 2001) and is secreted by AECII, Clara cells and alveolar macrophages. The expression of ET-1 is upregulated in IPF lungs, most intensely in the alveolar epithelium (Giaid et al., 1993; Saleh et al., 1997), in sera of IPF patients (Uguccioni et al., 1995) and BALF (Reichenberger et al., 2001). *In vitro* ET-1 promotes fibroblast proliferation and differentiation to myofibroblasts (Shahar et al., 1999), production of collagen and synthesis of extracellular matrix (Shi-wen et al., 2004; Simonson and Ismail-Beigi, 2011). Furthermore, ET-1 promotes fibroblasts and myofibroblasts resistance to apoptosis (Kulasekaran et al., 2009), which is a prominent feature of fibrotic fibroblasts. In animal models of pulmonary fibrosis inhibition of ET-1 receptors by bosentan has been shown to attenuate bleomycin-induced fibrosis (Park et al., 1997). In contrast, a study with bosentan in our laboratory did not show a reduction in collagen deposition and the severity of fibrosis in the bleomycin model (Mutsaers et al., 1998). Nonetheless, bosentan was taken into a clinical trial in IPF patients without pulmonary hypertension (King et al., 2008) but the trial was terminated early due to overall lack of beneficial effect.

Angiotensin II (ANG II) is converted from angiotensinogen by the angiotensin-converting enzyme (ACE) and signals via angiotensin receptor I and II (AT I and AT II) to promote tissue repair in normal wound healing. In IPF ANG II is upregulated in apoptotic alveolar epithelium and myofibroblasts (Li et al., 2006), which is matched by increased expression of AT I and ATII receptors in the interstitial mesenchymal cells (Königshoff et al., 2007). Furthermore, ACE polymorphism is associated with increased risk of development of pulmonary fibrosis (Uh et al., 2013) and angiotensinogen promoter polymorphism has been recently shown to predict the decline in lung function in IPF patients (Dang et al., 2013). Targeting ANG II receptors and ACE activity *in vivo* attenuated radiation- and bleomycin-induced fibrosis (Molteni et al. 2007; Wang et al. 2000) while local suppression of ANG II expression in the lung also resulted in protection from bleomycin-induced pulmonary fibrosis (Li et al., 2007). ANG II exerts a potent mitogenic effect on lung fibroblasts that can be inhibited by ATI receptor antagonist losartan (Marshall et al.,

2000). Furthermore, myofibroblasts from IPF patients have been shown to constitutively produce angiotensinogen and express increased level of TGFβ mRNA (Marshall et al., 2000; Uhal et al., 2007). Subsequently, high concentrations of ANG II and active TGFβ are detected in the supernatants from *in vitro* cultures of these cells. Blocking ANG II receptors abrogates the increase in TGFβ mRNA and active protein expression (Uhal et al., 2007). Furthermore, ANG II expression is induced *de novo* in the alveolar epithelium in pulmonary fibrosis and in an autocrine fashion promotes apoptosis of alveolar epithelium (Uhal et al. 1998) that again can be blocked by AT I inhibitor losartan (Wang et al. 1999). All these data confirm that ANG II is a prominent profibrotic mediator produced locally in the fibrotic lung and contributes to the pathogenesis of disease by stimulating mesenchymal cell proliferation, epithelial cell apoptosis and upregulating the expression and activation of TGFβ by means of ANG II/TGFβ autocrine positive feedback loop.

Connective tissue growth factor (CTGF) has also been shown to contribute to the pathogenesis of pulmonary fibrosis. CTGF is produced and secreted downstream of TGFβ activation and perpetuates ECM synthesis and deposition by fibroblasts and myofibroblasts. Increased levels of CTGF have been detected in the fibrotic tissue of IPF patients (Scotton and Chambers, 2007). Although CTGF alone does not induce fibrosis, it increases susceptibility to pulmonary fibrosis in BALB/c mice, a strain of laboratory animals that are inherently resistant to bleomycin-driven lung injury and fibrosis (Bonniaud et al., 2004a).

1.3.4.2 Transforming growth factor β

There is overwhelming evidence that TGFβ is a central mediator of pulmonary fibrosis in human disease and animal models (Coker et al., 1997, 2001; Khalil et al., 1991). TGFβ is a pleiotropic and ubiquitously expressed cytokine and elicits a wide range of cell- and tissue-specific responses, which include regulation of cell growth and survival, cell and tissue differentiation, developmental, inflammatory and haematopoietic processes, tissue remodelling and repair and synthesis of ECM (reviewed in Akhurst and Hata 2012). Primary function of TGFβ is immunomodulation and its importance is fully demonstrated in TGFβ1 knockout

mice, which develop postnatal lethal multifocal inflammatory syndrome that leads to tissue necrosis and organ failure (Shull et al., 1992). TGFβ has suppressive and anti-proliferative effects on cells of both innate and adaptive immunity (Akhurst and Hata, 2012). There are three TGFβ isoforms in humans: TGFβ1, TGFβ2 and TGFβ3. However, unlike TGFβ1, TGFβ3 overexpression does not lead to upregulation of TGFβ receptors and progressive fibrosis in the lung (Ask et al., 2008).

TGFβ gene expression is upregulated by inflammatory mediators such as TNFα (Sullivan et al., 2009) and ANGII as described previously. However, TGFβ activity is mostly regulated post-transcriptionally and the cytokine is secreted from cells in an inactive form and sequestered in ECM as part of a latent complex formed by the latency associated peptide (LAP) and latent TGFβ binding proteins (LTBP). This latent complex is covalently bound to the extracellular matrix and the dissociation of active TGFβ occurs following a conformational change in the LAP that can be triggered by a number of mechanisms of activation, including interaction with thrombospondin I or proteolytic activity exerted by matrix metalloproteinases, particularly MMP2 and MMP9. Changes in the environment such as low pH and mechanical stretch also contribute to the release of active TGFβ (Akhurst and Hata, 2012). However, current evidence suggests that the most relevant *in vivo* mechanism of TGFβ activation, particularly in the context of pulmonary fibrosis, occurs via integrins.

Integrins are transmembrane heterodimeric proteins and adhesion molecules that convey bidirectional communication between the cell and the environment. Different isoforms of α and β subunits assemble into 24 combinations of integrins, of which eight have arginine-glycine-aspartate (RGD) domain that is capable of binding the latent TGFβ complex (Munger et al. 1999). The intracellular domain of integrin connects with the actin cytoskeleton of cells while the extracellular domain interacts with extracellular matrix and LAP. The interaction between the LTBP and ECM is necessary for integrin-mediated TGFβ activation and the activity of TGFβ is greatly reduced when LTBP lacks the ECM binding domain (Annes et al., 2004). Integrins αvβ3, αvβ5, αvβ6 and αvβ8 have been shown to activate TGFβ *in vitro.*

Integrins αvβ6 and αvβ5 are physiologically most relevant to the injured lung responses as they are expressed on alveolar epithelium and fibroblasts, respectively, and hence can contribute to local activation of TGFβ in the lung (Scotton et al. 2009; Jenkins et al. 2006; Sheppard 2005; Munger et al. 1999). Although αvβ6 is expressed at low levels in a normal lung, it has been shown to be upregulated in pulmonary fibrosis (Xu et al., 2009). Furthermore, neutralising αvβ6 integrin *in vivo* attenuates pulmonary fibrosis (Puthawala et al., 2008). Another integrin implicated in pulmonary fibrosis is αvβ8 that has been shown to delay epithelial wound closure and inhibit bronchial epithelial cell proliferation *in vitro* (Neurohr et al., 2006).

The mechanism of integrin-mediated TGFβ activation can occur downstream of G-protein coupled receptor (GPCR) activation and reorganisation of cellular cytoskeleton. It was initially demonstrated that thrombin and direct PAR-1 activating peptide signal via Gαq and RhoA kinases to induce cytoskeletal re-arrangement, which in turn increases the degree of mechanical stress between the integrins and LAP, disrupting the latent complex and leading to release of active TGFβ (Jenkins et al., 2006; Scotton et al., 2009). Since then other GPCRs agonists, including lysophosphatidic acid (LPA), have been shown to also activate TGFβ via a similar integrin-mediated mechanism (Xu et al., 2009). Furthermore, both PAR-1 knockout mice and LPA receptor deficient mice are protected from bleomycin-induced pulmonary fibrosis and show reduced expression of TGFβ, α-smooth muscle actin (αSMA), collagen and fibronectin (Howell et al., 2005; Huang et al., 2013).

Active TGFβ signals in a paracrine manner via transmembrane serine/threonine kinase receptors type I and type II (TβRI and II) that form heterotetrameric complexes following agonist binding. TβRI is also termed activin receptor-like kinase receptor (ALK) and ALK5 in particular is widely expressed in different cell types in the lung and recruits Smad2 and Smad3 transcription activators. The canonical Smad-dependent signalling pathway involves phosphorylation of Smad2 and Smad3, which then form complexes with Smad4 and translocate to the nucleus.

Smad complexes act as transcription factors for regulation of expression of many genes (Massague, 2000). The canonical signalling pathway is negatively regulated by an inhibitory member of Smad family- Smad7.

TGFβ can also activate multiple Smad-independent signalling pathways, including all three mitogen-activate protein kinases (MAPK) pathways: p38, C-Jun N-terminal kinase (JNK) and extracellular signal regulation kinase (ERK). TGFβ can also interact with Rho kinases, nuclear factor kB (NF-kB), Wnt-β catenin and PI3-AKT signalling pathways (reviewed in Akhurst and Hata 2012; Biernacka et al. 2011).

The effect of TGFβ signalling on the progression of fibrosis has been extensively studied *in vivo.* Overexpression of TGFβ results in lung fibrosis while inhibition of TGFβ attenuates fibrosis in the bleomycin-induced model of pulmonary fibrosis (Giri et al. 1993). Furthermore, Smad3 knockout mice show enlarged airspace phenotype but are also protected from pulmonary fibrosis (Bonniaud et al., 2004b). Similarly, targeted knockout of TβRII in the alveolar epithelium causes emphysema but also offers protection from bleomycin-induced lung injury and fibrosis (Li et al., 2011). Integrin αvβ6-null mice show MMP-12-dependent enlargement of airspaces and reduced surfactant clearance (Koth et al., 2007; Morris et al., 2003).

Furthermore, *in vitro* studies have shown that TGFβ can activate multiple signalling pathways simultaneously, which can interplay to produce similar biological effect. TGFβ signalling leads to fibroblast to myofibroblast differentiation and TGFβ induces αSMA and collagen gene expression in Smad3-dependent manner (Hu et al., 2003). Smad3-null mice have reduced numbers of αSMA-positive myofibroblasts (Bonniaud et al., 2005a). However, non-canonical and MAPK-dependent TGFβ signalling pathways also play a role in fibroblast to myofibroblast differentiation. MAPK p38 activation is required for fibronectin expression and polymerisation (Dugina et al., 2001) and both p38 and ERK kinases induce αSMA expression (Hu et al., 2006a). C-Jun N-terminal kinase (JNK) has been shown to be phosphorylated in human lung fibroblast prior to αSMA induction (Hashimoto et al., 2001) while TGFβ-ERK signalling also induces collagen expression in fibroblasts (Caraci et al., 2008).

Furthermore, interaction between Smad3 and MAPK pathways promotes fibroblast survival (Horowitz et al., 2004).

Taken together these data strongly suggest that TGFβ plays a key role in the pathogenesis of fibrosis, as summarised in **Figure 1.3.,** but is also necessary for the development and maintenance of alveolar homeostasis.

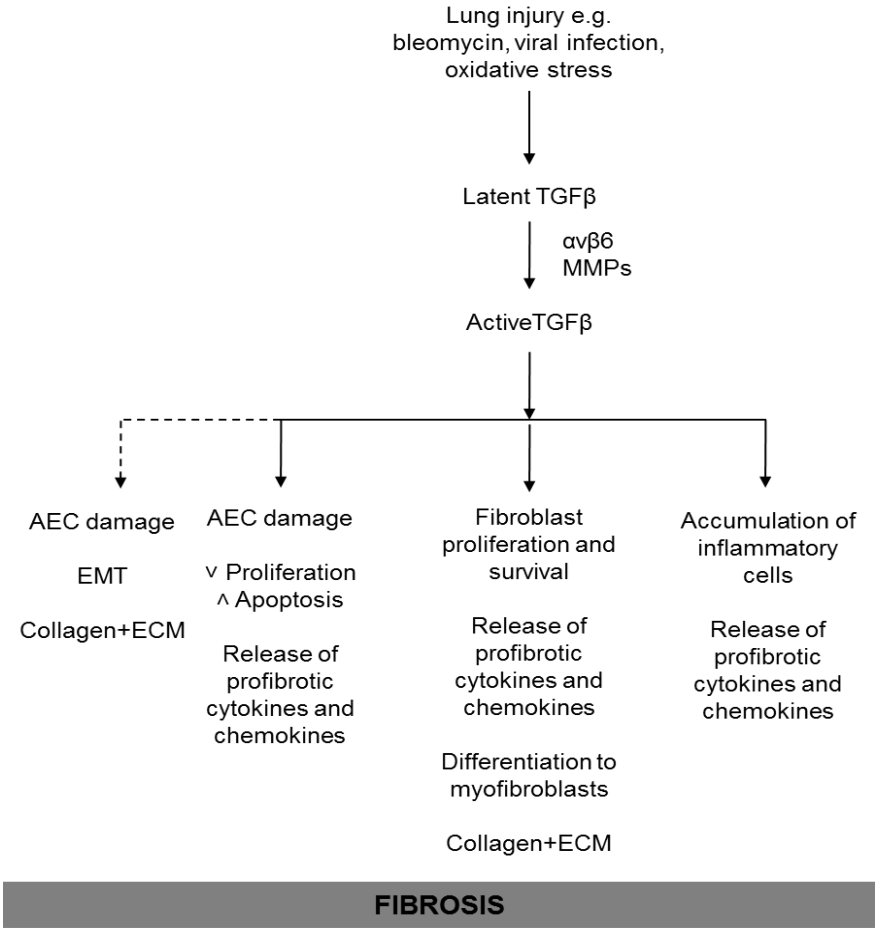

Figure 1.3 TGFβ-mediated profibrotic effects.

Following injury to the lung, mechanisms for the activation of TGFβ are set in motion. Subsequently, TGFβ acts in a paracrine mode on inflammatory cells, fibroblasts and epithelial cells in the lung and triggers ECM deposition. This perpetuation of a profibrotic environment can eventually lead to the development of fibroproliferative lung disease.

Mediator	Major Biological Activities					
	Target cell	Proliferation	Apoptosis	Chemotaxis	Collagen synthesis	Fibrogenic
TGFβ	Fibroblast	+	-	+	++	++
	Epithelium	-	+	-	+	+
PDGF	Fibroblast	++	0	+	+	+
FGF2	Fibroblast	+	0	+	+	+
TNFα	Fibroblast	+	+	0	+	+
IL-1β	Fibroblast	+	+	0	+	+
IL-4	Fibroblast	+	+	+	+	+
IL-10	Fibroblast	-	+	+	-	+
IL-13	Fibroblast	+	+	-	+	+
IFNγ	Fibroblast	-	+	+	-	-
CCL2/	Macrophage	-	-	+	+	+
MCP-1	Fibrocyte	+	-	+	+	+
CTGF	Fibroblast	+	0	+	+	+
Thrombin	Fibroblast	++	0	+	+	++
FXa	Fibroblast	++	0	-	+	++
ANG II	Fibroblast	+	-	0	+	++
	Epithelium	-	+	-	-	+
ET-1	Fibroblast	+	-	0	+	+

Table 1.2 Profibrotic mediators and their biological activity in pulmonary fibrosis. Updated from (Gharaee-Kermani et al. 2009; Gharaee-Kermani et al. 2007), ++, major role or strongly stimulatory, +, stimulatory, -, inhibitory, 0, no known effect.

1.3.4.3 Chemokines

Chemokines form an extensive family of proinflammatory mediators and chemoattractants that are released following injury to the lung and act to recruit neutrophils, lymphocytes, fibrocytes and other effector cells to the site of injury. Certain chemokines have been proposed as biomarkers for fibrotic lung disease. In experimental models of pulmonary fibrosis, CXCL11 has been demonstrated to attenuate bleomycin-induced fibrosis by preventing aberrant vascular remodelling (Burdick et al., 2005) and CXCL10 disrupts fibroblast migration (Jiang et al., 2010). Mice deficient in CXCL11 and CXCL10 receptor, CXCR3, have reduced levels of IFNγ and develop worse interstitial fibrosis following bleomycin administration (Jiang et al., 2004). CCL18 has also been shown to inversely correlates with the decline in pulmonary function (Prasse and Müller-Quernheim, 2009; Prasse et al., 2006).

Levels of CCL2 (monocyte chemoattractant protein 1, MCP-1) are increased in sera and bronchoalveolar lavage fluid from IPF patients (Baran et al., 2007; Suga et al., 1999) and fibroblasts from fibrotic lungs produce significantly higher levels of CCL2 (Deng et al., 2013). CCL2 is a potent chemoattractant of immune cells including neutrophils, monocytes, T-cells and immature dendritic cells. Moreover, CCL2 mediates recruitment of fibrocytes into the lung (Moore et al. 2006), their proliferation and differentiation into myofibroblasts (Ekert et al., 2011). CCL2 expression is induced by multiple profibrotic mediators including TGFβ and in an autocrine loop CCL2 subsequently upregulates TGFβ gene expression (Gharaee-Kermani et al. 1996). Cytokines IL-4, IL-13, IL-10 also mediate CCL2 release, which in turn propagates accumulation of Th2 lymphocytes and alternatively activated macrophages in the lung (Sun et al. 2011; Martinez et al. 2009; Ip et al. 2006). Alternatively activated macrophages are characterised by expression of arginase and mannose receptors and are involved in immunomodulation, tissue remodelling and angiogenesis. Furthermore, alternatively activated macrophages are potent producers of TGFβ and PDGF, can have a stimulatory effect on collagen production in normal lung fibroblasts and have been isolated from BALF of IPF patients (Prasse et al., 2006). CCL2 is also induced downstream of activation of extrinsic coagulation

cascade (Deng et al., 2008; Mercer et al., 2009), which will be discussed in more detail later in this thesis.

1.4 Viruses and IPF

There is accumulating evidence that viruses contribute to the pathogenesis of IPF and acute exacerbation of IPF. Hepatitis C virus and adenovirus have been linked with fibrosis but the strongest correlation has been described for the herpesvirus family (reviewed in Vannella and Moore 2008).

Herpesviruses have a double-stranded DNA genome, enclosed in icosapentahedral capsid that is surrounded by the amorphous protein layer called tegument, and finally enclosed in the glycoprotein envelope. The family is divided into three groups: α-herpesviruses include herpes simplex virus, β-herpesviruses, for example human cytomegalovirus (CMV) and human herpes virus 7 (HHV-7), and γ-herpesviruses such as Epstein Barr virus (EBV) and human herpes virus 8 (HHV-8). EBV infects asymptomatically 95% of the population, entering the organism via nasopharynx epithelium, where it replicates and migrates into lymph nodes to establish latency in the B-lymphocytes.

In experimental models, murine γ-herpesvirus-68 (γHV68) has been used to investigate the role of viral infection in the pathogenesis of pulmonary fibrosis (PF). Murine γHV68 is genetically co-linear with EBV and HHV-8 and occurs naturally following a similar infection pattern as human herpesviruses i.e. infects the respiratory system and persists in B-cells and epithelial cells (reviewed in Vannella and Moore 2008).

1.4.1 Detection of Herpesviruses in IPF patients

Evidence of persistent occult viral infections in the lungs of IPF patients have been reported by many studies. Lung tissue from IPF patients tested positive for herpes viruses in 97% cases, while in a control group composed of a cohort of patients with other lung conditions 36% harboured viral DNA (Tang et al., 2003). EBV, CMV, HHV-8 and HHV-7 were most commonly detected in the lungs of IPF patients, and 60% of

IPF patients harboured infection with 2 or more different types of herpesviruses (Tang et al., 2003). The findings of this study were also corroborated in another study, which showed that EBV genetic material was detected in IPF lung tissue with significant greater incidence (48%) than in control groups (12%) (Stewart et al., 1999). IPF patients have been shown to have increased serological levels of anti-EBV IgA and IgG in comparison to patients with pulmonary fibrosis of known aetiology (Vergnon et al., 1984) and the replicating virus is detected at higher frequency in alveolar epithelial cells in the lower respiratory system (Egan et al. 1995). Furthermore, EBV-positive IPF patients harboured virus with WZhet-rearranged genome containing a recombinant BZLF1 reactivation gene open reading frame, which allows the virus to spontaneously reactivate from latency, proliferate and spread between cells (Kelly et al., 2002). Indeed, detection of latent membrane 1 (LMP-1) of EBV virus is associated with a worse outcome and increased mortality in IPF patients (Tsukamoto et al., 2000).

It has also been postulated that the acute exacerbation of IPF can be a manifestation of an occult infection, not detected in the lung due to inadequate sensitivity of screening methods and a delay between onset of the symptoms and clinical presentation. A prospective study of BAL samples from IPF patients experiencing acute exacerbation and stable patients has shown that a third of exacerbating patients harboured viruses (Wootton et al., 2011). This study has employed three genetic screening methods to address the technological limitations of viral detection. By means of multiplex PCR, the presence of common respiratory viruses was detected in 9% of patients; pan-viral microarray revealed Torque teno virus (TTV) and herpesviruses in 35% of patients and finally the presence and identity of these viruses was also confirmed by DNA sequencing. Interestingly infection with two or more viruses was detected in a third of virally positive samples. Although this study found no significant correlation between the presence of viruses and incidence of acute exacerbations, patients harbouring viral infections required mechanical ventilation more often and had reduced lifespan post exacerbation (Wootton et al., 2011). Another study has previously identified TTV virus DNA in the blood sera of IPF patients, which was associated with increased

incidence of acute exacerbation and mortality (Bando et al., 2001). This virus is also detected at higher frequency in IPF patients that develop lung cancer when compared to IPF control and lung cancer control patients (Bando et al., 2008). A population of IPF patients that harbour TTV appear to have a poorer prognosis but more clinical evaluations and studies into the potential pathological mechanisms are required to establish a causative relationship between TTV infection and progression of IPF.

In contrast another study compared gene expression between IPF patients in a stable phase of disease and experiencing acute exacerbation and did not find any evidence of viral DNA presence (Konishi et al., 2009). However, the same study found upregulated markers of AECII damage and increased levels of mediators of innate immunity, α-defensins, which act as a broad spectrum endogenous antibiotics. In the lung α-defensins are secreted by the epithelium and inflammatory cells and display antimicrobial properties toward Gram-positive and Gram-negative bacteria, fungi and enveloped viruses (reviewed in Bals and Hiemstra 2004). Defensins also stimulate inflammatory cell recruitment into the lung by inducing the release of IL-8 from airway and alveolar epithelia (Wetering et al., 1997) and IFNγ, IL-6 and IL-10 from T-lymphocytes (Lillard et al., 1999). These data confirm that acute exacerbation is driven by injury to the epithelium that evokes inflammatory response, even though the potential infectious aetiology was not confirmed (Konishi et al., 2009).

1.4.2 Herpesvirus infection in experimental pulmonary fibrosis

Although evidence exists showing that herpesviruses are prevalent in patients with IPF, no definitive causal relationship between viral presence and the development of the human disease has been established. However, naturally-occurring equine γ-herpesvirus-5 has been associated with the development of interstitial pulmonary fibrosis in horses as a complication of viral pneumonia (Williams et al., 2007). Moreover, animal models of pulmonary fibrosis have been used to investigate the potential role of viruses in pulmonary fibrosis (PF).

The natural rodent pathogen, murine γHV68, shares 80% homology with human EBV and displays parallel invasive features: epithelial and B cell tropism, virus-driven B-cell activation and proliferation, and an acute infectious mononucleosis syndrome (Nash and Sunil-Chandra, 1994). Both EBV and γHV68 enter their respective hosts via oropharyngeal epithelium, preferentially replicate in the lung epithelium and traffic to lymphoid tissue where they establish a persistent, latent reservoir of the virus in B lymphocytes.

BALB/c mice are inherently resistant to bleomycin-induced pulmonary fibrosis and do not develop fibrosis following infection with γHV68. However, γHV68 infected mice develop pulmonary fibrosis when administered bleomycin (Lok et al., 2001). This two-hit model of pulmonary fibrosis in a resistant strain of mice demonstrates that a combination of pathological cues is required to trigger the fibroproliferative disease in the lung and validated viral infection as a potent contributor to the pathogenesis of pulmonary fibrosis. Furthermore, transgenic mice lacking the interferon gamma receptor (IFNγR) develop multi-organ fibrosis following infection with γHV68 (Ebrahimi et al., 2001) that can be attenuated by antiviral therapy. In these mice, the cytokine milieu is skewed towards T helper 2 (Th2) lymphocyte responses characterised by overproduction of profibrotic mediators, including TNF-α, TNF-β, IL-1β, TGF-β and lymphotactin. The IFNγR deficiency mimics the Th1-Th2 imbalance observed in IPF patients (Mora et al., 2007) and the results of this study support the notion that skewed immune responses can create a profibrotic environment in the lung that can act as cofactors for the development of fibrosis. Furthermore, adenoviral transfer of EBV transactivator protein Zta into mouse lungs caused neutrophilic inflammation, induced IL-13 production from alveolar epithelial cells prompting Th2 phenotype in the lung and increased secretion of profibrotic chemokines, mainly CCL2 from infiltrating immune cells (Guenther et al., 2010). In this study the inflammation resolved after four weeks with no fibrosis in the lung.

Animal models of pulmonary fibrosis concomitant with latent viral infection demonstrated aggravated fibrosis with a worse outcome in comparison to mice given a fibrotic stimulus only (Vannella et al., 2010a). Latent viral infection

augmented the response to the fibrotic injury and led to significantly increased collagen deposition in the lung, upregulation of CCL2 and CCL12 expression and release, increased fibrocyte recruitment, increased basal levels and activity of TGFβ. Also, infected mice were susceptible to sub-threshold doses of fibrotic stimuli (Vannella et al., 2010a). Furthermore, the virus has infected alveolar macrophages that produced large amounts of IFNγ, TNFα, CCL2, CCL12 as well as TGFβ four weeks after the infection (Stoolman et al., 2010). Mesenchymal cells isolated from the infected mice also showed long-lasting upregulation of profibrotic mediators, notably TGFβ and CCL2. These data suggest that the latent viral infection can prime the lung toward a profibrotic phenotype.

A link between viral infection and acute exacerbation of pulmonary fibrosis was also established in experimental model of fibrosis (McMillan et al., 2008). During the course of fluorescein isothiocyanate-induced (FITC) fibrosis mice were infected with γHV68 and displayed more rapid deterioration in comparison with mock-infected mice. Collagen deposition was significantly increased in infected mice as was CCL2 and CCL12 release and fibrocyte recruitment into the lung. In this study mice mounted a competent IFNγ-mediated antiviral response which showed that the virus is able to affect the progression of fibrosis independently of the cytokine environment. This observation was reinforced when this model of viral exacerbation of pulmonary fibrosis was repeated in Th1 biased mice deficient in the Th2 cytokines- IL-4 and IL-13 (McMillan et al., 2008).

Pulmonary fibrosis largely affects the ageing population and therefore the responses to viral infection have been investigated in aged mice to recapitulate the human disease better and to dissect any potential difference in fibrosis pattern that can be influenced by age. Aged mice have been shown to develop pulmonary fibrosis in response to gammaherpesvirus infection alone despite fully competent antiviral immune responses and control of the viral load (Naik et al., 2011). However, aged mice expressed higher levels of TGFβ concomitant with upregulation of TGFβ receptors on fibroblasts. An increase in fibroblast sensitivity to TGFβ and subsequent resistance to apoptosis was postulated as a mechanism for

development of fibrosis in these mice (Naik et al., 2011). Furthermore, viral infection in the lungs of aged mice was associated with increased markers of endoplasmic reticulum stress and AECII apoptosis (Torres-González et al., 2012). Aged mice also showed increased inflammation and TGFβ levels in the early phase of infection. Overall these data suggest that although young and aged mice can mount antiviral immunity to viral infection, there are marked differences in the resolution of inflammation and tissue repair mechanisms that in aged mice can lead to the development of fibroproliferative lung disease.

1.4.3 Viruses as cofactors in pulmonary fibrosis

Although herpesviruses preferentially infect B-lymphocytes, where they establish latency, they also display tissue tropism towards the alveolar epithelium. The virus is presumed to exist in a state of equilibrium, continuously shuttling between B lymphocytes, which is its main latency reservoir and epithelium, which is considered to be the main replication site. Furthermore, viral tropism is dictated by the specialised and discordant fusion proteins expressed by different cell types and necessary for the viral entry into cells. The viral glycoproteins B, H and L are essential for fusion with epithelial cells while glycoprotein gp42 is crucial for attachment to the HLA class II receptor present on B-lymphocytes. Subsequently progeny virions emerging from B-cell express more gBgHgL complexes which primes them for epithelial cell infection while epithelial cell released virions contain relatively more gp42 and target the B-cells (Borza and Hutt-Fletcher, 2002). In epithelial cells the auxiliary molecules required for the viral entry into the cell are integrins and particularly αvβ6 and αvβ8 have been shown to aid the viral entry into the epithelial cells (Chesnokova et al., 2009). As previously described in this thesis, both integrins are associated with pulmonary fibrosis as they have a high affinity for the latency associated peptide LAP-TGFβ complex and contribute to TGFβ activation (Goodwin and Jenkins, 2009; Sheppard, 2005). Furthermore, the αvβ6 integrin is expressed on normal lung epithelium at low levels and is upregulated in response to injury (Thomas et al., 2006). This may be a potential mechanism by which herpesviruses infection spreads to the alveolar epithelium in IPF patients.

Furthermore, alveolar epithelium expresses CD24 receptor, which EBV can also utilise as a co-receptor aiding the attachment and entry into the cell and this receptor is upregulated by IL-4 (Malizia et al., 2009a). This can lead to enhanced infection of AECII in Th2- skewed environment that is documented in IPF lung.

The viral life cycle is detrimental to infected cells. In the lytic phase virus attaches to the cell surface in order to enter the intracellular compartment. It subsequently hijacks and re-programmes host's replication and protein production machinery to produce viral structural components. Viral progeny assemble in the cytoplasm and trigger cell lysis in order to be released into the extracellular space, where the infection process can start again. Therefore viral infection leads to extensive epithelial cell damage as a direct result of the viral life cycle, which also produces an inflammatory responses that could lead to the remodelling of alveolar spaces and the development of fibrotic lesions similar to those observed in IPF (Mora et al., 2007). γHV68 has been shown to preferentially infect AEC II and may contribute to dysregulated cell repair and surfactant abnormalities associated with increased apoptosis of AECII and alveolar collapse (Mora et al., 2006).

Following invasion of the host cell and the incorporation of its genetic code into the host genome, viruses can switch into dormant mode and establish latency. This can create the potential for reactivation and be a source of repetitive epithelial injury, as implicated in the pathogenesis of IPF. Immunosuppression is a major trigger for viral reactivation and therefore IPF patients receiving steroids would be susceptible to recurring infections. Furthermore, the latent virus can alter the phenotype of infected cells. A study in human AECII shows that EBV latent membrane protein I (LMP-1) and TGFβ synergistically induce epithelial-mesenchymal transition (Sides et al., 2010). Also in the animal models it has been shown that latently infected epithelial cells upregulate TGFβ mRNA and protein expression and upon reactivation of the virus increase cell apoptosis (Malizia et al., 2008). Also, TGFβ has been shown to induce reactivation of the virus and promote phenotypic changes toward mesenchymal cells with loss of E-cadherin, increased cell proliferation, motility and invasion via Wnt/CUX-1 dependent mechanism (Malizia et al., 2009b).

CMV and parvovirus B19 infections induce microvascular injury (Magro et al., 2003), which is also a recognised feature of IPF and inevitably leads to activation of coagulation and fibrin deposition in alveolar spaces. Furthermore, human herpes simpex virus I (HSV I) and CMV have been shown to circumvent the host control of the coagulation cascade and activate it independently. HSV I and CMV express tissue factor and procoagulant phospholipids on their surface imitating the injury signal and providing a platform for the assembly of the TF-FVIIa-FXa complex leading to the generation of thrombin. These viruses also encode and express glycoprotein C which accelerates FVIIa-dependent activation of FXa, effectively improving the efficiency of the coagulation cascade (Sutherland et al., 1997). This viral behaviour is most likely an immune evasion strategy as it results in the virus being coated in host-derived proteins and hence hidden from the immune surveillance. However, thrombin has also been shown to enhance HSV I and CMV cell invasion in human umbilical vein endothelial cells (HUVEC) and human foreskin fibroblasts (HFF) (Sutherland et al. 2007). Herpesviruses can therefore directly contribute to excessive activation of coagulation implicated in the pathogenesis of pulmonary fibrosis, which will be the focus of the next section.

1.5 Coagulation in lung injury and fibrosis

The coagulation cascade is a host defence mechanism that plays a key role in restoration of homeostasis following an injury. The coagulation cascade is activated in response to loss of tissue integrity resulting from injury or infection. It leads to blood clot formation that acts as an impenetrable protective barrier preventing further blood loss and reducing the risk of infection. Historically two coagulation pathways have been described: extrinsic, initiated in the event of tissue damage and intrinsic, also known as contact activation pathway. It is increasingly recognised that the two pathways are intertwined and mutually interdependent. The current consensus of activation of coagulation identifies three steps: initiation that involves exposure of tissue factor to coagulation factors, amplification and clot formation. There is a large body of evidence suggesting that activation of the coagulation plays a role in acute lung injury (ALI), acute respiratory distress syndrome (ARDS) and pulmonary fibrosis.

1.5.1 Overview of coagulation and anticoagulant pathways

The extrinsic coagulation pathway is initiated by tissue factor (TF), which is a transmembrane glycoprotein constitutively expressed in the extravascular compartments in many different tissues and organs. TF is also expressed on quiescent endothelial cells but under normal physiological conditions TF is shielded from coagulation zymogens in the blood in the process of encryption, which is defined as post-translational suppression of the procoagulant activity. The exact mechanism of encryption is not fully elucidated and current theories postulate that TF requires anionic phospholipids (AP), such as phosphatidylserine (PS) for binding factor VIIa (FVIIa) and subsequent activation of factor X to factor Xa (FX to FXa) (Rao et al., 2012). Alternative hypothesis states that the coagulant activity of TF is regulated by the formation of allosteric cysteine disulphide bonds in the TF extracellular domain, which stabilises binding to FVIIa (Ruf, 2012). Bacterial lipopolysaccharide (Rivers et al., 1975), C-reactive protein (Cermak et al., 1993), PDGF and CCL2 (Ernofsson and Siegbahn, 1996) can all trigger unmasking of TF. These factors also alter the dynamic composition of the cell membrane and APs that

are normally expressed on the intracellular site of the cell membrane, flip to the extracellular part of the membrane. APs actively participate in the de-encryption process of TF and formation of the ternary complex (TF-FVIIa-FXa) through PS binding to FX and hence increasing the local concentration of the substrate for TF-FVIIa catalytic activity. It has also been suggested that PS can bind FVIIa and orientate it in the plasma membrane in the most efficient way for TF binding. Finally, it is possible that the electrostatic interactions between PS and TF can alter the quaternary structure of TF and position it in the cell membrane for the optimal alignment for assembly of the ternary complex (reviewed in Rao et al. 2012).

TF binds to FVIIa, of which small quantities constantly circulate in blood and facilitates further activation of factor VII (FVII). Although a fraction of active FVII is constitutively present in the circulation, it does not exhibit catalytic activity toward FX nor factor IX (FIX) until bound to TF. This extrinsic tenase complex (TF-FVIIa + APs) increases the rate of FXa generation 15-million fold (Bom and Bertina, 1990) and also activates FIX. The complete and active ternary complex TF-FVIIa-FXa proceeds to generate thrombin from prothrombin in a sufficient manner to trigger platelet activation, fibrin generation and activate factors V and VIII (FV, FVIII) (reviewed in Mann 2003). The small amounts of FIXa generated by the ternary complex combine with FVIIIa on the platelet surface forming the intrinsic tenase complex, which is 100-fold more efficient in cleaving FX and greatly amplifies the rate and amount of generated FXa. Combined with FVa, FXa forms a prothrombinase complex that proceeds to generate large amounts of thrombin (**Figure 1.4**). Primary function of thrombin is activation of platelets that involve their shape change, aggregation and assembly of a weak haemostatic plug that initiates clot formation. Thrombin then converts fibrinogen to fibrin, which forms cross-linked strands and provide the scaffold for stabilisation and reinforcement of the platelet plug, which altogether facilitate formation of a clot. Thrombin also exerts multiple cellular effects on many cell types by activating proteinase-activated receptors (PARs), in particular PAR-1 (described in detail in **section 1.6**). Thrombin also liberates FVIII bound to von Willebrand factor, which aids the switch from extrinsic to intrinsic coagulation cascade (Adams and Bird, 2009). It is generally

considered that the extrinsic coagulation is an initiation step in the thrombin generation cascade, while intrinsic coagulation activity serves as an amplification step to generated large quantities of thrombin.

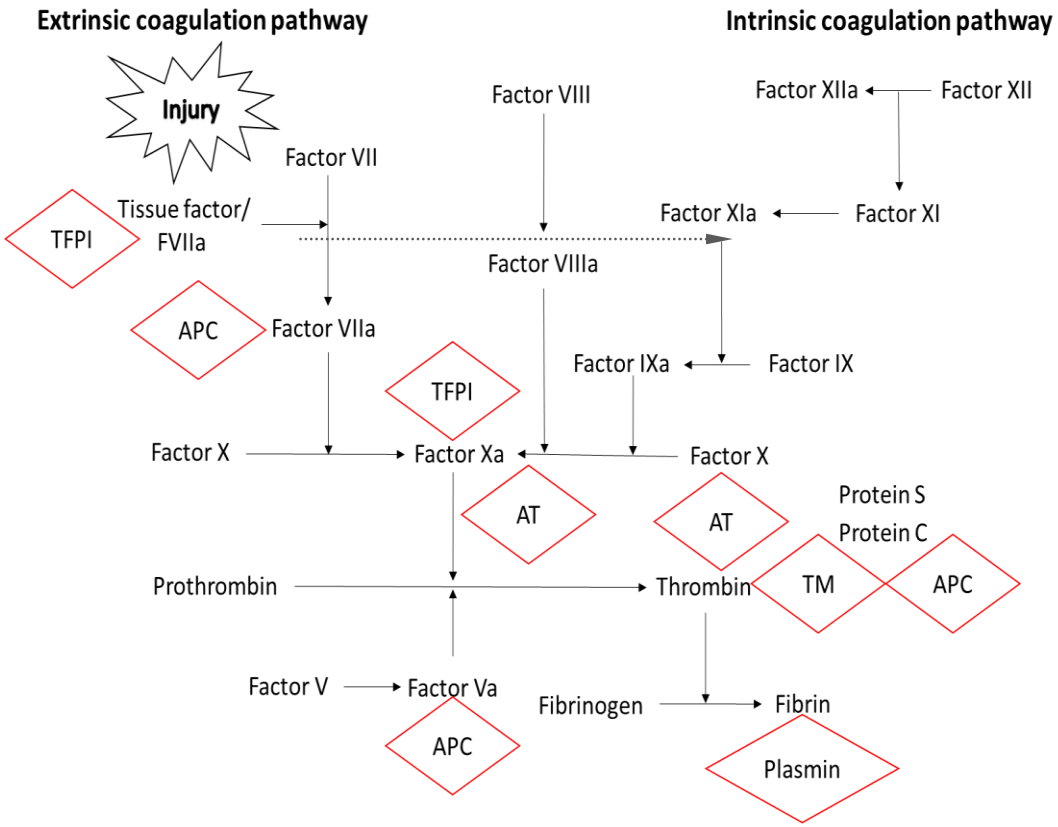

Figure 1.4 Overview of the coagulation cascade.

The extrinsic coagulation pathway is initiated by injury to the tissue that leads to upregulation of tissue factor (TF) and formation of the TF-FVIIa-FXa ternary complex. This complex triggers the conversion of prothrombin to thrombin and the subsequent generation of fibrin. The intrinsic coagulation pathway cascade is initiated upon assembly of the intrinsic tenase complex (FIXa-FVIIa) that greatly propagates FXa and thrombin generation hence amplifying the coagulation signal. This cascade is regulated by endogenous anticoagulants: TFPI- tissue factor pathway inhibitor, AT- antithrombin, TM- thrombomodulin, APC- activated protein C. Plasmin is a key regulator of reabsorption of the fibrin clot.

The coagulation cascade is tightly controlled by negative feedback loops and endogenous anticoagulants (**Figure 1.4**). Tissue factor pathway inhibitor (TFPI) is a key regulator of the extrinsic coagulation pathway through inhibition of the catalytic activity of the ternary complex. TFPI contains Kunitz-domains that first bind FXa and proceed to bind TF-FVIIa in a calcium-dependent mechanism forming a quaternary complex that prevents thrombin generation. In normal physiological conditions TFPI is constitutively produced by endothelial cells and around 80% remains bound to the cell surface. However, TFPI can also be induced in extravascular compartments in cell populations expressing tissue factor, including the activated alveolar epithelium and fibroblasts (Bajaj et al., 2001).

Thrombomodulin is present on endothelial cells where it binds thrombin and switches its activity from activation of the platelets and thrombus formation to activation of protein C. The potential of protein C activation is greatly enhanced when protein C is bound to the endothelial protein C receptor (EPCR), which is believed to spatially orientate protein C for optimal cleavage. Once activated, APC-EPCR complexes localise to caveolae and exert pleiotropic cytoprotective effects that will be described in more detail later in this thesis. The main anticoagulant function of APC is also to terminate thrombin generation by proteolytic inactivation of the components of the intrinsic coagulation pathway, namely FVa and FVIIa. Protein S is a major cofactor in this process by actively competing with FXa for binding to FVa (**Figure 1.4**) (Griffin et al., 2012).

Antithrombin is a circulating glycoprotein produced in the liver that inhibits a broad spectrum of coagulation factors including thrombin, FVIIa, FIXa, FXa, FXIa. The antithrombin inhibitory action is greatly potentiated by heparin or endogenous equivalent heparan glycosaminoglycans present on the cell surfaces. These molecules are essential for the efficient formation of antithrombin-thrombin complexes (Kubier and O'Brien, 2012).

The end result of the coagulation cascade is the formation of a fibrin clot that is subsequently reabsorbed in the tissue remodelling processes. Plasmin is the main executor of fibrinolysis and is generated from plasminogen by two types of

plasminogen activators (PA): tissue-type in the vasculature (tPA) and urokinase-type in the tissue (uPA). As well as dissolving the fibrin network, plasmin activates matrix metalloproteinases (MMPs) that are important in the remodelling of the extracellular matrix. The generation of plasmin is regulated by plasminogen activator inhibitors (PAI-1 and PAI-2), which irreversibly bind PA with high affinity. PAI expression is regulated by many growth factors including TGFβ, PDGF, inflammatory cytokines and endotoxins (Van De Craen et al., 2012).

1.5.2 Coagulation in lung injury and fibrosis

Acute lung injury (ALI) and the acute respiratory distress syndrome (ARDS) result from injury to the pulmonary epithelium and are characterised by diffuse alveolar damage (DAD), vascular leak and inflammation. TF is upregulated on the alveolar epithelium in the injured lung and co-localise with FVII and FX, strongly suggesting that extrinsic coagulation cascade is activated locally within the injured airspaces (Bastarache et al., 2007; Scotton et al., 2009). Furthermore, increased levels of TF are readily detected in the BALF from patients with ALI and ARDS (Idell, 2003a), both in a soluble form as well as associated with highly procoagulant microparticles (Bastarache et al., 2009). The current consensus states that locally activated extrinsic coagulation is then able to generate thrombin and subsequently form fibrin deposits from substrate coagulation zymogens present in the oedema fluid. Intraalveolar and interstitial fibrin deposition is a hallmark of ALI and manifests as hyaline membranes in alveolar spaces (reviewed in Chambers 2008; Idell 2003). Extensive fibrin deposition in the alveolar spaces leads to the collapse of alveoli (atelectasis) through inhibition of surfactant function (Seeger et al. 1993) and traction of remaining airspaces (honeycombing). Moreover, fibrin can act as a provisional matrix and a reservoir of growth factors and cytokines for the subsequent recruitment of inflammatory and mesenchymal cells. Inflammatory cytokines, namely IFNγ and TNFα, are released in abundance in ALI and have also been shown to upregulate the expression of TF by the alveolar epithelium (Bastarache et al., 2011) and hence perpetuate further the local activation of coagulation. ALI is also characterised by inadequate activation of intrinsic

anticoagulant and fibrinolysis pathways. Low levels of protein C and increased PAI levels in the serum of ALI patients are key features of the ALI biomarker profile and are predictive of poor clinical outcome (McClintock et al., 2008; Ware et al., 2007).

Similarly in pulmonary fibrosis there is strong evidence that the extrinsic coagulation pathway is activated in the intraalveolar compartment and may play a role in the disease pathogenesis. Tissue factor is upregulated on AEC II and alveolar macrophages in the vicinity of fibrin deposits in IPF lung and overlying fibrotic foci suggesting that extravascular coagulation plays a role in the pathology of IPF (Imokawa et al., 1997).

As already mentioned low levels of protein C are predictive of a poor outcome in ALI patients (McClintock et al., 2008; Ware et al., 2007). APC levels are also reduced in the lungs of patients with IPF and sarcoidosis as well as in collagen vascular disease-associated interstitial lung disease (Kobayashi et al. 1998). Deficient anticoagulant mechanisms also have been shown to correlate with abnormal collagen turnover in the intraalveolar space of patients with fibroproliferative lung diseases (Yasui et al., 2000).

Thrombin levels are increased in BALF fluid from patients with pulmonary fibrosis associated with systemic sclerosis (Hernández-Rodríguez et al., 1995) and chronic lung disease of prematurity (Dik et al., 2003). The importance of fibrin accumulation in the alveoli was investigated in animal models of pulmonary fibrosis with the use of transgenic mice over-expressing or deficient in plasminogen activator inhibitor-1 (PAI-1). PAI-1 is a negative regulator of the fibrinolytic pathway and inhibits plasminogen to plasmin conversion and hence prevents fibrin clearance. Mice over-expressing PAI-1 develop more severe fibrosis following bleomycin injury while PAI-1 knockout mice are protected (Eitzman et al., 1996). Interestingly, fibrinogen knockout mice are not protected from experimentally-induced pulmonary fibrosis, indicating that fibrin is most likely a symptomatic rather than a causative factor in the development of fibrosis in this animal model (Hattori et al., 2000).

1.5.3 Targeting coagulation in lung injury and fibrosis

Evidence from human and animal studies of lung injury and fibrosis suggest that the coagulation cascade is highly activated in these conditions whereas fibrinolytic pathways appear to be deficient. Several coagulation targeting approaches have been utilised over the years showing that inhibition of coagulation at different levels affects the progression of lung injury and fibrosis (**Tables 1.3 and 1.4**). In ALI models, concomitant administration of endotoxin and hirudin led to reduced lung inflammation (Bao et al., 2012). Administration of tissue factor neutralizing antibodies in the model of endotoxin-induced sepsis and indirect ALI attenuated inflammatory cell influx and oedema, reduced secretion of inflammatory cytokines IL-6 and IL-8 both systemically and in the alveolar compartment and prevented a decline in lung function and compliance (Welty-Wolf et al., 2006). In contrast, low tissue factor-expressing mice displayed increased inflammatory responses and alveolar haemorrhage in the model of direct ALI (Bastarache et al., 2012), pointing to a more complex role for the coagulation factors in lung injury.

In the bleomycin model of lung injury and fibrosis the coagulation cascade has been shown to be activated in the alveolar compartment with increased levels of thrombin detected from day three through to 21 after bleomycin administration (Yasui et al., 2001). This increase in coagulation proteinases levels can be reversed by administration of APC into the lung, which also reduces fibrotic alterations to the lung architecture (Yasui et al., 2001). Similarly, targeting tissue factor in the bleomycin model of pulmonary fibrosis by local overexpression of TFPI attenuates fibrosis (Kijiyama et al., 2006). Furthermore, administration of nebulised heparin and plasminogen activator (PA) has also had beneficial effects in pulmonary fibrosis in rabbits. The anticoagulant therapies attenuated the decline in lung compliance and respiratory physiology as reflected on molecular level by reduced collagen deposition in the lung (Günther et al., 2003).

As previously mentioned, FXa is upregulated locally in the lungs of IPF patients and in the experimental model of pulmonary fibrosis. Inhibition of FXa in the early phase of bleomycin model of pulmonary fibrosis attenuates lung collagen deposition

(Scotton et al., 2009). Direct thrombin inhibition has also been shown to reduce ECM proteins synthesis and deposition by fibroblasts and attenuate bleomycin-induced lung injury and fibrosis (Bogatkevich et al., 2011; Howell et al., 2001). Prophylactic (day 1) and therapeutic (day 8) thrombin inhibition reduced inflammation at day 14 post bleomycin instillation and reduced collagen deposition in the lung at day 21 post injury (Bogatkevich et al., 2011).

Systemic administration of APC also reduces the local activation of coagulation in the endotoxin-driven lung injury in humans. Following instillation of endotoxin into healthy volunteers, increased levels of thrombin and tissue factor are detected in the BALF and this effect is attenuated by APC (Poll et al., 2005). Furthermore, the fibrinolytic balance of the lung is disturbed with reduced levels of plasminogen activator PA and increased levels of plasminogen activator inhibitor, PAI-1. APC treatment restored this balance by blocking PAI-1 levels without affecting the PA levels (Poll et al., 2005).

The accumulated evidence that the coagulation cascade is activated in human lung disease and anticoagulant therapies reduce inflammation and fibrosis in the experimental models of lung injury and fibrosis provided a scientific rationale for two clinical trials that tested the effect of warfarin in IPF patients. A small, non-blinded, randomised study of IPF patients receiving standard prednisolone therapy supplemented with warfarin or heparin showed that anticoagulants extended the hospitalisation-free time and 3-year survival of IPF patients and significantly reduced the mortality from acute exacerbations (Kubo et al., 2005). Contrary to these results, a double-blinded, randomised, placebo-control clinical trial of warfarin in IPF was terminated early due to high mortality rate in the warfarin-treated patients (Noth et al., 2012). Almost 20% of patients given warfarin have died from respiratory-related causes and there was an overall trend pointing to anticoagulation having a detrimental effect on the progression of the disease (Noth et al., 2012).

Warfarin is a broad spectrum anticoagulant that inhibits vitamin K epoxide reductase, an enzyme that is responsible for recycling vitamin K from epoxide form.

Vitamin K is necessary for post-translational carboxylation of glutamate residues in key coagulation factors: thrombin, factors VII, IX and X. This process allows for the conformational change of these coagulation factors in the presence of calcium ions and interaction with anionic phospholipids, which is crucial for their bioactivity. Furthermore, key endogenous anticoagulants protein C and protein S are also vitamin K-dependent and their activity is inhibited by warfarin (Hirsh et al., 1995a). The imbalance between activation of coagulation and anticoagulant mechanisms is documented in pulmonary fibrosis and there is evidence suggesting that local activation of coagulation may have different effects from systemic activation of coagulation. The potential explanation for the rapid deterioration of IPF patients treated with warfarin may be that warfarin broad inhibition mechanism is further aggravating the already dysregulated homeostasis in IPF. Furthermore, warfarin did not prevent acute exacerbations in the first study but upon hospitalisation patients were given low-molecular-weight heparins, which then accounted for better recovery when compared to the control group (Kubo et al., 2005). Heparins are glycosaminoglycans that bind to antithrombin III and greatly increase the rate of thrombin and FXa inactivation (Hirsh et al., 1995b). Therefore, it is possible that warfarin is a “double-edged sword” and any benefit from blocking coagulation proteinases is offset by the inhibition of endogenous anticoagulants. It is also plausible that the contradictory results of the two studies stem from ethnic differences in the patient cohorts. The first study was performed in Asian IPF patients and the second clinical trial recruited patients of Caucasian and Afro-American origin. There are distinct differences in the disease progression and incidence of acute exacerbation between the two populations, most relevantly due to lower prevalence for cardiovascular disease and thromboembolism in Asian populations (reviewed in Song et al. 2011).

Furthermore, by inhibiting the coagulation factors, warfarin is also blocking a plethora of cellular effects that these factors exert via proteinase activated receptors PARs, as described in detail in the next section.

Target/ Anticoagulant	Model and outcome	Reference
Human studies		
APC administration	Reduced activation of intraalveolar coagulation and restoration of fibrinolytic balance in endotoxin-induced lung injury	(Poll et al., 2005)
Warfarin/ Heparin administration	Increased 3-year survival in IPF patients Hospitalised patients in the anticoagulant arm were administered low-molecular-weight heparin strongly associated with improved recovery and reduced mortality	(Kubo et al., 2005)
Warfarin administration	Increased mortality in IPF patients due to respiratory complications	(Noth et al., 2012)

Table 1.3 Anticoagulant therapies in lung injury and fibrosis- clinical studies

Target/ Anticoagulant	Model and outcome	Study
Animal studies		
Thrombin inhibition	Reduced inflammation and fibrosis in bleomycin-induced lung injury and fibrosis	(Bogatkevich et al., 2011; Howell et al., 2001)
Tissue factor inhibition	Attenuation of lung function abnormalities, reduced inflammation and oedema in LPS-induced sepsis-associated ARDS	(Welty-Wolf et al., 2006)
	Exacerbated inflammation and alveolar haemorrhage in ALI in TF-deficient mice	(Bastarache et al., 2012)
TFPI overexpression	Attenuation of bleomycin-induced lung injury and fibrosis following intratracheal TFPI gene transfer	(Kijiyama et al., 2006)
APC administration	Reduced extent of bleomycin-induced activation of coagulation and fibrosis	(Yasui et al., 2001)
Heparin administration	Attenuation of bleomycin-induced lung injury and fibrosis	(Günther et al., 2003)
Plasminogen activator administration	Attenuation of bleomycin-induced lung injury and fibrosis	(Günther et al., 2003)
FXa inhibition	Attenuation of collagen deposition in the bleomycin model	(Scotton et al., 2009)

Table 1.4 Anticoagulant therapies in experimental lung injury and fibrosis

1.6 Proteinase activated receptors in lung injury and fibrosis

Proteinase-activated receptors (PARs) are G-protein coupled receptors (GPCRs) activated via proteolytic cleavage of the external N-terminus (Coughlin, 2001). There are four members of the PAR family (**Table 1.5**), with PAR-1 and PAR-2 being most ubiquitously expressed. The main activators of PAR receptors are the proteinases of the extrinsic coagulation pathway. PAR-1 is the major high affinity thrombin receptor implicated in homeostasis and pathological processes and will be the main focus of this section.

	PAR-1	**PAR-2**	**PAR-3**	**PAR-4**
Activating proteases	Thrombin APC-EPCR TF-FVIIa-FXa Trypsin Plasmin Cathepsin G MMP-1 Granzyme A Bacterial gingipains	Trypsin Tryptase TF-FVIIa-FXa Der p1 Bacterial gingipains	Thrombin Trypsin	Thrombin Trypsin TF-FVIIa-FXa Cathepsin G Bacterial gingipains
Tethered ligand	SFLLRN (h) SFFLR (m,r)	SLIGKV (h) SLIGRL (m,r)	TFGRAP (h) SFNGGP (m)	GYPGQV (h) GYPGKV (m)
Inhibitory proteases	Cathepsin G Elastase Chymase Der p1	Elastase Chymase	Cathepsin G	Unknown
Chromosomal location	5q13	5q13	5q13	19p12
Main cleavage site	Arg41-Ser42	Arg36-Ser37	Lys38-Thr39	Arg47-Gly48
PAR-coupled- G proteins	$G\alpha_{i/o}$, $G\alpha_{q/11,}$ $G\alpha_{12/13}$	$G\alpha_{q/11,}$ $G\alpha_{12/13}$	$G\alpha_{o}$, $G\alpha_{q}$	$G\alpha_{q,}$ $G\alpha_{12/13}$
Expression in the lung	Airways, blood vessels, lung parenchyma	Airways, blood vessels, bronchial glands, lung parenchyma	Airways	Airways, blood vessels, cardiovascular system

Table 1.5 Characterisation of PARs

Updated from (Chambers 2008; Ramachandran and Hollenberg 2008; Steinhoff et al. 2005)

1.6.1 PAR-1 biological function

PAR-1 is ubiquitously expressed on a variety of cell types including human platelets, endothelial cells, epithelial cells, fibroblasts, monocytes, macrophages, lymphocytes, smooth muscle cells, skeletal muscle cells, mast cells, natural killer cells, neurons and glial cells and certain tumour cell lines (Steinhoff et al., 2005). PAR-1 influences a wide range of cellular responses including proliferation, differentiation, cytoskeletal rearrangements, apoptosis, migration and extracellular matrix production. In the lung, PAR-1 has been shown to be expressed by fibroblasts (Sokolova et al., 2005), endothelial cells (Ellis et al. 1999) and receptor expression is significantly upregulated in the lungs of IPF patients (Howell et al., 2001; Mercer et al., 2009).

Thrombin-mediated PAR-1 activation leads to activation and aggregation of platelets. In human platelets the initial burst of activity in response to thrombin is accounted for by PAR-1 receptor activation and signalling. PAR-4 is also expressed by human platelets and becomes activated when high concentrations of thrombin are present and is responsible for prolonged responses. Mouse platelets do not express PAR-1 but instead PAR-3 acts as a cofactor for PAR-4 activation by concentrating thrombin to the cell surface until a threshold concentration for PAR-4 activation is reached (Nakanishi-Matsui et al., 2000). PAR-3 and PAR-4 can form heterodimers reinforcing this mechanism (McLaughlin et al. 2007). Thrombin-PAR-1 signalling in platelets also leads to release of thromboxane A2, PDGF and TGFβ.

During acute lung injury, PAR-1 activation on endothelial cells leads to disruption of the endothelial-alveolar barrier and increased vascular permeability. High concentrations of thrombin act via PAR-1 and induce endothelial cell shape change and loss of tight junctions (Rabiet et al., 1996). PAR-1 signalling in endothelial cells also promotes tissue factor expression and the upregulation of adhesion molecule expression, such as intracellular adhesion molecules (ICAM), E-selectin and P-selectin. These molecules facilitate platelet aggregation and leukocyte adhesion as well as extravasation of inflammatory cells and coagulation factors to the site of

injury. This is the major mechanism that leads to extravascular leak and deposition of fibrin in alveolar spaces (Idell 2003) .

The role of inflammation in IPF is currently a highly debated subject, however PAR-1 activation exerts potent pro-inflammatory effects including promoting the production of cytokines: IL-1β, TNF-α, IL-8, IL-6 (reviewed in Chambers 2008). Thrombin-mediated PAR-1 signalling also leads to CCL2 release from macrophages, fibroblasts, endothelial cells, alveolar and bronchial epithelium (Baran et al., 2007; Deng et al., 2008; Goebeler et al., 2001; Mercer et al., 2009). CCL2 is a potent chemoattractant for inflammatory cells and fibrocytes (Moore et al. 2005) and is strongly implicated in the pathogenesis of pulmonary fibrosis. Furthermore, CCL2 induces the expression of TGFβ and suppresses the production of anti-fibrotic mediators, such as PGE_2 by lung fibroblasts (Moore et al. 2003).

Thrombin signalling via PAR-1 exerts potent mitogenic effects on lung fibroblasts (Trejo et al. 1996) and stimulates extracellular matrix production (Chambers et al. 1998). Thrombin levels are increased in BALF from patients with pulmonary fibrosis associated with systemic sclerosis. Subsequent application of this BALF to *in vitro* cultured fibroblasts leads to increased proliferation that can be inhibited by the thrombin inhibitor hirudin (Hernández-Rodríguez et al., 1995). PAR-1 signalling in fibroblasts also leads to the release of profibrotic growth factors, including CTGF (Chambers et al. 2000) and PDGF (Blanc-Brude et al. 2005), which further promote fibroblast proliferation.

PAR-1 signalling can also lead to integrin-mediated activation of latent TGFβ either via αvβ6 on epithelial cells (Jenkins et al. 2006) or αvβ5 on fibroblasts (Scotton et al. 2009) and hence contribute to the fibroblast to myofibroblast differentiation in a paracrine fashion. Mice lacking the β6 subunit are protected in the bleomycin-induced lung injury and fibrosis as well as lipopolysaccharide (LPS)-induced and ventilator-associated lung injury (Jenkins et al., 2006). Furthermore, thrombin-induced PAR-1 activation on fibroblasts also promotes α-SMA induction and differentiation to myofibroblasts (Bogatkevich et al., 2001). Finally, FXa signalling via PAR-1 also stimulates lung fibroblast procollagen production, proliferation, and

drives differentiation to myofibroblasts (Blanc-Brude et al., 2005; Scotton et al., 2009).

PAR-1 signalling also contributes to innate immunity in viral infection. PAR-1 activation, either with thrombin or specific agonist peptide, enhanced infection of endothelial cells and fibroblasts with herpes simplex I virus (Sutherland et al., 2007). Furthermore, human cytomegalovirus (CMV) increased expression of PAR-1 and PAR-3 at mRNA and protein levels in endothelial cells increasing their responsiveness to stimulation with thrombin (Popović et al., 2010).

PAR-1 knockout mice infected with cardiotropic coxsackievirus have been shown to have increased viral load in the heart and reduced level of interferon β (IFNβ) in the early phase of infection. This lack of early immunity was later over-compensated by increased recruitment of inflammatory cells into the heart and higher levels of IL-1β, TNFα, IL-6, which eventually resulted in extensive damage to the heart muscle (Antoniak et al., 2013). In contrast, mice over-expressing PAR-1 in cardiomyocytes had reduced viral infection-induced myocarditis (Antoniak et al., 2013). Furthermore, PAR-1 knockout mice had increased viral load in the lung following influenza A infection (Antoniak et al., 2013). PAR-1 and PAR-2 have also been shown to become upregulated in the airways following influenza infection and promote production of bronchodilatory prostanoids (Lan et al., 2004). Another study has demonstrated that activation of PAR-1 contributes to deleterious lung inflammation and decreased survival in influenza A infection in mice (Khoufache et al., 2013). PAR-1 agonist peptide has exacerbated the infection and increased mortality, while PAR-1 antagonist offered protection (Khoufache et al., 2013). These finding strongly suggest that PAR-1 plays a role in orchestrating responses to viral infection but further research is necessary to thoroughly dissect the mechanisms.

1.6.2 PAR-1 mechanisms of activation

PARs are seven-transmembrane-domain receptors, activated via irreversible proteolytic cleavage of the extracellular N-terminus that leads to the unmasking of a tethered ligand. The tethered ligand binds to the second extracellular loop (ECL2) of the receptor and this interaction induces a conformational change in the intracellular domains of the receptor allowing activation of the heterotrimeric G-proteins and downstream signalling (**Figure 1.5**). Interestingly, the amino acid sequence of the tethered ligand is a molecular signature of each PAR and has allowed the development of specific synthetic activating peptides. Their mechanism of action involves direct binding to ECL2 of appropriate PARs independently of proteolytic cleavage and they have proven invaluable tools for investigating biological functions of this group of receptors.

The N-terminus of PAR-1 contains an acidic hirudin-like sequence in the vicinity of the $LDPR_2S$ cleavage site that thrombin binds to with high affinity before cleaving the receptor. The newly formed tethered ligand contains a six-amino acid sequence SFLLRN that interacts with ECL2 and elicits downstream G-protein activation and signalling (**Figure 1.6**). The PAR-1 tethered ligand can also bind to ECL2 of PAR-2 and activate PAR-2 signalling pathways by unidirectional transactivation mechanism (O'Brien et al., 2001).

The remaining product of the PAR-1 N-terminal cleavage is a 41-amino-acid peptide termed parstatin. It is released into the extracellular milieu and may exert some biological activity. A study showed that parstatin inhibits VEGF and FGF-induced angiogenesis *in vitro* and *in vivo* (Zania et al., 2009) but the exact mechanism of action remains unclear.

Thrombin displays high affinity towards PAR-1 and cleaves the receptor with significantly higher efficiency in comparison to other activating proteinases (**Table 1.5**). In order to increase the potency of binding, other activating proteinases utilise cofactor molecules for efficacious PAR-1 cleavage. Factor Xa (FXa) cleaves PAR-1 five times more efficiently when bound within the ternary complex TF-FVIIa-FXa

(Riewald et al. 2001). Activated protein C (APC) binds to the endothelial protein C receptor (EPCR) and cleaves a subpopulation of PAR-1 localised to lipid rafts (Russo et al. 2009). The affinity of APC for PAR-1 is 500 times less than that of thrombin and APC fails to efficiently cleave PAR-1 if EPCR is blocked (Schuepbach et al., 2008). Furthermore, APC-EPCR cleaved PAR-1 can be retained on the cell surface suggestive of a possible desensitization mechanism and is highly protective of endothelial barrier integrity (Schuepbach et al., 2008). The APC-mediated protection of vascular integrity is PAR-1-dependent as confirmed in *in vivo* studies of endotoxin-induced acute lung injury, where PAR-1 knockout mice were not protected from vascular leak upon administration of exogenous APC (Schuepbach et al., 2009).

Deactivating proteinases have been described for PAR-1, PAR-2 and PAR-3 (**Table 1.5**). Their mechanism of action involves the cleavage of the receptors between N-terminus and tethered ligand and the loss of the latter yield the receptor insensitive to thrombin and other activating proteinases.

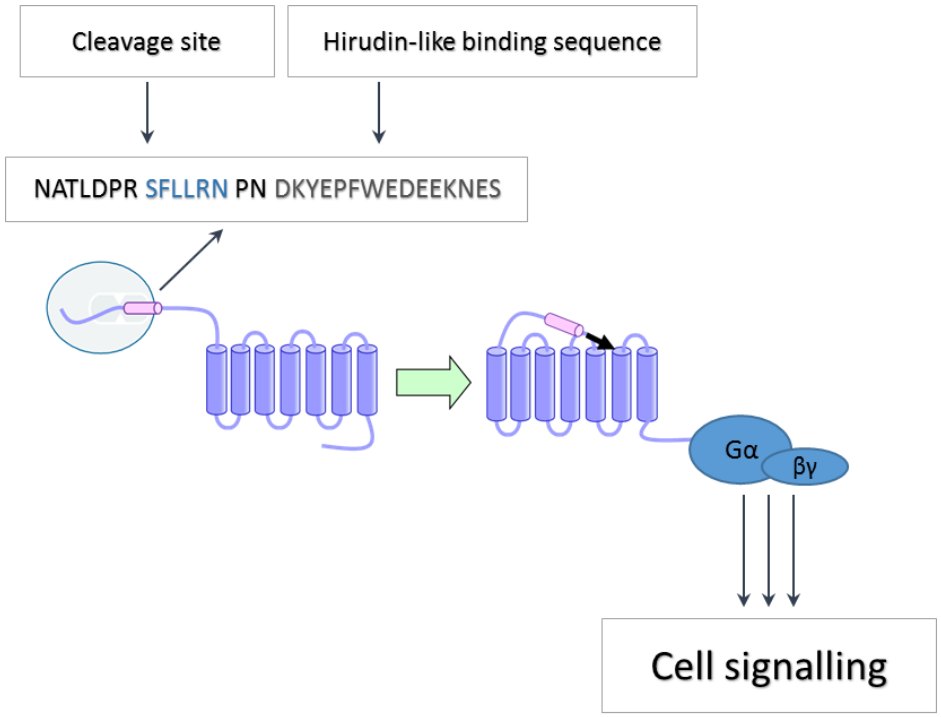

Figure 1.5 Mechanism of PAR-1 activation

PAR-1 is a seven-transmembrane-domain receptor. The extracellular N-terminus of PAR-1 contains thrombin binding site composed of a hirudin-like amino acid sequence that has high affinity for thrombin and hence facilitates its binding and cleavage of the receptor at the indicated cleavage site. Following proteolytic cleavage, the newly generated tethered ligand binds to the second extracellular loop of the receptor. This induces a conformational change in the receptor that is then able to interact with heterotrimeric G-proteins and elicit downstream cell signalling.

1.6.3 PAR-1 signalling via G-proteins

G-proteins are heterotrimeric guanine nucleotide-binding proteins that consist of α, β and γ subunits. There are four main classes of Gα-proteins: $G\alpha_{i/o}$, $G\alpha_{s}$, $G\alpha_{q/11}$, $G\alpha_{12/13}$ but only $G\alpha_{i/o}$, $G\alpha_{q/11}$, and $G\alpha_{12/13}$ form stable complexes with intracellular parts of PAR-1 receptor (McCoy et al., 2012). Upon PAR-1 activation the associated G-protein complex is phosphorylated and the Gα protein acts as a guanine exchange factor (GEF) that drives the GDP to GTP exchange. This leads to dissociation of Gβγ subunits and initiates downstream cell signalling. The coupling to specific G-protein dictates the nature of cellular response and the signalling is cell- and tissue-specific but the focus of this report will be PAR-1 signalling in the lung and potential impact on lung injury and pulmonary fibrosis.

PAR-1 preferentially couples to $G\alpha_{q/11}$ and $G\alpha_{i/o}$, and with less efficiency to $G\alpha_{12/13}$. $G\alpha_{q/11}$ interacts with the second intracellular loop (ICL2) (Verrall et al., 1997) and alanine scanning mutagenesis has revealed that one crucial amino acid (arginine R205A) in PAR-1 ICL2 sequence is essential for $G\alpha_{q/11}$ uncoupling and signalling (McCoy et al., 2012). However, other sites on the PAR-1 intracellular interface have also been shown to interact with G-proteins including the cytoplasmic tail (Swift et al., 2006) and first and third intracellular loops (ICL1 and ICL3) (Cisowski et al., 2011). These coupling sites were identified using pepducins, which are agonist or antagonist peptides specific to a GPCR. Pepducins have hydrophobic lipid moieties that allow them to anchor in the lipid membrane bilayer, be transported into cells and interact with the cognate receptor modulating the interaction with G-proteins (Covic et al., 2002). Pepducins targeting PAR-1 ICL1 and ICL3 had different effects on A549 cell behaviour. Both pepducins blocked cell motility but while ICL1 only partially suppressed calcium signalling, ICL3 completely blocked calcium signalling and ERK1/2 activation (Cisowski et al., 2011). These data strongly suggests that both ICL1 and ICL3 can couple to $G\alpha_{i/o}$, which downstream effects influence cell shape and migratory potential. In addition ICL3 is also capable of interacting with $G\alpha_{q/11}$. In conclusion, G-proteins utilise multiple intracellular sites for coupling to PAR-1 and the concomitant activation of different G-proteins can lead to the simultaneous

induction of various signalling pathways that can converge to produce a physiological effect (**Figure 1.6**).

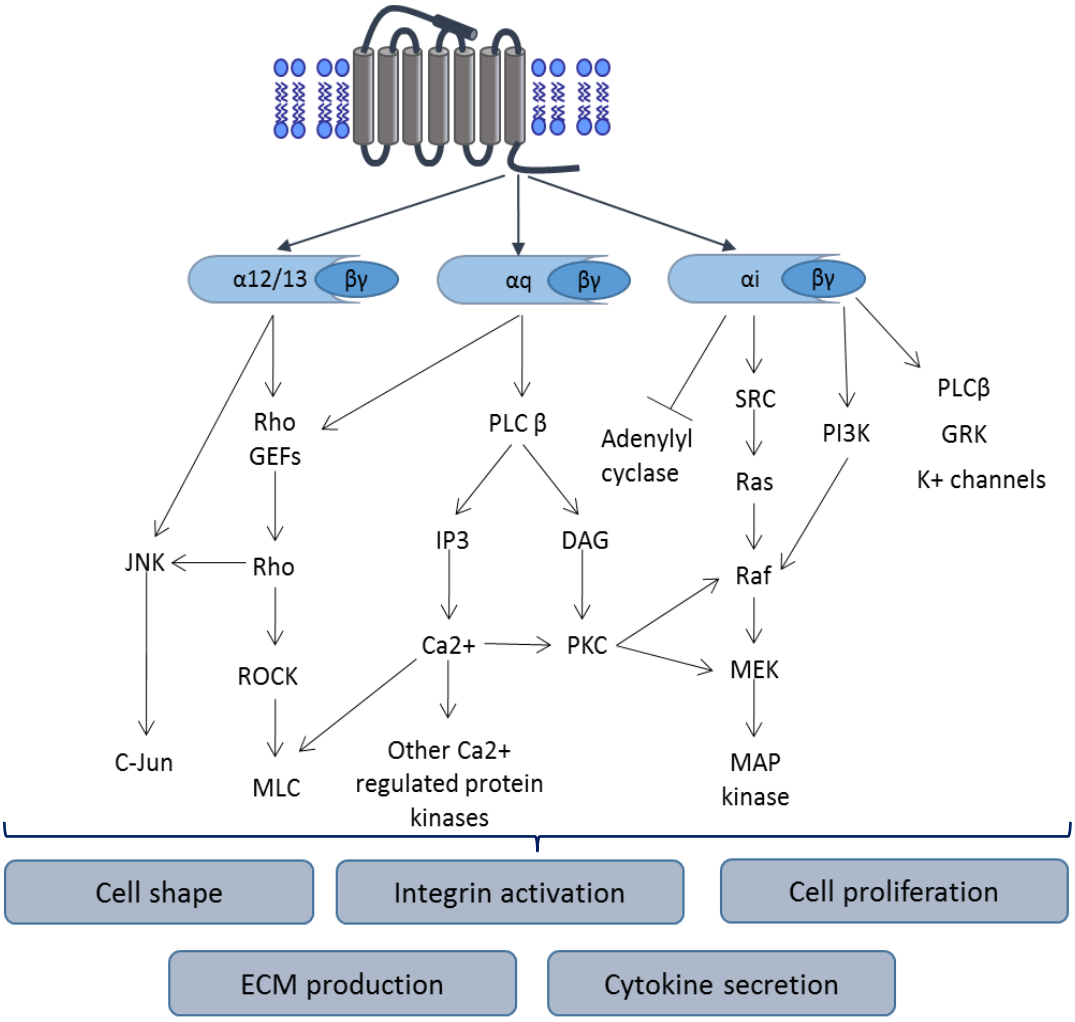

Figure 1.6 PAR-1 mediated G-protein signalling pathways

$G\alpha_{12/13}$ pathway couples to Rho guanine-nucleotide exchange factors GEFs, resulting in activation of Rho, Rho kinase ROCK, and myosin light chain (MLC) kinase; $G\alpha_q$ activates phospholipase C-β (PLC-β) to generate inositol triphosphate (IP3) and diacylglycerol (DAG), which in turn mobilises intracellular Ca^{2+} and activates protein kinase C (PKC); the $G\alpha_i$ pathway inhibits adenylyl cyclase; Gβγ subunits activate phosphoinositide 3-kinase (PI3K), PLCβ, G protein-coupled receptor kinases (GRK), K^+ channels; (updated from (Coughlin, 2001; McLaughlin et al., 2005).

PAR-1- $G\alpha_{i/o}$ signalling

Pertussis toxin-sensitive $G\alpha_{i/o}$ uncoupling following PAR-1 activation leads to the inhibition of adenylyl cyclase and reduced generation of cyclic adenosine monophosphate (cAMP) (Hung et al., 1992). This in turn leads to intracellular calcium ion mobilisation and cell shape change, which is an important mechanism in thrombin-induced platelet activation and aggregation at sites of injury (McLaughlin et al. 2005). In endothelial cells, PAR-1-$G\alpha_{i/o}$ coupling leads to an increase in expression of thrombospondin-1 and thrombin-mediated vascular permeability (Riewald and Ruf 2005).

PAR-1-$G\alpha_{i/o}$ also activates the Src tyrosine kinase pathway that stimulates Ras, Raf and the mitogen-activated protein kinases (MAPK). This pathway is important for thrombin- and FXa-induced fibroblast proliferation and transformation (Blanc-Brude et al., 2005; Della Rocca et al., 1999). Inhibition studies have also shown that blocking $G\alpha_{i/o}$ abrogates thrombin mitogenic effects on lung fibroblasts (Baffy et al., 1994; LaMorte et al., 1993).

PAR-1- $G\alpha_{q/11}$ signalling

$G\alpha_{q/11}$ signals via activation of β-isoforms of phospholipase C (PLC-β) (Babich et al. 1990), which triggers phosphoinositide (PIP_2) hydrolysis to generate inositol triphosphate (IP_3) and diacylglycerol (DAG). IP_3 regulates the mobilisation of intracellular calcium and activation of protein kinase C (PKC) (Berridge, 1993). Calcium ions and PKC act as second messengers and activate cascades of kinases and phosphatases, such as Ras GEFs and MAPK, respectively.

PAR-1- $G\alpha_q$ signalling also plays a role in fibroblast proliferation and differentiation. Blocking $G\alpha_q$ leads to a dramatic reduction in fibroblast DNA synthesis and inhibits calcium mobilisation following stimulation with thrombin (Baffy et al., 1994; LaMorte et al., 1993). It is also responsible for NFκB activation and ICAM-1 upregulation in endothelial cells following activation by thrombin (Rahman et al., 1999).

PAR-1 knockout mice have greatly reduced levels of CCL2 in the lung following bleomycin injury, which may contribute to the attenuation of fibrosis in this model (Howell et al. 2005). Further research in our laboratory has shown that thrombin induces CCL2 synthesis and release by murine fibroblasts via PAR-1-$G\alpha_q$ signalling (Deng et al., 2008). CCL2 gene transcription is upregulated as a result of thrombin-PAR-1-$G\alpha_q$ signalling via Ca^{2+}-independent pathway leading to PKC, c-Raf and ERK1/2 phosphorylation. CCL2 production and release is then mediated by Ca^{2+}-dependent PKC activation in response to a rise in intracellular Ca^{2+} concentration and subsequent Rho kinase activation. These results were confirmed using a selective PAR-1-$G\alpha_q$ signalling inhibitor, Q94, which blocked thrombin-mediated CCL2 upregulation both at the mRNA and protein levels (Deng et al., 2008).

PAR-1- $G\alpha_{12/13}$ signalling

$G\alpha_{12/13}$ downstream signalling leads to selective interactions with the small Rho GTPase- RAS superfamily that control the organisation of the actin cytoskeleton (Wennerberg et al. 2005). Thrombin-mediated activation of PAR-1-$G\alpha_{12/13}$ signalling induces calcium-independent platelet shape change and aggregation (Moers et al., 2003) and cytoskeletal re-organisation in endothelial cells.

Of particular importance to the pathogenesis of IPF, the thrombin- PAR-1- $G\alpha_{12/13}$ signalling axis plays a key role in TGFβ activation via αvβ6 integrins in epithelial cells (Jenkins et al. 2006) and αvβ5 integrins in fibroblasts (Scotton et al. 2009).

1.6.4 Signal termination, internalization and re-sensitization

Unlike other GPCRs, which are reversibly activated by small hydrophilic agonists, PAR-1 ligand is tethered to the receptor and unmasked by a permanent proteolytic cleavage. The post-translational modifications, phosphorylation and internalization are crucial for spatial and temporal control of PAR-1 signalling.

The phosphorylation of the PARs occurs rapidly after activation and effectively disrupts the receptor-G-protein interaction. Agonist-dependent internalisation of PAR-1 is critical for termination of signalling and involves phosphorylation of specific

C-terminal residues by G protein receptor kinases (GRKs) which require β-arrestins as cofactors (Yan et al. 1998). The receptors are then internalized in a clathrin-dependent mechanism and targeted for lysosomal degradation (Hoxie et al., 1993). Unlike other GPCRs, PARs are used only once and not recycled (Trejo et al. 1998), though a small fraction is transported back to the cell surface in a cleaved, inactive form (Hammes and Coughlin, 1999). PAR-1 also exhibits constitutive turnover at the cell surface that occurs at a slower rate and plays a role in maintaining cell sensitivity to activating proteinases. Agonist-induced and constitutive internalization of PAR-1 is regulated differently with constitutive internalization requiring clathrin adaptor protein complex-2 (AP2), whereas agonist-induced internalization of PAR-1 is controlled by AP-2 and ubiquitination (Wolfe et al. 2007).

Ubiquitination acts ultimately as a lysosomal sorting and degradation signal in mammalian GPCRs following covalent attachment of ubiquitin molecules to proteins by ligases. Agonist-induced ubiquitination of β2AR adrenergic receptor and CXCR4 chemokine receptor is critical for lysosomal degradation but is not required for internalization (reviewed in Wolfe et al. 2007). However, ubiquitination of PAR-1 seems to retain the receptor on the cell surface while deubiquitination targets the receptor for lysosomal degradation (Wolfe et al. 2007). The main site for ubiquitination in PAR-1 is the C-terminal tyrosine-based motif, which also appears to be a site for AP2 binding that is required for constitutive internalization. Maintaining this site ubiquitinated provides a mechanism to retain the majority of the receptors at the cell surface where they are readily available for proteolytic activation by extracellular proteinases (Wolfe et al. 2007).

N-linked glycosylation is another post-translational modification shown to regulate PAR-1 activation and trafficking to the cell surface. N-linked glycosylation is critical for correct protein folding and transport to the cell surface of many membrane-spanning receptors. The main site of PAR-1 N-linked glycosylation is at ECL2 and the N-terminus. The ECL2 site is essential for proper regulation of ligand-induced receptor activation and endocytosis whereas N-linked glycosylation at the N-terminus is responsible for PAR-1 trafficking to the cell surface (Soto and Trejo

2010). ECL2 N-linked glycosylation deficient PAR-1 showed increased signalling in response to thrombin or synthetic activating peptides and impaired trafficking in comparison to a wild-type receptor. This is an important observation since molecular pathologies of many conditions involve altered post-translational modifications of key receptors (Soto and Trejo 2010). The expression of PAR-1 is upregulated in many types of invasive cancers and defective receptor trafficking and persistent signalling may contribute to disease progression (Arora et al. 2008).

The mechanisms to maintain PAR-1 surface expression are cell-specific and include trafficking of the receptor from pre-formed intracellular pools or *de novo* receptor synthesis. Epithelial cells engage in *de novo* receptor synthesis following activation by thrombin while platelets do not become re-sensitized as once activated these cells are not reused. Endothelial cells and fibroblasts have abundant intracellular pools of PAR-1 and can become rapidly re-sensitized by mobilising these intracellular receptor stores and only engage in *de novo* receptor synthesis after prolonged exposure to activating proteinases (Paing et al. 2006; Blanc-Brude et al. 2005; Ellis et al. 1999).

1.6.5 PAR-1 gene expression and regulation

PAR-1 gene expression is differently regulated in homeostasis and disease, and displays cell- and tissue-specific variations. PAR-1 plays a role in early organogenesis and high levels of PAR-1 mRNA are detected in the murine mesenchymal cell populations at early stages of development (Soifer et al., 1994). Later in life, PAR-1 expression and regulation is tissue-specific. PAR-1 expression is upregulated in many pathological conditions including in breast (Boire et al., 2005), colonic (Darmoul et al., 2003) and prostatic (Chay et al. 2002) cancers and fibrotic conditions including pulmonary, liver, kidney and heart fibrosis.

PAR-1 is encoded by the *F2R* gene located on chromosome 5q13, between genes encoding PAR-2 and PAR-3 (Bahou et al., 1993). The gene has a two-exon structure, separated by a large intron. The first exon encodes the 5' untranslated region (UTR), the start codon and the signal peptide. The second exon encodes the mature

receptor with the activating proteolytic cleavage site and the 3'UTR. The immediate promoter region has two GC-rich cluster boxes where transcription factors bind and initiate PAR-1 gene expression.

The PAR-1 gene regulatory mechanisms are not well described and appear to be highly cell-specific (**Table 1.6**). In human melanoma cells, transcription factor AP-2 represses PAR-1 gene expression. AP-2 competes with a positive regulator, Sp1, for the binding site in the promoter region of *F2R* gene and the loss of AP-2 and predominant binding of Sp1 is linked to the overexpression of PAR-1 and the metastatic phenotype of cancer cells (Tellez et al., 2003). Mutations or loss of transcription factor p53 are documented in many cancer types and a positive correlation exists between p53 mutation or deficiency, upregulation of the PAR-1 gene expression and the metastatic phenotype of cancer cells (Salah et al. 2008). In malignant prostate cancer cells, PAR-1 mRNA levels are upregulated by the transcription factor early growth response-1 (Egr-1) (Salah et al. 2007). Egr-1 is a short-lived, immediate, early response gene that encodes a zinc finger transcription factor. The expression of Egr-1 is rapid and transient in many cell types, including cancer cells, injured fibroblast and endothelial cells. Egr-1 can be induced by cell stress, injury by cytokines, hypoxia, shear stress and ultraviolet light. Egr-1 knockout mice showed enhanced survival in response to vascular injury (Yan et al. 2000). Interestingly, TGFβ is a major inducer of Egr-1 in mesenchymal cells *in vitro* and *in vivo* and TGFβ- mediated collagen gene expression is regulated by Egr-1 downstream of Smad3-dependent and independent pathways (Chen et al. 2006).

The findings in cancer do not appear to extrapolate to other cell types. In human lung fibroblasts, inhibition of AP-2 or Sp1 does not affect PAR-1 gene transcription (Sokolova et al., 2005). However, in human fibroblasts, PAR-1 gene and protein expression are negatively regulated by prostaglandins. Activation of PAR-1 in human lung fibroblasts induces COX-2 mRNA expression and release of prostaglandin PGE_2, which in turn downregulates PAR-1 gene expression (Sokolova et al., 2005). PGE_2 also reduces PAR-1 surface expression and responsiveness to agonist and this effect is stable for 24 hours after fibroblast activation. PGE_2 exerts a range of anti-fibrotic

effects through the EP2 receptor including inhibition of collagen synthesis, fibroblast proliferation and cell migration (Sokolova et al. 2008; Keerthisingam et al. 2001). This negative feedback loop is disrupted in fibrotic fibroblasts that have a greatly reduced ability to upregulate COX-2 mRNA levels (Keerthisingam et al. 2001).

In human umbilical vein endothelial cells (HUVEC), microvascular endothelial cells (HMEC), and human arterial vascular smooth muscle cells PAR-1 mRNA and protein levels are downregulated following exposure to shear stress (Nguyen et al., 2001; Papadaki et al., 1998). Interestingly, these cells have intracellular PAR-1 reservoirs that rapidly replenish the receptor on the cell surface independently of *de novo* gene and protein expression. This can potentially explain the temporal separation between the PAR-1 gene expression and responsiveness to agonists at cellular level.

In endothelial cells stimulation with thrombin and PAR-1 activating peptides upregulate PAR-1 mRNA level in a positive feedback mechanism (Ellis et al. 1999). In rat osteoblast-like cells, TGFβ has been shown to significantly upregulate PAR-1 mRNA levels and increase the surface expression of the receptor. These effects translated to enhanced proliferative responses to thrombin in these cells (Abraham and MacKie, 1999).

Mediator/ Transcription factor	Cell type	PAR-1 expression	Reference
TGFβ	Rat osteoblast-like cells	**+**	(Abraham and MacKie, 1999)
IL-4	Human macrophages	**-**	(Colognato et al., 2003)
COX-2	Human fibroblasts	**-**	(Sokolova et al., 2005)
Thrombin	Human endothelial cells	**+**	(Ellis et al. 1999)
p53 **-wild type** **-mutant or lost**	 Human epithelial cells Human carcinoma	 **-** **+**	(Salah et al. 2008)
Sp1	Human melanoma	**+**	(Tellez et al., 2003)
AP2	Human melanoma	**-**	(Tellez et al., 2003)
Egr-1	Prostate cancer cells	**+**	(Salah et al. 2008)

Table 1.6 Regulation of PAR-1 expression

1.6.6 PAR-1 antagonism

PAR-1 is an attractive pharmacological target for blocking thrombin-mediated cellular effects without disrupting systemic coagulation pathways and fibrin generation. Studies with PAR-1 knockout mice demonstrate that blocking PAR-1 can be beneficial in injury and pulmonary fibrosis and can modulate viral infection in the lung. Several PAR-1 inhibitors are currently being tested in a clinical setting of cardiovascular disease as antiplatelet and antithrombotic agents (reviewed in Lang et al. 2010).

The first PAR-1 antagonists developed were peptide-mimetics that blocked the receptor by binding to the second extracellular loop independently of proteolytic cleavage. Indole-based, RWJ-56110 and indazole-based, RWJ-58259, were the first selective PAR-1 antagonists with antiplatelet properties. Out of the two, RWJ-58259 turned out to be more selective, potent and displayed a higher binding affinity with reduced side effects and was therefore developed further (Damiano et al., 2003). RWJ-58259 antithrombotic activity was validated *in vivo* in a cynomolgus monkey arterial injury models (Adams et al., 2011).

E5555 (Atopaxar) is a bicyclic amide-derivative PAR-1 antagonist developed for oral administration. The compound was validated in Phase I clinical study and shown to inhibit platelet aggregation without affecting bleeding time and tested safe and well-tolerated in patients (reviewed in Lang et al. 2010). In Phase II trials carried out in patients with established coronary artery disease (Wiviott et al., 2011) and acute coronary syndrome (O'Donoghue et al., 2011), a trend toward reduction in major adverse cardiovascular effects was observed in patients treated with E5555. However, these patients also showed increased incidence of minor bleeding events and elevated liver enzymes indicating potential hepatic toxicity of the drug (Goto et al., 2010; de Souza Brito and Tricoci, 2013).

Another class of PAR-1 antagonists is based on the core structure of the tetracycline piperidine alkaloid himbacine, naturally isolated from the bark of Australian magnolias. The most advanced compound, SCH530348 (Vorapaxar), is a synthetic

tricyclic 3-phenylpyridine that can be administered orally and inhibits thrombin-PAR1-mediated platelet aggregation with an IC_{50} of 47 nM (Adams et al., 2011). The compound has a half-life of 20 hours in humans, which is reflected in the inhibitory effect that lasts 24 to 48 hours. In vivo studies in non-human primates demonstrated antithrombotic efficacy of SCH530348 in arteriovenous shunt models and in thrombosis models without any alterations to bleeding time or surgical blood loss. Phase I safety and tolerability studies in human volunteers showed that the drug does not cause any adverse effects and that platelet aggregation is significantly inhibited for up to 72 hours. SCH530348 safety and efficacy was further confirmed in a Phase II study in patients undergoing elective coronary angiography, who were randomly administered SCH530348 or placebo and the treatment with the compound was not associated with risk of minor or major bleeding (Becker et al., 2009). The efficacy of SCH530348 was subsequently assessed in two large, randomised, multi-centre clinical trials. TRA 2P-TIMI tested SCH530348 in patients with atherosclerosis and history of myocardial infarction, ischemic stroke and peripheral arterial disease and TRACER investigated patients with acute coronary disease. Results from TRA 2P-TIMI trial showed that SCH530348 significantly reduces the risk of death from cardiovascular causes in patients with stable atherosclerosis (Morrow et al., 2012). A lesser protective effect was observed in patients with peripheral arterial disease although there was a significantly reduced risk of acute limb ischemia (Bonaca et al., 2013). However, in patients with history of ischemic stroke, addition of SCH530348 to the standard antiplatelet therapy was associated with increased the risk of intracranial haemorrhage without sufficient reduction in adverse vascular effects (Morrow et al., 2013). Furthermore, increased risk of bleeding was observed in all patients groups receiving SCH530348 in the TRA 2P-TIMI study (Morrow et al., 2012). Results of TRACER study also showed significant and long-lasting protection from myocardial infarction even though the trial failed to reach the primary endpoint of reduction in the rate of cardiovascular-related death (Leonardi et al., 2013; Tricoci et al., 2012). In both clinical studies increased risk of bleeding, particularly intracranial haemorrhage, was prominent in patients receiving SCH530348. However, patients in these studies were already

receiving standard antiplatelet therapy including thienpyridone (Clopidogrel) and therefore the bleeding risk could be a consequence of additive anticoagulant therapy with SCH530348.

Furthermore, a group of cell-penetrating allosteric modulators of G-protein interactions with the receptor are currently being used to investigate the possibility of targeting specific signalling pathways downstream of PAR-1 activation. An allosteric inhibitor, Q94, specifically inhibits PAR-1 coupling to $G\alpha_q$ with an IC_{50} of 916 nM and blocks signalling pathways that include intracellular calcium mobilisation and CCL2 release from fibroblasts (Deng et al. 2008). Also pepducins can be engineered to attach to different intracellular loops and so are excellent tools for investigating the different types of G proteins interactions with specific parts of the receptor. Blocking different sites at the intracellular interface of the receptor has been shown to have a varying impact of cell responses (Cisowski et al., 2011).

1.7 Hypothesis and aims

Pulmonary fibrosis is the end stage of a heterogeneous group of respiratory conditions characterised by excessive and disordered ECM deposition within the pulmonary interstitium leading to obliteration of alveolar architecture and respiratory insufficiencies. Current evidence suggests that in IPF dysregulated cross-talk between epithelial and mesenchymal cells following repetitive lung injury is a central mechanism driving the activation and persistence of fibroblasts and myofibroblasts. Furthermore, there is strong evidence showing that viral infections promote profibrotic and procoagulant responses in the lung and can therefore propagate the progression of fibrosis. The main feature of a profibrotic environment in the lung is an imbalance between the major inflammatory, coagulation and tissue repair pathways that perpetuate fibrogenesis.

PAR-1 is a ubiquitously expressed receptor, which pluripotent actions link the inflammatory and coagulation pathways. *In vivo* models of lung injury support the notion that PAR-1 promotes inflammation and thrombin-mediated profibrotic signalling.

This thesis will therefore address the following hypothesis:

Activation of the coagulation cascade in response to lung injury and viral infection promotes inflammation and fibrosis via PAR-1 signalling.

And the following aims:

- **Identify PARs responsible for coagulation proteinases signalling responses in human primary lung cells.**
- **Determine whether the coagulation cascade contributes to inflammatory and fibrogenic responses in the model of viral infection in pulmonary fibrosis.**

Chapter 2: Materials and Methods

Materials

2.1 General plastic ware, chemical and solvents

All chemicals were of analytical grade and obtained from Sigma Aldrich (UK) unless otherwise stated. All water used for the preparation of buffers was distilled and deionised using a Millipore Water Purification System (Millipore R010 followed by Milli-Q Plus; Millipore Ltd, UK). Sterile tissue culture flasks, plates and disposable pipettes were obtained from Nunc (Denmark). Sterile polypropylene centrifuge tubes were purchased from Falcon (New Jersey, USA). Dulbecco's Modified Eagle Medium (DMEM) was purchased from Gibco (UK). Foetal bovine serum (FBS), sterile tissue grade trypsin/EDTA and antibiotic (penicillin/ streptomycin) were obtained from Invitrogen (UK).

2.2 Reagents, antibodies and inhibitors

Human α-thrombin, human FXa and antithrombin III were purchased from Enzyme Research Laboratories, UK. Transforming growth factor β-1 (TGFβ-1) was purchased from R&D Biosystems, UK. PAR-1 agonist peptide TFLLR-NH_2, the control peptide RFLLT-NH_2, PAR-2 activating peptide SLIGKV-NH_2, PAR-2 control peptide VKGILS-NH_2, PAR-3 activating peptide TFRGAP-NH_2 and PAR-4 activation peptide AYPGKF-NH_2 were purchased from Bachem AG, Switzerland. Hirudin was purchased from Sigma, UK. MEK inhibitors, UO126 and PD98059, ALK5 inhibitor, SB431542, and JNK inhibitor, SP600126, were purchased from Calbiochem, UK. SB203580 p38 inhibitor was purchased from Cell Signalling Technology, UK. Antibodies used in these studies are listed in **Table 2.1**. PAR-1 inhibitor, RWJ58259, was a kind gift from Department of Chemistry, UCL. PAR-1 inhibitor, SCH530348, and PAR-2 inhibitor, GB83, were purchased from Axon Medchem, Netherlands.

Target	Antibody	Supplier	Concentration	Application
PAR-1	Mouse monoclonal ATAP2	Santa Cruz Biotechnology, USA	2 µg/ml	Immunocytofluorescence
PAR-2	Mouse monoclonal SAM11	Santa Cruz Biotechnology, USA	1 µg/ml	Immunocytofluorescence
Vimentin	Rabbit monoclonal	Abcam, UK	2 µg/ml	Immunocytofluorescence
αSMA	Mouse monoclonal	Sigma, UK	2 µg/ml	Immunocytofluorescence
E-cadherin	Rabbit polyclonal	Abcam, UK	4 µg/ml	Immunocytofluorescence
CK5	Rabbit polyclonal	Abcam, UK	1 µg/ml	Immunocytofluorescence
CK14	Mouse monoclonal LL02 clone	Abcam, UK	1 µg/ml	Immunocytofluorescence
PECAM	Goat polyclonal	Santa Cruz Biotechnology, USA	2 µg/ml	Immunocytofluorescence
vWF	Rabbit polyclonal	Santa Cruz Biotechnology, USA	2 µg/ml	Immunocytofluorescence
ProSurfactant protein C	Rabbit polyclonal	Millipore, USA	5 µg/ml	Immunocytofluorescence
ZO-1	Mouse monoclonal	Invitrogen	2.5 µg/ml	Immunocytofluorescence
Tissue factor	Rabbit polyclonal	Santa Cruz Biotechnology, USA	1 µg/ml	Immunohistochemistry
FX	Rabbit polyclonal	Santa Cruz Biotechnology, USA	2 µg/ml	Immunohistochemistry
Smad 2	Mouse monoclonal	Cell Signalling Technology, UK	0.05 µg/ml	Western blot
Smad 3	Rabbit Monoclonal	Cell Signalling Technology, UK	0.075 µg/ml	Western blot
βactin	Mouse monoclonal	Sigma, UK	0.2 µg/ml	Western blot

Table 2.1 Antibodies used for analysis of human and mouse cells and tissue.

2.3 Animals

BALB/c female and C57BL/6 male mice (Charles River Laboratories, UK) were housed at the Central Biological Services Unit, University College London; in a specific pathogen-free facility in individually ventilated cages, with free access to food and water (12 hour light/dark cycle, normal sodium dry fishmeal diet, temperature 18-20°C). All procedures were performed on BALB/c mice between 6 and 8 weeks of age and C57BL/6 mice between 10 and 12 weeks of age. All studies were ethically reviewed and carried out in accordance with the UK Home Office Animals for Scientific Procedures Act 1986.

2.4 Bleomycin model of pulmonary fibrosis

C57BL/6 male mice were used for the model of viral infection on the background of bleomycin-induced pulmonary fibrosis. Bleomycin (1 mg/kg of body weight in 50 µl of sterile 0.9% saline) or saline was administered by oropharyngeal instillation as previously described (Lakatos et al., 2006). Mice under light isofluorane-induced anaesthesia were suspended on an elastic band, their nose pinched shut and tongue held to prevent the swallow reflex and forcing the mouse to breathe through the mouth. Consequently saline/bleomycin was introduced to the back of their mouth with Gilson pipette and aspirated. Mice were sacrificed after 21 or 28 days by intraperitoneal injection of pentobarbitone and severing of the abdominal inferior vena cava.

For total collagen measurements and real-time RT-PCR the lungs were removed, blotted dry and immediately snap frozen in liquid nitrogen. Subsequently, the lungs were weighed and pulverised under liquid nitrogen. For µCT, histological and immunohistochemical analysis the trachea was cannulated and lungs insufflated with 4% paraformaldehyde in PBS at a pressure of 25 cm H_2O, excised and submerged in fresh fixative for 4 hours. Following the fixation, the lungs were kept in 15% sucrose over night at 4°C and transferred into 70% ethanol for storage. Lung

tissue homogenates were prepared by mixing the frozen lung powders with 0.5ml PBS with added proteinase inhibitors (Complete Mini, Roche Diagnostics, UK) and 1% Triton-X.

2.5 Viral infection in pulmonary fibrosis

Mice were administered bleomycin via oropharyngeal route as described in previous section and the injury and subsequent fibrosis allowed to develop for 14 days. Mice were then anaesthetised by intraperitoneal injection of ketamine and xylazine at a concentration of 100 mg/kg and 10 mg/kg, respectively, in 100 µl sterile saline. γHV68 (ATCC, USA) $1x10^5$ plaque forming units (PFU) was suspended in 20 µl sterile saline and inoculated intranasally, delivering 10 µl into each nostril. Mice were sacrificed after 7 or 14 days post inoculation by intraperitoneal injection of pentobarbitone and severing of the abdominal inferior vena cava.

Lungs were collected and processed as described in previous section. The spleens were also collected and snap frozen in liquid nitrogen, weighed and pulverised.

2.6 TGFβ and FXa inhibition studies

Pulmonary fibrosis and γHV68 infection were induced as described above. The highly selective small molecule ALK5 inhibitor, SB525334 was a kind gift from Novartis, Horsham, UK. Two weeks after bleomycin instillation and one day post-viral inoculation SB525334 (30 mg/kg in 100 µl acidified saline/0.2% Tween 80 pH 4.1) or vehicle (acidified saline/0.2% Tween 80 pH 4.1) was administered twice daily by oral gavage for the remaining duration of the experiment (**Figure 2.1**).

BAY 59-7939 (Rivaroxaban) was purchased from Selleckchem, USA. The therapeutic dosing of BAY 59-7939 (3 mg/kg in 100 µl polyethylene glycol 400/water 60/40% v/v) or vehicle (polyethylene glycol 400/water 60/40% v/v) started 14 days after bleomycin administration and one day post-viral inoculation out to 28 days post-bleomycin when the experiment was terminated (**Figure 2.1**).

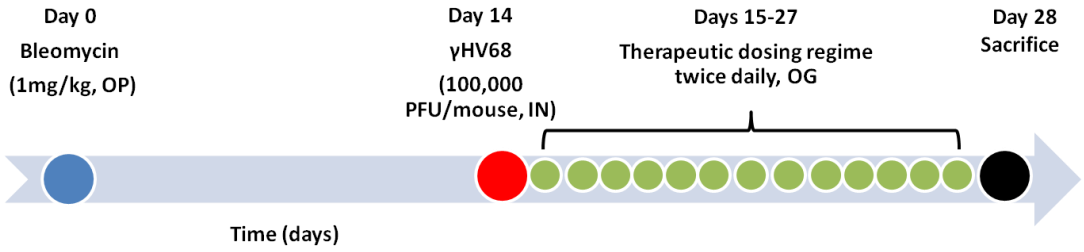

Figure 2.1. Experimental design of *in vivo* TGFβ and FXa inhibition studies

Bleomycin was administered via oropharyngeal (OP) route on day 0. γHV68 was inoculated intranasally (IN) on day 14. Mice received the compounds via oral gavage (OG) twice daily from day 15 to 27, and were sacrificed on day 28.

2.7 Determination of total lung collagen

2.7.1 HPLC

Total lung collagen was determined by measuring hydroxyproline content in aliquots of pulverised lung. Collagen contains 12.2% w/w hydroxyproline, which is detected and quantified by reverse-phase high performance liquid chromatography (HPLC) of 7-chloro-4-nitrobenzo-oxa-1,3-diazole (NBD-Cl)-derivatised acid hydrolysates. Hydroxyproline is a secondary amino acid that reacts with NBD-Cl to generate a chromophore detected at 495 nm wavelength. The specificity of the reaction is further ensured by keeping the derivation time to 20 minutes at 37°C, a time-point that has been confirmed experimentally to be maximal for hydroxyproline derivatisation with NBD-Cl for up to 20 nmol hydroxyproline.

2.7.1.1 Sample preparation

For each sample approximately 20 mg of lung powder was accurately weighed and hydrolysed in 2 ml 6 M HCl for 16 hours at 110° in a pyrex tube. Hydrolysates were decolourised with activated charcoal, filtered through 0.65 µm filter (Millipore Ltd., UK) and diluted 1 in 50. Aliquots (200 µl) of diluted hydrolysate were transferred to a microfuge tube and evaporated to dryness under vacuum on a Speedvac (Thermo Electron Corporation, UK). The resulting residue was reconstituted in 100 µl HPLC-grade water, buffered with 100 µl of 0.4 M potassium tetraborate (pH 9.5) and

reacted with 100 µl 36 mM NBD-Cl (in methanol) to a final concentration of 12 mM NBD-Cl. The samples were then incubated in a hot block at 37° for 20 minutes. The reaction was stopped by addition of 50 µl 1.5 M HCl. At this point 150 µl of 3.33x buffer A (**Table 2.2**) was also added. Samples were then filtered through an HPLC low dead-volume filter (0.22 µ, Millipore Ltd., UK) into a polypropylene insert within an Amber Snap Seal vial (Laboratory Sales Ltd., UK). These vials were then loaded onto the HPLC apparatus and the samples were sequentially injected onto the HPLC column and eluted with acetonitrile gradient as described below.

2.7.1.2 Chromatography conditions

The HPLC apparatus used for measurements was Agilent series 1100 (Agilent Technologies, USA) with a reverse-phase cartridge column (LiChroCART LiCrospher, 250mm length x 4 mm diameter, 5 µm particle size, 100 Rp-18; BDH/Merck, UK) protected by a directly coupled pre-column (LiChrosorb 4 mm x 4 mm, 5 µm particle size, 100 Rp-18; BDH/Merck, UK). The column was continuously maintained at 40°C in a heated column oven. At the beginning of each batch of samples, the HPLC system was equilibrated in running buffer A (**Table 2.2**) for minimum of 40 minutes. Hydroxyproline standards (equivalent to 50 pmol, Sigma) were subject to NBD-Cl derivatisation, processed alongside the samples and inserted at equal intervals throughout the run. NBD-Cl derivatives of samples and standards were individually injected onto the column and eluted with an acetonitrile gradient, which was achieved by changing the relative proportions of running buffers A and B over time. Chromatographic conditions and buffers used in this process are summarised in **Table 2.2**.

Post-column detection was achieved by monitoring absorbance at 495 using a flow-through variable wavelength monitor. Hydroxyproline elutes as a discreet peak between five and seven minutes following sample injection on the column, between glutamine (3.5 minutes) and serine (seven to nine minutes). The column running and regeneration time for each sample was 25 minutes.

The hydroxyproline content in each sample was determined by comparing peak areas of individual sample chromatograms with the average of the standard peak areas. This value represents the hydroxyproline level in the fraction of the acid hydrolysates of the pulverised lung and was used to calculate the total lung collagen based on the hydroxyproline content of the collagen, dilution factors at the processing steps, the weight of lung powder and the total lung weight.

Column	**LiChrospher, 100 RP-18, 250 x 4mm, 5µm**
Buffers	Buffer A- aqueous acetonitrile (8% v/v), 50mM sodium acetate, pH 6.4 Buffer B- aqueous acetonitrile (75% v/v)
Column flow	1 ml/min
Column temperature	40°C
Detection wavelength	495nm

Table 2.2 HPLC buffers and conditions.

2.7.2 Sircol collagen assay

Sircol collagen assay kit was purchased from Biocolor, UK and used according to the manufacturer's protocol. For each sample approximately 20 mg of pulverised lung powder was weighed out into 1.5 ml Eppendorf tube and soluble collagen extracted by an overnight incubation at 4°C in 1 ml of pepsin (0.1 mg/ml) in glacial acetic acid (0.5 M). Next day, the samples were centrifuged (16,100 RCF, 2 minutes) and supernatants removed to new tubes. Subsequently, 100 µl of Sircol acid neutralising reagent and 200 µl of Sircol isolation and concentration reagent were added to the supernatants before another overnight incubation at 4°C. Next day, the samples were centrifuged (13,300 RCF, 10 minutes) and supernatants removed revealing opaque concentrated collagen pellets. Collagen standards were diluted to a concentration range from 50 to 5 µg/ml collagen. Collagen in the standards and samples was then stained with Sircol dye reagent (1 ml) for 30 minutes with shaking

and excess dye was washed off with 750 µl of acid-salt wash. Standard and sample pellets were resuspended in Sircol alkali reagent and the absorbance measured at 555 nm wavelength. The total lung collagen was quantified based on soluble collagen content of each sample, weight of lung powder and weight of the whole lung.

2.8 µCT imaging

2.8.1 Sample preparation for µCT imaging

Fixed, insufflated lungs were incubated for two hours each in increasing concentration of ethanol: 70%, 80%, 90% and then in 100% ethanol overnight. Lungs were subsequently transferred to 100% hexamethyldisilazane for another two hours and air-dried. The lungs were then fixed on the tip of cannula for µCT scanning (**Figure 2.2**).

Figure 2.2. Lung preparation for µCT scanning.

2.8.2 µCT scanning

The lungs were subsequently scanned in a Skyscan 1072 µCT scanner (SkyScan, Belgium) at 40 kV/100 µA, without a filter, using two frame averaging at 0.49° angular rotation step size; on the typical measured 10% Modulation Transfer Function (MTF) with spatial resolution in the region of 20-30 µm. The voxel size was

set to 12.8 µm and a scan time of around 10 minutes to allow high resolution visualisation and good throughput. Reconstruction was carried out with the SkyScan NRecon software (SkyScan, Belgium).

2.8.3 µCT image analysis

Tissue segmentation analysis was performed using InForm^{TM} software (Caliper, PerkinElmer Company, UK). The software was "trained" to recognise areas of normal lung (green) and areas of abnormal lung (red) as well as other tissue (blue) that encompassed heart tissue, large airways and segments of oesophagus and trachea. Three representative µCT sections (8-bit greyscale) from each animal in the study were used for optimal training of the software until over 90% accuracy was achieved. All µCT sections (~900 sections per each lung) were subsequently segmented using the same training settings on a medium sample area at fine resolution. The output measurements were pixel area and pixel density for each category that were then compiled into a composite measurement of lung volume and greyscale density as described below.

Normal/Abnormal/Total absolute lung volume (mm^3) was calculated:

$$Sum\ of\ pixel\ area\ x\ voxel\ size\ ([12.8]^3)\ x\ 10^9$$

The percentage of normal and abnormal area of the lung volume was calculated:

$$Normal\ lung\ volume/\ Total\ lung\ volume\ x100$$

$$Abnormal\ lung\ volume/\ Total\ lung\ volume\ x100$$

Normal/Abnormal/Total voxel density was calculated:

$$Sum\ of\ pixel\ density\ x\ voxel\ size\ ([12.8]^3)\ x\ 10^9$$

Voxel density of the lungs was further analysed by generating composite 256-colour greyscale histograms (from 0= back to 255= white) representing the frequency distribution of pixel densities for each lung. The mean number of pixels in each bin (1 greyscale unit wide) was then calculated for each group, along with a t-test

distribution showing the p-value for the comparison between each animal group at each greyscale bin.

2.9 Histology and immunohistochemistry

2.9.1 Histology

Paraformaldehyde-insufflated mouse lungs or human biopsy were placed in processing cassettes, dehydrated through a serial alcohol gradient and embedded in paraffin wax blocks. Before standard histological processing 3-5 µm paraffin sections were cut, mounted on polylysine-coated glass slides and dewaxed. Two different staining methods were used to visualise the lung architecture. Hematoxylin and eosin stain (H&E stain) allows for discrimination of cellular components of the tissue. Heamatoxylin is a basic dye that interacts with nucleic acid and stains the nucleus blue. Eosin is an acidic dye that interacts with positively charged amino groups of proteins in the cytoplasm, staining it pink. A modified trichrome staining method (Martius Scarlet Blue (MSB)) was used to highlight collagen fibres deposition to visualise areas of fibrosis. This staining method relies on differential permeability of tissues to dyes of differing molecular size. The large Chicago Sky Blue 6GX dye permeates collagen fibrils causing areas of fibrosis to appear blue. Automated staining of sections was performed using a Sakura Tissue-Tek DRS 2000 Multiple Slide Stainer.

All sections were subsequently scanned on a Nanozoomer and images were captured using NDP.view v 1.2.36 (both from Hamamatsu Corporation, Japan).

Direct comparisons between µCT and histology were performed on the same set of lungs: post-Ct lungs were rehydrated through an ethanol gradient (100%, 90%, 80% and 70% for two hours in each) prior to standard processing.

2.9.2 Inflammatory cell aggregates counts

Inflammatory cell aggregates identified in H&E sections were quantified using Nuance FX Multispectral Tissue Imaging Software (Caliper, PerkinElmer Company,

UK). The software unmixed and analysed the areas of intense heamatoxilin staining that corresponded to the inflammatory cell aggregates and quantified them as regions of interest (ROI). The area of the lung section was then calculated using NDP.view v 1.2.36 software and the ROI expressed per mm^2 of the lung.

2.9.3 Immunohistochemistry

For mouse lung tissue, anitgens were unmasked by microwaving sections in 10 mM citrate buffer, pH 6.0 (2 x 10 minutes) before washing in TBS. Human lung tissue did not require any unmasking treatment. Endogenous peroxidises were blocked with 3% H_2O_2 for 20 minutes. Sections were subsequently incubated with normal goat or rabbit serum (Sigma), as determined by the origin of secondary antibody. Antigens were localized by overnight incubation with anti-FX (1:100 dilution) and anti-TF (1:200 dilution) for mouse lung sections and PAR-1 (1:100 dilution) and PAR-2 (1:200 dilution) for human lung section. Next day, sections were washed in TBS, incubated with a biotinylated goat anti-rabbit, rabbit anti-goat or goat anti-mouse secondary antibody (1:200 dilution; Invitrogen) for 1 hour, and washed again in TBS. Next, sections were incubated with a streptavidin/peroxidase complex (1:200 dilution; DAKO) for a further 30 minutes, followed by incubation with Impact NovaRed peroxidise substrate reagent (Vector Laboratories, UK) for colour development, as per manufacturer's instructions. Sections were washed, counterstained with Gill-2 hematoxylin (Thermo-Shandon), dehydrated, and mounted with DPX mountant (Merck). Control sections were incubated with an isotype-specific, nonimmune rabbit, goat, or mouse IgG primary antibody (DAKO).

All sections were subsequently scanned on a Nanozoomer and images were captured using NDP.view v 1.2.36 (both from Hamamatsu Corporation, Japan).

2.10 Tissue culture

2.10.1 Fibroblasts

Mouse lung fibroblasts were king gifts of Dr. Shaun Coughlin (Cardiovascular Research Institute, University of California, San Francisco, CA, USA) and used between passage 12 and 25 without noticeable alteration in phenotype.

Normal primary human adult lung fibroblasts were a kind gift of Dr. Robin McAnulty from our laboratory and used at passages below 10. Primary fibroblasts were initially grown from 1 mm^3 explants dissected from normal human lung tissue and fixed onto a tissue culture-treated Petri dish. The explants were cultured in 20% FBS Dulbecco's modification of Eagle's medium (DMEM) supplemented with penicillin (200 units/ml, Gibco), streptomycin (200 units/ml, Gibco), glutamine (4 mM, Gibco) and with added fungizone (Invitrogen). The culture medium was replaced with fresh medium one day after isolation and spiked with additional fungizone every three days for three weeks. The fibroblasts were collected by trypsinisation and propagated in a humidified atmosphere containing 10% CO_2 at 37°C. Fibroblasts were separated by morphological characterisation and by differential expression of a selection of cell markers including α-smooth muscle actin, vimentin and myosin.

Both mouse and human fibroblasts were subsequently maintained in static culture on 175 cm^2 triangular culture flasks. Cells were passaged by routine trypsinisation protocols when monolayer cultures reached 80-90% confluence.

2.10.2 Alveolar epithelial cells

A549 alveolar epithelial cells were purchased from ATCC and cultured in 10% FBS Kaighn's modification of Ham's F-12 medium (F12K, Gibco) medium supplemented with penicillin (200 units/ml, Gibco), streptomycin (200 units/ml, Gibco), glutamine (4 mM, Gibco). Cells were passaged by routine trypsinisation protocols when monolayer cultures reached 80-90% confluence.

Primary human type II alveolar epithelial cells (AEC II) were isolated from human lungs of grossly normal appearance, obtained through collaboration with Royal

Brompton Hospital and with approval of the Harefield Ethics Committee. Lung tissue was extensively washed and perfused with sterile 0.9% saline in order to remove blood and inflammatory cells. Subsequently, lung tissue was perfused with 0.25% trypsin in HBSS (3 x 15 minutes) at 37°C and 5% CO_2 in order to dissociate cells. Trypsin was promptly neutralised with FBS and DNase (250 µg/ml; Sigma-Aldrich) and lung tissue manually homogenised. A single cell suspension was obtained from the homogenised tissue by passing the mixture through progressively smaller filters (pore size 300 µm and 40 µm). Cells suspension was next centrifuged (290 RCF, 10 minutes, 20°C) and the resulting cell pellet was resuspended in DCCM-1 medium (Biological Industries, Kibbutz Beit Haemek, Israel) containing DNase (50 µg/ml). Cells were incubated in tissue culture flasks for 2 hours at 37°C in a humidified incubator to allow differential adherence of contaminating mononuclear cells and fibroblasts. Following the adherence step, non-adherent AECII in suspension were removed and centrifuged. The cell pellet was resuspended in red blood cell lysis buffer (Sigma-Aldrich) and incubated for 5 minutes at room temperature. Cell suspension was centrifuged once again and cell pellet resuspended in DCCM-1 medium supplemented with 10% FBS, 1% penicillin–streptomycin, glutamine and 1% fungizone. Cells were subsequently counted and seeded at a density of 1 x 10^6 in 12-well plates with Transwell inserts pre-coated with 1% collgen (PureCol, Nutacon). Cells reached confluence by 48 hours and were characterised by expression of surfactant C protein and zona occludens (ZO-1).

2.10.3 Bronchial epithelial cells

Immortalised bronchial epithelial cells (BEAS2B) were obtained from ATCC, cultured in 10% FBS DMEM and grown in humidified atmosphere containing 10% CO_2 at 37°C. Cells were passaged by routine trypsinisation protocols when monolayer cultures reached 80-90% confluence.

Human bronchial epithelial cells (HBECs) were grown out of human bronchial biopsies and used up to passage 5 in submerged cultures and up to passage 3 for air-liquid interface cultures. Cells were cultured in humidified atmosphere containing 5% CO_2 at 37°C in 1x bronchial epithelial growth medium (BEGM, Lonza,

Switzerland) containing 1x bronchial epithelial basal medium (BEBM) and BEGM Singlequots (Triiodothyronine (T3), human Epidermal Growth Factor (hEGF), Insulin, Transferrin, Hydrocortisone, Epinephrine, Gentamicin Sulphate/ Amphotericin-B (GA-1000), RA, Bovine Pituitary Extract (BPE)) (Lonza, Switzerland). One vial of P1 HBECs (1 ml at 660,000 cells/ml) was thawed in static flask 25 cm^2 at 3,500 cells/ cm^2 density in 3-5 ml of BEGM. The media was changed 6 hours after plating in order to remove the dimethyl sulfoxide (DMSO) in the freezing medium and unattached cells and debris. Subsequently, the medium was changed every 48 hours until 85-90% confluent. HBECs were washed briefly using 3-5 ml/25 cm^2 HANKs- Balanced Salt Solution (HBSS) and were subsequently passaged using 3 ml/25 cm^2 1x trypsin-EDTA at 37°C for 5 minutes. Equal volume of trypsin neutralising solution was added and cells centrifuged at 150 RCF for 5 minutes at room temperature. Cells were resuspendend in BEGM by mixing gently without pipetting up and down. Cells were then mixed 1:1 with 0.4% trypan blue to assess cell viability. Alive cells actively pump out trypan blue and appear white in microscopic field while dead cells are blue. White cells were counted in using haemocytometer and cells/ml calculated according to manufacturer's formula and accounting for dilution factor with trypan blue:

Total cell number = (average cell number counted/number of small squares counted) x 90,000 x 2

HBECs for air-liquid interface (ALI) were cultured on collagen IV from human placenta. Collagen IV was reconstituted with 0.25% acetic acid in ddH_2O at concentration of 0.66 µg/µl overnight at 4°C. The collagen IV stock was then mixed 1:1 with 100% ethanol and used to coat Transwell inserts overnight at concentration of 50 µg/cm^2. Cells at 2-3 passage were seeded apically at 70,000 cells/cm^2 density in 100 µl of BEGM medium on 0.4 µm pore size 24-well plate Transwell inserts. Basolaterally, 500 µl of BEGM was added to the well. The medium was changed every 2-3 days both apically and basolaterally until cells reached confluence, within 5-7 days. The media was then removed from apical site and cells were cultured for 21 days at ALI in differentiation medium which consisted of 50%

complete BEGM without T3, 50% DMEM and 500 µM All-Trans-Retinoic Acid (ATRA).

2.10.4 Endothelial cells

Human umbilical endothelial vein cells (HUVEC) and human lung microvascular endothelial cells (HMVEC) were purchased from Lonza, UK. Cells were cultured in humidified atmosphere containing 5% CO_2 at 37°C in 1x endothelial growth medium (EGM-2, Lonza, Switzerland) containing 1x endothelial basal medium (EBM-2) and EGM-2 Singlequots (human Epidermal Growth Factor (hEGF), Gentamicin Sulphate/ Amphotericin-B (GA-1000), Hydrocortisone, FBS, Vascular Endothelial Growth Factor (VEGF), human Fibroblast Growth Factor (hFGF-b), Insulin-like Growth Factor (IGF), Ascorbic Acid, Heparin) (Lonza, Switzerland). Cells were seeded in 175cm^2 tissue culture flasks at the density of 5000 cells/cm^2. The medium was changed every 48 hours until 85-90% confluent. HUVECs and HMVECs were washed briefly using 3-5 ml/25 cm^2 HANKs- Balanced Salt Solution (HBSS) and were subsequently passaged using 3 ml/25 cm^2 1x trypsin-EDTA at 37°C for 5 minutes. Equal volume of trypsin neutralising solution was added and cells centrifuged at 220 RCF for 5 minutes at room temperature. The cell pellets were re-suspended, counted and propagated accordingly.

2.11 RT-PCR and real-time RT-PCR analysis

2.11.1 Prevention of RNA degradation

For all the appropriate steps of RNA isolation protocol molecular biology grade chemicals were used and deionised water was pre-treated with 0.1% diethyl pyrocarbonate (DEPC) overnight at room temperature, and subsequently autoclaved to deactivate DEPC. All the equipment was thoroughly cleaned with RNaseZap (Sigma Aldrich, UK) and filtered, nuclease free pipette tips (Continental Lab Products, UK) were used to minimise RNA degradation.

2.11.2 RNA extraction

Total RNA from frozen powdered lung tissue or cells cultures was isolated with TRIzol reagent as per manufacturer's protocol (Invitrogen, UK). TRIzol is a solution of phenol and guanidine isothiocyanate which disrupts cell membrane and dissolves cell components leaving RNA integrity intact. The total RNA was isolated in single step as 1ml of TRIzol was added to 50-100 mg of lung tissue. For isolation from lung tissue 1 ml of TRIzol was added directly to the cell plate and cells scraped into TRIzol with 1 ml pipette tip and transferred to 1.5 ml Eppendorf tube.

To isolate mRNA from TRIzol the samples were left for 5 minutes at room temperature and then 200 µl of chloroform was added. The mixture was mixed vigorously and left for 10 minutes at room temperature to allow separation of upper aqueous and a lower organic layer. The samples were then centrifuged for 15 minutes at 16,100 RCF at 4°C and the aqueous phase containing RNA transferred to a new Eppendorf tube containing 500 µl isopropanol.

The RNA was allowed to precipitate for 10 minutes at room temperature and was then centrifuged at 16,100 RCF for 15 minutes at 4°C. The supernatants were discarded and the RNA pellet was resuspended in 900µl of ethanol (80%) (BDH VWR International, UK). Following further 15 minutes centrifugation at 16,100 RCF at 4°C the supernatants were discarded, the pellets air dried and then resuspended in 12.5 µl of nuclease free water (Ambion,UK).

Contaminating genomic DNA was removed using Ambion DNAfree kit. DNase I and RNase inhibitor were added to the total RNA and incubated at 37°C for 20 minutes. The DNase reaction was terminated by the addition of resin which was subsequently removed from the solution by centrifugation.

RNA quality was visualised on agarose gel containing 1 g agarose, 10 ml 10x MOPS (0.2 M 3-N-morpholino-propane sulphonic acid, 16 nM sodium acetate and 2 nM EDTA), 74 ml DEPC-treated water, 16 ml formaldehyde and 0.005% gel red. The mixture loaded on the gel was made up of 2 µl RNA and 2 µl loading buffer (48%

deionised formamide (Gibco BRL, UK), 6% formaldehyde (BDH, UK, 5% glycerol, 10 mM MOPS) made up to the volume of 10 µl with DEPC- treated water.

RNA bands were observed using a Syngene Gene Genius Bio-imaging system (Synoptics, UK). The analysis of 28S rRNA and 18S rRNA bands displaying intensities ratio of approximately 2:1 was unequivocal of non-degraded RNA. The RNA was quantified using Nanodrop 8000 spectrophotometer (Thermo Scientific, UK), by measuring the A_{260} and A_{260}/A_{280} ratio respectively. The A_{260}/A_{280} ratio was used as a guide to the purity of RNA sample and values between 1.7 and 2.0 were considered acceptable.

2.11.3 DNAse treatment

cDNA was prepared by reverse-transcription (RT) using qScript cDNA SuperMix ® kit (Quanta Biosciences, USA). Following manufacturer's instructions up to 1 µg of RNA sample was made up to volume of 16µl with nuclease-free water. 4 µl of qScript cDNA SuperMix ® (5X reaction buffer containing optimized concentrations of $MgCl_2$, dNTPs (dATP, dCTP, dGTP, dTTP), recombinant RNase inhibitor protein, qScript reverse transcriptase and random primers, was then added to each sample, to achieve a final volume of 20 µl. Samples were then incubated for 5 minutes at 25°C, 30 minutes at 42°C and 5 minutes at 85°C.

2.11.3 RT-PCR

Real time RT-PCR was conducted using the Platinum SYBR Green qPCR SuperMix UDG (Invitrogen, UK) with ~1 ng of cDNA, and forward and reverse primers each at a final concentration of 800 nM, on a Mastercycler EP Realplex (Eppendorf, Germany). Cycling conditions were as follows: activation of SYBR Green 95°C for 10 minutes; cDNA amplification 95°C for 5 seconds, 60°C for 45 seconds for 40 cycles; melting curve 95°C, 65°C for 15 seconds, 95°C.

The efficiency of each primer pair was assessed by determining the relationship of primer crossing point (Cp) values with cDNA concentration using a series of half-log dilutions of template cDNA. Cp values were defined as the earliest point of the

linear region of the logarithmic amplification plot reaching a threshold level of detection. The log of cDNA concentrations was plotted against Cp values, and the slope of the plot was used to ascertain primer efficiency. Primers efficiency was given by the equation: Efficiency= $10^{(-1/slope)}$ and were only used if the slope was close to 1 indicating PCR efficiency greater than 90%.

GeNorm algorithm was applied to obtain the optimal number of housekeeping genes. Geometric mean of two housekeeping genes was shown to produce optimal normalisation factor and out of 13 housekeeping genes tested, ATP synthase, H^+ transporting, mitochondrial F1 complex, beta polypeptide (ATP5B) and beta-2-microglobulin (B2M) showed highest reference target stability for human samples. Calnexin (CANX) and ATP5B have been identified as optimal housekeeping genes for mouse samples.

To examine the quantitative differences in target mRNA expression in each sample, Cp values were determined from the linear region of the logarithmic amplification plot. Each sample was also tested for the expression of the two housekeeping genes, the Cp value of which was used to normalise between samples. Fold change was subsequently calculated using the standard $2^{-\Delta\Delta Cp}$ approach. Statistical analysis was performed using the ΔCp values.

The specificity of the products obtained by PCR was confirmed by analysis of the melting curve. Double- stranded DNA has a melting temperature (Tm) defined as a temperature at which half of the DNA is denatured and its value is primarily dependent on the nucleotide sequence. The melting curve analysis is performed by measuring a decrease in fluorescence due to the dissociation of DNA helix as a function of temperature and a single melting curve is indicative of a single PCR product.

Human		
Gene	**Forward sequence**	**Reverse sequence**
hPAR-1	AGGCCAGAATCAAAAGCAAC	TCATCCTCCCAAAATGGTTC
hITGAV	TCTGTGCCGCGCCTTCAACC	AACATCCGGGAAGACGCGCTG
hITGB6	AAGTTGAGACCAGGTGGTGCGC	CCATGGAGGCGGAGAGGTCCAT
hSmad2	Primer Design, UK	Primer Design, UK
hSmad	Primer Design, UK	Primer Design, UK
Mouse		
Gene	**Forward sequence**	**Reverse sequence**
muTissue factor	AGCCCTTGGACATGGCGATCCT	TTCTCTGGAATGCCTGCACCCG
muITGAV	ACACTTTGGGCTGTGGAATCGCC	CGTACAGGATTGCGCTCTTGCCT
muITGB6	CCGGGAGCCAGAATGTGGAAGT	GCCAGGAGTGCCATCCCAATCA
muITGB5	GGAGCCTGCCTGAGAGCTCATT	ACAGGCAGACCAGCTCAATCCC
muCCL2	AGCTCTCTCTTCCTCCACCAC	CGTTAACTGCATCTGGTGA
muTGFb	GGATACCAACTATTGCTTCAGCTCC	AGGCTCCAAATATAGGGGAGGTC
muF10	CAGCGGTTACTTCCTGGGTA	GCCACAGACCTCTTCCTACG
muF7	GACTTTGAGGGTCGGAACTG	AGGTACGCTTGGTCCCTACA
muF5	ACCTCAGGCAGTCACACCACGA	GGCCTTGTTAGGCACTGGGCAT
muPAR-1	AGCCAGCCAGAATCAGAGAG	AGGGGGACCAGTTCAAATGTA
muPAR-2	CGGGACGCAACAACAGTAA	GTTCCACCGGAACCCCTTTC
muPAR-3	TGCCAAAGTGGCATAAATGT	TCCAGCCCTCTATGTCAGAA
muPAR-4	AGACCCCCAGCATCTACGA	GTCTGAGGACTTCGGCTCCT

Table 2.3 List of human and mouse primers

2.12 Transfection with siRNA

A549 cells were transfected following reverse transfection protocol. SMARTpool ONTARGETplus Human siRNA targeting Smad2 and Smad3 and the ONTARGETplus Nontargeting Pool (Thermo Scientific, UK) were reconstituted to 20 µM stock in RNA buffer. A range of siRNA concentrations (100 nM, 30 nM, 10 nM, 3 nM, 1 nM) was tested to optimise the conditions and combined with Interferin transfection reagent (Polypus, UK) as per manufacturer's protocol. Interferin is composed of non-liposomal amphiphilic molecules that form stable complexes with siRNA and transport it into the cell cytoplasm. Interferin can be used in the presence of serum and antibiotics and does not affect the cell viability. A549 cells were seeded at sufficient density to reach 80% confluence and the transfection mix was immediately added to the wells. Cells were then incubated for 24 hours, 48 hours and 72 hours. After each time the medium was removed and the samples collected for mRNA and protein analysis or replaced with serum-free medium for another 24 hours before cells were stimulated.

2.13 Western blot

Buffers: Cell lysis buffer: Phosphosafe extraction buffer (Merck Chemicals, UK), 1 tablet of protease inhibitor cocktail (Roche , UK) in per 10 ml; Laemmli buffer 5x: 100 mM dithiothreitol (DTT) 1 M Tris (pH 6.8), 10% sodium dodecyl sulphate (SDS), 20% glycerol, ddH_2O, 0.05% bromophenol blue; Running buffer 1x: 0.1 M Tris, 0.1 M Hepes, 0.1% SDS, TBS-Tween: 10 nM Tris (pH8), 150 nM NaCl, 0.1% Tween-20; Blocking buffer: 5% non fat milk powder in TBS-Tween.

2.13.1 Sample preparation

Cells were seeded in 24-well plates and following appropriate treatment, cells were washed with cold PBS and lysed in 100 µl of lysis buffer supplemented with a complete protease inhibitor cocktail. Viscous lysates were scraped and collected into labelled Eppendorf tubes and centrifuged for 10 minutes at 13,000 g in order to remove cell debris. The lysates were stored at -80°C prior to use.

2.13.2 Electrophoresis

BCA assay was used to calculate protein concentration in the cell lysates as described in **Section 2.14**. For electrophoresis, an aliquot of each sample equivalent to 8 µg of protein was mixed with Laemmli buffer supplemented with DTT and incubated for 10 minutes at 70°C. The samples were then loaded onto a pre-cast 4-12% polyacrylamide gel (Bolt Bis-Tris Plus gels, Novex, Life Technologies, UK). A Plus Prestained Protein Ladder (Fermentas, UK) with 10-25 kDa detection range was run in a separate lane to identify the molecular weights of individual proteins. Electrophoresis was performed at 165 V for 35 minutes.

Dry protein transfer onto polyvinyldene difluoride (PVDF) membrane was performed using iBlot Gel Transfer Device (Novex, Life Technologies, UK). The transfer sandwich was assembled using iBlot Transfer Stacks (Novex, Life Technologies, UK) containing PVDF membrane fixed onto the bottom anode stack, filter paper and top cathode stack. The transfer parameters were set to 20 V for 7 minutes. The quality of protein transfer was assessed by briefly staining with 2% Ponceau Red solution (Sigma) which was destained by a quick wash in double distilled water.

2.13.3 Detection of proteins

Following transfer, the membrane bearing the covalently bound proteins was incubated in blocking buffer (5% milk) for one hour at room temperature on a rotating platform. Then the membrane was incubated overnight at 4°C with specific antibodies for protein of interest diluted in blocking buffer. The next day the membrane was washed 3x 5 minutes in TBS-Tween and incubated for one hour at room temperature with specific horseradish peroxidise (HRP)- linked secondary antibody diluted in TBS-Tween. The membrane was washed again 3x5 minutes TBS-Tween and then developed by enhanced chemiluminescence (ECL) following manufacturer's instructions (Amersham). Immunoreactive protein bands were visualised by exposing the membrane to autoradiography film developer (Kodak, UK) and the exposure time adjusted to the strength of the signal.

Semi-quantitative analysis of Western blots was performed with densitometry. Blots underwent transmissive greyscale scanning at 300 dpi on a standard flatbed scanner (Epson, UK). The scanned images were transferred to the public domain NIH Image J 1.6 program (developed at the U.S. National Institutes of Health and available on the Internet) and the optical density of each protein band was calculated with reference to calibration curve, which was generated by scanning a Kodak photographic step Tablet (Kodak, UK) with known optical density, using the same setting as described above. The optical density of the band for the target protein was corrected for the loading control and therefore allowing a meaningful comparison between samples.

2.14 Protein detection

Bicinchoninic acid (BCA) protein assay (Pierce, USA) was used to measure protein content in lung homogenates and bronchoalveolar lavage fluid. The assay works on a basis of biuret reaction where protein reduces Cu^{2+} to Cu^{1+} in an alkaline medium. Two bicinchoninic acid molecules chelate with the reduced cuprous cation developing intense purple colour. The BCA- copper complex is water soluble and linearly proportioned to protein concentration and displaying strong absorbance at 562 nm. The assay was performed as per manufacturer's instructions and the results compared to a ten point standard curve of bovine serum albumin ranging from 2 mg/ml to 0.0039 mg/ml. The assay was conducted in 96-well plate format with 10 µl of sample in duplicate mixed with 200 µl freshly prepared BCA working reagent. The plate was incubated for 30min at 37°C and the absorbance measured at 550nm on a Titertek Multiscan MCC/340 plate reader (Labsystems, Finland).

2.15 Intracellular calcium measurement

The assay utilises a Ca^{2+}-binding dye fluo-4 acetoxymethyl ester (Fluo4-AM) to detect changes in cytosolic calcium concentration. The non-fluorescent precursor form of the dye is uncharged and hence cell permeable. Inside the cell, non-specific esterases render the dye sensitive to binding Ca^{2+} ions. Cation binding causes a conformational and energetic change in the molecule which leads to the emission

of fluorescence that is proportional to the intracellular Ca^{2+} concentration. Fluo-4 NW calcium assay kit was purchased from Invitrogen, UK and used as per manufacturer's instructions.

Cells were seeded 48 hours prior to experiment in black 96-well plates with a clear bottom. On the day of the assay 1 vial of Fluo 4-AM dye was resuspended in 10 ml of HBSS/Hepes assay buffer without calcium or magnesium. Cells were incubated with the dye, 100 µl/well, for 30 minutes at 37°C and calibrated for another 30 minutes at room temperature. The PAR antagonists used in this study were added and incubated with the dye for an hour prior to the experiment. PAR agonists were prepared at 3x final desired concentration in assay buffer and 50 µl per well of appropriate compound was added to a 96-well agonist plate.

Changes in the intracellular Ca^{2+} were monitored using a fluorescent image plate reader FLIPR Tetra (Molecular Devices, USA) and the results displayed and analysed using ScreenWorks software. The device is fitted with standard ECCM camera that records the fluorescent signal produced by light-emitting diodes (LED) that excites the Fluo-4AM dye at wavelength of 494 nm with emission at 516 nm. The fluorescence was monitored for 10 seconds before the agonists were simultaneously dispensed to the 96-well plate by the overhead pipettor. Two reading protocols were used depending on the cell type tested. Standard protocol recorded readings every second for first 60 seconds and every 6 seconds for the next 120 seconds. Extended protocol recorded readings every second for 180 seconds and every 6 seconds for another seven minutes. The change in intracellular calcium [Ca^{2+}] was quantified as an increase in relative fluorescence units (RFUs). The difference between maximum and minimum RFU was used to plot the results.

2.16 Immunocytofluorescence

Cells were seeded in 8-well chamber slides (Fisher Scientific, UK) and cultured for 48 hours in a humidified atmosphere with 5% or 10% CO_2 at 37°C. Depending on cell type, serum-starvation was carried out for 24 hours. Cells were subsequently

treated for another 24 hours or washed in PBS and fixed with 4% paraformaldehyde for 10 minutes at room temperature. Cells were washed and stored in PBS.

Cells were subsequently permeabilised in 0.4% Triton-X for 10 minutes and blocked in 3% bovine serum albumin (BSA), 5% goat serum in PBS for 1 hour. Following three washes with PBS, 2 minutes each, cells were incubated with appropriate antibodies, as listed in **Table 2.1,** for two hours. The primary antibodies were washed off in PBS and cells incubated with 1:100 dilution of secondary antibodies FITC- or PE-conjugated (Alexa Fluor 488 and Alexa Fluor 555, Invitrogen, UK) for another two hours. Again, three washes were performed and the side walls of the chambers carefully removed. Coverslips were mounted onto each slide using three drops of mounting medium containing 4,6-Diamidino-2-phenylindole (DAPI, 405) which is highly sensitive nucleic acid stain. Images were captured using confocal laser scanning microscopy Zeiss 700.

2.17 ELISA

DuoSet ELISA Development kits were purchased from R&D Systems, USA, and IFNγ and TNFα were bought from Biolegend, UK. Microtest TM 96-well ELISA plates were purchased from BD Biosciences, Pharmingen, USA. ELISA detections were performed according to manufacturer's instructions and a general standard protocol is described briefly. Microtest TM 96-well ELISA plates were coated with 50 µl capture antibody diluted in PBS and incubated overnight at 4°C. The next day plates were washed with the 0.05% Tween® in PBS wash buffer and blocked with 150 µl 1% BSA in PBS reagent diluent for minimum 1 hour. After the blocking step, plates were washed again and 50 µl of sample and the serial dilutions of the standard were added and incubated for 2 hours. Following incubation the plates were washed again and incubated for another 2 hours with detection antibody. Next Streptavidin-HRP (1:200 dilution) was added and plates incubated for 30 minutes. After the incubation and washing step, the plates were incubated with Tetramethylbenzidine (TMB, Invitrogen, UK)TMP Substrate for approximately 20 minutes and the reaction terminated with 1M H_2SO_4 stop solution. The optical

density was measured using a plate reader (Multiskan MCC/340, Titertek) at dual wavelength A1: 450nm and A2: 540nm.

2.18 Statystical analysis

All data in the figures are presented as mean values ± SEM, unless indicated otherwise. Statistical analysis was performed between two treatment groups by Student's t-test or Mann-Whitney U test, and between multiple treatment groups by one-way analysis of variance (ANOVA) with Tukey post-hoc testing or two-way ANOVA with Bonferroni post-hoc test, using Graphpad Prism 5 software. The mean values of various parameters were considered to be significantly different when the p value was calculated to be less than 0.05.

Chapter 3: Results

3.1 Characterisation of PAR-1 expression and signalling in human lung

3.1.1 Introduction

Coagulation factors, FXa and thrombin, can act as a danger signals and orchestrate inflammatory and tissue repair responses via activation of proteinase activated receptors PARs, particularly PAR-1 and PAR-2. Immunohistochemistry studies suggest that PAR-1 and PAR-2 are widely expressed in the normal and fibrotic lungs (Borensztajn et al., 2010; Mercer et al., 2009) and PAR-1 is overexpressed in lung cancer (Cisowski et al., 2011). In lung fibroblasts PAR-1 gene and protein expression has been shown to be regulated by a negative feedback mechanism, where PAR-1 activation induces prostaglandin PGE_2 release which in turn inhibits PAR-1 expression in a time-dependent manner (Sokolova et al., 2005). Furthermore, the transcriptional regulation of PAR-1 has been recently a focus in the context of cancer research as PAR-1 overexpression in carcinoma cells is associated with an aggressive and metastatic phenotype (Nierodzik and Karpatkin, 2006).

However, the mechanisms of PAR-1 expression and upregulation are not fully elucidated and the current findings suggest that PAR-1 regulation is both tissue- and cell-specific. Furthermore, our understanding of the role of PAR-1 and PAR-2 signalling in lung disease comes largely from experimental models of lung injury and fibrosis. Although some of the *in vivo* findings have been translated to human biology, there is a need to further understand PAR-1 signalling in human primary cells. Therefore, the aim of this study was to gain detailed insight into the relative importance of PAR-1 and PAR-2 signalling responses in human primary lung cells: fibroblasts, alveolar and bronchial epithelial cells, and lung microvascular endothelial cells. Furthermore, using selective pharmacological tools we tested the specificity of observed responses and began to dissect which cell types are the most important and relevant for potential therapeutic PAR targeting. Finally, PAR-1

activation directly leads to release of active TGFβ and we asked whether this key profibrotic cytokine affects PAR-1 expression and signalling in human primary lung cells.

3.1.2 PAR-1 expression and signalling in primary human lung fibroblasts

Thrombin is a potent mesenchymal cell mitogen (Furuhashi et al. 2008; Howell et al. 2001) and an inducer of fibroblast to myofibroblasts differentiation (Bogatkevich et al., 2001). It also stimulates production and secretion of collagen (Chambers et al., 1998), growth factors such as CTGF (Chambers et al., 2000), FGF2 (Duarte et al., 2006), chemokines and cytokines such as CCL2 (Deng et al., 2008; Ortiz-Stern et al., 2012).

Thrombin proteolytically cleaves the extracellular N-terminus of PAR-1 and unmasks the tethered ligand, which then interacts with the second extracellular loop of the receptor. This interaction causes a conformational change of the receptor, which in turn leads to uncoupling of G-protein bound to the intracellular part of the receptor and downstream signalling via multiple pathways. Gαq is one of three G-proteins types that form stable complexes with PAR-1 and upon uncoupling promotes the release of the intracellular calcium via phospholipase C and inositol trisphosphate-dependent mechanisms (McCoy et al., 2012). Mobilisation of calcium from intracellular stores leads to transient and robust increases in cytoplasmic concentration from 10^{-7} M to 10^{-3} M. Calcium as a second messenger influences multiple signalling pathways involved in fibroblasts proliferation (LaMorte et al., 1993), differentiation (Baffy et al., 1994), production and release of CCL2 (Deng et al., 2008; Ortiz-Stern et al., 2012). FXa is also able to cleave PAR-1 and has been shown to promote fibroblast proliferation and collagen production (Blanc-Brude et al., 2005; Scotton et al., 2009).

Previous research in our laboratory used single cell cytosolic calcium spectrofluorometry to demonstrate that thrombin and FXa signalling leads to release of intracellular calcium albeit there are marked differences in the kinetics,

magnitude and concentration of the agonist required to elicit the response (Blanc-Brude et al., 2005). Using a high throughput intracellular calcium monitoring assay, the aim of this study was to expand on these previous findings in primary human lung fibroblasts and to characterise PAR-1 and PAR-2 signalling responses in these cells. Furthermore, the effect of TGFβ stimulation on PARs responses was examined.

3.1.2.1 Intracellular calcium flux downstream of PAR-1 and PAR-2 activation in lung fibroblasts

In agreement with previous data, both thrombin and FXa elicit a calcium response in primary human lung fibroblasts. **Figure 3.1** shows representative traces of intracellular calcium flux in response to PAR-1 and PAR-2 agonists. The baseline was monitored for 10 seconds prior to exposure of fibroblasts to exogenous agonists. Addition of thrombin (10 nM) elicited an immediate response with a sharp increase suggestive of a simultaneous and synchronised release of intracellular calcium from a collective pool of cells. The calcium signal peaked 15 seconds after stimulation and lasted for approximately 60 seconds before returning to baseline (**Figure 3.1A**). In comparison, a 10-fold higher concentration of FXa was required to trigger a calcium response in fibroblasts. Following addition of FXa (100 nM) an increase in fluorescent signal was observed with a 20 second delay. The intracellular calcium release in response to FXa was of lower magnitude in comparison to the thrombin-mediated response and only of slightly extended duration (**Figure 3.1B**). As expected, the PAR-1 activating peptide, TFLLR, elicited a calcium flux of magnitude and duration equivalent to that observed for thrombin (**Figure 3.1C**). PAR-2 has also been shown to couple to Gαq (McCoy et al. 2010) and the PAR-2 activating peptide (SLIGKV) also triggered intracellular calcium release in fibroblasts (**Figure 3.1C**). However, the response to SLIGKV was of smaller magnitude than that of TFLLR and resembled the delayed activation wave observed with FXa.

The release of intracellular calcium in fibroblasts was agonist concentration-dependent. Cells were stimulated with a range of thrombin concentrations between 10 pM and 100 nM and intracellular calcium release was readily detected from 0.3 nM thrombin onwards, with an EC_{50} of 1.5 nM (**Figure 3.2A**). TFLLR also elicited an

intracellular calcium release in a concentration-dependent manner with an EC_{50} of 3.7 μM (**Figure 3.3A**). Exposure to TGFβ for 24 hours prior to thrombin or TFLLR stimulation did not affect the responsiveness of fibroblasts to thrombin (**Figures 3.2B and 3.3B**). The release of intracellular calcium in response to FXa stimulation was only observed at high FXa concentration with an EC_{50} of 150 nM (**Figure 3.4**).

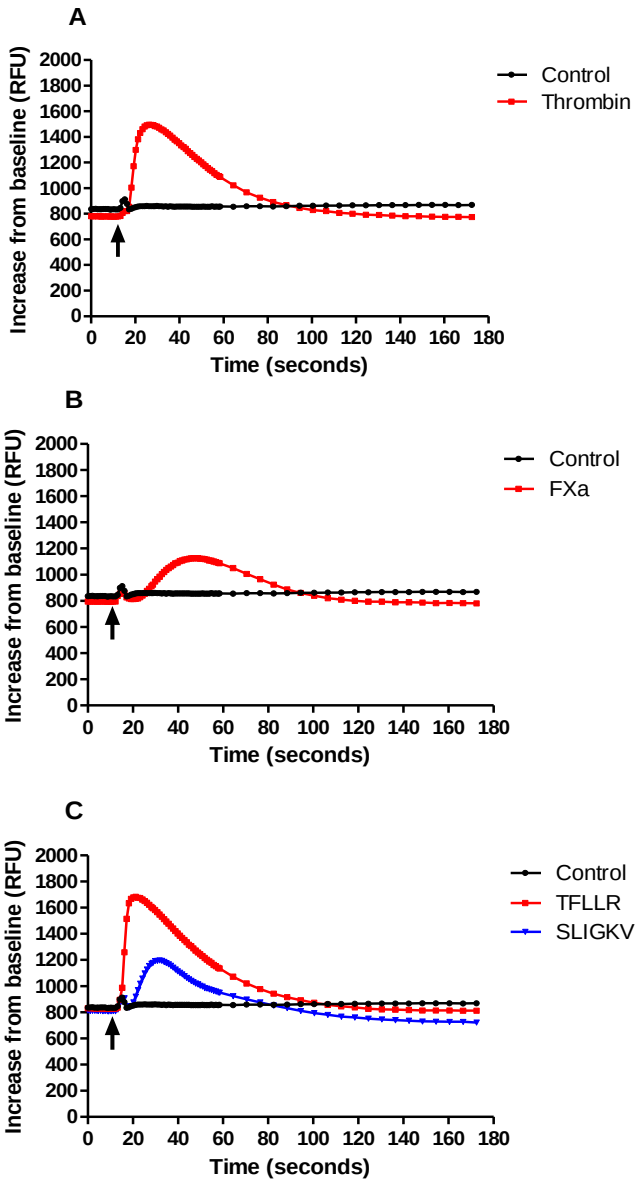

Figure 3.1. Intracellular calcium signalling in response to PAR-1 and PAR-2 agonists in primary human lung fibroblasts.

Primary human lung fibroblasts were seeded at a density of $1x10^4$ in 96-well plates, serum-starved for 24 hours and incubated with Fluo-4AM calcium binding dye for one hour prior to stimulation with thrombin (10 nM), FXa (100 nM), PAR-1 activating peptide TFLLR (100 µM), PAR-2 activating peptide SLIGKV (100 µM). The release of intracellular calcium was monitored by FLIPR® Tetra with baseline recorded for 10 seconds before agonist addition and responses measured for another 170 seconds. Data are represented as increase in relative fluorescence units (RFU) from the baseline. Panel A shows representative traces for thrombin-mediated calcium flux, panel B- FXa and panel C- TFLLR and SLIGKV. Each data point represents the mean +/- SEM of 3-4 replicate wells.

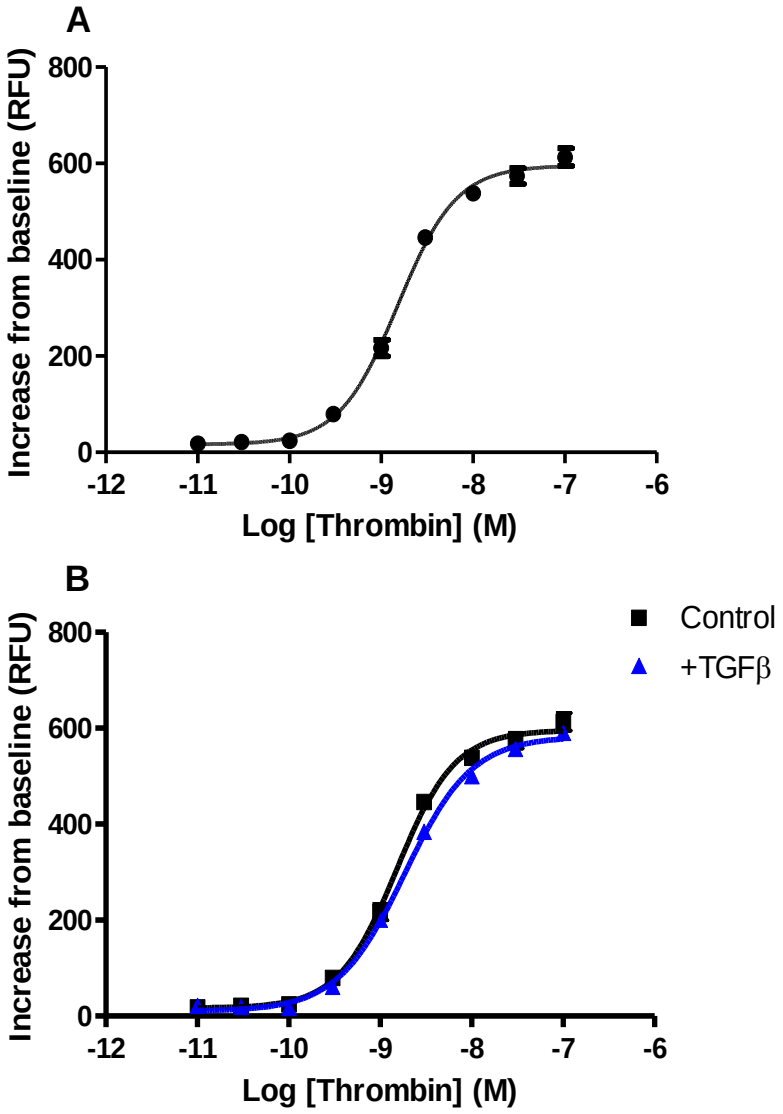

Figure 3.2. Concentration-response curve in primary human lung fibroblasts following thrombin stimulation.

Primary human lung fibroblasts were seeded at a density of $1x10^4$ in 96-well plates and serum-starved with or without TGFβ (1 ng/ml) for 24 hours. Cells were then incubated with Fluo-4AM calcium binding dye before being exposed to different concentrations of thrombin. The release of intracellular calcium was monitored by FLIPR® Tetra with calcium baseline recorded for 10 seconds before thrombin addition and responses measured for another 170 seconds. Data are represented as increase in relative fluorescence units (RFU) from the baseline. Panel A shows a concentration-response curve to thrombin and panel B is a comparison of response to thrombin when cells were pre-incubated with TGFβ. Each data point represents the mean +/- SEM of 3-4 replicate wells.

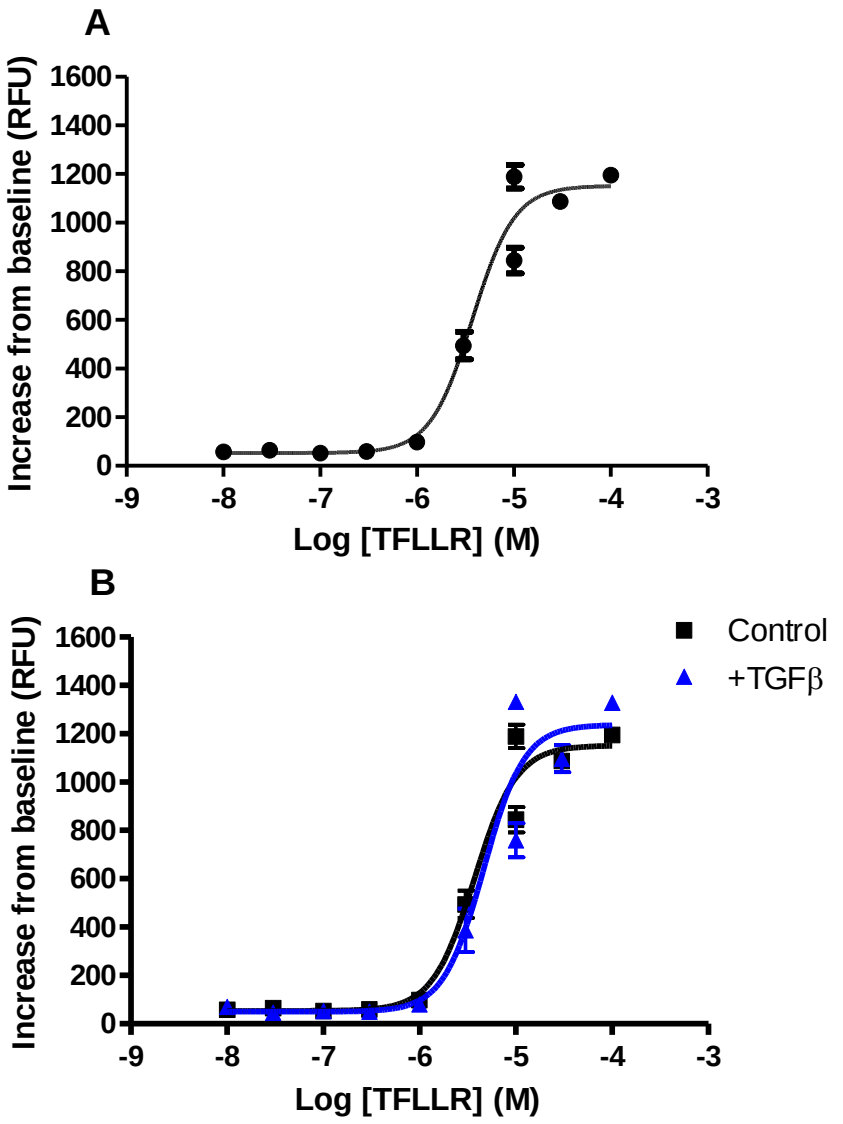

Figure 3.3. Concentration-response curve in primary human lung fibroblasts following TFLLR stimulation.

Primary human lung fibroblasts were seeded at a density of $1x10^4$ in 96-well plates and serum starved with or without TGFβ (1 ng/ml) for 24 hours. Cells were incubated with Fluo-4AM calcium binding dye before being exposed to different concentrations of PAR-1 activating peptide TFLLR. The release of intracellular calcium was monitored by FLIPR® Tetra with calcium baseline recorded for 10 seconds before TFLLR addition and responses measured for another 170 seconds. Data are represented as increase in relative fluorescence units (RFU) from the baseline. Panel A shows a concentration-response curve to TFLLR and panel B is a comparison of response when cells were pre-incubated with TGFβ. Each data point represents the mean +/- SEM of 3-4 replicate wells.

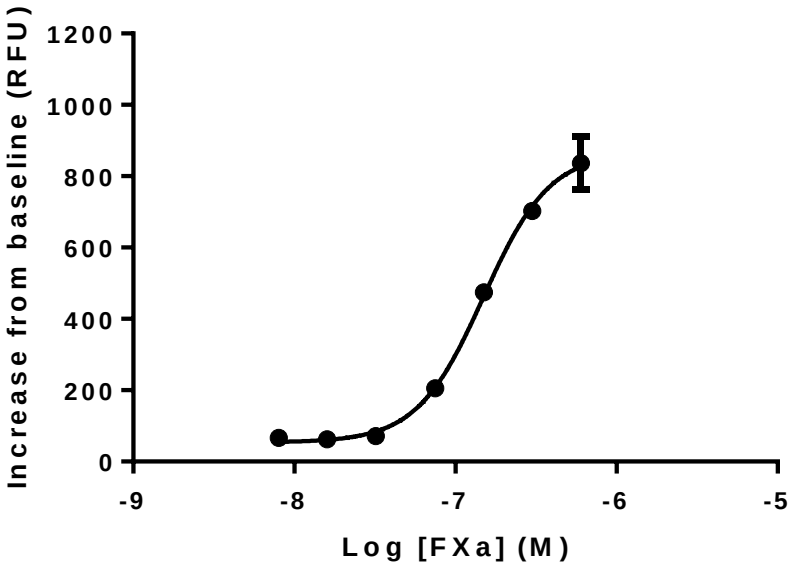

Figure 3.4. Concentration-response curve in primary human lung fibroblasts following FXa stimulation.

Primary human lung fibroblasts were seeded at a density of $1x10^4$ in 96-well plates and serum starved for 24 hours. Cells were incubated with Fluo-4AM calcium binding dye before being exposed to different concentrations of FXa. The release of intracellular calcium was monitored by FLIPR® Tetra with calcium baseline recorded for 10 seconds before FXa addition and responses measured for another 170 seconds. Data are represented as increase in relative fluorescence units (RFU) from the baseline. Data are presented as a concentration-response curve to FXa with each data point representing the mean +/- SEM of 3-4 replicate wells.

3.1.2.2 PAR-1 and PAR-2 expression in lung fibroblasts

PAR-1 and PAR-2 expression in primary human lung fibroblast was next assessed by immunocytofluorescence. Vimentin was used as mesenchymal cell markers and as shown in **Figure 3.5** fibroblasts intensely expressed vimentin and showed characteristic elongated shape. The intensity of PAR-1 was strong with the distribution of the receptor throughout the periphery of cells as well as within the cytoplasm and around the nucleus. Following stimulation of fibroblasts with TGFβ (1 ng/ml) for 24 hours, the intensity of PAR-1 staining did not change. Fibroblasts also expressed high levels of PAR-2 and the distribution of the receptor was similar to PAR-1 with expression in the periphery of cells as well as within the cytoplasm and around the nucleus (**Figure 3.6**). Again, the TGFβ treatment did not appear to have any effect on PAR-2 expression.

PAR-1 expression in human lung fibroblasts:

24 hours control

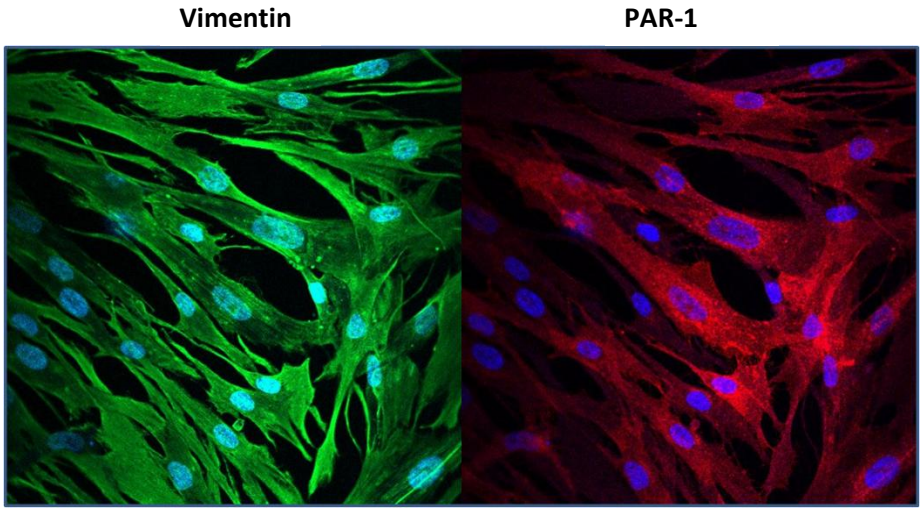

24 hours TGFβ

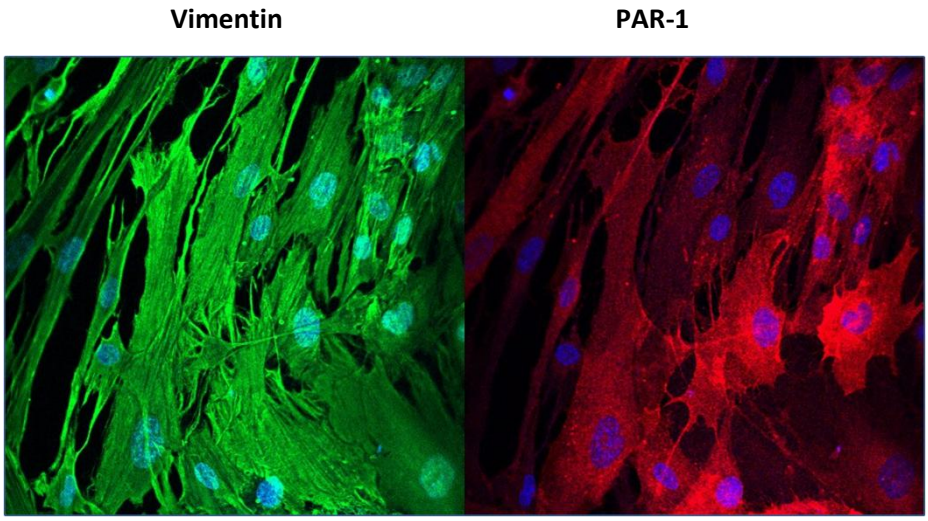

Figure 3.5. PAR-1 expression in primary human lung fibroblasts.

Primary human lung fibroblasts were seeded at a density of $3x10^4$ in chamber slides and allowed to reach over 80% confluence. Cells were serum starved with or without TGFβ (1 ng/ml) for 24 hours, fixed in paraformaldehyde and stained for PAR-1 (Alexa 555) and vimentin (Alexa 488). DAPI was used to visualise the nucleus. The top panel shows images for control cells and lower panels show the staining of TGFβ-stimulated cells, x20 original magnification.

PAR-2 expression in human lung fibroblasts:

24 hours control

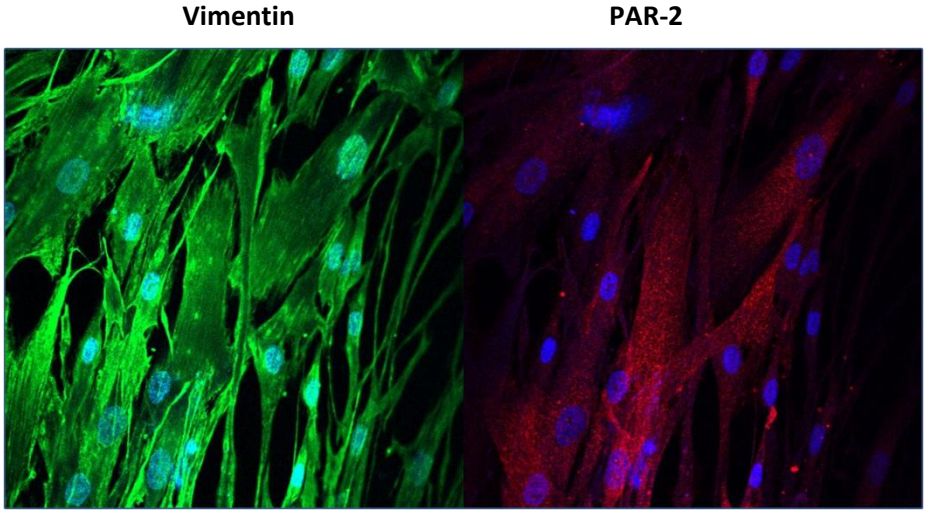

24 hours TGFβ

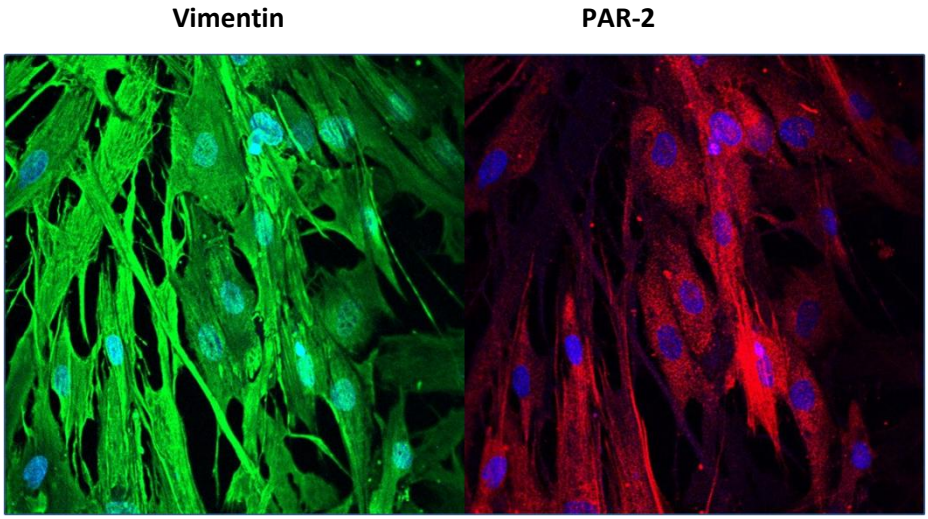

Figure 3.6. PAR-2 expression in primary human lung fibroblasts.

Primary human lung fibroblasts were seeded at a density of $3x10^4$ in chamber slides and allowed to reach over 80% confluence. Cells were serum starved with or without TGFβ (1 ng/ml) for 24 hours, fixed in paraformaldehyde and stained for PAR-2 (Alexa 555) and vimentin (Alexa 488). DAPI was used to visualise the nucleus. The top panel shows images for control cells and lower panels show the staining of TGFβ-stimulated cells, x20 original magnification.

3.1.2.3 Intracellular calcium release in lung fibroblasts is PAR-1-dependent and PAR-2-independent

Previous data from our laboratory have shown that in murine lung fibroblasts from PAR-1 knockout mice, thrombin and FXa fail to induce intracellular calcium release (Blanc-Brude et al., 2005). It has been challenging to recapitulate these findings in primary human lung fibroblasts, which express PAR-1 in abundance. We addressed the question of PAR-1 and PAR-2 contribution to intracellular calcium release in response to coagulation factors using PAR-1 specific antagonists, RWJ58259 and SCH530348, and the PAR-2 antagonist, GB83.

The specificity of the antagonists was validated first. RWJ58259 (Damiano et al., 2003) and GB83 (Suen et al., 2012) are small molecule antagonists that competitively bind to the second extracellular loop of PAR-1 and PAR-2, respectively, which are the sites of interaction between the tethered ligand and the receptor. TFLLR and SLIGKV are small mimetic peptides that activate PAR-1 and PAR-2, respectively, by binding also to the second extracellular loop. As shown in **Figure 3.7A**, TFLLR-mediated calcium responses were fully blocked by the PAR-1 antagonist and unaffected by the PAR-2 antagonist. In **Figure 3.7B** the calcium flux was induced by the PAR-2 activating peptide and consequently blocked by the PAR-2 antagonist. The PAR-1 antagonist did not affect PAR-2 activation by the agonist peptide.

As shown in **Figure 3.8**, thrombin-mediated PAR-1 activation elicited a significant increase in intracellular calcium flux and this response was dependent on thrombin enzymatic activity. Pre-incubation of thrombin with hirudin that yields it catalytically inert caused complete inhibition of calcium flux. PAR-1 antagonists (RWJ58259 and SCH580348) also completely blocked the release of intracellular calcium strongly suggesting that this response was entirely PAR-1 mediated. In contrast, the PAR-2 antagonist (GB83) did not affect the thrombin response.

Similarly FXa triggered a significant increase in intracellular calcium flux but the response was half the magnitude of the thrombin response. FXa-mediated calcium

flux was also fully inhibited by the PAR-1 antagonists but not by the PAR-2 inhibitor (**Figure 3.9**).

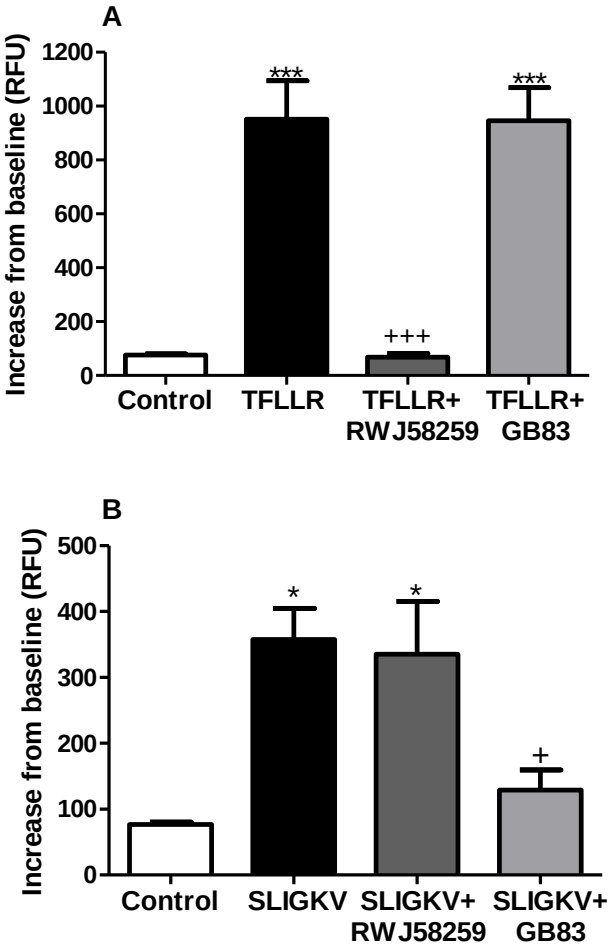

Figure 3.7. Selective antagonists block PAR-1- and PAR-2-mediated calcium signalling.

Primary human lung fibroblasts were seeded at a density of $1x10^4$ in 96-well plates and serum starved 24 hours prior to stimulation with TFLLR and SLIGKV (each at 100 µM). Cells were incubated with Fluo-4AM calcium binding dye with or without PAR-1 inhibitor RWJ58259 (3 µM) or PAR-2 antagonist GB83 (50 µM). The release of intracellular calcium was monitored by FLIPR® Tetra with calcium baseline recorded for 10 seconds before agonist addition and response measured for another 170 seconds. Data are represented as increase in relative fluorescence units (RFU) from the baseline. Panel A shows calcium responses in cells stimulated with TFLLR and panel B- SLIGKV. Each data point represents the mean +/- SEM of 3-4 replicate wells, one-way ANOVA, ***$p<0.01$ relative to control cells, +$p<0.05$, +++$p<0.01$ relative to TFLLR/SLIGKV responses.

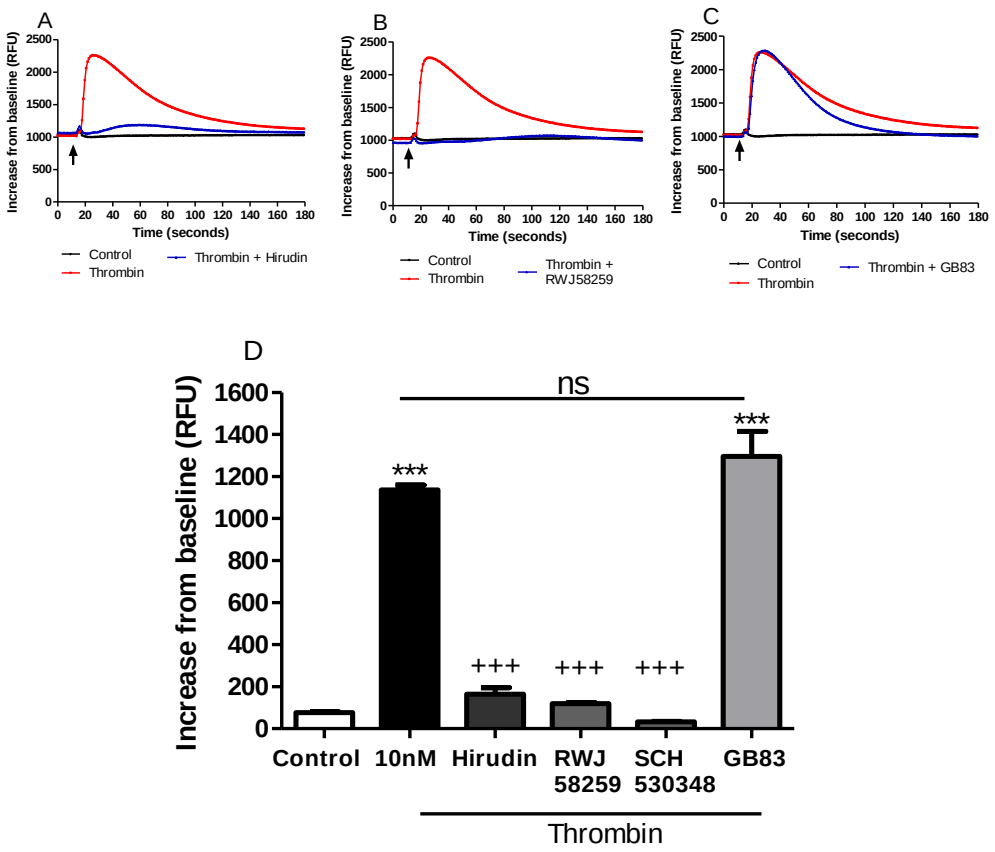

Figure 3.8. Thrombin-mediated intracellular calcium signalling in fibroblasts is PAR-1- dependent and PAR-2-independent.

Primary human lung fibroblasts were seeded at a density of $1x10^4$ in 96-well plates and serum starved 24 hours prior to stimulation with thrombin (10 nM) or thrombin (10 nM) pre-incubated with hirudin (50 nM). Cells were incubated with Fluo-4AM calcium binding dye with or without PAR-1 inhibitors RWJ58259 (3 µM) and SCH530348 (3 µM) or PAR-2 antagonist GB83 (50 µM). The release of intracellular calcium was monitored by FLIPR® Tetra with calcium baseline recorded for 10 seconds before thrombin addition and responses measured for another 170 seconds. Data are represented as increase in relative fluorescence units (RFU) from the baseline. Upper panel shows the representative intracellular calcium flux traces for hirudin inhibition-A, PAR-1 inhibition-B, PAR-2 inhibition-C. Panel D shows a graph of different treatments effect on calcium responses in cells stimulated with thrombin. Each data point represents the mean +/- SEM of 3-4 replicate wells, one-way ANOVA, ***p<0.01 relative to control cells, +++p<0.01 relative to thrombin responses, ns non-significant.

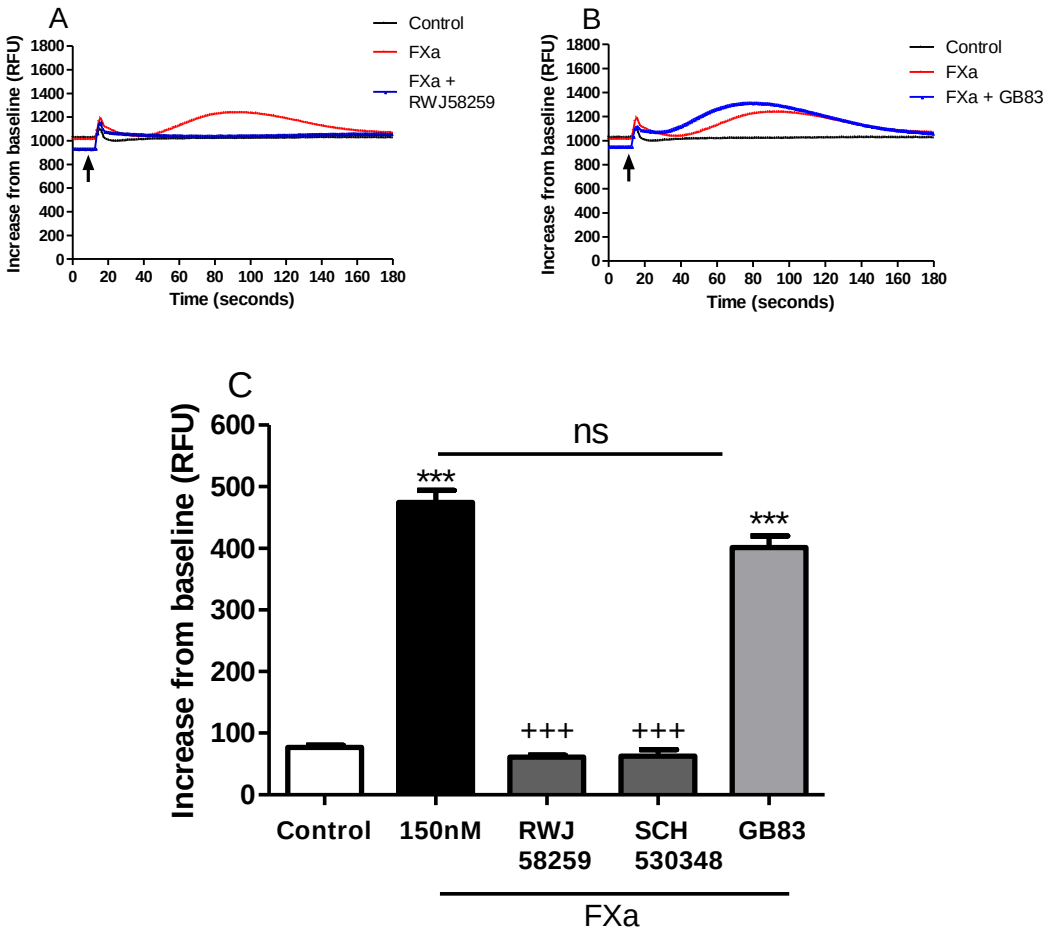

Figure 3.9. FXa-mediated intracellular calcium signalling in fibroblasts is PAR-1 dependent and PAR-2 independent.

Primary human lung fibroblasts were seeded at a density of $1x10^4$ in 96-well plates and serum starved 24 hours prior to stimulation with FXa (150 nM). Cells were incubated with Fluo-4AM calcium binding dye with or without PAR-1 inhibitors RWJ58259 (3 µM) and SCH530348 (3 µM) or PAR-2 antagonist GB83 (50 µM). The release of intracellular calcium was monitored by FLIPR® Tetra with calcium baseline recorded for 10 seconds before FXa addition and responses measured for another 170 seconds. Data are represented as increase in relative fluorescence units (RFU) from the baseline. Upper panel representative traces of intracellular calcium flux with PAR-1 inhibition-A and PAR-2 inhibition-B. Panel C shows the effect of different treatments on calcium responses in cells stimulated with FXa. Each data point represents the mean +/- SEM of 3 replicates, one-way ANOVA, ***p<0.01 relative to control cells, +++p<0.01 relative to FXa responses, ns non-significant.

3.1.2.4 Summary

- Human primary lung fibroblasts express PAR-1 and PAR-2 and activation of these receptors leads to a robust and transient increase in intracellular calcium release.
- The pro-fibrotic cytokine TGFβ does not affect PAR-1 signalling responses in fibroblasts.
- Fibroblasts elicit robust responses when PAR-1 is activated by thrombin, even at low nanomolar concentrations. In contrast high FXa concentration is required to trigger intracellular calcium responses. There are marked differences in the kinetics of intracellular calcium responses mediated by thrombin and FXa.
- Thrombin and FXa trigger intracellular calcium release in PAR-1-dependent and PAR-2-independent pathway as examined using specific antagonists.

3.1.3 PAR-1 expression and signalling in human alveolar epithelium

PAR-1 is abundantly expressed in primary human lung fibroblasts, which signal robustly to coagulation proteinases. In contrast, PAR-1 and PAR-2 signalling responses to thrombin and FXa are less characterised in alveolar epithelium and will be the focus of this section. The alveolar epithelium is composed of two cell types. Type I pneumocytes (alveolar epithelial cells type I; AECI) are simple squamous and non-proliferating epithelial cells that line the alveolar spaces and facilitate the gas exchange. Type II pneumocytes (alveolar epithelial cells type II; AECII) are cuboidal in shape and are highly synthetic for chemokines and cytokines as well as being the main source of surfactants in the lung necessary for maintaining lung compliance. AECII also have large regenerative potential and in case of injury to the epithelium can proliferate and differentiate into AECI to restore epithelial barrier integrity. Damage to the alveolar epithelium, particularly AECII is the first step in the development of multiple detrimental lung conditions, including acute lung injury and fibrosis. TGFβ, a central profibrotic cytokine, exerts pleiotropic effects on epithelial cells that is highly dependent on the local environment and can promote apoptosis (Degryse et al., 2011), epithelial to mesenchymal transition (Kim et al., 2007) and migration (Yu et al., 2008). In the fibrotic lung, PAR-1 is upregulated in the abnormal and hyperplastic epithelium in comparison to normal epithelium (Mercer et al., 2009). PAR-1 along with the remaining PAR receptors is also upregulated in endotoxin-induced model of acute lung injury (Jesmin et al., 2004, 2007).

In this series of experiments, PAR-1 expression and signalling in the alveolar epithelium was examined. Growing a fibrotic alveolar epithelium *in vitro* is currently not feasible due to lack of access to clinical specimens and technical limitations. However, in our laboratory we are able to isolate normal human alveolar epithelial cells from lung explants but the numbers of cells have always been limited and culturing them has been challenging. To date the most representative and widely used model of abnormal alveolar epithelium has been the A549 cell line, which is a hypotripoid human adenocarcinoma cell line. Although A549 cells have been

derived from a tumour, they display several characteristics of AECII including polygonal morphology, production of surfactants and the presence of cytoplasmic lamellar bodies (Lieber et al., 1976). A549 cells were therefore used in these experiments as an initial model of alveolar epithelial cells and responses found in A549 cell line were subsequently verified in freshly isolated normal human primary type II alveolar epithelial cells.

3.1.3.1 Intracellular calcium signalling in A549 in response to different agonist and following stimulation with TGFβ

Intracellular calcium release in A549 cells was measured in response to stimulation with coagulation enzymes and PAR activating peptides. In these cells, thrombin-induced calcium flux occurred within 20 seconds after stimulation and the signal lasted for approximately 100 seconds before returning to baseline. The magnitude of the response was lower when compared with the calcium flux observed in primary human lung fibroblasts and a higher concentration of thrombin (30 nM) was required to achieve consistent and reproducible responses. Stimulation of A549 cells with TGFβ (1 ng/ml) for 24 hours significantly changed the kinetics of the thrombin-mediated calcium response. The delay between the addition of the agonist and onset of the signal was reduced and the magnitude of intracellular calcium release in response to thrombin was increased (**Figure 3.10A**). All responses were inhibited with the PAR-1 specific antagonist, RWJ58259.

Similarly to fibroblasts, high concentrations of FXa were required to trigger calcium release in A549 cells. The response occurred with a 40 second delay from the addition of FXa, was of low magnitude and short duration. All the parameters of the intracellular calcium response to FXa were augmented with prior TGFβ stimulation for 24 hours (**Figure 3.10B**).

Figures 3.10C and 3.10D show that intracellular calcium responses to PAR-1 and PAR-2 activating peptides were robust in A549 cells. Furthermore, the onset of responses was similar between the two PAR activating peptides suggesting that in

A549 cells both PAR-1 and PAR-2 strongly couple to $G\alpha_q$ and hence trigger similar release of intracellular calcium. However, the magnitude of the intracellular calcium flux downstream of PAR-2 activation was greater in comparison to PAR-1 signalling, suggesting that A549 epithelial cells express more PAR-2 than PAR-1. Responses to PAR-1 and PAR-2 activating peptides were further enhanced with TGFβ pre-stimulation.

As summarised in **Figure 3.11A**, pre-stimulation of A549 cells with TGFβ significantly increased PAR-1 and PAR-2-mediated intracellular calcium fluxes in response to all agonists used: thrombin, FXa, TFLLR and SLIGKV. Thrombin enzymatic activity was again necessary to trigger the release of intracellular calcium and treatment with hirudin completely abolished this signalling response (**Figure 3.11B**). Furthermore, intracellular calcium release was inhibited by the PAR-1 antagonist, RWJ58259. The PAR-2 antagonist GB83 partially blocked thrombin-induced intracellular calcium release, which suggests that PAR-2 may be partially involved in thrombin-mediated signalling in A549 cells. It is possible that PAR-1 transactivates PAR-2 in the alveolar epithelium, an event that has been previously reported for endothelium (O'Brien et al., 2000).

Next the concentration range of thrombin capable of triggering calcium responses was investigated in A549 cells. Thrombin was found to induce intracellular calcium flux in A549 in a concentration-dependent manner with an EC_{50} of ~13 nM (**Figure 3.12A**). When cells had been pre-treated with TGFβ for 24 hours the EC_{50} was achieved at ~20 nM thrombin but the magnitude of response was 2.5 fold higher (**Figure 3.12B**). The significant increase in maximal response to thrombin with TGFβ pre-stimulation suggests that TGFβ increased PAR-1 expression in A549 cells.

At low concentrations FXa failed to elicit a detectable intracellular calcium release in A549 cells and the intracellular calcium response increased sharply at the highest concentrations of FXa. Pre-treatment with TGFβ for 24 hours again significantly increased the maximal response in A549 cells to FXa stimulation (**Figure 3.13**). In this experiment the concentration of FXa was taken up to 600 nM, at which point the calcium flux did not reach a plateau. However, this concentration greatly

exceeds the physiological concentrations of FXa that can be achieved in any body compartment as estimated by the total level of circulating FX being 174 nM (Mann, 1999). For that reason FXa was not used at higher concentration.

Taken together, these data show that calcium signalling downstream of specific PAR-1 activation is enhanced with TGFβ pre-treatment and that these responses are abolished with the PAR-1 specific inhibitor, RWJ58259. Therefore, the direct effect of TGFβ on PAR-1 expression was investigated further.

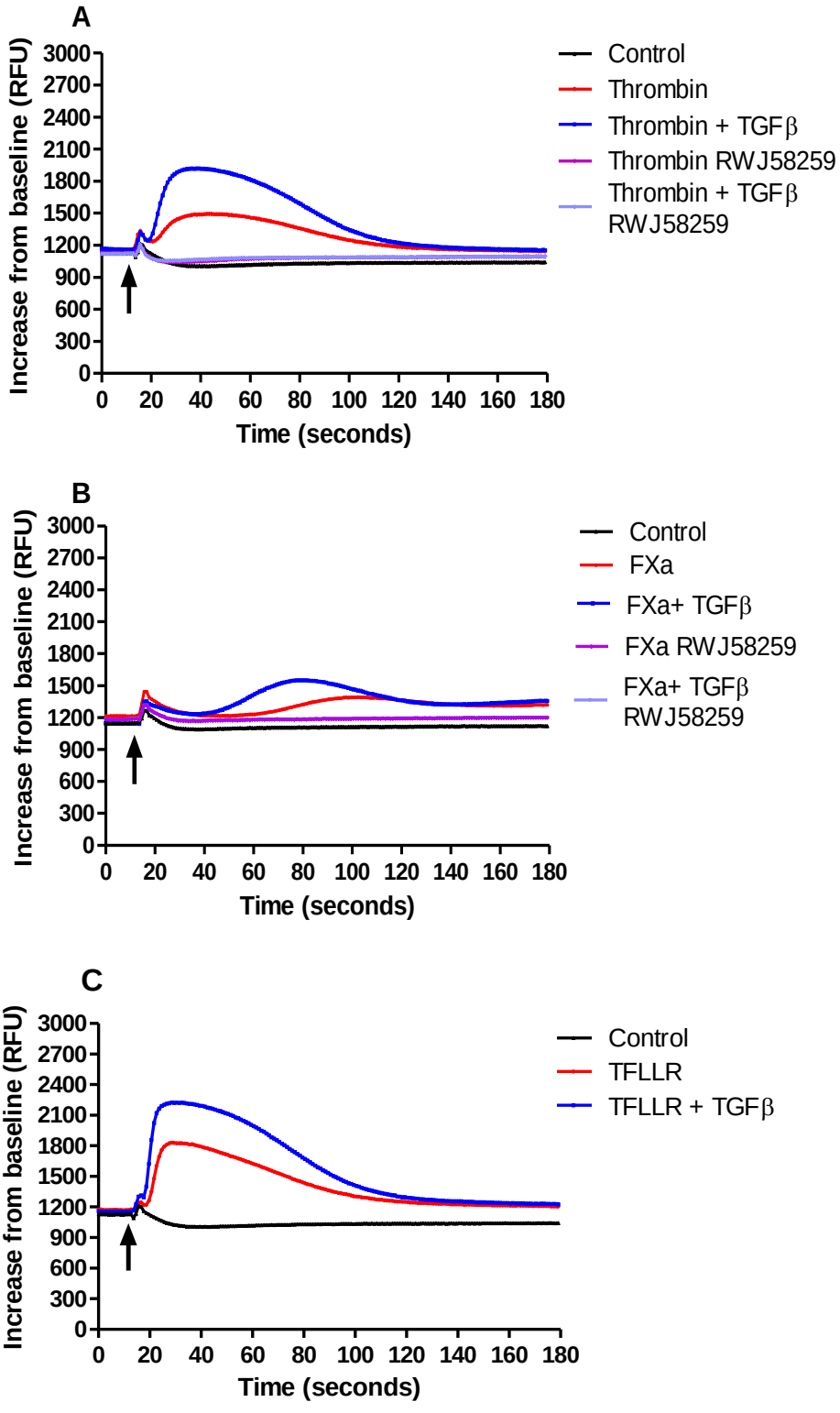
A
Increase from baseline (RFU)
3000
2700
2400
2100
1800
1500
1200
900
600
300
0
0 20 40 60 80 100 120 140 160 180
Time (seconds)
Control
Thrombin
Thrombin + TGFβ
Thrombin RWJ58259
Thrombin + TGFβ RWJ58259
B
Increase from baseline (RFU)
3000
2700
2400
2100
1800
1500
1200
900
600
300
0
0 20 40 60 80 100 120 140 160 180
Time (seconds)
Control
FXa
FXa+ TGFβ
FXa RWJ58259
FXa+ TGFβ RWJ58259
C
Increase from baseline (RFU)
3000
2700
2400
2100
1800
1500
1200
900
600
300
0
0 20 40 60 80 100 120 140 160 180
Time (seconds)
Control
TFLLR
TFLLR + TGFβ

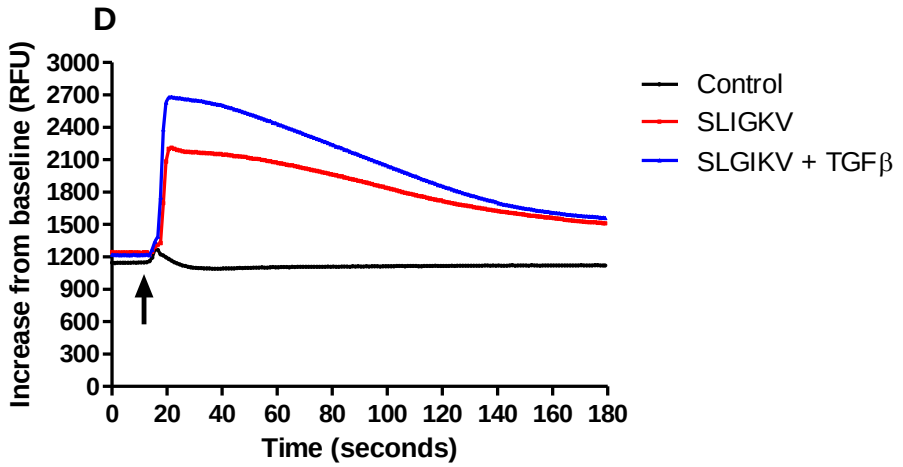

Figure 3.10. Intracellular calcium signalling in response to PAR-1 and PAR-2 agonists in A549 alveolar epithelial cells.

Human lung epithelial cells A549 were seeded at a density of $2x10^4$ in 96-well plates and serum-starved 24 hours with or without exposure to TGFβ (1 ng/ml), then incubated with Fluo-4AM calcium binding dye with or without PAR-1 inhibitor RWJ58259 (3 µM), prior to stimulation with thrombin (30 nM), FXa (100 nM), PAR-1 activating peptide TFLLR (100 µM), PAR-2 activating peptide SLIGKV (100 µM). The release of intracellular calcium was monitored by FLIPR® Tetra with calcium baseline recorded for 10 seconds before agonist addition and response measured for another 170 seconds. Data are represented as increase in relative fluorescence units (RFU) from the baseline. Panel A shows representative traces for thrombin-mediated calcium flux, panel B- FXa, panel C- TFLLR and panel D- SLIGKV. Each data point represents the mean +/- SEM of 3-4 replicate wells.

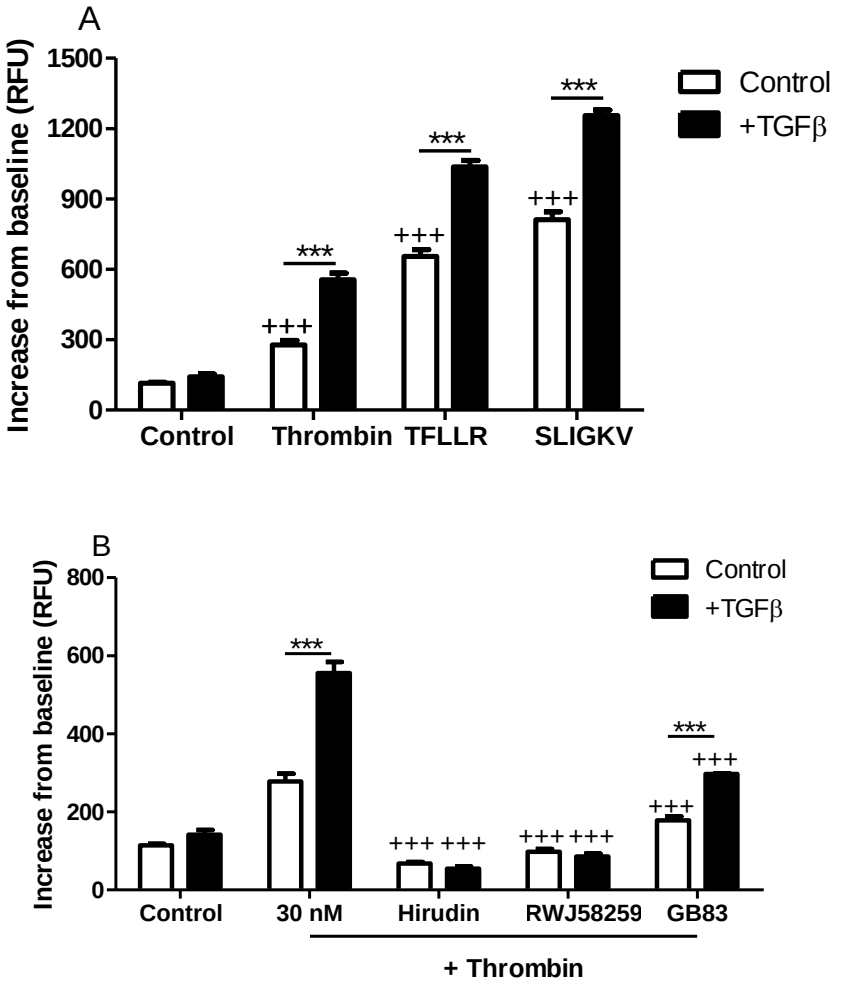

Figure 3.11. Pre-stimulation with TGFβ enhances PAR-1-mediated calcium signalling in human alveolar epithelial A549 cells.

Human epithelial cells A549 were seeded at a density of $2x10^4$ in 96-well plates and serum- starved with or without TGFβ (1 ng/ml) 24 hours and incubated with Fluo-4AM calcium binding dye for one hour with or without PAR-1 antagonist RWJ58259 (3 μM) and PAR-2 antagonist GB83 (50 μM) prior to stimulation with agonists: thrombin (30 nM), thrombin (30 nM) pre-incubated with hirudin (150 nM), TFLLR and SLIGKV (each at 100 μM). The release of intracellular calcium was monitored by FLIPR® Tetra with calcium baseline recorded for 10 seconds before agonist addition and response measured for another 170 seconds.Data are represented as increase in relative fluorescence units (RFU) from the baseline. Panel A shows intracellular calcium responses mediated by PAR-1 and PAR-2 agonists. Panel B shows effect of inhibitors on calcium signalling. Each data point represents the mean +/- SEM of 3-4 replicate wells, two-way ANOVA, ***p<0.001 comparison between control and TGFβ-pre-treated cells; +++p<0.001 comparison of treatments with relevant control.

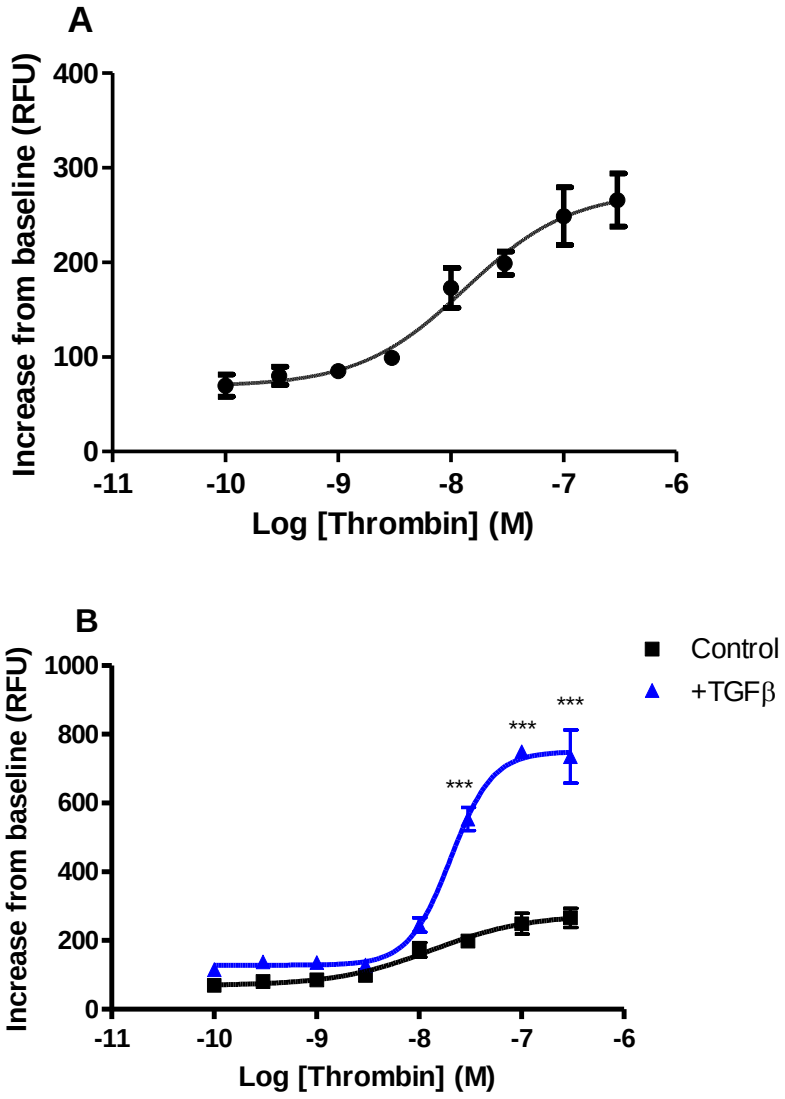

Figure 3.12. Concentration-response curve in A549 alveolar epithelial cells following thrombin stimulation.

Human epithelial A549 cells were seeded at a density of $2x10^4$ in 96-well plates and serum starved with or without TGFβ (1 ng/ml) 24 hours and incubated with Fluo-4AM calcium binding dye for one hour, prior to stimulation with different concentrations of thrombin. The release of intracellular calcium was monitored by FLIPR® Tetra with calcium baseline recorded for 10 seconds before thrombin addition and response measured for another 170 seconds. Data are represented as increase in relative fluorescence units (RFU) from the baseline. Panel A shows a concentration-response curve to thrombin and panel B is a comparison of response when cells were exposed to TGFβ for 24 hours. Each data point represents the mean +/- SEM of 3-4 replicate wells; Two-way ANOVA, ***p<0.001 comparison of control and TGFβ pre-treated cells.

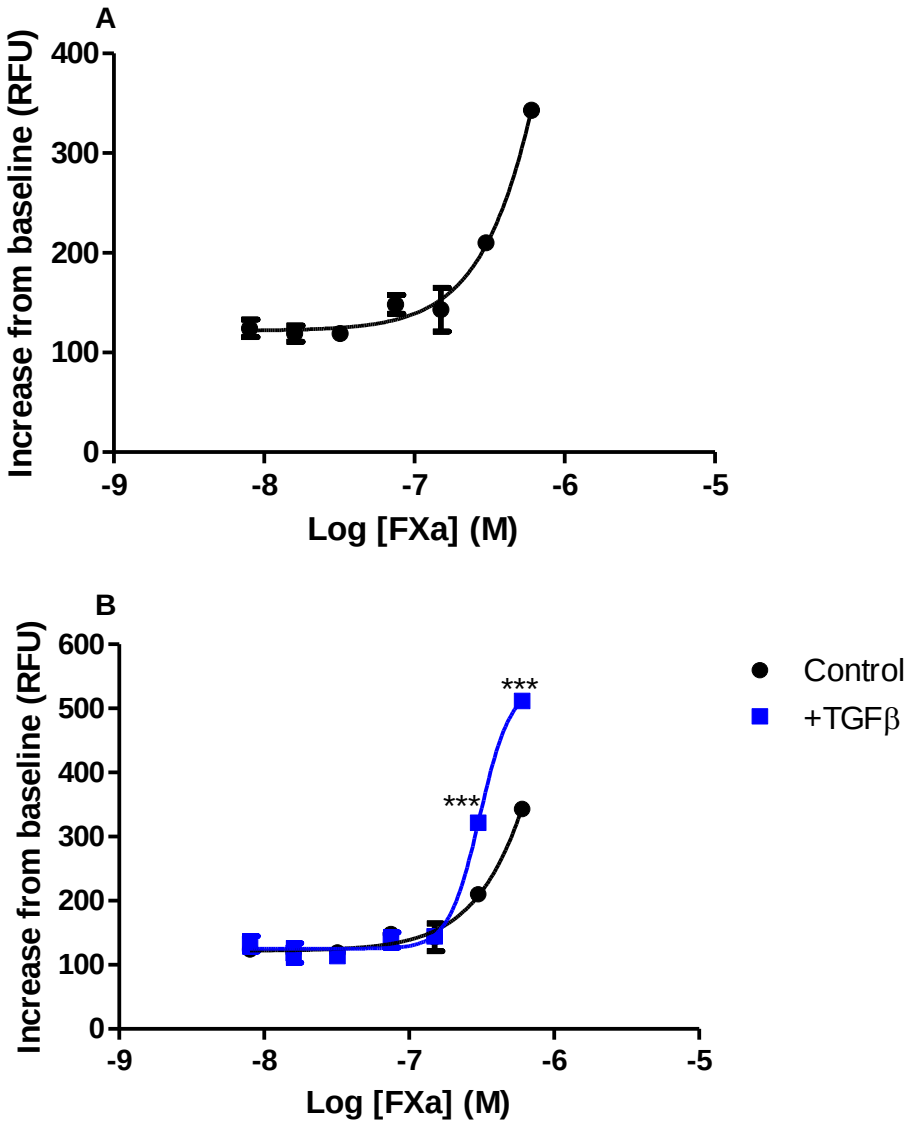

Figure 3.13. Concentration-response curve in A549 alveolar epithelial cells following FXa stimulation.

Human epithelial A549 cells were seeded at a density of $2x10^4$ in 96-well plates and serum starved with or without TGFβ (1 ng/ml) 24 hours and incubated with Fluo-4AM calcium binding dye for one hour, prior to stimulation with different concentrations of FXa. The release of intracellular calcium was monitored by FLIPR® Tetra with calcium baseline recorded for 10 seconds before FXa addition and response measured for another 170 seconds. Data are represented as increase in relative fluorescence units (RFU) from the baseline. Panel A shows a concentration-response curve to thrombin and panel B is a comparison of response when cells were exposed to TGFβ for 24 hours. Each data point represents the mean +/- SEM of 3-4 replicate wells; Two-way ANOVA, ***p<0.001 comparison of control and TGFβ pre-treated cells.

3.1.3.2 TGFβ upregulates PAR-1 expression in A549 alveolar epithelial cells

In order to examine the role of TGFβ in modulating PAR-1 signalling responses to thrombin, TGFβ concentration-response experiments were carried out next. A549 cells were incubated with different concentrations of TGFβ for 24 hours and subsequently stimulated with thrombin or TFLLR. TGFβ pre-treatment increased the magnitude of intracellular calcium signalling response in a concentration-dependent manner when A549 cells were stimulated with thrombin (EC_{50} of 0.15 ng/ml TGFβ) and TFLLR (EC_{50} of 2 ng/ml TGFβ) (**Figure 3.14**).

The effect of TGFβ stimulation on PAR-1 expression was subsequently investigated. As shown in **Figure 3.15**, unstimulated A549 cells were found to express PAR-1 on the cell surface at baseline and the expression was enhanced following exposure to TGFβ for 24 hours. A549 cells also expressed PAR-2 and the levels of PAR-2 were also further enhanced by TGFβ pre-treatment (**Figure 3.16**). It has previously been shown that TGFβ induces epithelial to mesenchymal transition (EMT) in epithelial and cancer cells and the hallmark of this phenotypic change is reduced expression of epithelial cell markers such as E-cadherin (Dubois-Marshall et al., 2011). In this immunocytofluorescence study E-cadherin was used as a marker of epithelial cell phenotype. **Figures 3.15 and 3.16** show that after exposure of A549 cells to TGFβ for 24 hours the intensity of E-cadherin staining diminished when compared to control but was still present. This suggests that although the levels of E-cadherin appear to be reduced, the A549 cells have not yet undergone change of phenotype. Therefore, increased PAR-1 expression could be an early TGFβ-mediated event but is not associated with a visible phenotypic change at this time point.

Stimulation of A549 with TGFβ also led to a significant upregulation of PAR-1 mRNA levels from 8 hours through to 24 hours, with a near 5-fold maximal increase at 16 hours (**Figure 3.17**). Research in our and other laboratories has shown that PAR-1 activation promotes the integrin-mediated activation of TGFβ via αvβ6 integrins on epithelial cells (Jenkins et al., 2006) and αvβ5 integrins on fibroblasts (Scotton et al., 2009). Therefore, the next question was whether PAR-1 upregulation in A549 cells

was also associated with increased expression of integrins. As shown in **Figure 3.18**, the αv subunit was significantly upregulated at the mRNA level from 6 hours of TGFβ stimulation (**Figure 3.18A**) and the β6 subunit mRNA level increased from 4 hours onwards (**Figure 18B**). Both integrin subunits remained significantly elevated throughout the duration of the experiment (24 hours).

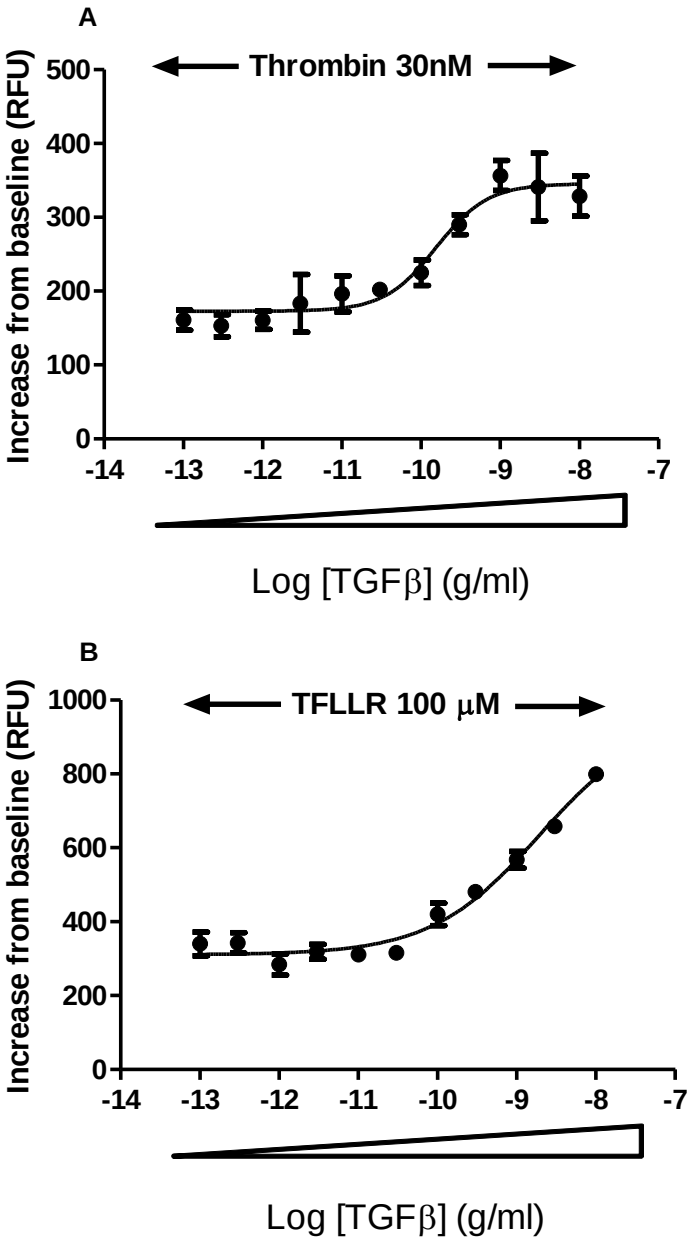

Figure 3.14. TGFβ concentration-response curves in A549 alveolar epithelial cells.

Human alveolar epithelial A549 cells were seeded at a density of $2x10^4$ in 96-well plates and serum starved with varying concentrations of TGFβ for 24 hours prior to stimulation with thrombin or TFLLR. Cells were incubated with Fluo-4AM calcium binding dye for one hour before being exposed to panel A- thrombin (30 nM) and panel B- TFLLR (100μM). The release of intracellular calcium was monitored by FLIPR® Tetra with calcium baseline recorded for 10 seconds before thrombin or TFLLR addition and response measured for another 170 seconds. Data are represented as increase in relative fluorescence units (RFU) from the baseline. Each data point represents the mean +/- SEM of 3-4 replicate wells.

PAR-1 expression in A549:

24 hours control

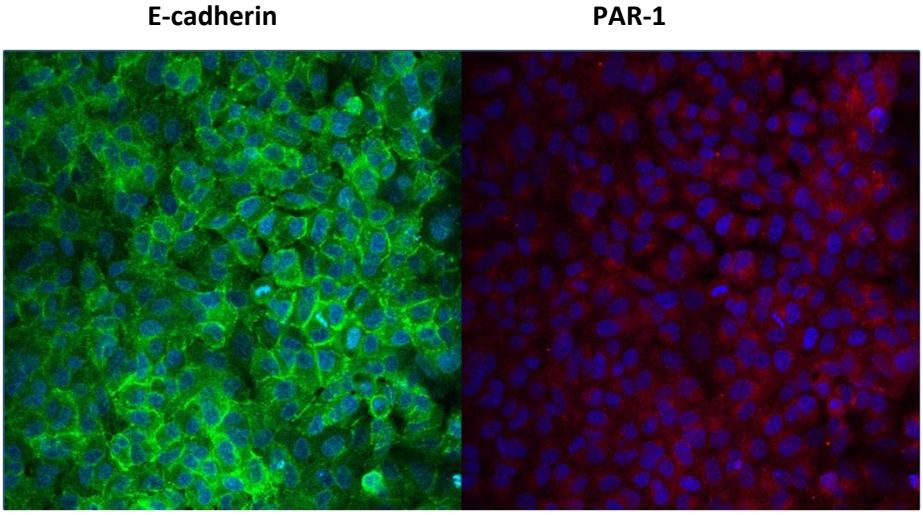

24 hours TGFβ

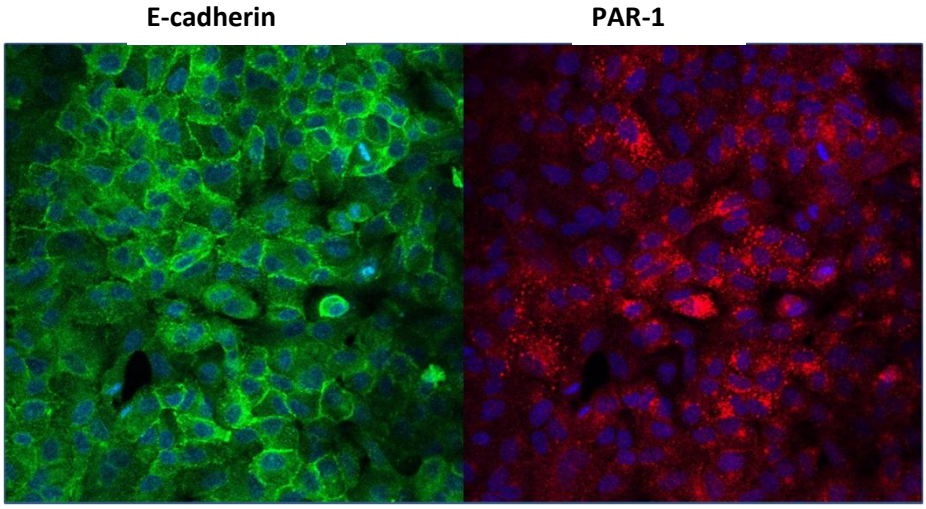

Figure 3.15. PAR-1 expression in A549 alveolar epithelial cells.

Human lung epithelial A549 cells were seeded at a density of $5x10^4$ in chamber slides and allowed to reach over 80% confluence. Cells were then serum starved with or without TGFβ (1 ng/ml) for 24 hours, fixed in paraformaldehyde and stained for PAR-1 (Alexa 555) and E-cadherin (Alexa 488), DAPI was used to visualise the nucleus. The top panel shows images for control cells and lower panel show the staining of TGFβ-stimulated cells, x20 original magnification.

PAR-2 expression in A549:

24 hours control

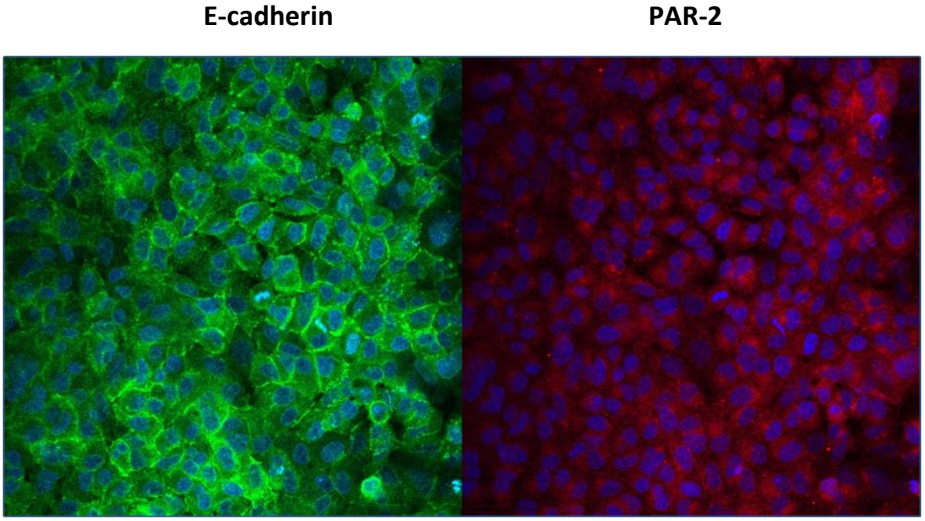

24 hours TGFβ

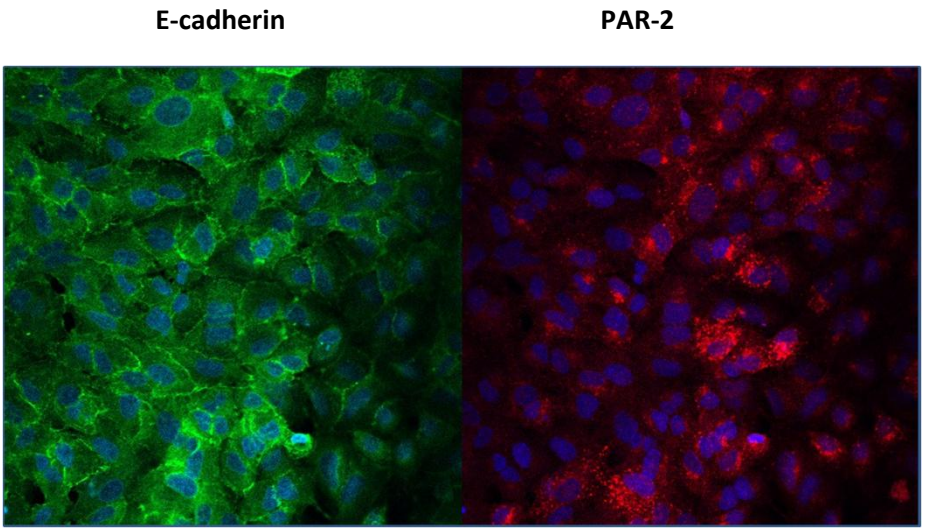

Figure 3.16. PAR-2 expression in A549 alveolar epithelial cells.

Human lung epithelial A549 cells were seeded at a density of $5x10^4$ in chamber slides and allowed to reach over 80% confluence. Cells were then serum starved with or without TGFβ (1 ng/ml) for 24 hours, fixed in paraformaldehyde and stained for PAR-2 (Alexa 555) and E-cadherin (Alexa 488), DAPI was used to visualise the nucleus. The top panel shows images for control cells and lower panel show the staining of TGFβ-stimulated cells, x20 original magnification.

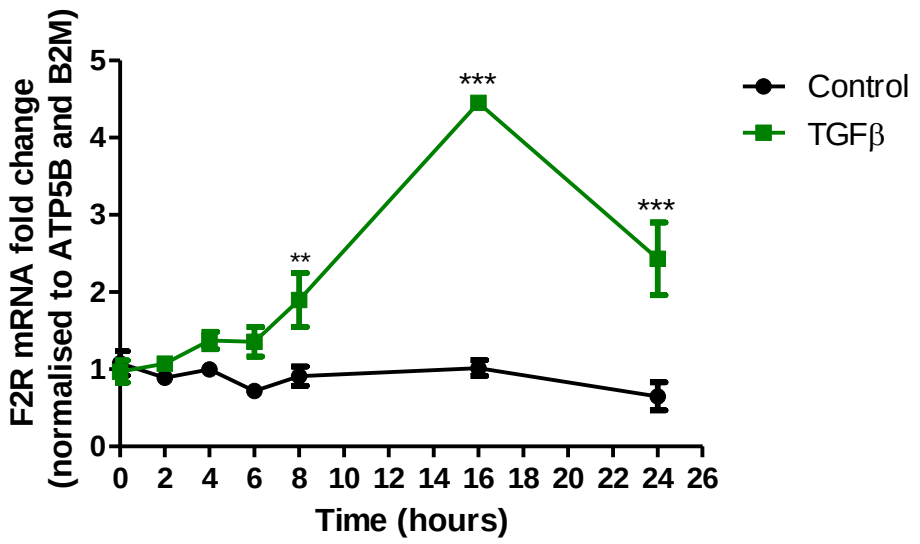

Figure 3.17. TGFβ upregulates F2R/PAR-1 mRNA levels in A549 alveolar epithelial cells.

Human alveolar epithelial A549 cells were seeded at a density of $5x10^4$ in 24-well plates and serum starved with or without TGFβ (1ng/ml) for 24 hours. The mRNA was collected at indicated times in the course of 24 hours. PAR-1 expression was quantified by real-time qPCR. Each data point represents the mean +/- SEM of 3 replicates, statistically analysed by Two-way ANOVA, **p<0.01, ***p<0.001 in comparison to control.

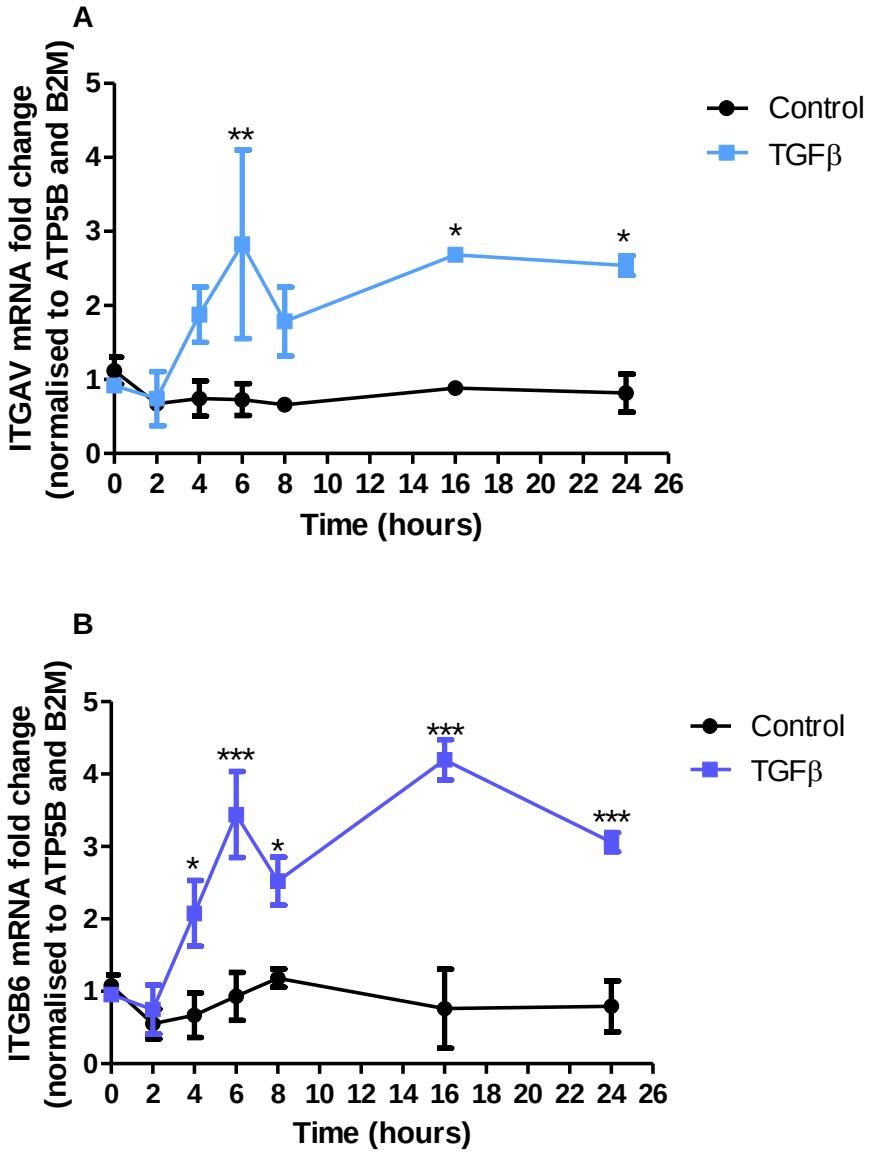

Figure 3.18. TGFβ upregulates mRNA levels of integrin subunits αv (ITGAV) and β6 (ITGB6) in A549 alveolar epithelial cells.

Human epithelial cells A549 were seeded at a density of $5x10^4$ in 24-well plates and serum- starved with or without TGFβ (1ng/ml) for 24 hours. The mRNA was collected at indicated times. Expression of integrin subunits αv- panel A and β6- panel B was quantified by real-time qPCR. Each data point represents the mean +/- SEM of 3 replicate wells, two-way ANOVA was performed for statistical analysis, *p<0.05, **p<0.01, ***p<0.001 comparison of TGFβ pre-treated vs control cells at each time point.

3.1.3.3 Mechanism of TGFβ-mediated upregulation of PAR-1 expression in A549 alveolar epithelial cells

In order to further investigate whether the observed responses are TGFβ-dependent, A549 cells were treated with the TGFβ ALK5 receptor inhibitor SB431542, for 30 minutes prior to addition of TGFβ. Intracellular calcium responses to thrombin were measured 24 hours later. SB431542 inhibited the TGFβ-mediated increase in thrombin-induced intracellular calcium flux in a concentration-dependent manner with an IC_{50} of 1.7 μM (**Figure 3.19**). TGFβ binding to the ALK5 receptor activates the canonical Smad2/3 signalling pathway. The TGFβ-Smad3 axis is critically involved in lung fibrosis as demonstrated by the observation that Smad3-null mice are protected from bleomycin induced pulmonary fibrosis (Zhao et al., 2002). The role of Smad2 and Smad3 in TGFβ-mediated PAR-1 upregulation was subsequently investigated using small interfering RNA (siRNA).

The silencing of Smad2 and Smad3 expression was validated at the mRNA (**Figure 3.20)** and protein levels **(Figure 3.21).** Smad3 mRNA levels were significantly reduced 48 hours post-transfection at high concentrations of siRNA and this effect persisted through to 72 hours post-transfection at which point a significant reduction in Smad3 mRNA level was detected at all siRNA concentrations (**Figure 3.20A**). Smad2 knockdown was achieved at all siRNA concentration from 24 hours through to 72 hours post-transfection (**Figure 3.20B**). Scrambled siRNA sequence did not reduce the expression of either Smad2 or Smad3 (**Figure 3.20C**). Total Smad3 protein levels were reduced by over 50% at 48 hours and 72 hours post-transfection with 1 nM and 3 nM of siRNA and completely blocked at higher concentrations of siRNA when compared to non-transfected control levels (**Figure 3.21A and B**). Total Smad2 protein expression was reduced by over 90% at all time points measured after transfection (**Figure 3.20C and D**). Since the reduction in Smad3 protein levels at 24 hours were modest, 48 hours and 72 hours post-transfection were chosen as time points to assess the effect of Smad2 and Smad3 expression knockdown on PAR-1 functional responses. As shown in **Figure 3.21 E,F and G** scrambled siRNA had a modest effect on the Smad2 and Smad3 protein levels at these two time points.

Figures 3.22A and B show that silencing of Smad3 expression significantly reduced the TGFβ-mediated increase in PAR-1 functional responses to thrombin in a concentration-dependent manner at 48 hours and 72 hours. Smad2 expression knockdown had small but significant reducing effect on TGFβ-mediated increase in PAR-1 signalling at 48 hours and siRNA concentrations of 10 nM and 30 nM. However, this effect was no longer detected at 72 hours and Smad2 knockdown did not overall inhibit the increase in TGFβ-mediated PAR-1 functional responsiveness to thrombin (**Figure 3.22C and D**).

TGFβ signalling expands beyond Smad-mediated pathways and can activate all three MAPK pathways: extracellular signal-regulated kinase (ERK), p38, and c-Jun-N-terminal kinase (JNK). These signalling pathways can subsequently influence Smad signalling or exert Smad-independent effects. ERK has been shown to have opposing effect on Smad phosphorylation depending on the cell type (Funaba et al. 2002; Kretzschmar et al. 1999), while p38 (Furukawa et al., 2003) and JNK (Yoshida et al., 2005) tend to promote Smad signalling. However, TGFβ-mediated direct activation of ERK has been shown to promote EMT (Zhang, 2009). The MEK1 and MEK2 inhibitors, UO126 and PD98059 were used to assess the effect of ERK inhibition on TGFβ-mediated increase in PAR-1 signalling responses. A549 cells were treated with different concentrations of the inhibitors 30 minutes prior to stimulation with TGFβ for 24 hours, at which point cells were stimulated with thrombin and intracellular calcium flux monitored. UO126 inhibited the TGFβ-mediated increase in intracellular calcium flux in response to thrombin stimulation in a concentration-dependent manner with an IC_{50} of 0.35 μM (**Figure 3.23A**). In contrast PD98059 had modest effect on the TGFβ-induced upregulation of PAR-1 functional responsiveness (**Figure 3.23B**). In contrast, Inhibition of JNK by SP600125 had no significant effect on TGFβ-mediated PAR-1 upregulation (**Figure 3.23C**). The p38 inhibitor, SB203580, did not block but appeared to increase the PAR-1 mediated intracellular flux (**Figure 3.23D**). This response was observed in TGFβ-stimulated cells and in control cells suggesting that the inhibitor has a non-specific, off-target effect or that p38 is involved in regulating PAR-1 at baseline in A549 cells.

TGFβ also activates Rho kinase signalling leading to stress fibre formation in epithelial cells (Bhowmick et al. 2004) and so the effect of Rho inhibition by Y-27632 on TGFβ-mediated increase in PAR-1 functional responses was also investigated. The highest concentrations of inhibitor increased baseline thrombin-mediated intracellular calcium flux and this response was more pronounced in TGFβ-stimulated cells (**Figure 3.23E**). These data could be explained by the inhibitor having a non-specific effect at high concentrations. Alternatively, Rho kinase signalling may affect PAR-1 expression and functional responsiveness in A549 cells.

Taken together these data suggest that TGFβ mediates increase in PAR-1 expression and functional responses in ALK5/-Smad3- and ERK-dependent mechanism.

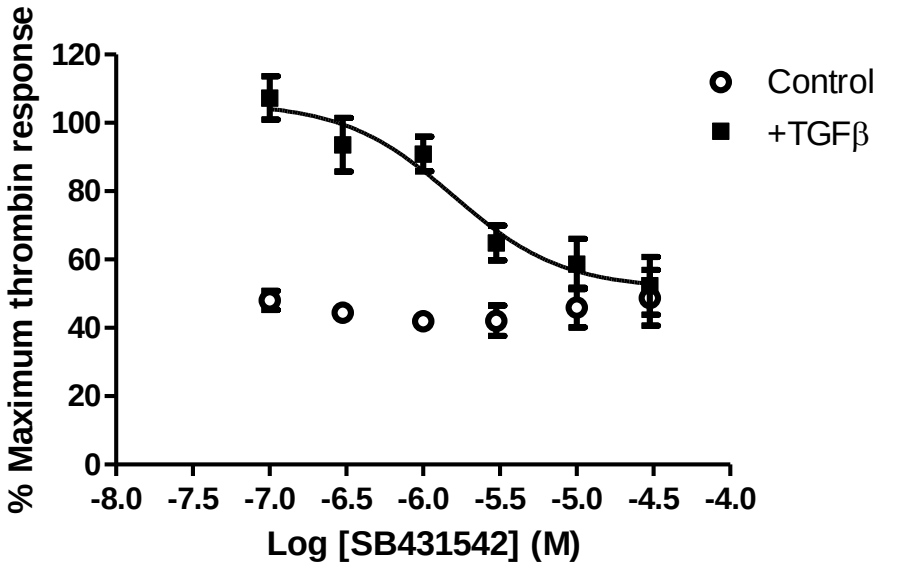

Figure 3.19. Targeting ALK5 TGFβ receptor prevents the increase in PAR-1 signalling in A549 alveolar epithelial cells.

Human alveolar epithelial A549 cells were seeded at a density of $2x10^4$ in 96-well plates and treated with varying concentrations of SB431542 for 30 minutes prior to stimulation with TGFβ (1 ng/ml) in serum-free medium for 24 hours. Cells were incubated with Fluo-4AM caclium binding dye for one hour before being exposed to thrombin (30 nM). The release of intracellular calcium was monitored by FLIPR® Tetra with calcium baseline recorded for 10 seconds before thrombin addition and response measured for another 170 seconds. Data are shown as a percentage of maximal thrombin response and the effect of SB431542 is presented as a concentration-inhibition curve. The open circles indicate the effect of the different concentrations of inhibitor on the calcium signalling in non-TGFβ treated and thrombin stimulated control cells. Each data point represents the mean +/- SEM of 4 replicate wells.

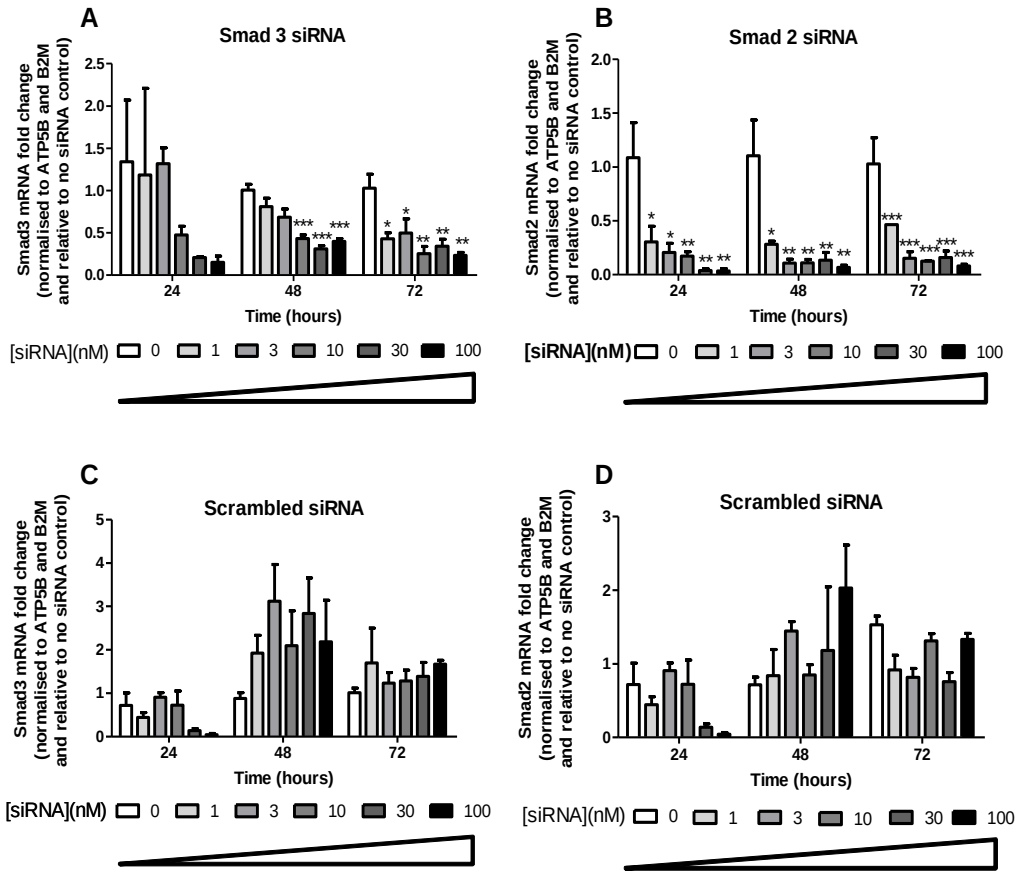

Figure 3.20. Validation of Smad3 and Smad2 mRNA knockdown.

Human alveolar epithelial A549 cells were seeded at a density of $5x10^4$ in 24-well plates and transfected with Smad3, Smad2 and scrambled siRNA in serum-free medium. The mRNA was collected 24, 48 and 72 hours post-transfection and the expression of Smad3-panel A and Smad2-panel B quantified by qPCR. Panel C and D- the effect of scrambled siRNA on Smad3 and Smad2 was also quantified by qPCR. Each data point represents the mean +/- SEM of 3 replicates; one-way ANOVA, *p<0.05, **p<0.01, ***p<0.001, relative to non-transfected control.

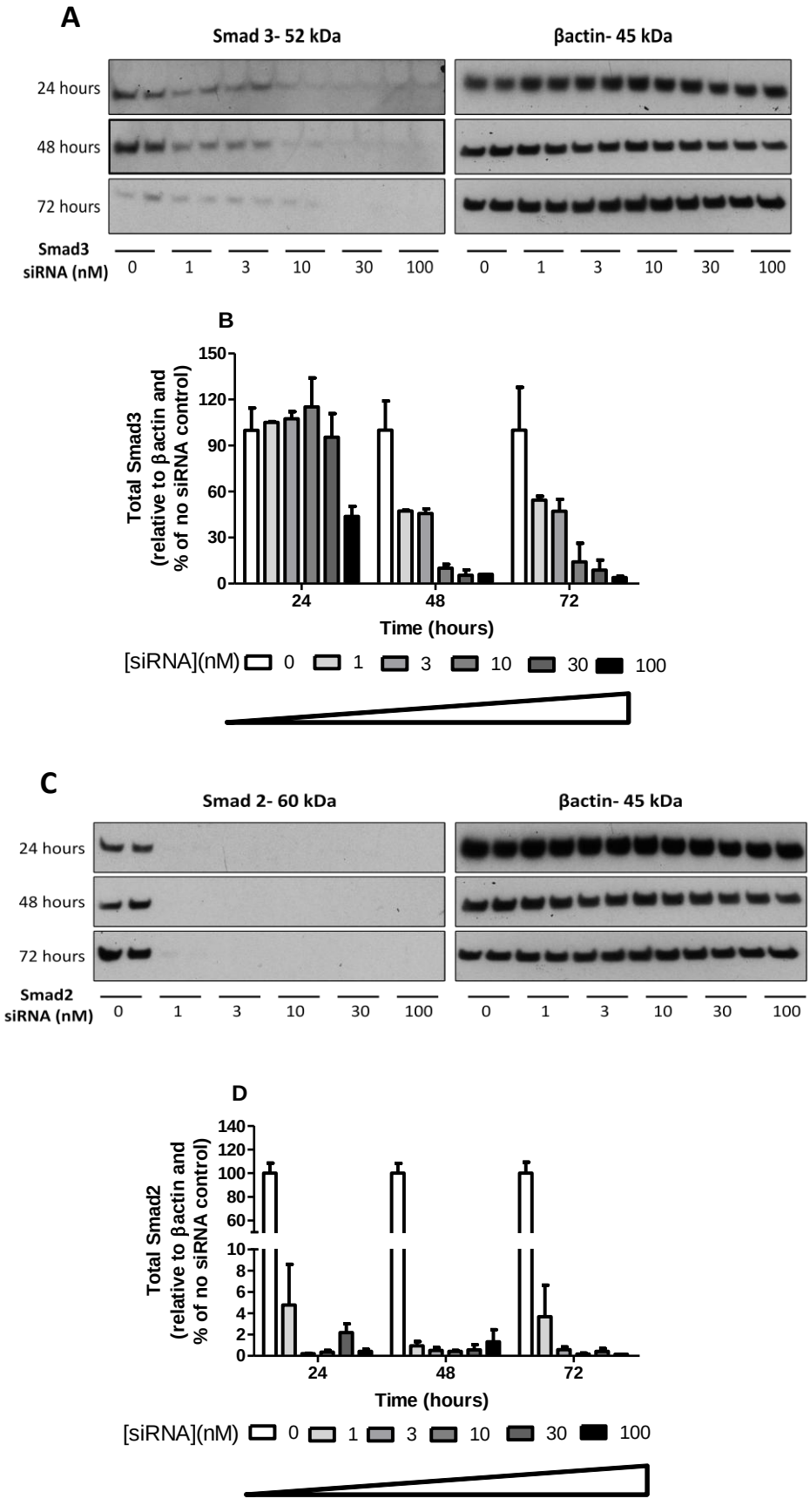
A
Smad 3- 52 kDa
βactin- 45 kDa
24 hours
48 hours
72 hours
Smad3 siRNA (nM)
0 1 3 10 30 100 0 1 3 10 30 100
B
Total Smad3 (relative to βactin and % of no siRNA control)
150
120
90
60
30
0
24
48
72
Time (hours)
[siRNA](nM) 0 1 3 10 30 100
C
Smad 2- 60 kDa
βactin- 45 kDa
24 hours
48 hours
72 hours
Smad2 siRNA (nM)
0 1 3 10 30 100 0 1 3 10 30 100
D
Total Smad2 (relative to βactin and % of no siRNA control)
140
120
100
80
60
10
8
6
4
2
0
24
48
72
Time (hours)
[siRNA](nM) 0 1 3 10 30 100

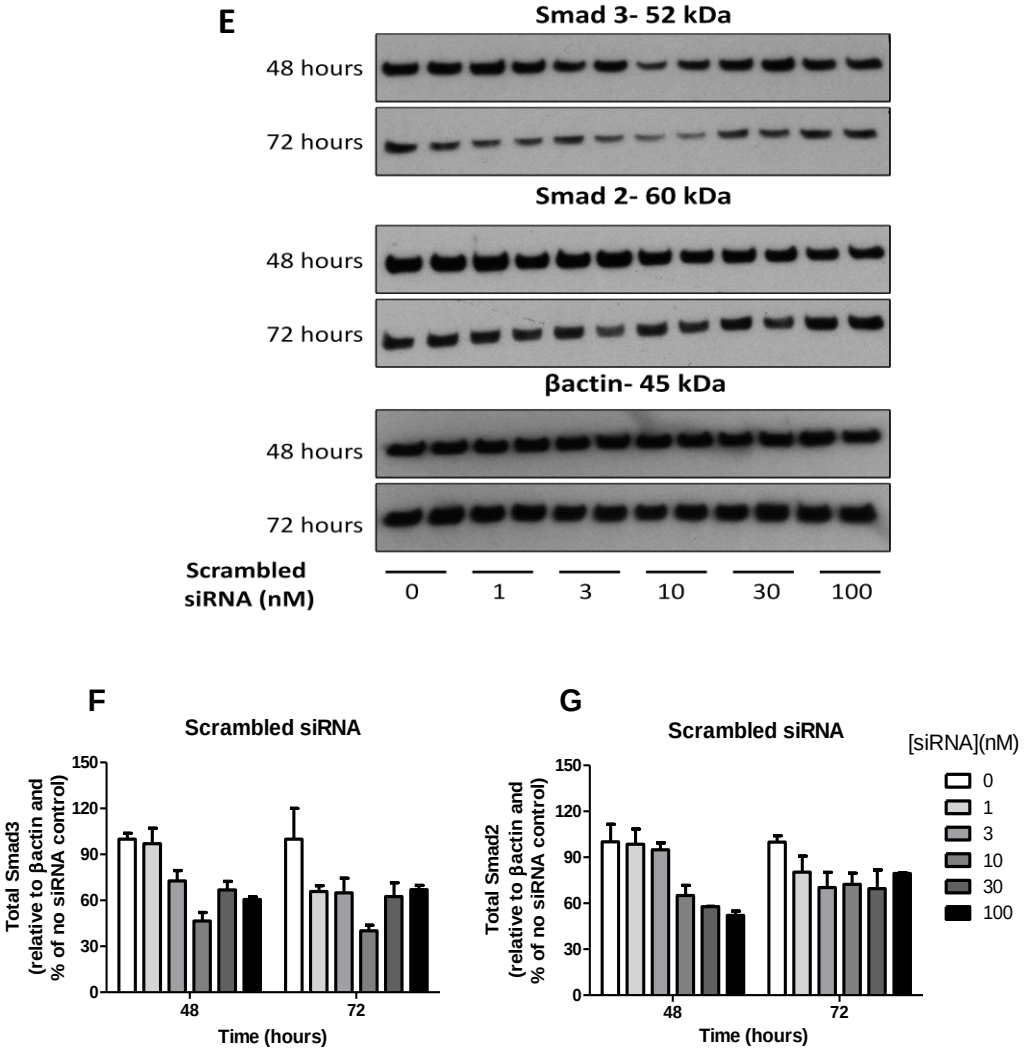

Figure 3.21. Validation of Smad3 and Smad2 protein knockdown.

Human alveolar epithelial A549 cells were seeded at a density of $5x10^4$ in 24-well plates and transfected with Smad3, Smad2 and scrambled siRNA in serum-free medium. The protein was collected 24, 48 and 72 hours post-transfection and the Smad3 and Smad2 total protein levels assessed by Western blotting. Panel A- Western blot of Smad3 and corresponding loading control at all time points; panel B- semi-quantitative densitometry analysis of the Smad3 total protein relative to the β-actin loading control; panel C- Western blot of Smad2 and corresponding loading control at all time points; panel D- semi-quantitative densitometry analysis the Smad2 total protein relative to the loading control; panel E- Western blot of Smad2 and Smad3 total protein in the samples transfected with scrambled siRNA at 48 and 72 hours with a corresponding loading control; panel F and G- semi-quantitative densitometry analysis of the Smad3 and Smad2, respectively, relative to the loading control at 48 and 72 hours. Each data point represents the mean +/- SEM of 2 replicates.

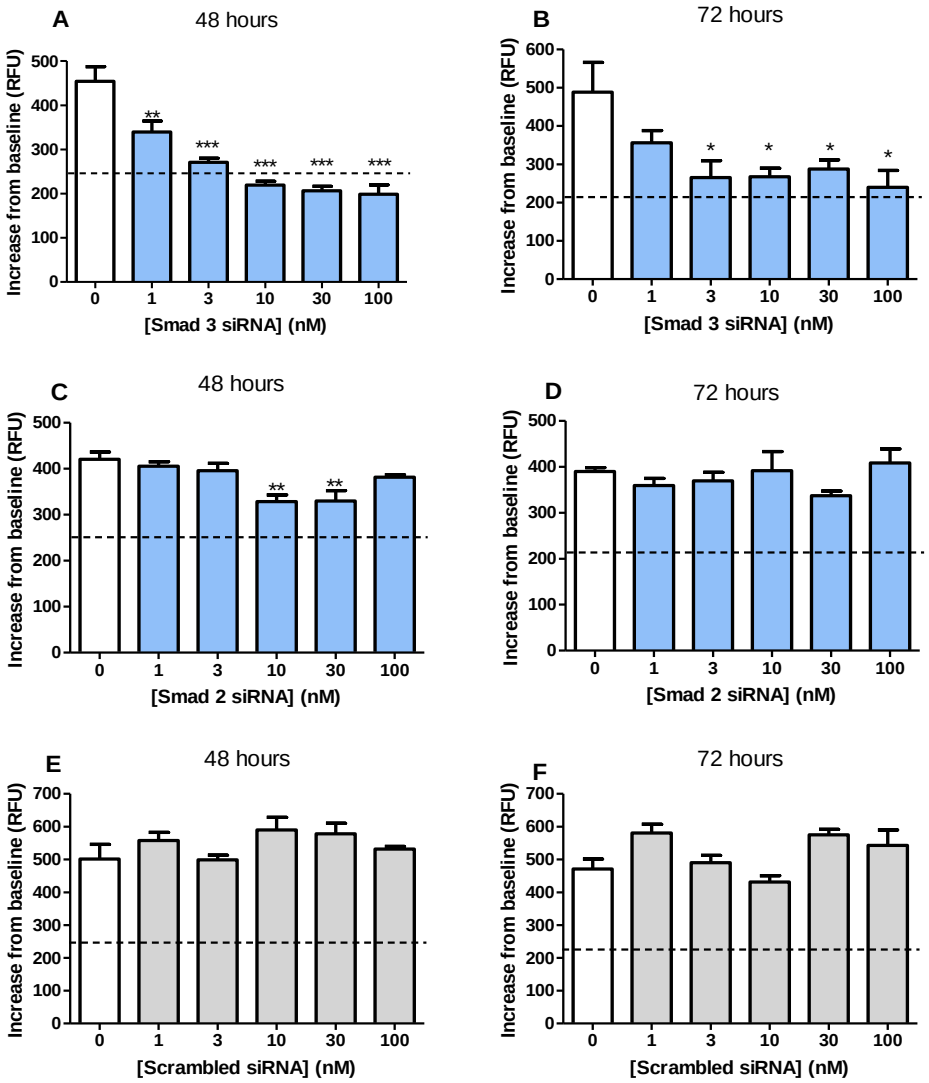

Figure 3.22. TGFβ-mediated increase in PAR-1 signalling in A549 alveolar epithelial cells is Smad3-dependent and Smad2-independent.

Human alveolar epithelial A549 cells were seeded at a density of $2x10^4$ in 96-well plates and treated with varying concentrations of Smad3- panel A and B, Smad2- panel C and D and scrambled siRNA- panel E and F, for 48 and 72 hours prior to stimulation with TGFβ (1 ng/ml) in serum-free medium for 24 hours. Cells were incubated with Fluo-4AM calcium binding dye for one hour before being exposed to thrombin (30 nM). The release of intracellular calcium was monitored by FLIPR® Tetra with calcium baseline recorded for 10 seconds before thrombin addition and response measured for another 170 seconds. Data are shown as an increase from baseline in relative fluorescence units (RFU) and the dotted line represent baseline response to thrombin in non-TGFβ stimulated A549 cells. Each data point represents the mean +/- SEM of 4 replicate wells, one-way ANOVA; *p<0.05, **p<0.01, ***p<0.001.

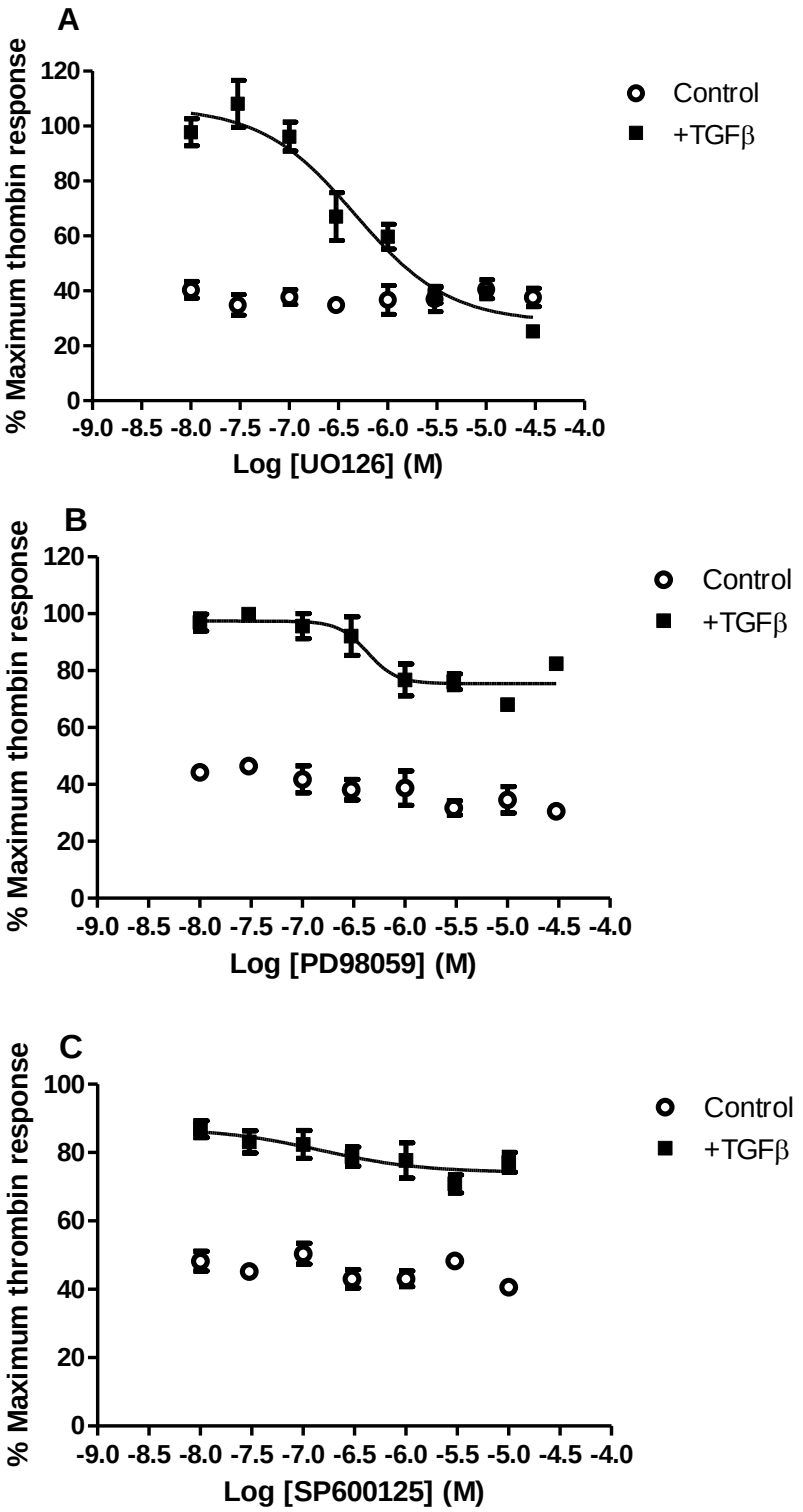
A
% Maximum thombin response
120
100
80
60
40
20
0
-9.0 -8.5 -8.0 -7.5 -7.0 -6.5 -6.0 -5.5 -5.0 -4.5 -4.0
Log [UO126] (M)
Control
+TGFβ
B
% Maximum thombin response
120
100
80
60
40
20
0
-9.0 -8.5 -8.0 -7.5 -7.0 -6.5 -6.0 -5.5 -5.0 -4.5 -4.0
Log [PD98059] (M)
Control
+TGFβ
C
% Maximum thrombin response
100
80
60
40
20
0
-9.0 -8.5 -8.0 -7.5 -7.0 -6.5 -6.0 -5.5 -5.0 -4.5 -4.0
Log [SP600125] (M)
Control
+TGFβ

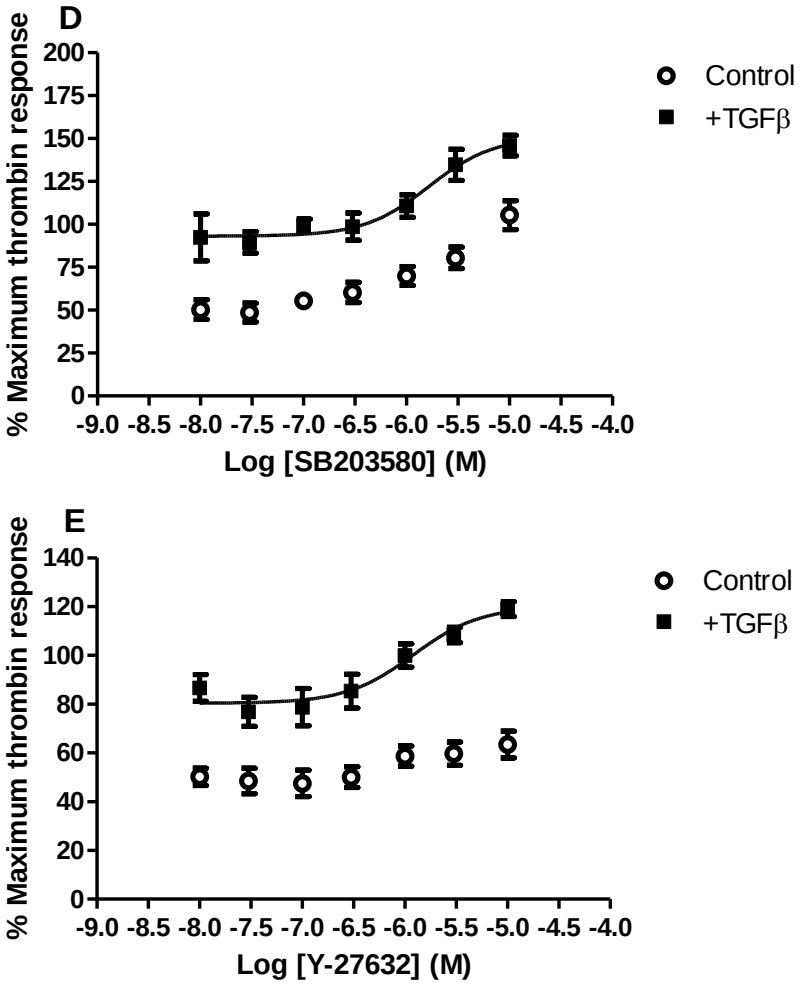

Figure 3.23. Investigation of the effect of non-Smad signalling pathways in the TGFβ-mediated increase in PAR-1 functional responses in A549 alveolar epithelial cells.

Human alveolar epithelial A549 cells were seeded at a density of $2x10^4$ in 96-well plates and treated with varying concentrations of specified inhibitors for 30 minutes prior to stimulation with TGFβ (1 ng/ml) in serum-free medium for 24 hours. Cells were incubated with Fluo-4AM calcium binding dye for one hour before being exposed to thrombin (30 nM). The release of intracellular calcium was monitored by FLIPR® Tetra with calcium baseline recorded for 10 seconds before thrombin addition and response measured for another 170 seconds. Data are shown as a percentage of maximal thrombin response and the effect of inhibitors is presented as a concentration-inhibition curve. The open circles indicate the effect of the different concentrations of inhibitor on the calcium signalling in non-TGFβ treated and thrombin stimulated control cells. Panel A- ERK1/2 inhibitor UO126, B- ERK1/2 inhibitor PD98059, C- JNK inhibitor SP600125, D- p38 inhibitor SB203580, E- Rho kinase inhibitor Y-27632. Each data point represents the mean +/- SEM of 4 replicate wells.

3.1.3.4 PAR-1 expression in primary alveolar type II epithelial cells

Following the characterisation of PAR-1 expression in A549 alveolar epithelial cells and the TGFβ-mediated upregulation of the receptor, it was next determined whether these findings are reflected in primary human type II alveolar epithelial cells (AECII). AECII were freshly isolated from lung explants and their phenotype confirmed by positive staining for zona occludens (ZO-1) tight junctions and cytoplasmic prosurfactant C protein (pro-SPC). As shown in **Figure 3.24A** ZO-1 tight junctions outlined the boarders of the AECII while pro-SPC accumulated largely in the cytoplasm. AECII were subsequently stimulated with TGFβ for 24 hours and PAR-1 expression visualised by immunocytofluorescence. As shown in **Figure 3.24B** low-intensity PAR-1 staining was detected in control cells and no visible changes were observed with TGFβ stimulation.

Cells were subsequently stimulated with thrombin, PAR-1 and PAR-2 activating peptides. Neither thrombin nor TFLLR stimulation of primary human AECII triggered a marked increase in intracellular calcium flux. In contrast, the PAR-2 activating peptide, SLIGKV, induced a significant calcium flux 20 seconds after the addition of the agonist. The signal lasted for approximately 100 seconds (**Figure 3.24C**). These data suggest that primary AECII are functionally responsive to PAR-2 but not PAR-1. Furthermore, stimulation with TGFβ for 24 hours did not change PAR-1 expression and functional responses in AECII.

A

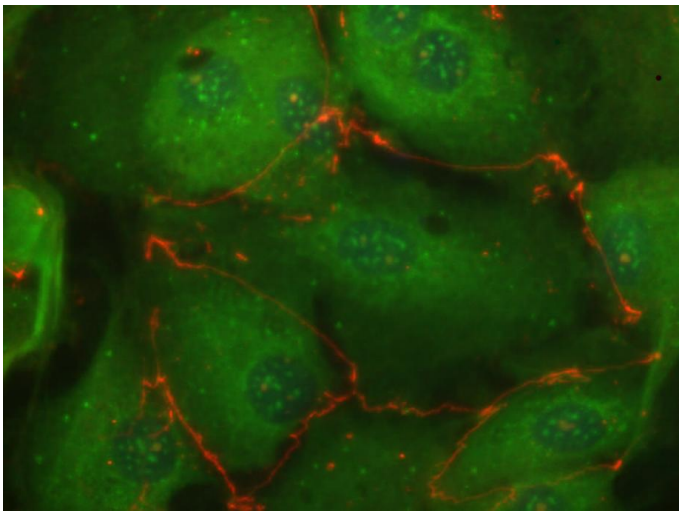

B

AEC II, 24 hours, control

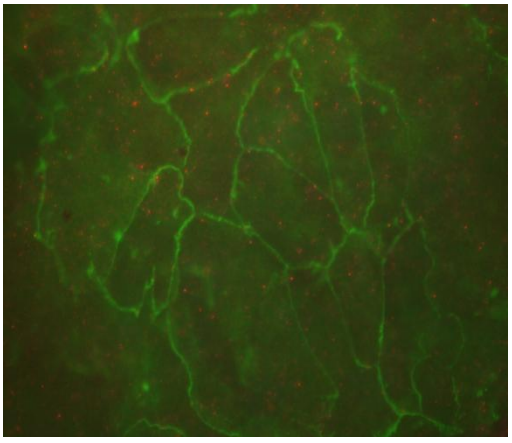

AEC II, 24 hours, TGFβ

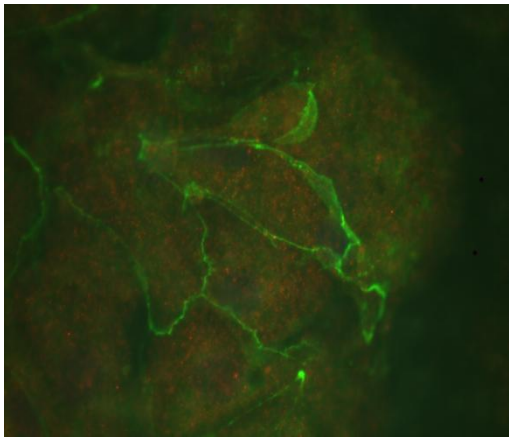

C

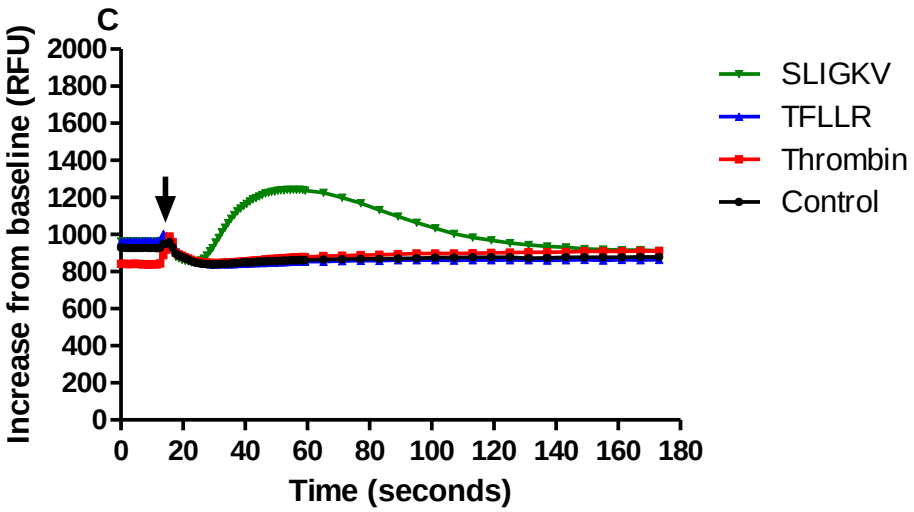

Figure 3.24. Characterisation of alveolar epithelial cells type II phenotype and responses.

Freshly isolated primary human alveolar epithelial cells were seeded in a collagen-coated 12-well plate at a density of $1x10^6$ or in 96-well plates at a density of $1x10^5$. Cells were cultured to 80% confluence. Panel A- cells were fixed with paraformaldehyde and stained for ZO-1 (red) and proSPC (green) (40x original magnification). Panel B- cells were stimulated with TGFβ for 24 hours and then fixed with paraformaldehyde and stained for ZO-1 (green) and PAR-1 (red) (20x original magnification). Panel C- cells were incubated with Fluo-4AM calcium binding dye before being exposed to thrombin (30 nM), PAR-1 activating peptide- TFLLR (100μM) and PAR-2 activating peptide- SLIGKV (100μM). Intracellular calcium was monitored by FLIPR® Tetra with calcium baseline recorded for 10 seconds before agonist addition and response measured for another 170 seconds. Data are represented as increase in relative fluorescence units (RFU) from the baseline. Each data point represents the mean +/- SEM of 4 replicates and the graph is representative of data obtained with cells from 4 different donors.

3.1.3.5 Summary

- PAR-1 and PAR-2 activation leads to intracellular calcium release in human A549 alveolar epithelial cells.
- Thrombin- and FXa-mediated calcium flux is fully blocked by PAR-1-antagonists in A549 cells.
- TGFβ pre-treatment for 24 hours leads to an increase in PAR-1 mRNA levels, protein expression and enhanced PAR-1-mediated calcium signalling.
- This increase in PAR-1 expression is mediated by TGFβ-ALK5-Smad3 signalling axis and is also ERK-dependent.
- TGFβ pre-treatment also increases αv and β6 integrin mRNA levels.
- Freshly isolated control primary human AECII elicit robust intracellular calcium release following stimulation with PAR-2 activating peptide but not PAR-1.

3.1.4 PAR-1 expression and signalling in human bronchial epithelium

The bronchial epithelium is a specialised, pseudostratified epithelium with distinct populations of cells including basal cells, terminally differentiated columnar ciliated cells, Clara cells and goblet cells, which are non-ciliated secretory cells producing mucus. The composition of the bronchial epithelium accounts for its main three functions: i) formation of a tight protective barrier preventing the penetration of noxious agents into lung tissue, ii) entrapment and mucociliary clearance of these potentially damaging agents and iii) secretion of antimicrobial and pro-inflammatory mediators to prevent injury and combat infection (Velden and Versnel, 1998). Bronchial epithelium has also been reported to express all PAR receptors (Knight et al., 2001).

Basal cells are a cytokeratin-14 and cytokeratin-5 (CK14 and CK5) positive cell population with large regenerative potential and are considered to be progenitor cells of other cell types present in mature bronchial epithelium (Hong et al., 2004). Furthermore, basal cells are key effector cells in the initiation of wound healing responses and depend on activation of the coagulation cascade and generation of fibrin scaffold (Perrio et al., 2007). Basal cells constitutively express tissue factor and hence have the potential capacity to assemble the TF-FVIIa-FXa ternary complex on their cell surface and locally activate the extrinsic coagulation cascade. The aim of this study was to assess the intracellular calcium responses in the primary bronchial epithelial cells following PAR-1 and PAR-2 activation in order to determine which PAR receptor is involved in mediating coagulation signalling responses in human bronchial epithelium.

Intracellular calcium release in response to thrombin stimulation was initially assessed in the immortalised bronchial epithelial cell line, BEAS2B. These cells responded to thrombin in a concentration-dependent manner with an EC_{50} of 0.7 nM (**Figure 3.25**). Pre-stimulation of cells with TGFβ slightly but significantly altered their responsiveness to thrombin. The intracellular calcium flux was significantly

reduced at lower thrombin concentration and increased at higher thrombin concentration.

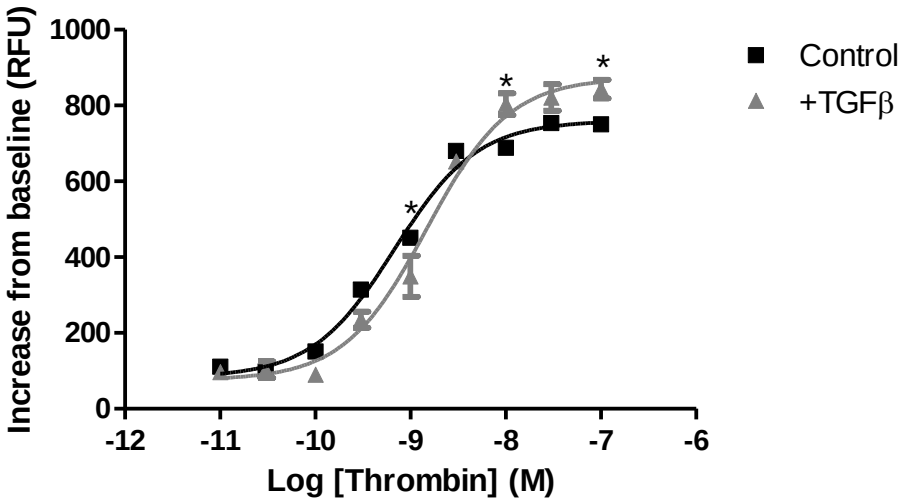

Figure 3.25. Concentration-response curve in BEAS2B cells following thrombin stimulation.

Bronchial epithelial cells BEAS2B were seeded at a density of $2x10^4$ in 96-well plates and serum starved with or without TGFβ (1ng/ml) 24 hours prior to stimulation with thrombin. Cells were incubated with Fluo-4AM calcium binding dye for one hour before being exposed to different concentration of thrombin. The release of intracellular calcium was monitored by FLIPR® Tetra with calcium baseline recorded for 10 seconds before thrombin addition and response measured for another 170 seconds. Data are represented as increase in relative fluorescence units (RFU) from the baseline. Panel A shows a concentration-response curve to thrombin and panel B is a comparison of response when cells were stimulated with TGFβ. Each data point represents the mean +/- SEM of 3 replicate wells.

3.1.4.1 PAR-1 expression and signalling in primary human basal epithelial cells

Following the encouraging results with BEAS2B cells, PAR responses were next assessed in primary bronchial epithelial cells (HBECs), which were grown in our laboratory from airways dissected from human lung explants, obtained from several donors. Primary human bronchial epithelial cells isolated from lung airway explants are composed primarily of CK14- and CK5-positive basal cells. As shown in **Figure 3.26**, PAR-1 activating peptide, TFLLR, triggered barely detectable intracellular calcium flux while PAR-2 activating peptide, SLIGKV, elicited a strong calcium response. Furthermore, thrombin did not elicit measurable intracellular calcium release suggesting that the basal cells either do not express much PAR-1 or PAR-1 activation does not induce intracellular calcium release in these cells.

Interestingly, intracellular calcium release was observed in primary HBECs following stimulation with FXa. This calcium response occurred with a 100 second delay and with a prolonged and sustained duration of 300 seconds. This pattern of intracellular calcium release in response to FXa stimulation in basal cells is unusual and shows different kinetics to the responses observed with other agonists and other lung cell populations. The intracellular calcium release was FXa concentration-dependent (**Figure 3.26B**) and fully blocked by the PAR-2 antagonist, GB83 (**Figure 3.27)**. Although the functional data suggest that HBECs do not express much PAR-1, the PAR-1 antagonist, RWJ58259, significantly reduced FXa-induced intracellular calcium release. Taken together, these data suggest that in bronchial epithelial cells FXa-induced calcium flux is both PAR-1- and PAR-2-dependent.

Subsequently PAR-1 and PAR-2 expression was visualised in basal cells by immunocytofluorescence. CK5 was used as a marker of the basal cell phenotype. As shown in **Figure 3.28** bronchial basal cells expressed little PAR-1 while PAR-2 was detected in abundance. Furthermore, this expression pattern was preserved in basal cells following differentiation at air-liquid interface for 3 weeks. As shown in **Figure 3.29** fully differentiated bronchial epithelium expressed large quantities of PAR-2 and low levels of PAR-1. A cross-section analysis of the cell layer reveals that

PAR-2 largely localised to the apical side of cells. Pre-incubation of the basal cells with TGFβ for 24 hours did not change the pattern of PAR-1 expression.

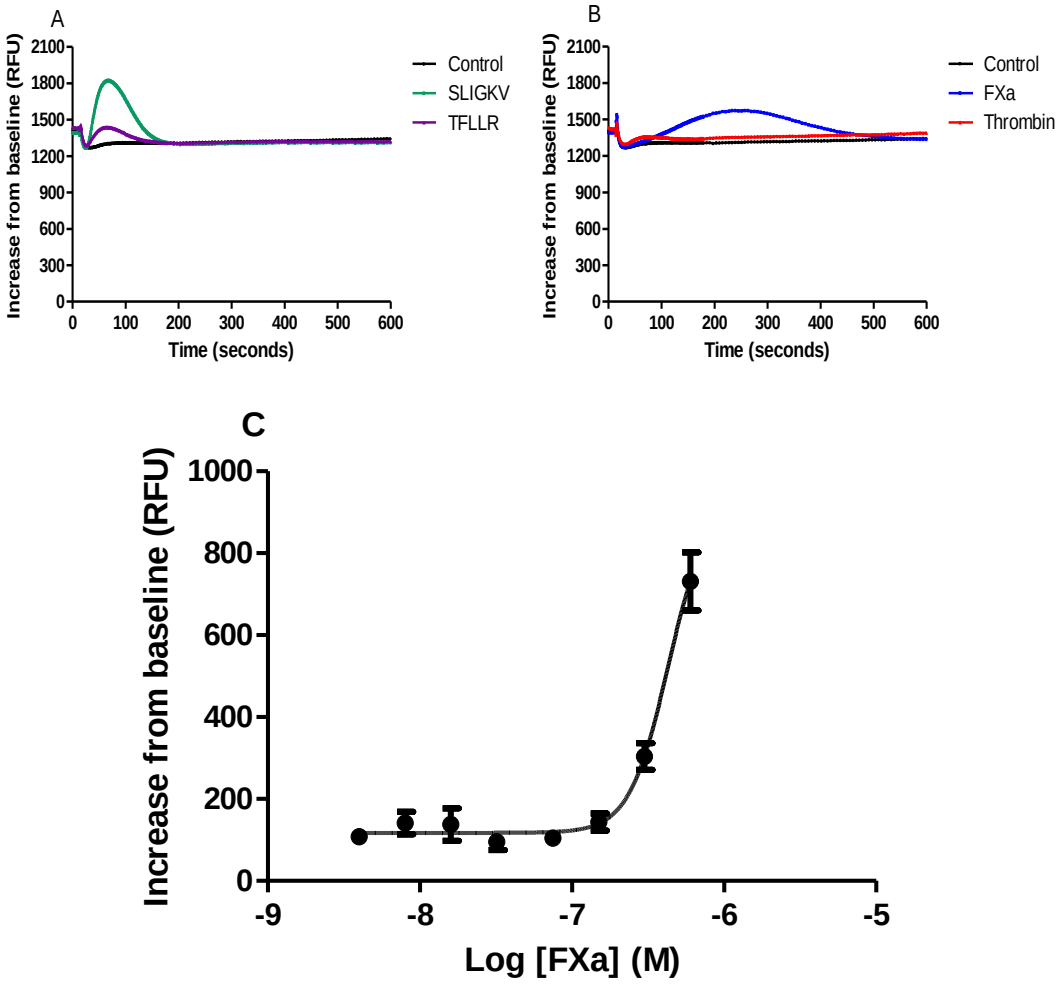

Figure 3.26. Characterisation of intracellular calcium responses in primary HBECs.

Human bronchial basal epithelial cells were seeded at a density of $3x10^4$ in 96-well plates coated with collagen IV and cultured for 48 hours. Cells were incubated with Fluo-4AM calcium binding dye for one hour before stimulation with PAR-1 and PAR-2 agonists. Panel A- representative traces for responses triggered thrombin (30 nM), FXa (200 nM), TFLLR (100 µM) and SLIGKV (100 µM). Panel B- concentration-response curve to FXa. The release of intracellular calcium was monitored by FLIPR® Tetra with calcium baseline recorded for 10 seconds before thrombin addition and response measured for another 700 seconds. Data are represented as increase in relative fluorescence units (RFU) from the baseline. Each data point represents the mean +/- SEM of 4 replicate wells.

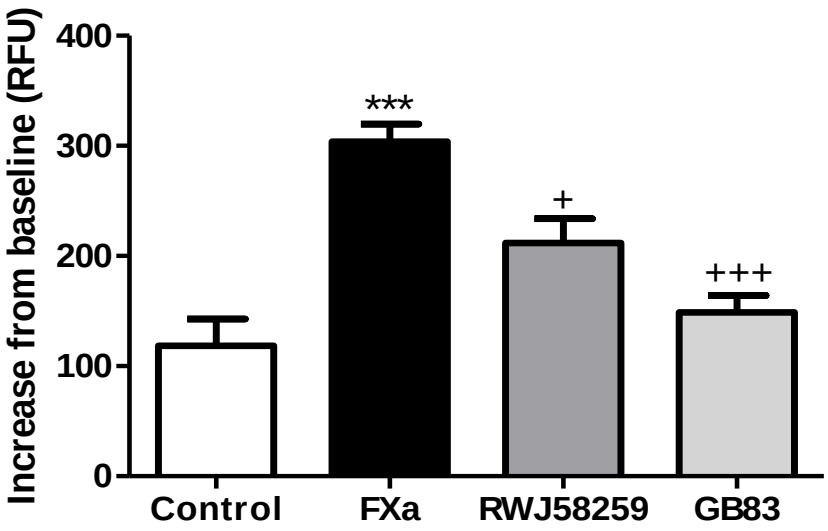

Figure 3.27. Intracellular calcium response in bronchial epithelial cells is PAR-2-dependent.

Human bronchial epithelial cells were seeded at a density of $3x10^4$ in 96-well plates coated with collagen IV and cultured for 48 hours. Cells were incubated with Fluo-4AM calcium binding dye with or without RWJ58258 (3 µM) or GB83 (50 µM) before being exposed to FXa (200 nM). The release of intracellular calcium was monitored by FLIPR® Tetra with calcium baseline recorded for 10 seconds before thrombin addition and response measured for another 700 seconds. Each data point represents the mean +/- SEM of 4 replicate wells, One-way ANOVA was performed for statistical analysis: ***$p<0.001$ relative to medium control; +++$p<0.001$, +<0.05 relative to FXa response.

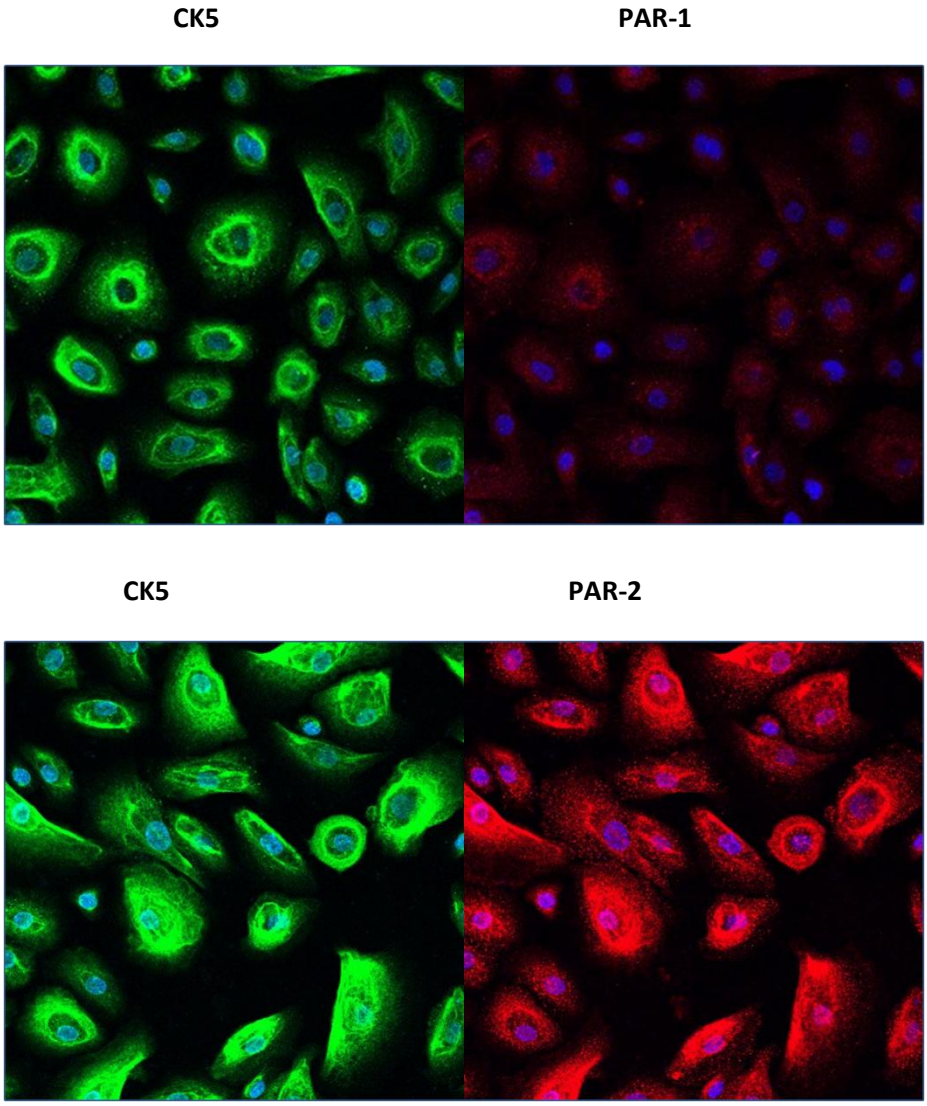

Figure 3.28. PAR-1 and PAR-2 expression in basal cells.

Bronchial basal cells were seeded at a density of $5x10^4$ in chamber slides and allowed to reach over 80% confluence. Cells were then fixed in paraformaldehyde and stained for PAR-1 (Alexa 555), PAR-2 (Alexa 555) and CK5 (Alexa 488), DAPI was used to visualise the nucleus. The top panel shows cells stained for PAR-1 cells and lower panel shows the staining for PAR-2 (20x original magnification).

PAR-1

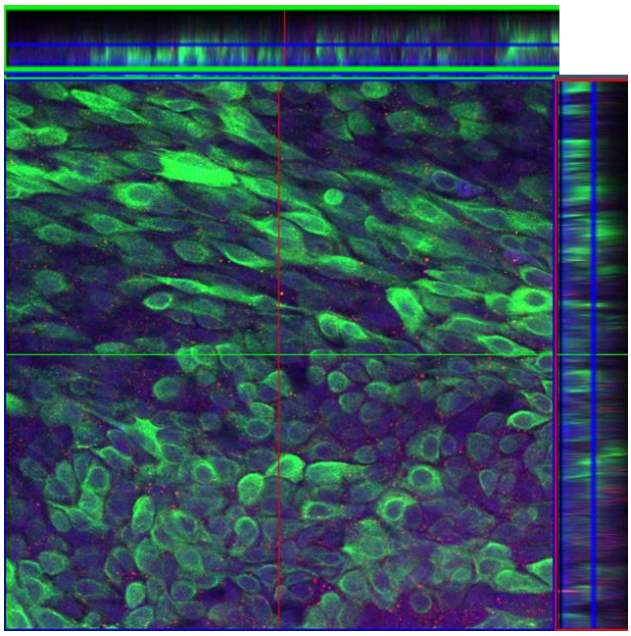

PAR-2

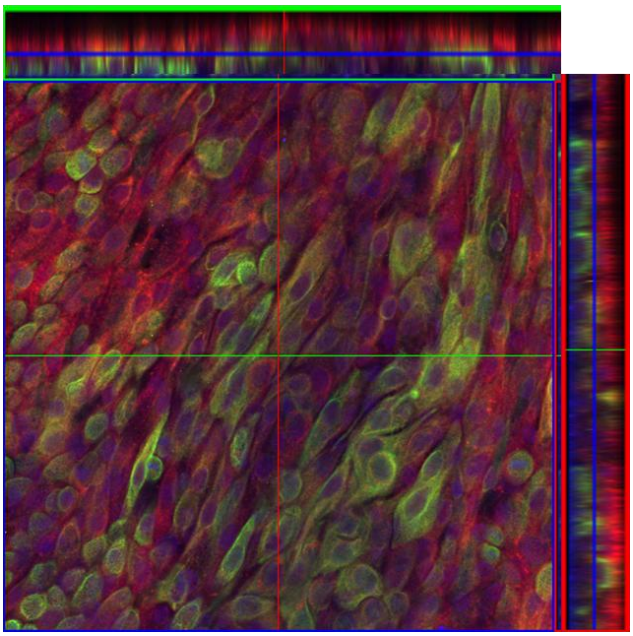

Figure 3.29. PAR-1 and PAR-2 expression in primary differentiated bronchial epithelium.

Bronchial epithelium was differentiated for 3 weeks at air-liquid interface. Cells were then fixed in paraformaldehyde and PAR-1 (red), PAR-2 (red) and CK14 (green) visualised by immunocytofluorescence, DAPI was used to visualise the nucleus. The top panel shows cells stained for PAR-1 cells and lower panel shows the staining for PAR-2. The side panels show cross-section analysis of the cell layer reconstructed from the z-stack images (20x original magnification).

3.1.4.2 Summary

- The BEAS2B bronchial epithelial immortalised cell line signals robustly to thrombin in a concentration-dependent manner.
- Robust intracellular calcium release is observed in primary HBECs in response to PAR-2 activation but not PAR-1.
- Primary basal cells express high levels of PAR-2 and low levels of PAR-1 in submerged culture and following differentiation into pseudostratified bronchial epithelium at air-liquid interface.

3.1.5 PAR-1 expression and signalling in lung endothelial cells

Similar to fibroblasts, endothelial cells have been reported to express PAR-1 in abundance both on the cell surface as well as in intracellular pools. Since activated PAR-1 is not recycled, the intracellular store of the receptor allows for quick mobilisation and cell re-sensitisation. Furthermore, a positive feedback mechanism has been identified in endothelial cells where thrombin and PAR-1 activating peptides upregulate PAR-1 mRNA levels between 3 and 6 hours following stimulation (Ellis et al. 1999). However, PAR-1 signalling has been primarily investigated in human umbilical vein endothelial cells (HUVECs) and large airway endothelial cells. In contrast, little is known about PAR-1 expression and signalling responses in lung microvascular endothelium. The aim of this set of experiments was to investigate intracellular calcium signalling in response to coagulation proteinases stimulation in human primary lung microvascular endothelial cells (HLMECs).

Distinct cellular effects have been described downstream of PAR-1 activation in the endothelium depending on the type of agonist and expression of co-factors. High levels of thrombin induce endothelial cell shape change and loss of tight junctions via activation of PAR-1 (Rabiet et al., 1996). Furthermore, PAR-1 signalling in endothelial cells promotes tissue factor expression and the upregulation of cytokine and adhesion molecule expression such as intracellular adhesion molecules (ICAM), E-selectin and P-selectin. These molecules facilitate platelet aggregation and leukocyte adhesion as well as extravasation of inflammatory cells and coagulation factors to the site of injury, which are the first steps of physiological inflammatory and tissue repair responses.

3.1.5.1 PAR-1 expression and signalling in human umbilical vein endothelial cells (HUVECs)

The aim of this part of this study was to investigate PAR-1 expression and signalling in endothelial cells of the lung. Intracellular calcium signalling and phospholipase C activation downstream of thrombin-mediated PAR-1 activation leads to cytoskeletal rearrangements and endothelial cell contraction that results in loss of endothelial barrier integrity and interstitial oedema (Tiruppathi et al., 2002). In the first series of experiments it was confirmed that PAR-1 and PAR-2 agonists trigger a robust increase in intracellular calcium release in HUVECs, which were used to model the responses in the large lung vessels. As shown in **Figure 3.30A** thrombin induced a transient intracellular calcium flux of high magnitude that occurred within 10 seconds following agonist stimulation, peaked rapidly and decreased to baseline over the next 200 seconds. In contrast, the kinetics of FXa-induced calcium signalling followed a different pattern with a delay between the addition of the agonists and onset of the response, lower magnitude of response and shorter duration (**Figure 3.30B**). The PAR-1 and PAR-2 activating peptides, TFLLR and SLIGKV, elicited robust release of intracellular calcium, with kinetics and magnitude of responses comparable to thrombin stimulation (**Figure 3.30C**). Upon quantification of these results (**Figure 3.30D)**, PAR-1 and PAR-2 agonists significantly increased the intracellular calcium concentration but FXa-induced calcium flux was 3-fold lower compared to that seen with thrombin. Furthermore, the responses were agonist-concentration dependent with EC_{50} of 5 nM and 150 nM, for thrombin and FXa respectively (**Figure 3.31**).

Subsequently, the responses to different agonists were investigated in the presence of specific PAR-1 and PAR-2 inhibitors. As shown in **Figure 3.32A**, thrombin enzymatic activity was necessary for triggering the calcium flux and no responses were detected when thrombin was yielded catalytically inert by pre-incubation with hirudin and antithrombin III (ATIII). Furthermore, thrombin signalling in HUVECS was PAR-1-mediated as PAR-1 antagonists, RWJ58259 and SCH530348, fully inhibited the calcium response (**Figure 3.32A**). PAR-2 antagonist, GB83, partially but

significantly attenuated thrombin-mediated calcium flux, which suggests a level of PAR-1 and PAR-2 interaction as previously described (O'Brien et al., 2000).

FXa proteolytic activity was also necessary for inducing the calcium flux in HUVECs and this response was inhibited by antithrombin III. The calcium response was reduced both by PAR-1 and PAR-2 inhibitors (**Figure 3.32B**), suggesting that at high concentration of FXa the calcium response in HUVECs is mediated via both receptors.

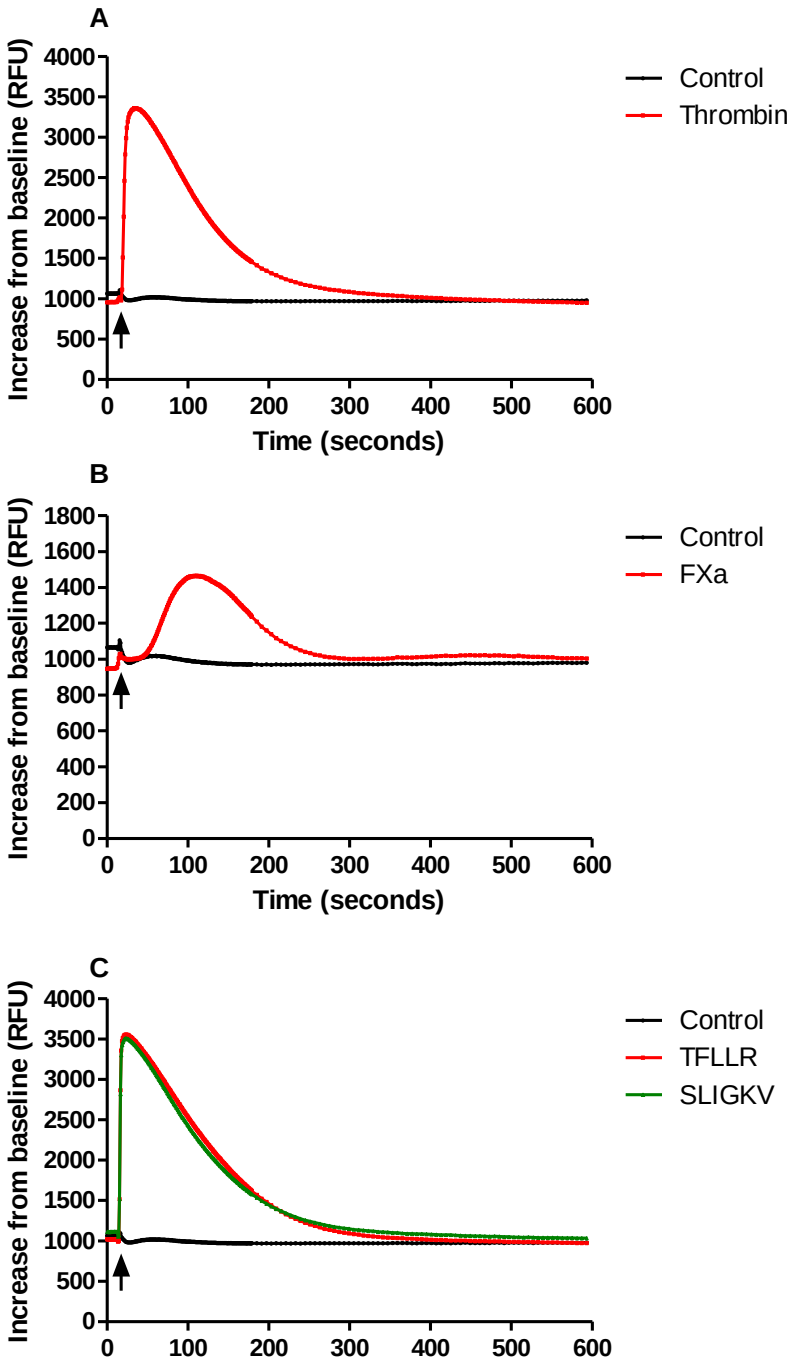
A
Increase from baseline (RFU)
4000
3500
3000
2500
2000
1500
1000
500
0
0
100
200
300
400
500
600
Time (seconds)
Control
Thrombin
B
Increase from baseline (RFU)
1800
1600
1400
1200
1000
800
600
400
200
0
0
100
200
300
400
500
600
Time (seconds)
Control
FXa
C
Increase from baseline (RFU)
4000
3500
3000
2500
2000
1500
1000
500
0
0
100
200
300
400
500
600
Control
TFLLR
SLIGKV

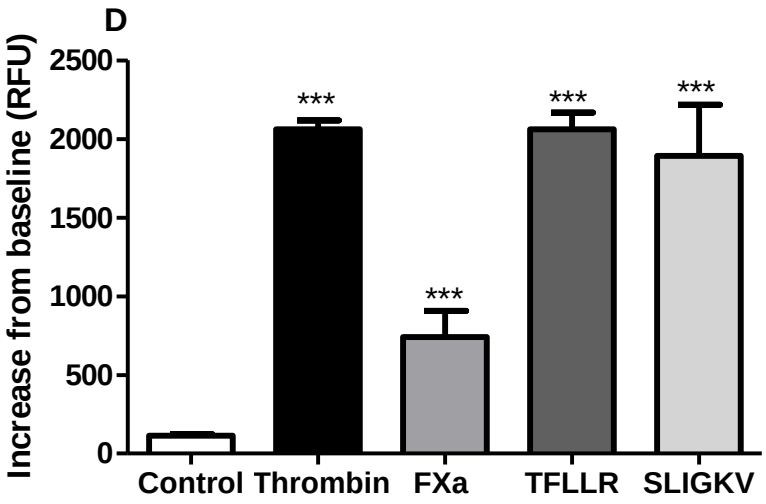

Figure 3.30. Calcium signalling in HUVECs in response to PAR-1 and PAR-2 activation

Primary human umbilical vein endothelial cells (HUVEC) were seeded at a density of $2x10^4$ in 96-well plates and allowed to reach confluence for 48 hours prior to stimulation with thrombin (10 nM), FXa (200 nM) and PAR-1 activating peptide TFLLR and PAR-2 activating peptide SLIGKV (100 μM). Cells were incubated with Fluo-4AM calcium binding dye for one hour and the release of intracellular calcium was monitored by FLIPR® Tetra with calcium baseline recorded for 10 seconds before agonist addition and response measured for up to 600 seconds. Data are represented as increase in relative fluorescence units (RFU) from the baseline. Panels A, B and C show representative traces for thrombin, FXa, TFLLR and SLIGKV-mediated calcium flux, panel D- quantification of calcium flux in response to PAR agonist. Data are expressed as an increase in relative fluorescence units (RFU) and each data point represents the mean +/- SEM of 3-4 replicate wells; one-way ANOVA was performed for statistical analysis. ***$p<0.001$ compared to baseline non-stimulated cells.

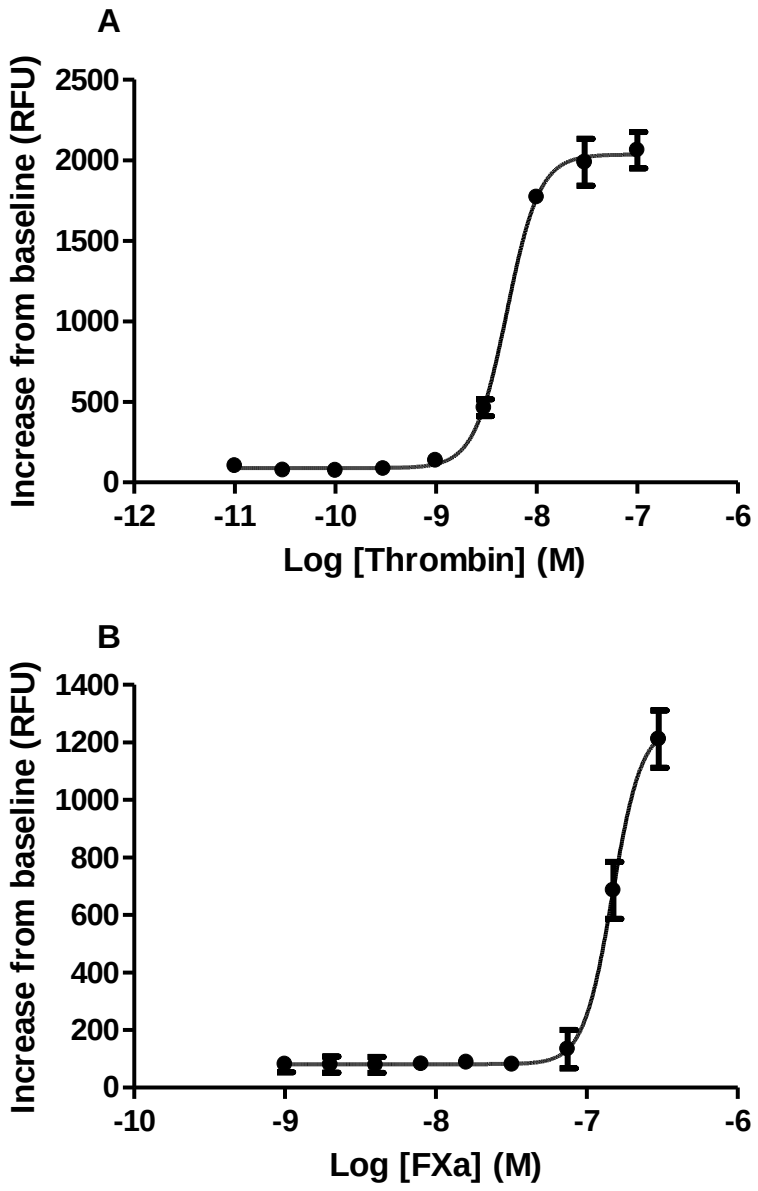

Figure 3.31. Concentration-response curve to thrombin and FXa in HUVECs.

Human umbilical vein endothelial cells (HUVEC) were seeded at a density of $2x10^4$ in 96-well plates and allowed to reach confluence for 48 hours prior to stimulation with different concentrations of thrombin- panel A and FXa- panel B. Cells were incubated with Fluo-4AM calcium binding dye for one hour and the release of intracellular calcium was monitored by FLIPR® Tetra with calcium baseline recorded for 10 seconds before agonist addition and response measured for up to 600 seconds. Data are represented as increase in relative fluorescence units (RFU) from the baseline. Each data point represents the mean +/- SEM of 3-4 replicates.

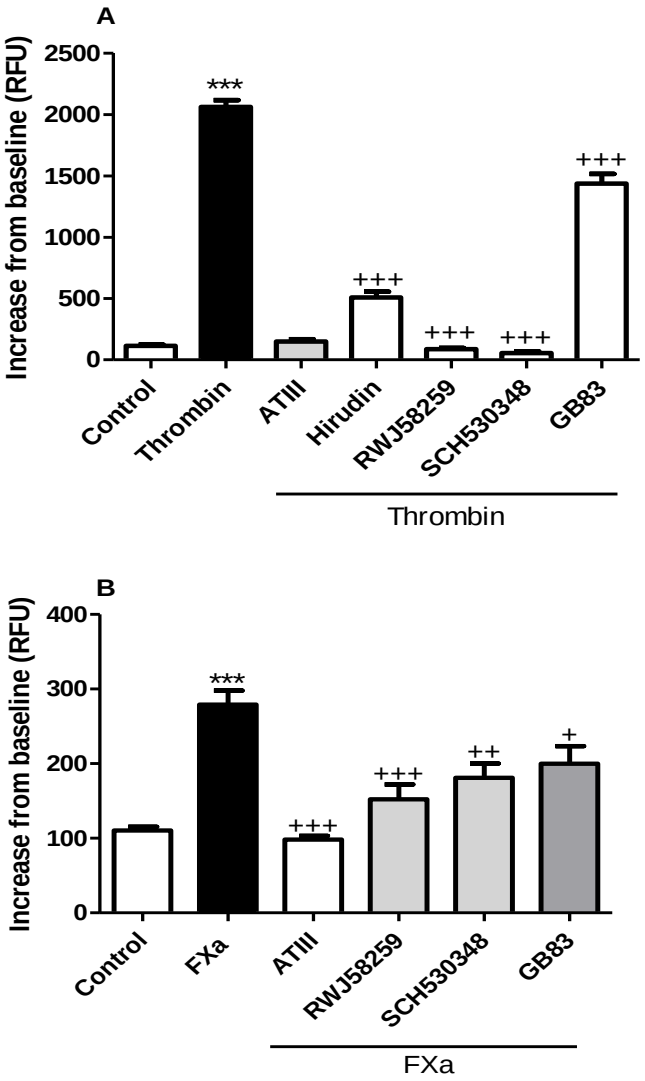

.

Figure 3.32. Thrombin and FXa mediated intracellular calcium release in HUVECs.

Human umbilical vein endothelial cells (HUVEC) were seeded at a density of $2x10^4$ in 96-well plates and allowed to reach confluence for 48 hours prior to stimulation with thrombin (10 nM), thrombin pre-incubated with hirudin (50 nM), thrombin pre-incubated with (100nM) antithrombin III/heparin, FXa (200 nM) and FXa pre-incubated in antithrombin III/heparin (2 µM). Cells were incubated with Fluo-4AM calcium binding dye for one hour with or without PAR-1 antagonists RWJ58259 and SCH530348 (3 µM) or GB83 at (50 µM) and the release of intracellular calcium was monitored by FLIPR® Tetra with calcium baseline recorded for 10 seconds before agonists addition and response measured for up to 600 seconds. Data are represented as increase in relative fluorescence units (RFU) from the baseline. Panels A shows the responses to thrombin and panel B- to FXA. Data represent the mean +/- SEM of 3-4 replicate wells; One-way ANOVA was performed for statistical analysis, ***$p<0.001$ relative to control, +++$p<0.001$ relative to agonist response.

3.1.5.2 PAR-1 expression and signalling in human lung microvascular endothelial cells (HLMEC)

The role of the thrombin-PAR-1 axis in inducing vascular permeability is well characterised in the large vessel endothelium but little is known about the effect of thrombin on human lung microvascular endothelium. It has been reported that in rat lung microvascular endothelium thrombin signalling via PAR-1 promotes endothelial integrity. Both thrombin and PAR-1 activating peptides increased transendothelial electrical resistance, reduced the formation of stress fibres and paracellular gaps (Troyanovsky et al., 2008). The aim of this study was to examine the intracellular calcium responses to PAR-1 and PAR-2 agonists in primary human lung microvascular endothelial cells (HLMECs).

Thrombin triggered a robust and transient intracellular calcium flux in HLMECs that occurred shortly after agonist addition and was maintained for 200 seconds before returning to baseline (**Figure 3.33A**). Both TFLLR and SLIGKV also elicited robust intracellular calcium flux, with PAR-1 activation inducing a response of higher magnitude than PAR-2 activation (**Figure 3.33B**). In contrast to responses observed in HUVECs, high concentrations of FXa elicited barely detectable intracellular calcium release in HLMECs (**Figure 3.33C**). Calcium fluxes in response to thrombin and TFLLR were found to be concentration-dependent with an EC_{50} of 7 nM and 36 µM, respectively (**Figure 3.34**). Pre-incubation of HLMEC with TGFβ did not have any effect on thrombin- and TFLLR-mediated intracellular calcium release downstream of PAR-1 activation (**Figure 3.34**). Furthermore, contrary to HUVECs, in HMLECs thrombin-mediated intracellular calcium flux was completely blocked by RWJ58259 (**Figure 3.35**), whereas PAR-2 antagonist GB83 did not have a significant effect on the response. This data suggests that in the HMLECs PAR-1 is a principal mediator of thrombin-mediated calcium signalling.

The expression of PAR-1 and PAR-2 was subsequently investigated by immunocytofluorescence (**Figure 3.36**). HMLECs phenotype was confirmed by staining for von Willebrand factor and platelet endothelial cell adhesion molecule PECAM. Representative PECAM staining is shown in **Figure 3.36**. PAR-1 and PAR-2

were found to be expressed in HLMECs and localised to the cytoplasm and periphery of cells.

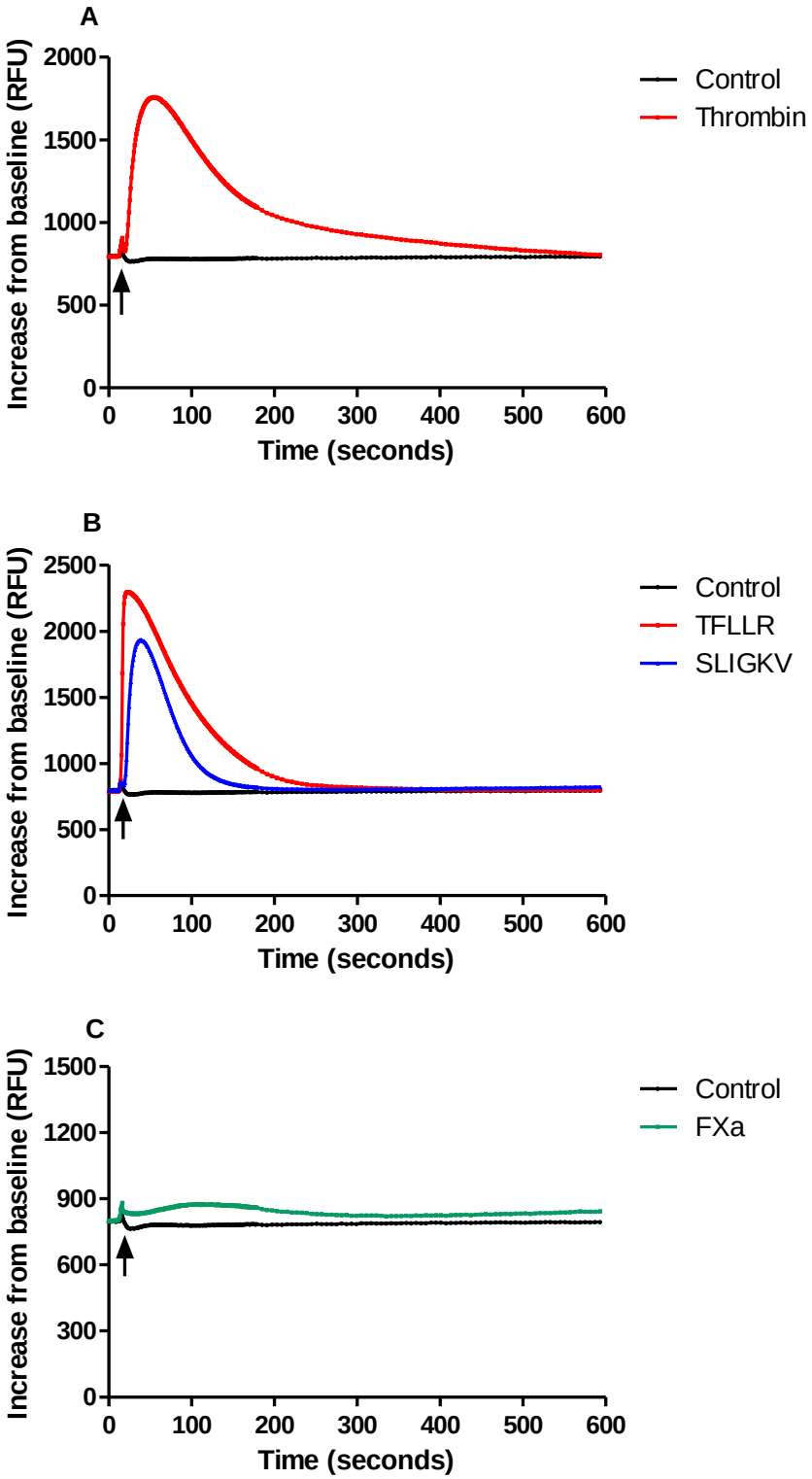

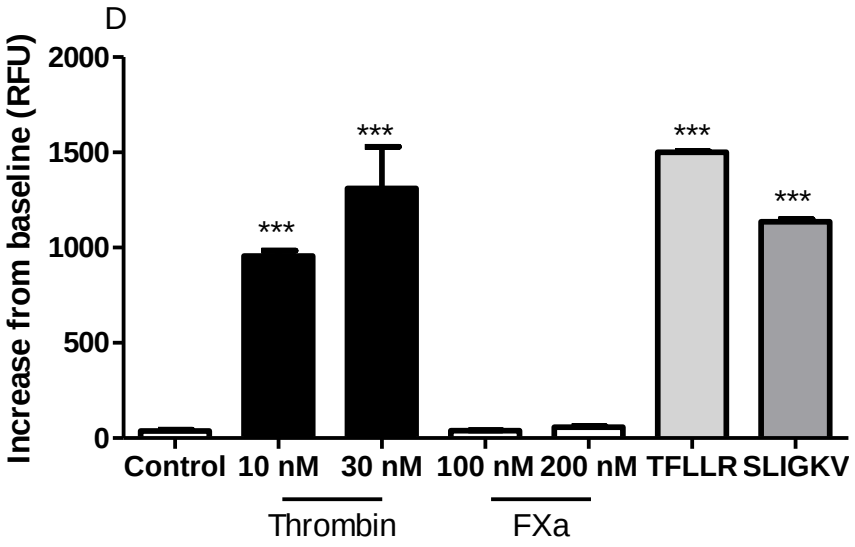

Figure 3.33. Intracellular calcium release in response to PAR-1 and PAR-2 agonists in HLMECs

Human lung microvascular endothelial cells (HLMEC) were seeded at a density of $3x10^4$ in 96-well plates and allowed to reach confluence for 48 hours prior to stimulation with thrombin (10 nM), FXa (200 nM)and PAR-1 activating peptide TFLLR and PAR-2 activating peptide SLIGKV (100 µM). Cells were incubated with Fluo-4AM calcium binding dye for one hour and the release of intracellular calcium was monitored by FLIPR® Tetra with calcium baseline recorded for 10 seconds before agonists addition and response measured for up to 600 seconds. Data are represented as increase in relative fluorescence units (RFU) from the baseline. Panels A, B and C show representative traces for thrombin, TFLLR and SLIGKV, and FXa-mediated calcium flux, panel D- quantification of calcium flux in response to PAR agonist. Each data point represents the mean +/- SEM of 3-4 replicates, one-way ANOVA was performed for statistical analysis, ***p<0.001.

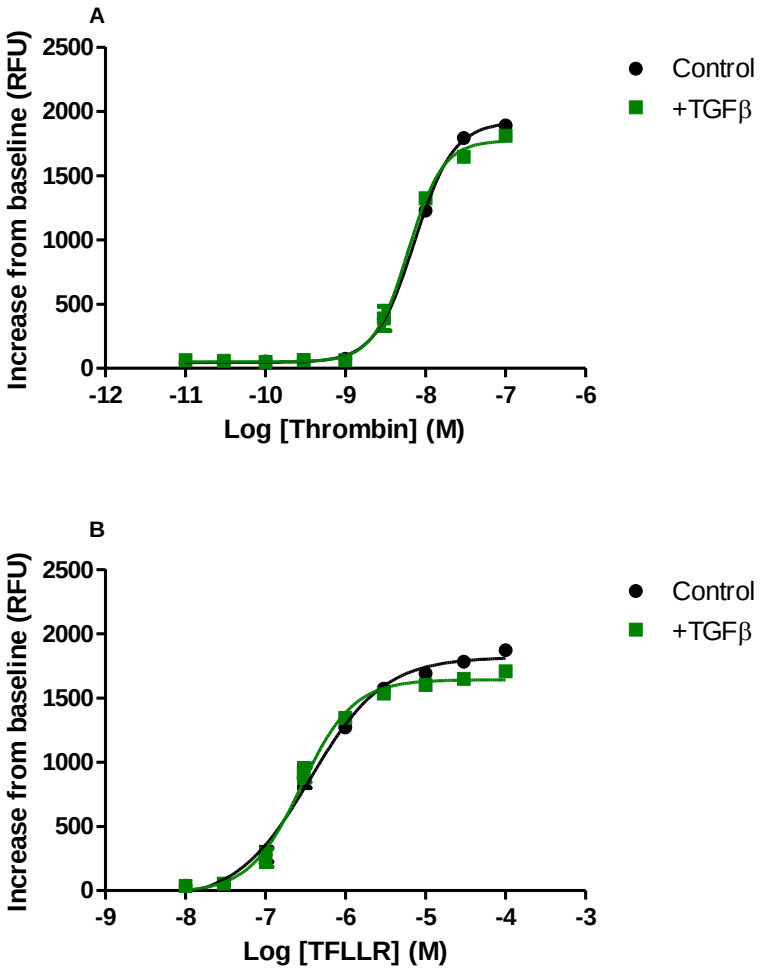

Figure 3.34. Concentration-response curve to thrombin and TFLLR in HLMEC

Human lung microvascular endothelial cells (HLMEC) were seeded at a density of $3x10^4$ in 96-well plates, allowed to reach confluence for 24 hours and incubated with or without TGFβ (1 ng/ml) for further 24 hours prior to stimulation with different concentrations of panel A- thrombin and panel B- TFLLR. Cells were incubated with Fluo-4AM calcium binding dye for one hour and the release of intracellular calcium was monitored by FLIPR® Tetra with calcium baseline recorded for 10 seconds before agonists addition and response measured for up to 600 seconds. Data are represented as increase in relative fluorescence units (RFU) from the baseline. Each data point represents the mean +/- SEM of 3-4 replicates.

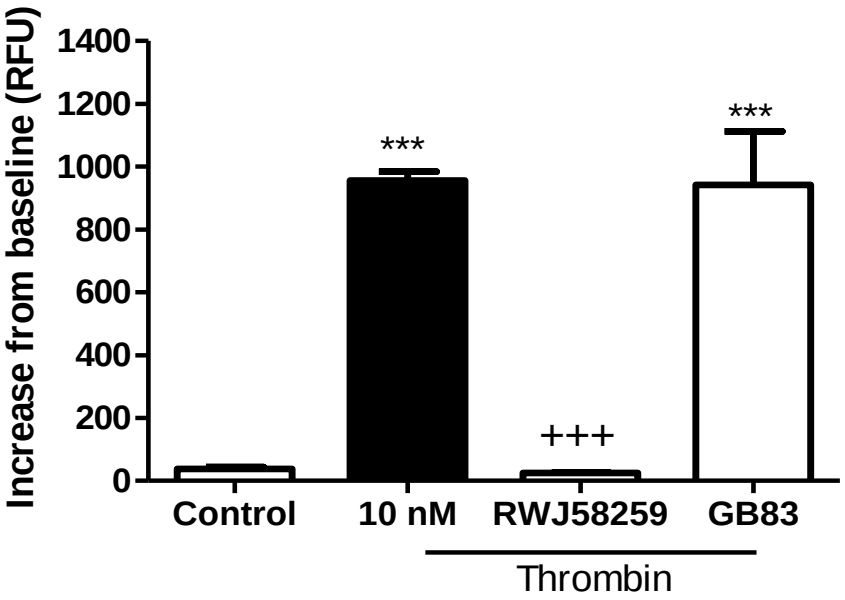

Figure 3.35. Thrombin-induced intracellular calcium signalling in HMLECs is PAR-1-dependent.

Human lung microvascular endothelial cells (HLMEC) were seeded at a density of $3x10^4$ in 96-well plates, allowed to reach confluence for 48 hours prior to stimulation with PAR-1 agonists. Cells were incubated with Fluo-4AM dye (Invitrogen) with or without RWJ58259 3µM or GB83 50µM for one hour and the release of intracellular calcium was monitored by FLIPR® Tetra with calcium baseline recorded for 10 seconds before agonists addition and response measured for up to 600 seconds. Each data point represents the mean +/- SEM of 3-4 replicates, One-way ANOVA was performed for statistical analysis, ***$p<0.001$ relative to control, +++$p<0.001$ relative to thrombin response.

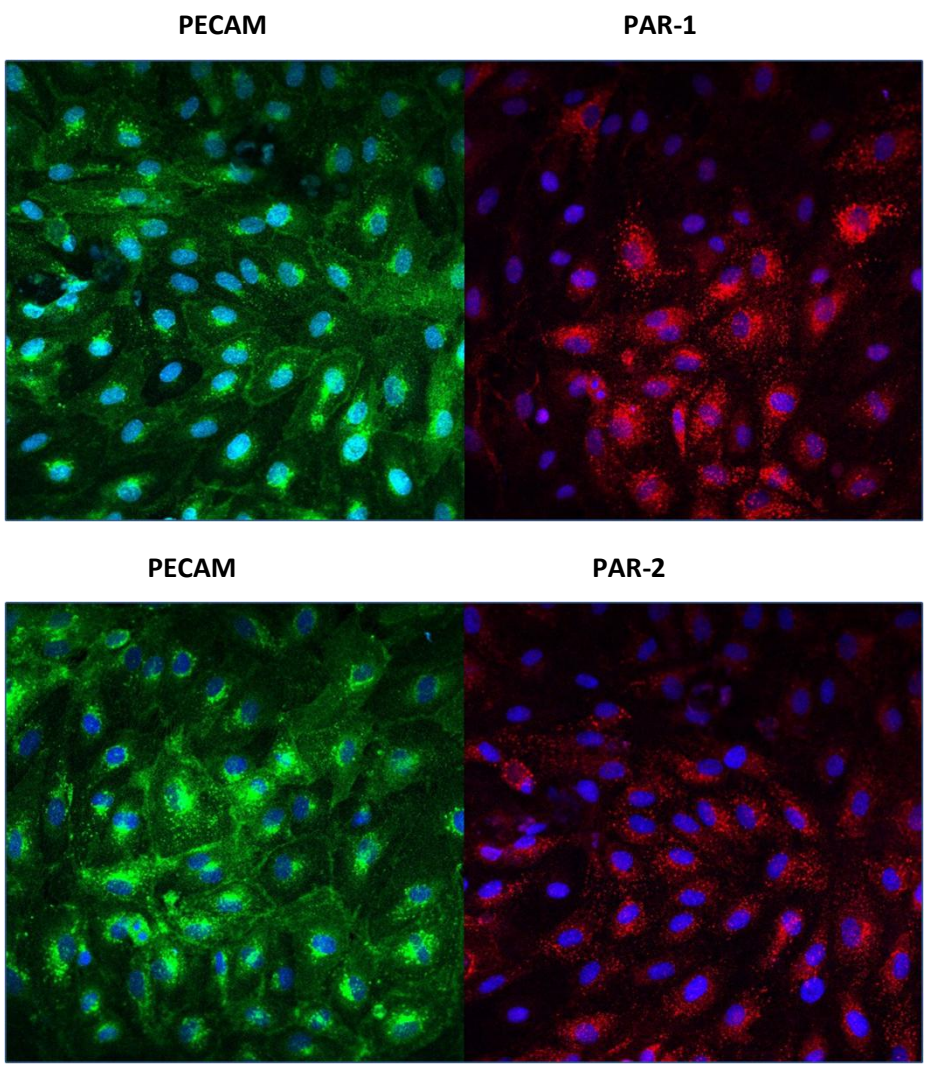

Figure 3.36. PAR-1 and PAR-2 expression in human lung microvascular cells.

Human lung microvascular endothelial cells were seeded at a density of $5x10^4$ in chamber slides and allowed to reach over 80% confluence. Cells were then fixed in paraformaldehyde and stained for PAR-1 (Alexa 555), PAR-2 (Alexa 555) and endothelial cells marker platelet endothelial cell adhesion molecule (PECAM, Alexa 488), DAPI was used to visualise the nucleus, 20x original magnification.

3.1.5.3 Summary

- PAR-1 and PAR-2 activation leads to rapid release of intracellular calcium in both HUVECs and HLMECs.
- Thrombin induces intracellular calcium release in HUVECs and HLMECs. This response is PAR-1- and PAR-2-dependent in HUVECs but entirely PAR-1-dependent in HLMEC.
- High concentrations of FXa trigger PAR-1- and PAR-2-dependent calcium flux in the HUVECs but in HLMECs FXa-mediated increase in intracellular calcium is barely detectable.

3.1.6 PAR-1 and PAR-2 expression in normal and fibrotic lung

In this section PAR-1 expression was investigated in several resident cell populations present in the lung. Fibroblasts and endothelial cells were found to express large amounts of PAR-1 and readily signal to PAR-1 activating peptide and thrombin. In contrast alveolar and bronchial epithelial cells signal robustly to PAR-2 activating peptide, which suggests that normal epithelium expresses primarily PAR-2. However, TGFβ upregulated PAR-1 in A549 alveolar epithelial cell line but not in primary AECII within the time-frame of the experiments presented in this study. Immunohistochemical analysis was subsequently performed in order to examine whether data collected in the *in vitro* experiments corresponded to the distribution of PAR-1 and PAR-2 in the human lung. Previous data from our laboratory have shown that PAR-1 is upregulated in abnormal and hyperplastic epithelium in the fibrotic lung (Mercer et al., 2009). However, in the control lung PAR-1 expression was detected at low levels on alveolar and bronchial epithelium. In contrast PAR-2 was readily on the alveolar epithelium (**Figure 3.37**- upper panel) and strongly positive on the apical site of bronchial epithelium (**Figure 3.37**- middle panel). In the fibrotic lung PAR-1 was a lot more readily detected and localised to fibroblasts within dense fibrotic areas (**Figure 3.37**- lower panel). PAR-2 was also detected in the fibrotic areas but the staining was of much lower intensity. Both PAR-1 and PAR-2 expression is readily expressed on the endothelium in both normal and fibrotic lungs.

Taken together, data presented in this study show that there are major differences in the PAR-1 and PAR-2 distributions between different cell populations in the lung and the expression of the coagulation receptors is likely to change in the disease. PAR-1 is a major signalling receptor in fibroblasts while in the control alveolar and bronchial epithelium PAR-2 appears to be the main signalling receptor. Whereas PAR-1 and PAR-2 are both expressed and functional in the endothelium of large vessels, PAR-1 appears to be the main signalling receptor in the microvascular endothelium.

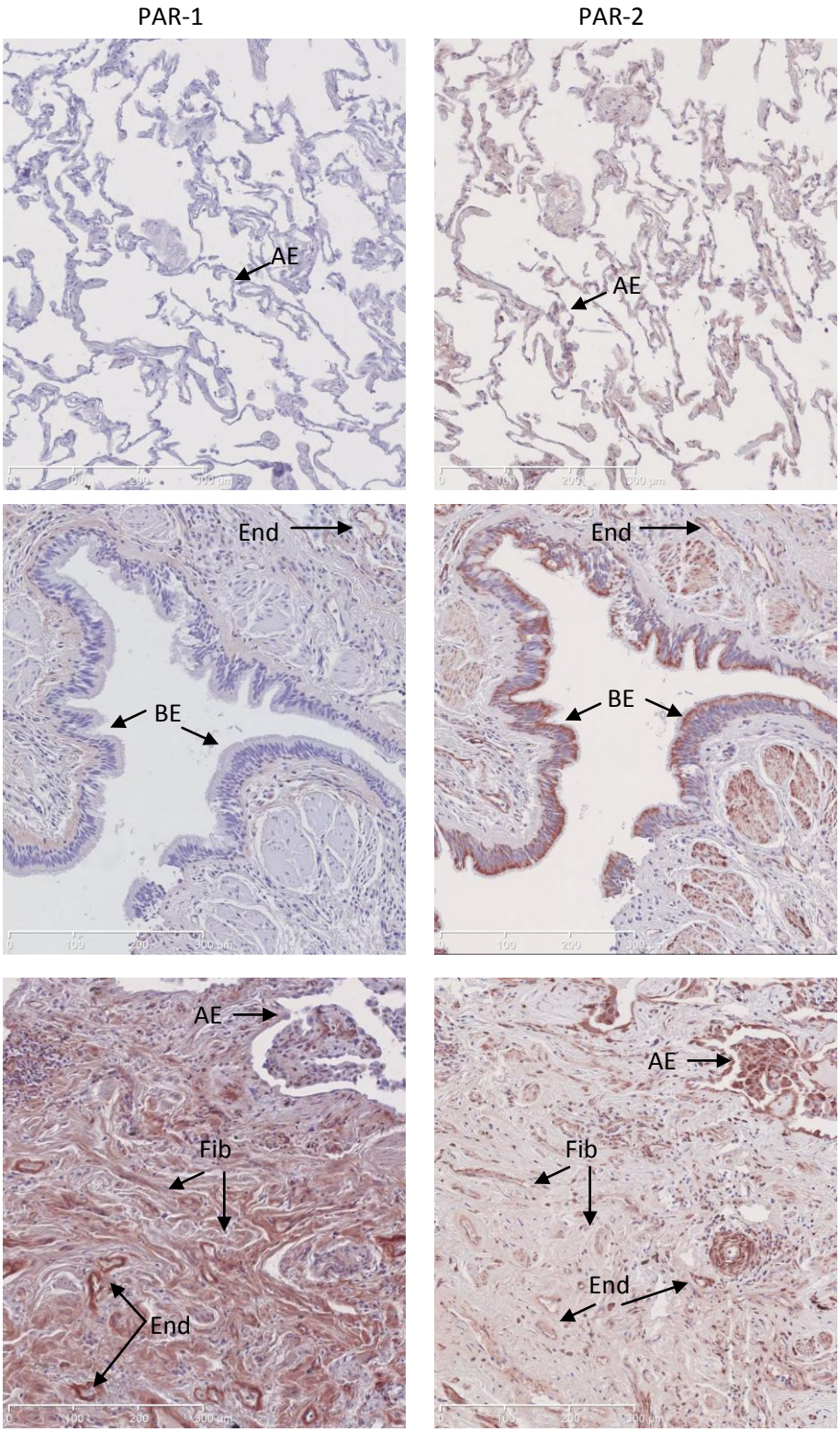

Figure 3.37. PAR-1 and PAR-2 expression in normal and fibrotic human lung.

Immunolocalisation of PAR-1 and PAR-2 in alveolar and bronchial epithelium in a normal lung- two upper panels and the distribution of the receptors in fibrotic lung- bottom panel. 10x original magnification, AE-alveolar epithelium, BE-bronchial epithelium, End- endothelium, Fib- fibroblasts.

3.1.7 Discussion

3.1.7.1 Overview

Substantial evidence supports the notion that over-exuberant activation of the extrinsic coagulation cascade plays a role in the pathogenesis of lung injury and pulmonary fibrosis. Apart from promoting fibrin deposition and clot formation, coagulation enzymes exert a plethora of cellular effects via the family of PAR receptors. Although thrombin can activate PAR-1, PAR-3 and PAR-4, PAR-1 is considered the main high-affinity thrombin receptor (Coughlin, 2000) and PAR-1 knockout mice are protected in the models of pulmonary injury and fibrosis (Howell et al. 2005). PAR-2 is the only receptor in PARs family that is not directly activated by thrombin but is efficiently cleaved by the components of the ternary complex, TF-FVII-FXa. PAR-2 is widely distributed in the lung and there is some evidence that PAR-2 may also contribute to the pathogenesis of pulmonary fibrosis (Wygrecka et al., 2011).

PAR signalling plays a significant role in inflammation, coagulation and restoration of tissue homeostasis. Increased expression of PAR-1 has been observed in many fibrotic diseases, including fibrosis of the lung (Howell et al. 2005), liver (Rullier et al., 2008), skin (Cevikbas et al., 2011) and also in cancer (Zigler et al., 2011). The aim of this study was to characterise PAR-1 and PAR-2 expression and calcium signalling responses in distinct human pulmonary cell population.

The expression of PAR-1 and PAR-2 receptors was assessed following stimulation with the major coagulation proteinases, thrombin and FXa, as well as in response to specific PAR agonist peptides. The mechanism of PAR activation is unusual among the family of GPCRs and it involves enzymatic cleavage and unmasking of a tethered ligand which subsequently binds to the orthosteric site on the second extracellular loop of the receptor. Each member of PAR family has a unique sequence of amino acids that form the active site of the tethered ligand. This property of the PAR receptors was used to develop specific and selective agonists and antagonists

against individual members of PAR family, which were used in this study to dissect PAR-1 and PAR-2- mediated calcium responses.

Similar to other GPCRs, PARs also display biased agonism. PARs can be activated by several agonists, with PAR-1 being activated by thrombin but also FXa and APC while PAR-2 is activated by FXa, trypsin and tryptase. Both PAR-1 and PAR-2 are also efficiently cleaved by the extrinsic coagulation cascade initiation complex, TF-FVIIa-FXa. Activation of the receptor by a specific agonist leads to stabilisation of distinct active conformations that facilitate binding to heterotrimeric G-proteins and allosteric modulators such as β-arrestins (Russo et al. 2009). This allows for functional selectivity and explains how PAR activation can initiate multiple signalling pathways and different cellular effects when activated by different agonists. Furthermore, PAR-1 tethered ligand is also an agonist of PAR-2, which was discovered when the original small activating peptide based on exact sequence of PAR-1 tethered ligand, SFLLRN, was found to also activate PAR-2 (Blackhart et al., 1996). The potential biological significance of this finding has been demonstrated *in vitro* in endothelial cells when the unmasked ligand of PAR-1 was shown to transactivate PAR-2 (O'Brien et al., 2001). Furthermore, PAR-1 and PAR-2 can form stable heterodimers on the cell surface that act as a functional unit, are jointly internalised and have been shown to modulate the responses to thrombin by preferentially recruiting β-arrestins and activating ERK1/2 (Lin and Trejo, 2013).

PAR-1 couples to $G\alpha_q$, $G\alpha_{i/0}$ and $G\alpha_{12/13}$ while PAR-2 couples to $G\alpha_q$ and $G\alpha_{12/13}$ (McCoy et al. 2010). Thrombin-mediated PAR-1 activation leads to $G\alpha_q$ uncoupling and robust intracellular calcium release and this functional response was used in the present study to evaluate PAR-1 signalling in different lung cell populations. Uncoupled $G\alpha_q$ leads to phospholipase C (PLCβ)-mediated generation of inositol trisphosphate (IP3), which interacts with IP3 receptors (IP3R) in the endoplasmic reticulum (ER). This interaction increases IP3R sensitivity to calcium and the receptor operates in a biphasic mode. At low cytoplasmic calcium concentrations the IP3R opens and allows efflux of calcium stored in the ER while high concentrations of cytoplasmic calcium negatively regulate IP3R permissiveness

(Berridge et al. 2003). The ER contains multiple IP3R clusters and upon activation of individual receptors blips of calcium are observed that summate into puffs that form a global wave of intracellular calcium (Bootman et al. 1997). The number of IP3R clusters activated influence the kinetics of the calcium wave and are proportionate to the upstroke velocity and the magnitude of the response. Calcium signalling regulates multiple cellular processes, including fertilisation of the egg, proliferation, differentiation, ion channel opening, cell contraction and shape changes. Cells respond to initial calcium waves but are also able to detect changes in frequency of calcium spikes and modulate the responses accordingly, which has been shown to regulate calcium-mediated exocytosis, mitochondrial function and gene expression (Bootman et al. 1997). The IP3/calcium axis also regulates synaptic plasticity in the brain involved in learning and memory (Berridge 1993). Abnormal calcium signalling has been linked to many pathologies, including cardiac hypertrophy, where overexpression of $G\alpha_q$ leads to a severe form of the disease in experimental models (Song et al., 2003). Furthermore, thrombin has been shown to directly affect the physiological responses of myocytes through increased calcium activation (Steinberg et al., 1991). Alzheimer's disease, schizophrenia and bipolar disease have also been associated with abnormal calcium fluxes (Berridge 2012).

In this study intracellular calcium release was monitored to investigate PAR-1 and PAR-2 signalling responses following stimulation with coagulation proteinases in primary human lung cells.

3.1.7.2 PAR-1 expression and signalling in lung fibroblasts

The current consensus for G-protein activation states that multiple subsets of G-proteins can become simultaneously uncoupled following receptor activation and trigger independent and converging cellular pathways. Thrombin exerts multiple stimulatory effects on fibroblasts, including promoting fibroblast to myofibroblast differentiation (Baffy et al., 1994; Bogatkevich et al., 2001), production and secretion of collagen (Chambers et al., 1998) and growth factors such as CTGF (Chambers et al., 2000), FGF2 (Duarte et al., 2006). Thrombin-mediated calcium release is a critical event for the coordination of many of these biological functions

in fibroblasts, including promoting DNA synthesis and cell proliferation (Baffy et al., 1994; LaMorte et al., 1993), production and release of CCL2 (Deng et al., 2008; Ortiz-Stern et al., 2012).

In the first part of this study, the relative contribution of PAR-1 and PAR-2 activation in response to coagulation proteinases was investigated in primary human lung fibroblasts by measuring $G\alpha_q$-mediated release of intracellular calcium. Thrombin is known to trigger IP3 accumulation within a few seconds after stimulation (Steinberg et al., 1991) which is followed by a robust calcium wave with high upstroke velocity and magnitude. This response suggests that thrombin can activate multiple PAR-1 receptors and lead to many $G\alpha_q$ uncoupling events in a short-time frame that allows for the generation of global long-lasting (approximately one minute) regenerative calcium waves. A similar pattern of calcium flux was observed with TFLLR and SLIGKV. TFLLR-mediated calcium flux occurred with an even steeper increase than observed with thrombin and reached higher magnitude, suggesting that the PAR-1 activating peptide modulates the response specifically toward $G\alpha_q$. PAR-2 activation with SLIGKV led to a sharp increase in intracellular calcium, although of lower magnitude than TFLLR. These data suggest that primary human lung fibroblasts express both PAR-1 and PAR-2, but PAR-1 appears to be more abundantly expressed than PAR-2. This observation was subsequently supported by immunocytofluorescence studies.

FXa can activate both PAR-1 and PAR-2 but in this study the calcium response was only detected with high concentrations of FXa and even then occurred with a delay and was of much lower magnitude when compared to thrombin response. Although, long-term exposure of lung fibroblasts to FXa produces similar responses as thrombin stimulation, i.e. differentiation to myofibroblasts and collagen production (Blanc-Brude et al., 2005; Scotton et al., 2009), it is possible that FXa activates different subset of G-proteins than thrombin and that PAR-1-$G\alpha_q$ is not the preferential signalling pathway downstream of FXa-mediated PAR-1 activation. Indeed, the delayed kinetics of the FXa-mediated calcium response may be caused by selective triggering of different or multiple signalling events. Furthermore,

previous studies have shown that high concentrations of FXa alone are required to elicit a response achievable at low nanomolar concentrations when FXa is bound to the TF-FVIIa-FXa ternary complex (Riewald and Ruf, 2001). TF-VIIa bind FX with high affinity, activate it to FXa and form a stable signalling unit that increases FXa efficiency to cleave PAR-1 and PAR-2 by up to 10-fold (Riewald and Ruf, 2001). All the components of the TF-FVIIa-FXa ternary complex are locally expressed in the lung and FX expression is increased within fibrotic foci (Scotton et al., 2009). It is therefore possible that in the lung FXa bound within the ternary complex is able to activate PAR-1 with greater efficiency and have profound effects on fibroblast biology via other signalling pathways that intracellular calcium release.

In this study, the PAR-1-mediated calcium response was inhibited by hirudin that yields thrombin catalytically inert. This clearly demonstrates that thrombin enzymatic activity is necessary for this response to occur. Furthermore, thrombin triggered the release of intracellular calcium at low concentrations of 0.3 nM and with a half-maximal response at 1.5 nM. Fibroblasts accumulate in the lung interstitium and by default are not considered to be exposed to thrombin unless there is injury followed by a vascular leak which leads to extravasation of prothrombin from the circulation and local thrombin activation. Furthermore, the TF-FVIIa-FXa ternary complex can assemble locally in the lung (Scotton et al., 2009) and facilitate generation of nanomolar concentrations of thrombin, which as reported in this study are sufficient to activate PAR-1 in lung fibroblasts.

Highly selective PAR-1 and PAR-2 antagonists were used next to investigate the contribution of PAR-1 and PAR-2 to calcium responses in fibroblasts following stimulation with coagulation proteinases. Thrombin- and FXa-mediated intracellular calcium fluxes were fully blocked by two PAR-1 antagonists but were unaffected by the PAR-2 inhibitor, which suggests that in lung fibroblasts calcium signalling downstream of coagulation proteinases stimulation is fully PAR-1-dependent. This observation does not exclude the possibility that FXa activates PAR-2 in primary human lung fibroblasts but suggests that all $G\alpha_q$-mediated responses are PAR-1-dependent.

TGFβ is a major pro-fibrotic cytokine that induces fibroblast to myofibroblast differentiation (Hinz, 2009) and fibrotic fibroblasts were reported to be more responsive to thrombin stimulation (Deng et al., 2013). Thrombin induced significantly higher CCL2 release in the fibrotic fibroblast when compared to the normal lung fibroblasts by increased binding of the transcription factors to the CCL2 promoter in the fibrotic fibroblasts (Deng et al., 2013). Therefore, the next question addressed in the present study was whether TGFβ affects PAR-1 expression and influences calcium functional responses in primary human lung fibroblasts. TGFβ pre-treatment did not affect the PAR-1-mediated calcium responses in human lung fibroblasts. However, PAR-1 is constitutively and abundantly expressed by lung fibroblasts and it is possible that the observed calcium responses are already maximally stimulated and cannot be further augmented by TGFβ.

In conclusion, PAR-1 and PAR-2 activation in primary human lung fibroblasts led to robust intracellular calcium signalling but the high responsiveness to thrombin stimulation was PAR-1-dependent.

3.1.7.3 PAR-1 expression and signalling in alveolar epithelial cells

Persistent and repetitive injury to the alveolar epithelium is considered to be the initiating step in the development of fibroproliferative lung disease. Furthermore, in acute exacerbation of IPF markers of alveolar epithelial injury are significantly upregulated (Collard et al., 2010), which supports the notion that the damage to the epithelium drives the fibrotic processes. Profibrotic TGFβ signalling in the epithelial cells is known to cause apoptosis (Martin et al., 2005) or the acquisition of abnormal phenotype characterised by hyperplasia and bronchiolisation (Chapman 2011). In IPF lung, strong PAR-1 immunopositivity is localised to the abnormal and hyperplastic epithelium (Mercer et al., 2009). PAR-1 is also upregulated in the lung epithelium in endotoxin-induced model of acute lung injury (Jesmin et al., 2004, 2007) and bleomycin-induced lung injury (Howell et al., 2005).

There are major technical limitations of growing fibrotic alveolar epithelial cells *in vitro* including lack of access to clinical specimens and lack of optimised culture

conditions. Culture of normal primary human alveolar epithelial cells isolated from lung explants is also challenging due to the low yield and finite life-span of AECII. In this study, a model A549 cell line representing abnormal alveolar epithelium was used to begin to characterise PAR-1 expression and functional responses in alveolar epithelial cells.

Thrombin stimulation of A549 epithelial cells produced a delayed calcium response of smaller magnitude when compared to the responses detected in the lung fibroblasts. Although, PAR-1 activation by TFLLR elicited a stronger calcium response than thrombin, the strongest calcium flux was observed following PAR-2 activation with SLIGKV. These data suggest that A549 cells express low levels of PAR-1 but abundant levels of PAR-2. This observation was subsequently confirmed by immunocytofluorescence study revealing that PAR-2 is highly expressed on the A549 cell surface while PAR-1 was barely detected. Calcium flux was also measured following stimulation of A549 cells with FXa but the response was delayed and of smaller magnitude, consistent with the low level response observed in fibroblasts. Again high concentrations of FXa were required to elicit a detectable calcium response.

Thrombin-mediated calcium responses in A549 cells were fully inhibited by hirudin and the PAR-1 antagonist RWJ58259. However, the response was also significantly reduced in the presence of PAR-2 antagonist, GB83, suggesting that PAR-1 might transactivate a subset of PAR-2 receptors to contribute to the calcium response. Unidirectional PAR-2 transactivation by PAR-1 has previously been described for endothelial cells (O'Brien et al., 2001). In order for transactivation to occur, the receptors need to be in close proximity and PAR-1 and PAR-2 are known to form heterodimers in certain cell types including vascular smooth muscle cells (Pawlinski and Holinstat, 2011). In this A549 cell study PAR-1 activation was found to be necessary for triggering downstream calcium release while PAR-2-$G\alpha_q$ signalling appeared to potentiate this response. Inhibition of PAR-2 signalling reduced the magnitude of response by approximately 50%. Further work is required to dissect the relationship between PAR-1 and PAR-2 on epithelial cell surface.

Pre-treatment with TGFβ increased the functional responsiveness of A549 that was both TGFβ and PAR-1 agonist concentration-dependent. Thrombin induced intracellular calcium flux in A549 with an EC_{50} of 13 nM and pre-treatment with TGFβ did not affect the threshold of activation. However, TGFβ increased the maximal response to thrombin by 2.5-fold which is consistent with increased PAR-1 expression following TGFβ stimulation. Potential explanations for the observed signalling pattern include the possibility that thrombin activation of PAR-1 can be affected by multiple factors such as thrombin concentration, spatial orientation of PAR-1 on the cell surface and localisation to lipid rafts, utilisation of co-receptors such as PAR-3, endothelial protein C receptor (EPCR), and the ability of thrombin to preferentially signal via different G-proteins (Feistritzer and Riewald 2005). All these signalling intricacies have been described for endothelial cells but further work will be required to investigate whether these mechanisms apply to alveolar epithelial cells.

TGFβ signalling in epithelial cells has been shown to induce phenotypic changes resembling epithelial to mesenchymal transition (EMT), which has been well-characterised for cancer cells. The hallmark of this phenotypic change is reduced expression of epithelial cell markers, such as E-cadherin, and increased expression of mesenchymal cell markers, such as vimentin and αSMA (Dubois-Marshall et al., 2011). In this study, TGFβ stimulation of A549 cells for 24 hours led to increased PAR-1 functional responses as measured by increased intracellular calcium flux and also increased surface expression as measured by immunocytofluorescence. This study also revealed that following 24 hour exposure to TGFβ, E-cadherin is still intensely expressed by A549 cells and hence TGFβ-mediated increase in PAR-1 expression occurred before the loss of epithelial markers associated with EMT.

Furthermore, TGFβ stimulation of A549 cells led to increased PAR-1 mRNA level from 8 hours onwards. Thrombin-PAR-1 signalling axis contributes to activation of latent TGFβ via integrins. Robust activation of TGFβ is triggered through the interaction of the TGFβ latency complex with αvβ6 integrins on epithelial cells (Jenkins et al., 2006) and αvβ5 integrins on fibroblasts (Scotton et al., 2009). As

previously described PAR-1 activation and signalling via the Rho-GTPase pathway leads to re-arrangement of the actin cytoskeleton resulting in cell contraction and redistribution of mechanical forces between the cell and the extracellular matrix. This in turn causes activation of surface integrins that are constitutively attached to the TGFβ latency complex, alters the interaction of these integrins with the TGFβ latency complex and results in the release of active TGFβ. The next question addressed in this study was whether increased PAR-1 expression and functional responsiveness to thrombin could be a part of a positive feedback mechanism that promotes further TGFβ activation. In order to examine this, mRNA levels of the integrin subunits αv and β6 were measured. Indeed, TGFβ stimulation led to a parallel upregulation in expression of both integrin subunits after 6 hours of stimulation. These data suggest a potential feedback loop in A549 cells where TGFβ controls the expression of crucial components of the machinery that actively contributes to activation of this cytokine. In order to test this hypothesis, future studies would involve assessing the surface expression of integrins and changes in the rate of TGFβ activation following pre-treatment of A549 cells with TGFβ for 24 hours and thrombin stimulation.

Active TGFβ has a high affinity for the type II receptor (TβRII) that is constitutively expressed on the cell surface. Ligand-TβRII complexes recruit the type I receptor/activin-receptor like kinase (TβRI/ALK). ALK5 is a ubiquitously expressed TβRI and the assembly of the heterotetramic ligand-receptor complex triggers the phosphorylation and activation of canonical Smad-dependent and non-canonical signalling pathways. Smad2 and Smad3 are substrates for ALK5 and following phosphorylation translocate to the nucleus together with the co-factor Smad4. The Smads then form transcriptional complexes recruiting co-activators such as Sp1 and AP-1 and regulate the expression of multiple target genes (Derynck and Zhang, 2003). There is strong evidence that the TGFβ-Smad3 pathway is essential for normal lung alveolarisation and for maintaining alveolar homeostasis but also contributes to the development of fibroproliferative lung disease (Gauldie et al., 2006). Smad3 knockout mice are protected from pulmonary fibrosis induced by overexpression of TGFβ (Bonniaud et al., 2004b) and administration of bleomycin

(Zhao et al., 2002). Furthermore, Smad3-null fibroblasts exhibit reduced contractile and migratory potential due to their inability to upregulate αSMA expression following TGFβ stimulation (Dobaczewski et al., 2010). Finally, inhibition of the ALK5 receptor is also protective in bleomycin-induced pulmonary fibrosis (Bonniaud et al., 2005b; Scotton et al., 2013). In the present study small molecule ALK5 inhibitor, SB431542, was used to investigate the mechanism of TGFβ-mediated PAR-1 upregulation. This compound fully blocked upregulation of PAR-1 expression and signalling. Furthermore, siRNA knockdown of the components of canonical signalling pathway, Smad2 and Smad3, has showed that the induction of PAR-1 is Smad3-dependent and Smad2-independent.

TGFβ bound to TβRII-ALK5 complexes leads to phosphorylation of serine and threonine residues on these receptors which activate Smad2 and Smad3 signalling but it can also lead to phosphorylation of tyrosine residues and recruitment of adaptor molecules necessary for the activation of MAPK kinases pathways (Zhang, 2009). TGFβ-activation of the ERK MAPK signalling pathway has been linked to EMT in cancer cells (Davies et al., 2005) and genetic profiling of TGFβ-mediated EMT revealed that ERK participates in the regulation of expression of cell-matrix adhesion and motility genes (Zavadil et al., 2001). Interestingly, activation of the ERK MAPK pathway has also been shown to lead to phosphorylation of Smad2 and Smad3 and differentially regulate their activity depending on cell type. ERK-mediated Smad3 phosphorylation has been reported to repress Smad3 transcriptional functions (Matsuura et al., 2005) but enhance Smad2-mediated gene expression (Funaba et al. 2002). In another study ERK signalling was found to negatively regulate Smad2 and Smad3 transcriptional activity and this was suggested as a mechanism for overriding TGFβ antiproliferative effect in epithelial cells (Kretzschmar et al., 1999b). The TGFβ-Smad-ERK-AP-1 axis has also been shown to be important for increased cancer cell motility (Davies et al., 2005). The other two MAPK signalling pathways, JNK and p38, can also co-operate with Smad-canonical pathways to induce TGFβ-mediated apoptosis and p38 has been shown to play a role in reorganisation of the cell cytoskeleton in the process of EMT (Zhang, 2009). TGFβ also leads to rapid activation of Rho-pathway that is necessary for the

formation of stress fibres during EMT (Bhowmick et al. 2001). Therefore, in the present study the role of MAPK and Rho pathways in TGFβ-mediated increase in PAR-1 expression was investigated. Inhibition of MEK-ERK signalling with UO126 completely inhibited TGFβ-mediated increase in PAR-1 calcium signalling responses. Another ERK inhibitor, PD98059 had modest effect on PAR-1 functional responses. Significant differences have been identified between the two inhibitors. While UO126 is a selective and potent MEK1 and MEK2 inhibitor, PD98059 has higher affinity for MEK1, which suggests that MEK2 may be important in TGFβ-mediated PAR-1 upregulation.

Inhibition of JNK did not affect the PAR-1 functional responses while p38 inhibition appeared to induce increased PAR-1 functional responses, both at baseline and following treatment with TGFβ, suggesting that at high concentrations the inhibitor may have non-specific off-target effects. Alternatively, p38 may play a role in regulating PAR-1 expression at baseline. Inhibition of Rho signalling pathway also enhanced PAR-1 functional responses, both at baseline and following TGFβ-stimulation. Further experiments need to be performed to validate the specificity of these inhibitors and their effect on PAR-1 expression.

The alveolar epithelium has been strongly implicated in the pathogenesis of pulmonary fibrosis and increased epithelial apoptosis, hyperplasia and bronchiolisation are key features of the abnormal wound healing response in IPF. In this study, we began to delineate a potential endogenous pathway which perpetuates the generation of active TGFβ. Next it was examined whether this mechanism is also observed in primary human type II alveolar epithelial cells (AEC II) isolated from donor lungs. The phenotype of AECII was confirmed by positive staining for zona occludens (ZO-1) tight junctions and cytoplasmic prosurfactant C protein (pro-SPC). In contrast to A549 cells, primary AECII did not elicit intracellular calcium release following thrombin stimulation. Furthermore, activation of PAR-1 and PAR-2 with specific agonist peptides clearly demonstrated that AECII release intracellular calcium in response to PAR-2 activation but not PAR-1. Immunocytofluorescence studies supported the notion that low levels of PAR-1 are

expressed in the primary AECII. Furthermore, stimulation of AECII with TGFβ for 24 hours did not augment surface expression and functional responses measured in this study. These results highlight clear differences in the expression of PAR-1 and functional responsiveness to PAR-1 and PAR-2 activation between primary control AECII and A549 cell line. There are several potential explanations for these findings. The AECII used in this study were isolated from non-fibrotic human lung tissue and young donors with no evident lung pathology. Previous laser capture microdissection studies in our laboratory have shown that normal human alveolar epithelium expresses low levels of PAR-1 mRNA that is significantly upregulated in IPF epithelium (Mercer et al., 2009). It is therefore plausible that increased PAR-1 expression is associated with the abnormal phenotype of alveolar epithelial cells and the enhancement of PAR-1 expression after TGFβ stimulation is a sign of further aberrant changes to the epithelial cells. In order to investigate whether increased PAR-1 expression in hyperplastic alveolar epithelium is a consequence of the chronic reparative phenotype in IPF, these *in vitro* studies will need to be performed in the cells isolated from the fibrotic epithelium. Unfortunately, this was not achievable in the scope of this study due to the lack of available IPF tissue. In order to isolate sufficient numbers of viable AECII a large lung specimen (<150 g) is required, which greatly exceeds the size of a regular biopsy. Furthermore, the time delay between sampling of the lung and the isolation procedure dramatically decreases the viability of AECII. Sufficient amount of tissue can only be obtained in the event of a lung transplant but the relative infrequency of these operations is a major limitation.

3.1.7.4 PAR-1 expression and signalling in primary bronchial epithelial cells

Previous immunohistochemistry studies reported that the bronchial epithelium expresses all PAR receptors (Knight et al., 2001). Furthermore, bronchial basal cells constitutively express tissue factor and can assemble the TF-FVIIa-FXa ternary complex on their cell surface (Perrio et al., 2007). This local activation of coagulation cascade was found to be essential to generate fibrin scaffold and initiate wound

healing response and restoration of bronchial epithelium integrity following injury (Perrio et al., 2007). Failure of tissue factor-initiated fibrin network formation, PAR-1 and PAR-2 activation has been shown to cause basal cell apoptosis, necrosis and inefficient wound healing responses of bronchial epithelium *in vitro* (Ahmad et al., 2013).

In this study, we investigated the responses in primary bronchial epithelial cells to thrombin stimulation. After determining that the bronchial cell line BEAS2B elicits intracellular calcium release following stimulation with thrombin in concentration-dependent manner and of magnitude comparable to the responses described for fibroblasts, the same response was evaluated in primary human bronchial epithelial cells (HBECs). HBECs were grown out from large airways excised from lung tissue processed in our laboratory. For experimental purposes HBECs were seeded on collagen IV, which is the major constituent of the basement membrane and enhances cell adhesion and proliferation.

Investigation of PAR-1 and PAR-2 expression in HBECs by immunocytofluorescence and measurements of intracellular calcium release following stimulation with PAR-1 and PAR-2 agonists have provided strong evidence that HBEC basal cells express low levels of PAR-1 and high levels of PAR-2. Thrombin failed to elicit intracellular calcium release from HBECs even at high concentrations and TFLLR produced a barely detectable response. In contrast, PAR-2 activation triggered a robust calcium flux. High concentrations of FXa were required to elicit delayed intracellular calcium flux of low magnitude albeit of prolonged duration. Furthermore, this response could be blocked with the PAR-2 antagonist, GB83, which suggests that in this system high FXa concentrations are capable of activating PAR-2-$G\alpha_q$ signalling. Interestingly, despite low PAR-1 expression in these cells, RWJ58259 significantly reduced the FXa-mediated calcium flux. This suggests that even at low expression levels, PAR-1 activation contributes to PAR-2-mediated calcium signalling responses.

Immunocytofluorescence studies further confirmed that expression of PAR-1 on the basal cell surface is sparse while PAR-2 is abundantly expressed. The mature bronchial epithelium is composed of different, specialised and fully-polarised cell

types and PAR expression may be different compared with that observed in submerged culture composed primarily of basal cells. In order to address this question, basal cells were cultured at air-liquid interface and differentiated into a pseudostratified cell layer. The differentiation process takes three weeks and once completed cells cannot be passaged and therefore it was impossible to perform intracellular calcium functional assay in the mature epithelium. Therefore, PAR expression was assessed by immunocytofluorescence only. As observed in basal cells, PAR-2 was found to be abundantly expressed in the differentiated bronchial epithelium and localised to apical side whereas PAR-1 expression remained consistently low in the bronchial epithelium. We concluded that PAR-2 is expressed at high levels both in basal cells and in fully differentiated bronchial epithelium while PAR-1 is scarcely detected. Immunocytofluorescence study of fully differentiated cells was also performed after exposure to TGFβ for 24 hours but there were no differences in PAR-1 and PAR-2 expression. It is possible that exposure to TGFβ for 24 hours is not sufficient to induce changes in PARs expression. It has been shown that HBECs undergo EMT after 72 hour exposure to TGFβ (Câmara and Jarai, 2010).

Previous studies have reported that HBECs secrete IL-6 and IL-8 following stimulation with PAR agonist peptides (Asokananthan et al., 2002). In this particular study HBECs were stimulated for 24 hours with TFLLR and SLIGKV and showed a modest increase in cytokine levels with PAR-1 activating peptide and a robust response with SLIGKV. These data are in agreement with our observations that PAR-2 is the main PAR receptor present on these cells.

Calcium signalling in the bronchial epithelium is essential for regulating airway tension (Borchers et al., 2003) as wells as for the release of inflammatory mediators. Interestingly in chronic lung disease and infection it has been shown that the hypersensitivity to GPCR-mediated intracellular calcium signalling can be achieved by expansion of the endoplasmic reticulum and hence calcium stores (Ribeiro, 2011). PAR-2 mediates multiple protective effects in the airway epithelium including promoting bronchodilation through induction of cyclooxygenase 2 (COX 2)

and stimulation of PGE_2 production (Cocks et al., 1999; Morello et al., 2005). Furthermore, PAR-2 is upregulated on the respiratory epithelium of asthmatic patients (Knight et al., 2001) and in animal models of allergic airway inflammation lack of PAR-2 protects from excessive inflammatory response while PAR-2 overexpression drives eosinophilia (Schmidlin et al., 2002). PAR-1 expression in the asthmatic bronchial epithelium remains low but thrombin-mediated PAR-1-activation in airways smooth muscle cells induces increase in cytosolic calcium and bronchoconstriction (Hauck et al., 1999). Moreover, lack of PAR-1 expression in the lung is protective from goblet cell metaplasia in the experimental model of COPD (Atzori et al., 2009). There is also evidence showing that both PAR-1 and PAR-2 are upregulated in the LPS-induced acute lung injury (Jesmin et al., 2007). It is possible that in the normal respiratory epithelium, including both bronchial and alveolar epithelium, PAR-2 is highly expressed at baseline and the expression increases in certain disease states, while PAR-1 is expressed at low levels in normal epithelial cells and the expression only increases following persistent and chronic injury to the epithelium.

3.1.7.5 PAR-1 expression and signalling in endothelial cells

Endothelial cells express all four PARs but signalling via PAR-1 and PAR-2 rather than PAR-3 and PAR-4 have been shown to contribute to most of the functional responses in health and disease (Bunnett, 2006). PAR-1 signalling in the endothelium has been shown to elicit different responses depending on the activating proteinases, as well as other cellular mechanisms set in place to control PAR-1-mediated functional responses. Intracellular calcium signalling downstream of thrombin-mediated PAR-1 activation leads to cytoskeletal rearrangement and endothelial cells contraction that results in loss of endothelial barrier integrity and interstitial oedema (Tiruppathi et al., 2002). Interestingly, while high thrombin concentrations increase vascular permeability, at low thrombin concentration PAR-1-mediated signalling is barrier protective (Feistritzer and Riewald 2005). Bioactive lipid sphingosine 1 phosphate (S1P) expressed on the cell surface and activated protein C (APC) have the capacity to modulate thrombin signalling and promote the

restoration of vascular barrier integrity (Feistritzer and Riewald 2005). APC can also cleave PAR-1 directly to elicit cytoprotective signalling (Yang et al., 2007) and cleaved PAR-1 is retained on the cell surface providing an endogenous desensitisation system (Schuepbach et al. 2008). APC and thrombin exert their enzymatic activity at distinct cleavage sites on PAR-1 N-terminus, which could also explain different cellular effects. Thrombin unmasks the tethered ligand at arginine 41 (R41) while APC cleaves PAR-1 at arginine 46 (R46) (Schuepbach et al. 2012). The affinity of thrombin to cleave PAR-1 is several magnitudes higher than for APC albeit APC augments PAR-1 signalling in other ways. Recruitment of PAR-1 to lipid rafts and interaction with APC bound to its receptor, EPCR, prevents excessive thrombin cleavage of PAR-1 and switches its function to being barrier protective (Bae et al. 2007). FXa has also been shown to exert protective responses in endothelial cells through the activation of PAR-2 but also by enhancing the interaction between EPCR and PAR-1 (Bae et al. 2010). Furthermore, FXa signalling in both PAR-1 and PAR-2 has been shown to counteract thrombin-induced vascular permeability (Feistritzer et al. 2005).

The intricacies of the spatial and temporal regulation of thrombin-PAR-1 signalling in the endothelial cells have been demonstrated *in vivo.* Infusion of PAR-1 agonist peptide into the circulation increases vascular permeability by 75% as measured by Evans blue dye-assessed pulmonary oedema (Kaneider et al., 2007). However, targeting of thrombin or PAR-1 signalling during the early phase of sepsis model offered protection and improved survival, while the same approaches applied during the late stages of sepsis proved detrimental. Moreover, therapeutic administration of PAR-1 agonists improved survival rate while PAR-1 antagonism exacerbated vascular leak and mortality in the model of sepsis. Interestingly, late PAR-1 cytoprotective effects have been linked to PAR-1-mediated PAR-2 transactivation (O'Brien et al., 2000) and selective activation of distinct G-proteins (Kaneider et al., 2007). The initial vascular leak occurs via activation of the thrombin-PAR-1-$G\alpha_{12/13}$-Rho GTPase signalling axis that orchestrates endothelial cell shape change. PAR-1-PAR-2 heterodimer formation and a shift towards activation of

the $G\alpha_i$-dependent pathway was associated with restoration of barrier integrity (Kaneider et al., 2007).

In the present study, HUVECs were used as model endothelial cells of large vessels and as expected showed robust intracellular calcium release following stimulation with thrombin in a concentration-dependent manner. PAR-1 and PAR-2 agonist peptides also elicited robust responses that were of similar magnitude and duration. Consistent with observations for other cell types, the FXa-mediated calcium flux was delayed and was of lower magnitude.

Specific PAR-1 and PAR-2 inhibitors were again used to investigate the contribution of PAR-1 and PAR-2 signalling responses in HUVECs. PAR-1 antagonists fully blocked the calcium response following thrombin stimulation but the PAR-2 inhibitor also significantly reduced it by around 25%. FXa-mediated signalling was fully blocked by the endogenous inhibitor, antithrombin III, and a partial block was obtained with PAR-1 and PAR-2 antagonists. As mentioned before, PAR-1 and PAR-2 can form heterodimers and have been shown to signal together in response to FXa (Feistritzer et al. 2005). The results presented in this section support the notion that thrombin- and FXa-mediated intracellular calcium release is an additive effect of signalling via both receptors.

Thrombin-PAR-1-signalling axis in large vessels has been thoroughly investigated but the nature of these responses in the primary human lung microvascular endothelial cells is not known. Injury to the microvascular endothelium in IPF has been described with evidence of areas of necrosis, denudation and collagen deposition in the basement membrane (Magro et al., 2006). Furthermore, these changes were found to be associated with the deposits of auto-antibodies in capillary vessels that showed reactivity to epitopes expressed by the microvascular endothelium, supporting the notion that the pathogenesis of IPF may have an autoimmune component (Magro et al., 2006). Although the question of autoimmunity as part of IPF pathogenesis is controversial, strong antibody reactions to endothelial epitopes correlate with pulmonary fibrosis secondary to systemic sclerosis (Ihn et al., 2000). In experimental pulmonary fibrosis bleomycin is also

highly cytotoxic for the microvascular endothelium (Patel et al., 2011). While in large vessel endothelial cells thrombin signalling is mainly barrier disruptive, different responses have been reported for microvascular endothelial cells. In rat lung microvascular endothelial cells thrombin and PAR-1 activating peptides increased the barrier integrity and reduced formation of stress fibres and paracellular gaps *in vitro* (Troyanovsky et al., 2008). In contrast, in LPS model of ALI targeting PAR-1 reduced vascular leak and neutrophilia (Mercer et al., 2013).

To our knowledge, PAR-1 and PAR-2 signalling responses to coagulation proteinases have never been evaluated in primary human lung microvascular endothelial cells and therefore the aim of this part of the present study was to examine the intracellular calcium response downstream of PAR-1 and PAR-2 activation in HMLECs. Thrombin elicited a robust signalling response that was concentration-dependent, while PAR-1 and PAR-2 agonist peptides also triggered strong signalling responses. The high level of PAR-1 and PAR-2 expression was also visualised by immunocytofluorescence. In contrast, FXa elicited a barely detectable wave of calcium signalling. The thrombin response was fully inhibited by the PAR-1 antagonist suggesting that in the lung microvascular endothelium the responsiveness to thrombin is PAR-1-mediated.

Taken together, this study has shown a differential distribution and levels of expression of PAR-1 receptor in the lung while PAR-2 appears to be expressed in all cell types tested. However, this study has highlighted that lung fibroblasts and lung microvascular endothelial cells are sensitive to low thrombin concentrations and respond to thrombin in entirely PAR-1-dependent manner. In contrast, normal bronchial and alveolar epithelial cells do not appear to express sufficient PAR-1 expression to be sensitive to thrombin signalling. PAR-1 expression can be upregulated in the abnormal alveolar epithelium in response to TGFβ-signalling. This response was ALK5/Smad3- and ERK-dependent.

3.1.7.6 Conclusion and future work

The aetiology of IPF remains enigmatic and current paradigms place lung epithelial cell injury as an initiating event in the development of fibrosis that is subsequently driven by dysregulated wound healing responses. Epithelial damage and destruction of the alveolar-capillary basement membrane allows fibroblast infiltration into the alveolar parenchyma, their proliferation, differentiation into myofibroblasts and excessive extracellular matrix protein deposition. Increasingly, bronchial epithelial dysfunction has also been implicated in the progression of fibrosis (Peljto et al., 2013). Markers of endothelial damage are detected in samples from IPF patients (Collard et al., 2010) and damage to the lung microvasculature and abnormal re-modelling of vessels often leads to the development of a common complication of IPF, namely pulmonary hypertension (Hanumegowda et. al 2012). Extensive evidence accumulated over the years highlights the complexity of intercellular interactions that contribute to the pathogenesis of IPF.

The persistent activation of the coagulation cascade and dysregulated fibrinolysis play key roles in the establishment and propagation of the fibrotic response to lung injury. The local activation of the coagulation cascade drives lung fibrosis independently of activation of the systemic coagulation (Scotton et al. 2009). Although the homeostatic alveolar environment is anticoagulant and pro-fibrinolytic (reviewed in Chambers 2008), it contains all the components required to trigger the extrinsic coagulation cascade. Tissue factor is upregulated on hyperplastic epithelial cells (Imokawa et al. 1997) and alveolar macrophages isolated from patients with sarcoidosis produce FVII (Chapman et al. 1985). Both alveolar and bronchial epithelia have been shown to synthesise and express FX/FXa. Therefore the ternary complex that initiates the extrinsic coagulation cascade and thrombin generation can be assembled in the alveolar microenvironment and indeed immunohistochemical analysis show colocalisation of TF/FVIIa/FXa in injured epithelium overlying fibrotic foci (Scotton et al. 2009).

PAR-1 mediates multiple cellular effects of coagulation proteinases and it is upregulated in the fibrotic lung (Mercer et al., 2009). PAR-2 is also activated by

coagulation proteinases and there is evidence supporting the role of PAR-2 in IPF (Wygrecka et al., 2011). The aim of this study was to investigate the PAR-1- and PAR-2-mediated signalling responses to thrombin and FXa in distinct primary human lung cell populations.

Coagulation proteinases can activate PAR-1 and elicit robust intracellular calcium response (Blanc-Brude et al., 2005). The calcium flux results from $G\alpha_q$ uncoupling and phospholipase C-mediated inositol trisphosphate (IP3) generation. IP3 binds to its receptor on the endoplasmic reticulum which opens the calcium store and leads to rapid increase in cytosolic calcium. The spatial and temporal distribution of the calcium wave is proportionate to surface expression of the receptor (Bootman et al., 1997a). In order to ensure that full activation of specific receptor was achieved, PAR-1 and PAR-2 agonist peptides were used and compared with thrombin and FXa signalling.

In this study, primary human lung fibroblasts and microvascular endothelial cells were identified as cells strongly responsive to thrombin stimulation and expressing high levels of PAR-1. All human cell populations investigated in this study expressed PAR-2 and in the alveolar and bronchial epithelium PAR-2 activation with the agonist peptide led to stronger calcium signalling responses when compared to PAR-1 activation by the agonist peptide. In alveolar epithelial cells PAR-1 expression was associated with abnormal phenotype and was further enhanced with TGFβ stimulation. The results of this study provide unique insights into the expression pattern of PAR-1 and PAR-2 in the normal lung setting, which was also confirmed by immunohistochemical analysis. This study also shows that the PAR-1 and PAR-2 expression pattern can change with exposure to a profibrotic mediator. Furthermore, these results highlight differences in the signalling pathways between the two major coagulation proteinases, thrombin and FXa.

Intracellular calcium release measured in this study was a summation of calcium waves generated through activation of many receptors over a short period of time. The number of receptors activated with high frequency and close functional coupling are proportionate to the upstroke velocity and magnitude of the response

(Bootman et al. 1997). TFLLR and SLIGKV specifically and directly activated PAR-1 and PAR-2, respectively, and produced the strongest and most rapid calcium fluxes that were consistent with the receptor expression pattern on the cell surface. While thrombin acted mainly through PAR-1-$G\alpha_q$, FXa consistently showed delayed responses of lower magnitude for all cell populations examined. This is consistent with the notion that FXa is a lower affinity agonist of the PAR-1 receptor and requires more time to efficiently dock and cleave the N-terminus. This would also explain the temporal delay and spatial decrease of the signal since low affinity agonists can act in an equivalent mode as low-concentration high affinity agonists. It has been previously reported that low affinity agonists trigger small calcium blips that fail to reach the frequency to generate a global wave (Bootman et al. 1997).

As the technology to measure and image cellular signalling is rapidly expanding, the traditional consensus stating that individual G-proteins uncouple from the receptor upon activation has now been replaced in favour of simultaneous activation of multiple G-proteins leading to concurrent activation of second messengers (McCoy et al., 2012). It is plausible that FXa causes uncoupling of multiple G-proteins from both PAR-1 and PAR-2 and $G\alpha_q$ uncoupling is a small fraction of the overall FXa-mediated signalling response, which could explain the lower magnitude of the observed response in comparison to thrombin. This reasoning is further supported by abundant evidence for biased agonism signalling properties of GPCRs (Mosnier et al. 2012; Vaidehi and Kenakin 2010; Russo at al. 2009). Furthermore, allosteric modulators, such as β-arrestin, have been shown to add another level of complexity to PAR signalling pathways by being able to affect G-protein uncoupling, second messenger recruitment, phosphorylation and internalisation of the receptor (Gao and Jacobson, 2013; Lin and Trejo, 2013).

Whilst the current study has explored the $G\alpha_q$-mediated release of intracellular calcium, a comprehensive assessment of other signalling pathways downstream of thrombin and FXa stimulation would provide a more complete scope of biological effects triggered by coagulation proteinases. Studies aimed at expanding the understanding of the relationship between PAR-1 and PAR-2 signalling, heterodimer

formation and the effect on activation and downstream signalling are also required in multiple lung cell types that are affected in disease.

3.2 Pro-inflammatory thrombin signalling in human lung fibroblasts.

3.2.1 Introduction

Previous work in our laboratory demonstrated that cultured human and murine fibroblasts constitutively secrete CCL2 over time. These responses increase dramatically upon stimulation with thrombin in a time- and concentration-dependent manner (Deng et al., 2008; Ortiz-Stern et al., 2012). The levels of CCL2 in fibroblast supernatants increase significantly from 6 hours onwards and this response is maintained until at least 24 hours post-stimulation. Furthermore, as little as 0.3 nM thrombin elicits significant upregulation of CCL2 production. Our laboratory also showed that in murine fibroblasts thrombin-mediated CCL2 release is entirely PAR-1-dependent and occurs downstream of $G\alpha_q$-induced calcium signalling (Deng et al., 2008). The aim of this study was to advance our understanding of thrombin-mediated CCL2 release by primary human lung fibroblasts. The results presented in this section form a part of publication: "PAR-1-dependent and PAR-independent pro-inflammatory signalling in human lung fibroblasts." A. Ortiz-Stern et al., Journal of Cellular Physiology, 2012, which is attached as **Appendix 2.**

3.2.2 Thrombin-mediated CCL2 release from human lung fibroblasts

In order to determine whether thrombin-mediated CCL2 release from human fibroblasts is PAR-1 dependent, two PAR-1 specific small molecule inhibitors were used: RWJ58259 (Damiano et al., 2003) and SCH530348 (Bonaca and Morrow, 2009). The dose of the RWJ58259 was previously optimised in our laboratory for both murine fibroblasts (Deng et al., 2008) and human fibroblasts **(Appendix 2, Figure 2C)**. In the first series of experiments, the efficacy of the antagonist in blocking CCL2 release was tested in both murine and human fibroblasts. As shown in **Figure 3.38A**, exposure of murine fibroblasts to thrombin (10 nM) for 6 hours led to a 2.5-fold increase in CCL2 levels in the supernatants and this response was fully

inhibited by both PAR-1 antagonists. In contrast, stimulation of human fibroblasts with thrombin (10 nM) for 6 hours led to a 10-fold increase in the amount of CCL2 released in the supernatants (**Figure 3.38B**). RWJ58259 and SCH530348 only partially inhibited this response.

Since both PAR-1 antagonists did not fully block CCL2 release by human lung fibroblasts, the next question was whether in human fibroblasts the CCL2 response is entirely thrombin-dependent. To address this question we first assessed whether thrombin enzymatic activity is necessary for the CCL2 response by using hirudin, a peptide naturally produced in the salivary glands of medicinal leeches, which forms non-covalent and irreversible bonds with thrombin and renders it catalytically inert. As previously observed thrombin stimulation of human fibroblasts for 6 hours significantly increased CCL2 release into the cell supernatants and this response was fully inhibited when thrombin enzymatic activity was inhibited by hirudin (**Figure 3.39**). Subsequently, the inhibitory effects of RWJ58259 and hirudin on CCL2 release by human fibroblasts were tested at different thrombin concentrations. RWJ58259 is a reversible PAR-1 antagonist that binds to the second extracellular loop of the receptor and thus does not interfere with thrombin-mediated cleavage of the tethered ligand. Another question addressed in this study was therefore whether the partial inhibition of the CCL2 release by RWJ58259 was a consequence of the displacement rate of the antagonist from the receptor and the tethered ligand triggering a response. In order to begin to examine this possibility, hirudin was added to fibroblasts after they had been exposed to thrombin for 30 minutes. As previously described thrombin induces CCL2 release in a concentration-dependent manner. Delayed thrombin inhibition by hirudin (added after 30 minutes) significantly reduced CCL2 levels by at least 70% at all thrombin concentrations tested (**Figure 3.40**) and following the short-term exposure to thrombin, CCL2 was only significantly elevated above the baseline at the highest thrombin concentration (10 nM). This suggests that the high CCL2 levels accumulated in the supernatants after 6 hours result from prolonged and constant thrombin stimulation. Consistent with previous experiments RWJ58259 did not fully block thrombin-induced CCL2 release by human lung fibroblasts at any concentration tested. In contrast,

combined treatment of RWJ58259 and hirudin achieved a similar level of inhibition of CCL2 release as observed with hirudin alone at all thrombin concentrations. Taken together, these data supported the previous results that the CCL2 release from human fibroblasts is thrombin-dependent but not exclusively mediated by PAR-1.

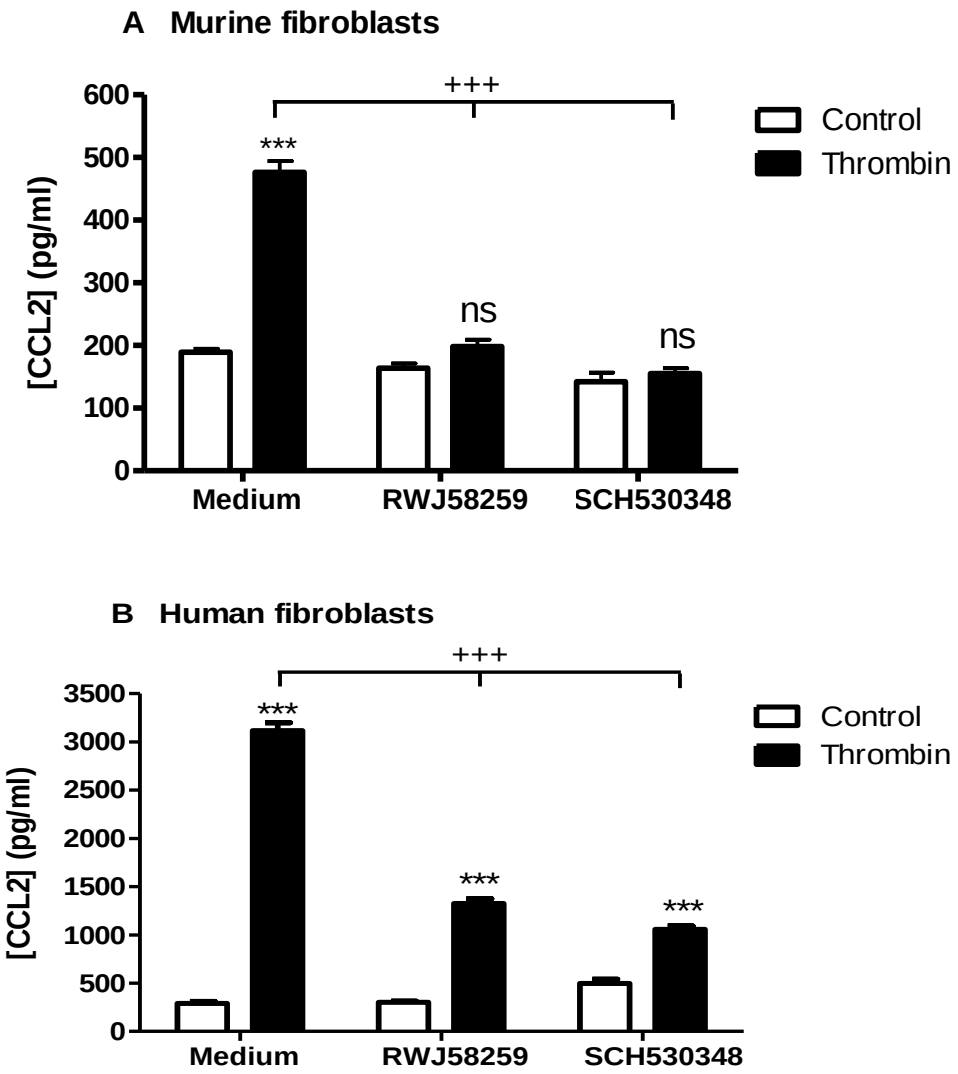

Figure 3.38. RWJ58259 and SCH530438 inhibit CCL2 release in murine and human lung fibroblasts.

Primary murine- panel A and human- panel B lung fibroblasts were seeded in 48-well plates at a density of $2x10^4$ cells/well and serum starved for 24 hours. Cells were pre-incubated with RWJ58259 or SCH530348 (3 µM) for 30 minutes before the addition of thrombin (10 nM). CCL2 levels in cell supernatants after 6 hours of incubation were quantified by ELISA. Data show mean +/- SEM of 6 replicates; two-way ANOVA ***p<0.001 comparison with basal CCL2 production, +++ p<0.001 comparison with thrombin stimulated cells.

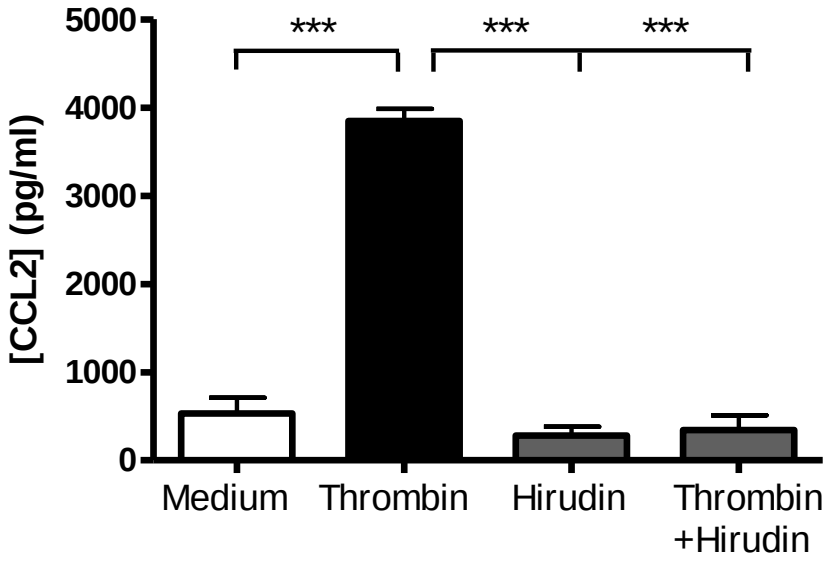

Figure 3.39. Inhibition of thrombin enzymatic activity by hirudin abolishes its stimulatory effect on CCL2 release by human lung fibroblasts.

Primary human lung fibroblasts were seeded in 48-well plates at a density of $2x10^4$ and serum-starved for 24 hours prior to the experiment. Cells were subsequently stimulated with thrombin (10 nM) or thrombin (10 nM) pre-incubated with (50 nM) hirudin for 1 hour. After 6 hours, cell supernatants were collected and CCL2 levels measured by ELISA. Data show mean +/- SEM of 4 replicates; one-way ANOVA, ***$p<0.001$ comparison with thrombin alone stimulated cells.

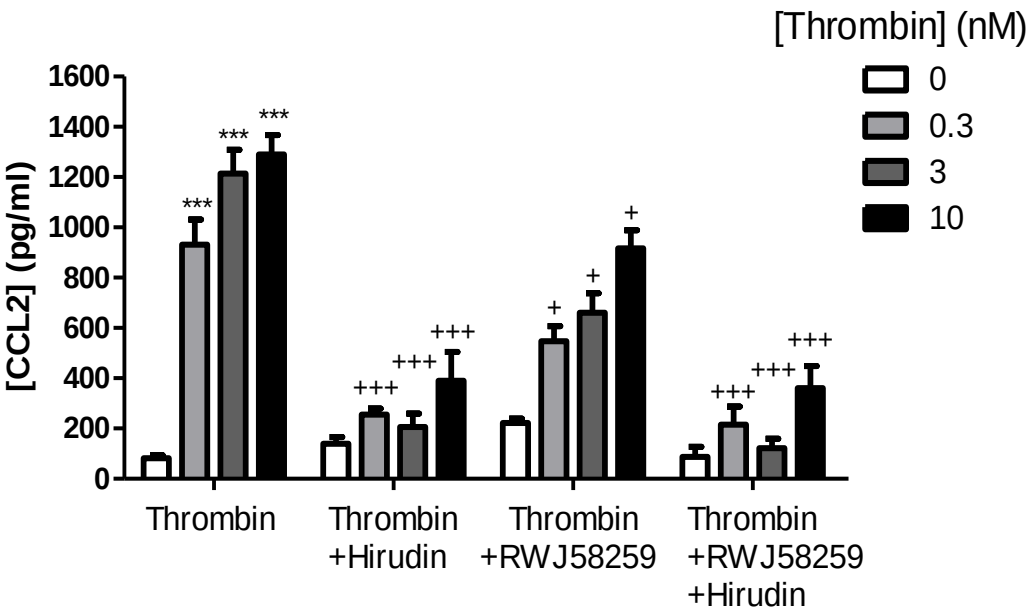

Figure 3.40. Delayed inhibition of thrombin catalytic activity abolishes CCL2 release while blocking PAR-1 only partially reduces CCL2 release in human lung fibroblasts.

Primary human lung fibroblasts were seeded in 96-well plates at a density of 10^4 cells/well and serum-starved for 24 hours. Cells were the pre-incubated with RWJ58259 (3 μM) for 30 minutes before addition of thrombin at indicated concentrations. Following another 30 minutes hirudin (50 nM) was added to designated wells. Level of CCL2 in the supernatants after 6 hours of incubation was quantified by ELISA. Data show mean +/- SEM of 4 replicates; two-way ANOVA, ***p<0.001 comparison with basal CCL2 production, +p<0.05, +++ p<0.001 comparison with thrombin alone at respective concentrations.

3.2.3 Thrombin-mediated intracellular calcium release in lung fibroblasts

As demonstrated in the previous section thrombin enzymatic activity is required for CCL2 release from primary human lung fibroblasts but PAR-1 specific antagonists do not fully block this response. The efficacy of the PAR-1 antagonists was subsequently tested in different PAR-1-mediated signalling responses. Both SCH530348 and RWJ58259 are small molecule competitive PAR-1 inhibitors but have different chemical properties that affect the nature of binding to the receptor. RWJ58259 is considered to be a reversible antagonist whereas SCH530348 binding to the receptor has been characterised to be virtually irreversible (Zhang et al., 2012). Considering that thrombin has a high affinity for the receptor and persists in the supernatant for up to 72 hours (Ortiz-Stern et al., 2012), it was possible that at high, yet standard, thrombin concentration (10 nM) RWJ58259 may be displaced by the activated tethered ligand at a fast enough rate to result in only partial inhibition of PAR-1 mediated CCL2 release. To pursue this question further, the efficiency of RWJ58259 inhibition was tested by monitoring the release of intracellular calcium, which is an immediate response that occurs within seconds of thrombin-mediated PAR-1 cleavage. Furthermore, in murine fibroblasts, intracellular calcium release downstream of PAR-1 activation was previously shown to be essential for CCL2 release (Deng et al., 2008).

As characterised in the previous chapter of this thesis and reproduced in **Figure 3.41A**, primary human lung fibroblasts signal robustly to thrombin and the magnitude of calcium response is thrombin concentration-dependent. At low concentration (0.3 nM) thrombin evoked a delayed intracellular calcium release of low magnitude and at high concentrations (3 nM and 10 nM) thrombin elicited a rapid and sharp signal. Nonetheless, at all thrombin concentrations RWJ58259 (3 µM) fully inhibited the release of intracellular calcium (**Figure 3.41B**).

Next, the PAR-1 antagonists, RWJ58259 and SCH530348, were tested over a range of concentrations in human and murine fibroblasts at fixed thrombin concentration (10 nM). As shown in **Figure 3.42,** both PAR-1 antagonists fully blocked intracellular

calcium release at a standard thrombin concentration of 10 nM with an IC_{50} of 12 nM and 0.9 nM in murine fibroblasts and 120 nM and 60 nM in human fibroblasts for RWJ58259 and SCH530348, respectively.

Taken together, these data support the notion that the antagonists used in this study are potent inhibitors of PAR-1-mediated intracellular calcium responses, regardless of thrombin concentration. It is therefore possible that the lack of full inhibition of CCL2 release observed in human lung fibroblasts is due to other non-PAR-1 signalling pathways contributing to thrombin-mediated CCL2 release.

In order to confirm that intracellular calcium release is essential for CCL2 release by human lung fibroblasts, the calcium chelator BAPTA-AM was used to inhibit the calcium flux and the levels of CCL2 measured subsequently. As shown in **Figure 3.43**, BAPTA-AM blocked CCL2 release in a concentration-dependent manner with complete inhibition observed at 2 μM.

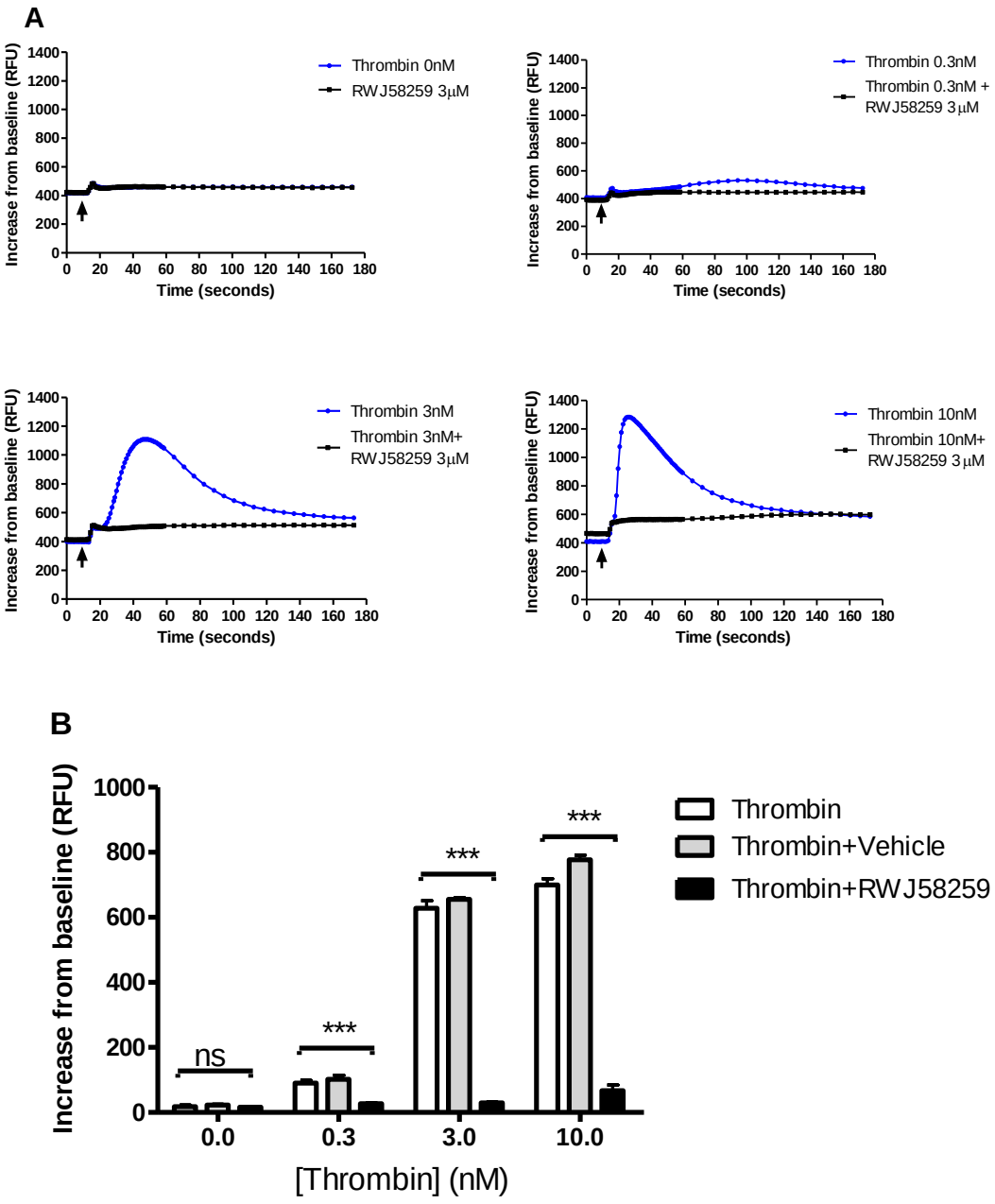
A
Increase from baseline (RFU)
Time (seconds)
Thrombin 0nM
RWJ58259 3μM
Thrombin 0.3nM
Thrombin 0.3nM + RWJ58259 3μM
Thrombin 3nM
Thrombin 3nM+ RWJ58259 3μM
Thrombin 10nM
Thrombin 10nM+ RWJ58259 3μM
B
Increase from baseline (RFU)
ns
***
***
***
0.0
0.3
3.0
10.0
[Thrombin] (nM)
Thrombin
Thrombin+Vehicle
Thrombin+RWJ58259

Figure 3.41. Thrombin-mediated intracellular calcium release in primary human lung fibroblasts is inhibited by the PAR-1 specific antagonist RWJ58259.

Primary human lung fibroblasts were seeded in 96-well plates at a density $1x10^4$ and serum starved for 24 hours. Cells were incubated with Fluo-4AM calcium binding alone or with addition of 3 µM RWJ58259 in 0.1% DMSO vehicle an hour before being exposed to thrombin at the indicated concentrations (0, 0.3, 3 and 10 nM). Intracellular calcium release was monitored by FLIPR® Tetra with calcium baseline recorded for 10 seconds before thrombin addition as indicated by the arrow and the response was measured for 170 seconds thereafter. Panel A shows representative calcium traces and panel B shows a quantification of the traces with data presented as increase from baseline in relative fluorescence units (RFU), mean +/- SEM of 4 replicates, two-way ANOVA, ***$p<0.001$ comparison to thrombin response.

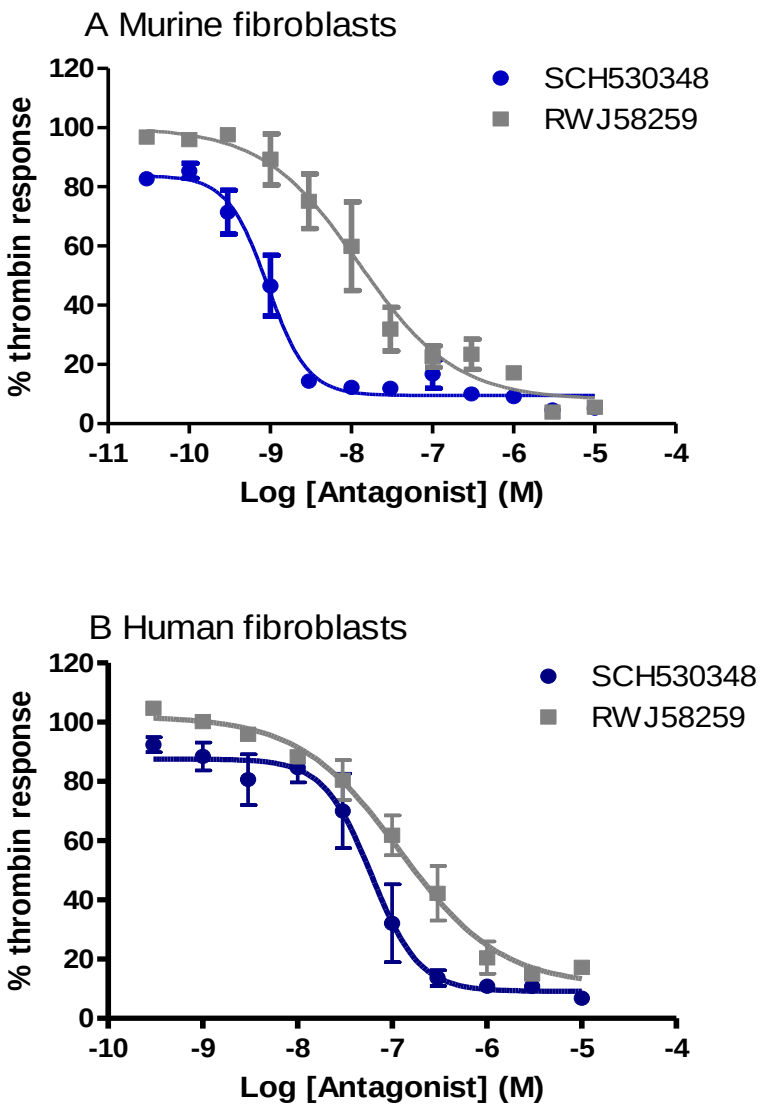

Figure 3.42. RWJ58259 and SCH530348 are potent inhibitors of PAR-1-mediated intracellular calcium release by human and murine fibroblasts.

Human and murine primary lung fibroblasts were seeded at a density of $1x10^4$ in 96-well plates and serum-starved 24 hours. Cells were incubated with Fluo-4AM calcium binding alone or with different concentrations of RWJ58259 and SCH530348, an hour before being exposed to thrombin (10 nM). The release of intracellular calcium was monitored by FLIPR® Tetra with calcium baseline recorded for 10 seconds before thrombin addition as indicated by the arrow and the response was measured for 170 seconds thereafter. Concentration-inhibition plots are presented for A- murine lung fibroblasts and B- human lung fibroblasts. Each data point represents the mean +/- SEM of 3 replicate wells.

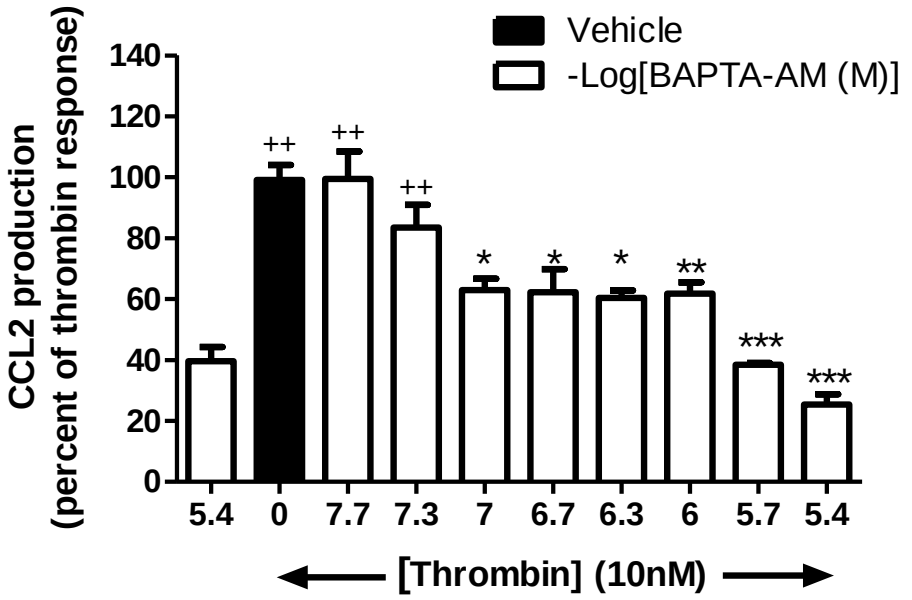

Figure 3.43. The intracellular calcium chelator BAPTA-AM abrogates thrombin-PAR-1 mediated CCL2 release in a concentration-dependent manner in primary human lung fibroblasts.

Primary human lung fibroblasts were seeded in 96-well plates at a density of 10^4 cells/well and serum starved for 24 hours. Cells were then pre-incubated with increasing concentrations of BAPTA-AM calcium chelator for 30 minutes before exposure to thrombin (10 nM) for 6 hours. Data are presented as a percentage of the maximal thrombin response. Inhibitor vehicle was 0.1% DMSO and was kept constant for all treatment conditions. The first bar represents the highest concentration of the inhibitor tested and shows no significant effect on basal CCL2 production. CCL2 levels in cell supernatants were quantified by an ELISA and one-way ANOVA was performed for statistical analysis. Data show mean +/- SEM of 3 replicates; ++$p<0.01$ comparison with vehicle control, ***$p<0.001$, **$p<0.01$, *$p<0.05$ comparison with thrombin alone.

3.2.4 Contribution of other PARs to thrombin-mediated signalling in lung fibroblasts

In order to further investigate the pathways leading to CCL2 release by human lung fibroblasts in response to thrombin, the contribution of other PAR receptors was examined. As reported by our group as well as in other studies, human lung fibroblasts express PAR receptors 1-3 at the mRNA level and low levels of PAR-4 (Ortiz-Stern et al., 2012; Ramachandran et al., 2007; Sokolova et al., 2005). We used PAR-specific small agonist peptides, which mimic the amino acid sequence of the tethered ligand inherent to each PAR receptor, to assess intracellular calcium flux and CCL2 release downstream of PAR activation. As demonstrated in **Figure 3.44A**, the PAR-1 activating peptide, TFLLR elicited a calcium response of the same magnitude and pattern as thrombin at standard concentration (10 nM). A reverse control peptide RLLFT had no effect on the response.

Although PAR-2 is not directly activated by thrombin, current evidence suggests that at high thrombin concentration the unmasked tethered ligand of PAR-1 can transactivate PAR-2 in endothelial cells (Kaneider et al., 2007; O'Brien et al., 2001). Furthermore, PAR-2 also couples to $G\alpha_q$ (McCoy et al. 2010) and hence is capable of triggering calcium signalling responses. As shown in **Figure 3.44B**, the PAR-2 activating peptide, SLIGKV, induced intracellular calcium release but the response was delayed and of lower magnitude when compared to thrombin at standard concentration or TFLLR (**Figure 3.44A)**. Furthermore, experiments performed by Dr Ortiz-Stern showed that SLIGKV triggered a small but significant increase in the CCL2 release from human lung fibroblasts after 24 hours of stimulation **(Appendix 2, Figure 3B)**. However, knocking down PAR-2 expression with siRNA in human lung fibroblasts did not alter the responsiveness of the cells to TFLLR and did not affect the inhibition level achieved with RWJ58259 **(Appendix 2, Figure 3C)**.

PAR-3 has a short cytoplasmic tail and is generally considered not to signal independently but act as a co-receptor and allosteric modulator to amplify signalling via other PARs (Madhusudhan et al. 2011; Vidwan et al. 2010; McLaughlin et al. 2007). However, other studies have indicated the possibility that PAR-3 is

capable of autonomous signalling (Ostrowska and Reiser, 2008). To test the signalling capacity of PAR-3 in human lung fibroblasts, the PAR-3 activating peptide, TFRGAP was used but failed to trigger intracellular calcium release (**Figure 3.44C**). Furthermore, PAR-3 activation had no impact on supernatant CCL2 levels at either 6 hours (**Figure 3.45A**) or after 16 hours (**Figure 3.45B**) of stimulation at a range of TFRGAP concentrations. In contrast, the PAR-1 activating peptide, TFLLR, induced a significant increase in CCL2 levels.

Finally, PAR-4 is expressed at low levels in fibroblasts and the AYPGKF activating peptide did not induce increase in intracellular calcium (**Figure 3.44D**) or CCL2 release over prolonged period of time **(Appendix 2, Figure 3E)**.

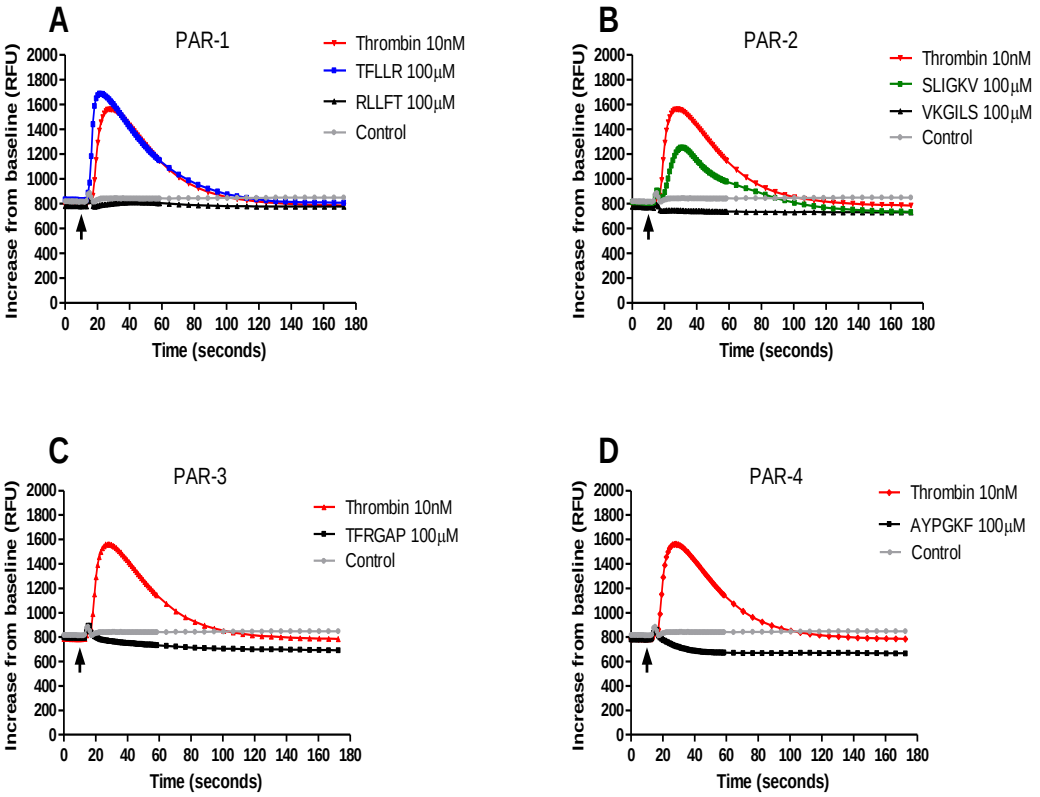

Figure 3.44. Activation of PAR-1 and PAR-2 but not PAR-3 and PAR-4 induces intracellular calcium fluxes in primary human lung fibroblasts.

Primary human lung fibroblasts were seeded in 96-well plates at density 1x10^4, serum starved for 24 hours and incubated with Fluo-4AM calcium binding for one hour prior to stimulation with thrombin (10 nM) or the respective PAR activating peptides- A- PAR-1 TFLLR, B- PAR-2 SLIGKV, C- PAR-3 TFRGAP, D- PAR-4 AYPGKF (each at 100 µM). PAR-1 and PAR-2 reverse control peptides were used to confirm specificity, RFLLT and VKGILS (each at 100 µM) respectively. Intracellular calcium release was monitored by FLIPR® Tetra with calcium baseline recorded for 10 seconds before thrombin addition as indicated by the arrow and measured for 170 seconds thereafter. Representative traces are presented as increase from baseline in relative fluorescence units (RFU) and represents the mean +/- SEM of 4 replicates.

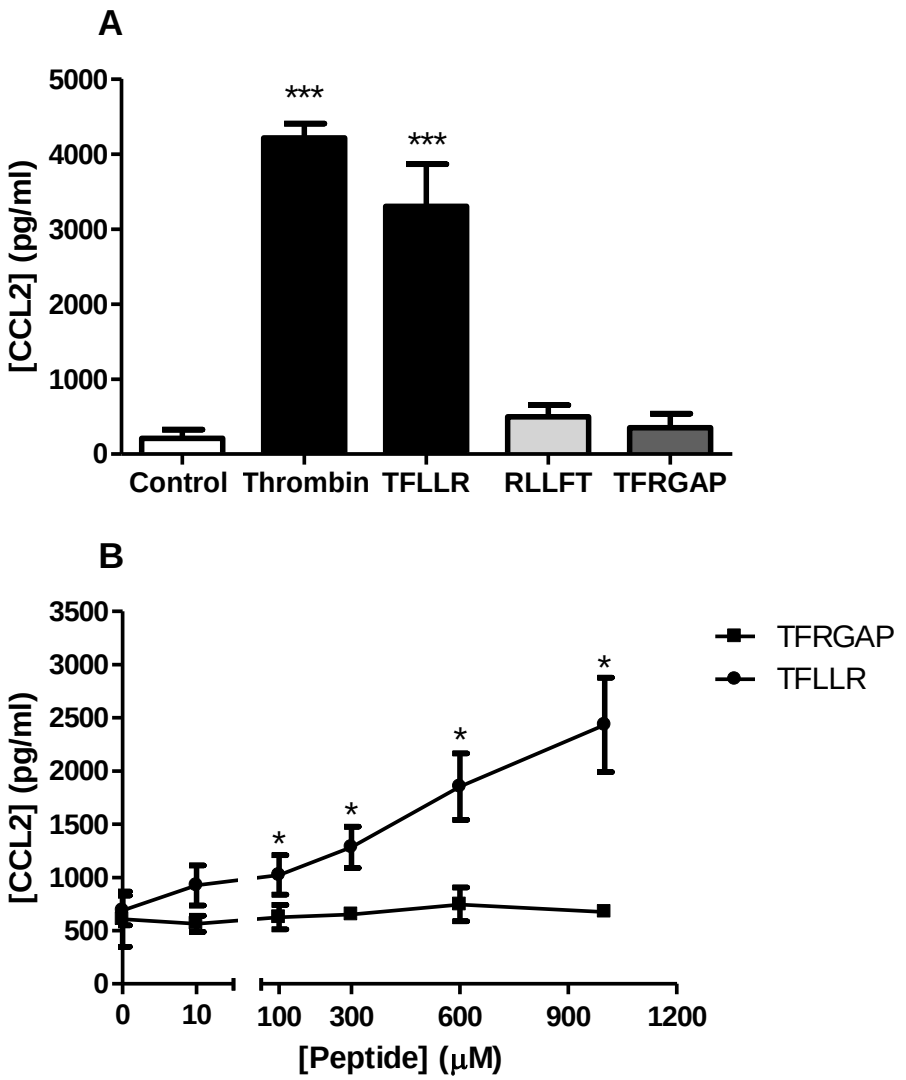

Figure 3.45. The PAR-3 activating peptide does not induce CCL2 release by human lung fibroblasts.

Panel A: Human lung fibroblasts were seeded in 48-well plates at a density $2x10^4$ cells/well, and serum-starved for 24 hours. Cells were subsequently stimulated with thrombin (10 nM), PAR-1 agonist- TFLLR, PAR-3 agonist- TFRGAP and RLLFT control peptide (each at 100 μM) for 6 hours. Panel B: Human lung fibroblasts were seeded in 96-well plates at a density of 10^4 cells/well, and serum-starved for 24 hours. Cells were subsequently exposed to a range of concentrations of PAR-1 and PAR-3 activating peptides, TFLLR and TFRGAP for 16 hours. CCL2 levels were measured in cell supernatants by ELISA. Data represent a mean +/- SEM of 4 replicates, analysed by A: one-way ANOVA ***$p<0.001$ versus unstimulated cells, B: two-way ANOVA *$p<0.05$ PAR-1 activating peptide versus PAR-3 activating peptide.

3.2.5 Summary

The aim of this study was to investigate the role of PAR-1 in thrombin-induced CCL2 release in primary human lung fibroblasts and the results show that:

- Thrombin-mediated activation of PAR-1 elicits a strong intracellular calcium response that is entirely PAR-1-dependent but the CCL2 response downstream of thrombin signalling is partially PAR-1-independent.
- PAR-1 and PAR-2 activation trigger robust intracellular calcium release but no calcium flux nor CCL2 release is detected after PAR-3 or PAR-4 activation.

3.2.6 Discussion

Thrombin signalling via PAR-1 has multiple effects on human lung fibroblasts biology including stimulation of proliferation (Della Rocca et al., 1999), differentiation into myofibroblasts (Blanc-Brude et al., 2005) and production of collagen (Chambers et al., 1998). CCL2 is a potent profibrotic chemokine and a chemoattractant of immune cells and fibrocytes (Moore et al. 2006). Furthermore, CCL2 can directly contribute to fibroproliferative processes by upregulating TGFβ gene expression (Gharaee-Kermani et al. 1996). CCL2 levels are also increased in serum and bronchoalveolar lavage fluid from IPF patients (Baran et al., 2007; Suga et al., 1999).

Previous work in our laboratory showed that in murine lung fibroblasts thrombin induces CCL2 gene transcription and protein production downstream of PAR-1-$G\alpha_q$-uncoupling and signalling via calcium-independent and ERK1/2-dependent pathways, while PAR-1-$G\alpha_q$-mediated calcium flux is required for the release of this chemokine from the cells (Deng et al., 2008). Recently, it has been demonstrated that in human lung fibroblasts thrombin signalling increases CCL2 gene transcription via two transcription factors. NFκB is involved in the rapid increase in the CCL2 mRNA levels while AP-1 promotes sustained CCL2 gene transcription (Deng et al., 2013). Furthermore, fibrotic lung fibroblasts were shown to secrete significantly more CCL2 at baseline and following stimulation with thrombin than control fibroblasts. This response is due to enhanced binding of transcription factors to the CCL2 promoter (Deng et al., 2013). Furthermore, a similar pattern of increased binding to the CCL2 promoter region also promotes high levels of CCL2 release in fibroblasts isolated from bleomycin-treated murine lungs (Deng et al., 2013).

In a collaborative study performed with Dr Alejandro Ortiz-Stern, we investigated CCL2 release by primary human lung fibroblasts and found that at low thrombin concentrations the CCL2 release occurs entirely downstream of PAR-1 activation. However, stimulation of human lung fibroblasts with high concentration of thrombin in the presence of two pharmacological agents directed against PAR-1, RWJ58259 (Damiano et al., 2003) and SCH530348 (Bonaca and Morrow, 2009),

significantly reduced but did not fully abolish CCL2 release. Importantly, the level of inhibition of CCL2 release with RWJ58259 was thrombin concentration-dependent but fully blocked when thrombin catalytic activity was inhibited by hirudin. ERK phosphorylation is known to occur within minutes of thrombin-mediated PAR-1 activation and is essential for CCL2 secretion (Goebeler et al., 2001) from different cell types including murine lung fibroblasts (Deng et al., 2008) and dendritic cells (Mitchell and Olive, 2010). In primary human lung fibroblasts, we found that at high thrombin concentration RWJ58259 did not block ERK phosphorylation (**Appendix 2, Figure 4**).

The ability of RWJ58259 and SCH530348 to block PAR-1-mediated signalling in human lung fibroblasts was subsequently confirmed using the intracellular calcium release assay. At all concentrations of thrombin tested both antagonists fully blocked the thrombin-induced intracellular calcium flux. Confidence in these pharmacological agents was further supported by data obtained with PAR-1 cleavage blocking antibodies which also failed to completely block CCL2 release from human lung fibroblasts (**Appendix 2, Figure 2F**). Importantly, intracellular calcium signalling was found to be essential for thrombin-mediated CCL2 release from human lung fibroblasts and this response was fully inhibited by the BAPTA calcium chelator. Taken together, this strongly suggests that thrombin-mediated CCL2 release from human lung fibroblasts is not exclusively PAR-1-mediated.

Following validation of the antagonists, the next plausible explanation was that with increasing thrombin concentration other PAR receptors are recruited and act independently or as co-receptors in order to enhance thrombin-mediated CCL2 release. Previous studies have shown that RWJ58259 efficiently blocks human platelet aggregation at low thrombin concentration but at high thrombin concentrations the inhibitory effect is overcome by the contribution of PAR-4 signalling (Damiano et al., 2003). PAR-4 is a low affinity thrombin receptor and high concentrations of thrombin are required to activate PAR-4 and convey signalling responses, while at low thrombin concentration PAR-1 mediates the majority of thrombin responses in human platelets. Combined PAR-1/PAR-4 activation and

signalling constitutes the primary mechanism of human platelet activation and aggregation (Kahn et al., 1999) and allows for cellular plasticity in response to different concentrations of thrombin, which can reach concentrations up to 140 nM in the proximity of a clot (Walz et al., 1985). Although, fibroblasts express low levels of PAR-4 mRNA at baseline, the expression of the receptor has been shown to be induced by LPS and TNFα in bronchial fibroblasts (Ramachandran et al., 2007). Furthermore, increased expression of PAR-4 is matched by the increased functional responses following activation of PAR-4 with specific agonist peptide (AYPGKF) and thrombin (Ramachandran et al., 2007). However, in the present study, PAR-4 specific activating peptide failed to induce intracellular calcium responses and CCL2 release from primary human lung fibroblasts. Therefore PAR-4 signalling as a contributing factor to CCl2 release following stimulation with high thrombin concentrations was disregarded.

PAR-3 is expressed by human lung fibroblasts but is considered to be incapable of autonomous signalling due to a short cytoplasmic tail, which is a recognised major site of G-protein coupling (Ishihara et al., 1997). Instead, PAR-3 is described as a co-factor receptor enhancing activation of other PARs (McLaughlin et al. 2007; Nakanishi-Matsui et al. 2000). The role of PAR-3 is best characterised as a PAR-4 co-receptor in mouse platelets where PAR-3 concentrates thrombin in the vicinity of PAR-4 and enhances PAR-4 activation by allowing efficient receptor cleavage and signalling at lower thrombin concentration (Nakanishi-Matsui et al., 2000). Furthermore, PAR-3 activation can modulate and potentiate PAR-1 signalling (Kaufmann et al., 2005) and the PAR-3 tethered ligand has been shown to directly trans-activate PAR-1 and PAR-2 to induce intracellular calcium signalling (Hansen et al. 2004). Furthermore, other reports suggest that PAR-3 can be functionally active (Ostrowska and Reiser, 2008) and this has been shown to be mechanistically plausible since other sites than just the cytoplasmic tail at the PAR receptors intracellular interface have been identified to bind the G-proteins, namely the intracellular loops (McCoy et al., 2012). However, in this study the PAR-3 specific activating peptide TFRGAP failed to initiate intracellular calcium flux or CCL2 release. Interestingly, in endothelial cells, PAR-3 forms heterodimers with PAR-1

and allosterically modulates PAR-1 interaction with G-proteins enhancing coupling and signalling via $G\alpha_{13}$ (McLaughlin et al. 2007). In endothelial cells, thrombin-PAR-1- $G\alpha_{13}$ signalling leads to increased endothelial permeability that is abolished when PAR-1 is silenced. However, PAR-3 allosterically modulates this effect by controlling the magnitude of response and in the event of PAR-3 knockdown, thrombin-PAR-1-induced endothelial permeability is reduced by 50% (McLaughlin et al. 2007). In contrast, thrombin-mediated activation of the PAR-1/PAR-3 heterodimer unit also triggers the release of intracellular calcium that is PAR-1-$G\alpha_q$-dependent and is unaffected by knockdown of PAR-3. Therefore, future work in this project will involve PAR-3 knockdown experiment to conclusively eliminate the possibility that PAR-3 contributes to CCL2 release from human lung fibroblasts.

PAR-2 is not directly activated by thrombin but the unmasked tethered ligand of PAR-1 can transactivate PAR-2 in endothelial cells (O'Brien et al., 2000). PAR-2 activation with the PAR-2 specific activating peptide SLIGKV leads to robust intracellular calcium release and induces a small but significant increase in CCL2 release over extended periods of time. However, the results obtained in the course of this study have shown that knockdown of PAR-2 in human lung fibroblasts did not affect the magnitude of thrombin-mediated CCL2 release and did not affect the inhibition level achieved with PAR-1-targeting strategies (Ortiz-Stern et al., 2012). The role for PAR-2 in thrombin-mediated CCL2 release is therefore highly unlikely.

As shown in the previous chapter of this thesis, human primary fibroblasts express high levels of PAR-1 and signal robustly to thrombin. This observation is also consistent with other studies showing that following desensitisation of fibroblasts with thrombin, the responsiveness to thrombin is rapidly restored (Blanc-Brude et al., 2005). Notably human lung fibroblasts secrete vastly more CCL2 than murine fibroblasts, which can be explained partially by inter-species variability. Moreover, the murine chemokine CCL12 has been shown to be more homologous to human CCL2 and is secreted in high levels in the context of pulmonary fibrosis (Moore et al. 2006). It is possible that levels of CCL2 are complemented by CCL12 release and both chemokines play convergent roles to promote pulmonary fibrosis in mice.

Furthermore, it is likely that RWJ58259, SCH530348 and PAR-1 blocking antibodies produce partial inhibition of CCL2 release due to high rate of PAR-1 turnover at the cell surface and mobilisation of the PAR-1 intracellular pool in the human lung fibroblasts. Silencing of PAR-1 by siRNA would provide final clarification for the thrombin-mediated CCL2 release in lung fibroblasts but we were unsuccessful in knocking down PAR-1 in these cells. This could be explained by the observation that human lung fibroblasts express PAR-1 in abundance.

CCL2 acts via G-protein coupled receptor CCR2 and CCL2/CCR2 signalling axis exerts multiple autocrine and paracrine cellular effects that involve activation of intracellular pathways, some of which overlap with thrombin signalling, including intracellular calcium release (Gouwy et al., 2008) and MAPK p38 signalling (Lin et al., 2012). In systemic sclerosis fibroblast expression of CCR2 was associated with overexpression of αSMA, CTGF and CCL2 in these cells (Carulli et al., 2005). Furthermore, CCR2 knockout mice are protected from bleomycin-induced pulmonary fibrosis (Moore et al. 2001) and the CCL2/CCR2 signalling axis has been shown to downregulate prostaglandin PGE_2 production in alveolar epithelial cells and promote fibroblast proliferation (Moore et al. 2003). Autocrine and paracrine signalling of CCR2/CCL2 axis extends beyond fibrosis and has been shown to promote expression of inflammatory mediators in different cell types including synovial fibroblasts (Giunti et al., 2006; Lin et al., 2012; Liu et al., 2007) and tumour cells to enhance survival and angiogenesis (Izhak et al. 2012). It is possible that CCL2 released following thrombin-mediated PAR-1 activation in human lung fibroblasts acts on CCR2 receptors and further propagates CCL2 release in PAR-1-independent manner. Future work to assess CCR2 expression in human lung fibroblasts and to investigate the existence of potential positive feedback regulation of CCL2 release downstream of thrombin signalling in human lung fibroblasts would test this possibility.

3.3 Herpesvirus infection in pulmonary fibrosis

3.3.1 Development of the model

3.3.1.1 Introduction

Gamma herpesvirus (γHV68) is a naturally occurring murine virus that shares homology with human gamma herpesviruses, especially Epstein-Barr virus (EBV) that, among other herpesviruses, has been implicated in the aetiology of IPF (Tang et al., 2003). γHV68 infection is persistent and occurs in a biphasic mode (Nash et al., 2001). The virus enters via respiratory routes and the primary site of infection and replication is the alveolar epithelium. Lytic infection is associated with extensive epithelial damage when the viral progeny are released and disseminated across lung tissue. The lytic phase peaks at day 7 post-infection and the virus subsequently establishes latency primarily in B lymphocytes but has been shown to persist in epithelial cells, macrophages and dendritic cells (Nash et al., 2001).

Damage to the epithelium is a well-recognised initiating factor in the development of pulmonary fibrosis. Furthermore, latent herpesvirus infection of the human alveolar epithelium increases its sensitivity to TGFβ and its potential to undergo epithelial to mesenchymal transition (Sides et al., 2011). Infection with γHV68 in the FITC model of pulmonary fibrosis has been reported to cause increased collagen deposition in the lung and overall worse outcome of fibrosis (McMillan et al., 2008).

The aim of this study was to establish a model of gamma herpesvirus infection on a background of bleomycin-induced pulmonary fibrosis. C57BL/6 male mice (aged 10-12 weeks) were administered bleomycin at 1 mg/kg via the oropharyngeal route. Two weeks later after the establishment of the fibrotic phase, mice where inoculated with 80,000-100,000 PFU γHV68 or given saline via the intranasal route. Mice were sacrificed at 21 days post-bleomycin administration and 7 days post viral inoculation (p.i.), which corresponds to the peak of the lytic phase of γHV68 infection (McMillan et al., 2008). The second group of mice was sacrificed 28 days post-bleomycin instillation and 14 days post-viral inoculation (p.i.).

3.3.1.2 The effect of bleomycin and viral infection on mouse body weight

The current study aimed to establish a "two-hit" injury model and therefore we reduced our standard bleomycin dose to 1 mg/kg. Mice were weighed every 2 days throughout the duration of the experiment (**Figure 3.46)**. The recorded weight loss corresponded temporally to the weight loss (on average 15% of starting body weight) observed with a "full" dose of bleomycin (2 mg/kg) routinely used in our laboratory, which occurs at the peak of inflammatory phase of bleomycin injury (between days 4-10) (Scotton et al., 2013). In this study maximum weight loss (on average 6% of starting body weight) was recorded 9 days after the bleomycin challenge. After this time, body weight stabilised and returned to the baseline values by day 14, when mice were infected with the virus. Following viral inoculation, infected mice ceased to gain weight and subsequently started losing weight again with a nadir around 7 days p.i., which corresponded to the peak of the lytic phase of infection. By 14 days post-infection all mice were gaining weight again.

3.3.1.3 The effect of fibrotic insult and viral infection on *ex vivo* lung and spleen weights

Normal mouse lungs weigh around 150 mg and following 2 mg/kg bleomycin injury this increases to 300 mg over the course of a four week model (Scotton et al., 2013). In this study with reduced bleomycin dose, the fibrotic lungs harvested at day 7 p.i. were on average 30% heavier than the historical baseline (**Figure 3.47A)**. The weight of virally-infected and bleomycin-challenged lungs was further significantly increased to 400 mg when compared to fibrotic only lungs. The weight of lungs harvested 14 days p.i. was lower for both control and virally-infected animals, although there was still a notable trend for virally-infected lungs to be heavier.

Murine γHV68 establishes latency primarily in B lymphocytes, which migrate to the spleen and hyperproliferate leading to splenomegaly that is usually established by two weeks post-infection (Nash et al., 2001). In this study we recorded the spleen weights as a surrogate indicator of infection. Normal mouse spleens weigh around 100 mg and the administration of bleomycin had no effect on spleen weights in this study. There was no difference in spleen weight between control and virally-infected animals at 7 days p.i. but 14 days p.i. spleen weight of virally-challenged mice was 3-fold higher (**Figure 3.47B**).

3.3.1.4 Viral gene expression in the lung and spleen

Viral infection was further confirmed by measuring the expression of viral genes in the lungs and spleens (**Figures 3.48 and 3.49)**. Expression of viral genes was quantified by qPCR and included genes encoding the M3 viral envelope protein (involved in the modulation of immune responses of the host), glycoprotein B (present on the viral envelope and involved in viral entry into the cell), and viral DNA polymerase (responsible for viral genome replication). Glycoprotein B and DNA polymerase gene expression is associated with the lytic phase of infection, while M3 is expressed throughout γHV68 infection (Vannella et al. 2010). At the peak of the lytic phase of the infection (7 days p.i.) the expression of all three genes was readily detectable in the lungs of infected animals. By day 14 post-infection, when the virus establishes latency, the expression of lytic genes in the lungs decreased to barely detectable levels (**Figure 3.48**). In the spleen glycoprotein B expression was detected at day 14 p.i., while both M3 and DNA polymerase expression was detected at day 7 and 14 post infection (**Figure 3.49**).

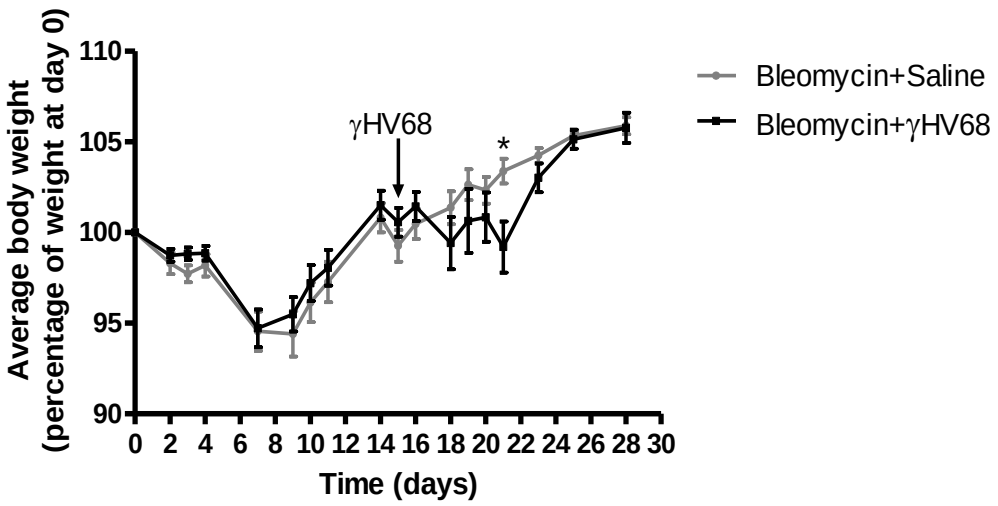

Figure 3.46. Changes in mouse body weights in the model of γHV68 infection on a background of bleomycin-induced pulmonary fibrosis.

C57BL/6 mice were administered bleomycin via oropharyngeal instillation at 1 mg/kg, followed by infection with 80,000 PFU γHV68 or saline intranasally on day 14 as indicated. Data represent percentage change in average mouse body weight relative to starting body weight at day 0 over the course of the experiment. Each point is representative of mean +/- SEM of n=7-9 animals per group; two-way ANOVA *$p<0.05$ at day 21 post-bleomycin challenge and 7 days post-inoculation with γHV68.

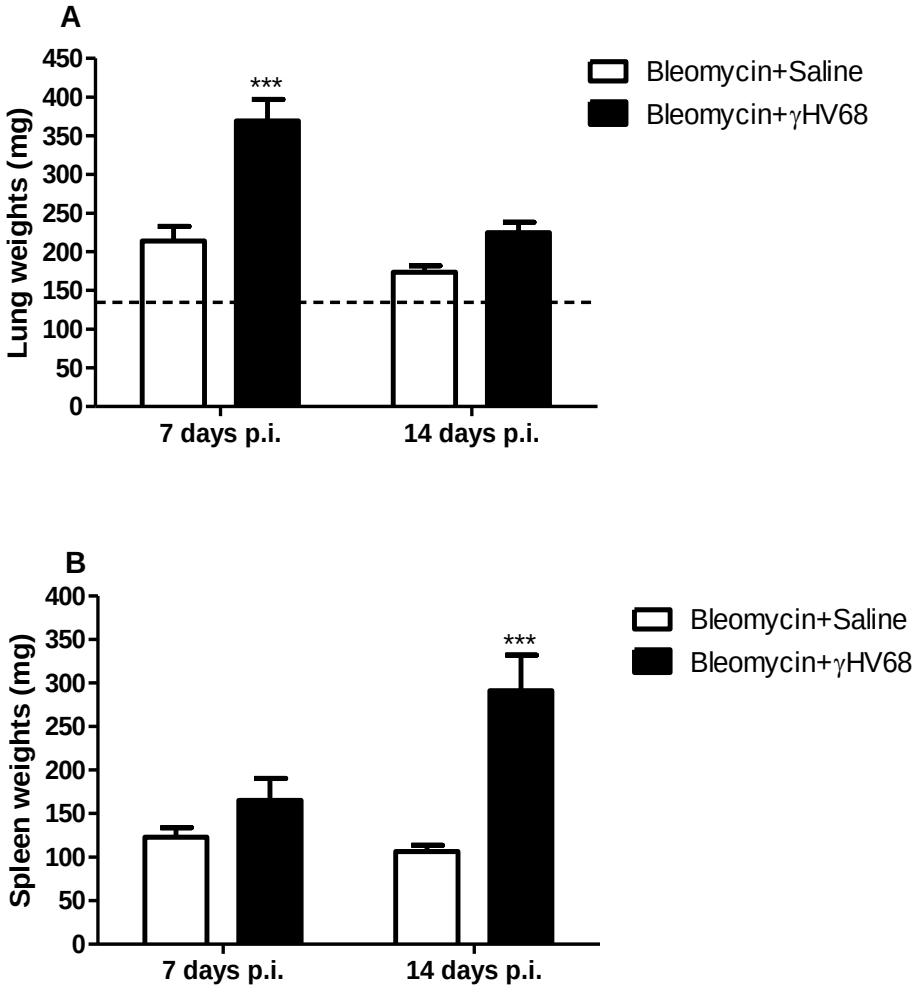

Figure 3.47. Effect of γHV68 infection on a background of bleomycin-induced pulmonary fibrosis on mouse lung and spleen weights.

C57BL/6 mice were administered bleomycin via oropharyngeal instillation at 1 mg/kg, followed by infection with 80,000 PFU γHV68 or saline intranasally on day 14. Panel A- data represent average mouse lung weights with the dotted line indicating historical baseline for a saline-treated mouse lung weights, representative of n=4-6 animals per group; and panel B- mouse spleen weights, representative of n=7-9 animals per group; measured ex vivo 7 and 14 days post infection; Two-way ANOVA, ***p<0.001.

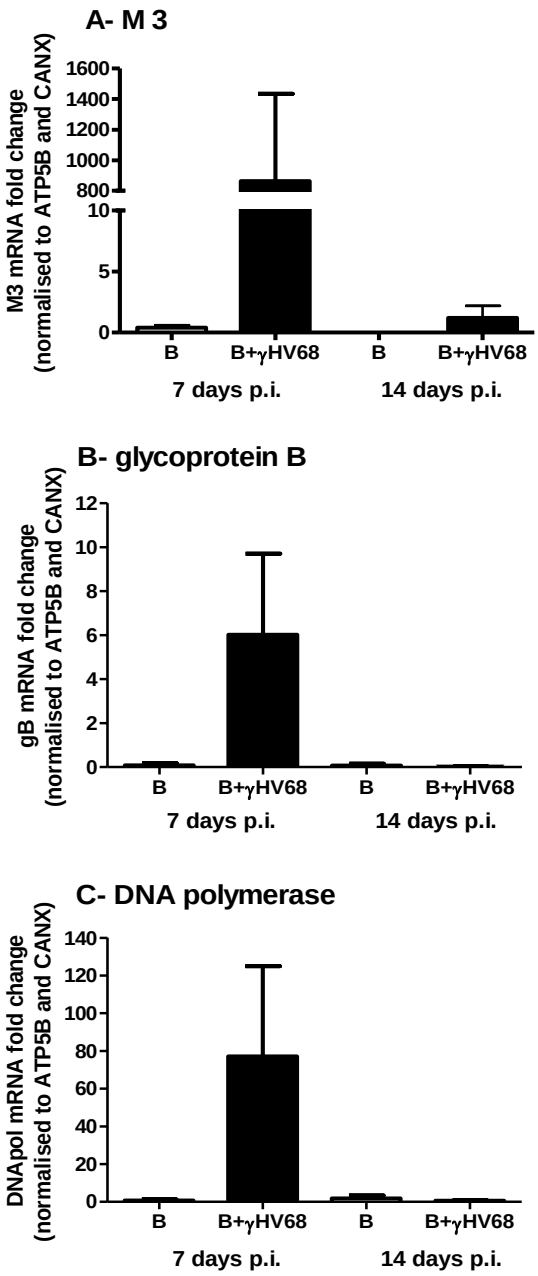

Figure 3.48. Determination of viral gene expression in the lungs.

C57BL/6 mice were administered bleomycin via oropharyngeal instillation at 1 mg/kg, followed by infection with 80,000 PFU γHV68 or saline intranasally on day 14. The expression of viral genes in the lungs at 7 days p.i. and 14 days p.i. was assessed by qPCR and data are presented as fold change in mRNA levels relative to two housekeeping genes ATP5B and CANX and representative of mean +/- SEM, n=4-6 animals per group. Panel A- M3; panel B- glycoprotein B; panel C- DNA polymerase.

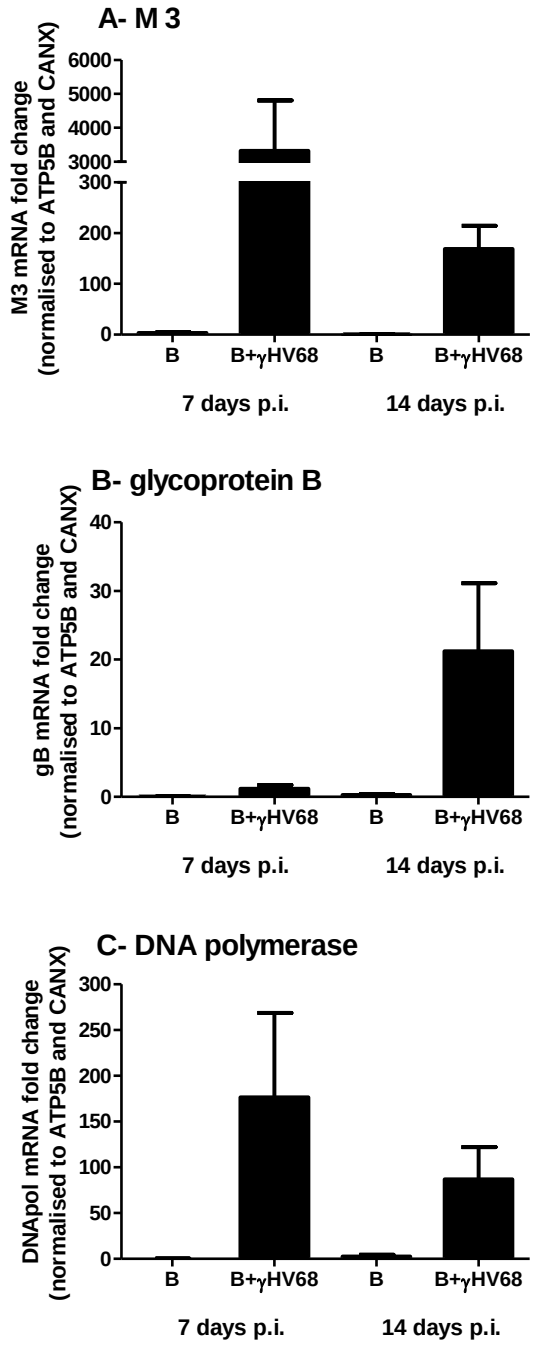

Figure 3.49. Determination of viral gene expression in the spleens.

C57BL/6 mice were administered bleomycin via oropharyngeal route at 1 mg/kg, followed by infection with 80,000 PFU γHV68 or saline intranasally on day 14. The expression of viral genes in the spleens at 7 days p.i. and 14 days p.i. was assessed by qPCR and data are presented as fold change in mRNA levels relative to two housekeeping genes ATP5B and CANX and representative of mean +/- SEM, n=4-6 animals per group. Panel A- M3; panel B- glycoprotein B; panel C- DNA polymerase.

3.3.1.5 Collagen expression and deposition following viral infection on a background of pulmonary fibrosis

Collagen deposition is a hallmark of fibroproliferative lung disease and marks the expansion of extracellular matrix in human disease and animal models of pulmonary fibrosis. Therefore, quantification of the lung collagen is the primary endpoint for the assessment of fibrosis in the lung. In order to evaluate the effect of viral infection on the development of fibrosis, total lung collagen protein and mRNA levels were measured.

Viral infection in the fibrotic lung led to a significant upregulation in collagen gene expression 7 days p.i. compared to the bleomycin alone levels. This upregulation was no longer significant at 14 days p.i. (**Figure 3.50**). Total lung collagen, based on hydroxyproline levels and measured by high performance liquid chromatography (HPLC), doubled following bleomycin challenge at 7 days p.i. compared to our historical baseline data for lung collagen levels in C57BL/6 mice. There was no difference in total lung collagen between mock- and virally-infected animals (**Figure 3.51A**). Published data from our laboratory revealed that in mice instilled with 2 mg/kg of bleomycin, lung collagen deposition continues to increase through to at least day 28 post-administration (Scotton et al., 2013). However, in the present study with a lower dose of bleomycin (1 mg/kg), we did not see a further increase in lung collagen accumulation at day 28 post-instillation in mock-infected mice (14 p.i.). Instead, we observed a trend towards a reduction in total lung collagen that may be indicative of an ongoing remodelling process. This trend was not observed in the bleomycin-challenged virally-infected animals in that total lung collagen remained significantly elevated and the difference was significant when compared to bleomycin-treated mock-infected animals (**Figure 3.51B**).

3.3.1.6 Histological characterisation of viral infection on a background of pulmonary fibrosis

The increase in collagen at days 21 and 28 post-bleomycin injury (7 and 14 p.i.) was corroborated by haematoxylin and eosin (H&E) and modified Martius Scarlett Blue staining (MSB) of sections from paraffin-embedded lungs (**Figures 3.52 and 3.53**). In all bleomycin-treated lungs, both mock- and virally-infected, we observed severe changes to the lung architecture 21 days into the study (7 days p.i.). The hallmark abnormalities included extensive extracellular matrix deposition with visible thick bands of collagen, abnormal appearance of the alveolar epithelium, thickening and obliteration of alveolar septae, and extensive infiltration of inflammatory cells (**Figure 3.52A**). In the virally-infected fibrotic lungs there were clear signs of acute lung injury superimposed on a background of extensive fibrosis. As identified in **Figure 3.52B** and **3.52C**, we observed pulmonary oedema, alveolar haemorrhage and greatly enhanced infiltration of inflammatory cells forming dense aggregates.

At day 28 (14 days p.i.), in bleomycin-treated and mock-infected mice, the fibrosis appeared to have a structured and condensed pattern with clearly defined borders distinguishing it from largely normal-looking lung (**Figure 3.53A**). The inflammatory cell infiltrates were also no longer evident. In contrast, in the fibrotic and virally-challenged lungs, extensive fibrosis was evident and collagen remained deposited in a disorganised manner. Although pulmonary oedema and haemorrhage appeared to have cleared, the dense inflammatory cells aggregates were still prominent (**Figure 3.53B** and **3.53C**).

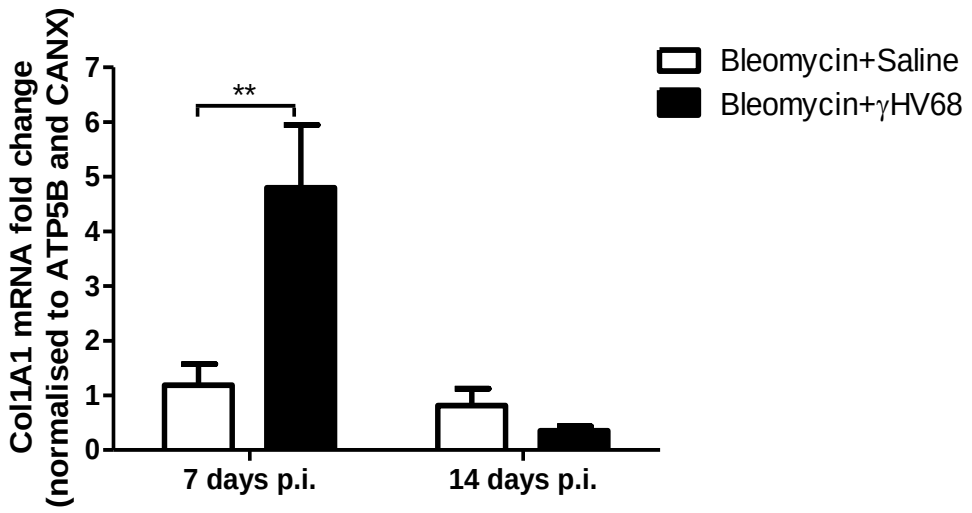

Figure 3.50. Effect of γHV68 infection in the model of pulmonary fibrosis on collagen gene expression.

C57BL/6 mice were administered bleomycin via oropharyngeal instillation at 1 mg/kg, followed by infection with 80,000 PFU γHV68 or saline intranasally on day 14. Col1A1 mRNA levels were measured by qPCR and normalised to two housekeeping genes ATP5B and CANX, and relative to bleomycin alone. Data are representative of mean +/- SEM, n=4-6 animals per group, two-way ANOVA, **p<0.01 comparison between bleomycin+γHV68 and bleomycin+saline.

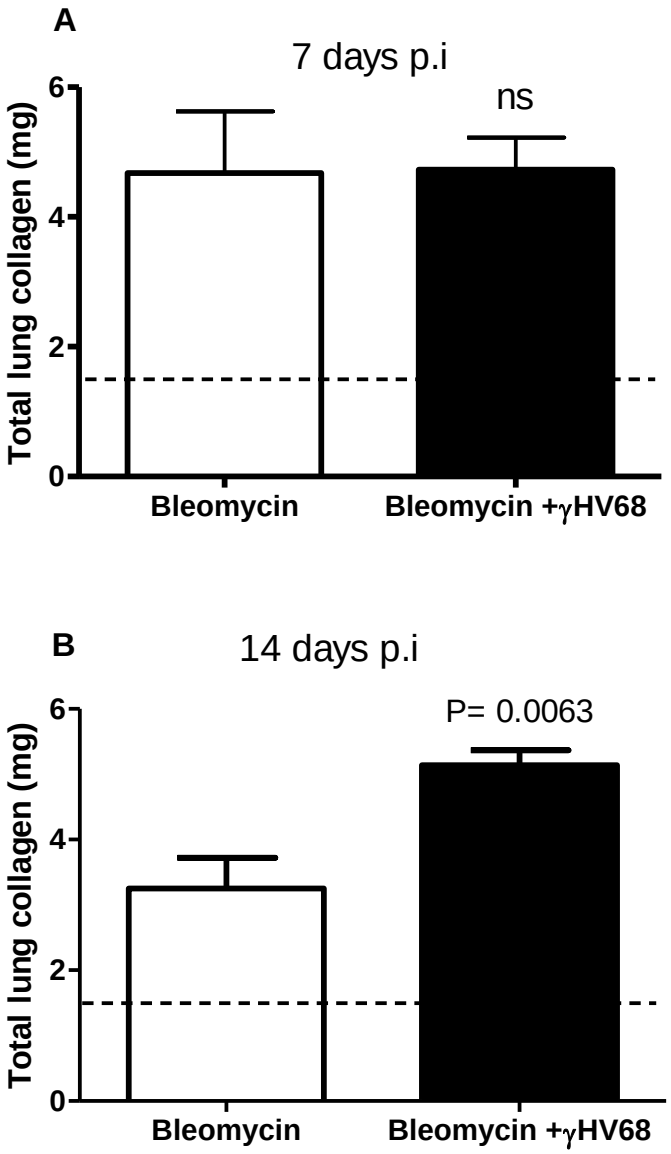

Figure 3.51. Effect of γHV68 infection on total lung collagen accumulation in the bleomycin-induced pulmonary fibrosis.

C57BL/6 mice were administered bleomycin via oropharyngeal instillation at 1 mg/kg, followed by infection with 80,000 PFU γHV68 or saline intranasally on day 14. Total lung collagen was measured by quantification of hydroxyproline by HPLC at A- 7 days p.i. and B- 14 days p.i. Data are representative of mean +/- SEM, n=4-6 animals per group, analysed by unpaired Student t-test.

A- Bleomycin

H&E

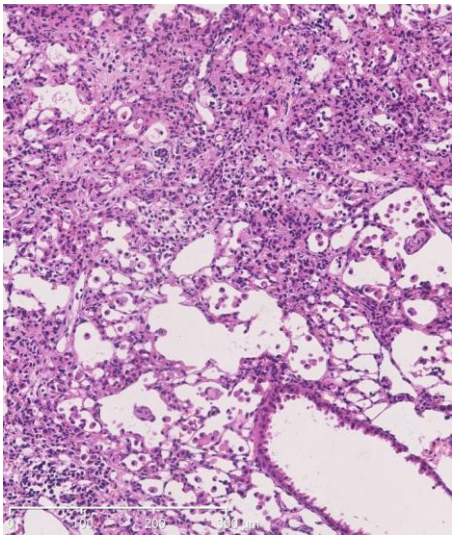

MSB

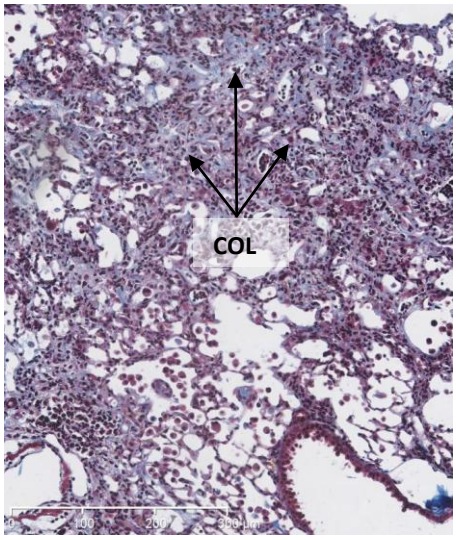

B- Bleomycin + γHV68

H&E

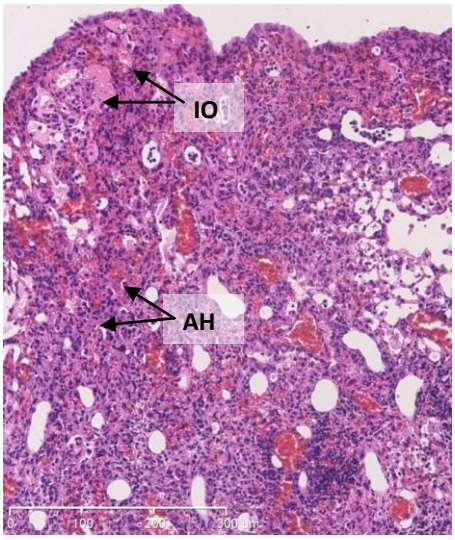

MSB

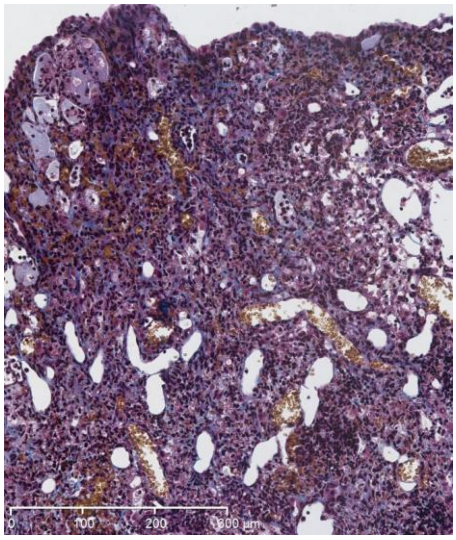

C- Bleomycin + γHV68

H&E

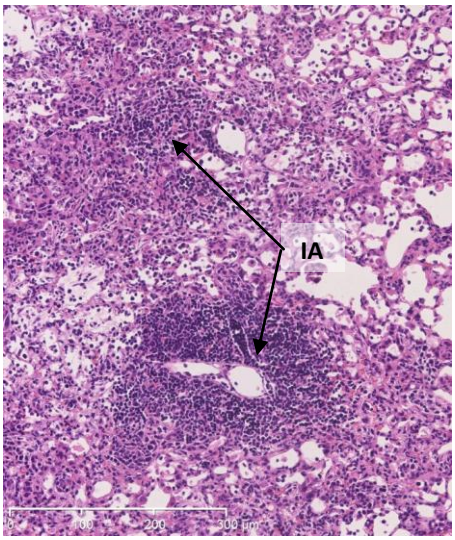

MSB

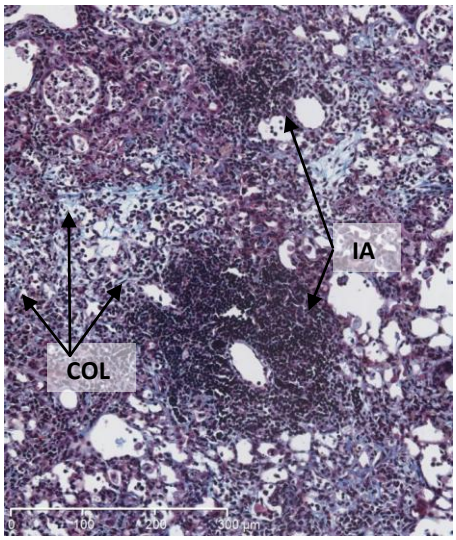

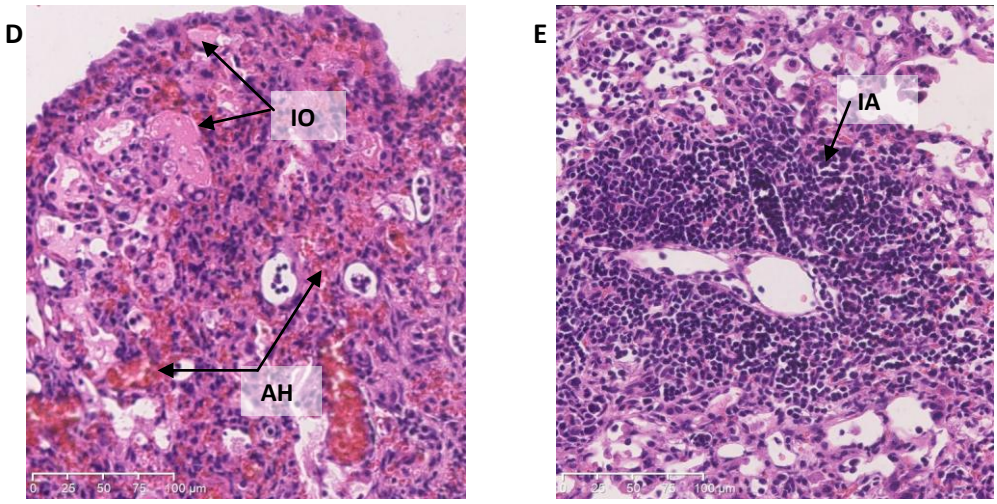

Figure 3.52. Histological analysis of virally-infected fibrotic lungs 7 days p.i.

Sections from paraffin-embedded lungs were stained with haematoxylin and eosin (H&E) (left column) and modified Martius Scarlett Blue method (MSB) revealing collagen fibres stained blue (right column). Panel A shows representative sections from a bleomycin-injured lung, panels B and C- γHV68-infected fibrotic lungs; the images are representative of n=3 animals per group; original magnification x10; panels D and E- H&E, x20 original magnification. IA- inflammatory aggregates, IO- interstitial oedema, AH- alveolar haemorrhage, COL- collagen.

A- Bleomycin

H&E

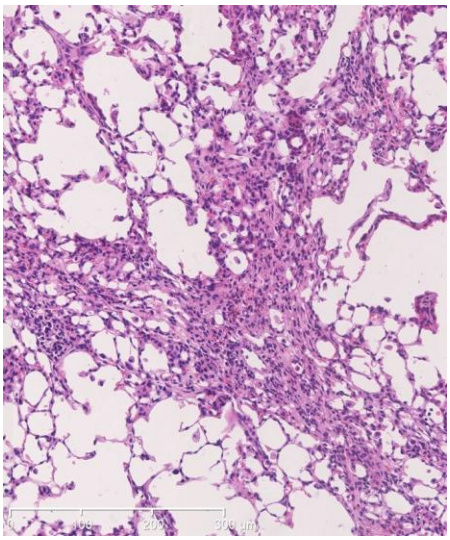

MSB

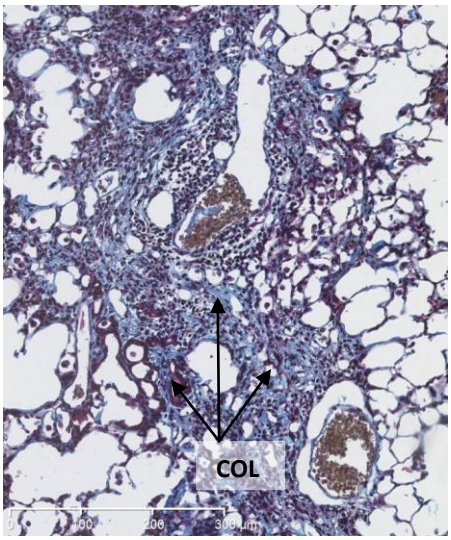

B- Bleomycin + γHV68

H&E

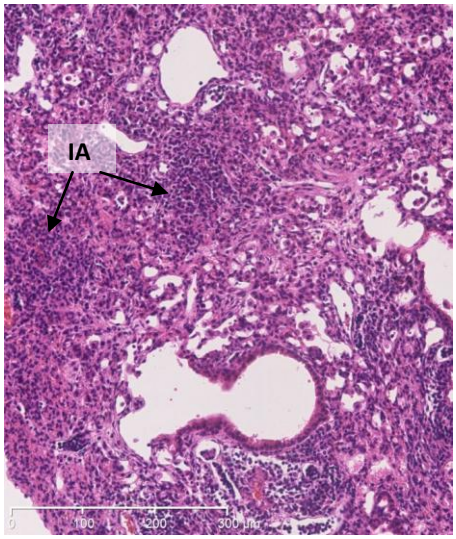

MSB

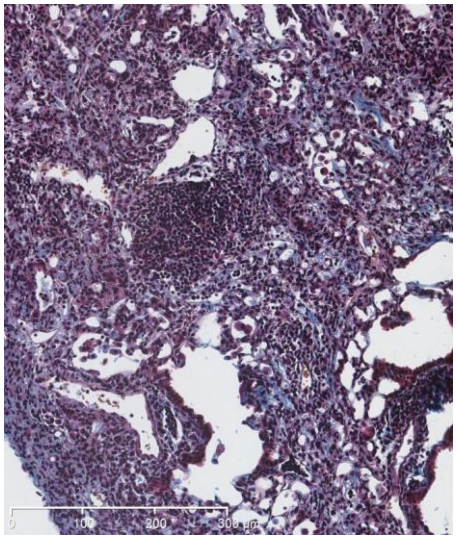

C- Bleomycin + γHV68

H&E

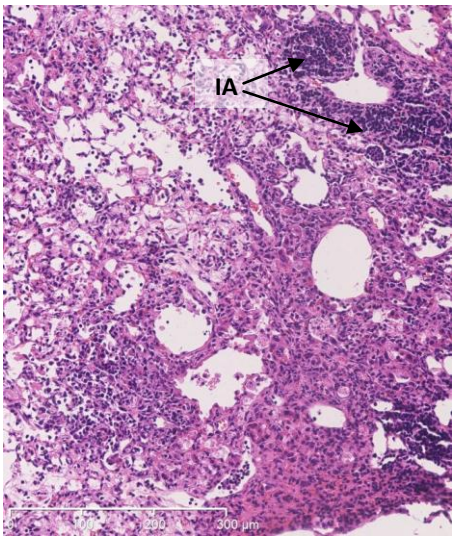

MSB

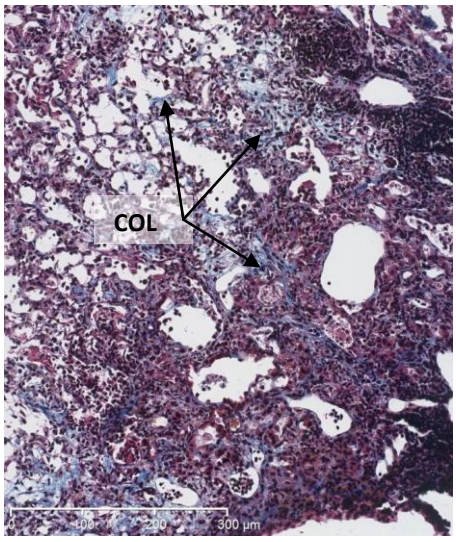

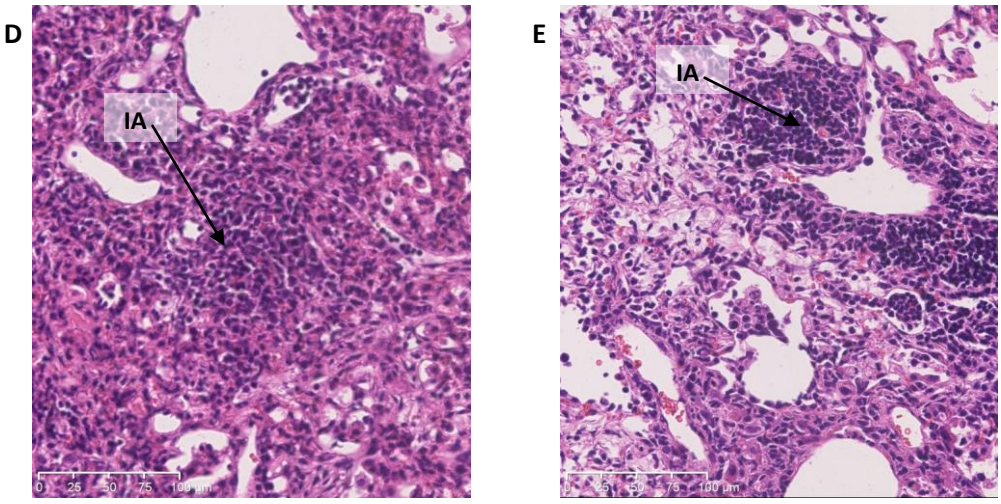

Figure 3.53. Histological analysis of virally-infected fibrotic lung 14 days p.i.

Sections from paraffin-embedded lungs were stained with haematoxylin and eosin (H&E) (left column) and modified Martius Scarlett Blue method (MSB) revealing collagen fibres stained blue (right column). Panel A shows representative sections from a bleomycin-treated lung, panels B and C- γHV68-infected fibrotic lungs; the images are representative of n=3 animals per group; original magnification x10; panels D and E- H&E, x20 original magnification. IA- inflammatory aggregates, COL- collagen.

3.3.1.7 Expression of inflammatory mediators in viral infection of existing pulmonary fibrosis

γHV68 infection is associated with a strong Th1-mediated and IFNγ-dependent antiviral response and a high lethality has been reported in IFNγ-deficient mice when infected with herpesviruses (Nash et al., 2001). Furthermore, IFNγ as well as TNFα levels have been shown to increase in the viral infection model of FITC-induced pulmonary fibrosis (McMillan et al., 2008). In the present study, the levels of these two cytokines in lung homogenates were quantified by ELISA. A significant increase in IFNγ levels with the viral infection was observed in comparison with mock-infected animals at 14 days p.i. (**Figure 3.54A**). The levels of TNFα were comparable between experimental groups both at day 7 and 14 p.i. with a small increase in the virally-infected mice that did not reached statistical significance (**Figure 3.54B**). Increased levels of interleukin IL-8 are predictive of poor prognosis in IPF patients (Richards et al., 2012) and IL-8 has been shown to be induced during herpesvirus infection (Sun et al., 2006). In this study, we found that levels of the murine equivalent of human IL-8, keratinocyte-derived chemokine KC, were increased at both 7 and 14 days p.i. but this response was variable for virally infected-mice at seven days p.i. and only reached statistical significance at day 14 p.i. when compared with bleomycin-alone treated mice (**Figure 3.54C**).

We next examined the expression of CCL2, which is elevated in IPF lung (Mercer et al., 2009) and increased levels of CCL2 and CCL12 were also reported in the model of herpesvirus infection in FITC-induced pulmonary fibrosis (McMillan et al., 2008). CCL2 mRNA level increased 15-fold 7 days p.i. in virally-infected fibrotic lungs when compared to the bleomycin-challenged lungs (**Figure 3.55A**). The CCL2 protein level was also significantly increased at both 7 and 14 days p.i. (**Figure 3.55B**).

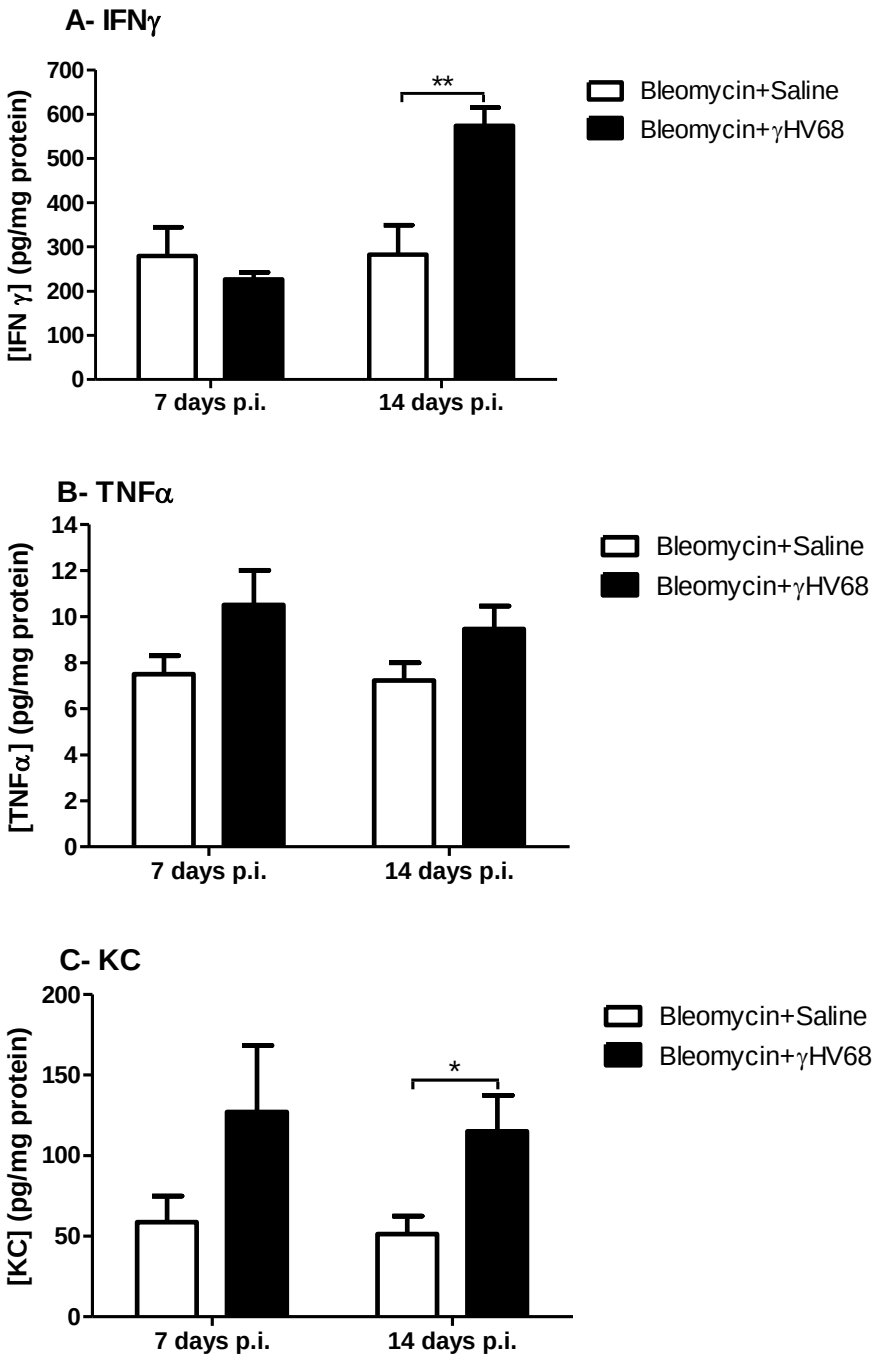

Figure 3.54. Expression of inflammatory mediators in virally-infected fibrotic lungs.

Cytokine and chemokine levels in lung homogenates were quantified by ELISA for A- IFNγ, B- TNFα and C- KC. Data are representative of mean +/- SEM, n=4-6 animals per group, two-way ANOVA, *p<0.05, **p<0.01 comparison between bleomycin+γHV68 and bleomycin+saline.

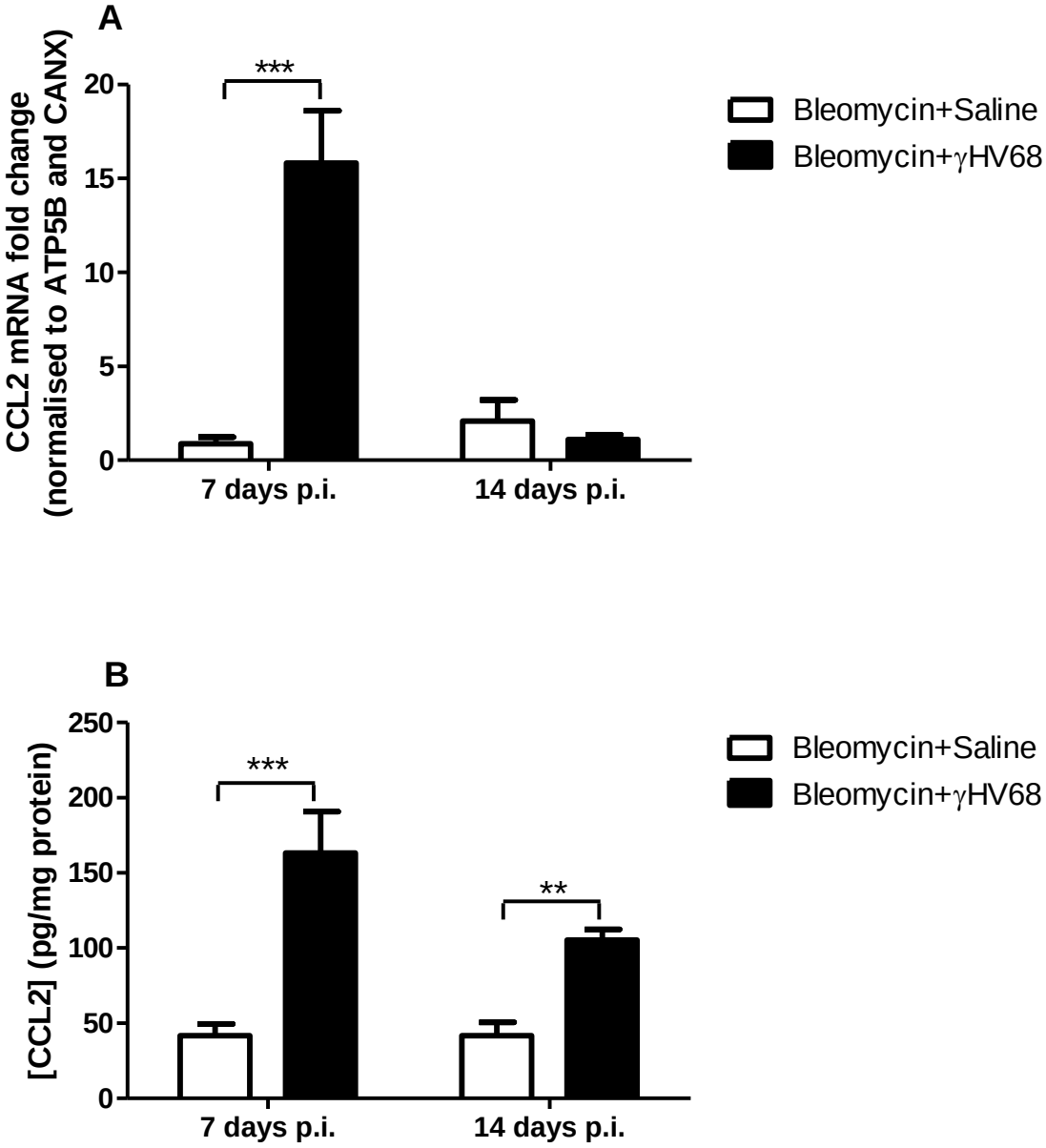

Figure 3.55. CCL2 expression in virally-infected fibrotic lungs.

CCL2 mRNA levels were measured by qPCR and normalised to two housekeeping genes ATP5B and CANX, and relative to bleomycin alone- panel A. Total CCL2 levels per mg of protein in lung homogenates was quantified by ELISA- panel B. Data are representative of mean +/- SEM, n=4-6 animals per group, two-way ANOVA, **p<0.01, ***p<0.001 comparison between bleomycin+γHV68 and bleomycin+saline.

3.3.1.8 Expression of coagulation factors in viral infection on a background of pulmonary fibrosis

Viral infection provides an injurious cue that can lead to the upregulation of tissue factor and trigger the activation of the extrinsic coagulation cascade. Research from our laboratory has shown that the components of the TF-FVIIa-FXa ternary complex are locally upregulated in both human and murine fibrotic lung and co-localise to areas of hyperplastic epithelium (Scotton et al., 2009). This creates a potential for increased thrombin generation in the event of lung injury and microvascular leak. Thrombin is mitogenic for mesenchymal cells and stimulates myofibroblast differentiation and the synthesis of extracellular matrix via PAR-1 mediated signalling (Chambers et al., 1998, 2000). Therefore, we next examined whether the coagulation factors are upregulated in this model of viral infection of bleomycin-induced pulmonary fibrosis. As shown in **Figure 3.56A** and **B**, γHV68 infection in the fibrotic lung led to a doubling in the tissue factor and FXa mRNA levels 7 days p.i relative to bleomycin-treated and mock infected lungs. This difference was lost by 14 days p.i.. In contrast, FVII mRNA levels were significantly reduced in virally-infected fibrotic lungs 7 days p.i. (**Figure 3.56C**).

Next, the immunohistochemical analysis of tissue factor and FX protein distribution in the lung was performed. As shown in **Figure 3.57,** tissue factor and FX were strongly expressed in both mock- and virally-infected bleomycin-treated lungs 7 days p.i. and co-localised to the bronchial epithelium and abnormal and hyperplastic alveolar epithelium. Macrophages and mesenchymal cells were also immunopositive for tissue factor and FX. **Figure 3.58** shows representative sections from lungs 14 days p.i. Panel A shows bleomycin-challenged lung with a dense fibrotic area that was weakly immunopositive for tissue factor and FX. In the γHV68-infected lungs (**Figure 3.57B**) the pattern of tissue factor and FX immunoreactivity is grossly similar to the sections from 7 days p.i. lungs with evidence of co-localisation to the bronchial epithelium, abnormal alveolar epithelium, macrophages and to lesser extent mesenchymal cells.

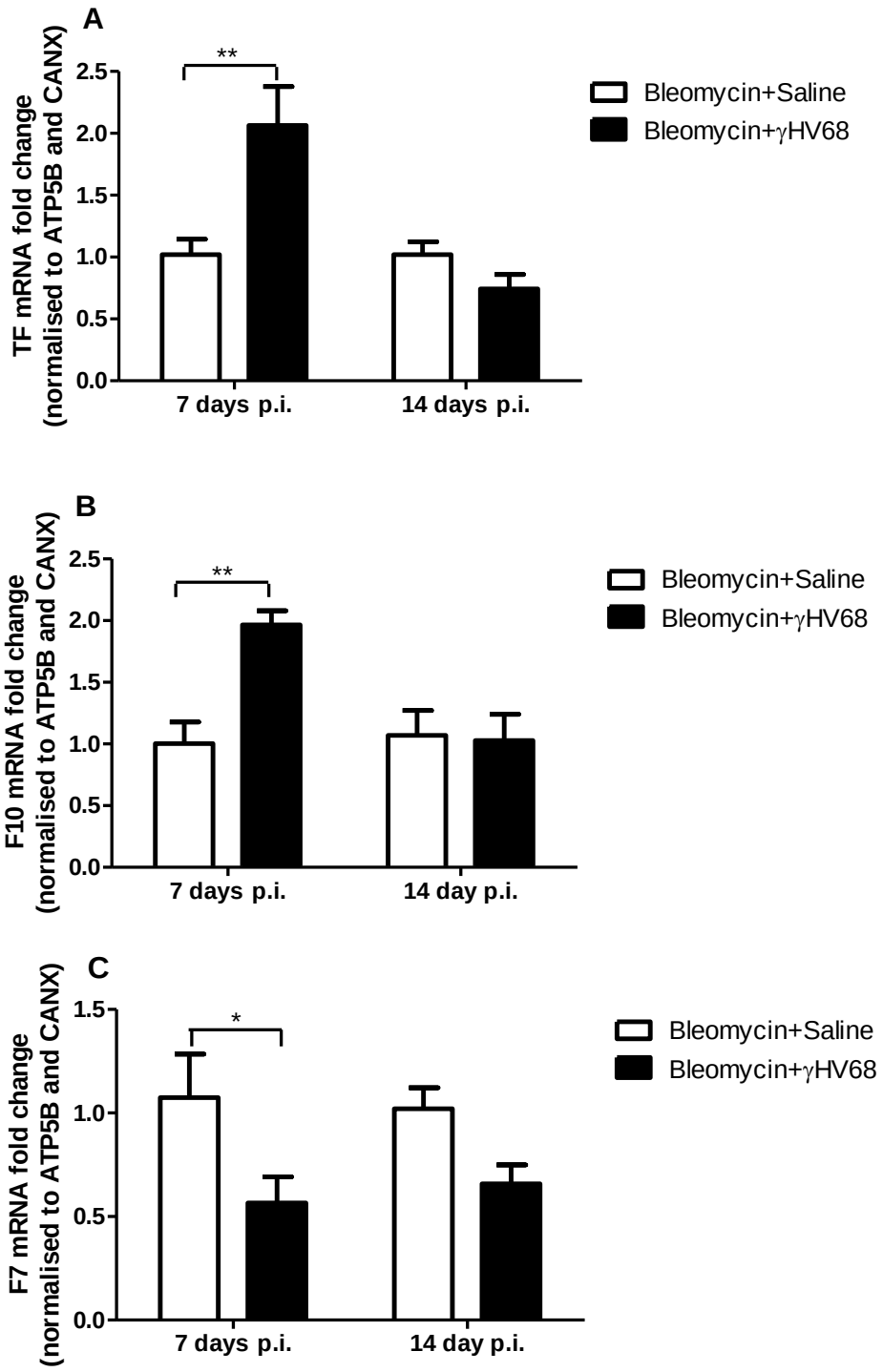

Figure 3.56. Expression of coagulation factors in viral infection of fibrotic lung.

Coagulation factors mRNA levels were measured by qPCR and normalised to two housekeeping genes ATP5B and CANX, and relative to bleomycin alone. Panel A- tissue factor (TF), panel B- factor X (F10), panel C- factor VII (F7). Presented data are representative of mean +/- SEM, n=4-6 animals per group, two-way ANOVA, *p<0.05, **p<0.01.

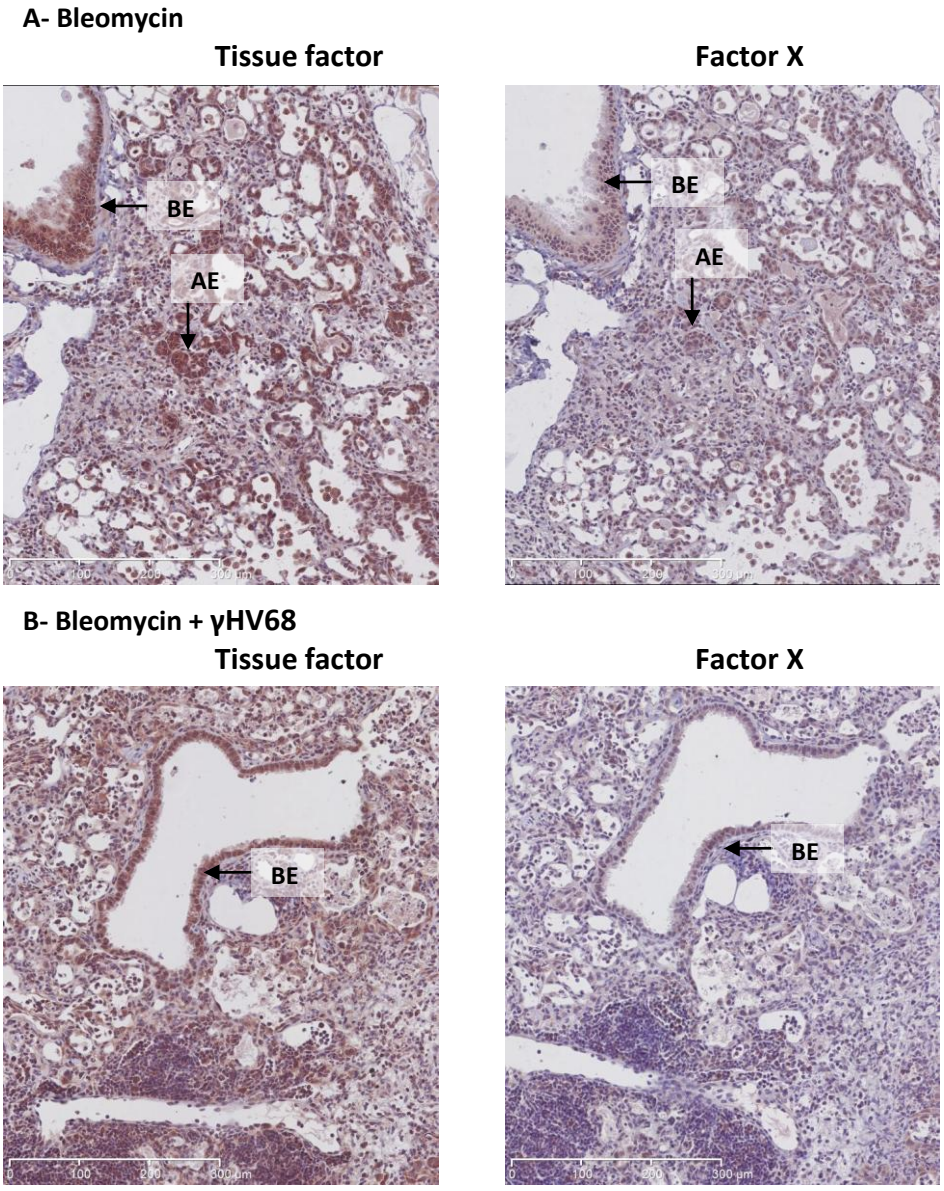

Figure 3.57. Immunodetection of coagulation factors in viral infection on a background of fibrosis 7 days p.i.

Sections from paraffin-embedded lungs were probed with antibodies for tissue factor (left column) and FX (right column). Panel A shows representative sections from a bleomycin-treated and mock-infected lung, panel B- γHV68-infected fibrotic lungs. BE- bronchial epithelium, AE- alveolar epithelium. The images are representative of n=3 animals per group; original magnification x10.

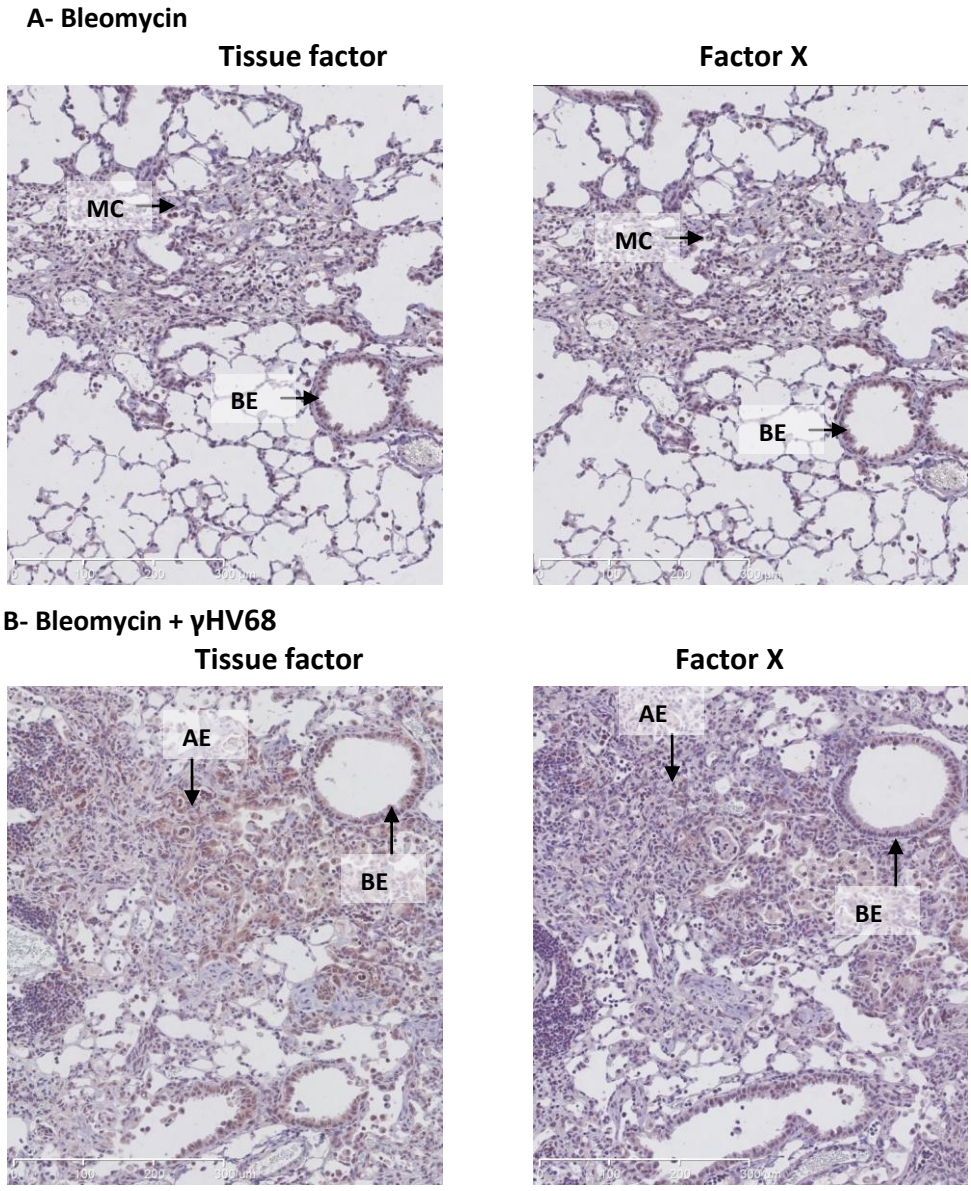

Figure 3.58. Immunodetection of coagulation factors in viral infection on a background of fibrosis 14 days p.i.

Sections from paraffin-embedded lungs were probed with antibodies for tissue factor (left column) and FX (right column). Panel A shows representative sections from a bleomycin- treated and mock infected lung, panel B- γHV68 infected fibrotic lungs. BE- bronchial epithelium, AE- alveolar epithelium, MC- mesenchymal cells. The images are representative of n=3 animals per group; original magnification x10.

Thrombin exerts a plethora of cellular effects via PAR-1 but can also activate PAR-3 and PAR-4, which are expressed in different lung cell populations and are considered to be modulators of PAR-1 signalling (McLaughlin et al. 2007). FXa, particularly when bound within the TF-FVIIa-FXa ternary complex, can also activate PAR-1 and PAR-2. Therefore, we next examined the expression of all four PARs at mRNA level. PAR-1 is known to be highly expressed by mesenchymal cells and is upregulated in the fibrotic epithelium in IPF (Mercer et al., 2009) while PAR-2 is the main PAR expressed on normal alveolar and bronchial epithelium. As shown in **Figure 3.59A** and **B**, PAR-1 (F2R) mRNA levels did not change significantly in the viral infection of fibrotic lung while PAR-2 (F2RL1) expression decreased significantly between day 7 p.i and 14 p.i. in virally-challenged fibrotic lungs only. As shown in Figure **3.59C** and **D** both PAR-3 (F2RL2) and PAR-4 (F2RL3) mRNA levels were significantly upregulated 7 days p.i. and an increase was also notable at 14 days p.i. in the virally-infected fibrotic lung when compared to bleomycin-treated and mock-infected lungs.

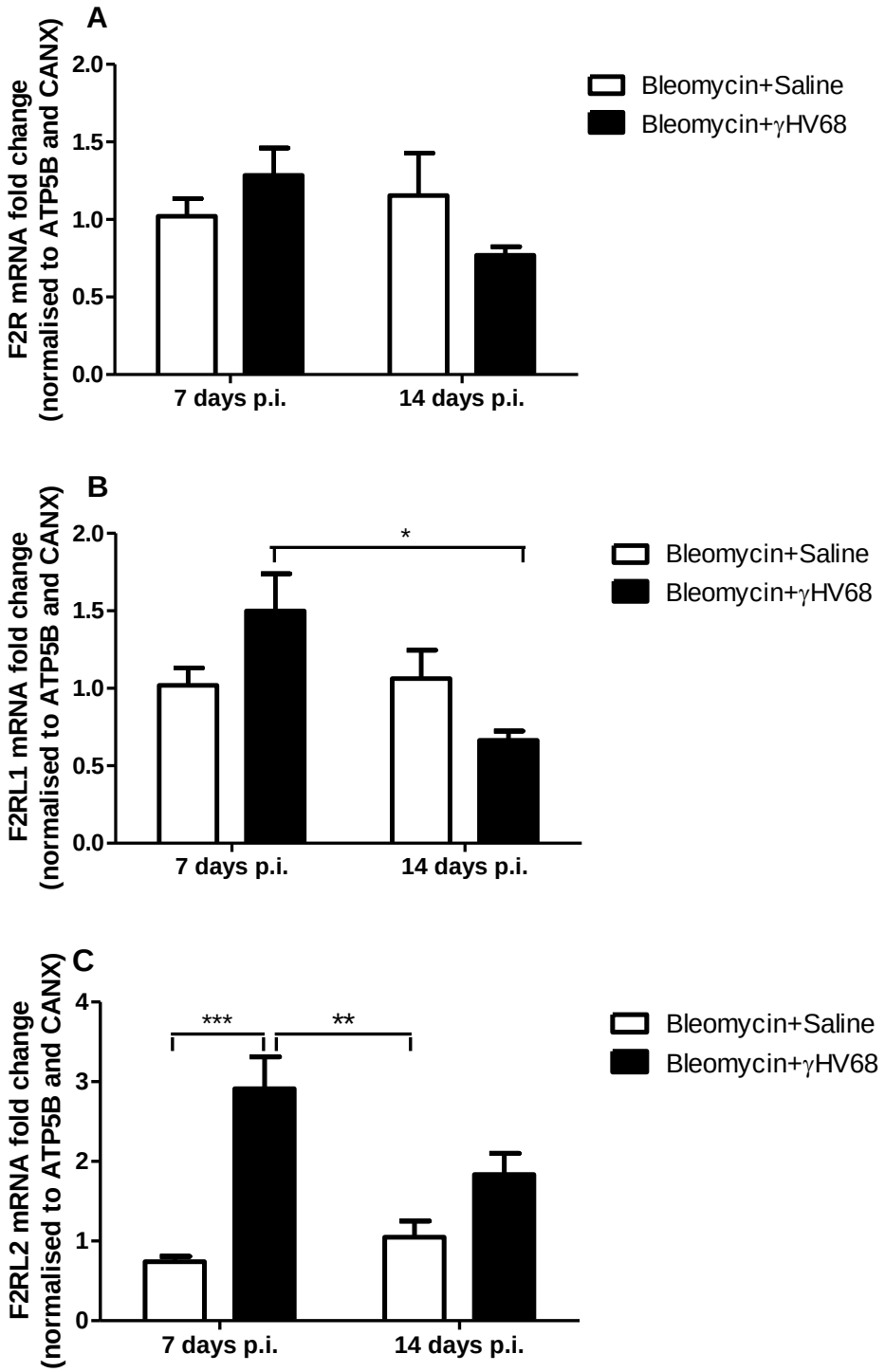
A
F2R mRNA fold change
(normalised to ATP5B and CANX)
2.0
1.5
1.0
0.5
0.0
7 days p.i.
14 days p.i.
Bleomycin+Saline
Bleomycin+γHV68
B
F2RL1 mRNA fold change
(normalised to ATP5B and CANX)
*
C
F2RL2 mRNA fold change
(normalised to ATP5B and CANX)
***
**
4
3
2
1
0

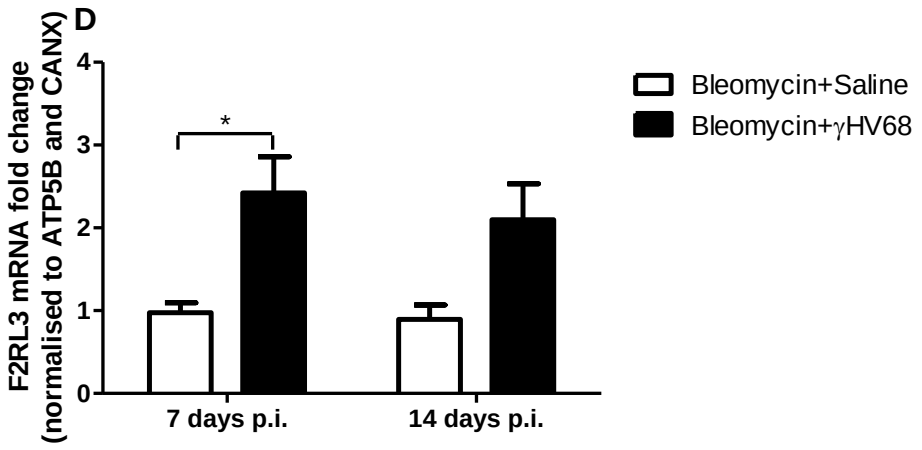

Figure 3.59. PAR receptors expression in viral infection on a background of fibrotic lung.

The mRNA expression of PAR receptors was measured by qPCR and normalised to two housekeeping genes ATP5B and CANX, and relative to bleomycin alone: panel A- PAR-1 (F2R), panel B- PAR-2 (F2RL1), panel C- PAR-3 (F2RL2), panel D- PAR-4 (F2RL3). Data are representative of mean +/- SEM, n=5-7 animals per group, one-way ANOVA, *p<0.05, **p<0.01, ***p<0.001.

3.3.1.9 Summary

- γHV68 infection on a background of bleomycin-induced fibrosis was confirmed by the expression of key viral genes in the lung and splenomegaly 14 days p.i.
- Bleomycin at a dose of 1 mg/kg increased total lung collagen 21 days post-administration but by day 28 the level of total collagen appeared to decrease. Viral infection prevented this reduction in total lung collagen accumulation at day 28 suggesting that viral infection prevents the resolution of fibrosis in this model rather than causing exacerbation of fibrosis.
- Viral infection of fibrotic lung induced a profound inflammatory response and acute lung injury superimposed on a background of fibrosis.
- γHV68 infection of fibrotic lung increased the expression of tissue factor and factor X at the mRNA level and with the protein distribution localised primarily to bronchial and abnormal alveolar epithelium.
- The expression of PAR-1 and PAR-2 was not affected by viral infection in the fibrotic lung but PAR-3 and PAR-4 mRNA levels were increased.

3.3 Herpesviruses infection in pulmonary fibrosis

3.3.2 Blocking TGFβ/ALK5 signalling in the model of viral infection on a background of pulmonary fibrosis

3.3.2.1 Introduction

Previous section showed that viral infection on the background of bleomycin-induced pulmonary fibrosis does not exacerbate fibrosis as assessed by measurements of total lung collagen, but rather prevents resolution of fibrotic response and triggers inflammatory responses. The aim of the next two sections was to investigate the potential role of TGFβ/ALK5 signalling and the role of coagulation cascade in this model of viral infection on a background of fibrosis.

There is an irrefutable link between TGFβ signalling and fibroproliferative lung disease. Multiple *in vitro* and *in vivo* studies have shown that TGFβ signalling promotes extracellular matrix production and deposition and fibroblast to myofibroblast differentiation (Bonniaud et al., 2004b; Decologne et al., 2007; Fernandez and Eickelberg, 2012). Targeting TGFβ signalling by inhibition of the TGFβ receptor TβRI/Activin receptor-like kinase 5 (ALK5) with the small molecule antagonist SB525334 attenuates experimental pulmonary fibrosis (Scotton et al. 2013; Bonniaud et al. 2005). Furthermore, a growing body of evidence strongly suggests that viral infection increases the rate of TGFβ activation (Stoolman et al. 2010; Vannella et al. 2010) and increases the cell responsiveness to TGFβ (Naik et al., 2011). Having established a model of viral infection on a background of pulmonary fibrosis, as described in the previous **Section 3.3.1** of this chapter, the aim of this study was to investigate whether TGFβ/ALK5 signalling plays a role in the development of fibrosis in this model.

C57BL/6 male mice (aged 10-12 weeks) were administered bleomycin at 1 mg/kg or saline via oropharyngeal route. Two weeks later, after the establishment of the fibrotic phase, mice were inoculated with 100,000 PFU γHV68 or given saline via

intranasal route. Mice were administered SB525334 at 30 mg/kg via oral gavage twice daily from the day after the inoculation until the end of the experiment 14 days later.

3.3.2.2 Effect of SB525334 treatment on mouse body weight and *ex vivo* lung and spleen weights

Following the oropharyngeal administration of 1 mg/kg bleomycin, mice lost on average 10% of starting body weight with a nadir at day 8, at which time the difference was significant for all bleomycin-challenged groups when compared to saline-instilled mice with stable body weight. After the initial weight loss, the weight stabilised and returned to the starting body weight by day 14, when mice were inoculated with the γHV68 virus (**Figure 3.60**). Treatment with SB525334 did not visibly influence mouse body weight in bleomycin-alone treated animals, but appeared to have abolished the second wave of the weight loss observed after administration of the virus. Mice in the bleomycin-γHV68-vehicle arm of the experiment lost approximately 5% body weight between days 18 and 24 of the experiment (**Figure 3.60B**). Saline control groups, mock- and γHV68-infected, continued to gain weight throughout the duration of the experiment and mice in all experimental groups gained weight by the end of the experiment.

Bleomycin administration and viral infection lead to an increase in *ex vivo* lung weight. Bleomycin-treated lungs were on average 30% heavier than control saline-administered lungs, while viral infection on a background of bleomycin-induced fibrosis caused a 40% increase in lung weights when compared to relevant control (**Figure 3.61A**). Administration of the virus in saline-treated mice caused a modest increase in lung weight. Treatment with SB525334 did not significantly affect the *ex vivo* lung weight although there is a notable trend towards a decrease in the bleomycin-alone treated lungs.

Consistently with the previous study presented in this thesis, at 14 days post-infection there was a significant splenomegaly observed in all experimental groups that have been infected with γHV68 (**Figure 3.61B**). Administration of bleomycin

alone did not affect the spleen weight but a double challenge with bleomycin and γHV68 virus significantly increased spleen weight when compared to γHV68 infection alone. Interestingly, treatment with SB525334 significantly reduced the spleen weight when compared to vehicle control.

In this study the expression of viral genes **(Figure 3.62)**, M3, glycoprotein B and DNA polymerase, was readily detected in the infected saline-treated lungs and infected fibrotic lungs 14 days p.i., which suggests an ongoing low-level viral replication in the lung.

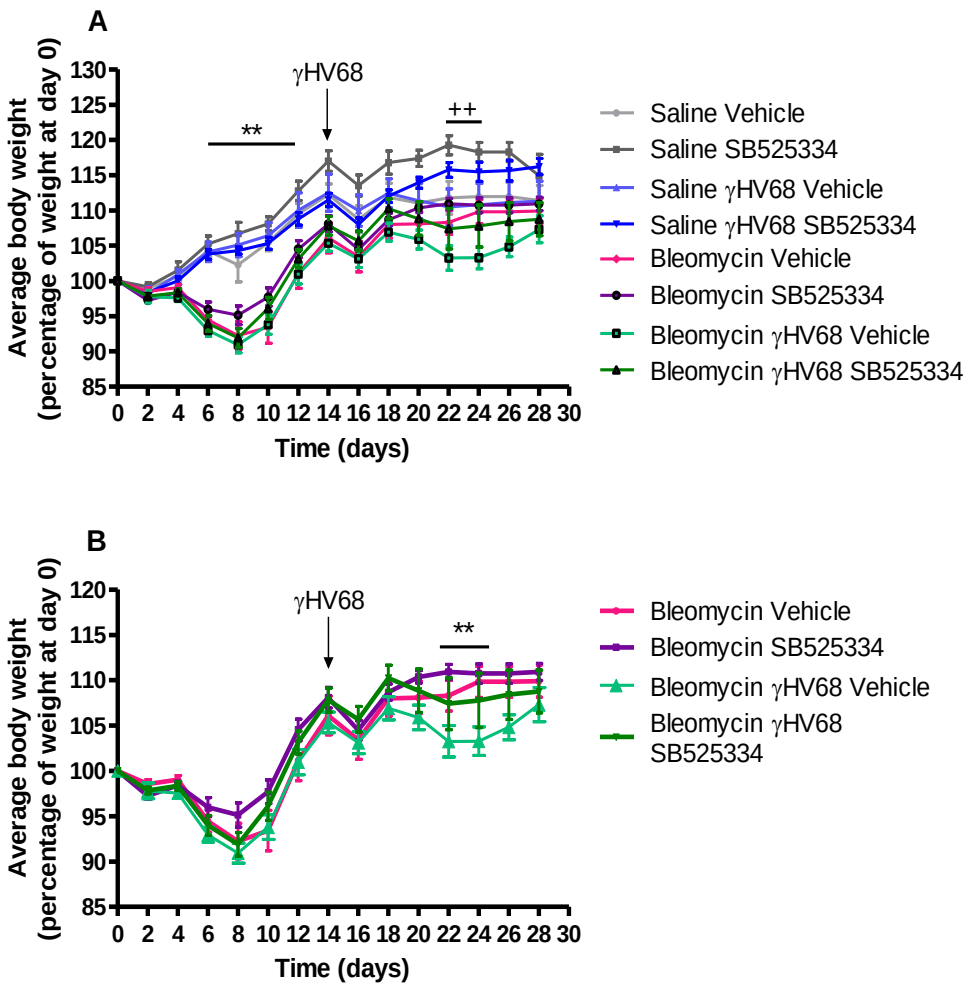

Figure 3.60. Effect of the viral infection on a background of lung fibrosis on mouse body weight.

C57BL/6 mice were administered bleomycin via oropharyngeal route at 1 mg/kg, followed by infection with 100,000 PFU γHV68 or saline intranasally on day 14. Between days 15 and 28, mice were administered SB525334 (30 mg/kg) twice daily via oral gavage. Data represent percentage change in average mouse body weight relative to weight at day 0 over the course of the experiment. Each time point represents mean +/- SEM of n=7-14 animals per group; two-way ANOVA was performed for statistical analysis. Panel A- all experimental groups, **p<0.01 bleomycin-challenged groups compared to saline-control groups, ++p<0.01 bleomycin+γHV68+vehicle compared to saline control groups; and panel B- comparison of bleomycin-treated mice only, **p<0.01 bleomycin+γHV68+vehicle group compared to bleomycin alone groups.

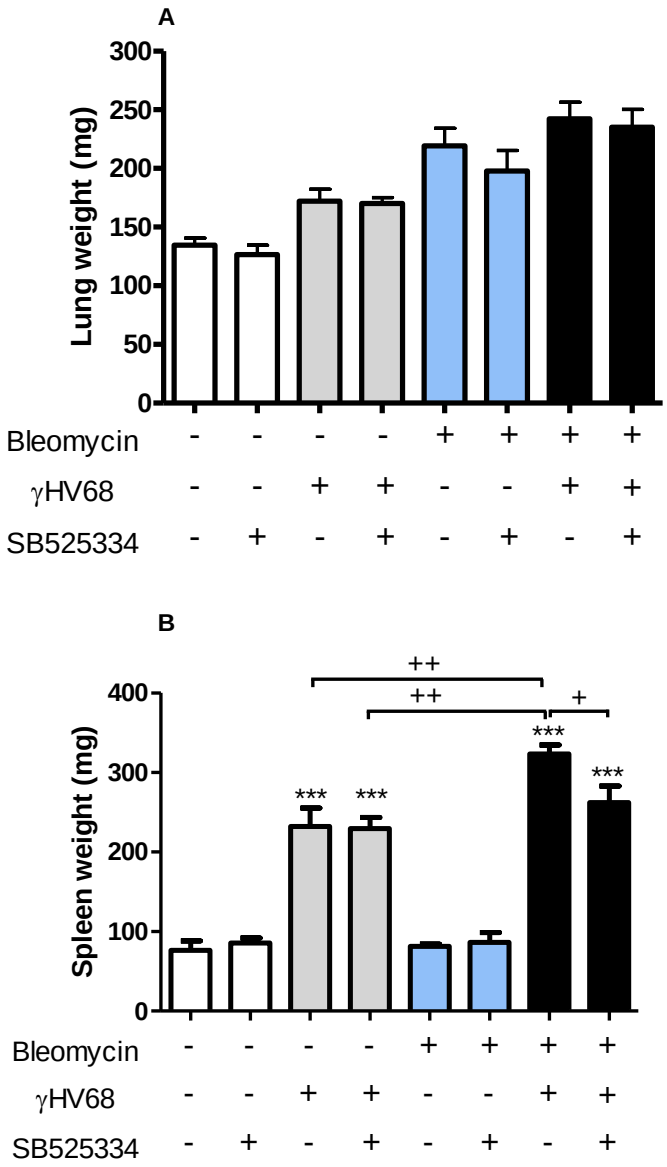

Figure 3.61. *Ex vivo* lung and spleen weights in γHV68 infection of bleomycin-induced pulmonary fibrosis.

C57BL/6 mice were administered bleomycin via oropharyngeal route at 1 mg/kg, followed by infection with 100,000 PFU γHV68 or saline intranasally on day 14. Between days 15 and 28 mice were administered SB525334 (30 mg/kg) twice daily via oral gavage. Data represent average weights of mouse lungs- panel A; and spleens- panel B; measured *ex vivo* 14 days post infection; representative of n=7-14 animals per group, One-way ANOVA statistical analysis, ***p<0.001 γHV68-infected groups versus each mock-infected groups; +p<0.05, ++p<0.01 comparison of γHV68-infected saline-treated groups and γHV68-infected bleomycin-challenged groups.

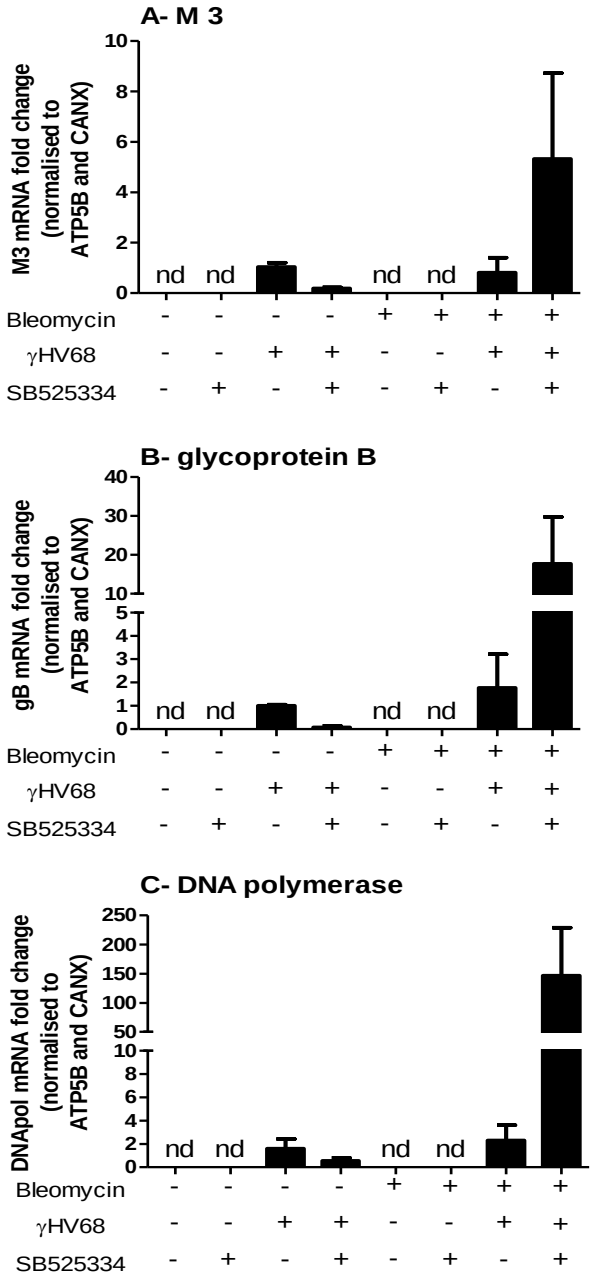

Figure 3.62. Determination of viral gene expression in the lungs.

C57BL/6 mice were administered bleomycin via oropharyngeal instillation at 1 mg/kg, followed by infection with 100,000 PFU γHV68 or saline intranasally on day 14. The expression of viral genes in the lungs 14 days p.i. was assessed by qPCR and data are presented as fold change in mRNA levels relative to two housekeeping genes ATP5B and CANX and representative of mean +/- SEM, n=3-8 animals per group. Panel A- M3; panel B- glycoprotein B; panel C- DNA polymerase; nd- not detected.

3.3.2.3 Collagen deposition in infected and fibrotic lungs.

In the pilot study of the γHV68 infection on a background of pulmonary fibrosis (**Section 3.3.1**), total lung collagen measured by hydroxyproline levels (HPLC) was increased 7 days p.i. and there was no difference between the mock- and virally-infected animals (**Figure 3.51A**). At 14 days p.i. and 28 days into the study total lung collagen in the bleomycin-alone group was reduced in comparison to day 7 p.i. while γHV68-infected mice continued to show significantly elevated total lung collagen (**Figure 3.51B**). As shown in **Figure 3.63A**, in this study, total lung collagen was significantly elevated in bleomycin mock- and bleomycin-γHV68-infected mice when compared to saline control groups at 14 days p.i.. However, viral infection did not further enhance collagen deposition in the lung when compared to the bleomycin alone group. The administration of SB525334 reduced the bleomycin-associated increase in lung collagen accumulation (unpaired Student t-test, $p=0.048$) but did not significantly reduce lung collagen accumulation in the γHV68-challenged mice.

Standard Sircol colorimetric assay was also performed to measure soluble collagen content in lung homogenates **(Figure 3.63B)**. The levels of collagen detected by Sircol were 20-fold lower than those detected by HPLC. Total lung collagen was elevated in all bleomycin-challenged groups compared to saline mock-infected groups. Treatment with SB525334 significantly reduced total lung collagen accumulation when compared to bleomycin-vehicle group. Infection with γHV68 in the fibrotic lung did not further increase collagen accumulation in the lungs and SB525334 treatment also did not have any effect on total lung collagen in the virally-infected fibrotic lungs. In contrast to the HPLC results, the Sircol results showed non-significant increase in collagen level in γHV68 infection alone.

It has been previously reported that serum proteins can interfere with Sircol collagen assay (Lareu et al., 2010) and discrepancies between the collagen levels in bleomycin-induced fibrosis as measured by HPLC and Sircol have also been reported (Scotton et al., 2013). It is therefore possible that the increase in collagen levels

detected by Sircol in γHV68-infected saline-treated group reflects serum proteins retained in the lungs after the clearance of vascular leak.

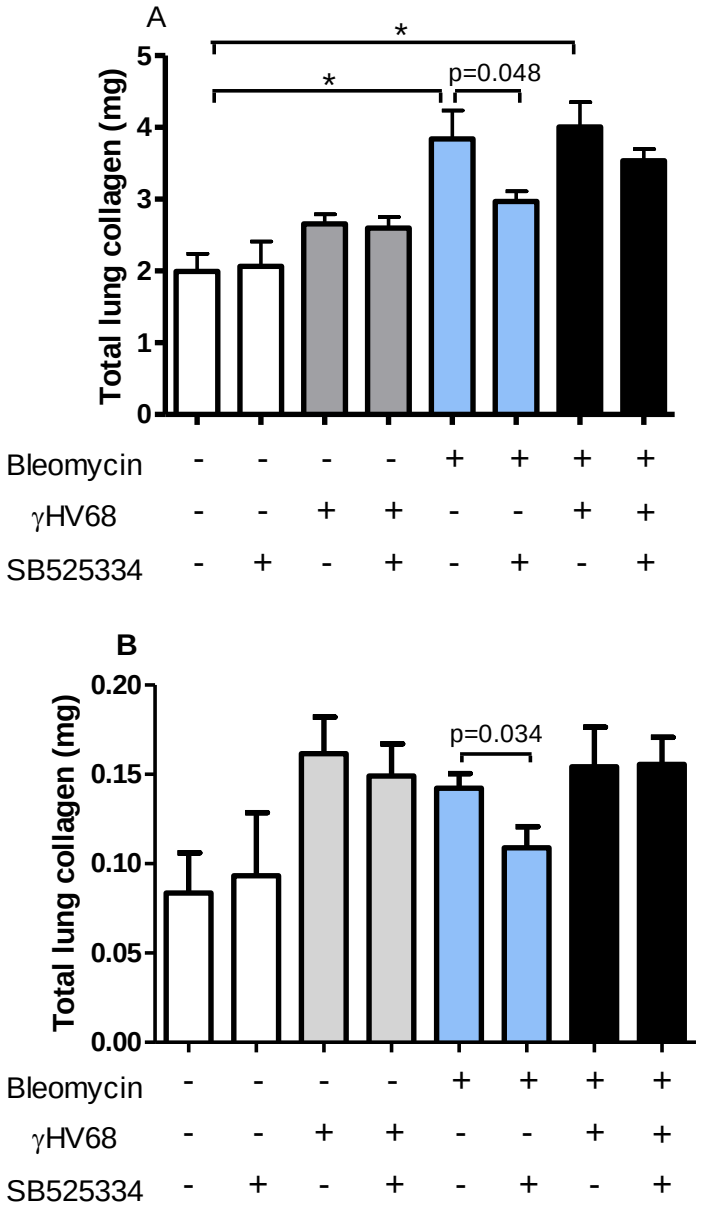

Figure 3.63. Effect of SB525334 treatment on total lung collagen accumulation in γHV68 infection of fibrotic lung.

C57BL/6 mice were administered bleomycin via oropharyngeal route at 1 mg/kg, followed by infection with 100,000 PFU γHV68 or saline intranasally on day 14. Between days 15 and 28 mice were given SB525334 (30 mg/kg) twice daily via oral gavage. The total collagen in the lungs was quantified by A-HPLC and B-Sircol. Data are representative of mean +/- SEM, n=3-8 animals per group and one-way ANOVA was performed for statistical analysis, *p<0.05, unpaired Student t-test was performed to compare bleomycin alone versus bleomycin+SB525334 groups.

3.3.2.4 *Ex vivo* µCT analysis of fibrosis and viral infection

A dose of 1 mg/kg bleomycin used in this study caused a significant increase of total lung collagen as measured by hydroxyproline levels in the lungs (HPLC) but the viral infection in bleomycin-treated lung did not further increase the level of lung collagen accumulation. As the traditional HPLC endpoint measurement used to evaluate fibrosis has a limited signal window, particularly when the lower dose of bleomycin is used, *ex vivo* micro-computed tomography (µCT) was used in conjunction with histological analysis to fully characterise the impact of viral infection on pulmonary fibrosis. µCT technology has been validated *in vivo* for repeated longitudinal studies of lung cancer (Namati et al., 2010) and *ex vivo* for investigating the lung architecture (Thiesse et al., 2010; Vasilescu et al., 2012) and as an endpoint for evaluating fibrosis (Rodt et al., 2010; Scotton et al., 2013). The aim of this part of the study was to evaluate whether viral infection adds to the pathology of fibrosis and whether µCT is an informative technique to quantify these changes.

All lungs were scanned at 13 µm resolution and representative reconstructed lung images from each experimental group are shown in **Figure 3.64**. The appearance of control lungs is homogenous and reveals a network of airways through a transparent parenchyma. In this experimental model of fibrosis peripheral areas of the lungs are mostly affected and dense lesions are clearly distinguishable on the dorsal side of bleomycin-challenged lungs. These lesions are noticeably dispersed in the SB525334 treated lungs. In γHV68-infected lungs with existing fibrosis these lesions appear to be more extensive and again are reduced in the SB525334-treated lungs. Virally-infected and saline-treated lungs have grossly normal appearance.

Pattern-recognition software was subsequently applied to quantify abnormal areas in the lungs. The software was first “trained” to discriminate between normal parenchyma and fibrotic lesions, excluding other tissue such as the heart. **Figure 3.65** shows representative coronal µCT scans matched with a segmentation map produced by the software and compared with histology for each experimental group. As exemplified by the saline control and saline-SB525334 treated lungs, µCT

provides a high resolution image of gross anatomy and architecture of the lung with clearly distinguishable airways and airspaces. As confirmed by histology, these lungs have normal morphology.

In contrast, µCT of bleomycin-injured lungs reveals dense fibrotic lesions. These areas of consolidation are largely concentrated around broncho-vascular bundles, consistent with the route of administration of bleomycin, and extend to the periphery of the lung. Prominent subpleural scarring and traction bronchiectasis appears to "ruffle" otherwise smooth edges of the lung. At the level of light microscopy, these abnormal areas correspond to fibrotic bands of elongated fibroblast bundles embedded in collagen fibres as visualised by modified Martius Scarlett Blue (MSB) staining. Lungs of mice treated with SB525334 displayed fewer areas of dense consolidation and less extensive scarring of the lung.

Inoculation with the γHV68 virus alone did not appear to cause any lasting alterations to the lung architecture. In contrast, γHV68 virus infection in mice injured with bleomycin led to increased areas of dense consolidation centred around airways. Furthermore, the infected lungs showed large areas with ground glass opacities suggestive of inflammatory cell infiltrates. Indeed, the histological analysis confirmed that next to dense fibrotic areas, multiple inflammatory cell aggregates were apparent in γHV68-infected lungs. µCT scanning and segmentation analysis revealed that SB525334 treatment appeared to have reduced these abnormal areas, which was also confirmed by histology. Although there was discernible reduction in pathological changes to the infected lungs with SB525334, the differences were not as dramatic as when fibrotic lungs were treated with the ALK5 inhibitor.

Saline

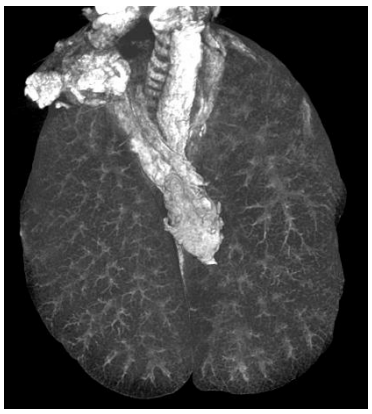

Saline + SB525334

Bleomycin

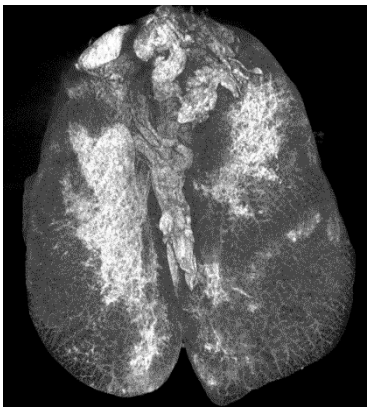

Bleomycin + SB525334

Saline γHV68

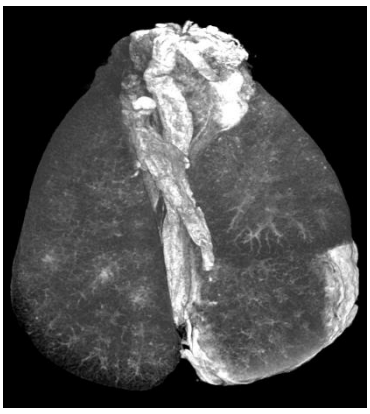

Saline γHV68 + SB525334

Bleomycin γHV68

Bleomycin γHV68 + SB525334

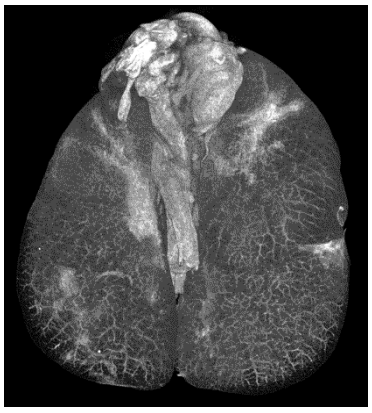

Figure 3.64. Reconstruction of µCT lung scans showing gross lung appearance. C57BL/6 mice were administered bleomycin via oropharyngeal route at 1 mg/kg, followed by infection with 100,000 PFU γHV68 or saline intranasally on day 14. Between days 15 and 28 mice were given SB525334 (30 mg/kg) twice daily via oral gavage. The lungs were insufflated, fixed and scanned at high resolution (13 µm). The figure shows representative 3D reconstructed images of the scanned lungs from all experimental groups.

Figure 3.65. Characterisation of the changes in lung morphology of virally infected fibrotic lungs.

C57BL/6 mice were administered bleomycin via oropharyngeal route at 1 mg/kg, followed by infection with 100,000 PFU γHV68 or saline intranasally on day 14. Between days 15 and 28 mice were given SB525334 (30mg/kg) twice daily via oral gavage. Panel A- representative coronal µCT scans with B- corresponding segmentation map showing normal parenchyma (green), abnormal lung areas (red) and other tissue (blue). Panel C- histology sections stained with haematoxylin and eosin (H&E) and panel D- modified Martius Scarlett Blue method (MSB) to visualise collagen fibres. Selected areas are shown in 100x magnification. Panel E and F- H&E and MSB sections at 200x magnification. Complete sets of images are shown for every experimental group as annotated. AE- alveolar epithelium, BE- bronchial epithelium, FB- fibroblasts, COL- collagen, IA- inflammatory aggregates.

Saline

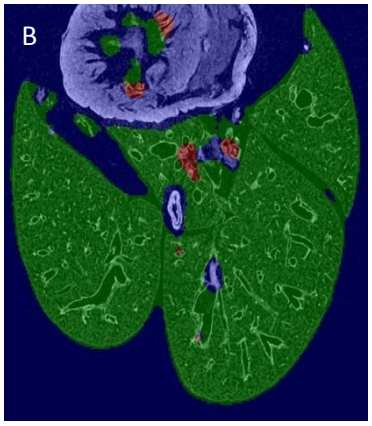

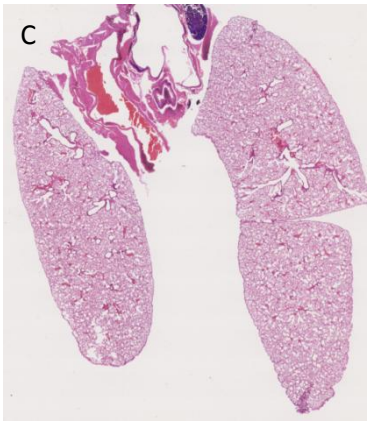

Saline, SB525334

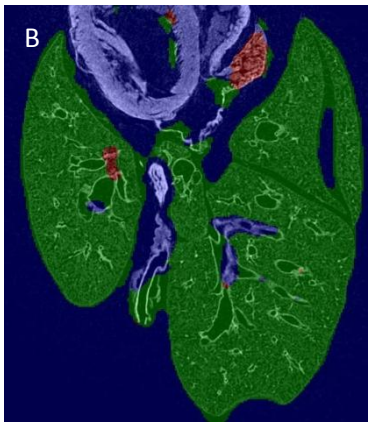

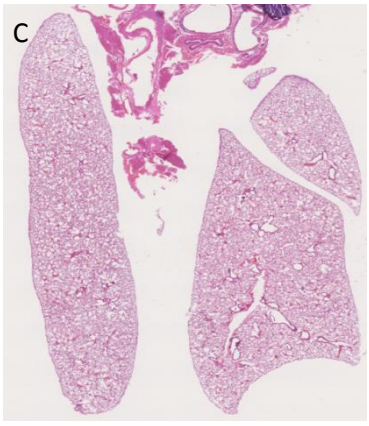

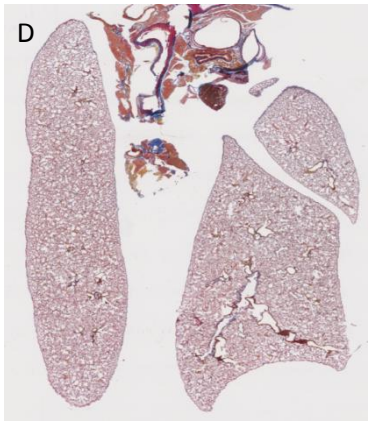

Saline, γHV68

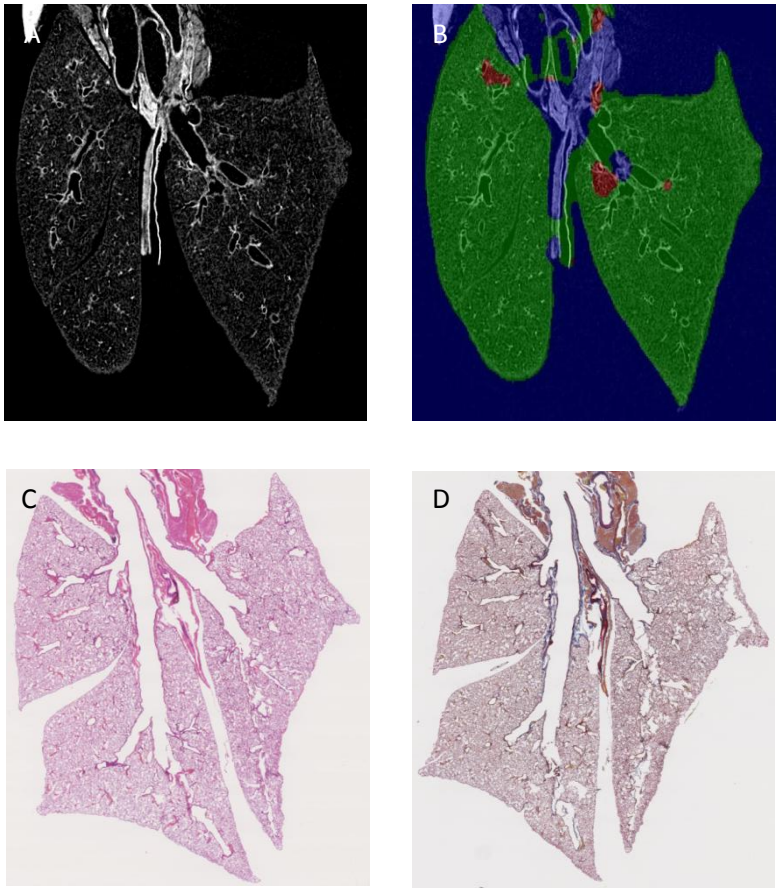

Saline, γHV68, SB525334

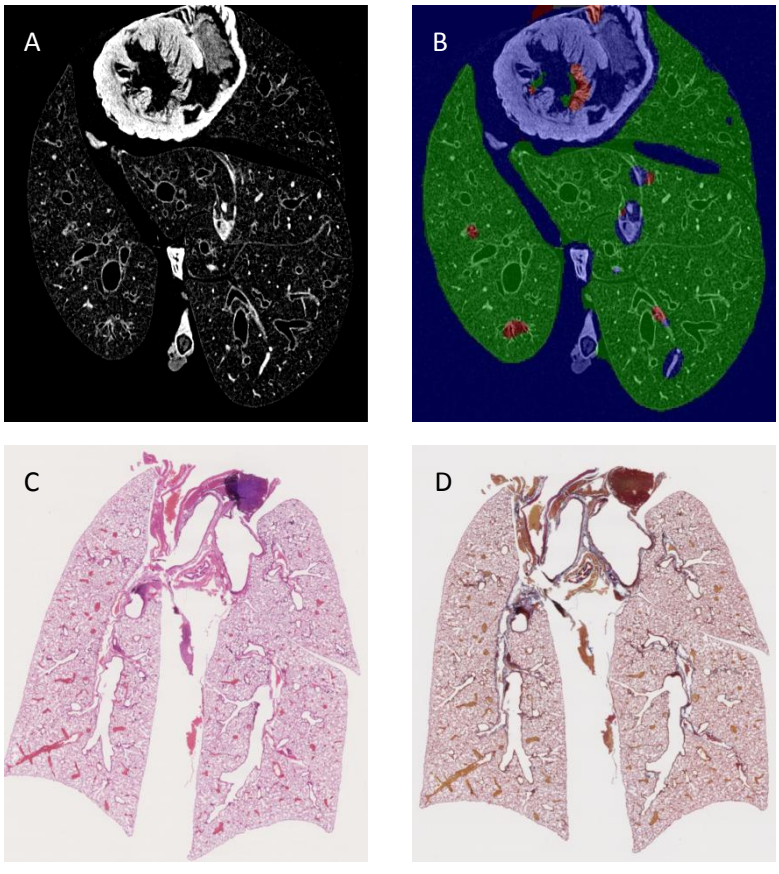

Bleomycin

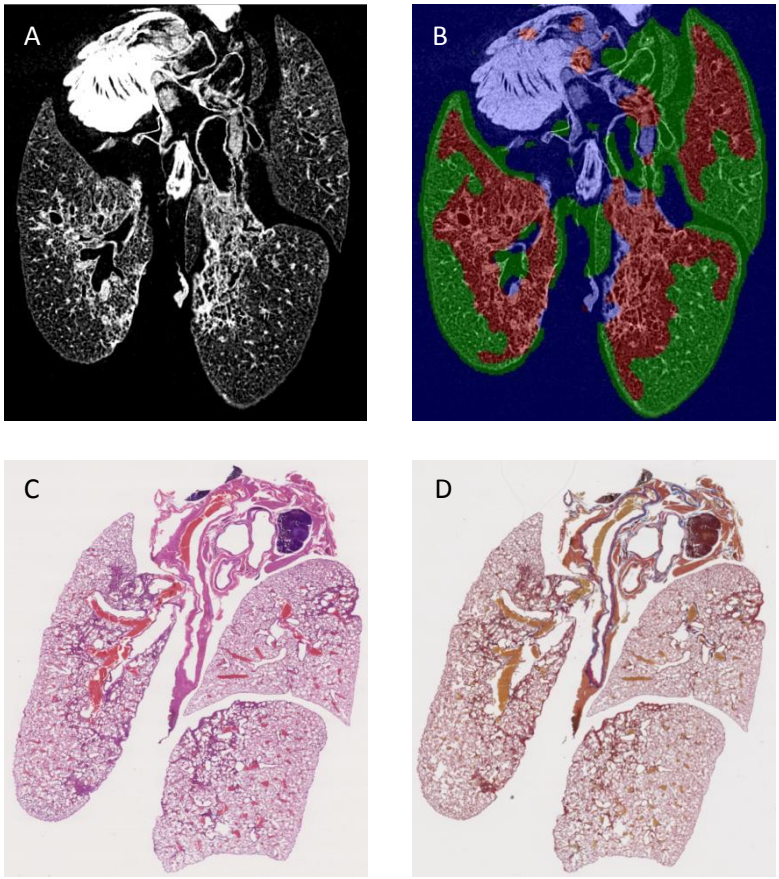

Bleomycin, SB525334

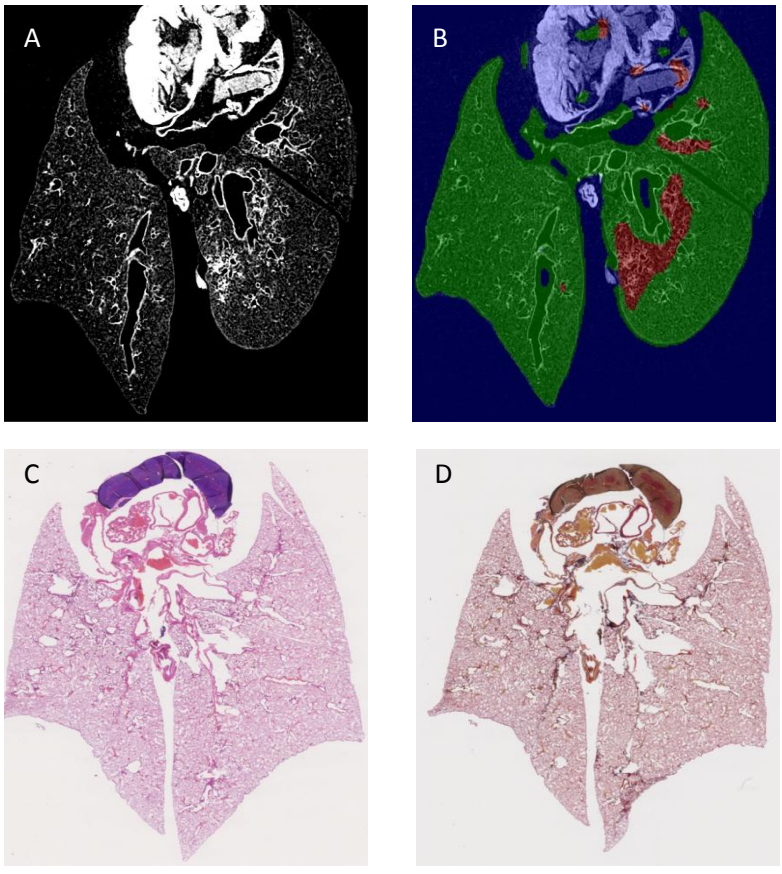

Bleomycin, γHV68

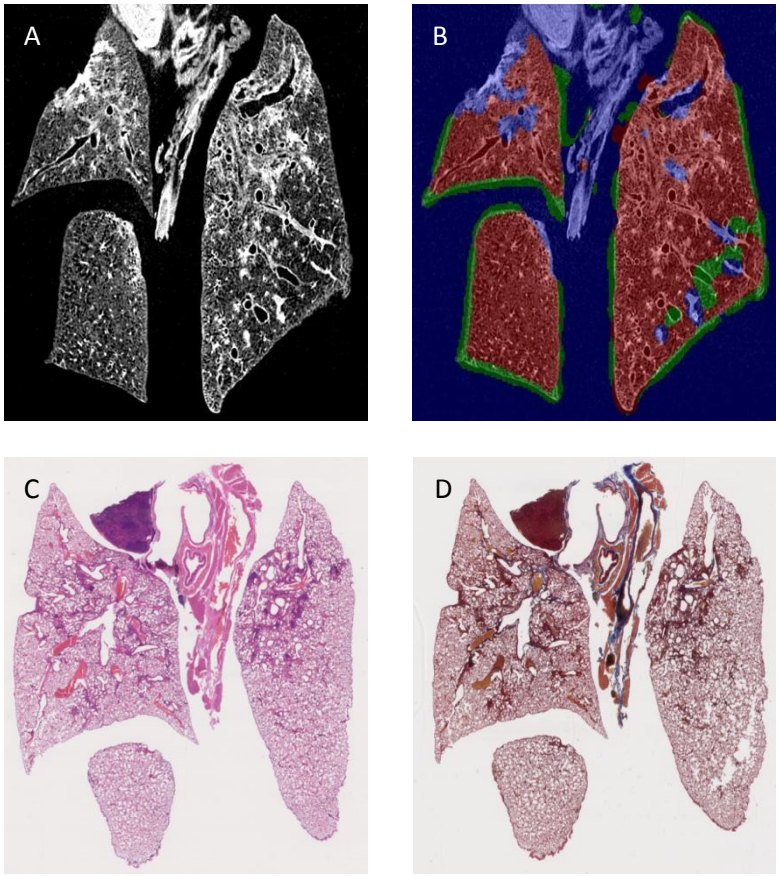

Bleomycin, γHV68, SB525334

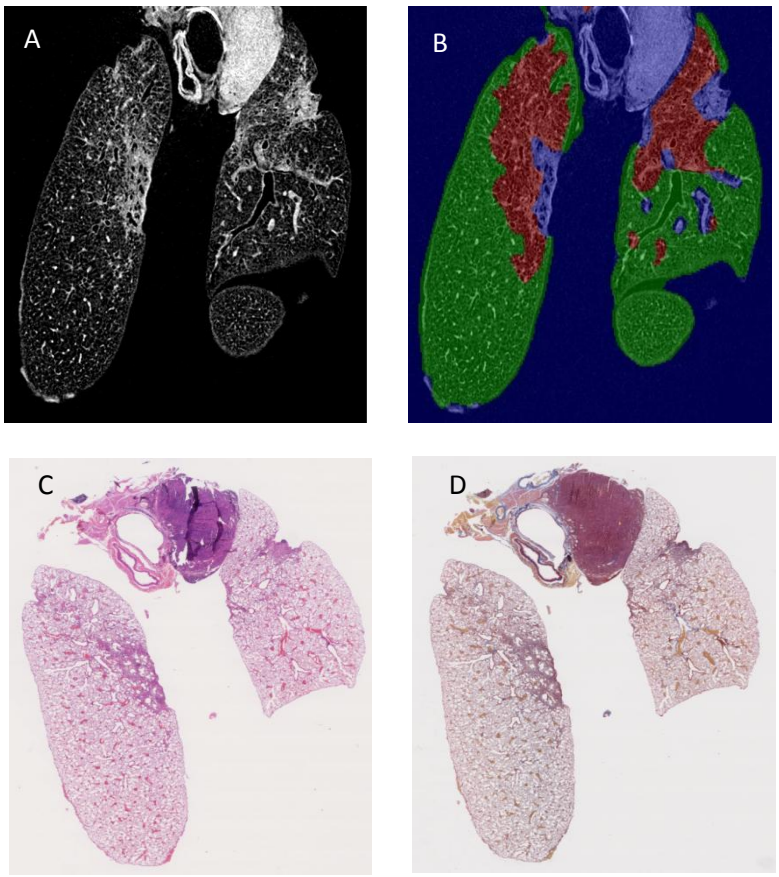

E Saline

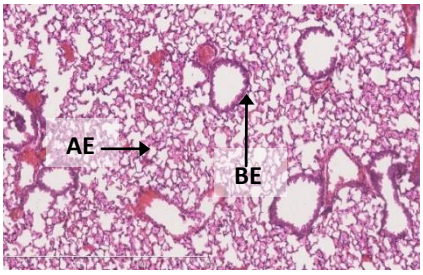

F

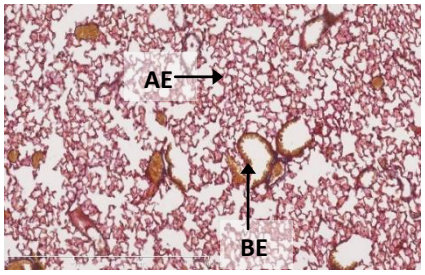

Saline, SB525334

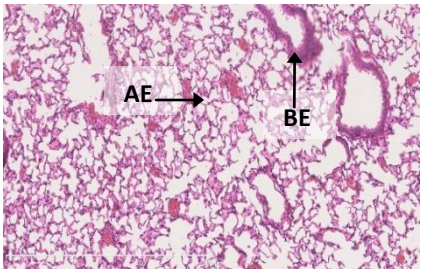

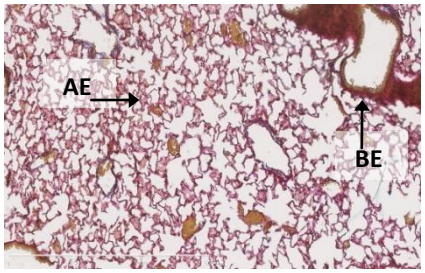

Saline, γHV68

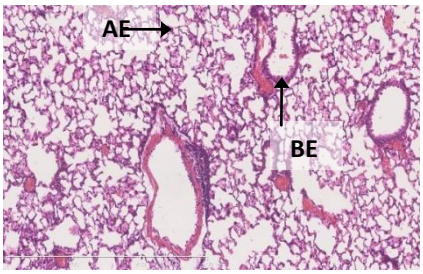

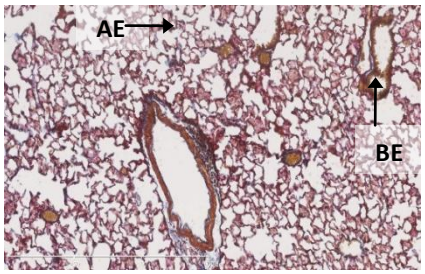

Saline, HV68, SB525334

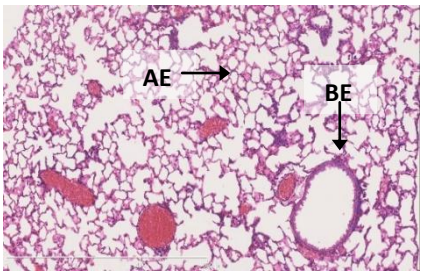

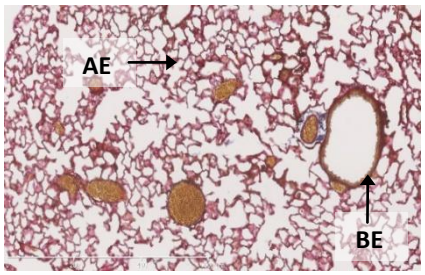

Bleomycin

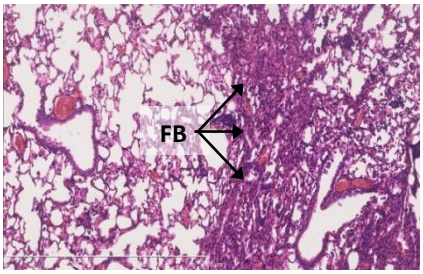

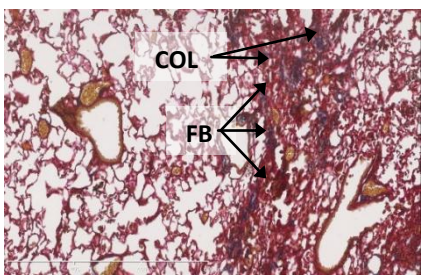

Bleomycin, SB525334

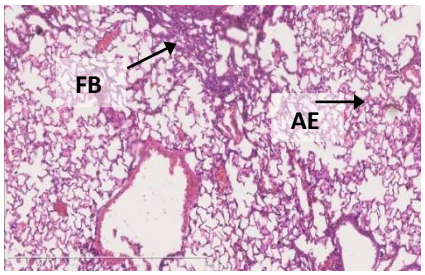

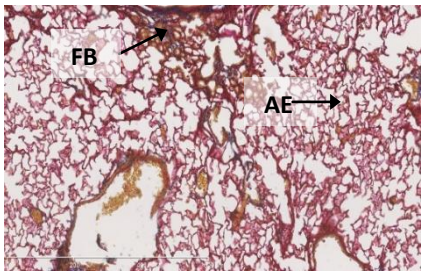

Bleomycin, γHV68

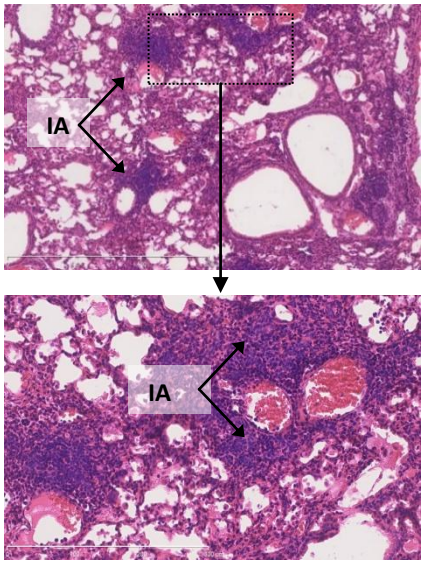

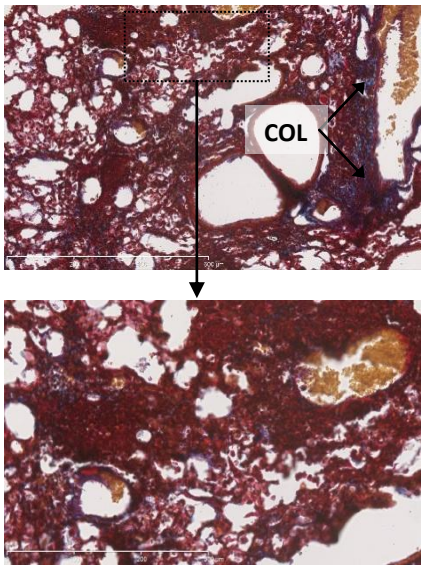

Bleomycin, γHV68, SB525334

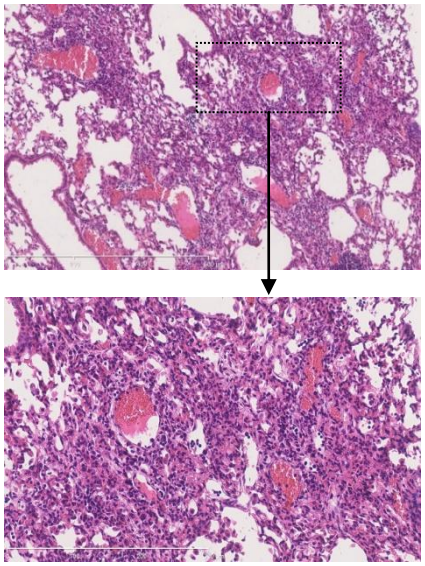

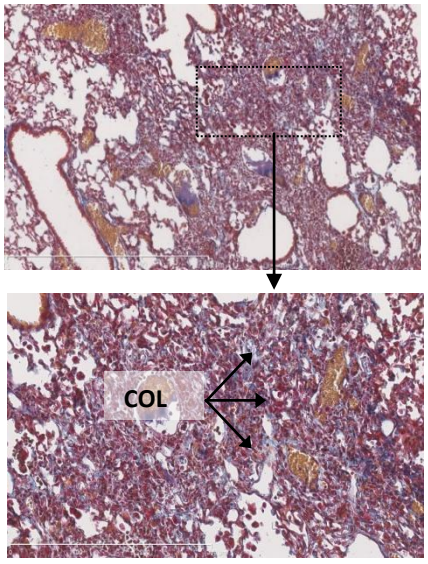

3.3.2.5 Quantification of µCT analysis of viral infection on a background of pulmonary fibrosis

The InForm analysis and segmentation of the µCT scans was subsequently used to quantify the extent of abnormal areas in the lungs. Whole lung volume was calculated first to confirm that the measurements were not affected by differences in lung insufflation and processing. As shown in **Figure 3.66** the average volumes of lungs did not differ between experimental groups.

The abnormal areas were subsequently expressed as a percentage of total lung volume for all experimental groups. As shown in **Figure 3.67** saline treated groups had less than 10% of areas segmented as abnormal by the software while lungs challenged with bleomycin showed an average of 40% abnormal areas. The lungs of animals treated with SB525334 showed 15% abnormal areas in the lung, which was a significant reduction when compared to all other bleomycin-challenged groups. Infection with γHV68 further increased the percentage of abnormal lung to an average of 50% but this trend fell short of statistical significance in comparison to the bleomycin-challenged group. Intervention with SB525334 in virally-infected fibrotic lung reduced the percentage of abnormal areas in the lung but this decrease was not as striking as observed in fibrotic lungs with the SB525334 treatment.

This pattern was corroborated by the analysis of associated densities for each lung. Abnormal density values in the bleomycin-injured lungs read 4500 voxels while normal lungs were below 1000 voxels **(Figure 3.68)**. SB525334 treatment reduced the fibrotic lung density to 2000 voxels, which was significantly lower when compared to fibrotic infected lungs and bleomycin-challenged lungs. Fibrotic lung density increased further following viral infection and reached 6000 voxels density but SB525334 only slightly reduced this increase in density in γHV68-infected fibrotic lungs. Taken together these data suggest that SB525334 blockade of TGFβ signalling in γHV68-infected fibrotic lungs may modulate the inflammatory response, which is detected by the software as a change in the appearance of the lungs (**Figure 3.67**). However, in γHV68-infected fibrotic lung SB525334 treatment did not appear to interfere with fibrotic responses.

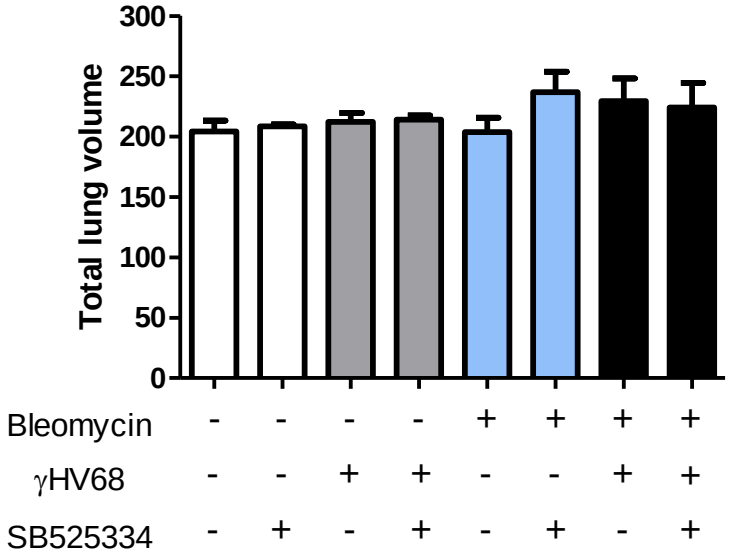

Figure 3.66. Total lung volume of µCT scanned lungs.

C57BL/6 mice were administered bleomycin via oropharyngeal route at 1 mg/kg, followed by infection with 100,000 PFU γHV68 or saline intranasally on day 14. Between days 15 and 28 mice were given SB525334 (30 mg/kg) twice daily via oral gavage. The graph shows an average of total volume of the lungs +/- SEM, processed for µCT and InForm analysis for each experimental group, n=2-5 mice.

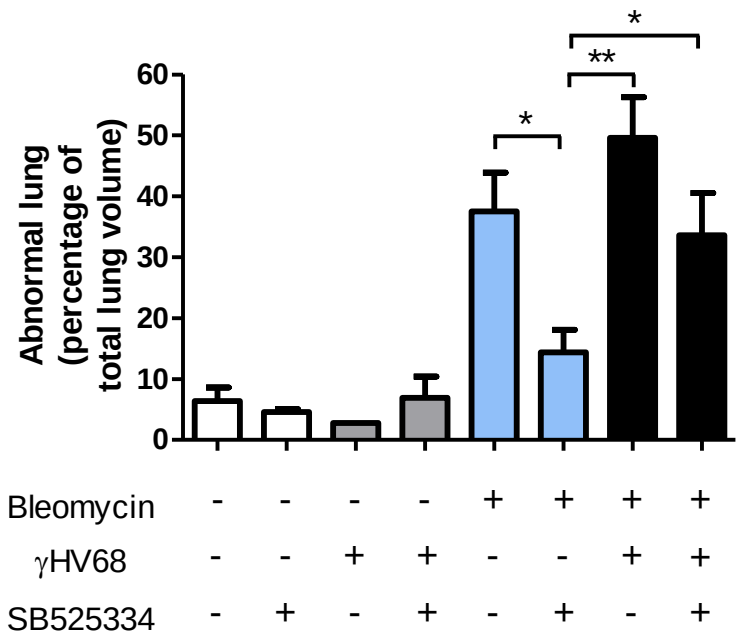

Figure 3.67. Quantification of abnormal lung area in viral infection on a background of pulmonary fibrosis.

C57BL/6 mice were administered bleomycin via oropharyngeal route at 1 mg/kg, followed by infection with 100,000 PFU γHV68 or saline intranasally on day 14. Between days 15 and 28 mice were given SB525334 (30 mg/kg) twice daily via oral gavage. The abnormal lung area were quantified by InForm analysis of µCT scans and are expressed as a percentage of total lung volume. Data are representative of n=2-5 animals per group, one-way ANOVA, *p<0.05, **p<0.01, comparison of all bleomycin-challenged groups (n=5).

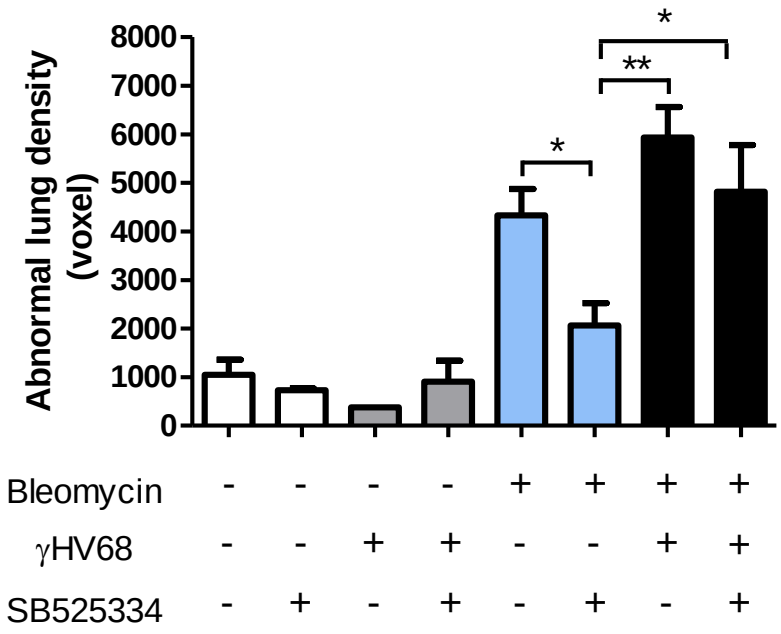

Figure 3.68. Quantification of lung density in viral infection on a background of pulmonary fibrosis.

C57BL/6 mice were administered bleomycin via oropharyngeal route at 1 mg/kg, followed by infection with 100,000 PFU γHV68 or saline intranasally on day 14. Between days 15 and 28 mice were given SB525334 at dose of 30 mg/kg twice daily via oral gavage. The abnormal lung densities were quantified by InForm analysis of µCT scans and are expressed as changes of density in the total lung. Data are representative of n=2-5 animals per group, one-way ANOVA, *p<0.05, **p<0.01, comparison of all bleomycin-challenged groups (n=5).

In order to support the segmentation analysis, voxel density analysis was performed which does not rely on the software segmentation output. Mean number of voxels per lung at each greyscale value (0 being least dense and 255 being most dense) for each experimental group is presented in the form of histograms and Student t-test was performed to compare individual groups and indicate statistically significant differences in the mean voxels numbers between the groups (**Figures 3.69** and **3.70**). **Figure 3.69** shows the histogram for all experimental groups and demonstrates a clear separation in density between saline controls, bleomycin alone and bleomycin and virus double-injured lungs. The majority of voxels in the virally infected saline lungs fall close to the saline control lungs and the bleomycin-injured lungs treated with SB525334 also have voxels of lower density. In the bleomycin alone and bleomycin and virally infected lungs there was a marked shift to the left indicating more voxels of higher density in comparison to saline controls, which corresponded to higher density on μCT scans.

Density histograms shown in **Figure 3.70A** demonstrate that for saline control groups and γHV68-inoculated saline control groups the greyscale density values were similar, which suggests that the viral infection alone did not affect the overall density of the lung. In contrast saline control lungs were visibly less dense than fibrotic lungs with a significant shift in pixel densities in a range of 50 to 110 (**Figure 3.70B).** SB525334 treatment did not affect the architecture of a normal lung but reduced the density of bleomycin-challenged lungs and there was no significant difference in pixel densities between saline control lungs and SB525334-treated fibrotic lungs. **Figure 3.70C** shows that a significant shift towards higher greyscale values was also observed between virally-infected saline lungs and virally-infected fibrotic lungs in a pixel density range of 50 to 150.

The pixel density range of 50 to 150 encompassed the differences in densities between the saline control, fibrotic and virally-infected groups and was chosen to demonstrate the distribution of density pixels in these lungs. As shown in **Figure 3.70E**, this greyscale range represented mainly airway walls in saline lungs and virally-infected saline lungs. In contrast, dense fibrotic areas were highlighted in the

bleomycin-challenged lungs. In virally infected fibrotic lungs the pixel range also covered abnormal changes in the lung parenchyma as well as fibrotic lesions.

Comparison of bleomycin-injured, fibrotic lungs showed a range of changes dependent on infection status and treatment status **(Figure 3.70D)**. Significant differences over a wide pixel range (50 to 115) were observed between bleomycin alone and bleomycin-γHV68 lungs. The distribution of pixels within this greyscale range highlighted fibrotic lesions and also extensive areas of parenchyma in the infected-fibrotic lungs **(Figure 3.70F).** Although SB525334 significantly reduced the density of the fibrotic lungs, the pixel range and distribution changed greatly in the γHV68-infected fibrotic lungs. ALK5 inhibition in the bleomycin-injured lungs reduced the extent and severity of fibrosis when compared with the bleomycin-vehicle lungs and this observation was further supported by the greyscale density differences in a range of 100 to 155, which localised to fibrotic lesions and airway walls in the lungs **(Figure 3.70F)**. In contrast, the range of significantly different pixels between bleomycin-γHV68 and bleomycin-γHV68-SB525334 was narrow (50 to 65) and distributed through parenchyma, which suggests that the ALK5 inhibitor in the environment of viral infection superimposed on a background of fibrosis primarily targets inflammatory changes **(Figure 3.70E)**.

In summary, these data show that SB525334 treatment in fibrotic lungs reduced the density of treated lungs, which suggests that blocking TGFβ signalling attenuates, but does not reverse, the development and course of fibrosis. Furthermore, a lack of statistical difference between saline and bleomycin-SB525334 treated lungs in pixel density further supports the rationale of targeting TGFβ in fibrosis. In contrast, the therapeutic effect of SB525334 was reduced in the event of viral infection on a background of pulmonary fibrosis.

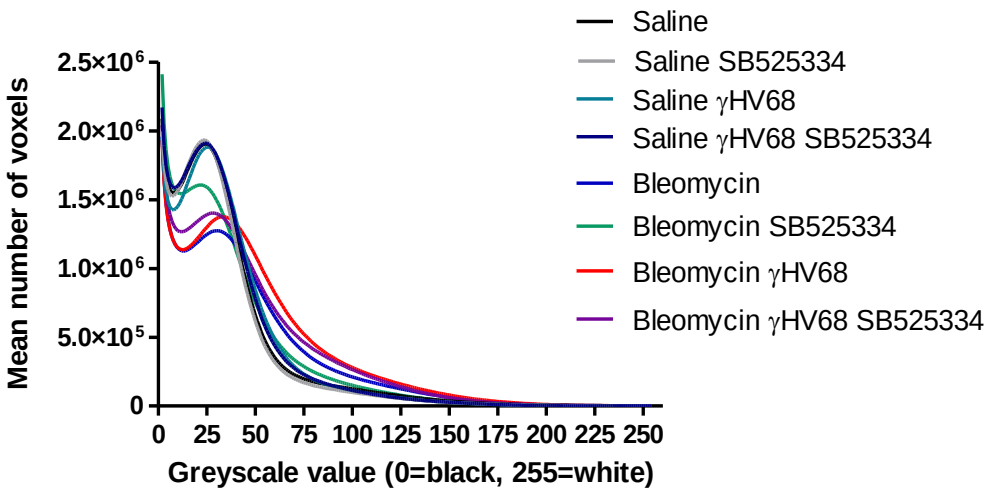

Figure 3.69. Voxel density histograms of µCT scanned lungs.

C57BL/6 mice were administered bleomycin via oropharyngeal route at 1 mg/kg, followed by infection with 100,000 PFU γHV68 or saline intranasally on day 14. Between days 15 and 28 mice were given SB525334 (30 mg/kg) twice daily via oral gavage. This density histogram shows distribution of voxels corresponding to each experimental groups plotted as a mean number of voxels against the greyscale values reflecting the density of the tissue, where 0 is black and 255 is white. Data are representative of an average of n=2-5 animals per group.

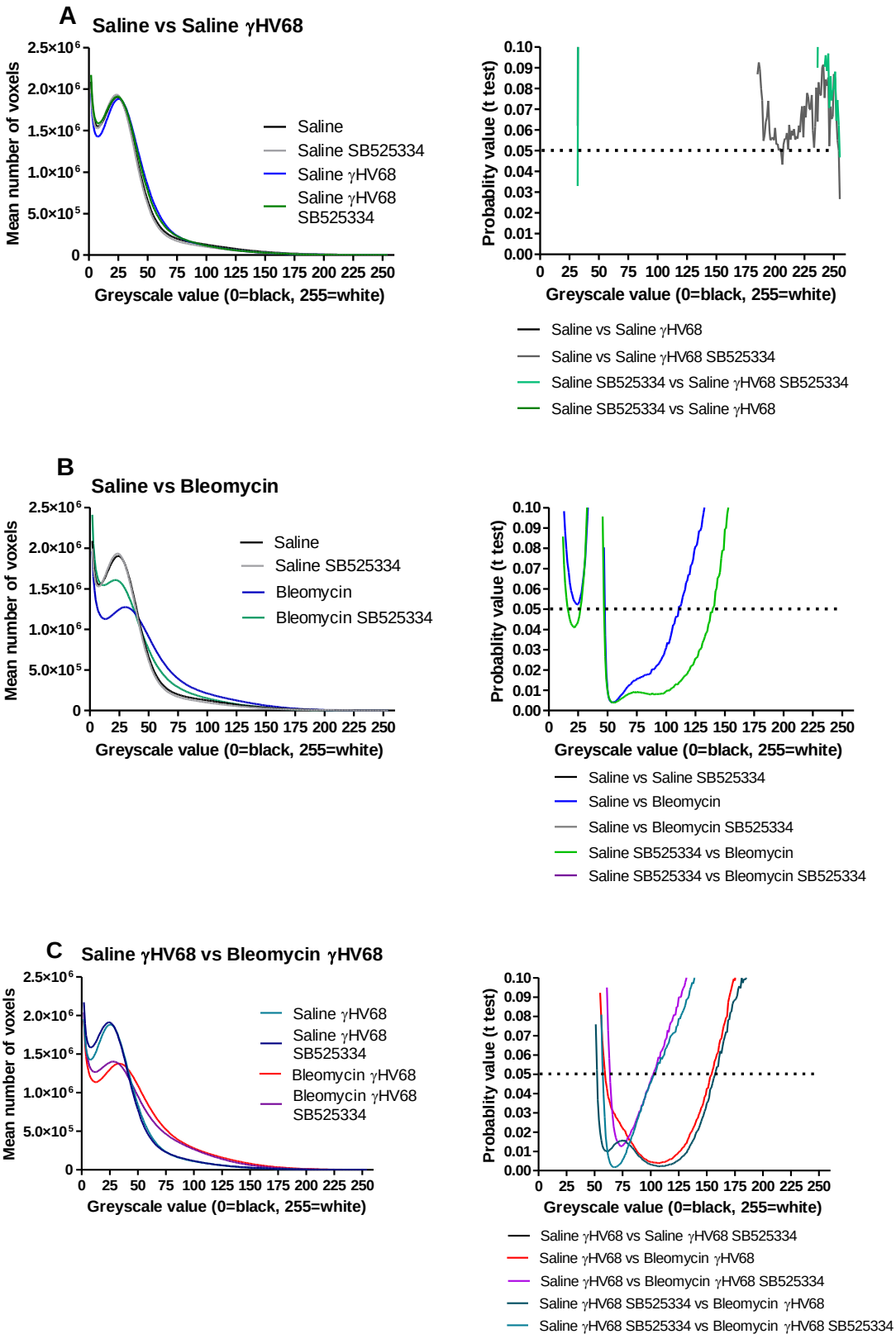
A
Saline vs Saline γHV68
Mean number of voxels
2.5×10⁶
2.0×10⁶
1.5×10⁶
1.0×10⁶
5.0×10⁵
0
0 25 50 75 100 125 150 175 200 225 250
Greyscale value (0=black, 255=white)
Saline
Saline SB525334
Saline γHV68
Saline γHV68 SB525334
Probablity value (t test)
0.10 0.09 0.08 0.07 0.06 0.05 0.04 0.03 0.02 0.01 0.00
Saline vs Saline γHV68
Saline vs Saline γHV68 SB525334
Saline SB525334 vs Saline γHV68 SB525334
Saline SB525334 vs Saline γHV68
B
Saline vs Bleomycin
Bleomycin
Bleomycin SB525334
Saline vs Saline SB525334
Saline vs Bleomycin
Saline vs Bleomycin SB525334
Saline SB525334 vs Bleomycin
Saline SB525334 vs Bleomycin SB525334
C
Saline γHV68 vs Bleomycin γHV68
Saline γHV68
Saline γHV68 SB525334
Bleomycin γHV68
Bleomycin γHV68 SB525334
Saline γHV68 vs Saline γHV68 SB525334
Saline γHV68 vs Bleomycin γHV68
Saline γHV68 vs Bleomycin γHV68 SB525334
Saline γHV68 SB525334 vs Bleomycin γHV68
Saline γHV68 SB525334 vs Bleomycin γHV68 SB525334

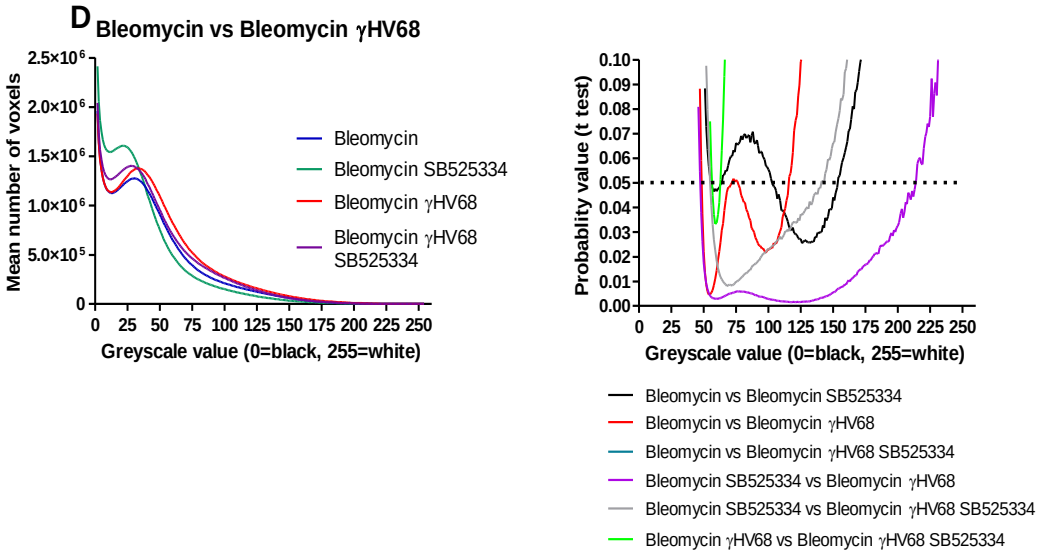

E **Pixel range 50-150**

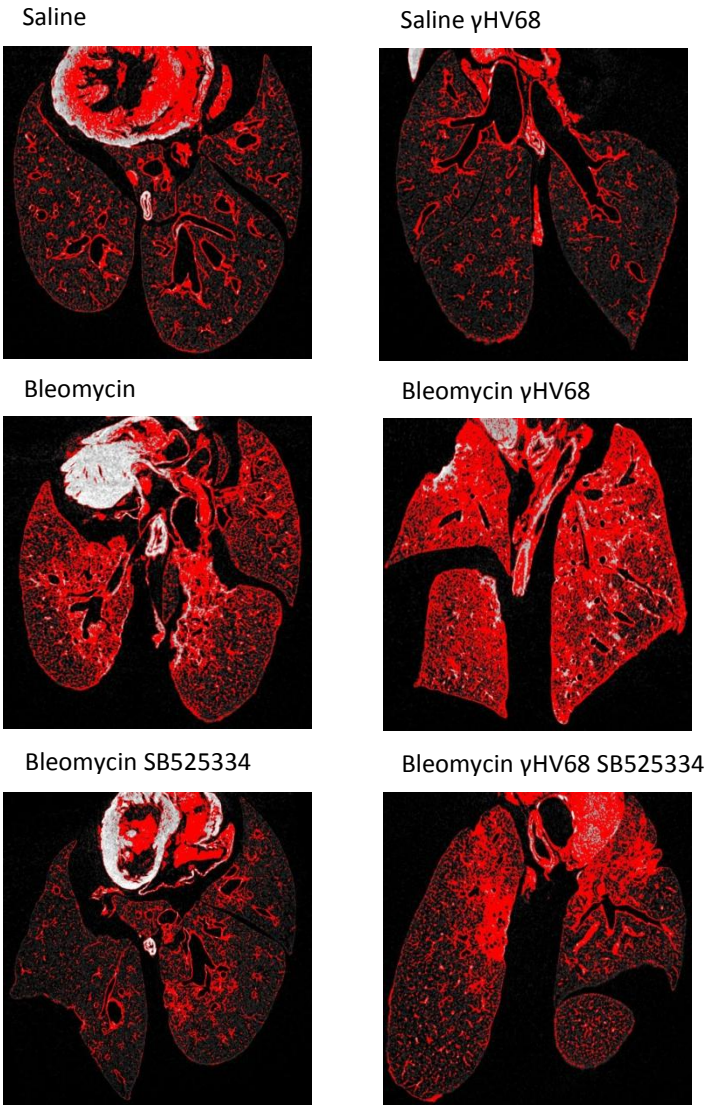

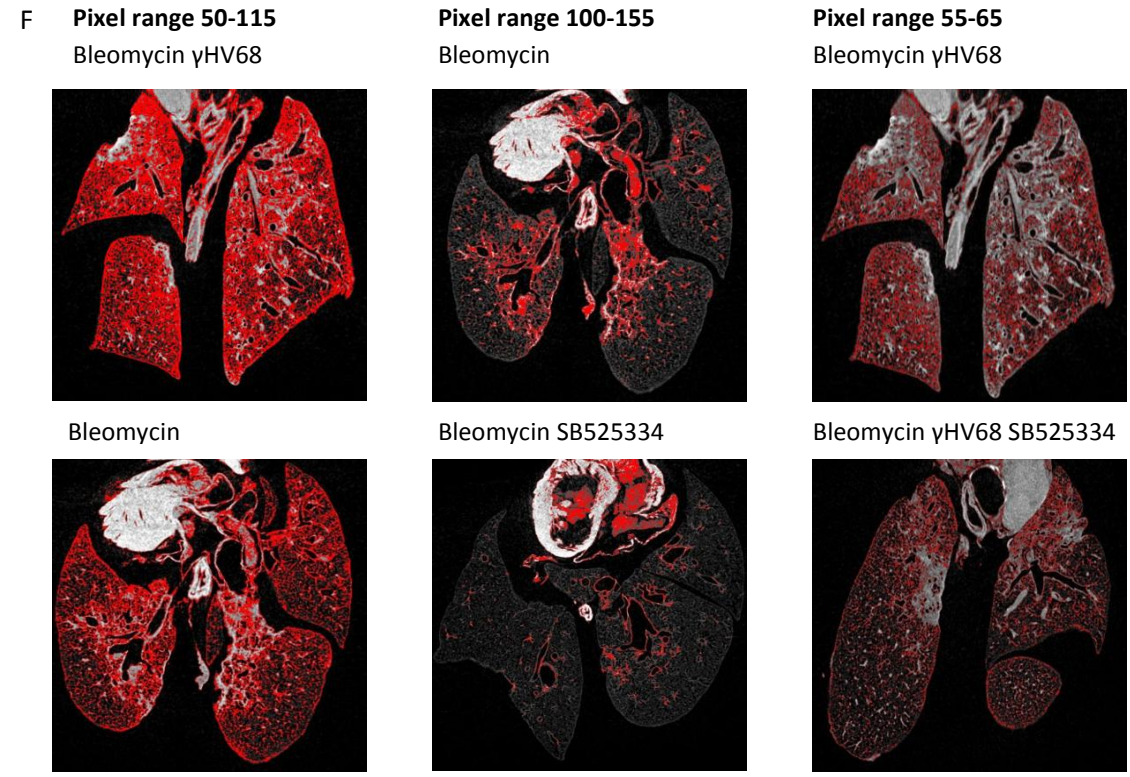

Figure 3.70. Density histograms analysis of µCT scanned lungs.

C57BL/6 mice were administered bleomycin via oropharyngeal route at 1 mg/kg, followed by infection with 100,000 PFU γHV68 or saline intranasally on day 14. Between days 15 and 28 mice were given SB525334 (30 mg/kg) twice daily via oral gavage. This figure shows density histograms corresponding to each experimental groups plotted as a mean number of voxels against the greyscale values reflecting the density of the tissue, where 0 is black and 255 is white. The histograms are matched with the Student t-test analysis of significance and represented as graphs of probability value of less than 0.1, where the significance cut off was set as 0.05 as indicated by the dotted line against the density denoting greyscale values. Panel A- comparison of saline groups with γHV68-infected saline groups and the statistical analysis plots; panel B- comparison of saline groups with bleomycin-challenged groups and the statistical analysis plots; panel C- comparison of γHV68-infected saline groups with γHV68-infected bleomycin-challenged groups and the statistical analysis plots; panel D- comparison of bleomycin challenged groups and γHV68-infected fibrotic groups and the statistical analysis plots; panel E- distribution of

pixels in a density range 50 to 150, highlighted in red between saline control and bleomycin-challenged and γHV68-infected saline and γHV68-infected fibrotic lungs; panel F- distribution of significantly different pixels highlighted in red between the γHV68-infected fibrotic lung and bleomycin only lung, fibrotic lung and fibrotic lung treated with SB525334 and γHV68-infected fibrotic and γHV68-infected fibrotic treated with SB525334. Data are representative of an average of n=2-5 animals per group.

Taken together, these data suggest a shift in the SB525334 therapeutic effect between the fibrotic lung and viral infection on a background of pulmonary fibrosis. In order to further dissect these differences, we quantified the numbers of prominent inflammatory cell aggregates observed in the lungs infected with γHV68 **(Figure 3.65E).** The inflammatory aggregates were formed by numerous mononuclear cell infiltrates that stained strongly with haematoxylin. Nuance multispectral tissue imaging software was used to enhance the areas in the lungs with high density of haematoxylin staining and count these areas as regions of interest per area of the lung section (ROI/mm^2) (**Figure 3.71A**). As shown in **Figure 3.71B,** no inflammatory aggregates were detected in the saline control lungs and low numbers were identified in bleomycin-challenged lungs. In contrast γHV68 infection on a background of pulmonary fibrosis significantly increased the number of inflammatory cell aggregates when compared to bleomycin challenged lungs. A trend towards reduction in inflammatory aggregates was evident with SB525334 treatment but the difference was not significant. A degree of variability was observed between the sections which may explain the lack of statistical difference. This pattern of inflammatory aggregates distribution was closely matched by CCL2 gene expression in the lungs (**Figure 3.71C**). Infection with γHV68 increased the expression of CCL2 in saline lungs compared to mock-infected saline and bleomycin-challenged lungs. This response was significantly increased in γHV68 infection on a background of existing pulmonary fibrosis and a trend towards a reduction of CCL2 expression was observed with SB525334 treatment.

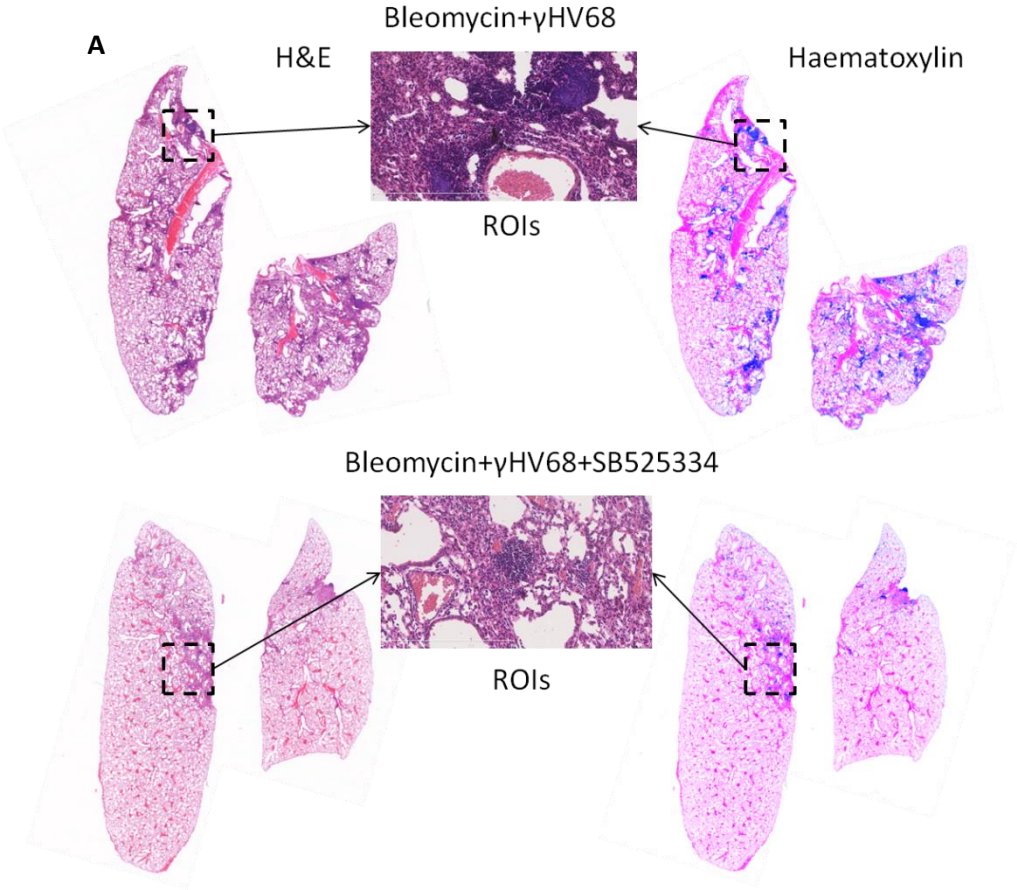
A
Bleomycin+γHV68
H&E
Haematoxylin
ROIs
Bleomycin+γHV68+SB525334
ROIs

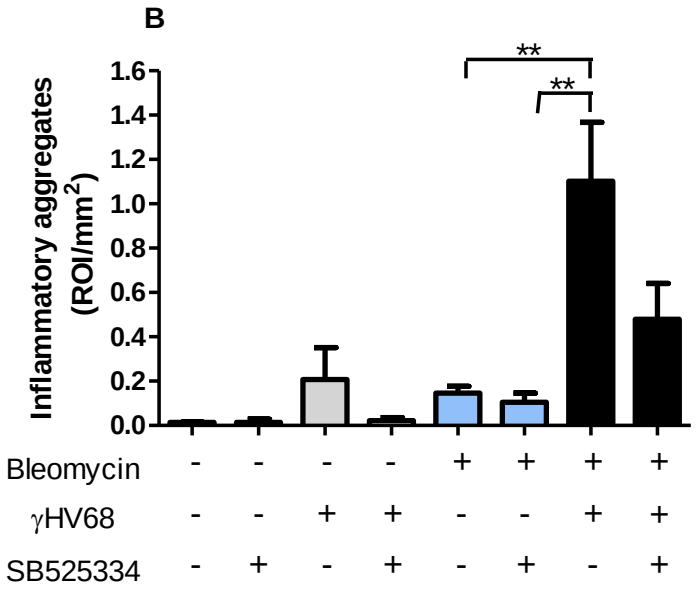
B
Inflammatory aggregates (ROI/mm2)
1.6
1.4
1.2
1.0
0.8
0.6
0.4
0.2
0.0
**
**
Bleomycin - - - - + + + +
γHV68 - - + + - - + +
SB525334 - + - + - + - +

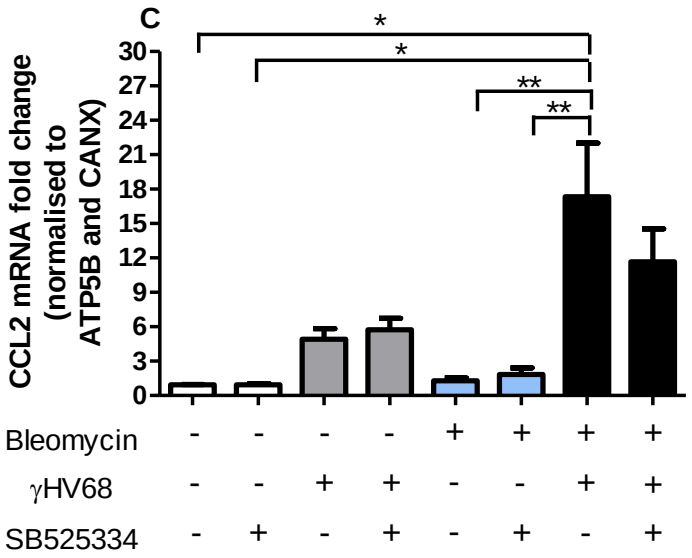

Figure 3.71. Inflammatory changes in the γHV68 infection on a background of pulmonary fibrosis.

C57BL/6 mice were administered bleomycin via oropharyngeal instillation at 1 mg/kg, followed by infection with 100,000 PFU γHV68 or saline intranasally on day 14. Panel A- inflammatory aggregates were identified as dense areas of haematoxylin staining by the Nuance software; Panel B- inflammatory aggregates were quantified and expressed as region of interest (ROI/mm^2), mean +/- SEM, n=2-5 animals per group. Panel C- expression of CCL2 in the lungs 14 days p.i. was assessed by qPCR and data are presented as fold change in mRNA levels relative to two housekeeping genes ATP5B and CANX and representative of mean +/- SEM, n=3-8 animals per group. One-way ANOVA was performed for statistical analysis, *$p<0.05$, **$p<0.01$.

3.3.2.6 Summary

The aim of this study was to investigate the role of TGFβ in the γHV68 infection on a background of pulmonary fibrosis.

- Infection with γHV68 caused weight loss in inoculated mice and increased *ex vivo* lung and spleen weights, as previously reported. Furthermore, expression of viral genes was readily detected in this study 14 day p.i.
- Assessment of total lung collagen by measuring hydroxyproline levels (HPLC) and soluble collagen (Sircol assay) showed no difference in collagen accumulation between fibrotic lung and γHV68 infected fibrotic lung. SB525334 reduced the collagen level in the mock-infected fibrotic lungs at day 28 post-bleomycin and 14 days p.i. but in virally-infected fibrotic lung the therapeutic effect of SB525334 was lost.
- Further analysis of the lungs was performed using μCT and InForm pattern recognition software analysis, which generated informative data that expanded on the HPLC and Sircol findings. Virally-infected fibrotic lungs had worse appearance on the μCT scans, had higher percentage of abnormal areas and increased lung densities when compared with bleomycin-challenged lungs. These findings were further corroborated by analysis of histology sections, which showed mature fibrotic lesions in bleomycin-challenged lungs while in the viral infection of fibrotic lungs there was evidence of inflammation superimposed on a background of existing fibrosis. Prominent inflammatory cell aggregates were quantified showing significantly increased numbers in the γHV68-infected fibrotic in comparison to bleomycin-challenged lungs. SB525334 treatment appeared to reduce the inflammation but this failed to reach statistical significance.
- Taken together, all the parameters analysed in this study support the conclusion that targeting TGFβ/ALK5 signalling in the bleomycin-model of pulmonary fibrosis attenuates fibrosis but in the virally infected fibrotic lungs SB525334 therapeutic effect appears to be re-directed towards dampening down the inflammatory response.

3.3 Herpesviruses infection in pulmonary fibrosis

3.3.3 Targeting coagulation in the viral infection on a background of pulmonary fibrosis

3.3.3.1 Introduction

Excessive activation of coagulation cascade has been strongly implicated in fibroproliferative lung disease. In experimental models of pulmonary fibrosis targeting either thrombin (Howell et al. 2001) or FXa (Scotton et al., 2009) has been reported to attenuate lung collagen accumulation and fibrosis. In contrast, global and non-specific anticoagulation therapy has been associated with increased mortality in patients with IPF (Noth et al., 2012). In Section 3.3.1 of this study we showed evidence for increased expression of tissue factor and factor X (FX) in response to γHV68 infection of a fibrotic lung. The aim of this study was to evaluate the effect of FXa inhibition in this model of viral infection on a background of pulmonary fibrosis using a direct and selective FXa inhibitor, BAY 59-7939 (marketed as Rivaroxaban or Xarelto). BAY 59-7939 has recently been tested in a clinical trial of acute coronary syndrome and proven efficacious in reducing adverse cardiovascular events (Fitchett, 2012).

C57BL/6 male mice (aged 10-12 weeks) were administered bleomycin at the reduced dose of 1 mg/kg or saline via oropharyngeal instillation. Two weeks later, when the fibrotic phase was established, mice where inoculated with 80,000-100,000 PFU γHV68 or given saline via intranasal route. Mice were administered BAY 59-7939 at 3 mg/kg via oral gavage twice daily for the remaining 14 days of the experiment.

3.3.3.2 Monitoring mouse body weight

Following the oropharyngeal administration of 1 mg/kg bleomycin, mice have lost on average 7% of starting body weight with a nadir at day 6 while the saline-treated mice continued to gain weight (**Figure 3.72**). By day 14, mice were gaining weight

again and were inoculated with γHV68 virus. During the first week of infection a second wave of weight loss was registered in all γHV68-infected-bleomycin-challenged groups, with a trend suggesting that treatment with BAY 59-7939 caused more weight loss. Saline groups both mock- and γHV68-infected continued to gain weight throughout the duration of the experiment and mice in all the experimental groups were gaining weight by the end of the experiment.

3.3.3.3 Effect of treatment with BAY59-7939 on *ex vivo* lung and spleen weights

Both bleomycin administration and viral infection lead to increase in *ex vivo* lung weights in comparison to saline control lungs. Consistent with previous experiments, bleomycin-challenged lungs were on average 30% heavier than saline-administered control lungs and an increase in lung weight with administration of the virus alone was also notable. Viral infection on a background of bleomycin-induced fibrosis led to a significant 50% increase in lung weight when compared to relevant control (**Figure 3.73A**). BAY 59-7939 did not affect *ex vivo* lung weight in either bleomycin alone or virally-infected and bleomycin-challenged experimental groups.

Consistent with previous observations, a significant splenomegaly was present at the end of the experiment (**Figure 3.74B)**. Bleomycin alone did not increase spleen weight but combined injury with bleomycin and γHV68 virus significantly increased spleen weight when compared to γHV68 infection alone groups.

Furthermore, in this study the expression of viral genes **(Figure 3.74)**, M3, glycoprotein B and DNA polymerase, was also readily detected in the lungs 14 days p.i.. This suggests a low-level, ongoing viral replication in the lung as observed in the previous study and the viral gene expression was increased in virally infected fibrotic lungs compared to viral infection in the saline treated lungs.

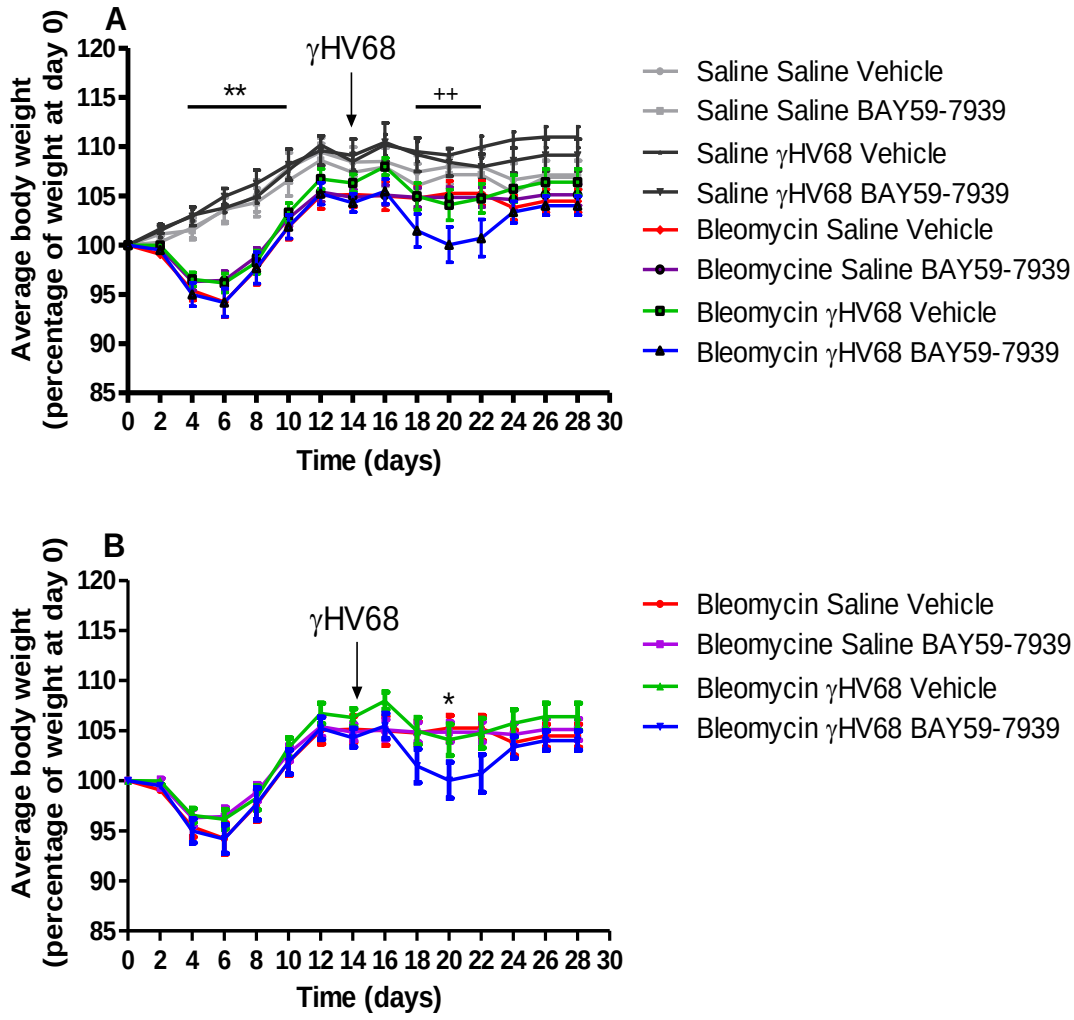

Figure 3.72. Monitoring mouse body weight in the viral infection of fibrotic lung.

C57BL/6 mice were administered bleomycin via oropharyngeal route at 1 mg/kg, followed by infection with 100,000 PFU γHV68 or saline intranasally on day 14. Between days 15 and 28 the mice were given BAY 59-7939 (3 mg/kg) twice daily via oral gavage. Data represent percentage change in average mouse body weight relative to starting weight at day 0 over the course of the experiment. Panel A- all experimental groups; **p<0.01 comparison of saline control group versus bleomycin-challenged groups, ++p<0.01 comparison of saline control group with bleomycin+γHV68+BAY 59-7939; and panel B- comparison of bleomycin-challenged groups only, *p<0.05 comparison of bleomycin+ γHV68+BAY 59-7939 with the remaining groups. Each point is representative mean +/- SEM of n=7-14 animals per group, two-way ANOVA statistical analysis.

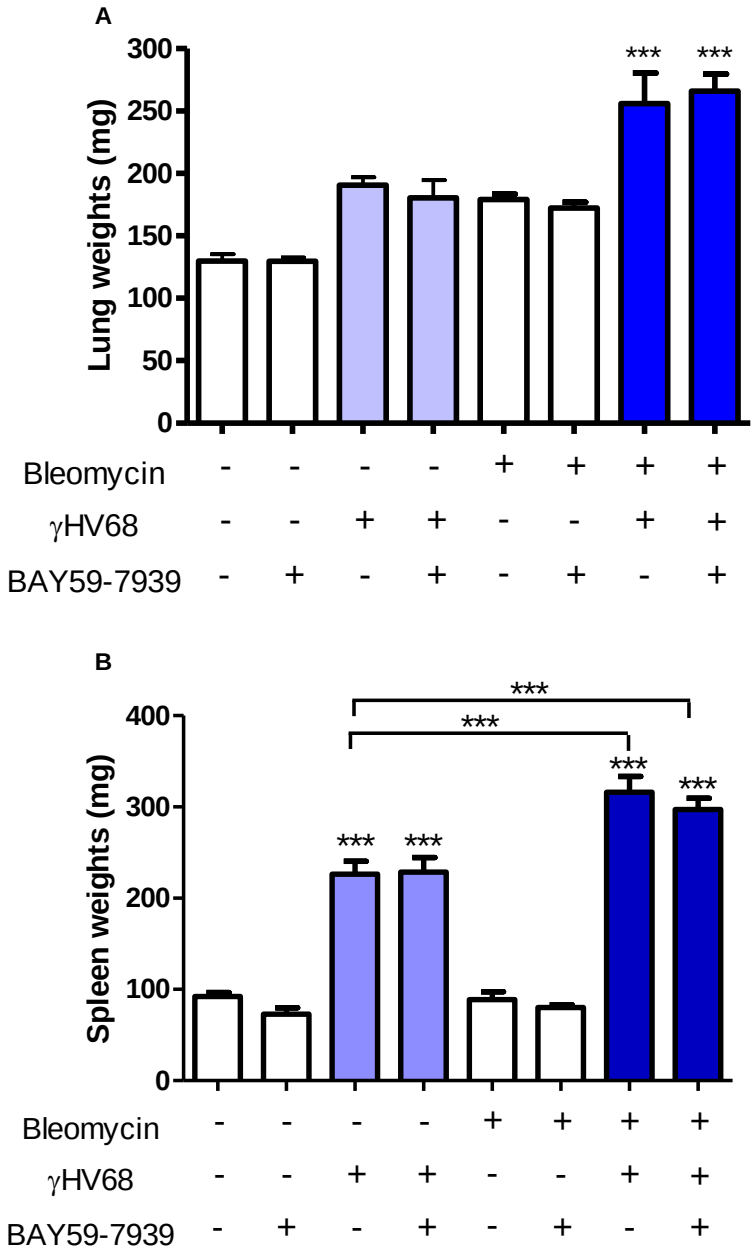

Figure 3.73. *Ex vivo* lung and spleen weights in γHV68 infection of bleomycin-induced pulmonary fibrosis.

C57BL/6 mice were administered bleomycin via oropharyngeal route at 1 mg/kg, followed by infection with 100,000 PFU γHV68 or saline intranasally on day 14. Between days 15 and 28 the mice were given BAY 59-7939 (3 mg/kg) twice daily via oral gavage. Data represent average weights of mouse lungs- panel A; and spleens- panel B; measured ex vivo 14 days post infection; representative of n=7-14 animals per group, one-way ANOVA, ***p<0.001.

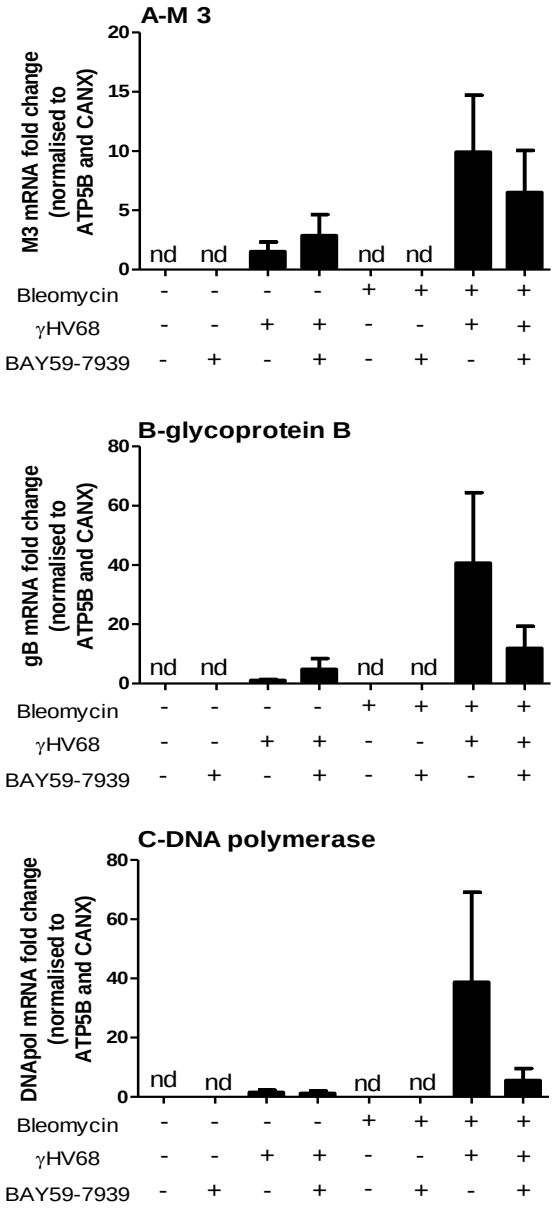

Figure 3.74. Determination of viral gene expression in the lungs.

C57BL/6 mice were administered bleomycin via oropharyngeal route at 1 mg/kg, followed by infection with 100,000 PFU γHV68 or saline intranasally on day 14. Between days 15 and 28 the mice were given BAY 59-7939 (3 mg/kg) twice daily via oral gavage. The expression of viral genes in the lungs 14 days p.i. was assessed by qPCR and data are presented as fold change in mRNA levels relative to two housekeeping genes ATP5B and CANX and representative of mean +/- SEM, n=3-8 animals per group. Panel A- M3; panel B- glycoprotein B; panel C- DNA polymerase; nd- not detected.

3.3.3.4 Collagen deposition in the viral infection of fibrotic lung

A dose of 1 mg/kg bleomycin alone caused a modest increase in total lung collagen of 30% as measured by HPLC that was significant when compared to saline control lungs (unpaired Studen t-test p=0.003). As observed in the previous study, viral infection in bleomycin-injured lung did not further increase the level of collagen deposition in the lung (**Figure 3.75A**). The greatest increase in collagen accumulation (40%) was observed in bleomycin-γHV68-BAY 59-7939 group. Measurement of soluble collagen by the standard Sircol colorimetric assay also showed no difference in lung collagen deposition between bleomycin alone and bleomycin-γHV68 challenged groups **(Figure 3.75B)**. As observed in the previous study, an increase in lung collagen was detected in γHV68 infected saline lungs, which may reflect cross-reaction of the Sircol assay with other non-collagenous proteins (Lareu et al., 2010). This suggests a possible vascular leak caused by the viral infection and there is a trend towards a reduction with BAY59-7939. µCT analysis was also performed in this study to expand on HPLC results and characterise fibrosis and viral infection.

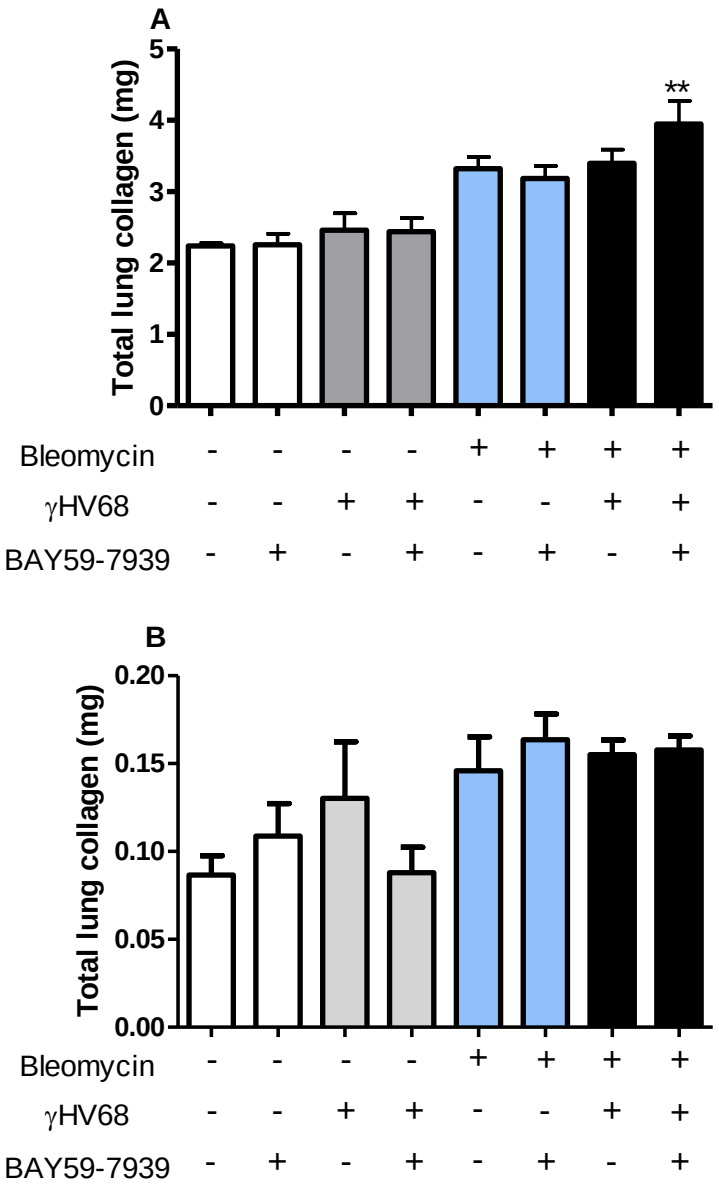

Figure 3.75. Total lung collagen accumulation in γHV68 infection on a background of pulmonary fibrosis.

C57BL/6 mice were administered bleomycin via oropharyngeal route at 1 mg/kg, followed by infection with 100,000 PFU γHV68 or saline intranasally on day 14. Between days 15 and 28 the mice were given BAY 59-7939 (3 mg/kg) twice daily via oral gavage. The total lung collagen was quantified by measurements of hydroxyproline by HPLC- panel A and soluble collagen by Sircol- panel B. Data are representative of mean +/- SEM, n=3-8 animals per group, one-way ANOVA, **p<0.01 comparison of bleomycin+γHV68+BAY59-7939 and all saline groups.

3.3.3.5 *Ex vivo* µCT analysis of viral infection in fibrotic lung.

A dose of 1 mg/kg bleomycin used in this experiment caused a 30% increase in total lung collagen as measured by HPLC and the bleomycin-γHV68-BAY59-7939 experimental group appeared to have further increased collagen deposition, although this difference did not reach statistical significance. As demonstrated in the previous study by µCT and histology analysis, viral infection of fibrotic lungs leads to a prominent inflammatory response superimposed on a background of existing fibrosis. The same analysis was subsequently performed in this study to assess the effect of FXa inhibition in the model of viral infection in fibrotic lung. **Figure 3.76** shows a representative reconstructed image of the dorsal side of the scanned lung from each experimental group. As observed in the previous study, saline treated lungs appear homogenous, with visible small airways. In contrast, bleomycin-injured lungs display areas of dense consolidation indicative of fibrosis. These areas are also prominent in γHV68-infected fibrotic lungs.

Figure 3.77 shows a representative µCT scan matched with a segmentation map produced by the InForm software and compared with histology for each experimental group. Analysis of saline control and saline-BAY59-7939 treated lungs shows that these lungs have normal appearance and morphology. In contrast, µCT analysis of bleomycin-challenged lungs reveals fibrotic lesions largely concentrated around broncho-vascular bundles as observed in the previous study and consistent with the route of administration of bleomycin. The fibrotic areas extend to the periphery of the lung and classic features of fibrosis are again notable, including subpleural scarring and traction bronchiectasis. Microscopically, these abnormal areas correspond to areas of high cellularity and increased deposition of extracellular matrix as visualised by MSB collagen staining. Treatment with BAY59-7939 did not appear to affect the macroscopic and microscopic pattern of fibrosis in bleomycin-injured lungs.

In this study minor alterations to the lung appearance were observed with γHV68 infection alone. The changes resembled glass ground opacities and interlobular septal thickening suggestive of inflammation and were identified by the analytical

software as “abnormal areas”. Microscopically, these lungs appeared largely normal but small areas of scar tissue and thickened alveolar walls could be seen. In contrast, γHV68 virus infection in mice challenged with bleomycin was associated with extensive areas of dense consolidation centred around airways and spreading to the lung periphery. The outline of the lung was visibly distorted. Furthermore, virally-infected lungs displayed large areas with ground glass opacities suggestive of inflammatory cell infiltrates (confirmed by histology) alongside extensive deposition of extracellular matrix. BAY59-7939 treatment appeared to be associated with marked inflammatory changes in the virally-infected fibrotic lungs, which were further confirmed by histological analysis that also revealed dense fibrotic changes with collagen deposition, cellular infiltrates and abnormal epithelium.

Saline

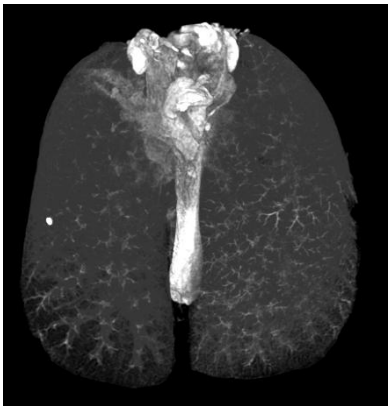

Saline + BAY59-7939

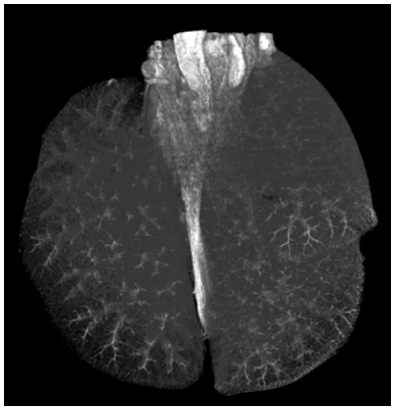

Bleomycin

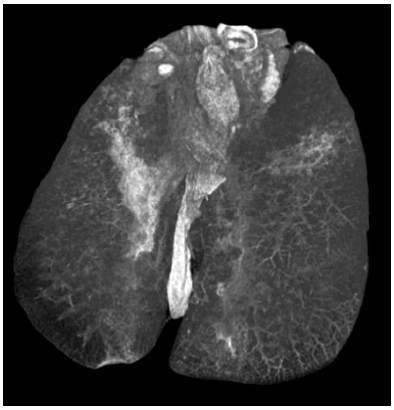

Bleomycin + BAY59-7939

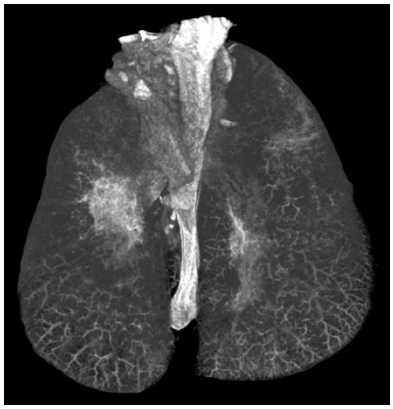

Saline γHV68

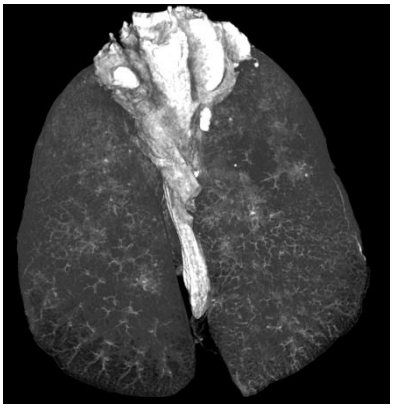

Saline γHV68 + BAY59-7939

Bleomycin γHV68

Bleomycin γHV68 + BAY59-7939

Figure 3.76. Reconstruction of µCT scans showing gross lung appearance.

C57BL/6 mice were administered bleomycin via oropharyngeal route at 1 mg/kg, followed by infection with 100,000 PFU γHV68 or saline intranasally on day 14. Between days 15 and 28 mice were given BAY59-7939 (3 mg/kg) twice daily via oral gavage. The lungs were insufflated, fixed and scanned at high resolution (13 µm). The figure shows representative 3D reconstructed images of the scanned lungs from all experimental groups.

Figure 3.77. Characterisation of the changes in lung morphology induced by bleomycin-challenge and γHV68 infection.

C57BL/6 mice were administered bleomycin via oropharyngeal route at 1 mg/kg, followed by infection with 100,000 PFU γHV68 or saline intranasally on day 14. Between days 15 and 28 mice were given BAY59-7939 (3 mg/kg) twice daily via oral gavage. Panel A- representative coronal µCT scans with B- corresponding segmentation map showing normal parenchyma (green), abnormal lung areas (red) and other tissue (blue). Panel C- histology sections stained with haematoxylin and eosin (H&E) and panel D- modified Martius Scarlett Blue method (MSB) to visualise collagen fibres. Selected areas are shown in 100x magnification. Panel E and F- H&E and MSB sections at 200x magnification. Complete sets of images are shown for every experimental group as annotated. AE- alveolar epithelium, BE- bronchial epithelium, FB- fibroblasts, COL- collagen, IA- inflammatory aggregates.

Saline

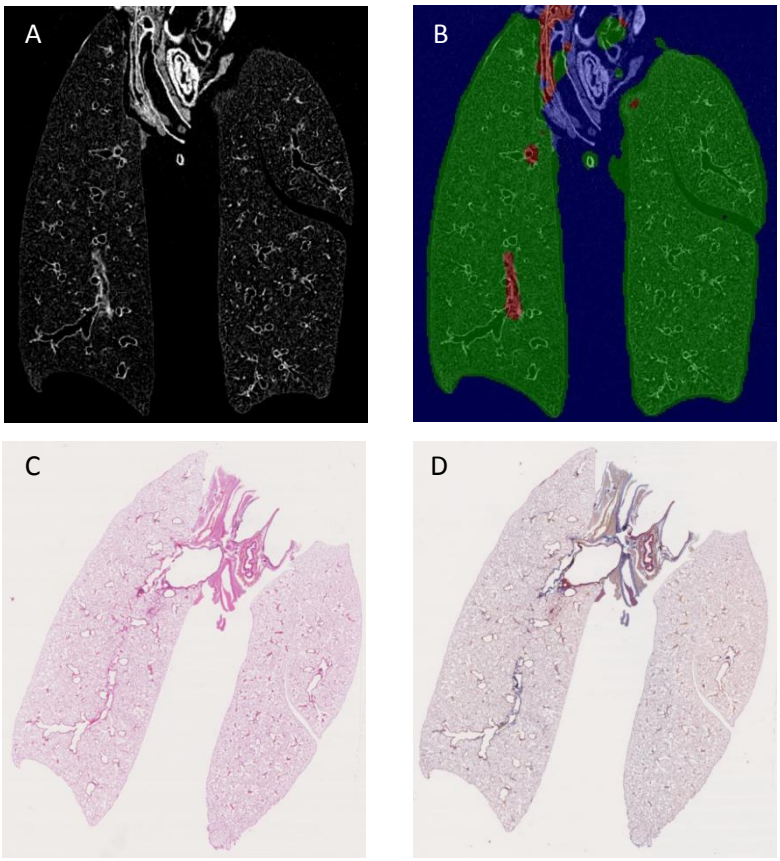

Saline, BAY 59-7939

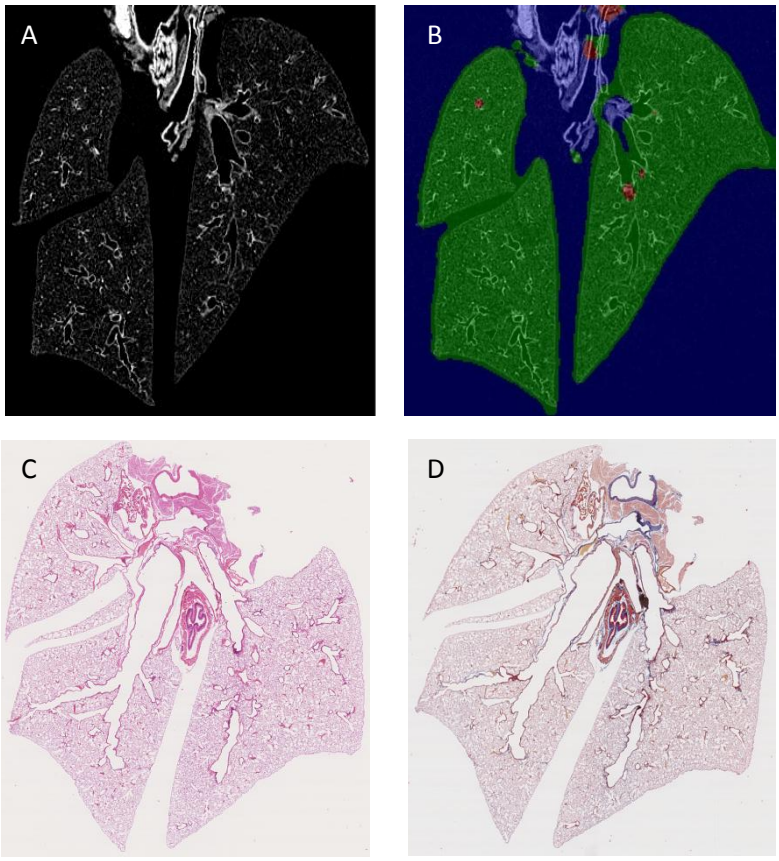

Saline, γHV68

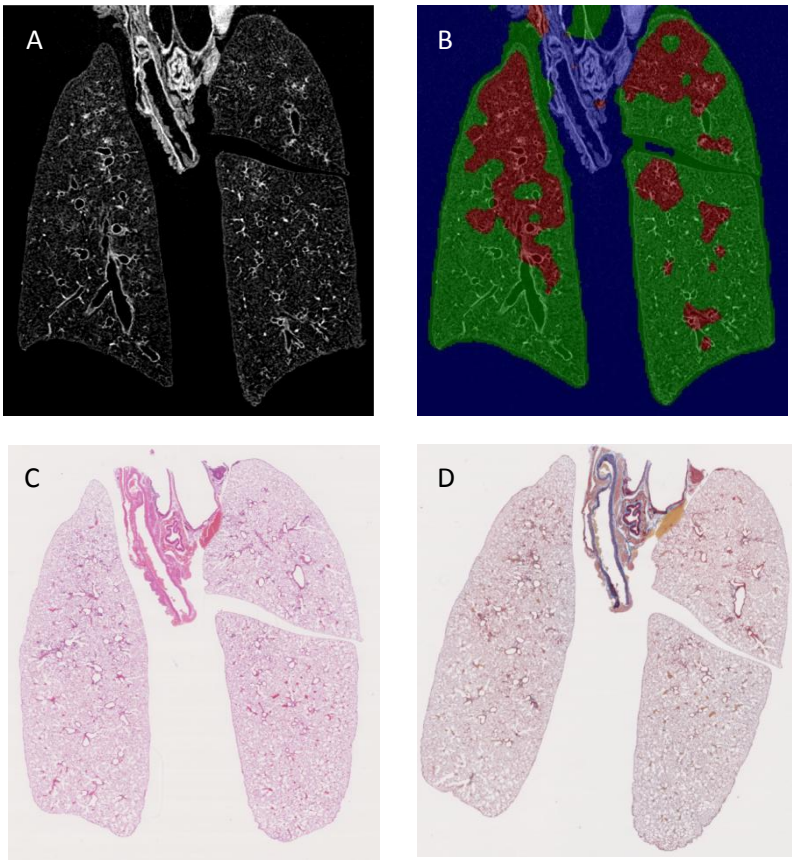

Saline, γHV68, BAY 59-7939

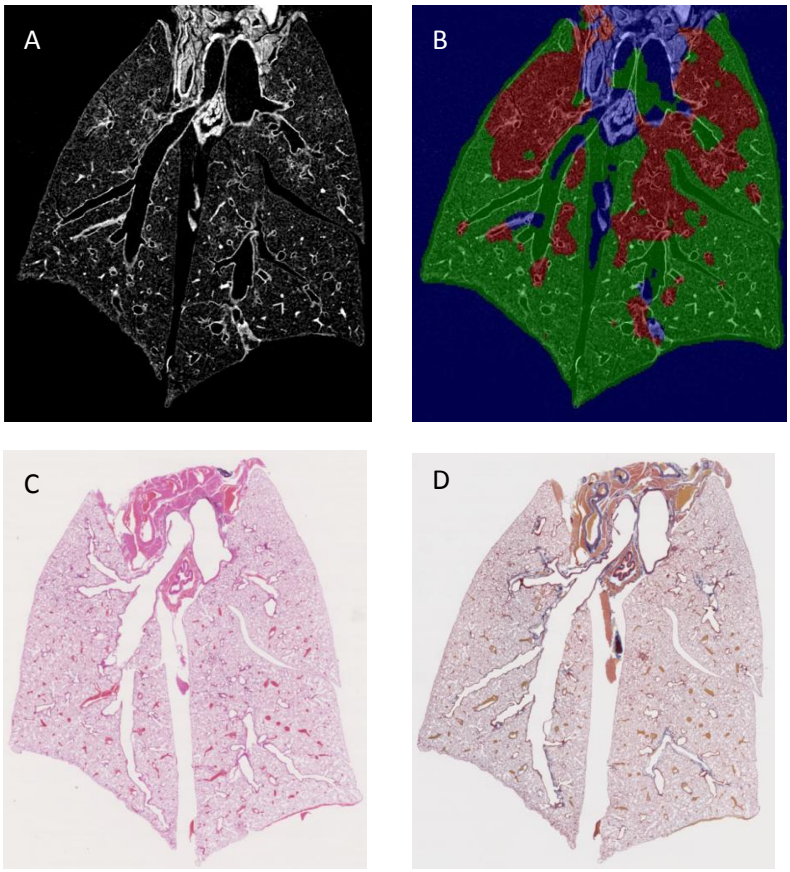

Bleomycin

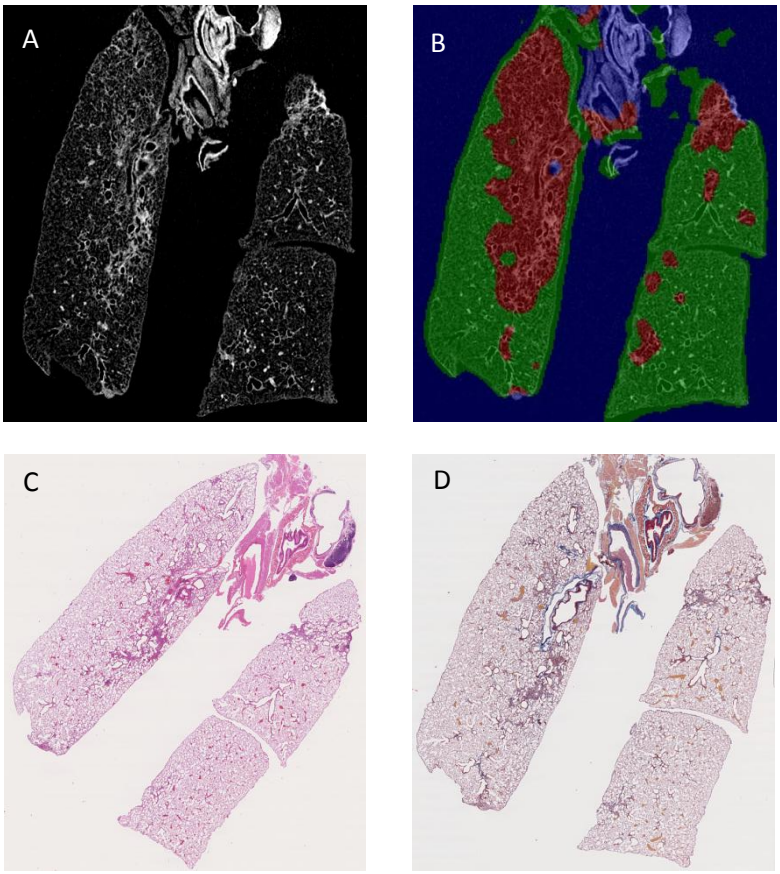

Bleomycin, BAY 59-7939

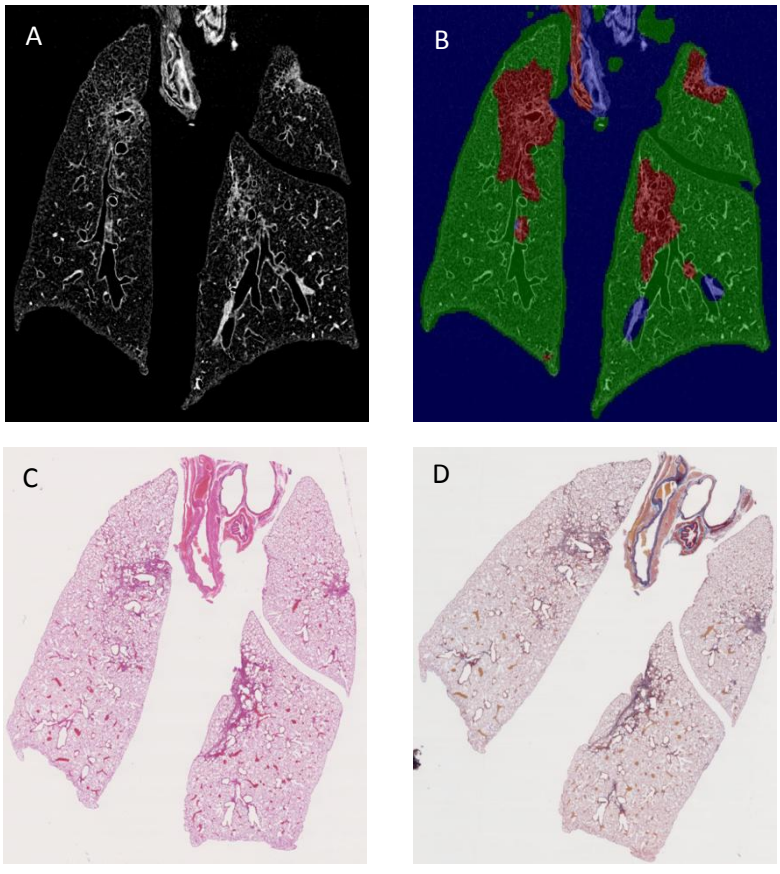

Bleomycin, γHV68

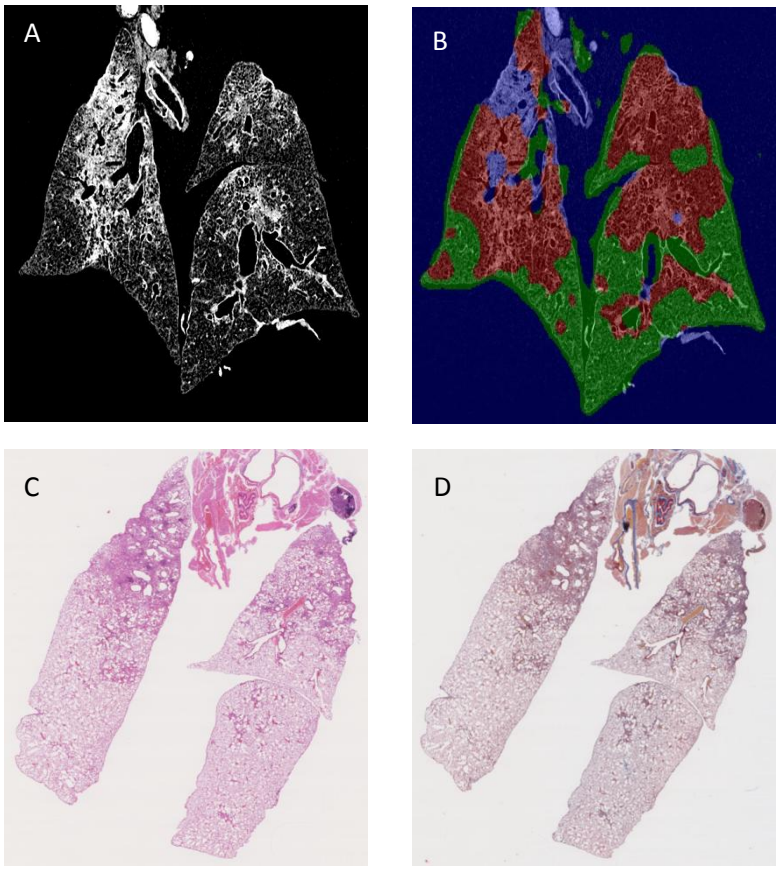

Bleomycin, γHV68, BAY 59-7939

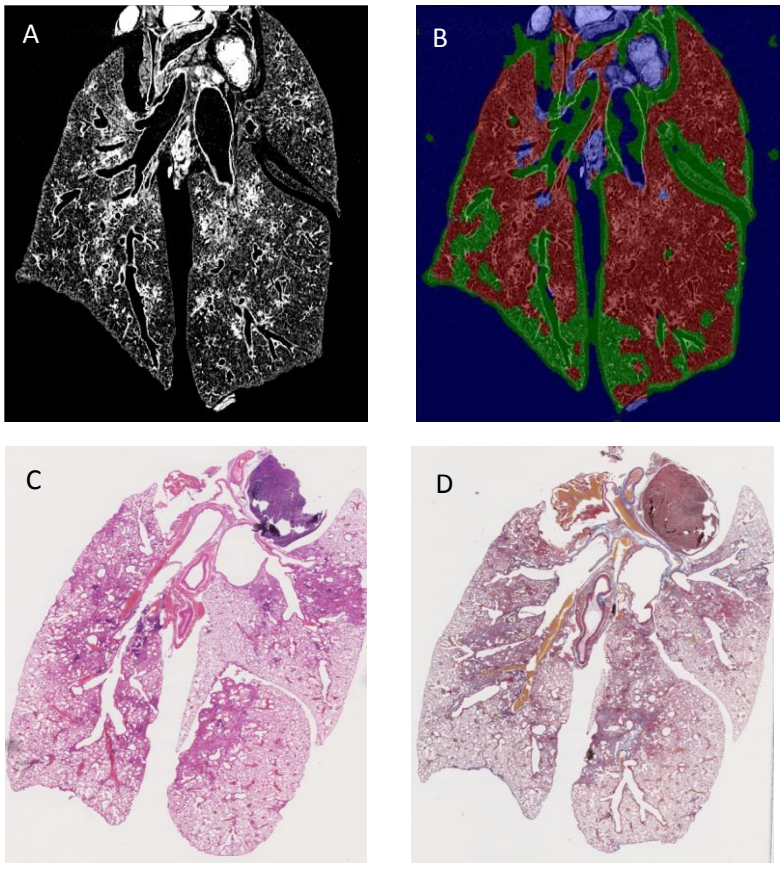

E **Saline**

F

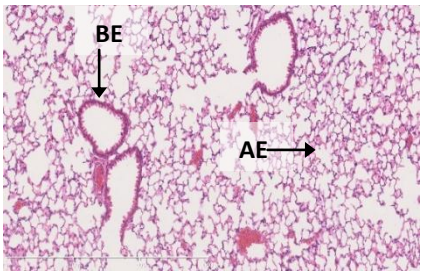

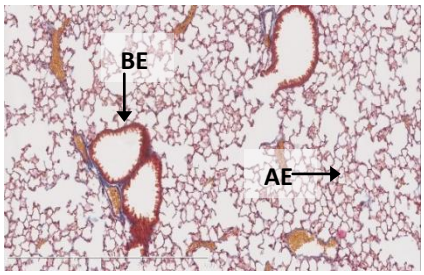

Saline, BAY59-7939

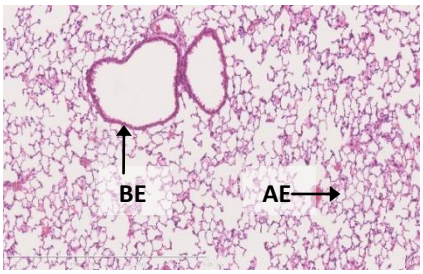

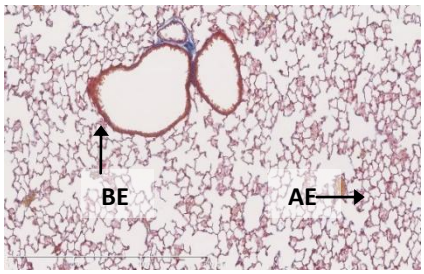

Saline, γHV68

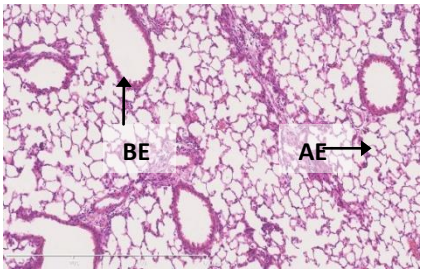

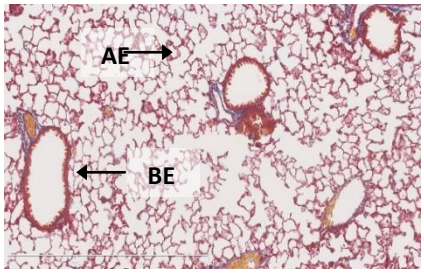

Saline, γHV68, BAY59-7939

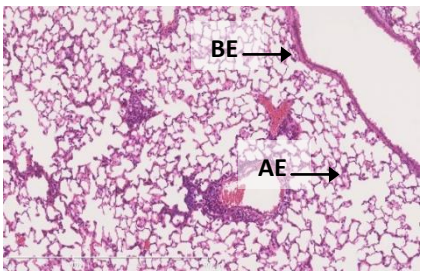

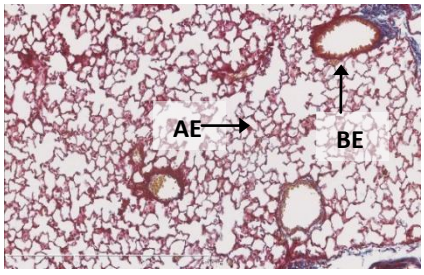

Bleomycin

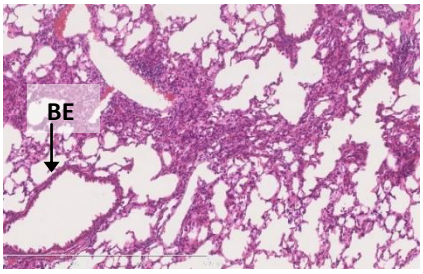

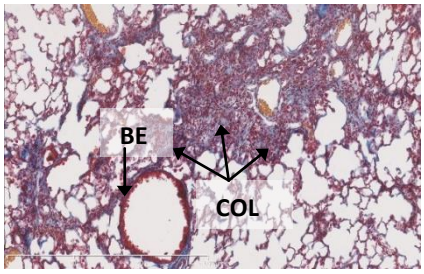

Bleomycin, BAY59-7939

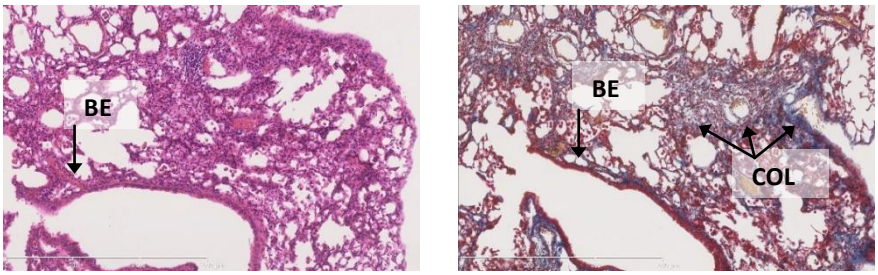

Bleomycin, γHV68

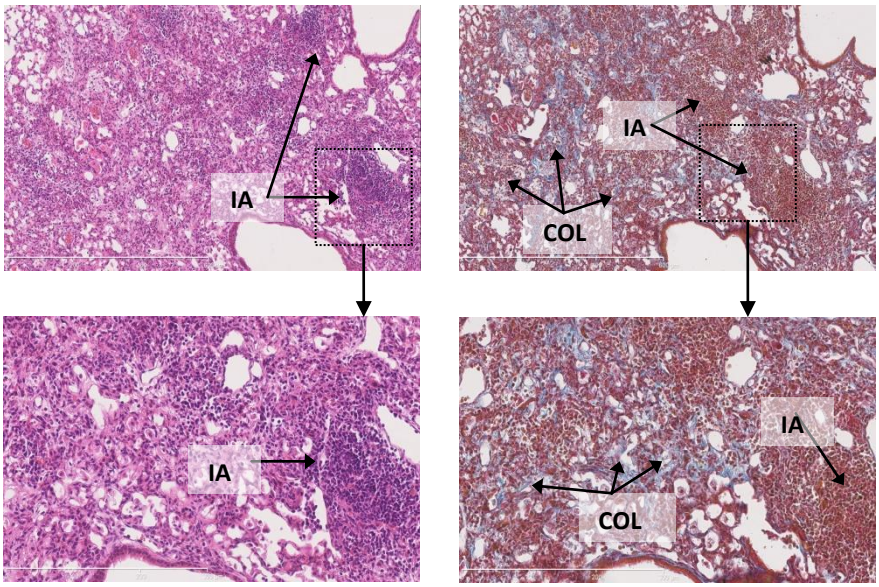

Bleomycin, γHV68, BAY59-7939

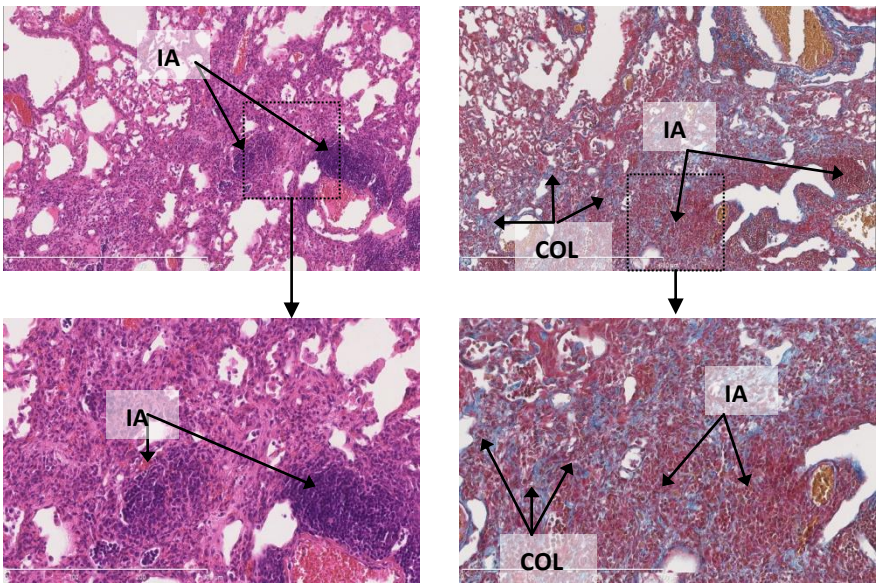

3.3.3.6 Quantification of *ex vivo* µCT analysis of fibrosis and viral infection

Abnormal lung areas and density were subsequently quantified based on the InForm segmentation analysis of µCT scans. **Figure 3.78** shows that total lung volumes across all experimental groups are comparable, which is consistent with homogenous lung insufflation and processing.

Figure 3.79 shows the percentage of abnormal lung area for all experimental groups. Saline control groups have less than 10% of abnormal lung area in the lungs but viral infection alone increased this percentage to 20%, which is consistent with abnormalities observed on the µCT scans. Bleomycin-induced fibrosis also amounted to 20% abnormal lung area and treatment with BAY59-7939 did not affect this response. Infection with γHV68 on a background of exiting fibrosis increased the abnormal lung area to 35%, again consistent with changes observed on µCT scans. The most extensive alterations to lung architecture were detected in the bleomycin-γHV68-BAY59-7939 group as reflected by the abnormal lung area reaching on average 45%, but the difference between bleomycin-γHV68-vehicle and bleomycin-γHV68-BAY59-7939 failed to reach statistical significance.

Consistent with the previous study, the saline control lungs register a density below 1000 voxels but there is an increase in density with viral infection alone. Bleomycin-injured lungs are 2500 voxels dense and treatment with BAY59-7939 did not affect lung density. Infected fibrotic lungs were nearly twice as dense as saline control lungs and treatment with BAY59-7939 further increased the density to an average of 6000 voxels. Taken together, these data suggests that viral infection in the fibrotic lung caused the most marked distortion of lung architecture when combined with BAY59-7939 therapy (**Figure 3.80**).

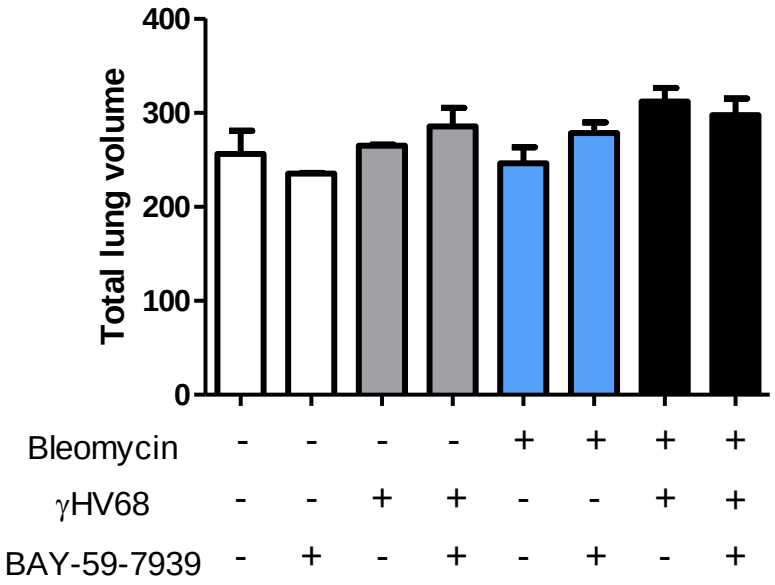

Figure 3.78. Total lung volume of µCT scanned lungs.

C57BL/6 mice were administered bleomycin via oropharyngeal route at 1 mg/kg, followed by infection with 100,000 PFU γHV68 or saline intranasally on day 14. Between days 15 and 28 the mice were given BAY59-7939 (3 mg/kg) twice daily via oral gavage. The graph shows an average of total volume of the lungs processed for µCT and InForm analysis for each experimental group, n=2-5 mice.

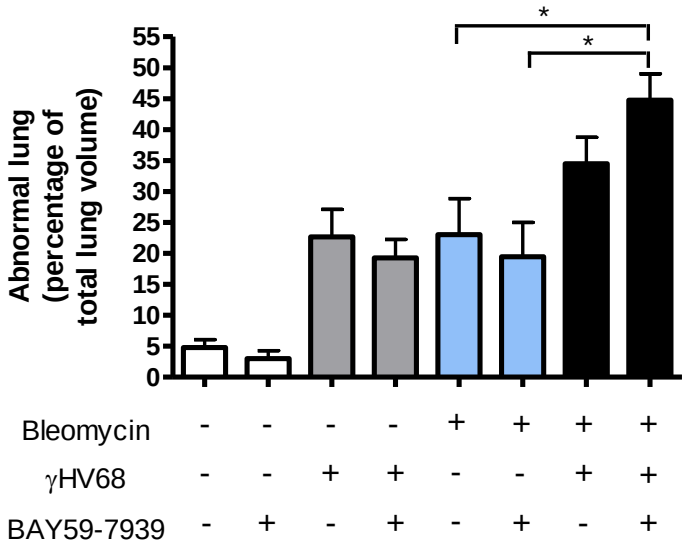

Figure 3.79. Quantification of abnormal lung area in viral infection on a background of pulmonary fibrosis

C57BL/6 mice were administered bleomycin via oropharyngeal route at 1 mg/kg, followed by infection with 100,000 PFU γHV68 or saline intranasally on day 14. Between days 15 and 28 the mice were given BAY59-7939 (3 mg/kg) twice daily via oral gavage. The abnormal areas in the lung were quantified by InForm analysis of µCT scans and are expressed as a percentage of total lung area. Data are representative of n=2-5 animals per group, one-way ANOVA, *$p<0.05$.

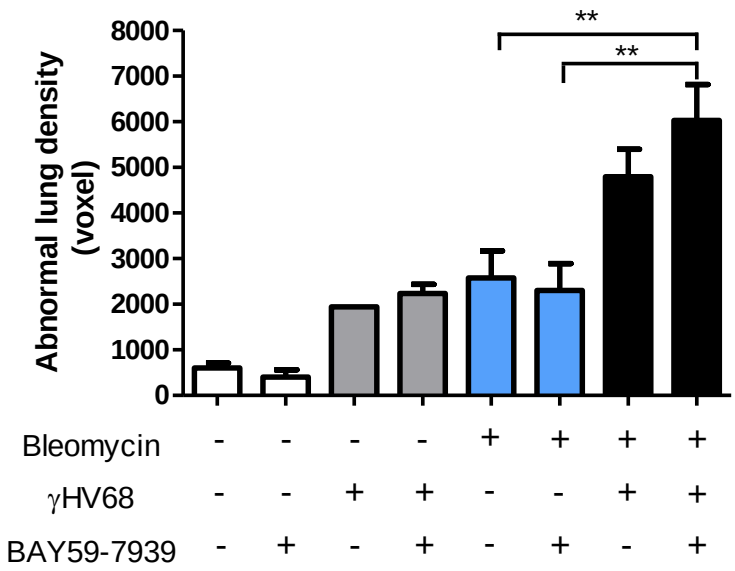

Figure 3.80. Quantification of lung density in viral infection on a background of pulmonary fibrosis

C57BL/6 mice were administered bleomycin via oropharyngeal route at 1 mg/kg, followed by infection with 100,000 PFU γHV68 or saline intranasally on day 14. Between days 15 and 28 the mice were given BAY59-7939 (3 mg/kg) twice daily via oral gavage. The changes in the lung were quantified by InForm analysis of µCT scans and are expressed as abnormal lung density in the total lung. Data are representative of n=2-5 animals per group, One-way ANOVA, **p<0.01.

In order to further examine data, voxel density analysis was performed which does not rely on the software segmentation output. The mean number of voxels per lung at each greyscale value (0 being least dense and 255 being most dense) for each experimental group is presented in the form of histograms and a Student t-test performed to compare individual groups (**Figures 3.81 and 3.82**). Density histograms of all experimental groups (**Figure 3.81**) show a clear separation into three groups. Saline control lungs have the lowest density voxels, virally-infected control lungs and bleomycin only challenged lungs are represented by voxels of intermediate density and virally-infected fibrotic lungs are shifted towards the high density end of the scale.

Figure 3.82A shows that lungs from saline control groups were less dense than lungs from γHV68 alone infected saline groups with significant differences in voxels numbers between 35 and 85 greyscale density values. Treatment with FXa inhibitor did not affect the lung densities in this group. **Figure 3.82B** demonstrates that a clear shift towards higher density voxels occurred in the bleomycin-challenged lungs when compared to saline controls with statistical difference observed between 40 to 150 greyscale pixel values. Viral infection in the fibrotic lung significantly shifted the density of the lungs towards higher end of the greyscale value when compared to infected lungs alone **(Figure 3.82C)**, with the mean voxels numbers significantly different between 40 and 90 greyscale values.

The distribution of density pixels over a range of 40 to 150, visualised in **Figure 3.82F,** reveals localisation to airway walls in saline control lungs and areas of parenchyma in virally-infected saline lungs. In all bleomycin-injured groups fibrotic lesions were highlighted. In bleomycin+γHV68 double injured lungs areas of parenchyma displaying extensive opacities were also identified as different from other experimental groups. Treatment with BAY59-7939 did not affect the lung density and pixel distribution in any of the groups.

In this study, infection with γHV68 caused density changes in the saline-treated lungs that appeared to be comparable to bleomycin-induced fibrosis when quantified as density and percentage abnormal lung area. However, a significant

difference in the greyscale pixels over a narrow range (35 to 45) was identified between γHV68-infected saline groups and bleomycin alone groups (**Figure 3.83D)**, which corresponded to changes within the lung parenchyma but not dense fibrotic lesions (**Figure 3.82G)**. These data support the µCT and histology findings that the virus alone did not cause formation of fibrotic lesion but instead an evidence of lung infection remains in the form of diffused increase in density of lung parenchyma. While the virally infected lungs show abundant opacities dispersed throughout the lung, the fibrotic lung has characteristic consolidation areas consistent with fibrotic lesions and localised around the airways and periphery of the lungs.

Comparison of bleomycin-injured, fibrotic lungs showed a range of changes dependent on infection status and treatment status (**Figure 3.82E**). Significant changes were observed between fibrotic lungs and γHV68 infected fibrotic lungs in a range of 30 to 140 greyscale values, which corresponded to pixels distributed throughout the parenchyma and fibrotic lesions **(Figure 3.82F)**. In this study targeting FXa with BA59-7939 in the model of viral infection on a background of bleomycin induced pulmonary fibrosis did not have a significant impact either on the density of the bleomycin only challenged lungs or infected fibrotic lungs. Nonetheless, the widest range of significantly different pixels (35 to 160) was identified between bleomycin challenged lungs and bleomycin-γHV68-BAY59-7939 lungs. Furthermore, a trend towards statistical significance was observed between bleomycin-γHV68 and bleomycin-γHV68-BAY59-7939 groups over low density pixels (20-30, **Figure 3.82E**) which localise to the lung parenchyma. These data suggest that FXa inhibition in this study did not affect the fibrotic processes in bleomycin-injured lungs and bleomycin-γHV68 double injured lungs and did not significantly influence the inflammatory response to the viral infection.

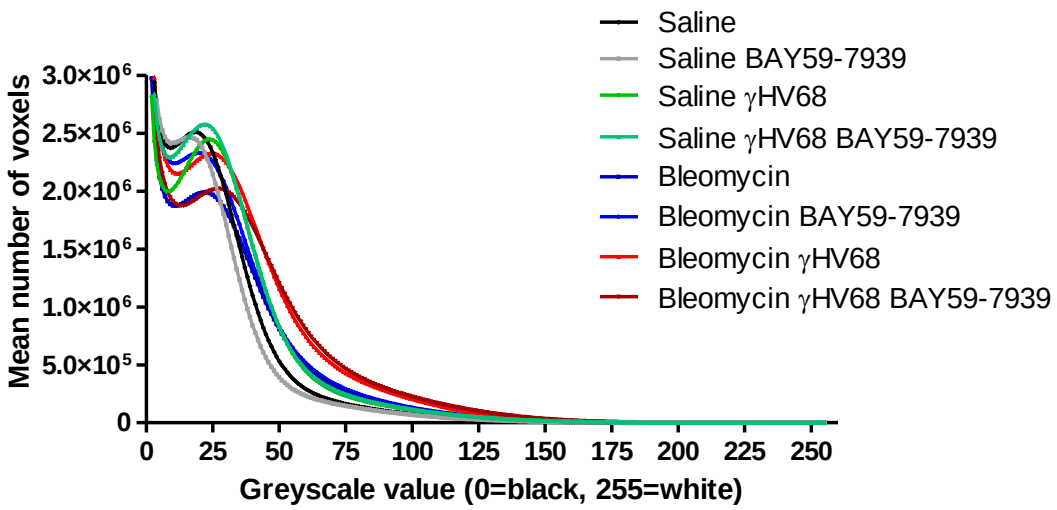

Figure 3.81. Voxel density histograms of µCT scanned lungs.

C57BL/6 mice were administered bleomycin via oropharyngeal route at 1 mg/kg, followed by infection with 100,000 PFU γHV68 or saline intranasally on day 14. Between days 15 and 28 the mice were given BAY59-7939 (3 mg/kg) twice daily via oral gavage. This figure shows density histograms corresponding to each experimental group plotted as a mean number of voxels against the greyscale values reflecting the density of the tissue, where 0 is black and 255 is white. Data are representative of an average of n=2-5 animals per group.

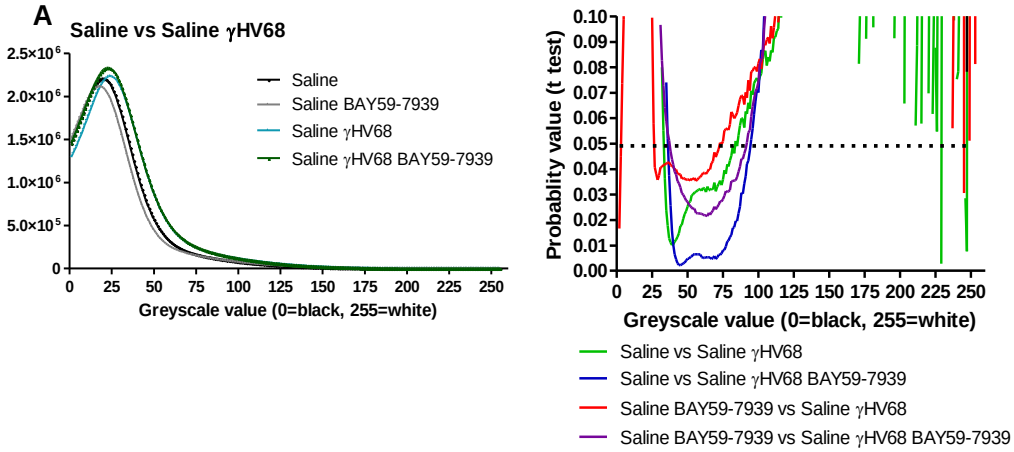
A
Saline vs Saline γHV68
Saline
Saline BAY59-7939
Saline γHV68
Saline γHV68 BAY59-7939
Greyscale value (0=black, 255=white)
Probablity value (t test)
Saline vs Saline γHV68
Saline vs Saline γHV68 BAY59-7939
Saline BAY59-7939 vs Saline γHV68
Saline BAY59-7939 vs Saline γHV68 BAY59-7939

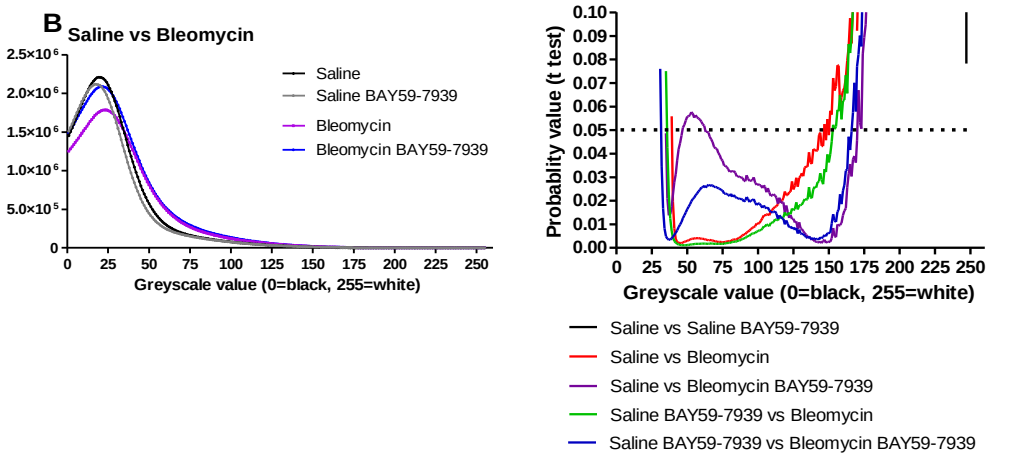
B
Saline vs Bleomycin
Saline
Saline BAY59-7939
Bleomycin
Bleomycin BAY59-7939
Greyscale value (0=black, 255=white)
Probablity value (t test)
Saline vs Saline BAY59-7939
Saline vs Bleomycin
Saline vs Bleomycin BAY59-7939
Saline BAY59-7939 vs Bleomycin
Saline BAY59-7939 vs Bleomycin BAY59-7939

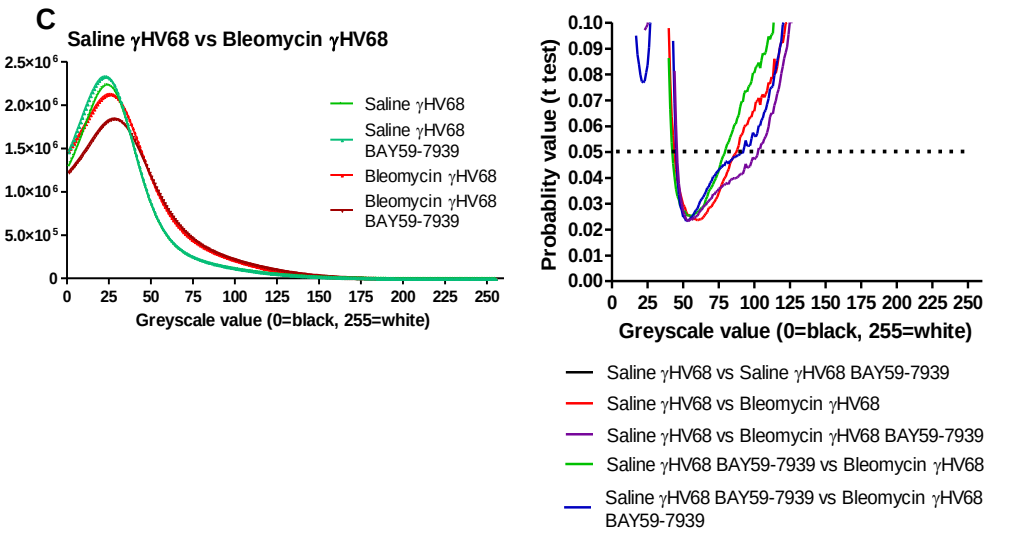
C
Saline γHV68 vs Bleomycin γHV68
Saline γHV68
Saline γHV68 BAY59-7939
Bleomycin γHV68
Bleomycin γHV68 BAY59-7939
Greyscale value (0=black, 255=white)
Probablity value (t test)
Saline γHV68 vs Saline γHV68 BAY59-7939
Saline γHV68 vs Bleomycin γHV68
Saline γHV68 vs Bleomycin γHV68 BAY59-7939
Saline γHV68 BAY59-7939 vs Bleomycin γHV68
Saline γHV68 BAY59-7939 vs Bleomycin γHV68 BAY59-7939

D

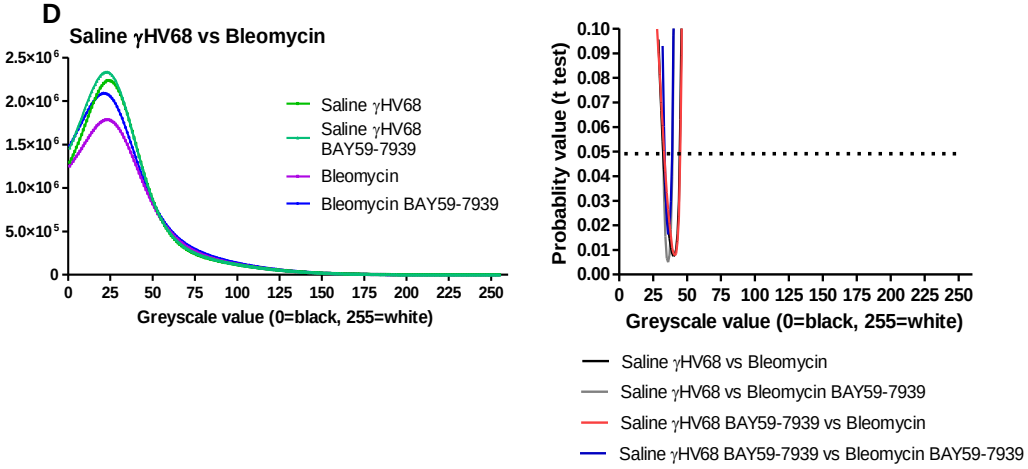
Saline γHV68 vs Bleomycin
2.5×10⁶
2.0×10⁶
1.5×10⁶
1.0×10⁶
5.0×10⁵
0
0 25 50 75 100 125 150 175 200 225 250
Greyscale value (0=black, 255=white)
Saline γHV68
Saline γHV68 BAY59-7939
Bleomycin
Bleomycin BAY59-7939
Probablity value (t test)
0.10 0.09 0.08 0.07 0.06 0.05 0.04 0.03 0.02 0.01 0.00
0 25 50 75 100 125 150 175 200 225 250
Greyscale value (0=black, 255=white)
Saline γHV68 vs Bleomycin
Saline γHV68 vs Bleomycin BAY59-7939
Saline γHV68 BAY59-7939 vs Bleomycin
Saline γHV68 BAY59-7939 vs Bleomycin BAY59-7939

E

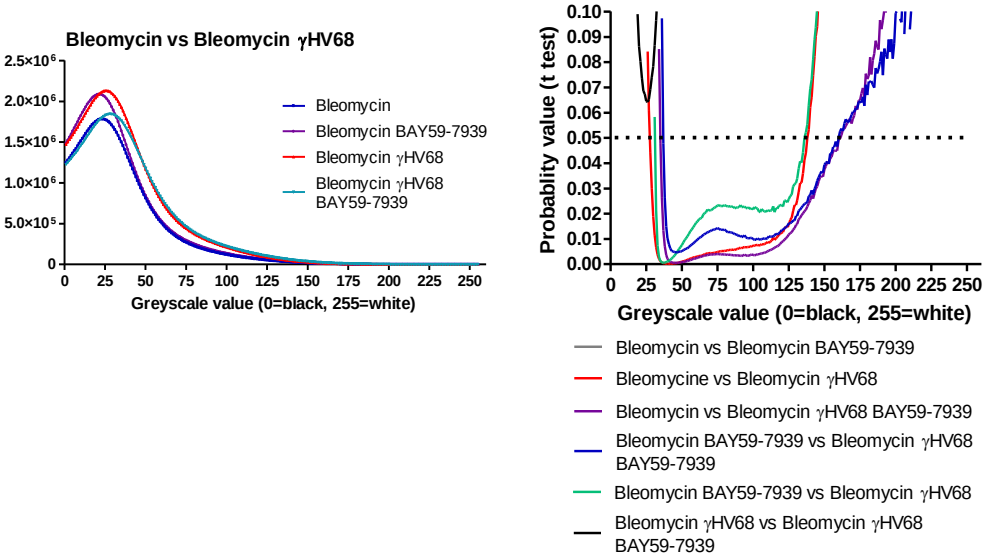
Bleomycin vs Bleomycin γHV68
2.5×10⁶
2.0×10⁶
1.5×10⁶
1.0×10⁶
5.0×10⁵
0
0 25 50 75 100 125 150 175 200 225 250
Greyscale value (0=black, 255=white)
Bleomycin
Bleomycin BAY59-7939
Bleomycin γHV68
Bleomycin γHV68 BAY59-7939
Probablity value (t test)
0.10 0.09 0.08 0.07 0.06 0.05 0.04 0.03 0.02 0.01 0.00
0 25 50 75 100 125 150 175 200 225 250
Greyscale value (0=black, 255=white)
Bleomycin vs Bleomycin BAY59-7939
Bleomycine vs Bleomycin γHV68
Bleomycin vs Bleomycin γHV68 BAY59-7939
Bleomycin BAY59-7939 vs Bleomycin γHV68 BAY59-7939
Bleomycin BAY59-7939 vs Bleomycin γHV68
Bleomycin γHV68 vs Bleomycin γHV68 BAY59-7939

F **Pixel range 40-150**

Saline

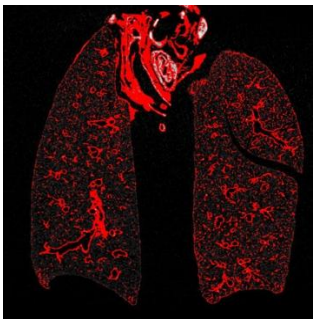

Saline γHV68

Bleomycin

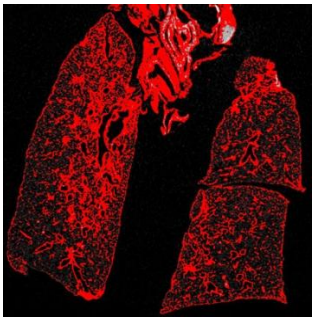

Bleomycin γHV68

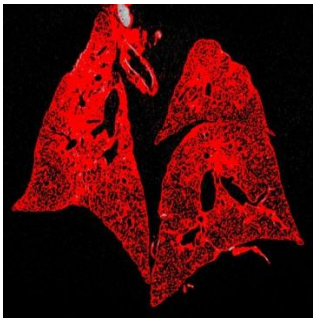

Bleomycin BAY59-3979

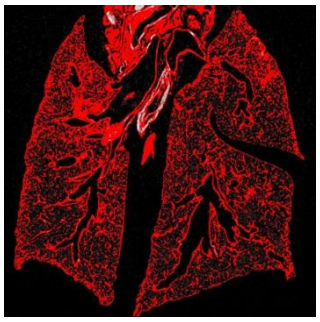

Bleomycin γHV68 BAY59-3979

G **Pixel range 35-45**

Saline γHV68

Bleomycin

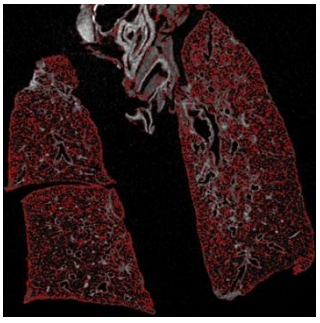

Figure 3.82. Density histograms analysis of µCT scanned lungs.

C57BL/6 mice were administered bleomycin via oropharyngeal route at 1 mg/kg, followed by infection with 100,000 PFU γHV68 or saline intranasally on day 14. Between days 15 and 28 the mice were given BAY59-7939 (3 mg/kg) twice daily via oral gavage. This figure shows density histograms corresponding to each experimental group plotted as a mean number of voxels against the greyscale values reflecting the density of the tissue, where 0 is black and 255 is white. The histograms are matched with the Student t-test analysis of significance and represented as graphs of probability value of less than 0.1, where the significance cut off was set as 0.05 as indicated by the dotted line against the density denoting greyscale values. Panel A- comparison of saline groups with γHV68-infected saline groups and the statistical analysis plots; panel B- comparison of saline groups with bleomycin-injured groups and the statistical analysis plots; panel B- comparison of saline groups with γHV68-infected bleomycin groups and the statistical analysis plots; panel C- distribution of significantly different pixels highlighted in red between the saline and bleomycin-challenged and saline and γHV68-infected fibrotic lungs; panel D- comparison of γHV68-infected saline groups with bleomycin groups and the statistical analysis plots; panel E- comparison of γHV68-infected saline groups with γHV68-infected bleomycin groups and the statistical analysis plots; panel F- distribution of significantly different pixels highlighted in red between the γHV68-infected saline and bleomycin-challenged and γHV68-infected saline and γHV68-infected fibrotic lungs; panel G- comparison of saline and γHV68-infected saline groups and the statistical analysis plots; panel H- comparison of bleomycin challenged groups and γHV68-infected fibrotic groups and the statistical analysis plots; panel I- distribution of significantly different pixels highlighted in red between the saline control lungs and γHV68-infected saline-treated lungs, and bleomycin only challenged lungs and γHV68-infected fibrotic lungs. Data are representative of an average of n=2-5 animals per group.

3.3.3.7 Investigation of inflammation in the viral infection of fibrotic lung

As previously mentioned FXa is a key component of the extrinsic coagulation cascade that leads to thrombin generation and can also directly activate both PAR-1 and PAR-2. In order to assess whether systemic inhibition of FXa affected the inflammation in the fibrotic lungs and γHV68 infected fibrotic lungs, inflammatory mediators were measured in lung homogenates and serum. Prominent dense inflammatory cell aggregates are consistent feature of the viral infection in the fibrotic lungs and were also quantified in this study as described in the previous, SB525334 study (**Figure 3.83B).** The inflammatory cell aggregates were detected at significantly higher frequency in bleomycin-γHV68 group and the numbers were further increased in bleomycin-γHV68-BAY59-7939 group. However, this difference fell short of statistical significance, which can be explained by a degree of variability between the histology sections.

Furthermore, increased CCL2 expression was detected in lung homogenates from all virally-infected groups. γHV68 infection alone caused a 7-fold upregulation in CCL2 mRNA levels and infection in the fibrotic lung further significantly increased CCL2 expression to 17-fold above the saline baseline (**Figure 3.83C**). A significant increase in CCL2 protein levels was also detected in the lung homogenates from all the virally infected groups when compared to mock-infected control groups (**Figure 3.83D**) and BAY59-7939 treatment did not affect CCL2 expression in the infected lungs.

Subsequently, the levels of CCL2, interferon γ (IFNγ) and keratinocyte chemoattractant (KC) inflammatory markers were assessed in serum collected in this study (**Figure 3.84**). In control mice and bleomycin-challenged mice 28 days post instillation the levels of CCL2 and IFNγ were below the detection range and the mouse IL-8 homolog-KC were low. In contrast, in virally-infected control lungs all these inflammatory mediators were significantly upregulated. In the bleomycin-treated and γHV68 infected lungs the levels of CCL2 and IFNγ were further significantly increased.

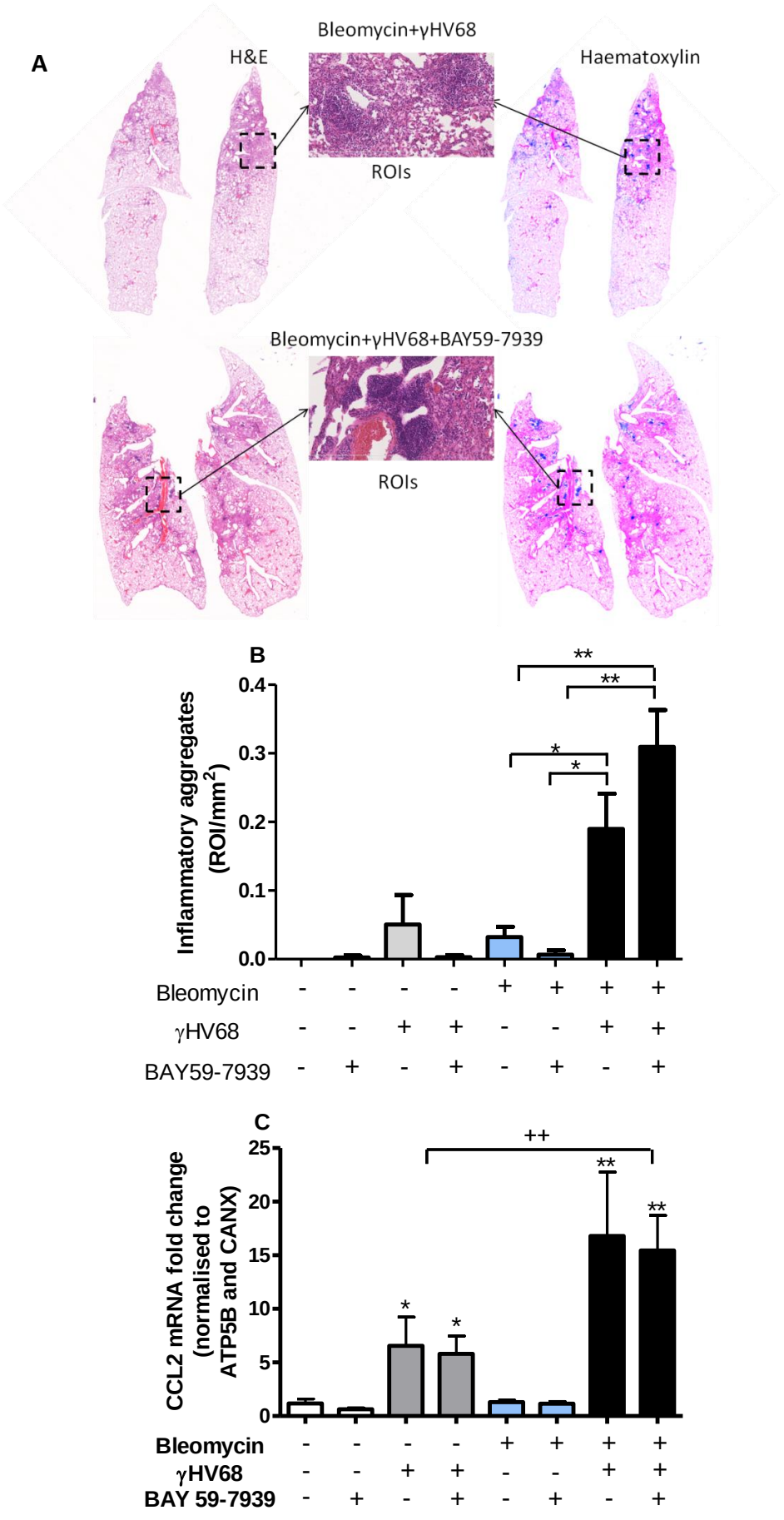
A
Bleomycin+γHV68
H&E
Haematoxylin
ROIs
Bleomycin+γHV68+BAY59-7939
ROIs
B
Inflammatory aggregates (ROI/mm²)
0.0
0.1
0.2
0.3
0.4
**
**
*
*
Bleomycin - - - - + + + +
γHV68 - - + + - - + +
BAY59-7939 - + - + - + - +
C
CCL2 mRNA fold change (normalised to ATP5B and CANX)
0
5
10
15
20
25
++
**
**
*
*
Bleomycin - - - - + + + +
γHV68 - - + + - - + +
BAY 59-7939 - + - + - + - +

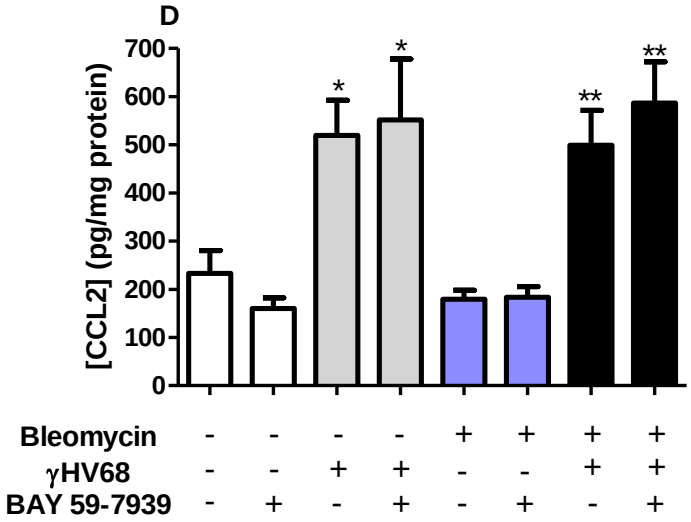

Figure 3.83. Inflammatory changes in the γHV68 infection on a background of pulmonary fibrosis.

C57BL/6 mice were administered bleomycin via oropharyngeal instillation at 1 mg/kg, followed by infection with 100,000 PFU γHV68 or saline intranasally on day 14. Between days 15 and 28 the mice were given BAY59-7939 (3 mg/kg) twice daily via oral gavage. Panel A- inflammatory aggregates were identified as dense areas of haematoxylin staining by the Nuance software and panel B- quantified as region of interest (ROI), mean +/- SEM, n=2-5 animals per group. Panel C- expression of CCL2 in the lungs 14 days p.i. was assessed by qPCR and data are presented as fold change in mRNA levels relative to two housekeeping genes ATP5B and CANX and representative of mean +/- SEM, n=3-8 animals per group; panel D- CCL2 protein levels in lung homogenates were quantified by ELISA. Data are representative of an average of n=4-8 animals per group. One-way ANOVA was performed for statistical analysis, *$p<0.05$, **$p<0.01$ relative to mock-infected saline and bleomycin groups; ++$p<0.01$ comparison of each γHV68-infected saline groups and each γHV68-infected fibrotic lungs.

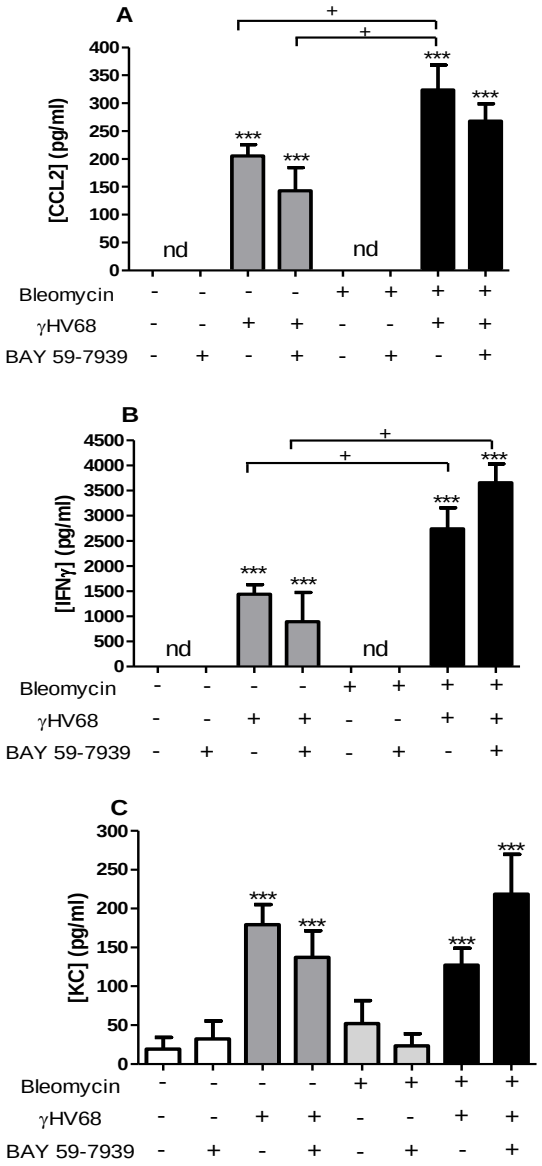

Figure 3.84. Assessment of serum inflammatory markers in the γHV68 infection on a background of pulmonary fibrosis.

C57BL/6 mice were administered bleomycin via oropharyngeal route at 1 mg/kg, followed by infection with 80,000 PFU γHV68 or saline intranasally on day 14. Between days 15 and 28 the mice were given BAY59-7939 at dose of 3 mg/kg twice daily via oral gavage. The serum levels of CCL2- panel A, IFNγ- panel B, and KC- panel C were assessed by ELISA. Data are representative of an average of n=6-14 animals per group and analysed with One-way ANOVA, *p<0.05, ***p<0.001 comparison between mock-infected and γHV68-infected groups; +p<0.05 comparison between γHV68-infected saline and fibrotic groups.

3.3.3.8 Summary

The aim of this study was to investigate the role of coagulation in the model of viral infection on a background of pulmonary fibrosis.

- As previously observed, infection with γHV68 caused a second wave of mouse body weight loss, increased ex vivo lung and spleen weight, and viral genes were still readily detected in the lungs.
- Hydroxyproline and Sircol measurement of collagen showed no difference in total lung collagen between fibrotic lung and infected fibrotic lung. BAY59-7939 did not affect lung collagen level either in bleomycin-challenged lungs or in bleomycin-γHV68 double-injured lungs.
- µCT and lung density analysis showed that in this study the γHV68 infection caused architectural changes in the saline infected lungs that were markedly different to the fibrosis induced by bleomycin. µCT scans revealed that infected fibrotic lungs displayed higher percentage of abnormal areas and increased lung density. Treatment with BAY59-7939 did not affect the development and course of fibrosis in bleomycin-challenged lungs and in γHV68 infected fibrotic lungs.
- Viral infection promoted the infiltration of inflammatory cells into the lung that formed dense aggregates, which were prominent 14 days p.i. Furthermore, γHV68 infection, both in saline and fibrotic lungs, led to a significant increase in CCL2 expression in the lung and CCL2, IFNγ and KC levels were found to be significantly increased in the systemic circulation 14 days p.i..

3.3.4 Discussion

3.3.4.1 Overview

Viral infections contribute to the pathogenesis of acute and chronic lung diseases. Infections with common respiratory viruses, for instance syncytial virus, rhinovirus and influenza virus, have been linked to exacerbations of asthma, chronic obstructive pulmonary disease (Holtzman et al., 2011) and cystic fibrosis (Asner et al., 2012). Herpes simplex virus infection is a risk factor for the development of ARDS in patients in intensive care (Bruynseels et al., 2003) and leads to increased complications and prolonged hospitalisation (Luyt et al., 2007). Cytomegalovirus reactivation is observed in septic surgical patients and is associated with increased incidence of fibroproliferative lung disease in these patients (Cook et al., 2006). Long-term antiviral therapy in post-lung transplant patients is protective from herpesviruses reactivation and transplant rejection (Finlen Copeland et al., 2011).

Current evidence of viral involvement in the progression of interstitial lung disease, particularly IPF, is conflicting but the γ-herpesviruses family have been strongly implicated in the pathogenesis of fibroproliferative lung disease. Epstein Barr virus (EBV) is the most common γ-herpesvirus detected in the lung tissue from IPF patients, next to HHV-8 and HHV-7 (Stewart et al., 1999; Tang et al., 2003). EBV asymptomatically infects 95% of the population. The virus gains entry via the nasopharynx epithelium, where it replicates and migrates into lymph nodes to establish latency in the B-lymphocytes. Detection of latent membrane 1 (LMP-1) of EBV virus is associated with worse outcome and increased mortality in IPF patients (Tsukamoto et al., 2000). The default programme of EBV is to establish latency in B-lymphocytes and the virus is not normally detected in the lungs of healthy individuals but in IPF patients EBV has been detected replicating in the lower respiratory epithelium (Egan et al. 1995). Furthermore, EBV-positive IPF patients harbour virus with increased capacity for spontaneous reactivation (Kelly et al., 2002). Presence of EBV in the lungs of IPF patients has also been associated with the

development of pulmonary hypertension, a major comorbidity that contributes to mortality in IPF patients (Calabrese et al., 2013).

In experimental models, murine γ-herpesvirus-68 (γHV68) has been used to investigate the role of viral infection in the pathogenesis of pulmonary fibrosis (PF). Murine γHV68 is genetically co-linear with human herpesviruses, EBV and HHV-8, and is natural pathogen of rodents that follows a similar infection pattern as human herpesviruses i.e. infects the respiratory epithelium and persists in B-cells, macrophages and epithelial cells (Nash et al., 2001).

Pulmonary fibrosis is a multifactorial disease and murine γHV68 has been shown to act as a contributing factor for the development and progression of experimental pulmonary fibrosis. Infection with γHV68 has been shown to prime otherwise resistant BALB/c mice to develop fibrosis following bleomycin injury (Lok et al., 2001). Transfection of EBV transactivation protein Zta into mouse lungs triggers neutrophilic inflammation, expression of Th2 profibrotic cytokines and alternatively activated macrophages, but this resolves without fibrosis (Guenther et al., 2010). In contrast, mice lacking IFNγ receptor and hence unable to mount antiviral responses develop multiorgan fibrosis following infection with γHV68 (Ebrahimi et al. 2001) that can be attenuated by antiviral therapy. Furthermore, pulmonary fibrosis in the latently-infected lungs develops in response to sub-threshold fibrotic stimulus and results in significantly increased lung collagen deposition and increased TGFβ activity (Vannella et al. 2010).

The aim of the studies presented in this thesis chapter was to establish a model of γHV68 infection on a background of existing pulmonary fibrosis and to investigate the impact of viral infection on the progression of disease. Furthermore, we aimed to examine the potential mechanisms by which viral infection promotes more severe disease by focusing on blocking TGFβ signalling and the coagulation cascade in this model.

3.3.4.2 Development of the model of γHV68 infection in pulmonary fibrosis

Infection with γHV68 of fluorescein isothiocyanate (FITC)-challenged mice has been shown to exacerbate pulmonary fibrosis (McMillan et al., 2008). In comparison with mock-infected mice, γHV68 infection led to inflammation, high levels of CCL2 and CCL12 release and significantly increased lung collagen accumulation.

In this study we aimed to develop a model of γHV68 infection on a background of bleomycin-induced pulmonary fibrosis. In our laboratory, we use oropharyngeal administration of bleomycin which reproducibly produces homogenous lung injury with evidence of vascular leak, monocytic and neutrophilic inflammation. Two weeks into the model peripheral and subpleural fibrotic lesions are detected in the lung and this point of established fibrosis was chosen to introduce the viral infection. Mice were inoculated with γHV68 via the intranasal route, which is considered to be a natural route of viral transmission. The initial study was designed to optimise and characterise the model of infection with γHV68 on a background of bleomycin-induced pulmonary fibrosis and hence two time points were chosen for data collection: 7 days post-infection (p.i.), described as the peak of inflammatory response to the infection (McMillan et al., 2008) and 14 days p.i. when lytic infection is cleared and virus establishes latency (Nash et al., 2001). Prominent splenomegaly was observed 14 days p.i. confirming successful infection. This was further confirmed by the detection of viral gene expression in infected lungs 7 day p.i. and 14 days p.i.

Following the administration of bleomycin, the acute phase of injury is associated with weight loss and in this study mice lost around 5% of the starting body weight (between days 4 and 12 post injury). Inoculation with γHV68 was associated with second wave of body weight loss (between days 3 and 7 post infection). Temporally the two waves of weight loss correspond to the inflammatory phases of bleomycin injury and viral infection. Furthermore, infection with γHV68 caused a significant increase in *ex vivo* lung weight in infected mice 7 days p.i. suggesting an ongoing inflammatory response and vascular leak. These inflammatory responses were

subsequently confirmed by the analysis of histological sections from virally-infected lungs, which in comparison to fibrosis only lungs, revealed widespread infiltration of inflammatory cells, which formed dense aggregates around airways and blood vessels, and remained prominent at day 14 p.i. Furthermore, at 7 days p.i. virally-infected fibrotic lungs showed evidence of disrupted alveolar architecture, alveolar leak and haemorrhage. These observations were consistent with the previous reports that γHV68 infection on a background of FITC-induced pulmonary fibrosis triggers a robust inflammatory response in the lung that is also associated with lung functional impediment, i.e. reduced total lung capacity, vital capacity and compliance (McMillan et al., 2008).

The extent of fibrosis was subsequently evaluated by measurement of total lung collagen in the viral infection on a background of pulmonary fibrosis. A time-course study in our laboratory characterised the collagen gene expression and protein accumulation in the lungs following oropharyngeal instillation of bleomycin at a dose of 2 mg/kg. Collagen mRNA levels increase from day 3 through to 28 post-injury whereas protein accumulation is stably detected between days 14 and 28 post-injury, and still significantly increased at day 84 post-injury when compared to saline-instilled control mice (Scotton et al., 2013). The current study aimed to develop a two-hit injury model and therefore a reduced dose of bleomycin of 1 mg/kg was used. An increase in total lung collagen was observed 7 days p.i. when compared to historical values for the saline control lung but no difference was observed between virus-challenged mice and bleomycin-alone treated animals. By day 14 p.i. (and 28 days after bleomycin instillation) total lung collagen in mock-infected fibrotic lungs decreased, which suggests that in this study bleomycin-induced injury and fibrosis followed different kinetics to the well-characterised 2 mg/kg bleomycin injury model established in our laboratory. However, at 7 days p.i. a 5-fold increase in collagen mRNA levels was detected in virally-infected fibrotic lungs when compared to bleomycin-only challenged lung. Collagen expression returned to baseline values by day 14 p.i. but total lung collagen remained elevated in virally infected fibrotic lungs 14 days p.i. and was significantly higher than in mock-infected fibrotic lungs. These observations were further corroborated by the

MSB collagen staining of the lung sections, where blue-stained collagen fibres formed condensed and well-defined bands running through otherwise normal lung architecture in the bleomycin-only treated lungs while in the virally-infected fibrotic lung the collagen appeared to be deposited in more dispersed fashion forming extensive fibrotic lesions with dense collagen bands.

The question whether bleomycin causes resolving injury has been controversial with different studies reporting contrasting observations. In one study bleomycin-induced fibrosis has been shown to completely resolve after three months (Degryse et al., 2010) while other groups report persistent and lasting fibrotic lesions up to six months after injury (Hodges et al., 2004; Scotton et al., 2013). In this pilot study of γHV68 infection on a background of pulmonary fibrosis, combined analysis of total lung collagen and histology supports the notion that at a lower dose of bleomycin the resulting lung fibrosis was being re-modelled four weeks post-injury and that viral infection appeared to impede on this process. Analysis of the histology sections from virally-infected fibrotic lungs 7 days p.i. revealed evidence of acute lung injury superimposed on existing fibrosis. This was associated with increased collagen and CCL2 mRNA levels 7 days p.i, which returned to levels detected in bleomycin-only lungs by 14 days p.i. However, collagen and CCL2 protein levels remained significantly higher in virally-infected fibrotic lungs 14 days p.i. when compared to fibrotic lungs. Taken together these data suggest that the inflammation triggered by γHV68 infection alters the kinetics of bleomycin-induced fibrosis in this model.

In contrast with previously reported data that γHV68 infection exacerbates FITC-induced pulmonary fibrosis (McMillan et al., 2008), our findings did not show increased lung collagen accumulation in virally-infected fibrotic lungs. However, this could be explained by several key differences between the two studies. There are intrinsic differences between FITC and bleomycin models of pulmonary fibrosis, particularly when administered via different routes (FITC- intratracheal, bleomycin-oropharyngeal). Bleomycin causes lung injury through direct DNA damage and oxidative stress, which evoke strong host inflammatory response characterised by

high levels of cytokines, TNFα and IL-1β, and chemokines, CCL12 and CCL2, infiltrations of inflammatory cells and vascular leak (Degryse and Lawson, 2011). Increased TGFβ activity by day 14 post-injury is associated with the development of fibrotic lesions. However, these responses are entirely host-mediated after bleomycin has been metabolised by bleomycin hydrolase. In contrast, FITC is a fine particle that attaches to the lung proteins and prolonged exposure to this agent causes chronic inflammatory and fibrotic responses. However, fibrotic lesions develop only in the areas of FITC deposition as visualised by immunofluorescence (Moore and Hogaboam, 2008). Therefore, the distribution and severity of the resultant fibrosis can potentially account for different responses to viral infection. Furthermore, in the FITC study lung collagen was measured only at day 7 days p.i., which corresponds to the peak of lytic infection and is characterised by a strong inflammatory response. Moreover, the assay used to measure lung collagen in this FITC study was colorimetric Sircol assay, which has been shown to also bind non-collagen serum proteins (Lareu et al., 2010). It is possible that the increased levels of collagen reported in that study may represent a combined measurement of collagen and protein leak in the lung.

The Th1-Th2 imbalance is well characterised in the IPF lung (Wuyts et al., 2012) and the classical Th2 cytokines, IL-4 and IL-13, are both fibrogenic. Chronic infection with γHV68 in IFNγR deficient mice is characterised by Th2-inflammation, alternatively activated macrophages and the development of pulmonary fibrosis with classical features of epithelial cell hyperplasia, myofibroblast transformation and activation of TGFβ (Gangadharan et al., 2008; Mora et al., 2005). Control of viral reactivation and antiviral therapy protect IFNγR deficient mice from developing severe pulmonary fibrosis (Mora et al., 2007). However, other studies have shown that γHV68 infection exacerbates pulmonary fibrosis in the presence of a strong IFNγ-driven antiviral response (McMillan et al., 2008). In the current study, IFNγ was found to be significantly elevated in lung homogenates of virally infected animals suggesting that the mice mounted a strong antiviral response to the γHV68 infection. However, this IFNγ response was only detected 14 days p.i., which again highlights differences between this model and the FITC model of viral exacerbation

(McMillan et al., 2008). The lack of an early IFNγ response in comparison to bleomycin alone could again be explained by intrinsic differences between bleomycin and the FITC fibrosis models. Murine γHV68 has been shown to latently infect alveolar macrophages that maintained production of large amounts of IFNγ, TNFα, CCL2, CCL12 as well as TGFβ four weeks after infection (Stoolman et al., 2010). CCL2 is a potent chemoattractant for immune cells as well as for precursor cells of fibroblasts, fibrocytes (Moore et al., 2005b) and is significantly upregulated in response to viral infection. Mesenchymal cells isolated from γHV68 infected mice also showed long-lasting upregulation of profibrotic mediators, notably TGFβ and CCL2 (Stoolman et al., 2010). In the present study, CCL2 gene expression was significantly increased 7 days p.i. and high CCL2 protein levels were detected both at 7 days p.i. and 14 days p.i., when compared to mock-infected fibrotic lungs. These findings suggest that in this model of two-hit lung injury viral infection leads to persistent inflammation that is ongoing 14 days p.i. and after the virus has established latency.

Excessive activation of the coagulation cascade has been strongly implicated in the progression of pulmonary fibrosis. The ternary complex, TF-FVIIa-FXa, can be assembled and activated locally in human and murine lungs (Scotton et al., 2009), while thrombin is considered to enter the lung as a result of a microvascular leak. Herpesvirus infection has previously been shown to trigger the activation of the coagulation cascade (Sutherland et al., 1997). Human cytomegalovirus (CMV) and parvovirus B19 infections induce microvascular injury (Magro et al., 2003) while human herpes simpex virus I (HSV I) and CMV have been shown to “hijack” the coagulation cascade in an immune evasion strategy. HSV I and CMV express tissue factor and procoagulant phospholipids on their surface providing a platform for the assembly of the TF-FVIIa-FXa complex leading to further activation of the coagulation cascade and thrombin generation (Sutherland et al., 1997). Furthermore, HSV I surface glycoprotein C has been shown to directly bind FX (Livingston et al., 2006). Thrombin has also been shown to enhance HSV I and CMV adhesion and cell entry in human umbilical vein endothelial cells (HUVEC) and human foreskin fibroblasts (HFF) (Sutherland et al. 2007). During the lytic phase,

viral infection causes extensive damage to the respiratory epithelium which is consistent with the mechanism of activation of the extrinsic coagulation cascade. In the current study we evaluated mRNA levels of three components of the ternary complex. Both tissue factor and FX mRNA levels were significantly increased 7 days p.i. when compared to the bleomycin alone treated lungs. FVII was significantly downregulated 7 days p.i. but the physiological importance of this result is difficult to evaluate as small amount of FVII are required to assemble the ternary complex. However, it is possible that downregulation of FVII is an intrinsic protective mechanism preventing excessive activation of the coagulation cascade. It has been previously shown that low-FVII-expressing mice are protected from acute inflammation and coagulopathy in the model of endotoxemia, which was also associated with reduced mortality (Xu et al. 2006). Immunolocalisation of the tissue factor and FX revealed that both proteins were expressed primarily in bronchial and alveolar epithelium and the intensity of staining was stronger in the virally-infected fibrotic lungs 14 days p.i. relative to fibrotic only lung. Finally, thrombin expression was not evaluated in this study as the general consensus is that the main source of prothrombin and active thrombin is the lung circulation.

The coagulation cascade exerts a plethora of cellular effects via PAR receptors. The high-affinity thrombin receptors, PAR-1, plays an important role in immunity to viruses. PAR-1 knockout mice infected with cardiotropic virus coxsackievirus 3 showed increased viral loads in the heart and liver, worse heart injury and a higher incidence of heart failure (Antoniak et al., 2013). This was accompanied by significant upregulation of the highly inflammatory cytokines TNFα, IL1β and increased accumulation of inflammatory cells in the heart. However, PAR-1 knockout mice showed reduced levels of cytokines involved in the antiviral responses, CXCL10 and IFNβ, and significantly reduced recruitment of NK cells into the heart in the early phase of infection. Moreover, lack of PAR-1 on non-haematopoietic cells was found to contribute to decreased antiviral immunity (Antoniak et al., 2013). In contrast, mice with cardiomyocytes overexpressing PAR-1 were protected from virally-induced heart injury while the cardiac fibroblasts

showed synergistic activation of PAR-1 and TLR3 in response to the virus *in vitro* (Antoniak et al., 2013).

In contrast, PAR-1 activation in mice infected with influenza virus was found to increase the viral replication and inflammation in the lungs resulting in higher mortality in this model (Khoufache et al., 2013). PAR-1 deficiency and PAR-1 antagonism were found to protect mice from infection and inflammation-related lung injury. Expression of all PARs in respiratory epithelium and airway smooth muscle cells has been shown to change following influenza infection and particularly increased expression of PAR-1 and PAR-2 significantly augmented the antiviral responses in these cells (Lan et al., 2004). These studies strongly suggest that PAR-1 plays greatly different roles in antiviral immunity depending on the infecting agent.

In the current study mRNA levels of PAR receptors in total lung homogenates were assessed but there was no change in PAR-1 and PAR-2 expression in any of the treatment groups. However, these receptors are widely expressed in the lung and it is possible that subtle changes in the expression measured in the lung homogenates may be missed. In contrast, the expression of PAR-3 and PAR-4 in the lung at baseline is low but was significantly increased at day 7 p.i. and this increase was maintained at day 14 p.i. Murine platelets express PAR-3 and PAR-4 and histological analysis of the virally-infected lungs showed evidence of alveolar haemorrhage. It is therefore possible that the increase in PAR-3 and PAR-4 expression is associated with the platelet influx into the lungs. Furthermore, PAR-4 has been shown to mediate neutrophilia and disseminated intravascular coagulation in the model of endotoxemia (Slofstra et al., 2007). CMV virus has been shown to increase mRNA levels of all PAR receptor in endothelial cells increasing their responsiveness to thrombin (Popović et al., 2010). Both PAR-3 and PAR-4 are activated by thrombin and hence could contribute to procoagulant signalling in response to viral infection in the lung.

Taken together, the results of this study demonstrate that reduced dose of bleomycin (1 mg/kg) caused mild fibrosis. γHV68 infection did not increase the lung collagen accumulation but interfered with the re-modelling process observed in

bleomycin-challenged lungs 14 days p.i.. However, strong inflammatory and antiviral responses were mounted in the infected fibrotic lung and persisted until day 14 p.i..

3.3.4.3 Effect of TGFβ inhibition on γHV68 infection in fibrotic lung

TGFβ is ubiquitously expressed in the normal lung and has been shown to be significantly upregulated in bleomycin induced pulmonary fibrosis (Santana et al., 1995). Disruption of TGFβ activation and signalling through direct cytokine inhibition (Giri et al. 1993), Smad3 knockout (Bonniaud et al. 2004), ALK5 receptor knockout (Li et al. 2011), integrin αvβ6 knockout (Koth et al., 2007; Morris et al., 2003) offers protection in experimental models of pulmonary fibrosis. TGFβ activates multiple cellular signalling pathways to exert its profibrotic effects including inducing fibroblast to myofibroblast differentiation and induction of αSMA and collagen gene expression, which are Smad3-dependent manner (Hu et al. 2003) but also rely on signalling via p38 and ERK kinases (Hu et al. 2006). Interaction between Smad3 and MAPK pathways also promotes fibroblast survival (Horowitz et al. 2004). Furthermore, TGFβ prevents extracellular matrix degradation by inducing the expression of tissue inhibitors of MMPs (TIMPs) (Edwards et al., 1987; Kwak et al., 2006) and the plasminogen-activator inhibitor PAI-1 (reviewed in Samarakoon 2013).

TGFβ also plays an important role in modulation of immune and inflammatory responses during herpesviruses infection. TGFβ signalling has been shown to cause activation of latent EBV infection (Liang et al., 2002). TGFβ-Smad canonical signalling pathway leads to re-activation of the latent Epstein Barr virus as lytic viral genes contain multiple Smad-binding elements in promoter region (Iempridee et al., 2011). Furthermore, TGFβ-mediated signalling through NFκB also promotes viral replication through downregulation of inducible nitric oxide synthase (iNOS) and ERK phosphorylation that was necessary for activation of viral genes (Oussaief et al., 2011). Upon infection of epithelial cells with EBV the level of TGFβ increases and

apoptosis markers are initially upregulated (Malizia et al., 2008) but in chronic infection epithelial cells infected with EBV are resistant to TGFβ-induced apoptosis (Fukuda et al., 2001). Latently infected epithelial cells can be reactivated by TGFβ and activate the programme for epithelial to mesenchymal transition (Malizia et al., 2009b). Latent virus LMP-1 protein has also been shown to act synergistically with TGFβ to promote EMT (Sides et al., 2010).

In this study the pharmacological inhibitor of the TGFβ ALK5 receptor, SB525334 was used to investigate the role of TGFβ in γHV68 infection on a background of existing pulmonary fibrosis. The compound was administered according to a therapeutic dosing regimen, from day 15 after bleomycin injury and day one after viral inoculation through to day 28 (14 p.i.), when the study was ended. As observed in the previous study, a reduced dose of bleomycin caused lung injury initially reflected by an early weight loss (between day 4 and 10 post-injury). The second wave of weight loss was recorded after the inoculation with γHV68 and the bleomycin+γHV68+vehicle mouse group showed the greatest body weight loss. Consistent with previous studies with higher dose of bleomycin (Scotton et al., 2013), SB525334 significantly attenuated lung collagen accumulation as measured by hydroxyproline (HPLC) in the bleomycin alone injured lungs. However, there was no difference in the total lung collagen between the mock-infected fibrotic lungs and virally-infected fibrotic lungs 14 days p.i.. Furthermore, the therapeutic effect of SB525334 appeared to be lost in bleomycin+γHV68 double-injured mice. Sircol assay was also performed in this study to measure the content of soluble collagen in lung homogenates, as this assay was employed by the previous studies of viral exacerbation in the FITC model (McMillan et al., 2008). Although the levels of total lung collagen quantified by Sircol were 20-fold lower than the levels measured by HPLC, the pattern of collagen accumulation within experimental groups was similar. SB525334 treatment decreased lung collagen accumulation in response to bleomycin injury alone but the therapeutic effect of the drug was again lost in the viral infection of fibrotic lung. The only difference between the two assays was observed in the collagen levels in the virally infected saline lungs, which showed higher collagen levels than saline control lungs. However, this difference was not

detected in any other assay analysed in this study to evaluate inflammatory and fibrotic changes in the lung and it was most likely due to Sircol assay cross-reacting with non-collagen proteins as has been previously reported (Lareu et al., 2010).

Successful viral infection was again confirmed by prominent splenomegaly 14 days p.i.. Spleen weight was significantly increased in virally infected saline-treated groups and further increased in virally infected fibrotic lungs. Interestingly, the increase in spleen weight with viral infection was significantly attenuated by SB525334 treatment in fibrotic lungs, but not in saline-treated lungs. Furthermore, all three viral genes were readily detected in the lungs 14 days p.i., which suggests that there was still ongoing viral replication in the lung at the time. Taken together, these data suggest that despite established latency in the spleen, γHV68 is still replicating in the lungs 14 days p.i..

In order to further analyse the effect of targeting TGFβ in this model of viral infection on a background pulmonary fibrosis, we used *ex vivo* μCT technology to investigate changes in lung morphology. The μCT technology for live animal imaging has been validated *in vivo* for repeated longitudinal studies of lung cancer (Namati et al., 2010) but the resolution was restricted by the respiratory movement and cardiac motion. This technique has also been applied for *ex vivo* investigation of the lung architecture (Thiesse et al., 2010; Vasilescu et al., 2012) and as an endpoint for evaluating fibrosis (Rodt et al., 2010; Scotton et al., 2013). The main advantage of μCT technology is that it allows whole-lung scanning and hence avoids the potential sampling error associated with standard histological analysis of tissue sections. In current study the μCT scans were analysed using pattern recognition software and matched with histological sections from the same lungs. Saline control lungs showed normal morphology while bleomycin-challenged lungs showed condensed fibrotic lesions, interlobular septal thickening, and traction bronchiectasis in areas of subpleural scarring. These fibrotic changes were significantly reduced by SB525334 treatment in bleomycin-challenged lungs. However, the appearance of lungs infected with the virus on a background of fibrosis clearly indicated that inflammation was still prominent in these lungs. The inflammatory features that

were readily identifiable on the μCT scans included diffuse ground-glass opacities and consolidation superimposed on the areas of fibrotic changes. These features are also commonly reported in acute exacerbation of IPF (Collard et al., 2007) and the scans of virally-infected fibrotic lungs bore resemblance to the scans of exacerbated IPF patients. Histological analysis of virally-infected fibrotic lungs revealed extensive thickening and distortion of alveolar septae, and dense aggregates of inflammatory cells, clearly visible around the airways and vasculature. These inflammatory cell aggregates were quantified revealing that bleomycin+γHV68 lungs had significantly higher numbers of inflammatory cells aggregates than all saline groups and mock-infected fibrotic lungs. Furthermore, there was a trend towards a reduction in the number of aggregates with SB525334 treatment. Taken together, these data suggest that in this study, 14 days p.i. there was still significant level of inflammation persistent in the γHV68-infected fibrotic lungs.

The output of μCT scans was subsequently quantified using "trainable" pattern recognition software. This software was trained to distinguish between normal lung architecture and fibrosis and to quantify these areas based on pixel density. Inflammatory cell infiltrations appear on the scans as areas of intermediate density between the dense fibrotic consolidations and normal lung parenchyma. To increase the accuracy of the analysis, areas different from normal lung parenchyma were grouped together as "abnormal lung". The quantification of abnormal lung areas and lung densities confirmed that μCT analysis offers an increased therapeutic window to detect the effect of SB525334 when compared with HPLC, as previously shown (Scotton et al., 2013). These data also show that 28 days into this model and 14 days p.i. on average 50% of fibrotic lungs showed abnormal appearance and this was modestly increased with viral infection on a background of fibrosis. SB525334 treatment significantly reduced abnormal lung area in bleomycin alone injured lungs but this therapeutic effect was consistently lost in the virally infected fibrotic lungs. Furthermore, a detailed greyscale analysis of lung densities independent of the segmentation output confirmed that bleomycin injury increased lung density and this increase was attenuated with SB525334 treatment in mock-infected

fibrosis group. Viral infection on a background of pulmonary fibrosis lungs further increased lung density when compared to bleomycin-challenged lungs and ALK5 inhibition impacted on the lung density but to a lesser degree than in the fibrosis alone groups. Furthermore, the statistical analysis of lung densities identified the pixel density range that was significantly different between the experimental groups and corresponded to specific areas in the lung. The pixel density range that in the saline-treated lungs corresponded to dense airway walls, in fibrotic lung localised to fibrotic lesions while in virally infected fibrotic lung encompassed fibrotic lesions and ground-glass opacities dispersed throughout the parenchyma. Interestingly, the range of significantly different density pixels between the bleomycin-injured lung and bleomycin+SB525334 lung localised directly to areas of fibrosis supporting the notion that blocking TGFβ signalling actively prevents formation of fibrotic lesions. This observation is consistent with HPLC and Sircol data showing attenuation of fibrosis in mock-infected bleomycin-challenged lungs. In contrast, in virally-infected fibrotic lung and bleomycin+γHV68+SB525334 lung the range of significantly different density pixels was narrower and distributed throughout the parenchyma, suggesting that in the viral infection of fibrotic lung the therapeutic effect of SB525334 is targeted against the inflammatory response rather than fibrotic response.

While SB525334 had a therapeutic effect in reducing fibrosis in bleomycin-alone injured lungs, in virally infected fibrotic lungs the TGFβ/ALK5 inhibition appeared to reduce infiltration of the inflammatory cells into the lung. There are several potential explanations for this finding. TGFβ exerts potent anti-inflammatory effects and it is possible that inhibition of TGFβ signalling early in the infection allowed for a stronger antiviral response in SB525334-treated mice. This would be associated with more efficient clearance of the virus as well as reduced capacity of the virus to establish latency. This explanation would be consistent with significantly reduced splenomegaly reported in this study in bleomycin+γHV68+SB525334 experimental group.

TGFβ exerts pleiotropic regulatory effects on immune and antiviral responses that depend on the site and cause of infection. In the model of eye infection with Herpes simplex I virus (HSV) inhibition of TGFβ signalling in innate immune cells reduces viral replication in the cornea while blocking TGFβ in T-cells reduces viral replication at the latency site, the trigeminal nerve (Allen et al., 2011). However, inhibition of TGFβ signalling in innate immune cells does not affect the viral replication in the trigeminal nerve, secondary site of infection and established latency (Allen et al., 2011), suggesting that different mechanism, TGFβ-dependent and -independent may be involved in viral clearance at different physiological sites. However, inhibition of TGFβ signalling in both innate and adaptive immune cells reduces the viral capacity to establish latency and reduces the number of immune cells infiltrations into the primary site of infection as wells as to the site of latency (Allen et al., 2011). TGFβ is generally immunosuppressive and this effect has been shown to converge with the viral immune evasion strategies. Herpesviruses downregulate the major histocompatibility complexes MHC class I and MHC class II that are required for mounting efficient adaptive immunity against infection. Murine γHV68 has been shown to ubiqitinate the MHC class I complex targeting it for degradation and preventing the upregulation on the cell surface and hence evading the recognition of infected cells by T-cells (Boname et al., 2004). TGFβ has also been shown to downregulate MHC class I and II and induce T-regulatory cells differentiation that dampen the immune response. Moreover, TGFβ-independent downregulation of MHC class I and II by virus also has inhibitory effect on T-cell activation and proliferation (Odeberg and Söderberg-Nauclér, 2001). Blocking TGFβ may therefore contribute to increased T-cell responsiveness and hence clearance of the virus. Furthermore, inhibition of TGFβ leads to expansion of NK cells and increased IFNγ production and hence better control of viral infection (Allen et al., 2011).

In this model of γHV68 infection in the fibrotic lungs targeting ALK5 reduced splenomegaly, a hallmark of γHV68 established latency, and reduced the number of inflammatory cell aggregates in the lungs. Interestingly, ALK5 inhibition did not affect the size of the spleen in virally-infected saline group. These data potentially

suggest that inhibition of TGFβ signalling in virally-infected fibrotic lung affects the course of infection and inflammatory responses in this model. It has been previously reported that viral infection in a lung with pre-existing injury triggers different host responses. In bone marrow transplantation model, post-transplant mice have been reported to be more susceptible to γHV68 infection in the lung and the latent infection led to chronic and persistent pneumonitis and fibrosis (Coomes et al., 2011). Furthermore, γHV68-infection in post-transplant lungs led to accumulation of alternatively activated macrophages and triggered influx of neutrophils and lymphocytes into the lung, with the latter being dominated by CD8 and CD4 T-cells (Coomes et al., 2011). Blocking TGFβ signalling in T lymphocytes led to attenuation of inflammation and fibrosis in that model (Coomes et al., 2010, 2011).

In conclusion, the findings of this study show that in the γHV68 infection on a background of pulmonary fibrosis viral infection leads to strong inflammatory response that persists in the lung 14 days p.i. Furthermore, data suggest that in the fibrotic lung the SB525334 effect is strictly anti-fibrotic while in the viral infection of fibrotic lung the anti-TGFβ therapy modulates inflammation and influences the course of infection.

3.3.4.4 Effect of coagulation inhibition on γHV68 infection in fibrotic lung

In the initial study of viral infection described in this thesis an increase in tissue factor and FX mRNA levels was recorded 7 days p.i. while the infected lungs were strongly immunoreactive for TF and FX protein 14 days p.i.. In the second study, an extensive inflammation was observed to continue through to 14 days p.i. in virally infected fibrotic lung. The aim of this study was to assess whether targeting coagulation in the model of viral infection on a background of pulmonary fibrosis, through inhibition of FXa, affects inflammatory and fibrotic responses in the lung. Previous studies performed in our laboratory have shown that prophylactic treatment of bleomycin injured mice with the FXa inhibitor (ZK807834) is protective from developing pulmonary fibrosis (Scotton et al., 2009). In the present study, the

clinically approved, orally available and direct FXa inhibitor BAY59-7939 (Gulseth et al. 2008) was administered twice daily from day 15 after bleomycin instillation and one day after viral inoculation to investigate the role of FXa in this two-hit model of viral infection and fibrosis.

As reported in the SB525334 study, this two-hit model of viral infection in fibrotic lung is reflected by two waves of weight loss. An early weigh loss (between days 2 and 8) is associated with bleomycin administration while the second wave is recorded post viral inoculation (3 to 7 days p.i.). Mice in bleomycin/γHV68/BAY59-7939 group experienced the biggest body weight loss in the virus-associated, second wave of weight loss. An increase in *ex vivo* lung weight was observed with the virus alone and matched the increase observed in the bleomycin alone group. In contrast, weights of virally-infected fibrotic lungs were further, significantly increased in comparison to all other groups. These results potentially suggest that this group of mice mounted a stronger inflammatory response to infection with γHV68. Consistent with the previous studies, prominent splenomegaly was observed in the virus alone infected animals and this was significantly increased in bleomycin+γHV68 groups. Furthermore, viral gene expression was again readily detected in the virally-infected fibrotic lungs.

Measurement of total lung collagen by HPLC did not show a significant difference between the bleomycin alone group and bleomycin+γHV68 group. Furthermore, targeting FXa did not affect total lung collagen level. This pattern was mirrored by Sircol quantification of collagen levels. As observed in the previous study, the collagen levels detected by Sircol were 20-fold lower when compared to measurement based on hydroxyproline analysis by HPLC but there was no difference in collagen levels between the bleomycin-challenged groups and bleomycin/γHV68 groups.

Further analysis of lungs by µCT and tissue segmentation software was subsequently performed. Fibrotic lungs were accurately segmented based on dense fibrotic lesions. In contrast, viral infection of fibrotic lung presented as diffuse ground-glass opacities and consolidation superimposed on the background of

fibrosis. Histological analysis confirmed prominent inflammatory cell aggregates together with disorganised collagen deposition and abnormal appearing epithelium in virally-infected fibrotic lung. These aggregates were quantified as previously described and virally-infected fibrotic lungs displayed greater numbers of inflammatory cell aggregates when compared to mock-infected groups. Furthermore, a trend was identified towards higher number of aggregates with BAY59-7939 treatment. The pathological changes in the lung morphology and density were also significantly increased in the bleomycin+γHV68+BAY59-7939 when compared to bleomycin alone challenged lungs but the difference was not statistically different when compared to the bleomycin+γHV68+vehicle group. The histogram analysis of lung densities showed clear separation into three groups. Saline control lungs were the least dense. Viral infection in saline control lungs and bleomycin alone challenged lungs showed the same extent of density changes in the lung, despite clear differences in pixel distribution on µCT scans as well as marked differences in histological appearance. Statistical analysis and distribution of pixel density range between saline+γHV68 and mock-infected bleomycin groups revealed that the significantly different pixels were dispersed throughout the parenchyma and did not localise to evident fibrotic lesions in the bleomycin-injured lung. Finally, virally-infected fibrotic lungs showed the most pronounce shift toward dense pixels and there was no significant separation between the treatment and the vehicle control. Taken together, the µCT analysis revealed that the viral infection leads to inflammatory response that is superimposed on a background of fibrosis and increases the pathological changes in the lung. The FXa inhibitor did not significantly affect the inflammatory and fibrotic responses in this study.

It was noted in the previous study that inflammation appears more elusive on µCT scans and cannot be separated from fibrosis. In the current study the markers of local and systemic inflammation were measured in lung homogenates and serum, respectively, 14 days p.i.. The level of CCL2 was significantly increased in the lung compartment of all γHV68-infected groups when compared to saline and fibrotic lungs and there was no difference between the treatment and vehicle groups. However, at the mRNA level, viral infection in the fibrotic lung significantly further

increased CCL2 expression when compared to viral infection alone. Systemic CCL2 levels were also higher in infected fibrotic lungs in comparison to viral infection alone. Viral infection also led to systemic increase in levels of IFNγ and KC as measured in the serum from γHV68 infected saline control mice with a further significant increase detected in virally infected fibrotic lungs.

In conclusion, these data suggest that viral infection in the lung triggers inflammatory responses and the inflammatory markers are readily detected locally in the lung and systemically in the serum 14 days p.i. and after the virus established latency. Furthermore, γHV68 infection on a background of fibrosis amplifies the inflammatory responses to viral infection. FXa inhibitor did not affect the inflammatory responses in this study.

3.3.4.5 Conclusion and future work

This body of work investigated the contribution of viral infection to the development of experimental pulmonary fibrosis. IPF is a complex lung disease displaying a range of heterogeneous phenotypes. A number of environmental and genetic cues have been identified to promote persistent epithelial injury, which combined with aberrant wound healing response can lead to the development of fibroproliferative lung disease. Several studies have shown that occult viral infections are detected in IPF patients. Particularly γ-herpesviruses have been implicated in the progression of IPF but the causative link remains to be established. It is considered highly unlikely that viral infection alone is able to induce lung fibrosis but viruses can influence fibrotic responses by promoting a profibrotic phenotype in latently infected cells as well as by low levels of re-activation and associated chronic damage to the alveolar epithelium. EBV latency membrane protein LMP-1 is associated with the transforming capacity of EBV and protects infected B-cells from apoptosis (Ackermann, 2006). LMP-1 also inhibits the terminal differentiation of the epithelial cells (Dawson et al 1990) and promotes their motility (Dawson et al. 2008). Furthermore, a study in human alveolar epithelial cells have shown that EBV LMP-1 and TGFβ synergistically induce epithelial-mesenchymal transition (Sides et al., 2010).

In this series of studies murine γHV68 was used to investigate the outcome of viral infection in bleomycin-induced pulmonary fibrosis. Bleomycin is an antimicrobial agent with anticancer properties but the chemotherapy with this drug is associated with high risk of pulmonary toxicity (Muggia et al. 1983). The mechanism of action of bleomycin involves interference with the cell cycle, DNA damage and oxidative stress, which evokes an inflammatory response, activation of fibroblasts and fibrosis. The lungs are particularly susceptible to developing fibrosis following exposure to bleomycin because they express low levels of bleomycin hydrolase, an enzyme required to metabolise the drug (Degryse and Lawson, 2011; Moeller et al., 2008). Administration of bleomycin in mice leads to initial acute lung injury phase characterised by extensive inflammation and vascular leak. By 14 days post instillation dense fibrotic lesions develop associated with fibroblast proliferation and deposition of collagen-rich extracellular matrix. Two weeks post injury, significant increase in total lung collagen can be detected by measurements of hydroxyproline in lung homogenates (Scotton et al., 2009, 2013). This phase of bleomycin-induced fibroproliferative lung disease was chosen to be the most suitable for introduction of the second injurious factor as the aim of this study was to develop a two-hit model of viral infection on a background of existing pulmonary fibrosis.

The natural rodent pathogen, murine γHV68, shares 80% homology with EBV and displays parallel invasive features: epithelial and B cell tropism, virus-driven B-cell activation and proliferation, and an acute infectious mononucleosis syndrome (Nash and Sunil-Chandra 1994). Murine γHV68 promotes activation, survival and proliferation of infected B-lymphocytes (Madureira et al., 2005). Furthermore, γHV68 can infect other cell types including alveolar macrophages and fibroblasts and induce profibrotic phenotype associated with increased expression and sensitivity to TGFβ (Stoolman et al., 2010). Notably, in the model of FITC-mediated pulmonary fibrosis, infection with γHV68 has been reported to exacerbate fibrosis by increasing total lung collagen 7 days post infection (McMillan et al., 2008).

The results of the first study presented in this section showed that γHV68 leads to a robust inflammatory response 7 days p.i. that persists to 14 days p.i.. Since this model was designed as a two-hit injury model, a reduced dose of bleomycin of 1 mg/kg was used since the standard dose of 2 mg/kg routinely used in our laboratory induces a maximal fibrotic response in C57BL/6 mice within the acceptable severity range. Despite strong evidence from our laboratory that emphasises non-resolving nature of bleomycin-induced injury and fibrosis at a dose of 2 mg/kg, in this initial study we observed a degree of scar tissue re-modelling by day 28 post bleomycin instillation (14 days p.i.). Prominent fibrotic lesions in the bleomycin-injured lungs were evident in histological analysis of lung sections and MSB collagen fibres staining revealed organised and consolidated collagen deposition in these lungs. However, the areas of fibrosis appeared to be reduced in comparison to histological analysis of lung sections from day 7 p.i. in this study and also when compared to section from lungs challenged with 2 mg/kg bleomycin in the previous studies performed in our laboratory. Assessment of hydroxyproline in lung homogenates by HPLC reflected the lesser degree of fibrosis 28 days post-bleomycin challenge when compared to day 21. This suggests an ongoing scar tissue re-modelling process in these lungs. In contrast, there was no difference in collagen deposition in the virally-infected fibrotic lungs between days 21 (7 days p.i.) and 28 (14 days p.i.) and at both time-points extensive fibrotic areas with high collagen content were detected by histological analysis and HPLC. Analysis of histological sections also highlighted extensive inflammatory changes at 7 days p.i. in virally infected fibrotic lungs when compared to mock-infected fibrotic lungs. Viral infection of fibrotic lung appeared to have caused acute lung injury with hallmark evidence of vascular leak, alveolar haemorrhage and prominent inflammatory cell infiltrates superimposed on the background of extensive fibrotic lesions. By day 14 p.i. the pulmonary oedema and the haemorrhage have been largely cleared but the dense inflammatory cell aggregates were still evident and localised around airways and blood vessels. Taken together, these data show that in this experiment the viral infection has caused extensive inflammatory changes in the lung that interfered with the potential scar tissue re-modelling process observed in the mock-infected fibrotic lungs. This

process appears to be responsible for the differences in the total lung collagen levels detected at day 14 p.i. between mock-infected and γHV68-infected fibrotic lungs.

Persistent inflammation in the lungs was also characterised by increased expression of inflammatory markers in the lungs (CCL2, IFNγ and KC) at day 14 p.i.. Furthermore, 7 days p.i. expression of coagulation factors (tissue factor and FX) was increased and the protein was found to strongly localise to bronchial and alveolar epithelium 14 days p.i.. Tissue factor is upregulated in response to infection and injury and strong immunoreactivity in the lung 14 days p.i. suggests potential ongoing damage to the epithelium. Taken together, these data suggest that a reduced dose of bleomycin (1 mg/kg) induces lung injury and fibrosis that appeared to be controlled by day 28 post-bleomycin instillation but viral infection in the fibrotic environment evokes persistent inflammatory response that is associated with lasting changes to the gross lung appearance.

The second study in this chapter was carried out with the aim of evaluating the role of TGFβ/ALK5 signalling in the model of viral infection on a background of pulmonary fibrosis. Furthermore, the analysis of this model was expanded by the use of *ex vivo* μCT imaging technology. The μCT analysis of the lung scans provided an informative tool to characterise changes in lung architecture. As thoroughly characterised in our laboratory, μCT scans accurately differentiate between the normal lung morphology and dense fibrotic lesions in the bleomycin model (Scotton et al., 2013) and show specific pattern of bronchiocentric and subpleural distribution of fibrotic lesions. However, μCT analysis of the scans from virally-infected fibrotic lungs revealed diffuse ground-glass opacities and dense consolidation spreading from the airways and major vessels, superimposed on existing fibrosis. The advantage of this model is that these μCT appear to resemble the HRCT scans of IPF patients with acute exacerbation, as previously characterised (Collard et al., 2007). From an analysis point of view, a new challenge was posed when the scans were segmented by the pattern recognition software. The software is trained to discriminate between normal lung areas and fibrotic areas based on

differences in the number and density of pixels as defined by the training process. The wide spectrum of changes in density between the relatively widely dispersed inflammatory changes and dense mature fibrotic lesions made it difficult for the software to accurately discriminate between inflammation and fibrosis in infected fibrotic lungs. Therefore, all the changes were grouped as “abnormal lung” areas with the full appreciation of the fact that in the bleomycin only injured lungs the abnormal areas represent fibrotic changes while in virally-infected fibrotic lungs abnormal areas represent both inflammation and fibrosis. Moreover, in this study heart tissue was not dissected out in order to help to preserve the integrity of the processed lung during the scanning process. Although the heart muscle was gated out as “other tissue” during the software training process, some of the mature fibrotic lesions of high density were also identified as other tissue because of overlapping density spectra. Another method of analysis was therefore applied and density histograms were generated based on voxel (cubic pixel) distribution on the greyscale of the scans and independent of the segmentation output. These histograms displayed the lung density distribution with saline control lungs being the least dense, closely followed by virally-infected saline lungs. A clear shift towards higher density voxels was recorded in the fibrotic lungs and the infected fibrotic lungs shifted further towards increased density voxels. The μCT scans analysis was then matched with histological analysis of the same lungs, which confirmed that the dense fibrotic areas corresponded to fibrotic tissue with abundant collagen deposition while the dispersed inflammatory changes were associated with inflammatory infiltrates.

In this study with the ALK5 inhibitor, SB525334, reduced dose of bleomycin was used again and it was consequently found that a smaller degree of lung collagen accumulation was detected when compared to historical data. However, viral infection of fibrotic lung did not affect the lung collagen levels as measured by hydroxyproline levels (HPLC). This result was subsequently confirmed by measurement of soluble collagen by Sircol assay. Worse appearance of virally-infected lungs in this model was associated primarily with inflammation superimposed on existing fibrosis and in the time frame of this study no changes in

the fibrotic endpoint readout are evident. This contrasts with the previous reports that active γHV68 infection exacerbates FITC-induced pulmonary fibrosis (McMillan et al., 2008). This result could be potentially explained by the differences in bleomycin and FITC models of pulmonary fibrosis. Bleomycin-induced fibrosis is not progressive and a degree of scar tissue re-modelling has been observed in the initial study with reduced dose of bleomycin. In contrast, FITC-induced fibrosis results from a persistent injury caused by FITC deposition in the lung. It is possible that the discrepancy in responses to viral infection between bleomycin- and FITC-challenged lungs is driven by the different nature of the original injury.

As previously observed, ALK5 inhibition attenuated the pulmonary fibrosis as evaluated by both total lung collagen and μCT analysis (Scotton et al., 2013). In this study, SB525334 inhibition of TGFβ/ALK5 signalling significantly reduced lung collagen accumulation in mock-infected bleomycin-challenged lungs but this therapeutic effect was lost in virally-infected fibrotic lungs. Interestingly, lung density analysis revealed the density pixel range affected by the SB525334 treatment that localised to fibrotic lesions in bleomycin alone challenged lungs, but in viral infection of fibrotic lungs pixels affected by the drug were distributed throughout the parenchyma. This suggests that the therapeutic target of SB525334 is significantly different in fibrotic lungs when compared to virally-infected fibrotic lungs and in the latter appeared to have affected the inflammation. This conclusion is further supported by the fact that SB525334 reduced the numbers of inflammatory cell aggregates in the lung and significantly attenuated splenomegaly.

In this study we observed that the inflammation caused by the virus appeared to persist 14 days p.i., despite the previous reports showing that the lytic phase of infection is cleared by that time (Vannella et al. 2010; Nash et al. 2001). Furthermore, despite prominent splenomegaly suggestive of established latent infection, viral gene expression continued to be detected in the virally infected fibrotic lungs 14 days p.i.. The infection with γHV68 is well characterised. Murine γHV68 infects the respiratory epithelium and the lytic phase is predominantly cleared by day 14 p.i. but a low level of replication can persist in the lung (Nash et

al., 2001). The murine virus is more lytic than the human counterpart but eventually establishes latency in B-lymphocytes and macrophages. Infected B-lymphocytes become a vehicle for systemic spread of the virus and establishment of latency at the preferred site, the spleen. Similarly to EBV, γHV68 enters naïve B-cells and programmes them to become long-lived memory B-cell. Studies with B-cell deficient mice demonstrated that the virus can persists in macrophages as well (Weck et al., 1997).

Components of innate and adaptive immune system are involved in mounting antiviral responses. Innate immunity to γHV68 involves activation of TLR9, which recognises bacterial and viral genome unmethylated CpG nucleotides. Interferons α and β (IFNα and IFNβ) are essential for the early containment of the infection while IFNγ and IL-6 are the main cytokines that sharply increase during infection (Doherty et al., 2001). Levels of IFNα, IL-12 and IL-5 are reduced in TLR9 knockout mice, which leads to greatly increased levels of viral load both in lytic and latent phase following intraperitoneal administration of the virus (Guggemoos et al., 2008). Furthermore, IFNβ is also decreased in these mice which is associated with increased fibroblast proliferation and collagen deposition in the lung (Luckhardt et al., 2011). Infection with γHV68 has also been associated with alternatively activated macrophages that suppress inflammation and promote wound healing responses (Gangadharan et al., 2008; Mora et al., 2006). These macrophages are characterised by expression of arginase I and insulin-like growth factors IGF-1 and stimulate expression of ECM protein, as well as high levels of TGFβ. High levels of arginase I are detected in IPF lungs (Mora et al., 2006).

A strong cytotoxic CD8 T-cell response has been reported in the BALF obtained from γHV68 infected mice throughout the lytic phase (Hardy et al., 2001). CD8 cytotoxic T-cells are necessary for clearance of the original infection but cannot control reactivation of the latent infection and subsequent infections. CD8 T-cells display effector memory phenotype and mount efficient immune responses to γHV68 challenge through large capacity to produce IFNγ, TNFα next to the cytotoxic abilities (Cush and Flaño, 2011). The most prominent feature of γHV68 infection is

splenomegaly that peaks 14 to 31 days after the infection and is caused by CD4 T-lymphocyte-mediated stimulation of B-cell clonal expansion (Nash et al., 2001). In the spleen, dendritic cells and macrophages are additional reservoirs of latent murine γHV68. In the lung, the virus can infect multiple cell types but long-term latency is only detected in B-lymphocytes and the alveolar epithelium. EBV and murine γHV68 both can infect alveolar epithelium and fibroblasts (Adachi et al., 2001). EBV has been shown to infect human lung fibroblasts and increase production of IL1β and FGF from these cells (Adachi et al., 2001). Viral entry into the non-immune cells involves the interaction between viral capsid glycoproteins gHgL and the integrins, with αvβ6, αvβ8 and αvβ5 best described targets (Chesnokova and Hutt-Fletcher 2011; Chesnokova et al. Hutt-Fletcher 2009). Integrin αvβ6 is upregulated in pulmonary fibrosis (Thomas et al. 2006) and strongly associated with activation of latent TGFβ (Wipff and Hinz, 2008). Human cytomegalovirus has also been shown to induce the TGFβ activation and expression of αvβ6 integrin in human umbilical vein endothelial cells and lung microvascular endothelial cells (Tabata et al., 2008). Both in the lung and spleen low level of persistent lytic replication can also be detected (Flaño et al., 2003).

Antiviral responses are crucial for effective infection control and the presence of inflammatory cell aggregates in the lung is prominent in all studies described in this section of the thesis. In terms of future work, it will be important to analyse the cellular components of these inflammatory aggregates and further characterise how bleomycin-induced fibrosis affects antiviral responses in the lung. This question was partly addressed in the final study where inflammatory mediators were measured locally in the lung and systemically in the serum. Viral infection in the fibrotic lung significantly augmented systemic inflammation with high levels of IFNγ and CCL2 detected in the serum. High levels of CCL2 and CCL12 have previously been shown to be produced in response to viral infection and can actively contribute to fibrogenesis by facilitating fibrocyte recruitment into the lung (McMillan et al., 2008). Furthermore, expression of immunomodulatory M3 viral protein at the mRNA level has been detected in all studies 14 days p.i. M3 has been shown to disrupt the chemokine gradient and prevent trafficking of the

inflammatory cells into the site of infection (Alexander-Brett and Fremont, 2007). M3 has also been shown to sequester macrophage inflammatory protein α and CCL2 in an immune evasion strategy (Berkel et al., 2000). The high levels of CCL2 protein and mRNA observed in these studies might also reflect the inadequate immune response to the virus.

Coagulation cascade has also been shown to be activated in response to viral infection. Injury to the lung leads to upregulation of tissue factor and in this study, mRNA levels of tissue factor and FX were increased 7 days p.i. and showed strong immunolocalisation to bronchial and alveolar epithelium 14 days p.i.. The ternary complex, TF-FVIIa-FXa, can be assembled locally in the lung (Scotton et al., 2009) and there is evidence for vascular leak in the initial study 7 days p.i. which creates the potential for prothrombin extravasation from the circulation and local activation of thrombin. HSV I and CMV express tissue factor and procoagulant phospholipids on their surface providing a platform for the assembly of the TF-FVIIa-FXa complex leading to the generation of thrombin (Sutherland et al., 1997). Thrombin has also been shown to enhance HSV I and CMV cell invasion in human umbilical vein endothelial cells (HUVEC) and human foreskin fibroblasts (HFF) (Sutherland et al. 2007).

We next used a direct FXa inhibitor, BAY59-7939, to investigate whether activation of coagulation cascade plays a role in the γHV68 infection on a background of pulmonary fibrosis. Previous study prophylactically targeting FXa in an early phase of bleomycin-induced lung injury and fibrosis showed attenuation of pulmonary fibrosis (Scotton et al., 2009). However, in the current study systemic targeting of FXa, using BAY59-7939, in the fibrotic phase of bleomycin-induced lung injury and viral infection of fibrotic lung did not affect lung collagen accumulation. Furthermore, targeting FXa in viral infection of fibrotic lung showed no effect on local and systemic inflammation as determined by measuring levels of inflammatory markers in lung homogenates and serum. In contrast, BAY59-7939 treatment appeared to increase inflammatory cell infiltrates in the lungs. Consequently, μCT analysis revealed that inhibition of the coagulation cascade in virally-infected

fibrotic lungs appeared to have increased inflammatory changes in the lungs evident as ground glass opacities. However, this observation did not correlate with lung density analysis and the density histograms showed no difference between the virally-infected fibrotic lung treated with vehicle and BAY59-7939. In conclusion, this final study in this chapter corroborated the findings of the previous two studies, that the viral infection on a background of pulmonary fibrosis evokes strong and long-lasting inflammatory response. Local and systemic inflammatory markers remained significantly upregulated 14 days p.i. and exceeded the levels observed in viral infection in the saline control.

PAR-1 signalling downstream of activation of coagulation cascade has been implicated in the fibroproliferative processes and PAR-1 knockout mice are protected from bleomycin-induced pulmonary fibrosis (Howell et al. 2005). An interesting next step in dissecting the role of viral infection in pulmonary fibrosis would be to experiment with this two-hit model in PAR-1 deficient mice. Multiple questions could be addressed in this potential study including whether PAR-1 knockout mice can be primed by the γHV68 infection to develop more severe fibrosis and whether PAR-1 deficiency affects the inflammatory and antiviral responses. The last points are of particular interest as PAR-1 signalling has been shown to play different roles in antiviral immunity and promote markedly different inflammatory responses that were dependent on the type of the virus and site of infection (Antoniak et al., 2013; Khoufache et al., 2013). Interestingly, herpesviruses show capacity to trigger exacerbation of pulmonary fibrosis but adenovirus infection did not affect the progression of the disease (McMillan et al., 2008). Similarly, herpesvirus infection has been shown to drive the pathology of atherosclerosis (Alber et al. 2000) by infecting and transforming endothelial cells (Flore et al., 1998). The identified pathogenic mechanisms revolve around systemic inflammation combined with responses of infected cells at the site of injury. Again, exacerbation of atherosclerosis was virus-specific and infection with other viruses failed to worsen the condition (Alber et al. 2002).

The pathology of γHV68 infection also differs between young and old mice (Naik et al., 2011), with old mice developing spontaneous fibrosis following viral challenge, despite fully immunocompetent immune responses and viral clearance. A robust fibrotic response in the aged mice was associated with increased levels of TGFβ and increased responsiveness of fibroblasts to TGFβ signalling leading to expression of α-SMA and collagen synthesis. Since pulmonary fibrosis affects ageing people, it would be relevant to assess the role of coagulation activation in response to viral infection on a background of pulmonary fibrosis in the aged mice.

Acute exacerbation of IPF is marked by epithelial cell injury and increased levels of mediators of innate immunity (Konishi et al., 2009). Moreover, antiviral therapy has been shown to benefit a small cohort of IPF patients (Egan et al., 2011). Abundant *in vitro* and *in vivo* evidence describes multiple mechanisms by which γ-herpesviruses contribute to the pathogenesis of pulmonary fibrosis. The aim of these studies was to investigate the impact of γHV68 infection on bleomycin-induced pulmonary fibrosis. In the time-frame of these experiments there were no changes in fibrosis endpoints, as assessed by measurement of total lung collagen, between bleomycin challenged and virally-infected fibrotic lungs. However, this study has shown in three independent experiments that the two-hit model of viral infection on a background of bleomycin-induced pulmonary fibrosis caused robust and extensive inflammatory responses that were severe and persisted in the fibrotic lungs. Furthermore, the therapeutic effect of the ALK5 inhibitor, SB525334, in attenuating pulmonary fibrosis was lost in viral infection on a background of existing fibrosis and the drug appeared to target the inflammation in response to viral infection. These data suggest that TGFβ/ALK5 signalling exerts greatly different effects in the context of fibrosis alone and when fibrosis is concomitant with viral infection. Moreover, in the third study in this chapter we evaluated systemic inflammation and significantly increased levels of inflammatory (CCL2, KC) and antiviral (IFNγ) mediators were still detected 14 days p.i. locally in the lung. Targeting the activation of coagulation cascade by FXa inhibition did not affect inflammatory and fibrotic responses in this model of viral infection on a background of pulmonary fibrosis. Finally, using μCT technology we demonstrated that the viral infection on a background of pulmonary

fibrosis bears close resemblance to HRCT scans of IPF patients experiencing acute exacerbation with a hallmark inflammatory changes superimposed on existing fibrosis (Collard et al., 2007).

Chapter 4: Final summary and implications

The studies presented in this thesis addressed the following hypothesis:

Activation of the coagulation cascade in response to lung injury and viral infection promotes inflammation and fibrosis via PAR-1 signalling.

And the following aims:

- **Identify PARs responsible for coagulation proteinases signalling responses in human primary lung cells.**
- **Determine whether the coagulation cascade contributes to inflammatory and fibrogenic responses in the model of viral infection in pulmonary fibrosis.**

The first aim of this study was addressed in **Chapter 3.1** of this thesis, where PAR-1 expression and signalling was assessed in different human lung cell populations. The results showed that lung fibroblasts and lung microvascular endothelial cells express the highest levels of PAR-1 and responded robustly to thrombin, even at low nanomolar concentrations. In contrast, the normal respiratory epithelium does not express much PAR-1 and is non-responsive to thrombin stimulation. Interestingly, primary normal human bronchial and alveolar epithelial cells signalled robustly following PAR-2 activation. In contrast, PAR-1 expression is increased in abnormal alveolar epithelium represented by A549 cells. Furthermore, fibroblasts and lung microvascular endothelial cells signal to coagulation proteinases in PAR-1-dependent and PAR-2-independent manner whereas in epithelial cells and large vessel endothelial cells PAR-2 signalling can modulate the magnitude of PAR-1-mediated calcium responses. The interaction between PAR-1 and PAR-2 signalling in epithelial cells requires further investigation and potentially poses an interesting challenge when targeting PAR-1 and PAR-2 in lung disease.

TGFβ, ubiquitous and pleiotropic profibrotic cytokine, further increases PAR-1 expression in A549 cells, which is associated with a concurrent upregulation of αv

and β6 integrin subunit expression. In this study we also demonstrate a novel signalling axis in A549 cells that involves TGFβ/ALK5-mediated and Smad3- and ERK1/2-dependent PAR-1 upregulation. PAR-1 signalling has been shown to promote TGFβ activation via αvβ6 integrins in epithelial cells and αvβ5 in fibroblasts (Scotton et al. 2009; Jenkins 2008). The results of this study suggest that fibroblasts constitutively express high levels of PAR-1 and can readily respond to coagulation proteinases. Furthermore, in an abnormal wound healing microenvironment the alveolar epithelium may become increasingly responsive to the local procoagulant environment and may further propagate the pathologic milieu by means of a self-amplifying PAR-1-integrin-TGFβ feedback loop, as summarised in **Figure 4.1**.

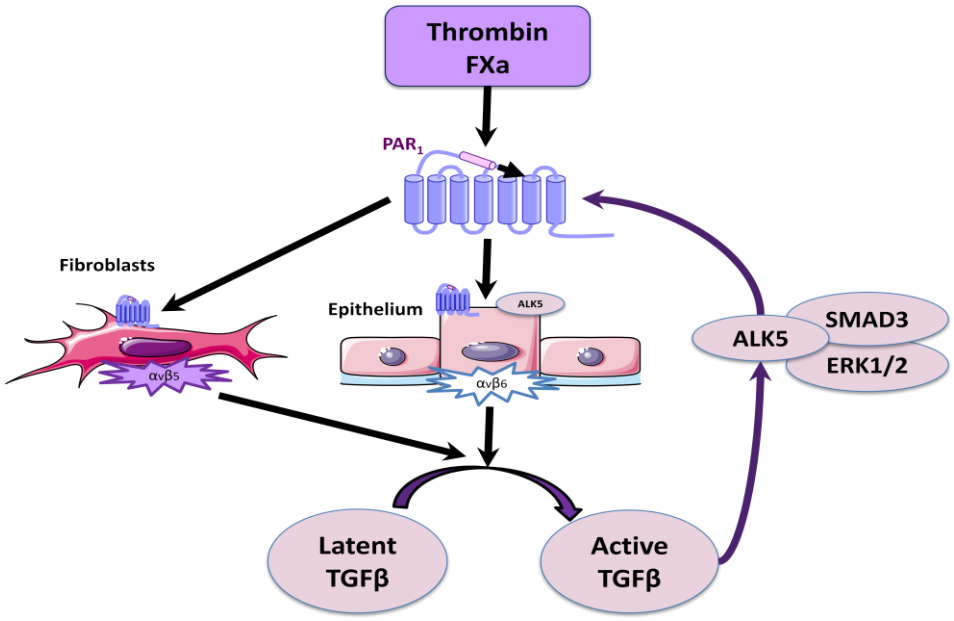

Figure 4.1. **PAR-1-integrin-TGFβ feedback loop.**

Activation of PAR-1 on fibroblasts and abnormal alveolar epithelium leads to TGFβ activation via integrins αvβ5 and αvβ6, respectively. TGFβ signalling via ALK5 receptor, Smad3 phosphorylation and activation of ERK1/2 signalling pathways leads to upregulation of PAR-1 expression in the abnormal alveolar epithelium.

Fibroblasts constitutively express high levels of PAR-1, which also leads to robust pro-fibrotic signalling following thrombin stimulation. As shown in **Chapter 3.2** and **Appendix 2**, fibroblasts secreted large amounts of pro-inflammatory chemokine,

CCL2, in response to thrombin stimulation. However, at high thrombin concentration this effect was only partially PAR-1 mediated which suggests that thrombin can influence fibroblast responses in a PAR-1-independent manner.

Activation of PAR-1 leads to convergence of coagulation signalling, inflammatory responses and TGFβ activation, which makes it a potential attractive therapeutic target in lung injury and fibrosis. PAR-1 knockout mice are protected from bleomycin-induced lung injury and fibrosis (Howell et al., 2005) and a recent study using pepducins to block PAR-1 signalling showed attenuation of bleomycin-induced fibrosis (Lin et al., 2013). In **Chapters 3.1 and 3.2** we used small molecule PAR-1 antagonists, RWJ58259 and SCH530348, to investigate PAR-1 distribution and responsiveness to thrombin. Although these antagonists are specific and potent PAR-1 inhibitors, there are limitations for their *in vivo* application in the setting of chronic diseases due to short half-life and consequent need for frequent administration. In this study we purified and began to characterise a novel murine PAR-1 neutralising antibody as described in **Appendix 1**. Therapeutic antibodies have high specificity and affinity for the target, longer half-life *in vivo* and reduced off-target effects. Although further work is required to optimise the purification of the antibody, we demonstrated that mPAR-1 neutralising antibody efficiently blocks PAR-1 signalling *in vitro,* which makes it a potential tool for investigating the therapeutic effects of blocking PAR-1 in long-term experimental models of pulmonary fibrosis.

The second aim of this study was addressed in **Chapter 3.3.** In a series of three independent experiments we showed that γ-herpesvirus infection on the background of bleomycin-induced pulmonary fibrosis did not exacerbate fibrosis as measured by collagen deposition in the lungs but triggered strong and persistent inflammatory responses. Several hallmark features of acute lung injury were observed in virally-infected fibrotic lungs at the peak of viral lytic cycle (7 days p.i.) including interstitial oedema, alveolar haemorrhage and inflammatory cells infiltrates. This was associated with increased expression of inflammatory mediators, including CCL2 and IFNγ, and components necessary for the activation of

the coagulation cascade, TF and FX. Persistent inflammation was also reflected by increased levels of inflammatory markers in the sera of infected mice with pre-existing fibrosis. Furthermore, viral gene expression was readily detected in the infected fibrotic lungs 14 days p.i. and the spleen weights were significantly increased when compared to virally-infected control mice, suggestive of continuing level of viral replication in the infected and fibrotic lungs and increased capacity to establish latency. The pathologic changes in the lungs were further investigated by analysis of μCT scans, which revealed ground glass opacities and consolidation concurrent with fibrotic lesions in viral infection on a background of pulmonary fibrosis. Importantly, several features recognised by μCT scanning resembled the findings in HRCT scans from IPF patients experiencing acute exacerbation.

We next investigated the role of TGFβ/ALK5 signalling in viral infection of fibrotic lung. The findings of this study agreed with previous reports that inhibition of TGFβ receptor, ALK5, attenuates fibrosis in bleomycin model of pulmonary fibrosis. In contrast, the therapeutic effect of SB525334 shifted from antifibrotic action in fibrotic lungs to anti-inflammatory action in virally infected fibrotic lungs. The analysis of μCT scans, lung density and histology supported the notion that while in bleomycin-challenged lungs ALK5 inhibitor targeted the fibrotic lesions, in the viral infection of fibrotic lung blocking TGFβ/ALK5 signalling appeared to modulate the inflammatory responses to infection, as summarised in **Figure 4.2**. TGFβ plays critical role in mediating vascular leak and inhibition of TGFβ signalling in models of lung injury protects from pulmonary oedema (Pittet et al. 2001). It is possible that inhibition of vascular leak in the early phase of lytic viral infection and lung injury impacts on inflammatory responses and lymphocyte trafficking in this model. The results of this study highlight pleiotropic nature of TGFβ in lung fibrosis and infection and advocate caution when predicting therapeutic effect of blocking TGFβ signalling in human disease.

Finally, we investigated whether inhibition of the activation of the coagulation cascade by blocking FXa, affects fibrosis and inflammation in viral infection of pulmonary fibrosis. Targeting FXa with specific inhibitor, BAY59-3979, did not

significantly augment fibrosis or viral infection on a background of existing pulmonary fibrosis in this model.

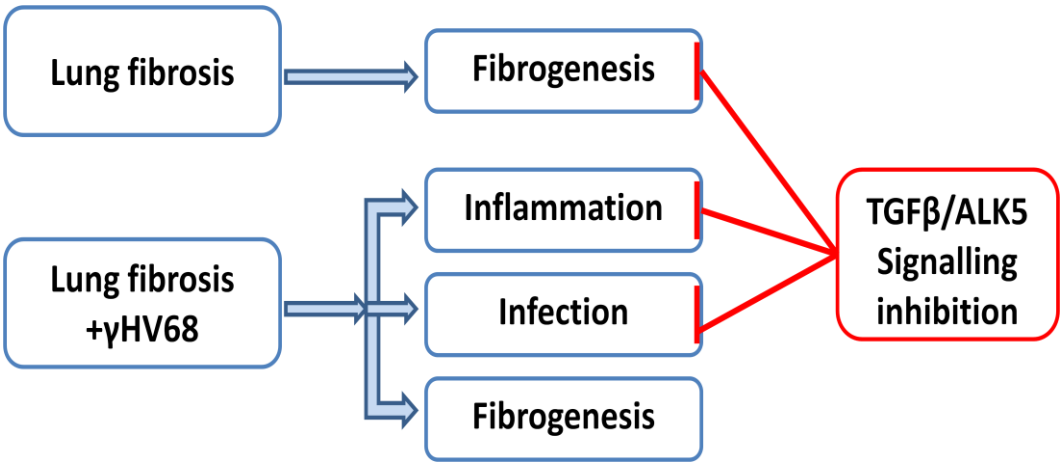

Figure 4.2. Different therapeutic effect of TGFβ/ALK5 signalling inhibition in fibrotic lung versus viral infection of fibrotic lung.

Viral infection in a lung with a pre-existing injury can trigger different and exaggerated host responses. Herpes simplex virus infection is a risk factor for the development of ARDS in patients in intensive care (Bruynseels et al. 2003) and leads to increased complications and prolonged hospitalisation (Luyt et al. 2007). Cytomegalovirus reactivation is observed in septic surgical patients and is associated with increased incidence of fibroproliferative lung disease in these patients (Cook et al. 2006). In bone marrow transplantation model, post-transplant mice are more susceptible to γHV68 infection in the lung and the latent infection leads to chronic and persistent pneumonitis and fibrosis (Coomes et al. 2011).

In this two-hit model of viral infection on a background of bleomycin-induced pulmonary fibrosis we observed increased local expression of TF and FX concomitant with evidence of vascular leak and haemorrhage, which are considered to be major sources of thrombin in the injured lung. Altogether, this can lead to enhanced procoagulant state and local activation of coagulation cascade in the lung. As characterised in **Chapter 3.1** and proposed in **Figure 4.1,** in an abnormal fibrotic microenvironment both mesenchymal cells and the epithelium can become more responsive to coagulation signalling via PAR-1 receptor. Increased expression

of all PARs in the respiratory epithelium and airway smooth muscle cells has been reported in influenza infection and particularly increased expression of PAR-1 and PAR-2 significantly augmented the antiviral responses in these cells (Lan et al., 2004). Furthermore, PAR-1-integrin-TGFβ activation and signalling axis can contribute to the progression of viral infection in the lung. Integrins αvβ5 on mesenchymal cells and αvβ6 on epithelial cells are major activators of latent TGFβ (Scotton et al. 2009; Jenkins et al. 2006) and are also utilised by the herpesviruses as auxiliary molecules to facilitate viral entry into the cell (Chesnokova et al. 2009). It is possible that in the injured lung profibrotic and procoagulant environment facilitates increased viral infectivity, which in turn evokes persistent inflammatory response and exacerbates existing injury.

Thus, major part of future studies of viral infection on a background of bleomycin-induced pulmonary fibrosis would involve: i) full characterisation of the persistent inflammatory response observed in this model, ii) dissecting further the mechanisms of differential TGFβ therapeutic effect between bleomycin-only challenged mice and γHV68-infected bleomycin-injured mice in this model, and iii) investigation of the role of PAR-1 in the viral infection of pulmonary fibrosis.

References

Abraham, L.A., and MacKie, E.J. (1999). Modulation of osteoblast-like cell behavior by activation of protease-activated receptor-1. J. Bone Miner. Res. Off. J. Am. Soc. Bone Miner. Res. *14*, 1320–1329.

Ackermann, M. (2006). Pathogenesis of gammaherpesvirus infections. Vet. Microbiol. *113*, 211–222.

Adachi, H., Saito, I., Horiuchi, M., Ishii, J., Nagata, Y., Mizuno, F., Nakamura, H., Yagyu, H., Takahashi, K., and Matsuoka, T. (2001). Infection of human lung fibroblasts with Epstein-Barr virus causes increased IL-1beta and bFGF production. Exp. Lung Res. *27*, 157–171.

Adams, R.L.C., and Bird, R.J. (2009). Review article: Coagulation cascade and therapeutics update: Relevance to nephrology. Part 1: Overview of coagulation, thrombophilias and history of anticoagulants. Nephrology *14*, 462–470.

Adams, M.N., Ramachandran, R., Yau, M.-K., Suen, J.Y., Fairlie, D.P., Hollenberg, M.D., and Hooper, J.D. (2011). Structure, function and pathophysiology of protease activated receptors. Pharmacol. Ther.

Ahmad, S., Ahmad, A., Rancourt, R.C., Neeves, K.B., Loader, J.E., Hendry-Hofer, T., Di Paola, J., Reynolds, S.D., and White, C.W. (2013). Tissue factor signals airway epithelial basal cell survival via coagulation and protease-activated receptor isoforms 1 and 2. Am. J. Respir. Cell Mol. Biol. *48*, 94–104.

Akhurst, R.J., and Hata, A. (2012). Targeting the TGFβ signalling pathway in disease. Nat. Rev. Drug Discov. *11*, 790–811.

Alber, D.G., Powell, K.L., Vallance, P., Goodwin, D.A., and Grahame-Clarke, C. (2000). Herpesvirus infection accelerates atherosclerosis in the apolipoprotein E-deficient mouse. Circulation *102*, 779–785.

Alber, D.G., Vallance, P., and Powell, K.L. (2002). Enhanced atherogenesis is not an obligatory response to systemic herpesvirus infection in the apoE-deficient mouse: comparison of murine gamma-herpesvirus-68 and herpes simplex virus-1. Arterioscler. Thromb. Vasc. Biol. *22*, 793–798.

Alexander-Brett, J.M., and Fremont, D.H. (2007). Dual GPCR and GAG mimicry by the M3 chemokine decoy receptor. J. Exp. Med. *204*, 3157–3172.

Allen, S.J., Mott, K.R., Wechsler, S.L., Flavell, R.A., Town, T., and Ghiasi, H. (2011). Adaptive and Innate Transforming Growth Factor {beta} Signaling Impact Herpes Simplex Virus 1 Latency and Reactivation. J. Virol. *85*, 11448–11456.

Annes, J.P., Chen, Y., Munger, J.S., and Rifkin, D.B. (2004). Integrin alphaVbeta6-mediated activation of latent TGF-beta requires the latent TGF-beta binding protein-1. J. Cell Biol. *165*, 723–734.

Antoniak, S., Owens, A.P., 3rd, Baunacke, M., Williams, J.C., Lee, R.D., Weithäuser, A., Sheridan, P.A., Malz, R., Luyendyk, J.P., Esserman, D.A., et al. (2013). PAR-1 contributes to the innate immune response during viral infection. J. Clin. Invest.

Antoniou, K.M., Nicholson, A.G., Dimadi, M., Malagari, K., Latsi, P., Rapti, A., Tzanakis, N., Trigidou, R., Polychronopoulos, V., and Bouros, D. (2006). Long-term clinical effects of interferon gamma-1b and colchicine in idiopathic pulmonary fibrosis. Eur. Respir. J. Off. J. Eur. Soc. Clin. Respir. Physiol. *28*, 496–504.

Arora, P., Cuevas, B.D., Russo, A., Johnson, G.L., and Trejo, J. (2008). Persistent transactivation of EGFR and ErbB2/HER2 by protease-activated receptor-1 promotes breast carcinoma cell invasion. Oncogene *27*, 4434–4445.

Ask, K., Bonniaud, P., Maass, K., Eickelberg, O., Margetts, P.J., Warburton, D., Groffen, J., Gauldie, J., and Kolb, M. (2008). Progressive pulmonary fibrosis is mediated by TGF-beta isoform 1 but not TGF-beta3. Int. J. Biochem. Cell Biol. *40*, 484–495.

Asner, S., Waters, V., Solomon, M., Yau, Y., Richardson, S.E., Grasemann, H., Gharabaghi, F., and Tran, D. (2012). Role of respiratory viruses in pulmonary exacerbations in children with cystic fibrosis. J. Cyst. Fibros. Off. J. Eur. Cyst. Fibros. Soc. *11*, 433–439.

Asokananthan, N., Graham, P.T., Fink, J., Knight, D.A., Bakker, A.J., McWilliam, A.S., Thompson, P.J., and Stewart, G.A. (2002). Activation of protease-activated receptor (PAR)-1, PAR-2, and PAR-4 stimulates IL-6, IL-8, and prostaglandin E2 release from human respiratory epithelial cells. J. Immunol. Baltim. Md 1950 *168*, 3577–3585.

Atzori, L., Lucattelli, M., Scotton, C.J., Laurent, G.J., Bartalesi, B., De Cunto, G., Lunghi, B., Chambers, R.C., and Lungarella, G. (2009). Absence of proteinase-activated receptor-1 signaling in mice confers protection from fMLP-induced goblet cell metaplasia. Am. J. Respir. Cell Mol. Biol. *41*, 680–687.

Babich, M., King, K.L., and Nissenson, R.A. (1990). Thrombin stimulates inositol phosphate production and intracellular free calcium by a pertussis toxin-insensitive mechanism in osteosarcoma cells. Endocrinology *126*, 948–954.

Bae, J.-S., Yang, L., Manithody, C., and Rezaie, A.R. (2007). The ligand occupancy of endothelial protein C receptor switches the protease-activated receptor 1-dependent signaling specificity of thrombin from a permeability-enhancing to a barrier-protective response in endothelial cells. Blood *110*, 3909–3916.

Bae, J.-S., Yang, L., and Rezaie, A.R. (2010). Factor X/Xa elicits protective signaling responses in endothelial cells directly via PAR-2 and indirectly via endothelial protein C receptor-dependent recruitment of PAR-1. J. Biol. Chem. *285*, 34803–34812.

Baffy, G., Yang, L., Raj, S., Manning, D.R., and Williamson, J.R. (1994). G protein coupling to the thrombin receptor in Chinese hamster lung fibroblasts. J. Biol. Chem. *269*, 8483–8487.

Bahou, W.F., Nierman, W.C., Durkin, A.S., Potter, C.L., and Demetrick, D.J. (1993). Chromosomal assignment of the human thrombin receptor gene: localization to region q13 of chromosome 5. Blood *82*, 1532–1537.

Bajaj, M.S., Birktoft, J.J., Steer, S.A., and Bajaj, S.P. (2001). Structure and biology of tissue factor pathway inhibitor. Thromb. Haemost. *86*, 959–972.

Bals, R., and Hiemstra, P.S. (2004). Innate immunity in the lung: how epithelial cells fight against respiratory pathogens. Eur. Respir. J. *23*, 327–333.

Bando, M., Ohno, S., Oshikawa, K., Takahashi, M., Okamoto, H., and Sugiyama, Y. (2001). Infection of TT virus in patients with idiopathic pulmonary fibrosis. Respir. Med. *95*, 935–942.

Bando, M., Takahashi, M., Ohno, S., Hosono, T., Hironaka, M., Okamoto, H., and Sugiyama, Y. (2008). Torque teno virus DNA titre elevated in idiopathic pulmonary fibrosis with primary lung cancer. Respirology *13*, 263–269.

Bao, Y., Geng, Y., and Jing, H. (2012). Effect of hirudin on the levels of acute lung injury rat tumor necrosis factor-α and matrix metalloproteinase-12. Mol. Med. Rep. *5*, 873–875.

Baran, C.P., Opalek, J.M., McMaken, S., Newland, C.A., O'Brien, J.M., Hunter, M.G., Bringardner, B.D., Monick, M.M., Brigstock, D.R., Stromberg, P.C., et al. (2007). Important Roles for Macrophage Colony-stimulating Factor, CC Chemokine Ligand 2,

and Mononuclear Phagocytes in the Pathogenesis of Pulmonary Fibrosis. Am J Respir Crit Care Med *176*, 78–89.

Bastarache, J.A., Wang, L., Geiser, T., Wang, Z., Albertine, K.H., Matthay, M.A., and Ware, L.B. (2007). The alveolar epithelium can initiate the extrinsic coagulation cascade through expression of tissue factor. Thorax *62*, 608–616.

Bastarache, J.A., Fremont, R.D., Kropski, J.A., Bossert, F.R., and Ware, L.B. (2009). Procoagulant alveolar microparticles in the lungs of patients with acute respiratory distress syndrome. Am. J. Physiol. Lung Cell. Mol. Physiol. *297*, L1035–1041.

Bastarache, J.A., Sebag, S.C., Grove, B.S., and Ware, L.B. (2011). Interferon-γ and tumor necrosis factor-α act synergistically to up-regulate tissue factor in alveolar epithelial cells. Exp. Lung Res. *37*, 509–517.

Bastarache, J.A., Sebag, S.C., Clune, J.K., Grove, B.S., Lawson, W.E., Janz, D.R., Roberts, L.J., 2nd, Dworski, R., Mackman, N., and Ware, L.B. (2012). Low levels of tissue factor lead to alveolar haemorrhage, potentiating murine acute lung injury and oxidative stress. Thorax *67*, 1032–1039.

Bauman, K.A., Wettlaufer, S.H., Okunishi, K., Vannella, K.M., Stoolman, J.S., Huang, S.K., Courey, A.J., White, E.S., Hogaboam, C.M., Simon, R.H., et al. (2010). The antifibrotic effects of plasminogen activation occur via prostaglandin E2 synthesis in humans and mice. J. Clin. Invest. *120*, 1950–1960.

Baumgartner, K.B., Samet, J.M., Stidley, C.A., Colby, T.V., and Waldron, J.A. (1997). Cigarette smoking: a risk factor for idiopathic pulmonary fibrosis. Am. J. Respir. Crit. Care Med. *155*, 242–248.

Becker, R.C., Moliterno, D.J., Jennings, L.K., Pieper, K.S., Pei, J., Niederman, A., Ziada, K.M., Berman, G., Strony, J., Joseph, D., et al. (2009). Safety and tolerability of SCH 530348 in patients undergoing non-urgent percutaneous coronary intervention: a randomised, double-blind, placebo-controlled phase II study. Lancet *373*, 919–928.

Behr, J., Demedts, M., Buhl, R., Costabel, U., Dekhuijzen, R.P.N., Jansen, H.M., MacNee, W., Thomeer, M., Wallaert, B., Laurent, F., et al. (2009). Lung function in idiopathic pulmonary fibrosis--extended analyses of the IFIGENIA trial. Respir. Res. *10*, 101.

Berkel, V. van, Barrett, J., Tiffany, H.L., Fremont, D.H., Murphy, P.M., McFadden, G., Speck, S.H., and Virgin, H.W. (2000). Identification of a Gammaherpesvirus Selective Chemokine Binding Protein That Inhibits Chemokine Action. J. Virol. *74*, 6741–6747.

Berridge, M.J. (1993). Inositol trisphosphate and calcium signalling. Nature *361*, 315–325.

Berridge, M.J. (2012). Calcium signalling remodelling and disease. Biochem. Soc. Trans. *40*, 297–309.

Berridge, M.J., Bootman, M.D., and Roderick, H.L. (2003). Calcium signalling: dynamics, homeostasis and remodelling. Nat. Rev. Mol. Cell Biol. *4*, 517–529.

Bhowmick, N.A., Ghiassi, M., Bakin, A., Aakre, M., Lundquist, C.A., Engel, M.E., Arteaga, C.L., and Moses, H.L. (2001). Transforming growth factor-beta1 mediates epithelial to mesenchymal transdifferentiation through a RhoA-dependent mechanism. Mol. Biol. Cell *12*, 27–36.

Bhowmick, N.A., Chytil, A., Plieth, D., Gorska, A.E., Dumont, N., Shappell, S., Washington, M.K., Neilson, E.G., and Moses, H.L. (2004). TGF-beta signaling in fibroblasts modulates the oncogenic potential of adjacent epithelia. Science *303*, 848–851.

Biernacka, A., Dobaczewski, M., and Frangogiannis, N.G. (2011). TGF-β signaling in fibrosis. Growth Factors Chur Switz. *29*, 196–202.

Blackhart, B.D., Emilsson, K., Nguyen, D., Teng, W., Martelli, A.J., Nystedt, S., Sundelin, J., and Scarborough, R.M. (1996). Ligand Cross-reactivity within the Protease-activated Receptor Family. J. Biol. Chem. *271*, 16466–16471.

Blanc-Brude, O.P., Archer, F., Leoni, P., Derian, C., Bolsover, S., Laurent, G.J., and Chambers, R.C. (2005). Factor Xa stimulates fibroblast procollagen production, proliferation, and calcium signaling via PAR1 activation. Exp. Cell Res. *304*, 16–27.

Bogatkevich, G.S., Tourkina, E., Silver, R.M., and Ludwicka-Bradley, A. (2001). Thrombin differentiates normal lung fibroblasts to a myofibroblast phenotype via the proteolytically activated receptor-1 and a protein kinase C-dependent pathway. J. Biol. Chem. *276*, 45184–45192.

Bogatkevich, G.S., Tourkina, E., Abrams, C.S., Harley, R.A., Silver, R.M., and Ludwicka-Bradley, A. (2003). Contractile activity and smooth muscle alpha-actin organization in thrombin-induced human lung myofibroblasts. Am. J. Physiol. Lung Cell. Mol. Physiol. *285*, L334–343.

Bogatkevich, G.S., Ludwicka-Bradley, A., and Silver, R.M. (2009). Dabigatran, a direct thrombin inhibitor, demonstrates antifibrotic effects on lung fibroblasts. Arthritis Rheum. *60*, 3455–3464.

Bogatkevich, G.S., Ludwicka-Bradley, A., Nietert, P.J., Akter, T., van Ryn, J., and Silver, R.M. (2011). Antiinflammatory and antifibrotic effects of the oral direct thrombin inhibitor dabigatran etexilate in a murine model of interstitial lung disease. Arthritis Rheum. *63*, 1416–1425.

Boire, A., Covic, L., Agarwal, A., Jacques, S., Sherifi, S., and Kuliopulos, A. (2005). PAR1 is a matrix metalloprotease-1 receptor that promotes invasion and tumorigenesis of breast cancer cells. Cell *120*, 303–313.

Bokemeyer, C. (2008). Bleomycin in Testicular Cancer: Will Pharmacogenomics Improve Treatment Regimens? J. Clin. Oncol. *26*, 1783–1785.

Bom, V.J., and Bertina, R.M. (1990). The contributions of Ca2+, phospholipids and tissue-factor apoprotein to the activation of human blood-coagulation factor X by activated factor VII. Biochem. J. *265*, 327–336.

Bonaca, M.P., and Morrow, D.A. (2009). SCH 530348: a novel oral thrombin receptor antagonist. Future Cardiol. *5*, 435–442.

Bonaca, M.P., Scirica, B.M., Creager, M.A., Olin, J., Bounameaux, H., Dellborg, M., Lamp, J.M., Murphy, S.A., Braunwald, E., and Morrow, D.A. (2013). Vorapaxar in patients with peripheral artery disease: results from TRA2{degrees}P-TIMI 50. Circulation *127*, 1522–1529, 1529e1–6.

Boname, J.M., de Lima, B.D., Lehner, P.J., and Stevenson, P.G. (2004). Viral degradation of the MHC class I peptide loading complex. Immunity *20*, 305–317.

Bonner, J.C. (2004). Regulation of PDGF and its receptors in fibrotic diseases. Cytokine Growth Factor Rev. *15*, 255–273.

Bonniaud, P., Martin, G., Margetts, P.J., Ask, K., Robertson, J., Gauldie, J., and Kolb, M. (2004a). Connective tissue growth factor is crucial to inducing a profibrotic environment in “fibrosis-resistant” BALB/c mouse lungs. Am. J. Respir. Cell Mol. Biol. *31*, 510–516.

Bonniaud, P., Kolb, M., Galt, T., Robertson, J., Robbins, C., Stampfli, M., Lavery, C., Margetts, P.J., Roberts, A.B., and Gauldie, J. (2004b). Smad3 null mice develop airspace enlargement and are resistant to TGF-beta-mediated pulmonary fibrosis. J. Immunol. Baltim. Md 1950 *173*, 2099–2108.

Bonniaud, P., Margetts, P.J., Ask, K., Flanders, K., Gauldie, J., and Kolb, M. (2005a). TGF-beta and Smad3 signaling link inflammation to chronic fibrogenesis. J. Immunol. Baltim. Md 1950 *175*, 5390–5395.

Bonniaud, P., Margetts, P.J., Kolb, M., Schroeder, J.A., Kapoun, A.M., Damm, D., Murphy, A., Chakravarty, S., Dugar, S., Higgins, L., et al. (2005b). Progressive transforming growth factor beta1-induced lung fibrosis is blocked by an orally active ALK5 kinase inhibitor. Am. J. Respir. Crit. Care Med. *171*, 889–898.

Bonniaud, P., Margetts, P.J., Kolb, M., Schroeder, J.A., Kapoun, A.M., Damm, D., Murphy, A., Chakravarty, S., Dugar, S., Higgins, L., et al. (2005c). Progressive transforming growth factor beta1-induced lung fibrosis is blocked by an orally active ALK5 kinase inhibitor. Am. J. Respir. Crit. Care Med. *171*, 889–898.

Bootman, M., Niggli, E., Berridge, M., and Lipp, P. (1997a). Imaging the hierarchical Ca2+ signalling system in HeLa cells. J. Physiol. *499 (Pt 2)*, 307–314.

Bootman, M.D., Berridge, M.J., and Lipp, P. (1997b). Cooking with Calcium: The Recipes for Composing Global Signals from Elementary Events. Cell *91*, 367–373.

Borchers, M.T., Biechele, T., Justice, J.P., Ansay, T., Cormier, S., Mancino, V., Wilkie, T.M., Simon, M.I., Lee, N.A., and Lee, J.J. (2003). Methacholine-induced airway hyperresponsiveness is dependent on Galphaq signaling. Am. J. Physiol. Lung Cell. Mol. Physiol. *285*, L114–120.

Borensztajn, K., Bresser, P., van der Loos, C., Bot, I., van den Blink, B., den Bakker, M.A., Daalhuisen, J., Groot, A.P., Peppelenbosch, M.P., von der Thüsen, J.H., et al. (2010). Protease-activated receptor-2 induces myofibroblast differentiation and tissue factor up-regulation during bleomycin-induced lung injury: potential role in pulmonary fibrosis. Am. J. Pathol. *177*, 2753–2764.

Borza, C.M., and Hutt-Fletcher, L.M. (2002). Alternate replication in B cells and epithelial cells switches tropism of Epstein-Barr virus. Nat. Med. *8*, 594–599.

Breuss, J.M., Gillett, N., Lu, L., Sheppard, D., and Pytela, R. (1993). Restricted distribution of integrin beta 6 mRNA in primate epithelial tissues. J. Histochem. Cytochem. *41*, 1521–1527.

Breuss, J.M., Gallo, J., DeLisser, H.M., Klimanskaya, I.V., Folkesson, H.G., Pittet, J.F., Nishimura, S.L., Aldape, K., Landers, D.V., and Carpenter, W. (1995). Expression of the beta 6 integrin subunit in development, neoplasia and tissue repair suggests a role in epithelial remodeling. J. Cell Sci. *108 (Pt 6)*, 2241–2251.

Bruynseels, P., Jorens, P.G., Demey, H.E., Goossens, H., Pattyn, S.R., Elseviers, M.M., Weyler, J., Bossaert, L.L., Mentens, Y., and Ieven, M. (2003). Herpes simplex virus in the respiratory tract of critical care patients: a prospective study. Lancet *362*, 1536–1541.

Bunnett, N.W. (2006). Protease-activated receptors: how proteases signal to cells to cause inflammation and pain. Semin. Thromb. Hemost. *32 Suppl 1*, 39–48.

Burdick, M.D., Murray, L.A., Keane, M.P., Xue, Y.Y., Zisman, D.A., Belperio, J.A., and Strieter, R.M. (2005). CXCL11 attenuates bleomycin-induced pulmonary fibrosis via inhibition of vascular remodeling. Am. J. Respir. Crit. Care Med. *171*, 261–268.

Calabrese, F., Kipar, A., Lunardi, F., Balestro, E., Perissinotto, E., Rossi, E., Nannini, N., Marulli, G., Stewart, J.P., and Rea, F. (2013). Herpes Virus Infection Is Associated with Vascular Remodeling and Pulmonary Hypertension in Idiopathic Pulmonary Fibrosis. PLoS ONE *8*, e55715.

Câmara, J., and Jarai, G. (2010). Epithelial-mesenchymal transition in primary human bronchial epithelial cells is Smad-dependent and enhanced by fibronectin and TNF-alpha. Fibrogenesis Tissue Repair *3*, 2.

Caraci, F., Gili, E., Calafiore, M., Failla, M., La Rosa, C., Crimi, N., Sortino, M.A., Nicoletti, F., Copani, A., and Vancheri, C. (2008). TGF-β1 targets the GSK-3β/β-catenin pathway via ERK activation in the transition of human lung fibroblasts into myofibroblasts. Pharmacol. Res. *57*, 274–282.

Carulli, M.T., Ong, V.H., Ponticos, M., Shiwen, X., Abraham, D.J., Black, C.M., and Denton, C.P. (2005). Chemokine receptor CCR2 expression by systemic sclerosis fibroblasts: Evidence for autocrine regulation of myofibroblast differentiation. Arthritis Rheum. *52*, 3772–3782.

Cermak, J., Key, N.S., Bach, R.R., Balla, J., Jacob, H.S., and Vercellotti, G.M. (1993). C-reactive protein induces human peripheral blood monocytes to synthesize tissue factor. Blood *82*, 513–520.

Cevikbas, F., Seeliger, S., Fastrich, M., Hinte, H., Metze, D., Kempkes, C., Homey, B., and Steinhoff, M. (2011). Role of protease-activated receptors in human skin fibrosis and scleroderma. Exp. Dermatol. *20*, 69–71.

Chambers, R.C. (2008). Procoagulant signalling mechanisms in lung inflammation and fibrosis: novel opportunities for pharmacological intervention? Br. J. Pharmacol. *153 Suppl 1*, S367–378.

Chambers, R.C., Dabbagh, K., McAnulty, R.J., Gray, A.J., Blanc-Brude, O.P., and Laurent, G.J. (1998). Thrombin stimulates fibroblast procollagen production via proteolytic activation of protease-activated receptor 1. Biochem. J. *333 (Pt 1)*, 121–127.

Chambers, R.C., Leoni, P., Blanc-Brude, O.P., Wembridge, D.E., and Laurent, G.J. (2000). Thrombin is a potent inducer of connective tissue growth factor production via proteolytic activation of protease-activated receptor-1. J. Biol. Chem. *275*, 35584–35591.

Chapman, H.A. (2011). Epithelial-mesenchymal interactions in pulmonary fibrosis. Annu. Rev. Physiol. *73*, 413–435.

Chapman, H.A., Allen, C.L., Stone, O.L., and Fair, D.S. (1985). Human alveolar macrophages synthesize factor VII in vitro. Possible role in interstitial lung disease. J. Clin. Invest. *75*, 2030–2037.

Chaudhary, N.I., Schnapp, A., and Park, J.E. (2006). Pharmacologic Differentiation of Inflammation and Fibrosis in the Rat Bleomycin Model. Am. J. Respir. Crit. Care Med. *173*, 769–776.

Chay, C.H., Cooper, C.R., Gendernalik, J.D., Dhanasekaran, S.M., Chinnaiyan, A.M., Rubin, M.A., Schmaier, A.H., and Pienta, K.J. (2002). A functional thrombin receptor (PAR1) is expressed on bone-derived prostate cancer cell lines. Urology *60*, 760–765.

Chen, D., Carpenter, A., Abrahams, J., Chambers, R.C., Lechler, R.I., McVey, J.H., and Dorling, A. (2008). Protease-activated receptor 1 activation is necessary for monocyte chemoattractant protein 1-dependent leukocyte recruitment in vivo. J. Exp. Med. *205*, 1739–1746.

Chen, S.-J., Ning, H., Ishida, W., Sodin-Semrl, S., Takagawa, S., Mori, Y., and Varga, J. (2006). The early-immediate gene EGR-1 is induced by transforming growth factor-beta and mediates stimulation of collagen gene expression. J. Biol. Chem. *281*, 21183–21197.

Chesnokova, L.S., and Hutt-Fletcher, L.M. (2011). Fusion of Epstein-Barr virus with epithelial cells can be triggered by αvβ5 in addition to αvβ6 and αvβ8, and integrin binding triggers a conformational change in glycoproteins gHgL. J. Virol. *85*, 13214–13223.

Chesnokova, L.S., Nishimura, S.L., and Hutt-Fletcher, L.M. (2009). Fusion of epithelial cells by Epstein-Barr virus proteins is triggered by binding of viral glycoproteins gHgL to integrins alphavbeta6 or alphavbeta8. Proc. Natl. Acad. Sci. U. S. A. *106*, 20464–20469.

Cisowski, J., O'Callaghan, K., Kuliopulos, A., Yang, J., Nguyen, N., Deng, Q., Yang, E., Fogel, M., Tressel, S., Foley, C., et al. (2011). Targeting protease-activated receptor-1 with cell-penetrating pepducins in lung cancer. Am. J. Pathol. *179*, 513–523.

Cocks, T.M., Fong, B., Chow, J.M., Anderson, G.P., Frauman, A.G., Goldie, R.G., Henry, P.J., Carr, M.J., Hamilton, J.R., and Moffatt, J.D. (1999). A protective role for protease-activated receptors in the airways. Nature *398*, 156–160.

Coker, R.K., Laurent, G.J., Shahzeidi, S., Lympany, P.A., du Bois, R.M., Jeffery, P.K., and McAnulty, R.J. (1997). Transforming growth factors-beta 1, -beta 2, and -beta 3 stimulate fibroblast procollagen production in vitro but are differentially expressed during bleomycin-induced lung fibrosis. Am. J. Pathol. *150*, 981–991.

Coker, R.K., Laurent, G.J., Jeffery, P.K., du Bois, R.M., Black, C.M., and McAnulty, R.J. (2001). Localisation of transforming growth factor beta1 and beta3 mRNA transcripts in normal and fibrotic human lung. Thorax *56*, 549–556.

Collard, H.R., Moore, B.B., Flaherty, K.R., Brown, K.K., Kaner, R.J., King, T.E., Lasky, J.A., Loyd, J.E., Noth, I., Olman, M.A., et al. (2007). Acute Exacerbations of Idiopathic Pulmonary Fibrosis. Am. J. Respir. Crit. Care Med. *176*, 636–643.

Collard, H.R., Calfee, C.S., Wolters, P.J., Song, J.W., Hong, S.-B., Brady, S., Ishizaka, A., Jones, K.D., King, T.E., Matthay, M.A., et al. (2010). Plasma biomarker profiles in acute exacerbation of idiopathic pulmonary fibrosis. Am. J. Physiol. Lung Cell. Mol. Physiol. *299*, L3–7.

Colognato, R., Slupsky, J.R., Jendrach, M., Burysek, L., Syrovets, T., and Simmet, T. (2003). Differential expression and regulation of protease-activated receptors in human peripheral monocytes and monocyte-derived antigen-presenting cells. Blood *102*, 2645–2652.

Cook, C.H., Zhang, Y., Sedmak, D.D., Martin, L.C., Jewell, S., and Ferguson, R.M. (2006). Pulmonary cytomegalovirus reactivation causes pathology in immunocompetent mice. Crit. Care Med. *34*, 842–849.

Coomes, S.M., Wilke, C.A., Moore, T.A., and Moore, B.B. (2010). Induction of TGF-beta 1, not regulatory T cells, impairs antiviral immunity in the lung following bone marrow transplant. J. Immunol. Baltim. Md 1950 *184*, 5130–5140.

Coomes, S.M., Farmen, S., Wilke, C.A., Laouar, Y., and Moore, B.B. (2011). Severe Gammaherpesvirus-Induced Pneumonitis and Fibrosis in Syngeneic Bone Marrow Transplant Mice Is Related to Effects of Transforming Growth Factor-β. Am. J. Pathol.

Coughlin, S.R. (2000). Thrombin signalling and protease-activated receptors. Nature *407*, 258–264.

Coughlin, S.R. (2001). Protease-activated receptors in vascular biology. Thromb. Haemost. *86*, 298–307.

Covic, L., Gresser, A.L., Talavera, J., Swift, S., and Kuliopulos, A. (2002). Activation and inhibition of G protein-coupled receptors by cell-penetrating membrane-tethered peptides. Proc. Natl. Acad. Sci. U. S. A. *99*, 643–648.

Cush, S.S., and Flaño, E. (2011). KLRG1+NKG2A+ CD8 T cells mediate protection and participate in memory responses during γ-herpesvirus infection. J. Immunol. Baltim. Md 1950 *186*, 4051–4058.

Damiano, B.P., Derian, C.K., Maryanoff, B.E., Zhang, H., and Gordon, P.A. (2003). RWJ-58259: A Selective Antagonist of Protease Activated Receptor-1. Cardiovasc. Drug Rev. *21*, 313–326.

Dang, M.-T.T., Gu, C., Klavanian, J.I., Jernigan, K.A., Friderici, K.H., Cui, Y., Molina-Molina, M., Ancochea, J., Xaubet, A., and Uhal, B.D. (2013). Angiotensinogen Promoter Polymorphisms Predict Low Diffusing Capacity in U.S. and Spanish IPF Cohorts. Lung *191*, 353–360.

Daniels, C.E., Wilkes, M.C., Edens, M., Kottom, T.J., Murphy, S.J., Limper, A.H., and Leof, E.B. (2004). Imatinib mesylate inhibits the profibrogenic activity of TGF-beta and prevents bleomycin-mediated lung fibrosis. J. Clin. Invest. *114*, 1308–1316.

Daniels, C.E., Lasky, J.A., Limper, A.H., Mieras, K., Gabor, E., and Schroeder, D.R. (2010). Imatinib treatment for idiopathic pulmonary fibrosis: Randomized placebo-controlled trial results. Am. J. Respir. Crit. Care Med. *181*, 604–610.

Darmoul, D., Gratio, V., Devaud, H., Lehy, T., and Laburthe, M. (2003). Aberrant expression and activation of the thrombin receptor protease-activated receptor-1 induces cell proliferation and motility in human colon cancer cells. Am. J. Pathol. *162*, 1503–1513.

Datta, A., Scotton, C.J., and Chambers, R.C. (2011). Novel Therapeutic Approaches for Pulmonary Fibrosis. Br. J. Pharmacol.

Davies, M., Robinson, M., Smith, E., Huntley, S., Prime, S., and Paterson, I. (2005). Induction of an epithelial to mesenchymal transition in human immortal and malignant keratinocytes by TGF-beta1 involves MAPK, Smad and AP-1 signalling pathways. J. Cell. Biochem. *95*, 918–931.

Dawson, C.W., Rickinson, A.B., and Young, L.S. (1990). Epstein-Barr virus latent membrane protein inhibits human epithelial cell differentiation. Nature *344*, 777–780.

Dawson, C.W., Laverick, L., Morris, M.A., Tramoutanis, G., and Young, L.S. (2008). Epstein-Barr virus-encoded LMP1 regulates epithelial cell motility and invasion via the ERK-MAPK pathway. J. Virol. *82*, 3654–3664.

Van De Craen, B., Declerck, P.J., and Gils, A. (2012). The Biochemistry, Physiology and Pathological roles of PAI-1 and the requirements for PAI-1 inhibition in vivo. Thromb. Res. *130*, 576–585.

Decologne, N., Kolb, M., Margetts, P.J., Menetrier, F., Artur, Y., Garrido, C., Gauldie, J., Camus, P., and Bonniaud, P. (2007). TGF-beta1 induces progressive pleural scarring and subpleural fibrosis. J. Immunol. Baltim. Md 1950 *179*, 6043–6051.

Degryse, A.L., and Lawson, W.E. (2011). Progress toward improving animal models for idiopathic pulmonary fibrosis. Am. J. Med. Sci. *341*, 444–449.

Degryse, A.L., Tanjore, H., Xu, X.C., Polosukhin, V.V., Jones, B.R., McMahon, F.B., Gleaves, L.A., Blackwell, T.S., and Lawson, W.E. (2010). Repetitive intratracheal bleomycin models several features of idiopathic pulmonary fibrosis. Am. J. Physiol. Lung Cell. Mol. Physiol. *299*, L442–452.

Degryse, A.L., Tanjore, H., Xu, X.C., Polosukhin, V.V., Jones, B.R., Boomershine, C.S., Ortiz, C., Sherrill, T.P., McMahon, F.B., Gleaves, L.A., et al. (2011). TGFβ signaling in lung epithelium regulates bleomycin-induced alveolar injury and fibroblast recruitment. Am. J. Physiol. Lung Cell. Mol. Physiol. *300*, L887–897.

Della Rocca, G.J., Maudsley, S., Daaka, Y., Lefkowitz, R.J., and Luttrell, L.M. (1999). Pleiotropic coupling of G protein-coupled receptors to the mitogen-activated protein kinase cascade. Role of focal adhesions and receptor tyrosine kinases. J. Biol. Chem. *274*, 13978–13984.

Demedts, M., Behr, J., Buhl, R., Costabel, U., Dekhuijzen, R., Jansen, H.M., MacNee, W., Thomeer, M., Wallaert, B., Laurent, F., et al. (2005). High-dose acetylcysteine in idiopathic pulmonary fibrosis. N. Engl. J. Med. *353*, 2229–2242.

Deng, X., Mercer, P.F., Scotton, C.J., Gilchrist, A., and Chambers, R.C. (2008). Thrombin induces fibroblast CCL2/JE production and release via coupling of PAR1 to Galphaq and cooperation between ERK1/2 and Rho kinase signaling pathways. Mol. Biol. Cell *19*, 2520–2533.

Deng, X., Xu, M., Yuan, C., Yin, L., Chen, X., Zhou, X., Li, G., Fu, Y., Feghali-Bostwick, C.A., and Pang, L. (2013). Transcriptional regulation of increased CCL2 expression in pulmonary fibrosis involves nuclear factor-κB and activator protein-1. Int. J. Biochem. Cell Biol. *45*, 1366–1376.

Derynck, R., and Zhang, Y.E. (2003). Smad-dependent and Smad-independent pathways in TGF-beta family signalling. Nature *425*, 577–584.

Desmoulière, A., Geinoz, A., Gabbiani, F., and Gabbiani, G. (1993). Transforming growth factor-beta 1 induces alpha-smooth muscle actin expression in granulation tissue myofibroblasts and in quiescent and growing cultured fibroblasts. J. Cell Biol. *122*, 103–111.

Diaz, K.T., Skaria, S., Harris, K., Solomita, M., Lau, S., Bauer, K., Smaldone, G.C., and Condos, R. (2012). Delivery and safety of inhaled interferon-γ in idiopathic pulmonary fibrosis. J. Aerosol Med. Pulm. Drug Deliv. *25*, 79–87.

Dik, W.A., Zimmermann, L.J.I., Naber, B.A., Janssen, D.J., van Kaam, A.H.L.C., and Versnel, M.A. (2003). Thrombin contributes to bronchoalveolar lavage fluid mitogenicity in lung disease of the premature infant. Pediatr. Pulmonol. *35*, 34–41.

Distler, J.H.W., Jüngel, A., Huber, L.C., Schulze-Horsel, U., Zwerina, J., Gay, R.E., Michel, B.A., Hauser, T., Schett, G., Gay, S., et al. (2007). Imatinib mesylate reduces production of extracellular matrix and prevents development of experimental dermal fibrosis. Arthritis Rheum. *56*, 311–322.

Distler, J.H.W., Manger, B., Spriewald, B.M., Schett, G., and Distler, O. (2008). Treatment of pulmonary fibrosis for twenty weeks with imatinib mesylate in a patient with mixed connective tissue disease. Arthritis Rheum. *58*, 2538–2542.

Dobaczewski, M., Bujak, M., Li, N., Gonzalez-Quesada, C., Mendoza, L.H., Wang, X.-F., and Frangogiannis, N.G. (2010). Smad3 Signaling Critically Regulates Fibroblast Phenotype and Function in Healing Myocardial Infarction. Circ. Res. *107*, 418–428.

Doherty, P.C., Christensen, J.P., Belz, G.T., Stevenson, P.G., and Sangster, M.Y. (2001). Dissecting the host response to a gamma-herpesvirus. Philos. Trans. R. Soc. Lond. B. Biol. Sci. *356*, 581–593.

Duarte, M., Kolev, V., Soldi, R., Kirov, A., Graziani, I., Oliveira, S.M., Kacer, D., Friesel, R., Maciag, T., and Prudovsky, I. (2006). Thrombin induces rapid PAR1-mediated non-classical FGF1 release. Biochem. Biophys. Res. Commun. *350*, 604–609.

Dubois-Marshall, S., Thomas, J.S., Faratian, D., Harrison, D.J., and Katz, E. (2011). Two possible mechanisms of epithelial to mesenchymal transition in invasive ductal breast cancer. Clin. Exp. Metastasis.

Dugina, V., Fontao, L., Chaponnier, C., Vasiliev, J., and Gabbiani, G. (2001). Focal adhesion features during myofibroblastic differentiation are controlled by intracellular and extracellular factors. J. Cell Sci. *114*, 3285–3296.

Ebrahimi, B., Dutia, B.M., Brownstein, D.G., and Nash, A.A. (2001). Murine gammaherpesvirus-68 infection causes multi-organ fibrosis and alters leukocyte trafficking in interferon-gamma receptor knockout mice. Am. J. Pathol. *158*, 2117–2125.

Edwards, D.R., Murphy, G., Reynolds, J.J., Whitham, S.E., Docherty, A.J., Angel, P., and Heath, J.K. (1987). Transforming growth factor beta modulates the expression of collagenase and metalloproteinase inhibitor. EMBO J. *6*, 1899–1904.

Egan, J.J., Stewart, J.P., Hasleton, P.S., Arrand, J.R., Carroll, K.B., and Woodcock, A.A. (1995). Epstein-Barr virus replication within pulmonary epithelial cells in cryptogenic fibrosing alveolitis. Thorax *50*, 1234–1239.

Egan, J.J., Adamali, H.I., Lok, S.S., Stewart, J.P., and Woodcock, A.A. (2011). Ganciclovir antiviral therapy in advanced idiopathic pulmonary fibrosis: an open pilot study. Pulm. Med. *2011*, 240805.

Eitzman, D.T., McCoy, R.D., Zheng, X., Fay, W.P., Shen, T., Ginsburg, D., and Simon, R.H. (1996). Bleomycin-induced pulmonary fibrosis in transgenic mice that either lack or overexpress the murine plasminogen activator inhibitor-1 gene. J. Clin. Invest. *97*, 232–237.

Ekert, J.E., Murray, L.A., Das, A.M., Sheng, H., Giles-Komar, J., and Rycyzyn, M.A. (2011). Chemokine (C-C motif) ligand 2 mediates direct and indirect fibrotic responses in human and murine cultured fibrocytes. Fibrogenesis Tissue Repair *4*, 23.

Ellis, C.A., Malik, A.B., Gilchrist, A., Hamm, H., Sandoval, R., Voyno-Yasenetskaya, T., and Tiruppathi, C. (1999a). Thrombin induces proteinase-activated receptor-1 gene expression in endothelial cells via activation of Gi-linked Ras/mitogen-activated protein kinase pathway. J. Biol. Chem. *274*, 13718–13727.

Ellis, C.A., Tiruppathi, C., Sandoval, R., Niles, W.D., and Malik, A.B. (1999b). Time course of recovery of endothelial cell surface thrombin receptor (PAR-1) expression. Am. J. Physiol. *276*, C38–45.

Ernofsson, M., and Siegbahn, A. (1996). Platelet-derived growth factor-BB and monocyte chemotactic protein-1 induce human peripheral blood monocytes to express tissue factor. Thromb. Res. *83*, 307–320.

Farkas, L., Farkas, D., Ask, K., Möller, A., Gauldie, J., Margetts, P., Inman, M., and Kolb, M. (2009). VEGF ameliorates pulmonary hypertension through inhibition of endothelial apoptosis in experimental lung fibrosis in rats. J. Clin. Invest. *119*, 1298–1311.

Feistritzer, C., and Riewald, M. (2005). Endothelial barrier protection by activated protein C through PAR1-dependent sphingosine 1-phosphate receptor-1 crossactivation. Blood *105*, 3178–3184.

Feistritzer, C., Lenta, R., and Riewald, M. (2005). Protease-activated receptors-1 and -2 can mediate endothelial barrier protection: role in factor Xa signaling. J. Thromb. Haemost. JTH *3*, 2798–2805.

Fernandez, I.E., and Eickelberg, O. (2012). The impact of TGF-β on lung fibrosis: from targeting to biomarkers. Proc. Am. Thorac. Soc. *9*, 111–116.

Finlen Copeland, C.A., Davis, W.A., Snyder, L.D., Banks, M., Avery, R., Davis, R.D., and Palmer, S.M. (2011). Long-term efficacy and safety of 12 months of valganciclovir prophylaxis compared with 3 months after lung transplantation: a single-center, long-term follow-up analysis from a randomized, controlled cytomegalovirus prevention trial. J. Heart Lung Transplant. Off. Publ. Int. Soc. Heart Transplant. *30*, 990–996.

Firszt, R., Francisco, D., Church, T.D., Thomas, J.M., Ingram, J.L., and Kraft, M. (2013). Interleukin-13 induces collagen type-1 expression through matrix metalloproteinase-2 and transforming growth factor-β1 in airway fibroblasts in asthma. Eur. Respir. J. Off. J. Eur. Soc. Clin. Respir. Physiol.

Fitchett, D.H. (2012). Potential role of rivaroxaban in patients with acute coronary syndrome. Drug Des. Devel. Ther. *6*, 349–357.

Flaherty, K.R., Travis, W.D., Colby, T.V., Toews, G.B., Kazerooni, E.A., Gross, B.H., Jain, A., Strawderman, R.L., Flint, A., Lynch, J.P., et al. (2001). Histopathologic variability in usual and nonspecific interstitial pneumonias. Am. J. Respir. Crit. Care Med. *164*, 1722–1727.

Flaño, E., Kim, I.-J., Moore, J., Woodland, D.L., and Blackman, M.A. (2003). Differential gamma-herpesvirus distribution in distinct anatomical locations and cell

subsets during persistent infection in mice. J. Immunol. Baltim. Md 1950 *170*, 3828–3834.

Flore, O., Rafii, S., Ely, S., O'Leary, J.J., Hyjek, E.M., and Cesarman, E. (1998). Transformation of primary human endothelial cells by Kaposi's sarcoma-associated herpesvirus. Nature *394*, 588–592.

Fukuda, M., Ikuta, K., Yanagihara, K., Tajima, M., Kuratsune, H., Kurata, T., and Sairenji, T. (2001). Effect of transforming growth factor-beta1 on the cell growth and Epstein-Barr virus reactivation in EBV-infected epithelial cell lines. Virology *288*, 109–118.

Funaba, M., Zimmerman, C.M., and Mathews, L.S. (2002a). Modulation of Smad2-mediated Signaling by Extracellular Signal-regulated Kinase. J. Biol. Chem. *277*, 41361–41368.

Funaba, M., Zimmerman, C.M., and Mathews, L.S. (2002b). Modulation of Smad2-mediated signaling by extracellular signal-regulated kinase. J. Biol. Chem. *277*, 41361–41368.

Furuhashi, I., Abe, K., Sato, T., and Inoue, H. (2008). Thrombin-stimulated proliferation of cultured human synovial fibroblasts through proteolytic activation of proteinase-activated receptor-1. J. Pharmacol. Sci. *108*, 104–111.

Furukawa, F., Matsuzaki, K., Mori, S., Tahashi, Y., Yoshida, K., Sugano, Y., Yamagata, H., Matsushita, M., Seki, T., Inagaki, Y., et al. (2003). p38 MAPK mediates fibrogenic signal through Smad3 phosphorylation in rat myofibroblasts. Hepatol. Baltim. Md *38*, 879–889.

Gangadharan, B., Hoeve, M.A., Allen, J.E., Ebrahimi, B., Rhind, S.M., Dutia, B.M., and Nash, A.A. (2008). Murine gammaherpesvirus-induced fibrosis is associated with the development of alternatively activated macrophages. J. Leukoc. Biol. *84*, 50–58.

Gao, Z.-G., and Jacobson, K.A. (2013). Allosteric modulation and functional selectivity of G protein-coupled receptors. Drug Discov. Today Technol. *10*, e237–e243.

Gauldie, J., Kolb, M., Ask, K., Martin, G., Bonniaud, P., and Warburton, D. (2006). Smad3 Signaling Involved in Pulmonary Fibrosis and Emphysema. Proc. Am. Thorac. Soc. *3*, 696–702.

Gharaee-Kermani, M., Denholm, E.M., and Phan, S.H. (1996a). Costimulation of fibroblast collagen and transforming growth factor beta1 gene expression by

monocyte chemoattractant protein-1 via specific receptors. J. Biol. Chem. *271*, 17779–17784.

Gharaee-Kermani, M., Denholm, E.M., and Phan, S.H. (1996b). Costimulation of fibroblast collagen and transforming growth factor beta1 gene expression by monocyte chemoattractant protein-1 via specific receptors. J. Biol. Chem. *271*, 17779–17784.

Gharaee-Kermani, M., Gyetko, M.R., Hu, B., and Phan, S.H. (2007). New insights into the pathogenesis and treatment of idiopathic pulmonary fibrosis: a potential role for stem cells in the lung parenchyma and implications for therapy. Pharm. Res. *24*, 819–841.

Gharaee-Kermani, M., Hu, B., Phan, S.H., and Gyetko, M.R. (2009). Recent advances in molecular targets and treatment of idiopathic pulmonary fibrosis: focus on TGFbeta signaling and the myofibroblast. Curr. Med. Chem. *16*, 1400–1417.

Giaid, A., Michel, R.P., Stewart, D.J., Sheppard, M., Corrin, B., and Hamid, Q. (1993). Expression of endothelin-1 in lungs of patients with cryptogenic fibrosing alveolitis. Lancet *341*, 1550–1554.

Giri, S.N., Hyde, D.M., and Hollinger, M.A. (1993). Effect of antibody to transforming growth factor beta on bleomycin induced accumulation of lung collagen in mice. Thorax *48*, 959–966.

Giunti, S., Pinach, S., Arnaldi, L., Viberti, G., Perin, P.C., Camussi, G., and Gruden, G. (2006). The MCP-1/CCR2 system has direct proinflammatory effects in human mesangial cells. Kidney Int. *69*, 856–863.

Goebeler, M., Gillitzer, R., Kilian, K., Utzel, K., Bröcker, E.B., Rapp, U.R., and Ludwig, S. (2001). Multiple signaling pathways regulate NF-kappaB-dependent transcription of the monocyte chemoattractant protein-1 gene in primary endothelial cells. Blood *97*, 46–55.

Goodwin, A., and Jenkins, G. (2009). Role of integrin-mediated TGFbeta activation in the pathogenesis of pulmonary fibrosis. Biochem. Soc. Trans. *37*, 849–854.

Goto, S., Ogawa, H., Takeuchi, M., Flather, M.D., and Bhatt, D.L. (2010). Double-blind, placebo-controlled Phase II studies of the protease-activated receptor 1 antagonist E5555 (atopaxar) in Japanese patients with acute coronary syndrome or high-risk coronary artery disease. Eur. Heart J. *31*, 2601–2613.

Gouwy, M., Struyf, S., Noppen, S., Schutyser, E., Springael, J.-Y., Parmentier, M., Proost, P., and Van Damme, J. (2008). Synergy between coproduced CC and CXC

chemokines in monocyte chemotaxis through receptor-mediated events. Mol. Pharmacol. *74*, 485–495.

Gribbin, J., Hubbard, R.B., Jeune, I.L., Smith, C.J.P., West, J., and Tata, L.J. (2006). Incidence and mortality of idiopathic pulmonary fibrosis and sarcoidosis in the UK. Thorax *61*, 980–985.

Griffin, J.H., Zlokovic, B.V., and Mosnier, L.O. (2012). Protein C anticoagulant and cytoprotective pathways. Int. J. Hematol. *95*, 333–345.

Guenther, J.F., Cameron, J.E., Nguyen, H.T., Wang, Y., Sullivan, D.E., Shan, B., Lasky, J.A., Flemington, E.K., and Morris, G.F. (2010). Modulation of lung inflammation by the Epstein-Barr virus protein Zta. Am. J. Physiol. Lung Cell. Mol. Physiol. *299*, L771–784.

Guggemoos, S., Hangel, D., Hamm, S., Heit, A., Bauer, S., and Adler, H. (2008). TLR9 contributes to antiviral immunity during gammaherpesvirus infection. J. Immunol. Baltim. Md 1950 *180*, 438–443.

Gulseth, M.P., Michaud, J., and Nutescu, E.A. (2008). Rivaroxaban: an oral direct inhibitor of factor Xa. Am. J. Health-Syst. Pharm. AJHP Off. J. Am. Soc. Health-Syst. Pharm. *65*, 1520–1529.

Günther, A., Lübke, N., Ermert, M., Schermuly, R.T., Weissmann, N., Breithecker, A., Markart, P., Ruppert, C., Quanz, K., Ermert, L., et al. (2003). Prevention of bleomycin-induced lung fibrosis by aerosolization of heparin or urokinase in rabbits. Am. J. Respir. Crit. Care Med. *168*, 1358–1365.

Gura, T. (2002). Therapeutic antibodies: Magic bullets hit the target. Nature *417*, 584–586.

Gurujeyalakshmi, G., and Giri, S.N. (1995). Molecular mechanisms of antifibrotic effect of interferon gamma in bleomycin-mouse model of lung fibrosis: downregulation of TGF-beta and procollagen I and III gene expression. Exp. Lung Res. *21*, 791–808.

Hamada, N., Kuwano, K., Yamada, M., Hagimoto, N., Hiasa, K., Egashira, K., Nakashima, N., Maeyama, T., Yoshimi, M., and Nakanishi, Y. (2005). Anti-vascular endothelial growth factor gene therapy attenuates lung injury and fibrosis in mice. J. Immunol. Baltim. Md 1950 *175*, 1224–1231.

Hammes, S.R., and Coughlin, S.R. (1999). Protease-activated receptor-1 can mediate responses to SFLLRN in thrombin-desensitized cells: evidence for a novel

mechanism for preventing or terminating signaling by PAR1's tethered ligand. Biochemistry (Mosc.) *38*, 2486–2493.

Hansen, K.K., Saifeddine, M., and Hollenberg, M.D. (2004). Tethered ligand-derived peptides of proteinase-activated receptor 3 (PAR3) activate PAR1 and PAR2 in Jurkat T cells. Immunology *112*, 183–190.

Hanumegowda, C., Farkas, L., and Kolb, M. (2012). Angiogenesis in pulmonary fibrosis: too much or not enough? Chest *142*, 200–207.

Hardy, C.L., Flaño, E., Cardin, R.D., Kim, I.J., Nguyen, P., King, S., Woodland, D.L., and Blackman, M.A. (2001). Factors controlling levels of CD8+ T-cell lymphocytosis associated with murine gamma-herpesvirus infection. Viral Immunol. *14*, 391–402.

Hashimoto, S., Gon, Y., Takeshita, I., Matsumoto, K., Maruoka, S., and Horie, T. (2001). Transforming growth Factor-beta1 induces phenotypic modulation of human lung fibroblasts to myofibroblast through a c-Jun-NH2-terminal kinase-dependent pathway. Am. J. Respir. Crit. Care Med. *163*, 152–157.

Hattori, N., Degen, J.L., Sisson, T.H., Liu, H., Moore, B.B., Pandrangi, R.G., Simon, R.H., and Drew, A.F. (2000). Bleomycin-induced pulmonary fibrosis in fibrinogen-null mice. J. Clin. Invest. *106*, 1341–1350.

Hauck, R.W., Schulz, C., Schömig, A., Hoffman, R.K., and Panettieri, R.A. (1999). alpha-Thrombin stimulates contraction of human bronchial rings by activation of protease-activated receptors. Am. J. Physiol. *277*, L22–29.

Hernández-Rodríguez, N.A., Cambrey, A.D., Harrison, N.K., Chambers, R.C., Gray, A.J., Southcott, A.M., duBois, R.M., Black, C.M., Scully, M.F., and McAnulty, R.J. (1995). Role of thrombin in pulmonary fibrosis. Lancet *346*, 1071–1073.

Hetzel, M., Bachem, M., Anders, D., Trischler, G., and Faehling, M. (2005). Different effects of growth factors on proliferation and matrix production of normal and fibrotic human lung fibroblasts. Lung *183*, 225–237.

Hinz, B. (2009). Tissue stiffness, latent TGF-beta1 activation, and mechanical signal transduction: implications for the pathogenesis and treatment of fibrosis. Curr. Rheumatol. Rep. *11*, 120–126.

Hinz, B. (2010). The myofibroblast: paradigm for a mechanically active cell. J. Biomech. *43*, 146–155.

Hinz, B. (2012). Mechanical Aspects of Lung Fibrosis.

Hinz, B., and Gabbiani, G. (2003). Mechanisms of force generation and transmission by myofibroblasts. Curr. Opin. Biotechnol. *14*, 538–546.

Hirsh, J., Dalen, J.E., Deykin, D., Poller, L., and Bussey, H. (1995a). Oral anticoagulants. Mechanism of action, clinical effectiveness, and optimal therapeutic range. Chest *108*, 231S–246S.

Hirsh, J., Raschke, R., Warkentin, T.E., Dalen, J.E., Deykin, D., and Poller, L. (1995b). Heparin: mechanism of action, pharmacokinetics, dosing considerations, monitoring, efficacy, and safety. Chest *108*, 258S–275S.

Hisatomi, K., Mukae, H., Sakamoto, N., Ishimatsu, Y., Kakugawa, T., Hara, S., Fujita, H., Nakamichi, S., Oku, H., Urata, Y., et al. (2012). Pirfenidone inhibits TGF-β1-induced over-expression of collagen type I and heat shock protein 47 in A549 cells. BMC Pulm. Med. *12*, 24.

Hodges, R.J., Jenkins, R.G., Wheeler-Jones, C.P.D., Copeman, D.M., Bottoms, S.E., Bellingan, G.J., Nanthakumar, C.B., Laurent, G.J., Hart, S.L., Foster, M.L., et al. (2004). Severity of lung injury in cyclooxygenase-2-deficient mice is dependent on reduced prostaglandin E(2) production. Am. J. Pathol. *165*, 1663–1676.

Holtzman, M., Patel, D., Kim, H.J., Kim, H., You, Y., and Zhang, Y. (2011). Hypersusceptibility to respiratory viruses as a shared mechanism for asthma, chronic obstructive pulmonary disease, and cystic fibrosis. Am. J. Respir. Cell Mol. Biol. *44*, 739–742.

Hong, K.U., Reynolds, S.D., Watkins, S., Fuchs, E., and Stripp, B.R. (2004). Basal cells are a multipotent progenitor capable of renewing the bronchial epithelium. Am. J. Pathol. *164*, 577–588.

Horan, G.S., Wood, S., Ona, V., Li, D.J., Lukashev, M.E., Weinreb, P.H., Simon, K.J., Hahm, K., Allaire, N.E., Rinaldi, N.J., et al. (2008). Partial Inhibition of Integrin αvβ6 Prevents Pulmonary Fibrosis without Exacerbating Inflammation. Am. J. Respir. Crit. Care Med. *177*, 56–65.

Horowitz, J.C., Lee, D.Y., Waghray, M., Keshamouni, V.G., Thomas, P.E., Zhang, H., Cui, Z., and Thannickal, V.J. (2004). Activation of the Pro-survival Phosphatidylinositol 3-Kinase/AKT Pathway by Transforming Growth Factor-β1 in Mesenchymal Cells Is Mediated by p38 MAPK-dependent Induction of an Autocrine Growth Factor. J. Biol. Chem. *279*, 1359–1367.

Howell, D.C., Goldsack, N.R., Marshall, R.P., McAnulty, R.J., Starke, R., Purdy, G., Laurent, G.J., and Chambers, R.C. (2001). Direct thrombin inhibition reduces lung

collagen, accumulation, and connective tissue growth factor mRNA levels in bleomycin-induced pulmonary fibrosis. Am. J. Pathol. *159*, 1383–1395.

Howell, D.C.J., Johns, R.H., Lasky, J.A., Shan, B., Scotton, C.J., Laurent, G.J., and Chambers, R.C. (2005). Absence of proteinase-activated receptor-1 signaling affords protection from bleomycin-induced lung inflammation and fibrosis. Am. J. Pathol. *166*, 1353–1365.

Hoxie, J.A., Ahuja, M., Belmonte, E., Pizarro, S., Parton, R., and Brass, L.F. (1993). Internalization and recycling of activated thrombin receptors. J. Biol. Chem. *268*, 13756–13763.

Hu, B., Wu, Z., and Phan, S.H. (2003). Smad3 mediates transforming growth factor-beta-induced alpha-smooth muscle actin expression. Am. J. Respir. Cell Mol. Biol. *29*, 397–404.

Hu, Y., Peng, J., Feng, D., Chu, L., Li, X., Jin, Z., Lin, Z., and Zeng, Q. (2006a). Role of Extracellular Signal-Regulated Kinase, p38 Kinase, and Activator Protein-1 in Transforming Growth Factor-β1–Induced Alpha Smooth Muscle Actin Expression in Human Fetal Lung Fibroblasts In Vitro. Lung *184*, 33–42.

Hu, Y., Peng, J., Feng, D., Chu, L., Li, X., Jin, Z., Lin, Z., and Zeng, Q. (2006b). Role of Extracellular Signal-Regulated Kinase, p38 Kinase, and Activator Protein-1 in Transforming Growth Factor-β1–Induced Alpha Smooth Muscle Actin Expression in Human Fetal Lung Fibroblasts In Vitro. Lung *184*, 33–42.

Huang, L.S., Fu, P., Patel, P., Harijith, A., Sun, T., Zhao, Y., Garcia, J.G.N., Chun, J., and Natarajan, V. (2013). Lysophosphatidic Acid Receptor 2 Deficiency Confers Protection Against Bleomycin-Induced Lung Injury and Fibrosis in Mice. Am. J. Respir. Cell Mol. Biol.

Hubbard, R., Johnston, I., Coultas, D.B., and Britton, J. (1996). Mortality rates from cryptogenic fibrosing alveolitis in seven countries. Thorax *51*, 711–716.

Hung, D.T., Wong, Y.H., Vu, T.K., and Coughlin, S.R. (1992). The cloned platelet thrombin receptor couples to at least two distinct effectors to stimulate phosphoinositide hydrolysis and inhibit adenylyl cyclase. J. Biol. Chem. *267*, 20831–20834.

Idell, S. (2003a). Coagulation, fibrinolysis, and fibrin deposition in acute lung injury. Crit. Care Med. *31*, S213–220.

Idell, S. (2003b). Coagulation, fibrinolysis, and fibrin deposition in acute lung injury. Crit. Care Med. *31*, S213–220.

Iempridee, T., Das, S., Xu, I., and Mertz, J.E. (2011). Transforming growth factor beta-induced reactivation of Epstein-Barr virus involves multiple Smad-binding elements cooperatively activating expression of the latent-lytic switch BZLF1 gene. J. Virol. *85*, 7836–7848.

Ihn, H., Sato, S., Fujimoto, M., Igarashi, A., Yazawa, N., Kubo, M., Kikuchi, K., Takehara, K., and Tamaki, K. (2000). Characterization of autoantibodies to endothelial cells in systemic sclerosis (SSc): association with pulmonary fibrosis. Clin. Exp. Immunol. *119*, 203–209.

Imokawa, S., Sato, A., Hayakawa, H., Kotani, M., Urano, T., and Takada, A. (1997). Tissue factor expression and fibrin deposition in the lungs of patients with idiopathic pulmonary fibrosis and systemic sclerosis. Am. J. Respir. Crit. Care Med. *156*, 631–636.

Inoue, Y., King, T.E., Jr, Barker, E., Daniloff, E., and Newman, L.S. (2002). Basic fibroblast growth factor and its receptors in idiopathic pulmonary fibrosis and lymphangioleiomyomatosis. Am. J. Respir. Crit. Care Med. *166*, 765–773.

Ip, W.K., Wong, C.K., and Lam, C.W.K. (2006). Interleukin (IL)-4 and IL-13 up-regulate monocyte chemoattractant protein-1 expression in human bronchial epithelial cells: involvement of p38 mitogen-activated protein kinase, extracellular signal-regulated kinase 1/2 and Janus kinase-2 but not c-Jun NH2-terminal kinase 1/2 signalling pathways. Clin. Exp. Immunol. *145*, 162–172.

Ishihara, H., Connolly, A.J., Zeng, D., Kahn, M.L., Zheng, Y.W., Timmons, C., Tram, T., and Coughlin, S.R. (1997). Protease-activated receptor 3 is a second thrombin receptor in humans. Nature *386*, 502–506.

Iwano, M. (2002). Evidence that fibroblasts derive from epithelium during tissue fibrosis. J. Clin. Invest. *110*, 341–350.

Izhak, L., Wildbaum, G., Jung, S., Stein, A., Shaked, Y., and Karin, N. (2012). Dissecting the autocrine and paracrine roles of the CCR2-CCL2 axis in tumor survival and angiogenesis. PloS One *7*, e28305.

Janick-Buckner, D., Ranges, G.E., and Hacker, M.P. (1989). Alteration of bronchoalveolar lavage cell populations following bleomycin treatment in mice. Toxicol. Appl. Pharmacol. *100*, 465–473.

Jenkins, G. (2008). The role of proteases in transforming growth factor-beta activation. Int. J. Biochem. Cell Biol. *40*, 1068–1078.

Jenkins, G., Hart, S.L., Hodges, R.J., Meng, Q.-H., Kinnon, C., Laurent, G.J., and McAnulty, R.J. (2002). Cyclooxygenase-2 overexpression, using an integrin-targeted gene delivery system (the LID vector), inhibits fibroblast proliferation in vitro and leads to increased prostaglandin E(2) in the lung. Chest *121*, 102S–104S.

Jenkins, R.G., Su, X., Su, G., Scotton, C.J., Camerer, E., Laurent, G.J., Davis, G.E., Chambers, R.C., Matthay, M.A., and Sheppard, D. (2006). Ligation of protease-activated receptor 1 enhances alpha(v)beta6 integrin-dependent TGF-beta activation and promotes acute lung injury. J. Clin. Invest. *116*, 1606–1614.

Jesmin, S., Gando, S., Matsuda, N., Sakuma, I., Kobayashi, S., Sakuraya, F., and Hattori, Y. (2004). Temporal changes in pulmonary expression of key precoagulant molecules in rabbits with endotoxin-induced acute lung injury: elevated expression levels of protease-activated receptors. Thromb. Haemost.

Jesmin, S., Gando, S., Zaedi, S., and Sakuraya, F. (2007). Differential expression, time course and distribution of four PARs in rats with endotoxin-induced acute lung injury. Inflammation *30*, 14–27.

Jiang, D., Liang, J., Hodge, J., Lu, B., Zhu, Z., Yu, S., Fan, J., Gao, Y., Yin, Z., Homer, R., et al. (2004). Regulation of pulmonary fibrosis by chemokine receptor CXCR3. J. Clin. Invest. *114*, 291–299.

Jiang, D., Liang, J., Campanella, G.S., Guo, R., Yu, S., Xie, T., Liu, N., Jung, Y., Homer, R., Meltzer, E.B., et al. (2010). Inhibition of pulmonary fibrosis in mice by CXCL10 requires glycosaminoglycan binding and syndecan-4. J. Clin. Invest. *120*, 2049–2057.

Kage, H., and Borok, Z. (2012). EMT and interstitial lung disease: a mysterious relationship. Curr. Opin. Pulm. Med. *18*, 517–523.

Kahn, M.L., Nakanishi-Matsui, M., Shapiro, M.J., Ishihara, H., and Coughlin, S.R. (1999). Protease-activated receptors 1 and 4 mediate activation of human platelets by thrombin. J. Clin. Invest. *103*, 879–887.

Kalluri, R., and Neilson, E.G. (2003). Epithelial-mesenchymal transition and its implications for fibrosis. J. Clin. Invest. *112*, 1776–1784.

Kaneider, N.C., Leger, A.J., Agarwal, A., Nguyen, N., Perides, G., Derian, C., Covic, L., and Kuliopulos, A. (2007). “Role reversal” for the receptor PAR1 in sepsis-induced vascular damage. Nat. Immunol. *8*, 1303–1312.

Kapanci, Y., Desmouliere, A., Pache, J.C., Redard, M., and Gabbiani, G. (1995). Cytoskeletal protein modulation in pulmonary alveolar myofibroblasts during

idiopathic pulmonary fibrosis. Possible role of transforming growth factor beta and tumor necrosis factor alpha. Am. J. Respir. Crit. Care Med. *152*, 2163–2169.

Katzenstein, A.-L.A., Zisman, D.A., Litzky, L.A., Nguyen, B.T., and Kotloff, R.M. (2002). Usual interstitial pneumonia: histologic study of biopsy and explant specimens. Am. J. Surg. Pathol. *26*, 1567–1577.

Kaufmann, R., Schulze, B., Krause, G., Mayr, L.M., Settmacher, U., and Henklein, P. (2005). Proteinase-activated receptors (PARs)—the PAR3 Neo-N-terminal peptide TFRGAP interacts with PAR1. Regul. Pept. *125*, 61–66.

Kedzierski, R.M., and Yanagisawa, M. (2001). Endothelin system: the double-edged sword in health and disease. Annu. Rev. Pharmacol. Toxicol. *41*, 851–876.

Keerthisingam, C.B., Jenkins, R.G., Harrison, N.K., Hernandez-Rodriguez, N.A., Booth, H., Laurent, G.J., Hart, S.L., Foster, M.L., and McAnulty, R.J. (2001). Cyclooxygenase-2 deficiency results in a loss of the anti-proliferative response to transforming growth factor-beta in human fibrotic lung fibroblasts and promotes bleomycin-induced pulmonary fibrosis in mice. Am. J. Pathol. *158*, 1411–1422.

Keizer, R.J., Huitema, A.D.R., Schellens, J.H.M., and Beijnen, J.H. (2010). Clinical pharmacokinetics of therapeutic monoclonal antibodies. Clin. Pharmacokinet. *49*, 493–507.

Kelly, B.G., Lok, S.S., Hasleton, P.S., Egan, J.J., and Stewart, J.P. (2002). A rearranged form of Epstein-Barr virus DNA is associated with idiopathic pulmonary fibrosis. Am. J. Respir. Crit. Care Med. *166*, 510–513.

Khalil, N., O'Connor, R.N., Unruh, H.W., Warren, P.W., Flanders, K.C., Kemp, A., Bereznay, O.H., and Greenberg, A.H. (1991). Increased production and immunohistochemical localization of transforming growth factor-beta in idiopathic pulmonary fibrosis. Am. J. Respir. Cell Mol. Biol. *5*, 155–162.

Khoufache, K., Berri, F., Nacken, W., Vogel, A.B., Delenne, M., Camerer, E., Coughlin, S.R., Carmeliet, P., Lina, B., Rimmelzwaan, G.F., et al. (2013). PAR1 contributes to influenza A virus pathogenicity in mice. J. Clin. Invest. *123*, 206–214.

Kijiyama, N., Ueno, H., Sugimoto, I., Sasaguri, Y., Yatera, K., Kido, M., Gabazza, E.C., Suzuki, K., Hashimoto, E., and Takeya, H. (2006). Intratracheal gene transfer of tissue factor pathway inhibitor attenuates pulmonary fibrosis. Biochem. Biophys. Res. Commun. *339*, 1113–1119.

Kim, D.S., Park, J.H., Park, B.K., Lee, J.S., Nicholson, A.G., and Colby, T. (2006a). Acute exacerbation of idiopathic pulmonary fibrosis: frequency and clinical features. Eur. Respir. J. Off. J. Eur. Soc. Clin. Respir. Physiol. *27*, 143–150.

Kim, J.H., Jang, Y.S., Eom, K.-S., Hwang, Y.I., Kang, H.R., Jang, S.H., Kim, C.H., Park, Y.B., Lee, M.G., Hyun, I.G., et al. (2007). Transforming growth factor beta1 induces epithelial-to-mesenchymal transition of A549 cells. J. Korean Med. Sci. *22*, 898–904.

Kim, K.K., Kugler, M.C., Wolters, P.J., Robillard, L., Galvez, M.G., Brumwell, A.N., Sheppard, D., and Chapman, H.A. (2006b). Alveolar epithelial cell mesenchymal transition develops in vivo during pulmonary fibrosis and is regulated by the extracellular matrix. Proc. Natl. Acad. Sci. U. S. A. *103*, 13180–13185.

King, T.E., Jr, Behr, J., Brown, K.K., du Bois, R.M., Lancaster, L., de Andrade, J.A., Stähler, G., Leconte, I., Roux, S., and Raghu, G. (2008). BUILD-1: a randomized placebo-controlled trial of bosentan in idiopathic pulmonary fibrosis. Am. J. Respir. Crit. Care Med. *177*, 75–81.

King, T.E., Jr, Albera, C., Bradford, W.Z., Costabel, U., Hormel, P., Lancaster, L., Noble, P.W., Sahn, S.A., Szwarcberg, J., Thomeer, M., et al. (2009). Effect of interferon gamma-1b on survival in patients with idiopathic pulmonary fibrosis (INSPIRE): a multicentre, randomised, placebo-controlled trial. Lancet *374*, 222–228.

Knight, D.A., Lim, S., Scaffidi, A.K., Roche, N., Chung, K.F., Stewart, G.A., and Thompson, P.J. (2001). Protease-activated receptors in human airways: upregulation of PAR-2 in respiratory epithelium from patients with asthma. J. Allergy Clin. Immunol. *108*, 797–803.

Kobayashi, H., Gabazza, E.C., Taguchi, O., Wada, H., Takeya, H., Nishioka, J., Yasui, H., Kobayashi, T., Hataji, O., Suzuki, K., et al. (1998). Protein C anticoagulant system in patients with interstitial lung disease. Am. J. Respir. Crit. Care Med. *157*, 1850–1854.

Kolb, M., Margetts, P.J., Anthony, D.C., Pitossi, F., and Gauldie, J. (2001). Transient expression of IL-1beta induces acute lung injury and chronic repair leading to pulmonary fibrosis. J. Clin. Invest. *107*, 1529–1536.

Kolodsick, J.E., Toews, G.B., Jakubzick, C., Hogaboam, C., Moore, T.A., McKenzie, A., Wilke, C.A., Chrisman, C.J., and Moore, B.B. (2004). Protection from fluorescein isothiocyanate-induced fibrosis in IL-13-deficient, but not IL-4-deficient, mice results from impaired collagen synthesis by fibroblasts. J. Immunol. Baltim. Md 1950 *172*, 4068–4076.

Königshoff, M., Wilhelm, A., Jahn, A., Sedding, D., Amarie, O.V., Eul, B., Seeger, W., Fink, L., Günther, A., Eickelberg, O., et al. (2007). The angiotensin II receptor 2 is expressed and mediates angiotensin II signaling in lung fibrosis. Am. J. Respir. Cell Mol. Biol. *37*, 640–650.

Konishi, K., Gibson, K.F., Lindell, K.O., Richards, T.J., Zhang, Y., Dhir, R., Bisceglia, M., Gilbert, S., Yousem, S.A., Song, J.W., et al. (2009). Gene expression profiles of acute exacerbations of idiopathic pulmonary fibrosis. Am. J. Respir. Crit. Care Med. *180*, 167–175.

Kontermann, R.E. (2009). Strategies to extend plasma half-lives of recombinant antibodies. BioDrugs Clin. Immunother. Biopharm. Gene Ther. *23*, 93–109.

Koth, L.L., Alex, B., Hawgood, S., Nead, M.A., Sheppard, D., Erle, D.J., and Morris, D.G. (2007). Integrin beta6 mediates phospholipid and collectin homeostasis by activation of latent TGF-beta1. Am. J. Respir. Cell Mol. Biol. *37*, 651–659.

Kottmann, R.M., Hogan, C.M., Phipps, R.P., and Sime, P.J. (2009). Determinants of initiation and progression of idiopathic pulmonary fibrosis. Respirol. Carlton Vic *14*, 917–933.

Kretzschmar, M., Doody, J., Timokhina, I., and Massagué, J. (1999a). A mechanism of repression of TGFβ/ Smad signaling by oncogenic Ras. Genes Dev. *13*, 804–816.

Kretzschmar, M., Doody, J., Timokhina, I., and Massagué, J. (1999b). A mechanism of repression of TGFbeta/ Smad signaling by oncogenic Ras. Genes Dev. *13*, 804–816.

Kubier, A., and O'Brien, M. (2012). Endogenous Anticoagulants. Top. Companion Anim. Med. *27*, 81–87.

Kubo, H., Nakayama, K., Yanai, M., Suzuki, T., Yamaya, M., Watanabe, M., and Sasaki, H. (2005). Anticoagulant therapy for idiopathic pulmonary fibrosis. Chest *128*, 1475–1482.

Kulasekaran, P., Scavone, C.A., Rogers, D.S., Arenberg, D.A., Thannickal, V.J., and Horowitz, J.C. (2009). Endothelin-1 and Transforming Growth Factor-β1 Independently Induce Fibroblast Resistance to Apoptosis via AKT Activation. Am. J. Respir. Cell Mol. Biol. *41*, 484–493.

Kuwano, K., Kunitake, R., Kawasaki, M., Nomoto, Y., Hagimoto, N., Nakanishi, Y., and Hara, N. (2012). P21Waf1/Cip1/Sdi1 and p53 expression in association with DNA strand breaks in idiopathic pulmonary fibrosis.

Kwak, H.-J., Park, M.-J., Cho, H., Park, C.-M., Moon, S.-I., Lee, H.-C., Park, I.-C., Kim, M.-S., Rhee, C.H., and Hong, S.-I. (2006). Transforming Growth Factor-β1 Induces Tissue Inhibitor of Metalloproteinase-1 Expression via Activation of Extracellular Signal-Regulated Kinase and Sp1 in Human Fibrosarcoma Cells. Mol. Cancer Res. *4*, 209 –220.

Lakatos, H.F., Burgess, H.A., Thatcher, T.H., Redonnet, M.R., Hernady, E., Williams, J.P., and Sime, P.J. (2006). OROPHARYNGEAL ASPIRATION OF A SILICA SUSPENSION PRODUCES A SUPERIOR MODEL OF SILICOSIS IN THE MOUSE WHEN COMPARED TO INTRATRACHEAL INSTILLATION. Exp. Lung Res. *32*, 181–199.

LaMorte, V.J., Harootunian, A.T., Spiegel, A.M., Tsien, R.Y., and Feramisco, J.R. (1993). Mediation of growth factor induced DNA synthesis and calcium mobilization by Gq and Gi2. J. Cell Biol. *121*, 91–99.

Lan, R.S., Stewart, G.A., Goldie, R.G., and Henry, P.J. (2004). Altered expression and in vivo lung function of protease-activated receptors during influenza A virus infection in mice. Am. J. Physiol. Lung Cell. Mol. Physiol. *286*, L388–398.

Lang, N.N., Guðmundsdóttir, I.J., and Newby, D.E. (2010). Vascular PAR-1: Activity and Antagonism. Cardiovasc. Ther.

Lareu, R.R., Zeugolis, D.I., Abu-Rub, M., Pandit, A., and Raghunath, M. (2010). Essential modification of the Sircol Collagen Assay for the accurate quantification of collagen content in complex protein solutions. Acta Biomater. *6*, 3146–3151.

Lawson, W.E., Crossno, P.F., Polosukhin, V.V., Roldan, J., Cheng, D.-S., Lane, K.B., Blackwell, T.R., Xu, C., Markin, C., Ware, L.B., et al. (2008). Endoplasmic reticulum stress in alveolar epithelial cells is prominent in IPF: association with altered surfactant protein processing and herpesvirus infection. Am. J. Physiol. Lung Cell. Mol. Physiol. *294*, L1119–1126.

Lawson, W.E., Loyd, J.E., and Degryse, A.L. (2011). Genetics in pulmonary fibrosis--familial cases provide clues to the pathogenesis of idiopathic pulmonary fibrosis. Am. J. Med. Sci. *341*, 439–443.

Lee, C.G., Homer, R.J., Zhu, Z., Lanone, S., Wang, X., Koteliansky, V., Shipley, J.M., Gotwals, P., Noble, P., Chen, Q., et al. (2001). Interleukin-13 induces tissue fibrosis by selectively stimulating and activating transforming growth factor beta(1). J. Exp. Med. *194*, 809–821.

Lee, C.G., Cho, S.J., Kang, M.J., Chapoval, S.P., Lee, P.J., Noble, P.W., Yehualaeshet, T., Lu, B., Flavell, R.A., Milbrandt, J., et al. (2004). Early growth response gene 1-

mediated apoptosis is essential for transforming growth factor beta1-induced pulmonary fibrosis. J. Exp. Med. *200*, 377–389.

Leonardi, S., Tricoci, P., White, H.D., Armstrong, P.W., Huang, Z., Wallentin, L., Aylward, P.E., Moliterno, D.J., Van de Werf, F., Chen, E., et al. (2013). Effect of vorapaxar on myocardial infarction in the thrombin receptor antagonist for clinical event reduction in acute coronary syndrome (TRA{middle dot}CER) trial. Eur. Heart J. *34*, 1723–1731.

Ley, B., Collard, H.R., and King, T.E., Jr (2011). Clinical course and prediction of survival in idiopathic pulmonary fibrosis. Am. J. Respir. Crit. Care Med. *183*, 431–440.

Li, M., Abdollahi, A., Gröne, H.-J., Lipson, K.E., Belka, C., and Huber, P.E. (2009). Late treatment with imatinib mesylate ameliorates radiation-induced lung fibrosis in a mouse model. Radiat. Oncol. Lond. Engl. *4*, 66.

Li, M., Krishnaveni, M.S., Li, C., Zhou, B., Xing, Y., Banfalvi, A., Li, A., Lombardi, V., Akbari, O., Borok, Z., et al. (2011). Epithelium-specific deletion of TGF-β receptor type II protects mice from bleomycin-induced pulmonary fibrosis. J. Clin. Invest. *121*, 277–287.

Li, X., Molina-Molina, M., Abdul-Hafez, A., Ramirez, J., Serrano-Mollar, A., Xaubet, A., and Uhal, B.D. (2006). Extravascular sources of lung angiotensin peptide synthesis in idiopathic pulmonary fibrosis. Am. J. Physiol. Lung Cell. Mol. Physiol. *291*, L887–895.

Li, X., Zhuang, J., Rayford, H., Zhang, H., Shu, R., and Uhal, B.D. (2007). Attenuation of bleomycin-induced pulmonary fibrosis by intratracheal administration of antisense oligonucleotides against angiotensinogen mRNA. Curr. Pharm. Des. *13*, 1257–1268.

Liang, C.-L., Chen, J.-L., Hsu, Y.-P.P., Ou, J.T., and Chang, Y.-S. (2002). Epstein-Barr virus BZLF1 gene is activated by transforming growth factor-beta through cooperativity of Smads and c-Jun/c-Fos proteins. J. Biol. Chem. *277*, 23345–23357.

Lieber, M., Todaro, G., Smith, B., Szakal, A., and Nelson-Rees, W. (1976). A continuous tumor-cell line from a human lung carcinoma with properties of type II alveolar epithelial cells. Int. J. Cancer *17*, 62–70.

Lillard, J.W., Boyaka, P.N., Chertov, O., Oppenheim, J.J., and McGhee, J.R. (1999). Mechanisms for induction of acquired host immunity by neutrophil peptide defensins. Proc. Natl. Acad. Sci. *96*, 651–656.

Lin, H., and Trejo, J. (2013). Transactivation of the PAR1-PAR2 heterodimer by thrombin elicits β-arrestin-mediated endosomal signaling. J. Biol. Chem.

Lin, C., Duitman, J., Daalhuisen, J., Ten Brink, M., von der Thüsen, J., van der Poll, T., Borensztajn, K., and Spek, C.A. (2013). Targeting protease activated receptor-1 with P1pal-12 limits bleomycin-induced pulmonary fibrosis. Thorax.

Lin, Y.-M., Hsu, C.-J., Liao, Y.-Y., Chou, M.-C., and Tang, C.-H. (2012). The CCL2/CCR2 axis enhances vascular cell adhesion molecule-1 expression in human synovial fibroblasts. PloS One *7*, e49999.

Liu, J.Y., Sime, P.J., Wu, T., Warshamana, G.S., Pociask, D., Tsai, S.Y., and Brody, A.R. (2001). Transforming growth factor-beta(1) overexpression in tumor necrosis factor-alpha receptor knockout mice induces fibroproliferative lung disease. Am. J. Respir. Cell Mol. Biol. *25*, 3–7.

Liu, X., Das, A.M., Seideman, J., Griswold, D., Afuh, C.N., Kobayashi, T., Abe, S., Fang, Q., Hashimoto, M., Kim, H., et al. (2007). The CC chemokine ligand 2 (CCL2) mediates fibroblast survival through IL-6. Am. J. Respir. Cell Mol. Biol. *37*, 121–128.

Livingston, J.R., Sutherland, M.R., Friedman, H.M., and Pryzdial, E.L.G. (2006). Herpes simplex virus type 1-encoded glycoprotein C contributes to direct coagulation factor X-virus binding. Biochem. J. *393*, 529–535.

Lok, S.S., Stewart, J.P., Kelly, B.G., Hasleton, P.S., and Egan, J.J. (2001). Epstein-Barr virus and wild p53 in idiopathic pulmonary fibrosis. Respir. Med. *95*, 787–791.

Luckhardt, T.R., Coomes, S.M., Trujillo, G., Stoolman, J.S., Vannella, K.M., Bhan, U., Wilke, C.A., Moore, T.A., Toews, G.B., Hogaboam, C., et al. (2011). TLR9-induced interferon β is associated with protection from gammaherpesvirus-induced exacerbation of lung fibrosis. Fibrogenesis Tissue Repair *4*, 18.

Luyt, C.-E., Combes, A., Deback, C., Aubriot-Lorton, M.-H., Nieszkowska, A., Trouillet, J.-L., Capron, F., Agut, H., Gibert, C., and Chastre, J. (2007). Herpes simplex virus lung infection in patients undergoing prolonged mechanical ventilation. Am. J. Respir. Crit. Care Med. *175*, 935–942.

Madhusudhan, T., Wang, H., Straub, B.K., Gröne, E., Zhou, Q., Shahzad, K., Müller-Krebs, S., Schwenger, V., Gerlitz, B., Grinnell, B.W., et al. (2011). Cytoprotective signaling by activated protein C requires protease activated receptor-3 in podocytes. Blood.

Madureira, P.A., Matos, P., Soeiro, I., Dixon, L.K., Simas, J.P., and Lam, E.W.-F. (2005). Murine gamma-herpesvirus 68 latency protein M2 binds to Vav signaling

proteins and inhibits B-cell receptor-induced cell cycle arrest and apoptosis in WEHI-231 B cells. J. Biol. Chem. *280*, 37310–37318.

Magro, C.M., Allen, J., Pope-Harman, A., Waldman, W.J., Moh, P., Rothrauff, S., and Ross, P. (2003). The role of microvascular injury in the evolution of idiopathic pulmonary fibrosis. Am. J. Clin. Pathol. *119*, 556–567.

Magro, C.M., Waldman, W.J., Knight, D.A., Allen, J.N., Nadasdy, T., Frambach, G.E., Ross, P., and Marsh, C.B. (2006). Idiopathic pulmonary fibrosis related to endothelial injury and antiendothelial cell antibodies. Hum. Immunol. *67*, 284–297.

Maher, T.M., Evans, I.C., Bottoms, S.E., Mercer, P.F., Thorley, A.J., Nicholson, A.G., Laurent, G.J., Tetley, T.D., Chambers, R.C., and McAnulty, R.J. (2010). Diminished prostaglandin E2 contributes to the apoptosis paradox in idiopathic pulmonary fibrosis. Am. J. Respir. Crit. Care Med. *182*, 73–82.

Malizia, A.P., Keating, D.T., Smith, S.M., Walls, D., Doran, P.P., and Egan, J.J. (2008). Alveolar epithelial cell injury with Epstein-Barr virus upregulates TGFbeta1 expression. Am. J. Physiol. Lung Cell. Mol. Physiol. *295*, L451–460.

Malizia, A.P., Egan, J.J., and Doran, P.P. (2009a). IL-4 increases CD21-dependent infection of pulmonary alveolar epithelial type II cells by EBV. Mol. Immunol. *46*, 1905–1910.

Malizia, A.P., Lacey, N., Walls, D., Egan, J.J., and Doran, P.P. (2009b). CUX1/Wnt signaling regulates epithelial mesenchymal transition in EBV infected epithelial cells. Exp. Cell Res. *315*, 1819–1831.

Malyala, P., and Singh, M. (2008). Endotoxin limits in formulations for preclinical research. J. Pharm. Sci. *97*, 2041–2044.

Mann, K.G. (1999). Biochemistry and physiology of blood coagulation. Thromb. Haemost. *82*, 165–174.

Mann, K.G. (2003). THrombin formation*. CHEST J. *124*, 4S–10S.

Marchal-Sommé, J., Uzunhan, Y., Marchand-Adam, S., Kambouchner, M., Valeyre, D., Crestani, B., and Soler, P. (2007). Dendritic cells accumulate in human fibrotic interstitial lung disease. Am. J. Respir. Crit. Care Med. *176*, 1007–1014.

Marshall, R.P., McAnulty, R.J., and Laurent, G.J. (2000). Angiotensin II is mitogenic for human lung fibroblasts via activation of the type 1 receptor. Am. J. Respir. Crit. Care Med. *161*, 1999–2004.

MARSHALL, R., BELLINGAN, G., and LAURENT, G. (1998). The acute respiratory distress syndrome: fibrosis in the fast lane. Thorax *53*, 815–817.

Martin, T.R., Hagimoto, N., Nakamura, M., and Matute-Bello, G. (2005). Apoptosis and Epithelial Injury in the Lungs. Proc. Am. Thorac. Soc. *2*, 214–220.

Martinet, Y., Rom, W.N., Grotendorst, G.R., Martin, G.R., and Crystal, R.G. (1987). Exaggerated spontaneous release of platelet-derived growth factor by alveolar macrophages from patients with idiopathic pulmonary fibrosis. N. Engl. J. Med. *317*, 202–209.

Martinez, F.O., Helming, L., and Gordon, S. (2009). Alternative activation of macrophages: an immunologic functional perspective. Annu. Rev. Immunol. *27*, 451–483.

Massague, J. (2000). How cells read TGF-[beta] signals. Nat Rev Mol Cell Biol *1*, 169–178.

Matsuura, I., Wang, G., He, D., and Liu, F. (2005). Identification and characterization of ERK MAP kinase phosphorylation sites in Smad3. Biochemistry (Mosc.) *44*, 12546–12553.

McAnulty, R.J., Chambers, R.C., and Laurent, G.J. (1995). Regulation of fibroblast procollagen production. Transforming growth factor-beta 1 induces prostaglandin E2 but not procollagen synthesis via a pertussis toxin-sensitive G-protein. Biochem. J. *307 (Pt 1)*, 63–68.

McClintock, D., Zhuo, H., Wickersham, N., Matthay, M.A., and Ware, L.B. (2008). Biomarkers of inflammation, coagulation and fibrinolysis predict mortality in acute lung injury. Crit. Care Lond. Engl. *12*, R41.

McCoy, K.L., Traynelis, S.F., and Hepler, J.R. (2010a). PAR1 and PAR2 couple to overlapping and distinct sets of G proteins and linked signaling pathways to differentially regulate cell physiology. Mol. Pharmacol. *77*, 1005–1015.

McCoy, K.L., Traynelis, S.F., and Hepler, J.R. (2010b). PAR1 and PAR2 couple to overlapping and distinct sets of G proteins and linked signaling pathways to differentially regulate cell physiology. Mol. Pharmacol. *77*, 1005–1015.

McCoy, K.L., Gyoneva, S., Vellano, C.P., Smrcka, A.V., Traynelis, S.F., and Hepler, J.R. (2012). Protease-activated receptor 1 (PAR1) coupling to G(q/11) but not to G(i/o) or G(12/13) is mediated by discrete amino acids within the receptor second intracellular loop. Cell. Signal. *24*, 1351–1360.

McLaughlin, J.N., Shen, L., Holinstat, M., Brooks, J.D., Dibenedetto, E., and Hamm, H.E. (2005). Functional selectivity of G protein signaling by agonist peptides and thrombin for the protease-activated receptor-1. J. Biol. Chem. *280*, 25048–25059.

McLaughlin, J.N., Patterson, M.M., and Malik, A.B. (2007). Protease-activated receptor-3 (PAR3) regulates PAR1 signaling by receptor dimerization. Proc. Natl. Acad. Sci. U. S. A. *104*, 5662–5667.

McMillan, T.R., Moore, B.B., Weinberg, J.B., Vannella, K.M., Fields, W.B., Christensen, P.J., van Dyk, L.F., and Toews, G.B. (2008). Exacerbation of established pulmonary fibrosis in a murine model by gammaherpesvirus. Am. J. Respir. Crit. Care Med. *177*, 771–780.

Mercer, P.F., Johns, R.H., Scotton, C.J., Krupiczojc, M.A., Konigshoff, M., Howell, D.C.J., McAnulty, R.J., Das, A., Thorley, A.J., Tetley, T.D., et al. (2009). Pulmonary Epithelium Is a Prominent Source of Proteinase-activated Receptor-1-inducible CCL2 in Pulmonary Fibrosis. Am J Respir Crit Care Med *179*, 414–425.

Mercer, P.F., Williams, A.E., Scotton, C.J., José, R.J., Sulikowski, M., Moffatt, J.D., Murray, L.A., and Chambers, R.C. (2013). Proteinase-Activated Receptor-1, CCL2 and CCL7 Regulate Acute Neutrophilic Lung Inflammation. Am. J. Respir. Cell Mol. Biol.

Miki, H., Mio, T., Nagai, S., Hoshino, Y., Tsutsumi, T., Mikuniya, T., and Izumi, T. (2000). Glucocorticoid-induced contractility and F-actin content of human lung fibroblasts in three-dimensional culture. Am. J. Physiol. Lung Cell. Mol. Physiol. *278*, L13–18.

Mitchell, D., and Olive, C. (2010). Regulation of Toll-like receptor-induced chemokine production in murine dendritic cells by mitogen-activated protein kinases. Mol. Immunol. *47*, 2065–2073.

Moeller, A., Ask, K., Warburton, D., Gauldie, J., and Kolb, M. (2008). The bleomycin animal model: a useful tool to investigate treatment options for idiopathic pulmonary fibrosis? Int. J. Biochem. Cell Biol. *40*, 362–382.

Moers, A., Nieswandt, B., Massberg, S., Wettschureck, N., Grüner, S., Konrad, I., Schulte, V., Aktas, B., Gratacap, M.-P., Simon, M.I., et al. (2003). G13 is an essential mediator of platelet activation in hemostasis and thrombosis. Nat. Med. *9*, 1418–1422.

Molteni, A., Wolfe, L.F., Ward, W.F., Ts'ao, C.H., Molteni, L.B., Veno, P., Fish, B.L., Taylor, J.M., Quintanilla, N., Herndon, B., et al. (2007). Effect of an angiotensin II receptor blocker and two angiotensin converting enzyme inhibitors on transforming

growth factor-beta (TGF-beta) and alpha-actomyosin (alpha SMA), important mediators of radiation-induced pneumopathy and lung fibrosis. Curr. Pharm. Des. *13*, 1307–1316.

Moodley, Y.P., Scaffidi, A.K., Misso, N.L., Keerthisingam, C., McAnulty, R.J., Laurent, G.J., Mutsaers, S.E., Thompson, P.J., and Knight, D.A. (2003). Fibroblasts isolated from normal lungs and those with idiopathic pulmonary fibrosis differ in interleukin-6/gp130-mediated cell signaling and proliferation. Am. J. Pathol. *163*, 345–354.

Moore, B.B., and Hogaboam, C.M. (2008). Murine models of pulmonary fibrosis. Am. J. Physiol. Lung Cell. Mol. Physiol. *294*, L152–160.

Moore, B.B., Paine, R., Christensen, P.J., Moore, T.A., Sitterding, S., Ngan, R., Wilke, C.A., Kuziel, W.A., and Toews, G.B. (2001). Protection from pulmonary fibrosis in the absence of CCR2 signaling. J. Immunol. Baltim. Md 1950 *167*, 4368–4377.

Moore, B.B., Peters-Golden, M., Christensen, P.J., Lama, V., Kuziel, W.A., Paine, R., and Toews, G.B. (2003). Alveolar epithelial cell inhibition of fibroblast proliferation is regulated by MCP-1/CCR2 and mediated by PGE2. Am. J. Physiol. Lung Cell. Mol. Physiol. *284*, L342–349.

Moore, B.B., Ballinger, M.N., White, E.S., Green, M.E., Herrygers, A.B., Wilke, C.A., Toews, G.B., and Peters-Golden, M. (2005a). Bleomycin-induced E prostanoid receptor changes alter fibroblast responses to prostaglandin E2. J. Immunol. Baltim. Md 1950 *174*, 5644–5649.

Moore, B.B., Kolodsick, J.E., Thannickal, V.J., Cooke, K., Moore, T.A., Hogaboam, C., Wilke, C.A., and Toews, G.B. (2005b). CCR2-mediated recruitment of fibrocytes to the alveolar space after fibrotic injury. Am. J. Pathol. *166*, 675–684.

Moore, B.B., Murray, L., Das, A., Wilke, C.A., Herrygers, A.B., and Toews, G.B. (2006). The role of CCL12 in the recruitment of fibrocytes and lung fibrosis. Am. J. Respir. Cell Mol. Biol. *35*, 175–181.

Mora, A.L., Woods, C.R., Garcia, A., Xu, J., Rojas, M., Speck, S.H., Roman, J., Brigham, K.L., and Stecenko, A.A. (2005). Lung infection with gamma-herpesvirus induces progressive pulmonary fibrosis in Th2-biased mice. Am. J. Physiol. Lung Cell. Mol. Physiol. *289*, L711–721.

Mora, A.L., Torres-González, E., Rojas, M., Corredor, C., Ritzenthaler, J., Xu, J., Roman, J., Brigham, K., and Stecenko, A. (2006). Activation of alveolar macrophages via the alternative pathway in herpesvirus-induced lung fibrosis. Am. J. Respir. Cell Mol. Biol. *35*, 466–473.

Mora, A.L., Torres-González, E., Rojas, M., Xu, J., Ritzenthaler, J., Speck, S.H., Roman, J., Brigham, K., and Stecenko, A. (2007). Control of virus reactivation arrests pulmonary herpesvirus-induced fibrosis in IFN-gamma receptor-deficient mice. Am. J. Respir. Crit. Care Med. *175*, 1139–1150.

Morello, S., Vellecco, V., Roviezzo, F., Maffia, P., Cuzzocrea, S., Cirino, G., and Cicala, C. (2005). A protective role for proteinase activated receptor 2 in airways of lipopolysaccharide-treated rats. Biochem. Pharmacol. *71*, 223–230.

Morris, D.G., Huang, X., Kaminski, N., Wang, Y., Shapiro, S.D., Dolganov, G., Glick, A., and Sheppard, D. (2003). Loss of integrin alpha(v)beta6-mediated TGF-beta activation causes Mmp12-dependent emphysema. Nature *422*, 169–173.

Morrow, D.A., Braunwald, E., Bonaca, M.P., Ameriso, S.F., Dalby, A.J., Fish, M.P., Fox, K.A.A., Lipka, L.J., Liu, X., Nicolau, J.C., et al. (2012). Vorapaxar in the Secondary Prevention of Atherothrombotic Events. N. Engl. J. Med. *366*, 1404–1413.

Morrow, D.A., Alberts, M.J., Mohr, J.P., Ameriso, S.F., Bonaca, M.P., Goto, S., Hankey, G.J., Murphy, S.A., Scirica, B.M., Braunwald, E., et al. (2013). Efficacy and safety of vorapaxar in patients with prior ischemic stroke. Stroke J. Cereb. Circ. *44*, 691–698.

Mosnier, L.O., Sinha, R.K., Burnier, L., Bouwens, E.A., and Griffin, J.H. (2012). Biased agonism of protease-activated receptor 1 by activated protein C caused by noncanonical cleavage at Arg46. Blood *120*, 5237–5246.

Muggia, F.M., Louie, A.C., and Sikic, B.I. (1983). Pulmonary toxicity of antitumor agents. Cancer Treat. Rev. *10*, 221–243.

Munger, J.S., Huang, X., Kawakatsu, H., Griffiths, M.J., Dalton, S.L., Wu, J., Pittet, J.F., Kaminski, N., Garat, C., Matthay, M.A., et al. (1999a). The integrin alpha v beta 6 binds and activates latent TGF beta 1: a mechanism for regulating pulmonary inflammation and fibrosis. Cell *96*, 319–328.

Munger, J.S., Huang, X., Kawakatsu, H., Griffiths, M.J., Dalton, S.L., Wu, J., Pittet, J.F., Kaminski, N., Garat, C., Matthay, M.A., et al. (1999b). The integrin alpha v beta 6 binds and activates latent TGF beta 1: a mechanism for regulating pulmonary inflammation and fibrosis. Cell *96*, 319–328.

Mutsaers, S.E., Marshall, R.P., Goldsack, N.R., Laurent, G.J., and McAnulty, R.J. (1998). Effect of endothelin receptor antagonists (BQ-485, Ro 47-0203) on collagen deposition during the development of bleomycin-induced pulmonary fibrosis in rats. Pulm. Pharmacol. Ther. *11*, 221–225.

Naik, P.N., Horowitz, J.C., Moore, T.A., Wilke, C.A., Toews, G.B., and Moore, B.B. (2011). Pulmonary Fibrosis Induced by γ-Herpesvirus in Aged Mice Is Associated With Increased Fibroblast Responsiveness to Transforming Growth Factor-β. J. Gerontol. A. Biol. Sci. Med. Sci.

Nakanishi-Matsui, M., Zheng, Y.W., Sulciner, D.J., Weiss, E.J., Ludeman, M.J., and Coughlin, S.R. (2000). PAR3 is a cofactor for PAR4 activation by thrombin. Nature *404*, 609–613.

Namati, E., Thiesse, J., Sieren, J.C., Ross, A., Hoffman, E.A., and McLennan, G. (2010). Longitudinal assessment of lung cancer progression in the mouse using in vivo micro-CT imaging. Med. Phys. *37*, 4793–4805.

Narayanan, A.S., Whithey, J., Souza, A., and Raghu, G. (1992). Effect of gamma-interferon on collagen synthesis by normal and fibrotic human lung fibroblasts. Chest *101*, 1326–1331.

Nash, A.A., and Sunil-Chandra, N.P. (1994). Interactions of the murine gammaherpesvirus with the immune system. Curr. Opin. Immunol. *6*, 560–563.

Nash, A.A., Dutia, B.M., Stewart, J.P., and Davison, A.J. (2001). Natural history of murine gamma-herpesvirus infection. Philos. Trans. R. Soc. Lond. B. Biol. Sci. *356*, 569–579.

Nash, J.R., McLaughlin, P.J., Butcher, D., and Corrin, B. (1993). Expression of tumour necrosis factor-alpha in cryptogenic fibrosing alveolitis. Histopathology *22*, 343–347.

Neurohr, C., Nishimura, S.L., and Sheppard, D. (2006). Activation of Transforming Growth Factor-? by the Integrin ?v?8 Delays Epithelial Wound Closure. Am. J. Respir. Cell Mol. Biol. *35*, 252–259.

Nguyen, K.T., Eskin, S.G., Patterson, C., Runge, M.S., and McIntire, L.V. (2001). Shear stress reduces protease activated receptor-1 expression in human endothelial cells. Ann. Biomed. Eng. *29*, 145–152.

Nierodzik, M.L., and Karpatkin, S. (2006). Thrombin induces tumor growth, metastasis, and angiogenesis: Evidence for a thrombin-regulated dormant tumor phenotype. Cancer Cell *10*, 355–362.

Nissen, L.J., Cao, R., Hedlund, E.-M., Wang, Z., Zhao, X., Wetterskog, D., Funa, K., Bråkenhielm, E., and Cao, Y. (2007). Angiogenic factors FGF2 and PDGF-BB synergistically promote murine tumor neovascularization and metastasis. J. Clin. Invest. *117*, 2766–2777.

Noble, P.W., Albera, C., Bradford, W.Z., Costabel, U., Glassberg, M.K., Kardatzke, D., King, T.E., Jr, Lancaster, L., Sahn, S.A., Szwarcberg, J., et al. (2011). Pirfenidone in patients with idiopathic pulmonary fibrosis (CAPACITY): two randomised trials. Lancet *377*, 1760–1769.

Noth, I., Anstrom, K.J., Calvert, S.B., de Andrade, J., Flaherty, K.R., Glazer, C., Kaner, R.J., and Olman, M.A. (2012). A Placebo-Controlled Randomized Trial of Warfarin in Idiopathic Pulmonary Fibrosis. Am. J. Respir. Crit. Care Med. *186*, 88–95.

O'Brien, P.J., Prevost, N., Molino, M., Hollinger, M.K., Woolkalis, M.J., Woulfe, D.S., and Brass, L.F. (2000). Thrombin responses in human endothelial cells. Contributions from receptors other than PAR1 include the transactivation of PAR2 by thrombin-cleaved PAR1. J. Biol. Chem. *275*, 13502–13509.

O'Brien, P.J., Molino, M., Kahn, M., and Brass, L.F. (2001). Protease activated receptors: theme and variations. Oncogene *20*, 1570–1581.

O'Donoghue, M.L., Bhatt, D.L., Wiviott, S.D., Goodman, S.G., Fitzgerald, D.J., Angiolillo, D.J., Goto, S., Montalescot, G., Zeymer, U., Aylward, P.E., et al. (2011). Safety and tolerability of atopaxar in the treatment of patients with acute coronary syndromes: the lessons from antagonizing the cellular effects of Thrombin–Acute Coronary Syndromes Trial. Circulation *123*, 1843–1853.

Odeberg, J., and Söderberg-Nauclér, C. (2001). Reduced expression of HLA class II molecules and Iinterleukin-10- and transforming growth factor beta1-independent suppression of T-cell proliferation in human cytomegalovirus-infected macrophage cultures. J. Virol. *75*, 5174–5181.

Ortiz, L.A., Lasky, J., Lungarella, G., Cavarra, E., Martorana, P., Banks, W.A., Peschon, J.J., Schmidts, H.L., Brody, A.R., and Friedman, M. (1999). Upregulation of the p75 but not the p55 TNF-alpha receptor mRNA after silica and bleomycin exposure and protection from lung injury in double receptor knockout mice. Am. J. Respir. Cell Mol. Biol. *20*, 825–833.

Ortiz-Stern, A., Deng, X., Smoktunowicz, N., Mercer, P.F., and Chambers, R.C. (2012). PAR-1-dependent and PAR-independent pro-inflammatory signaling in human lung fibroblasts exposed to thrombin. J. Cell. Physiol. *227*, 3575–3584.

Ostrowska, E., and Reiser, G. (2008). The protease-activated receptor-3 (PAR-3) can signal autonomously to induce interleukin-8 release. Cell. Mol. Life Sci. CMLS *65*, 970–981.

Oussaief, L., Ramírez, V., Hippocrate, A., Arbach, H., Cochet, C., Proust, A., Raphaël, M., Khelifa, R., and Joab, I. (2011). NF-kappaB-mediated modulation of inducible nitric oxide synthase activity controls induction of the Epstein-Barr virus productive cycle by transforming growth factor beta 1. J. Virol. *85*, 6502–6512.

Paing, M.M., Johnston, C.A., Siderovski, D.P., and Trejo, J. (2006). Clathrin adaptor AP2 regulates thrombin receptor constitutive internalization and endothelial cell resensitization. Mol. Cell. Biol. *26*, 3231–3242.

Pan, L.-H., Yamauchi, K., Uzuki, M., Nakanishi, T., Takigawa, M., Inoue, H., and Sawai, T. (2001). Type II alveolar epithelial cells and interstitial fibroblasts express connective tissue growth factor in IPF. Eur. Respir. J. *17*, 1220–1227.

Papadaki, M., Ruef, J., Nguyen, K.T., Li, F., Patterson, C., Eskin, S.G., McIntire, L.V., and Runge, M.S. (1998). Differential regulation of protease activated receptor-1 and tissue plasminogen activator expression by shear stress in vascular smooth muscle cells. Circ. Res. *83*, 1027–1034.

Park, S.H., Saleh, D., Giaid, A., and Michel, R.P. (1997). Increased endothelin-1 in bleomycin-induced pulmonary fibrosis and the effect of an endothelin receptor antagonist. Am. J. Respir. Crit. Care Med. *156*, 600–608.

Patel, R.B., Kotha, S.R., Sherwani, S.I., Sliman, S.M., Gurney, T.O., Loar, B., Butler, S.O., Morris, A.J., Marsh, C.B., and Parinandi, N.L. (2011). Pulmonary fibrosis inducer, bleomycin, causes redox-sensitive activation of phospholipase D and cytotoxicity through formation of bioactive lipid signal mediator, phosphatidic acid, in lung microvascular endothelial cells. Int. J. Toxicol. *30*, 69–90.

Pawlinski, R., and Holinstat, M. (2011). We can do it together: PAR1/PAR2 heterodimer signaling in VSMCs. Arterioscler. Thromb. Vasc. Biol. *31*, 2775–2776.

Peljto, A.L., Zhang, Y., Fingerlin, T.E., Ma, S.-F., Garcia, J.G.N., Richards, T.J., Silveira, L.J., Lindell, K.O., Steele, M.P., Loyd, J.E., et al. (2013). Association between the MUC5B promoter polymorphism and survival in patients with idiopathic pulmonary fibrosis. JAMA J. Am. Med. Assoc. *309*, 2232–2239.

Perrio, M.J., Ewen, D., Trevethick, M.A., Salmon, G.P., and Shute, J.K. (2007). Fibrin formation by wounded bronchial epithelial cell layers in vitro is essential for normal epithelial repair and independent of plasma proteins. Clin. Exp. Allergy *37*, 1688–1700.

Pierce, E.M., Carpenter, K., Jakubzick, C., Kunkel, S.L., Flaherty, K.R., Martinez, F.J., and Hogaboam, C.M. (2007). Therapeutic targeting of CC ligand 21 or CC chemokine

receptor 7 abrogates pulmonary fibrosis induced by the adoptive transfer of human pulmonary fibroblasts to immunodeficient mice. Am. J. Pathol. *170*, 1152–1164.

Pittet, J.F., Griffiths, M.J., Geiser, T., Kaminski, N., Dalton, S.L., Huang, X., Brown, L.A., Gotwals, P.J., Koteliansky, V.E., Matthay, M.A., et al. (2001). TGF-beta is a critical mediator of acute lung injury. J. Clin. Invest. *107*, 1537–1544.

Plataki, M., Koutsopoulos, A.V., Darivianaki, K., Delides, G., Siafakas, N.M., and Bouros, D. (2005). Expression of apoptotic and antiapoptotic markers in epithelial cells in idiopathic pulmonary fibrosis. Chest *127*, 266–274.

Poll, T. van der, Levi, M., Nick, J.A., and Abraham, E. (2005). Activated Protein C Inhibits Local Coagulation after Intrapulmonary Delivery of Endotoxin in Humans. Am. J. Respir. Crit. Care Med. *171*, 1125–1128.

Popović, M., Paskas, S., Zivković, M., Burysek, L., and Laumonnier, Y. (2010). Human cytomegalovirus increases HUVEC sensitivity to thrombin and modulates expression of thrombin receptors. J. Thromb. Thrombolysis *30*, 164–171.

Prasse, A., and Müller-Quernheim, J. (2009). Non-invasive biomarkers in pulmonary fibrosis. Respirol. Carlton Vic *14*, 788–795.

Prasse, A., Pechkovsky, D.V., Toews, G.B., Jungraithmayr, W., Kollert, F., Goldmann, T., Vollmer, E., Müller-Quernheim, J., and Zissel, G. (2006). A Vicious Circle of Alveolar Macrophages and Fibroblasts Perpetuates Pulmonary Fibrosis via CCL18. Am. J. Respir. Crit. Care Med. *173*, 781–792.

Puthawala, K., Hadjiangelis, N., Jacoby, S.C., Bayongan, E., Zhao, Z., Yang, Z., Devitt, M.L., Horan, G.S., Weinreb, P.H., Lukashev, M.E., et al. (2008). Inhibition of Integrin αvβ6, an Activator of Latent Transforming Growth Factor-β, Prevents Radiation-induced Lung Fibrosis. Am. J. Respir. Crit. Care Med. *177*, 82–90.

Rabiet, M.J., Plantier, J.L., Rival, Y., Genoux, Y., Lampugnani, M.G., and Dejana, E. (1996). Thrombin-induced increase in endothelial permeability is associated with changes in cell-to-cell junction organization. Arterioscler. Thromb. Vasc. Biol. *16*, 488–496.

Raghu, G., Brown, K.K., Bradford, W.Z., Starko, K., Noble, P.W., Schwartz, D.A., and King, T.E., Jr (2004). A placebo-controlled trial of interferon gamma-1b in patients with idiopathic pulmonary fibrosis. N. Engl. J. Med. *350*, 125–133.

Raghu, G., Anstrom, K.J., King, T.E., Jr, Lasky, J.A., and Martinez, F.J. (2012). Prednisone, azathioprine, and N-acetylcysteine for pulmonary fibrosis. N. Engl. J. Med. *366*, 1968–1977.

Rahman, A., Anwar, K.N., True, A.L., and Malik, A.B. (1999). Thrombin-Induced p65 Homodimer Binding to Downstream NF-κB Site of the Promoter Mediates Endothelial ICAM-1 Expression and Neutrophil Adhesion. J. Immunol. *162*, 5466 – 5476.

Ramachandran, R., and Hollenberg, M.D. (2008). Proteinases and signalling: pathophysiological and therapeutic implications via PARs and more. Br. J. Pharmacol. *153 Suppl 1*, S263–282.

Ramachandran, R., Sadofsky, L.R., Xiao, Y., Botham, A., Cowen, M., Morice, A.H., and Compton, S.J. (2007). Inflammatory mediators modulate thrombin and cathepsin-G signaling in human bronchial fibroblasts by inducing expression of proteinase-activated receptor-4. Am. J. Physiol. Lung Cell. Mol. Physiol. *292*, L788–798.

Rao, L.V.M., Kothari, H., and Pendurthi, U.R. (2012). Tissue Factor encryption and decryption: Facts and controversies. Thromb. Res. *129, Supplement 2*, S13–S17.

Reichenberger, F., Schauer, J., Kellner, K., Sack, U., Stiehl, P., and Winkler, J. (2001). Different expression of endothelin in the bronchoalveolar lavage in patients with pulmonary diseases. Lung *179*, 163–174.

Renzoni, E.A., Walsh, D.A., Salmon, M., Wells, A.U., Sestini, P., Nicholson, A.G., Veeraraghavan, S., Bishop, A.E., Romanska, H.M., Pantelidis, P., et al. (2003). Interstitial vascularity in fibrosing alveolitis. Am. J. Respir. Crit. Care Med. *167*, 438–443.

Ribeiro, C.M.P. (2011). Measurements of intracellular calcium signals in polarized primary cultures of normal and cystic fibrosis human airway epithelia. Methods Mol. Biol. Clifton NJ *742*, 113–126.

Richards, T.J., Kaminski, N., Baribaud, F., Flavin, S., Brodmerkel, C., Horowitz, D., Li, K., Choi, J., Vuga, L.J., Lindell, K.O., et al. (2012). Peripheral blood proteins predict mortality in idiopathic pulmonary fibrosis. Am. J. Respir. Crit. Care Med. *185*, 67–76.

Richeldi, L., Costabel, U., Selman, M., Kim, D.S., Hansell, D.M., Nicholson, A.G., Brown, K.K., Flaherty, K.R., Noble, P.W., Raghu, G., et al. (2011). Efficacy of a tyrosine kinase inhibitor in idiopathic pulmonary fibrosis. N. Engl. J. Med. *365*, 1079–1087.

Riewald, M., and Ruf, W. (2001). Mechanistic coupling of protease signaling and initiation of coagulation by tissue factor. Proc. Natl. Acad. Sci. U. S. A. *98*, 7742–7747.

Riewald, M., and Ruf, W. (2005). Protease-activated receptor-1 signaling by activated protein C in cytokine-perturbed endothelial cells is distinct from thrombin signaling. J. Biol. Chem. *280*, 19808–19814.

Riewald, M., Kravchenko, V.V., Petrovan, R.J., O'Brien, P.J., Brass, L.F., Ulevitch, R.J., and Ruf, W. (2001). Gene induction by coagulation factor Xa is mediated by activation of protease-activated receptor 1. Blood *97*, 3109–3116.

Rivers, R.P.A., Hathaway, W.E., and Weston, W.L. (1975). The Endotoxin-induced Coagulant Activity of Human Monocytes. Br. J. Haematol. *30*, 311–316.

Rock, J.R., Barkauskas, C.E., Cronce, M.J., Xue, Y., Harris, J.R., Liang, J., Noble, P.W., and Hogan, B.L.M. (2011). Multiple stromal populations contribute to pulmonary fibrosis without evidence for epithelial to mesenchymal transition. Proc. Natl. Acad. Sci. U. S. A.

Rodt, T., von Falck, C., Dettmer, S., Halter, R., Maus, R., Ask, K., Kolb, M., Gauldie, J., Länger, F., Hoy, L., et al. (2010). Micro-computed tomography of pulmonary fibrosis in mice induced by adenoviral gene transfer of biologically active transforming growth factor-β1. Respir. Res. *11*, 181.

Rosas, I.O., Ren, P., Avila, N.A., Chow, C.K., Franks, T.J., Travis, W.D., McCoy, J.P., May, R.M., Wu, H.-P., Nguyen, D.M., et al. (2007). Early Interstitial Lung Disease in Familial Pulmonary Fibrosis. Am. J. Respir. Crit. Care Med. *176*, 698–705.

Rosenbloom, J., Feldman, G., Freundlich, B., and Jimenez, S.A. (1984). Transcriptional control of human diploid fibroblast collagen synthesis by γ-interferon. Biochem. Biophys. Res. Commun. *123*, 365–372.

Ruf, W. (2012). Role of thiol pathways in TF procoagulant regulation. Thromb. Res. *129, Supplement 2*, S11–S12.

Rullier, A., Gillibert-Duplantier, J., Costet, P., Cubel, G., Haurie, V., Petibois, C., Taras, D., Dugot-Senant, N., Deleris, G., Bioulac-Sage, P., et al. (2008). Protease-activated receptor 1 knockout reduces experimentally induced liver fibrosis. Am. J. Physiol. Gastrointest. Liver Physiol. *294*, G226–235.

Russo, A., Soh, U.J.K., Paing, M.M., Arora, P., and Trejo, J. (2009a). Caveolae are required for protease-selective signaling by protease-activated receptor-1. Proc. Natl. Acad. Sci. U. S. A. *106*, 6393–6397.

Russo, A., Soh, U.J.K., and Trejo, J. (2009b). Proteases display biased agonism at protease-activated receptors: location matters! Mol. Interv. *9*, 87–96.

Salah, Z., Maoz, M., Pizov, G., and Bar-Shavit, R. (2007). Transcriptional regulation of human protease-activated receptor 1: a role for the early growth response-1 protein in prostate cancer. Cancer Res. *67*, 9835–9843.

Salah, Z., Haupt, S., Maoz, M., Baraz, L., Rotter, V., Peretz, T., Haupt, Y., and Bar-Shavit, R. (2008). p53 controls hPar1 function and expression. Oncogene *27*, 6866–6874.

Saleh, D., Furukawa, K., Tsao, M.S., Maghazachi, A., Corrin, B., Yanagisawa, M., Barnes, P.J., and Giaid, A. (1997). Elevated expression of endothelin-1 and endothelin-converting enzyme-1 in idiopathic pulmonary fibrosis: possible involvement of proinflammatory cytokines. Am. J. Respir. Cell Mol. Biol. *16*, 187–193.

Samarakoon, R., Overstreet, J.M., and Higgins, P.J. (2013). TGF-β signaling in tissue fibrosis: Redox controls, target genes and therapeutic opportunities. Cell. Signal. *25*, 264–268.

Santana, A., Saxena, B., Noble, N.A., Gold, L.I., and Marshall, B.C. (1995). Increased expression of transforming growth factor beta isoforms (beta 1, beta 2, beta 3) in bleomycin-induced pulmonary fibrosis. Am. J. Respir. Cell Mol. Biol. *13*, 34–44.

Schmidlin, F., Amadesi, S., Dabbagh, K., Lewis, D.E., Knott, P., Bunnett, N.W., Gater, P.R., Geppetti, P., Bertrand, C., and Stevens, M.E. (2002). Protease-Activated Receptor 2 Mediates Eosinophil Infiltration and Hyperreactivity in Allergic Inflammation of the Airway. J. Immunol. *169*, 5315–5321.

Schuepbach, R.A., Feistritzer, C., Brass, L.F., and Riewald, M. (2008). Activated protein C-cleaved protease activated receptor-1 is retained on the endothelial cell surface even in the presence of thrombin. Blood *111*, 2667–2673.

Schuepbach, R.A., Feistritzer, C., Fernández, J.A., Griffin, J.H., and Riewald, M. (2009). Protection of vascular barrier integrity by activated protein C in murine models depends on protease-activated receptor-1. Thromb. Haemost. *101*, 724–733.

Scotton, C.J., and Chambers, R.C. (2007). Molecular targets in pulmonary fibrosis: the myofibroblast in focus. Chest *132*, 1311–1321.

Scotton, C.J., Krupiczojc, M.A., Königshoff, M., Mercer, P.F., Lee, Y.C.G., Kaminski, N., Morser, J., Post, J.M., Maher, T.M., Nicholson, A.G., et al. (2009). Increased local expression of coagulation factor X contributes to the fibrotic response in human and murine lung injury. J Clin Invest *119*, 2550–2563.

Scotton, C.J., Hayes, B., Alexander, R., Datta, A., Forty, E.J., Mercer, P.F., Blanchard, A., and Chambers, R.C. (2013). Ex vivo μCT analysis of bleomycin-induced lung fibrosis for pre-clinical drug evaluation. Eur. Respir. J. Off. J. Eur. Soc. Clin. Respir. Physiol.

Seeger, W., Elssner, A., Günther, A., Krämer, H.J., and Kalinowski, H.O. (1993). Lung surfactant phospholipids associate with polymerizing fibrin: loss of surface activity. Am. J. Respir. Cell Mol. Biol. *9*, 213–220.

Seibold, M.A., Wise, A.L., Speer, M.C., Steele, M.P., Brown, K.K., Loyd, J.E., Fingerlin, T.E., Zhang, W., Gudmundsson, G., Groshong, S.D., et al. (2011). A Common MUC5B Promoter Polymorphism and Pulmonary Fibrosis. N. Engl. J. Med. *364*, 1503–1512.

Sempowski, G.D., Beckmann, M.P., Derdak, S., and Phipps, R.P. (1994). Subsets of murine lung fibroblasts express membrane-bound and soluble IL-4 receptors. Role of IL-4 in enhancing fibroblast proliferation and collagen synthesis. J. Immunol. Baltim. Md 1950 *152*, 3606–3614.

Sevastos, J., Kennedy, S.E., Davis, D.R., Sam, M., Peake, P.W., Charlesworth, J.A., Mackman, N., and Erlich, J.H. (2007). Tissue factor deficiency and PAR-1 deficiency are protective against renal ischemia reperfusion injury. Blood *109*, 577–583.

Shahar, I., Fireman, E., Topilsky, M., Grief, J., Schwarz, Y., Kivity, S., Ben-Efraim, S., and Spirer, Z. (1999). Effect of endothelin-1 on alpha-smooth muscle actin expression and on alveolar fibroblasts proliferation in interstitial lung diseases. Int. J. Immunopharmacol. *21*, 759–775.

Sheppard, D. (2005). Integrin-mediated activation of latent transforming growth factor beta. Cancer Metastasis Rev. *24*, 395–402.

Shi-wen, X., Howat, S.L., Renzoni, E.A., Holmes, A., Pearson, J.D., Dashwood, M.R., Bou-Gharios, G., Denton, C.P., Bois, R.M. du, Black, C.M., et al. (2004). Endothelin-1 Induces Expression of Matrix-associated Genes in Lung Fibroblasts through MEK/ERK. J. Biol. Chem. *279*, 23098–23103.

Shull, M.M., Ormsby, I., Kier, A.B., Pawlowski, S., Diebold, R.J., Yin, M., Allen, R., Sidman, C., Proetzel, G., and Calvin, D. (1992). Targeted disruption of the mouse transforming growth factor-beta 1 gene results in multifocal inflammatory disease. Nature *359*, 693–699.

Sides, M.D., Klingsberg, R.C., Shan, B., Gordon, K.A., Nguyen, H.T., Lin, Z., Takahashi, T., Flemington, E.K., and Lasky, J.A. (2010). The Epstein-Barr Virus LMP 1 and TGF-

{beta}1 Synergistically Induce EMT in Lung Epithelial Cells. Am. J. Respir. Cell Mol. Biol.

Sides, M.D., Klingsberg, R.C., Shan, B., Gordon, K.A., Nguyen, H.T., Lin, Z., Takahashi, T., Flemington, E.K., and Lasky, J.A. (2011). The Epstein-Barr virus latent membrane protein 1 and transforming growth factor--β1 synergistically induce epithelial--mesenchymal transition in lung epithelial cells. Am. J. Respir. Cell Mol. Biol. *44*, 852–862.

Sikic, B.I., Young, D.M., Mimnaugh, E.G., and Gram, T.E. (1978). Quantification of Bleomycin Pulmonary Toxicity in Mice by Changes in Lung Hydroxyproline Content and Morphometric Histopathology. Cancer Res. *38*, 787–792.

Sime, P.J., Marr, R.A., Gauldie, D., Xing, Z., Hewlett, B.R., Graham, F.L., and Gauldie, J. (1998). Transfer of tumor necrosis factor-alpha to rat lung induces severe pulmonary inflammation and patchy interstitial fibrogenesis with induction of transforming growth factor-beta1 and myofibroblasts. Am. J. Pathol. *153*, 825–832.

Simonson, M.S., and Ismail-Beigi, F. (2011). Endothelin-1 increases collagen accumulation in renal mesangial cells by stimulating a chemokine and cytokine autocrine signaling loop. J. Biol. Chem. *286*, 11003–11008.

Sisson, T.H., Mendez, M., Choi, K., Subbotina, N., Courey, A., Cunningham, A., Dave, A., Engelhardt, J.F., Liu, X., White, E.S., et al. (2010). Targeted injury of type II alveolar epithelial cells induces pulmonary fibrosis. Am. J. Respir. Crit. Care Med. *181*, 254–263.

Slofstra, S.H., Bijlsma, M.F., Groot, A.P., Reitsma, P.H., Lindhout, T., Cate, H. ten, and Spek, C.A. (2007). Protease-activated receptor-4 inhibition protects from multiorgan failure in a murine model of systemic inflammation. Blood *110*, 3176–3182.

Soifer, S.J., Peters, K.G., O'Keefe, J., and Coughlin, S.R. (1994). Disparate temporal expression of the prothrombin and thrombin receptor genes during mouse development. Am. J. Pathol. *144*, 60–69.

Sokolova, E., Grishina, Z., Bühling, F., Welte, T., and Reiser, G. (2005). Protease-activated receptor-1 in human lung fibroblasts mediates a negative feedback downregulation via prostaglandin E2. Am. J. Physiol. Lung Cell. Mol. Physiol. *288*, L793–802.

Sokolova, E., Hartig, R., and Reiser, G. (2008). Downregulation of protease-activated receptor-1 in human lung fibroblasts is specifically mediated by the prostaglandin E receptor EP2 through cAMP elevation and protein kinase A. FEBS J. *275*, 3669–3679.

Song, J.W., Hong, S.-B., Lim, C.-M., Koh, Y., and Kim, D.S. (2011). Acute exacerbation of idiopathic pulmonary fibrosis: incidence, risk factors and outcome. Eur. Respir. J. *37*, 356–363.

Song, Q., Schmidt, A.G., Hahn, H.S., Carr, A.N., Frank, B., Pater, L., Gerst, M., Young, K., Hoit, B.D., McConnell, B.K., et al. (2003). Rescue of cardiomyocyte dysfunction by phospholamban ablation does not prevent ventricular failure in genetic hypertrophy. J. Clin. Invest. *111*, 859–867.

Soto, A.G., and Trejo, J. (2010). N-linked glycosylation of protease-activated receptor-1 second extracellular loop: a critical determinant for ligand-induced receptor activation and internalization. J. Biol. Chem. *285*, 18781–18793.

De Souza Brito, F., and Tricoci, P. (2013). Novel anti-platelet agents: focus on thrombin receptor antagonists. J Cardiovasc. Transl. Res. *6*, 415–424.

Steele, M.P., Speer, M.C., Loyd, J.E., Brown, K.K., Herron, A., Slifer, S.H., Burch, L.H., Wahidi, M.M., Phillips, J.A., Sporn, T.A., et al. (2005). Clinical and Pathologic Features of Familial Interstitial Pneumonia. Am. J. Respir. Crit. Care Med. *172*, 1146–1152.

Steinberg, S.F., Robinson, R.B., Lieberman, H.B., Stern, D.M., and Rosen, M.R. (1991). Thrombin modulates phosphoinositide metabolism, cytosolic calcium, and impulse initiation in the heart. Circ. Res. *68*, 1216–1229.

Steinhoff, M., Buddenkotte, J., Shpacovitch, V., Rattenholl, A., Moormann, C., Vergnolle, N., Luger, T.A., and Hollenberg, M.D. (2005). Proteinase-activated receptors: transducers of proteinase-mediated signaling in inflammation and immune response. Endocr. Rev. *26*, 1–43.

Stewart, J.P., Egan, J.J., Ross, A.J., Kelly, B.G., Lok, S.S., Hasleton, P.S., and Woodcock, A.A. (1999). The detection of Epstein-Barr virus DNA in lung tissue from patients with idiopathic pulmonary fibrosis. Am. J. Respir. Crit. Care Med. *159*, 1336–1341.

Stoolman, J.S., Vannella, K.M., Coomes, S.M., Wilke, C.A., Sisson, T.H., Toews, G.B., and Moore, B.B. (2010). Latent Infection by Gammaherpesvirus Stimulates Pro-fibrotic Mediator Release from Multiple Cell Types. Am. J. Physiol. Lung Cell. Mol. Physiol.

Strieter, R.M., and Mehrad, B. (2009). New Mechanisms of Pulmonary Fibrosis. Chest *136*, 1364–1370.

Strieter, R.M., Starko, K.M., Enelow, R.I., Noth, I., and Valentine, V.G. (2004). Effects of interferon-gamma 1b on biomarker expression in patients with idiopathic pulmonary fibrosis. Am. J. Respir. Crit. Care Med. *170*, 133–140.

Suen, J.Y., Barry, G.D., Lohman, R.J., Halili, M.A., Cotterell, A.J., Le, G.T., and Fairlie, D.P. (2012). Modulating human proteinase activated receptor 2 with a novel antagonist (GB88) and agonist (GB110). Br. J. Pharmacol. *165*, 1413–1423.

Suga, M., Iyonaga, K., Ichiyasu, H., Saita, N., Yamasaki, H., and Ando, M. (1999). Clinical significance of MCP-1 levels in BALF and serum in patients with interstitial lung diseases. Eur. Respir. J. *14*, 376–382.

Suganuma, H., Sato, A., Tamura, R., and Chida, K. (1995). Enhanced migration of fibroblasts derived from lungs with fibrotic lesions. Thorax *50*, 984–989.

Sullivan, D.E., Ferris, M., Nguyen, H., Abboud, E., and Brody, A.R. (2009). TNF-alpha induces TGF-beta1 expression in lung fibroblasts at the transcriptional level via AP-1 activation. J. Cell. Mol. Med. *13*, 1866–1876.

Sun, L., Louie, M.C., Vannella, K.M., Wilke, C.A., LeVine, A.M., Moore, B.B., and Shanley, T.P. (2011). New concepts of IL-10-induced lung fibrosis: fibrocyte recruitment and M2 activation in a CCL2/CCR2 axis. Am. J. Physiol. Lung Cell. Mol. Physiol. *300*, L341–353.

Sun, Q., Matta, H., Lu, G., and Chaudhary, P.M. (2006). Induction of IL-8 expression by human herpesvirus 8 encoded vFLIP K13 via NF-κB activation. Oncogene *25*, 2717–2726.

Sutherland, M.R., Raynor, C.M., Leenknegt, H., Wright, J.F., and Pryzdial, E.L. (1997). Coagulation initiated on herpesviruses. Proc. Natl. Acad. Sci. U. S. A. *94*, 13510–13514.

Sutherland, M.R., Friedman, H.M., and Pryzdial, E.L.G. (2007). Thrombin enhances herpes simplex virus infection of cells involving protease-activated receptor 1. J. Thromb. Haemost. JTH *5*, 1055–1061.

Swift, S., Leger, A.J., Talavera, J., Zhang, L., Bohm, A., and Kuliopulos, A. (2006). Role of the PAR1 receptor 8th helix in signaling: the 7-8-1 receptor activation mechanism. J. Biol. Chem. *281*, 4109–4116.

Swigris, J.J., Olson, A.L., Huie, T.J., Fernandez-Perez, E.R., Solomon, J., Sprunger, D., and Brown, K.K. (2012). Ethnic and racial differences in the presence of idiopathic pulmonary fibrosis at death. Respir. Med. *106*, 588–593.

Tabata, T., Kawakatsu, H., Maidji, E., Sakai, T., Sakai, K., Fang-Hoover, J., Aiba, M., Sheppard, D., and Pereira, L. (2008). Induction of an epithelial integrin alphavbeta6 in human cytomegalovirus-infected endothelial cells leads to activation of transforming growth factor-beta1 and increased collagen production. Am. J. Pathol. *172*, 1127–1140.

Tang, Y.-W., Johnson, J.E., Browning, P.J., Cruz-Gervis, R.A., Davis, A., Graham, B.S., Brigham, K.L., Oates, J.A., Jr, Loyd, J.E., and Stecenko, A.A. (2003). Herpesvirus DNA is consistently detected in lungs of patients with idiopathic pulmonary fibrosis. J. Clin. Microbiol. *41*, 2633–2640.

Tellez, C., McCarty, M., Ruiz, M., and Bar-Eli, M. (2003). Loss of activator protein-2alpha results in overexpression of protease-activated receptor-1 and correlates with the malignant phenotype of human melanoma. J. Biol. Chem. *278*, 46632–46642.

Thiesse, J., Namati, E., Sieren, J.C., Smith, A.R., Reinhardt, J.M., Hoffman, E.A., and McLennan, G. (2010). Lung structure phenotype variation in inbred mouse strains revealed through in vivo micro-CT imaging. J. Appl. Physiol. Bethesda Md 1985 *109*, 1960–1968.

Thomas, D., Yang, H., Boffa, D.J., Ding, R., Sharma, V.K., Lagman, M., Li, B., Hering, B., Mohanakumar, T., Lakey, J., et al. (2002). Proapoptotic Bax is hyperexpressed in isolated human islets compared with antiapoptotic Bcl-2. Transplantation *74*, 1489–1496.

Thomas, G.J., Nyström, M.L., and Marshall, J.F. (2006). Alphavbeta6 integrin in wound healing and cancer of the oral cavity. J. Oral Pathol. Med. Off. Publ. Int. Assoc. Oral Pathol. Am. Acad. Oral Pathol. *35*, 1–10.

Tiruppathi, C., Minshall, R.D., Paria, B.C., Vogel, S.M., and Malik, A.B. (2002). Role of Ca2+ signaling in the regulation of endothelial permeability. Vascul. Pharmacol. *39*, 173–185.

Torres-González, E., Bueno, M., Tanaka, A., Krug, L.T., Cheng, D.-S., Polosukhin, V.V., Sorescu, D., Lawson, W.E., Blackwell, T.S., Rojas, M., et al. (2012). Role of endoplasmic reticulum stress in age-related susceptibility to lung fibrosis. Am. J. Respir. Cell Mol. Biol. *46*, 748–756.

Trejo, J., Connolly, A.J., and Coughlin, S.R. (1996). The cloned thrombin receptor is necessary and sufficient for activation of mitogen-activated protein kinase and mitogenesis in mouse lung fibroblasts. Loss of responses in fibroblasts from receptor knockout mice. J. Biol. Chem. *271*, 21536–21541.

Trejo, J., Hammes, S.R., and Coughlin, S.R. (1998). Termination of signaling by protease-activated receptor-1 is linked to lysosomal sorting. Proc. Natl. Acad. Sci. U. S. A. *95*, 13698–13702.

Tricoci, P., Huang, Z., Held, C., Moliterno, D.J., Armstrong, P.W., Van de Werf, F., White, H.D., Aylward, P.E., Wallentin, L., Chen, E., et al. (2012). Thrombin-receptor antagonist vorapaxar in acute coronary syndromes. N. Engl. J. Med. *366*, 20–33.

Troyanovsky, B., Alvarez, D.F., King, J.A., and Schaphorst, K.L. (2008). Thrombin enhances the barrier function of rat microvascular endothelium in a PAR-1-dependent manner. Am. J. Physiol. Lung Cell. Mol. Physiol. *294*, L266–275.

Tsukamoto, K., Hayakawa, H., Sato, A., Chida, K., Nakamura, H., and Miura, K. (2000). Involvement of Epstein-Barr virus latent membrane protein 1 in disease progression in patients with idiopathic pulmonary fibrosis. Thorax *55*, 958–961.

Uguccioni, M., Pulsatelli, L., Grigolo, B., Facchini, A., Fasano, L., Cinti, C., Fabbri, M., Gasbarrini, G., and Meliconi, R. (1995). Endothelin-1 in idiopathic pulmonary fibrosis. J. Clin. Pathol. *48*, 330–334.

Uh, S.-T., Kim, T.-H., Shim, E.-Y., Jang, A.-S., Park, S.-W., Park, J.-S., Park, B.-L., Choi, B.W., Shin, H.D., Kim, D.S., et al. (2013). Angiotensin-Converting Enzyme (ACE) Gene Polymorphisms are Associated with Idiopathic Pulmonary Fibrosis. Lung *191*, 345–351.

Uhal, B.D., Joshi, I., Hughes, W.F., Ramos, C., Pardo, A., and Selman, M. (1998). Alveolar epithelial cell death adjacent to underlying myofibroblasts in advanced fibrotic human lung. Am. J. Physiol. - Lung Cell. Mol. Physiol. *275*, L1192–L1199.

Uhal, B.D., Kim, J.K., Li, X., and Molina-Molina, M. (2007). Angiotensin-TGF-beta 1 crosstalk in human idiopathic pulmonary fibrosis: autocrine mechanisms in myofibroblasts and macrophages. Curr. Pharm. Des. *13*, 1247–1256.

Ulloa, L., Doody, J., and Massagué, J. (1999). Inhibition of transforming growth factor-β/SMAD signalling by the interferon-γ/STAT pathway. Nature *397*, 710–713.

Usuki, J., and Fukuda, Y. (1995). Evolution of three patterns of intra-alveolar fibrosis produced by bleomycin in rats. Pathol. Int. *45*, 552–564.

Vaidehi, N., and Kenakin, T. (2010). The role of conformational ensembles of seven transmembrane receptors in functional selectivity. Curr. Opin. Pharmacol. *10*, 775–781.

Vannella, K.M., and Moore, B.B. (2008). Viruses as co-factors for the initiation or exacerbation of lung fibrosis. Fibrogenesis Tissue Repair *1*, 2.

Vannella, K.M., Luckhardt, T.R., Wilke, C.A., van Dyk, L.F., Toews, G.B., and Moore, B.B. (2010a). Latent herpesvirus infection augments experimental pulmonary fibrosis. Am. J. Respir. Crit. Care Med. *181*, 465–477.

Vannella, K.M., Luckhardt, T.R., Wilke, C.A., van Dyk, L.F., Toews, G.B., and Moore, B.B. (2010b). Latent herpesvirus infection augments experimental pulmonary fibrosis. Am. J. Respir. Crit. Care Med. *181*, 465–477.

Varga, J., Olsen, A., Herhal, J., Constantine, G., Rosenbloom, J., and Jimenez, S.A. (1990). Interferon-γ reverses the stimulation of collagen but not fibronectin gene expression by transforming growth factor-β in normal human fibroblasts. Eur. J. Clin. Invest. *20*, 487–493.

Vasilescu, D.M., Knudsen, L., Ochs, M., Weibel, E.R., and Hoffman, E.A. (2012). Optimized murine lung preparation for detailed structural evaluation via micro-computed tomography. J. Appl. Physiol. Bethesda Md 1985 *112*, 159–166.

Velden, V.H., and Versnel, H.F. (1998). Bronchial epithelium: morphology, function and pathophysiology in asthma. Eur. Cytokine Netw. *9*, 585–597.

Vergnon, J.M., Vincent, M., de Thé, G., Mornex, J.F., Weynants, P., and Brune, J. (1984). Cryptogenic fibrosing alveolitis and Epstein-Barr virus: an association? Lancet *2*, 768–771.

Verrall, S., Ishii, M., Chen, M., Wang, L., Tram, T., and Coughlin, S.R. (1997). The thrombin receptor second cytoplasmic loop confers coupling to Gq-like G proteins in chimeric receptors. Additional evidence for a common transmembrane signaling and G protein coupling mechanism in G protein-coupled receptors. J. Biol. Chem. *272*, 6898–6902.

Vidwan, P., Pathak, A., Sheth, S., Huang, J., Monroe, D.M., and Stouffer, G.A. (2010). Activation of protease-activated receptors 3 and 4 accelerates tissue factor-induced thrombin generation on the surface of vascular smooth muscle cells. Arterioscler. Thromb. Vasc. Biol. *30*, 2587–2596.

Vuorinen, K., Gao, F., Oury, T.D., Kinnula, V.L., and Myllärniemi, M. (2007). Imatinib mesylate inhibits fibrogenesis in asbestos-induced interstitial pneumonia. Exp. Lung Res. *33*, 357–373.

Walz, D.A., Anderson, G.F., Ciaglowski, R.E., Aiken, M., and Fenton, J.W. (1985). Thrombin-elicited contractile responses of aortic smooth muscle. Proc. Soc. Exp. Biol. Med. Soc. Exp. Biol. Med. N. Y. N *180*, 518–526.

Wang, A., Yokosaki, Y., Ferrando, R., Balmes, J., and Sheppard, D. (1996). Differential regulation of airway epithelial integrins by growth factors. Am. J. Respir. Cell Mol. Biol. *15*, 664–672.

Wang, R., Zagariya, A., Ibarra-Sunga, O., Gidea, C., Ang, E., Deshmukh, S., Chaudhary, G., Baraboutis, J., Filippatos, G., and Uhal, B.D. (1999). Angiotensin II induces apoptosis in human and rat alveolar epithelial cells. Am. J. Physiol. *276*, L885–889.

Wang, R., Ibarra-Sunga, O., Verlinski, L., Pick, R., and Uhal, B.D. (2000). Abrogation of bleomycin-induced epithelial apoptosis and lung fibrosis by captopril or by a caspase inhibitor. Am. J. Physiol. Lung Cell. Mol. Physiol. *279*, L143–151.

Wang, X., Gao, X.-H., Li, X., Hong, Y., Qi, R., Chen, H.-D., Zhang, L., and Wei, H. (2009). Local hyperthermia induces apoptosis of keratinocytes in both normal skin and condyloma acuminata via different pathways. Apoptosis Int. J. Program. Cell Death *14*, 721–728.

Ware, L.B., Matthay, M.A., Parsons, P.E., Thompson, B.T., Januzzi, J.L., and Eisner, M.D. (2007). Pathogenetic and prognostic significance of altered coagulation and fibrinolysis in acute lung injury/acute respiratory distress syndrome. Crit. Care Med. *35*, 1821–1828.

WARE, L.B., and MATTHAY, M.A. (2001). Alveolar Fluid Clearance Is Impaired in the Majority of Patients with Acute Lung Injury and the Acute Respiratory Distress Syndrome. Am J Respir Crit Care Med *163*, 1376–1383.

Weck, K.E., Dal Canto, A.J., Gould, J.D., O'Guin, A.K., Roth, K.A., Saffitz, J.E., Speck, S.H., and Virgin, H.W. (1997). Murine gamma-herpesvirus 68 causes severe large-vessel arteritis in mice lacking interferon-gamma responsiveness: a new model for virus-induced vascular disease. Nat. Med. *3*, 1346–1353.

Welty-Wolf, K.E., Carraway, M.S., Ortel, T.L., Ghio, A.J., Idell, S., Egan, J., Zhu, X., Jiao, J., Wong, H.C., and Piantadosi, C.A. (2006). Blockade of tissue factor-factor X binding attenuates sepsis-induced respiratory and renal failure. Am. J. Physiol. - Lung Cell. Mol. Physiol. *290*, L21–L31.

Wennerberg, K., Rossman, K.L., and Der, C.J. (2005). The Ras superfamily at a glance. J. Cell Sci. *118*, 843–846.

Wetering, S.V., Mannesse-Lazeroms, S.P., Sterkenburg, M.A.V., Daha, M.R., Dijkman, J.H., and Hiemstra, P.S. (1997). Effect of defensins on interleukin-8 synthesis in airway epithelial cells. Am. J. Physiol. - Lung Cell. Mol. Physiol. *272*, L888–L896.

Williams, K.J., Maes, R., Del Piero, F., Lim, A., Wise, A., Bolin, D.C., Caswell, J., Jackson, C., Robinson, N.E., Derksen, F., et al. (2007). Equine multinodular pulmonary fibrosis: a newly recognized herpesvirus-associated fibrotic lung disease. Vet. Pathol. *44*, 849–862.

Willis, B.C., Liebler, J.M., Luby-Phelps, K., Nicholson, A.G., Crandall, E.D., du Bois, R.M., and Borok, Z. (2005). Induction of epithelial-mesenchymal transition in alveolar epithelial cells by transforming growth factor-beta1: potential role in idiopathic pulmonary fibrosis. Am. J. Pathol. *166*, 1321–1332.

Wilson, M.S., and Wynn, T.A. (2009). Pulmonary fibrosis: pathogenesis, etiology and regulation. Mucosal Immunol. *2*, 103–121.

Wipff, P.-J., and Hinz, B. (2008). Integrins and the activation of latent transforming growth factor beta1 - an intimate relationship. Eur. J. Cell Biol. *87*, 601–615.

Wiviott, S.D., Flather, M.D., O'Donoghue, M.L., Goto, S., Fitzgerald, D.J., Cura, F., Aylward, P., Guetta, V., Dudek, D., Contant, C.F., et al. (2011). Randomized trial of atopaxar in the treatment of patients with coronary artery disease: the lessons from antagonizing the cellular effect of Thrombin–Coronary Artery Disease Trial. Circulation *123*, 1854–1863.

Wolfe, B.L., Marchese, A., and Trejo, J. (2007). Ubiquitination differentially regulates clathrin-dependent internalization of protease-activated receptor-1. J. Cell Biol. *177*, 905–916.

Wootton, S.C., Kim, D.S., Kondoh, Y., Chen, E., Lee, J.S., Song, J.W., Huh, J.W., Taniguchi, H., Chiu, C., Boushey, H., et al. (2011). Viral infection in acute exacerbation of idiopathic pulmonary fibrosis. Am. J. Respir. Crit. Care Med. *183*, 1698–1702.

Wuyts, W.A., Agostini, C., Antoniou, K., Bouros, D., Chambers, R., Cottin, V., Egan, J., Lambrecht, B., Lories, R., Parfrey, H., et al. (2012). The pathogenesis of pulmonary fibrosis: a moving target. Eur. Respir. J. Off. J. Eur. Soc. Clin. Respir. Physiol.

Wygrecka, M., Kwapiszewska, G., Jablonska, E., von Gerlach, S., Henneke, I., Zakrzewicz, D., Guenther, A., Preissner, K.T., and Markart, P. (2011). Role of

protease-activated receptor-2 in idiopathic pulmonary fibrosis. Am. J. Respir. Crit. Care Med. *183*, 1703–1714.

Wynn, T.A. (2004). Fibrotic disease and the T(H)1/T(H)2 paradigm. Nat. Rev. Immunol. *4*, 583–594.

Xu, H., Ploplis, V., and Castellino, F. (2006). A coagulation factor VII deficiency protects against acute inflammatory responses in mice. J. Pathol. *210*, 488–496.

Xu, M.Y., Porte, J., Knox, A.J., Weinreb, P.H., Maher, T.M., Violette, S.M., McAnulty, R.J., Sheppard, D., and Jenkins, G. (2009). Lysophosphatidic acid induces alphavbeta6 integrin-mediated TGF-beta activation via the LPA2 receptor and the small G protein G alpha(q). Am. J. Pathol. *174*, 1264–1279.

Yan, S.F., Fujita, T., Lu, J., Okada, K., Shan Zou, Y., Mackman, N., Pinsky, D.J., and Stern, D.M. (2000). Egr-1, a master switch coordinating upregulation of divergent gene families underlying ischemic stress. Nat. Med. *6*, 1355–1361.

Yan, W., Tiruppathi, C., Lum, H., Qiao, R., and Malik, A.B. (1998). Protein kinase C beta regulates heterologous desensitization of thrombin receptor (PAR-1) in endothelial cells. Am. J. Physiol. *274*, C387–395.

Yang, L., Bae, J.-S., Manithody, C., and Rezaie, A.R. (2007). Identification of a specific exosite on activated protein C for interaction with protease-activated receptor 1. J. Biol. Chem. *282*, 25493–25500.

Yasui, H., Gabazza, E.C., Taguchi, O., Risteli, J., Risteli, L., Wada, H., Yuda, H., Kobayashi, T., Kobayashi, H., Suzuki, K., et al. (2000). Decreased protein C activation is associated with abnormal collagen turnover in the intraalveolar space of patients with interstitial lung disease. Clin. Appl. Thromb. Off. J. Int. Acad. Clin. Appl. Thromb. *6*, 202–205.

Yasui, H., Gabazza, E.C., Tamaki, S., Kobayashi, T., Hataji, O., Yuda, H., Shimizu, S., Suzuki, K., Adachi, Y., and Taguchi, O. (2001). Intratracheal administration of activated protein C inhibits bleomycin-induced lung fibrosis in the mouse. Am. J. Respir. Crit. Care Med. *163*, 1660–1668.

Yoshida, K., Matsuzaki, K., Mori, S., Tahashi, Y., Yamagata, H., Furukawa, F., Seki, T., Nishizawa, M., Fujisawa, J., and Okazaki, K. (2005). Transforming Growth Factor-β and Platelet-Derived Growth Factor Signal via c-Jun N-Terminal Kinase-Dependent Smad2/3 Phosphorylation in Rat Hepatic Stellate Cells after Acute Liver Injury. Am. J. Pathol. *166*, 1029–1039.

Yu, H., Königshoff, M., Jayachandran, A., Handley, D., Seeger, W., Kaminski, N., and Eickelberg, O. (2008). Transgelin is a direct target of TGF-beta/Smad3-dependent epithelial cell migration in lung fibrosis. FASEB J. Off. Publ. Fed. Am. Soc. Exp. Biol. *22*, 1778–1789.

Zambruno, G., Marchisio, P.C., Marconi, A., Vaschieri, C., Melchiori, A., Giannetti, A., and De Luca, M. (1995). Transforming growth factor-beta 1 modulates beta 1 and beta 5 integrin receptors and induces the de novo expression of the alpha v beta 6 heterodimer in normal human keratinocytes: implications for wound healing. J. Cell Biol. *129*, 853–865.

Zania, P., Gourni, D., Aplin, A.C., Nicosia, R.F., Flordellis, C.S., Maragoudakis, M.E., and Tsopanoglou, N.E. (2009). Parstatin, the cleaved peptide on proteinase-activated receptor 1 activation, is a potent inhibitor of angiogenesis. J. Pharmacol. Exp. Ther. *328*, 378–389.

Zavadil, J., Bitzer, M., Liang, D., Yang, Y.C., Massimi, A., Kneitz, S., Piek, E., and Bottinger, E.P. (2001). Genetic programs of epithelial cell plasticity directed by transforming growth factor-beta. Proc. Natl. Acad. Sci. U. S. A. *98*, 6686–6691.

Zhang, Y.E. (2009). Non-Smad pathways in TGF-beta signaling. Cell Res. *19*, 128–139.

Zhang, C., Srinivasan, Y., Arlow, D.H., Fung, J.J., Palmer, D., Zheng, Y., Green, H.F., Pandey, A., Dror, R.O., Shaw, D.E., et al. (2012). High-resolution crystal structure of human protease-activated receptor 1. Nature.

Zhang, Y., Lee, T.C., Guillemin, B., Yu, M.C., and Rom, W.N. (1993). Enhanced IL-1 beta and tumor necrosis factor-alpha release and messenger RNA expression in macrophages from idiopathic pulmonary fibrosis or after asbestos exposure. J. Immunol. *150*, 4188–4196.

Zhao, J., Shi, W., Wang, Y.-L., Chen, H., Bringas, P., Datto, M.B., Frederick, J.P., Wang, X.-F., and Warburton, D. (2002). Smad3 deficiency attenuates bleomycin-induced pulmonary fibrosis in mice. Am. J. Physiol. - Lung Cell. Mol. Physiol. *282*, L585–L593.

Zhu, Z., Lee, C.G., Zheng, T., Chupp, G., Wang, J., Homer, R.J., Noble, P.W., Hamid, Q., and Elias, J.A. (2001). Airway inflammation and remodeling in asthma. Lessons from interleukin 11 and interleukin 13 transgenic mice. Am. J. Respir. Crit. Care Med. *164*, S67–70.

Zhu, Z., Ma, B., Zheng, T., Homer, R.J., Lee, C.G., Charo, I.F., Noble, P., and Elias, J.A. (2002). IL-13-induced chemokine responses in the lung: role of CCR2 in the

pathogenesis of IL-13-induced inflammation and remodeling. J. Immunol. Baltim. Md 1950 *168*, 2953–2962.

Ziesche, R., Hofbauer, E., Wittmann, K., Petkov, V., and Block, L.H. (1999). A preliminary study of long-term treatment with interferon gamma-1b and low-dose prednisolone in patients with idiopathic pulmonary fibrosis. N. Engl. J. Med. *341*, 1264–1269.

Zigler, M., Kamiya, T., Brantley, E.C., Villares, G.J., and Bar-Eli, M. (2011). PAR-1 and thrombin: the ties that bind the microenvironment to melanoma metastasis. Cancer Res. *71*, 6561–6566.

Zuo, F., Kaminski, N., Eugui, E., Allard, J., Yakhini, Z., Ben-Dor, A., Lollini, L., Morris, D., Kim, Y., DeLustro, B., et al. (2002). Gene expression analysis reveals matrilysin as a key regulator of pulmonary fibrosis in mice and humans. Proc. Natl. Acad. Sci. U. S. A. *99*, 6292–6297.

(2002). American Thoracic Society/European Respiratory Society International Multidisciplinary Consensus Classification of the Idiopathic Interstitial Pneumonias . This Joint Statement of the American Thoracic Society (ATS), and the European Respiratory Society (ERS) was adopted by the ATS Board of Directors, June 2001 and by The ERS Executive Committee, June 2001. Am J Respir Crit Care Med *165*, 277–304.

Appendix: Publications and awards

Publications:

PAR-1-dependent and PAR-independent pro-inflammatory signalling in human lung fibroblasts exposed to thrombin. (2012) Ortiz-Stern A, Deng X, Smoktunowicz N, Mercer PF, Chambers RC., Journal of Cellular Physiology, 227(11):3575-84.

Abtract publications:

S128 The Extrinsic Coagulation Pathway is Locally Upregulated in an Experimental Model of Viral Exacerbation of Pulmonary Fibrosis, N Smoktunowicz[1], R Alexander[1], L Franklin[1], AE Williams[1], G Jarai[2], CJ Scotton[1], PF Mercer[1], RC Chambers[1], *Thorax* 2012;67:A61 doi:10.1136/thoraxjnl-2012-202678.133

Transforming Growth Factor Beta1 (TGFBeta1) Upregulates Proteinase Activated Receptor-1 (PAR-1) Expression And Functional Signalling Responses In Alveolar Epithelial Cells N.K. Smoktunowicz, A. Ortiz-Stern, A. Datta, G. Jarai, P.F. Mercer, R.C. Chambers, American Journal of Respiratory and Critical Care Medicine, Volume 185, May 2012

Characterization Of Proteinase Activated Receptor 1 (PAR-1) Expression In Primary Human Bronchial Epithelial Cells M. Plate, N.K. Smoktunowicz, A. Varanou, P.F. Mercer, J.R. Hurst, R.C. Chambers, American Journal of Respiratory and Critical Care Medicine, Volume 185, May 2012

Academic achievements:

Winner of the Young Investigator Poster Competition at the 19th Annual Summer Meeting of the British Association of Lung Research (BALR), Southampton, 2012

Winner of the best MPhil to PhD Upgrade talk Competition for the UCL Division of Medicine in the academic year 2010-2011

Appendix 1: PAR-1neutralising antibody

A1.1 Introduction

Previous work from our laboratory has shown that lack of PAR-1 offers protection in a number of lung conditions including bleomycin model of acute lung injury and fibrosis (Howell et al., 2005) and experimental model of chronic obstructive pulmonary disease (Atzori et al., 2009). The aim of this study was to support these finding with a pharmacological targeting of PAR-1 receptor. We have used RWJ58259 and SCH530348 to investigate the biological responses *in vitro* as described in **Chapter 3.1** of this thesis and *in vivo* in LPS model of acute lung injury (Mercer et al., 2013). However, both molecules have a short half life *in vivo* and have to be administered frequently at a relatively high dose to fully engage the target receptor and produce a significant biological response. Furthermore, neither antagonist prevents cleavage of the PAR-1 N- terminus and release of the tethered ligand. The inhibitors occupy the second extracellular loop of the receptor where the tethered ligand binds and while that blocks PAR-1 activation there is still potential to transactivate PAR-2 receptor, which has recently been shown to play a role in idiopathic pulmonary fibrosis (Wygrecka et al., 2011).

In order to find novel ways of targeting PAR-1 receptor in a long term pulmonary fibrosis model the aim of this part of the project was to purify a murine PAR-1 neutralising antibody from the hybridoma cell supernatant and assess its effect on thrombin-mediated intracellular calcium release and inflammatory responses in murine lung fibroblasts.

The second aim of this study was to test the efficacy of the mPAR-1 neutralising antibody in LPS model of acute lung injury. Main clinical features of acute lung injury (ALI) include disruption of the pulmonary epithelium and endothelium manifested as diffuse alveolar damage (DAD) (reviewed in Chambers 2008). This leads to increased vascular permeability and subsequent protein leak into the lung. The resultant oedema is potentiated by impaired fluid clearance in the injured lung

(Ware and Matthay 2001). Acute inflammation is also hallmark of ALI, manifested by the neutrophillic alveolitis and increased concentration of inflammatory cytokines in the lung (Ware and Matthay 2001). The model of LPS-induced acute lung injury is a widely used model that recapitulates the two main hallmarks of human condition, namely neutrophilic inflammation and vascular leak. Research in our laboratory has shown that blocking PAR-1 with a small molecule antagonist, RWJ58259, significantly reduced neutrophilia and vascular leak in the *in vivo* LPS-model of acute lung injury (Mercer et al., 2013).

A1.2 Methods

A1.2.1 Hybridoma cell culture

Armenian hamster derived hybridoma cells producing anti-mouse PAR-1 neutralising antibodies were kindly provided by Novartis Research Centre (Horsham, UK). The cells were maintained in DMEM/10% FCS in 250 cm^2 tissue culture flaks. When cells were 80-90% confluent (every 2-3 days) the supernatant was collected and the remaining cells passaged at 1 in 3 ratio. The cells were lightly adherent or floating and no trypsin was required for detachment.

The purification and characterisation approach was chosen based on data available for the human PAR-1 neutralising antibody that was also developed and described by Novartis. The extracellular N-terminus domain of PAR-1 was cloned and expressed in a fusion protein used to immunise laboratory animals- mice for human anti-PAR-1 and Armenian hamsters for murine anti-PAR-1. B lymphocytes producing antibodies against these fusion proteins were isolated from spleens of the immunised animals and transformed by fusion with myeloma cells. This technology, described in 1975 by Kohler and Milstein, allows for creation of immortal hybridoma cell lines secreting monoclonal antibodies against a specific peptide (reviewed in Gura 2002).

The anti-human PAR-1 and anti-murine PAR-1 antibodies were developed in tandem but the detailed procedure and thorough characterisation was described by Novartis for anti-human PAR-1 antibodies only. As shown in **Figure A1.2.1.** the human PAR-1 neutralising antibody inhibited thrombin-mediated calcium release in concentration-dependent manner in human colon cancer and prostate cancer cells. Thrombin-mediated IL-8 release from human umbilical vein endothelial cells (HUVECs) was reduced by the human PAR-1 neutralising antibody.

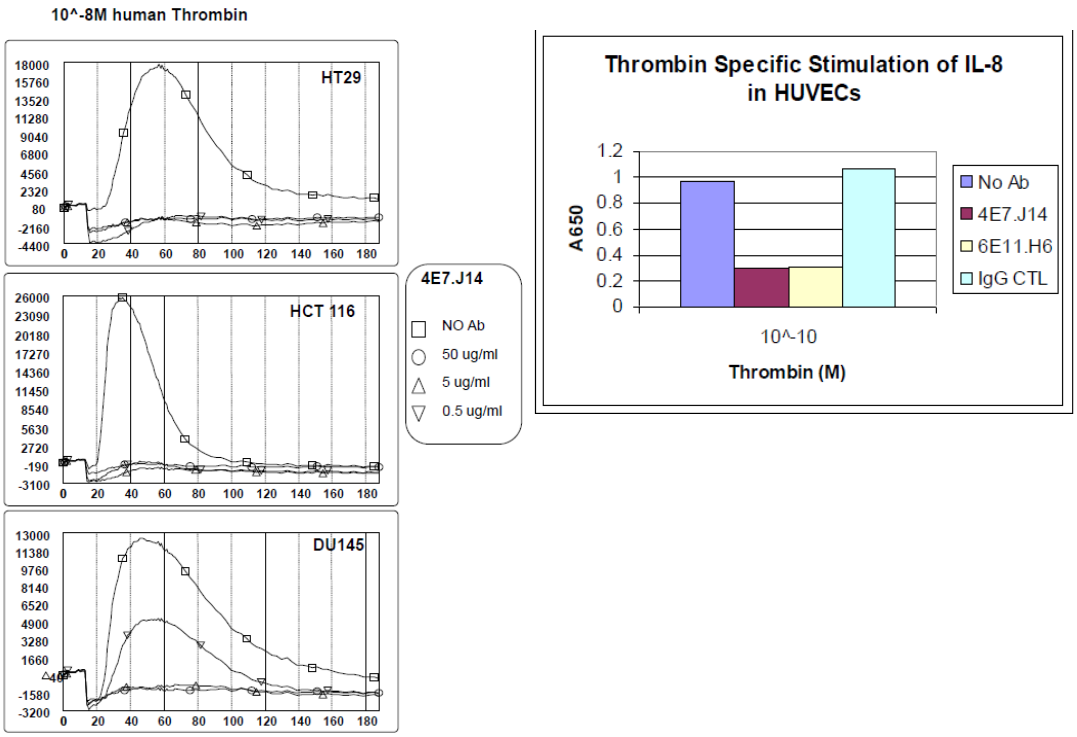

Figure A1.2.1 Characterisation of human PAR-1 neutralising antibody.

Left panel- anti-human PAR-1 antibody inhibits thrombin-induced calcium release in a concentration-dependent manner in colon HT29, HCT 116 and prostate DU145 cell lines; right panel shows reduction in thrombin-induced IL-8 release from human umbilical vein endothelial cells (HUVECs) following treatment with two clones of anti-human PAR-1 antibody. (Reproduced from Cohen and Nasoff, 2008)

A1.2.2 Affinity chromatography

Buffers: Wash buffer: 30% isopropanol in 10 mM phosphate buffer pH=7.2, Elution buffer: 100 mM glycine pH=2.7.

The murine PAR-1 neutralising antibody was purified in a process of affinity chromatography using 1 ml HiTrap™ Protein G High Performance columns (GE Healthcare). The HiTrap™ column is pre-packed with protein G linked to sepharose matrix (highly cross-linked agarose beads). Protein G is a bacterial cell surface protein of Group G *Streptococci* that binds the Fc region of an IgG antibody in a pH-dependent mechanism. Protein G binds IgG over a wide range of pH with optimal binding achieved at pH 7. In order to release the antibody the elution buffer pH must be lowered to 2.5-3. The recombinant protein G in the HiTrap™ column is produced in *E.coli* and contains two IgG binding regions. The albumin binding region of native protein G has been genetically deleted to avoid cross-reactivity. As per manufacturer's description the protein G binding capacity for human IgG is approximately 25mg IgG per ml of solution and the affinity for hamster IgG is in medium range.

The automated chromatography system Aktaprime™plus (GE Healthcare Lifesciences) was used to perform the purification process. Supernatant from the hybridoma cells was collected, centrifuged for 5 minutes at 200 RCF and filtered through Nalgene 0.2 micron sterile filter unit (Thermo Scientific) to remove cell debris. All subsequent steps were performed at 4°C. The HiTrap™ column was equilibrated with 20 column volumes (CV) of PBS, pH=7.4 prior to running the supernatant. The column was then washed with 10 CV of wash buffer and the bound protein eluted with 20 CV of elution buffer. Forty 0.5 ml fractions containing the protein were collected in the sterile 12ml BD Falcon tubes aligned on the Aktaprime™plus collector. A real-time chromatogram was plotted and purification process evaluated using PrimeView™ software.

A1.2.3 Coomassie staining

In order to investigate the presence and purity of protein small aliquots from individual fractions were mixed with the loading dye (Invitrogen), with or without reducing agent (DTT), and separated in the course of gel electrophoresis. The protein was then visualised using Coomassie brilliant blue dye (Invitrogen), which binds non-specifically to all proteins. Anionic form of the Coomassie dye interacts with basic amino acids, chiefly with arginine residues and weakly with histidine, lysine, tyrosine, tryptophan and phenylalanine residues. This interaction causes colour change of the solution from reddish brown to bright blue when the protein is present.

A1.2.4 Dialysis

The individual purification fractions were pooled together and dialyzed into storage buffer (10% glycerol, 0.004% Tween-80 in PBS) using Slide-A-Lyzer® Dialysis Cassette (Thermo Scientific). The molecular weight cut off of the semi- permeable membrane was 20,000 Daltons allowing small molecules and salts to diffuse out of the solution and into the buffer. The dialysis cassette was used as per manufacturer's instructions. Briefly, the sample was gently injected between the membranes of the cassette that was then left floating in a storage buffer, 200 times the volume of the sample. The buffer was changed once after 3 hours and the sample dialyzed overnight at 4°C. The following day the sample was gently extracted from the cassette and stored in sterile BD Falcon tube.

A1.2.5 Endotoxin detection

Endotoxin levels in the antibody stock were detected using the Endpoint Chromogenic Limulus Amebocyte Lysate (LAL) (Lonza, UK) with a sensitivity range of 0.1 EU/ml - 1.0 EU/ml. The assay was developed based on reaction between a Gram-negative bacterial endotoxin and a coagulation factor in the blood of the horseshoe crab (*Limulus polyphemus*) that initiates fatal intra-vascular clot formation. The current LAL method is based on the endotoxin-mediated lysate

activation that exerts enzymatic activity on the synthetic substrate releasing p-nitroaniline (pNA) (**Figure A1.2.2**), which leads to the chromogenic change of the solution that can then be quantified by measuring absorbance at the wavelength of 410 nm. The absorbance is directly proportionate to the amount of endotoxin present and its concentration can be calculated from a standard curve.

The kit was used as per manufacturer's instructions. Briefly, each sample was mixed with the LAL and incubated at 37°C (±1°C) for 10 minutes. A substrate solution was then added and incubated at 37°C (±1°C) for an additional 6 minutes. The reaction was then stopped with stop reagent and the absorbance measured at 410 nm.

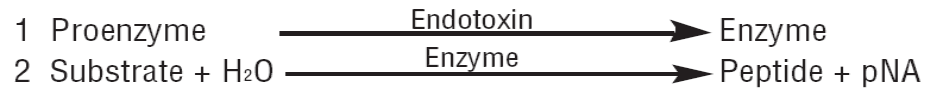

Figure A1.2.2 Principle of Limulus Amebocyte Lysate LAL assay.

Endotoxin initiates enzymatic reaction leading to release of pNA that causes colour change of the sample; there is linear correlation between the level of endotoxin and released chromogen.

A1.2.6 Endotoxin removal

The Detoxi-Gel Endotoxin Removing Columns (Thermo Scientific) were used to remove the endotoxin contamination from the antibody preparation. This method utilises immobilized polymyxin B, which belongs to the polymyxins family of antibiotics that bind the most conserved domain of bacterial lipopolysaccharide-lipid A.

The gravity-flow columns were washed 3-5 times with 1% sodium deoxycholate followed by washes with endotoxin-free water to remove the detergent. The columns were then equilibrated with the antibody storage buffer. The sample was then applied on the column and flow- through collected.

A1.2.7 Acute lung injury

BALB/c female mice, between 6 and 8 weeks of age (Charles River Laboratories, UK), were housed at the Central Biological Services Unit, University College London; in a specific pathogen-free facility in individually ventilated cages, with free access to food and water (12 hour light/dark cycle, normal sodium dry fishmeal diet, temperature 18-20°C). All studies were ethically reviewed and carried out in accordance with the UK Home Office Animals for Scientific Procedures Act 1986.

LPS (125 µg/kg, *E.coli* 0127:B8, Sigma) or saline were administered intranasally by placing 50 µl on the nose of a mouse under light isofluorane-induced anaesthesia and allowing it to be inhaled. The PAR-1 neutralising antibody (0.5 mg/kg) or Armenian hamster IgG isotype control (BioLegend, UK) were administered by intraperitoneal injection 30 minutes or 24 hours prior to LPS insult. The injury was allowed to develop for three hours and the mice were then sacrificed by intraperitoneal injection of pentobarbitone and severing of the abdominal inferior vena cava.

A1.2.8 Bronchoalveolar lavage fluid (BALF)

BALF was collected by inserting a cannula into trachea and washing the lungs with 1 ml PBS. BALF was then stored on ice for further processing. The lungs were dissected and snap frozen in liquid nitrogen.

Total cell counts (cells/ml) were obtained using a haemocytometer following cell staining with crystal violet in 0.1% acetic acid. Inflammatory cells from a 200 µl volume of BALF were pelleted onto microscope slides by centrifugation and left to dry. The cells were subsequently fixed in methanol and stained with eosin and methylene blue (Diffquick). Representative numbers of neutrophils and monocytes were counted in a total population of approximately 200 giving a respective differential ratio. The total neutrophil and monocyte counts (cells/ml) were calculated by multiplying the fraction of the neutrophils/monocytes in the sample population by the total cell counts. Total protein level in BALF was measured with BCA assay as described in **Material and Methods section 2.14**.

A1.3 Results

A1.3.1 Purification and characterisation of the mPAR-1 neutralising antibody

The mPAR-1 neutralising monoclonal antibody was isolated from the supernatant of Armenian hamster-derived hybridoma cells. These immortal cells are a sustainable source of the monoclonal antibodies and a litre of supernatant was harvested every three days when the cells were propagated. A total of 8 litres of supernatant were used for the purpose of this study.

The mPAR-1 neutralising antibody was isolated by affinity chromatography. Optimized conditions and maximal efficiency of the process was achieved by the use of an automated protein purification system (Aktaprime, GE Healthcare). The antibody was purified by exploiting the affinity interactions between protein G and immunoglobulins. Protein G is a bacterial cell surface protein of Group G *Streptococci* that binds the Fc region of an IgG antibody in a pH-dependent mechanism. Commercially-available recombinant protein G contains two IgG binding regions and displays medium affinity towards hamster IgG. Optimal binding occurs at pH 7 and the antibody is released when the pH is rapidly decreased to pH 2.5-3 by the elution buffer. In the course of a purification run changes in UV absorbance are monitored and plotted as a chromatogram. **Figure A1.3.1** shows a representative chromatogram that illustrates stages of the isolation process and allows for the qualitative evaluation of the collected protein. The single peak observed in the graph indicates the presence of only one elution product. The area under the peak is proportionate to the amount of the protein present and the fractions collected in that area contain significant concentration of protein.

The purity and the correct size of the collected protein were confirmed by Coomassie dye staining. The anionic form of the Coomassie dye interacts with basic amino acids and causes a colour change of the solution from reddish brown to bright blue, which is indicative of protein presence. **Figure A1.3.2A** shows a representative Coomassie-stained gel of the protein isolated during the purification

run. The non-reduced protein is visualised as a single band of 150 kDa, which corresponds to the molecular weight of an antibody. Treatment with a reducing agent disrupts the disulphide bonds that bind covalently the polypeptide chains forming an antibody. This is visualised by two bands corresponding to the light chain (25 kDa) and heavy chain (50 kDa). The isolated antibody was further identified to be Armenian hamster IgG by Western blot (**Figure A1.3.2B**).

The antibody preparation subsequently underwent overnight dialysis, which facilitates removal of small contaminants by selective and passive diffusion through a semi-permeable membrane. Furthermore, dialysis allows changing of the elution buffer to a storage buffer composed of 10% glycerol and 0.04% Tween-80 in PBS. The antibody concentration was quantified by BCA assay.

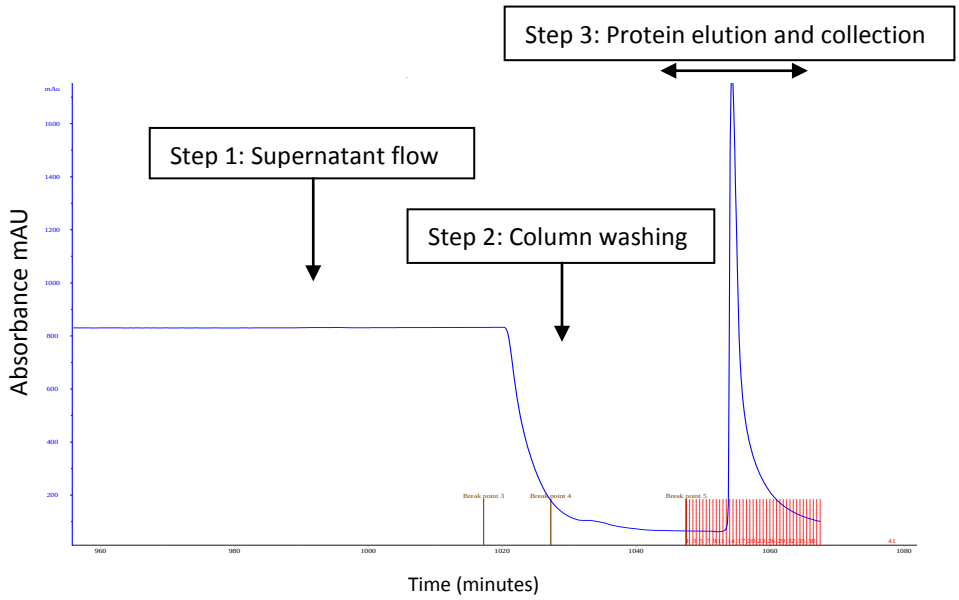

Figure A1.3.1. Isolation of IgG from hybridoma cells supernatant.

Figure shows a representative chromatogram plotted from the UV absorbance changes during the antibody purification run in a process of automated affinity chromatography (Aktaprime, GE Healthcare). A litre of supernatant collected from antibody-producing hybridoma cells was filtered and optimised to pH 7. Step 1- The supernatant was applied to a protein G column at a constant flow rate of 1 ml/minute. Step 2- Following the supernatant flow, the column was washed as indicated and the antibody eluted with elution buffer, pH 2.7. Step 3- Protein was detected and visualised by the peak and collected in forty 0.5 ml fractions.

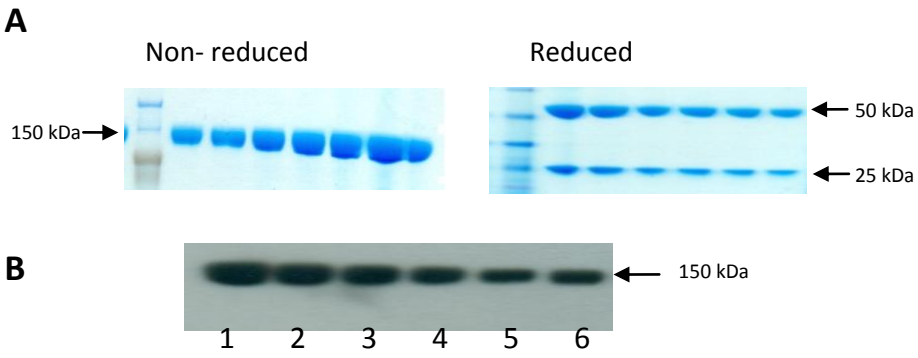

Figure A1.3.2. Identification of Armenian hamster IgG.

Panel A shows representative Coomassie staining of protein collected during automated affinity chromatography. A small aliquot from each fraction was subjected to gel electrophoresis under reducing (left) and non-reducing (right) conditions. The gel was subsequently fixed and stained with Coomassie dye. Panel B shows a Western blot in non-reducing conditions of IgG detected with anti-Armenian Hamster secondary antibody.

A1.3.2 Effect of the mPAR-1 neutralising antibody on thrombin-mediated intracellular calcium mobilisation

Following successful purification of the Armenian hamster IgG from the hybridoma cell supernatants, the next series of experiments aimed to assess the effect of this antibody on thrombin-mediated PAR-1 activation and cellular responses. Firstly, murine PAR-1 neutralising antibody effect on intracellular calcium flux was investigated in murine lung fibroblasts.

The cells were pre-incubated with the antibody at a concentration range from 90 µg/ml to 0.1 µg/ml, before being stimulated with thrombin (10 nM) or the PAR-1 activating peptide, TFLLR (100 µM). As shown in **Figure A1.3.3A**, the antibody inhibited thrombin-mediated intracellular calcium flux in a concentration-dependent manner and IC_{50} of 1.6 µg/ml. The antibody did not affect the TFLLR-mediated response (**Figure A1.3.3B**). The PAR-1 activating peptide TFLLR is a highly selective PAR-1 peptide agonist that activates PAR-1 independently of proteolytic cleavage by direct binding to the second extracellular loop of the receptor. In this experiment TFLLR was used as a positive control to demonstrate that the intracellular calcium release in murine lung fibroblasts is PAR-1-mediated and also to confirm a different mechanism of PAR-1 blocking as predicted for this antibody. As characterised by Novartis, the antibody was generated against the N-terminus of the receptor.

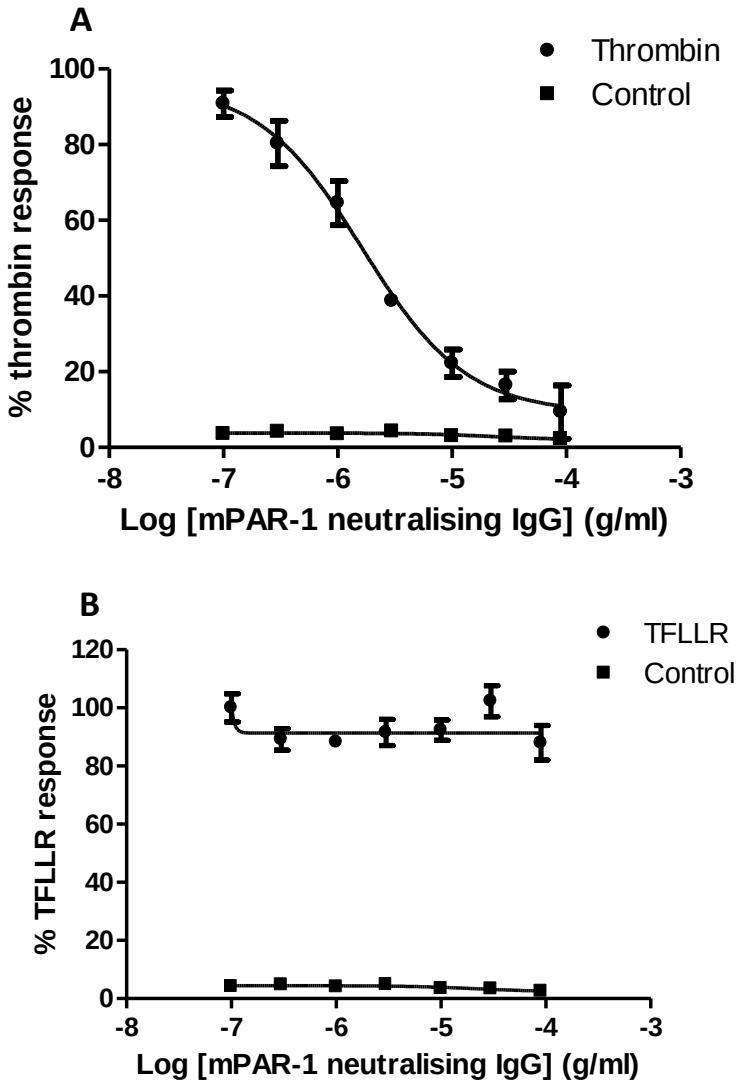

Figure A1.3.3. PAR-1 neutralising antibody inhibits thrombin but not TFLLR-induced intracellular calcium release.

Murine lung fibroblasts were incubated with mPAR-1 neutralising antibody, at a concentration range from 90 µg/ml to 0.1 µg/ml and Fluo4-AM calcium binding dye an hour prior to the agonist stimulation. A- Concentration-inhibition curve with thrombin; B- Concentration-inhibition curve with TFLLR; data are presented as a percentage of thrombin response and values represent mean ± SEM of 3 replicate wells.

A1.3.3 Effect of the mPAR-1 neutralising antibody on thrombin-mediated CCL2 release

The characterisation of the human PAR-1 neutralising antibody showed its potential to inhibit thrombin-mediated intracellular calcium release and reduce IL-8 release from endothelial cells (**Figure A1.2.1**). In the previous section, it was demonstrated that the murine PAR-1 neutralising antibody inhibits thrombin-mediated intracellular calcium release in a concentration-dependent manner in murine lung fibroblasts. As described in detail in **Chapter 3.2**, thrombin-mediated PAR-1 signalling leads to CCL2 synthesis and release from murine lung fibroblasts and hence the effect of mPAR-1 neutralising antibody on CCL2 release was investigated next. As shown in **Figure A1.3.4** treatment of fibroblasts with mPAR-1 neutralising antibody at concentrations of 50 μg/ml, 5 μg/ml and 0.5 μg/ml prior to stimulation with thrombin (10 nM) led to an increase in CCL2 release from the cells. Furthermore, the control cells pre-treated with different concentrations of antibody alone showed a concentration-dependent increase in CCL2 release.

The results of this experiment were opposite to expected and potential explanations were considered. CCL2 is a potent inflammatory chemokine induced and released in response to tissue injury and infection. A potent mediator of CCL2 release is bacterial endotoxin, which binds to Toll-like receptor 4 (TLR 4) and activates signalling pathways via the NFκB pathway. Endotoxin is also a common contaminant in the process of antibody generation and purification. The antibody preparation was subsequently tested for endotoxin levels and was found to be contaminated with endotoxin (approximately 300 endotoxin units per ml (EU/ml), equivalent to 30 ng/ml).

Due to the high levels of endotoxin present, the antibody stock was unsafe for further *in vitro* and *in vivo* use. Commercially- available endotoxin removal kits were used to eliminate the contamination. Following endotoxin removal treatment the contamination level was reduced to 10 EU/ml (1 ng/ml). At this concentration the antibody did not induce CCL2 release from murine lung fibroblasts.

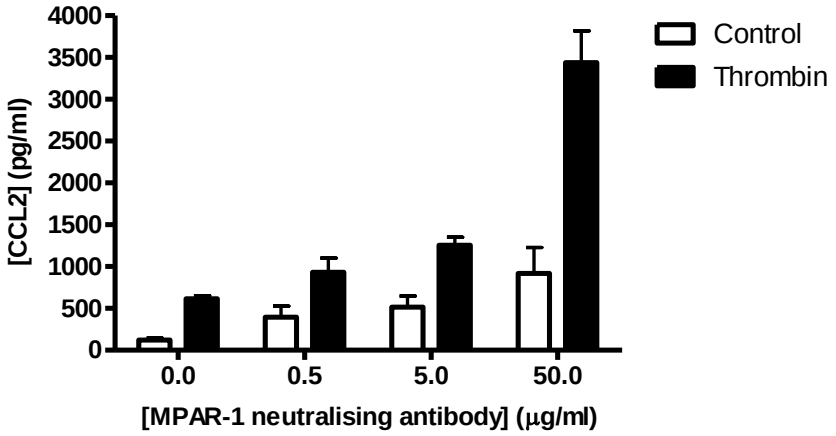

Figure A1.3.4. Effect of mPAR-1 neutralising antibody on CCL2 release from murine lung fibroblasts.

Murine lung fibroblasts were pre-treated for an hour with mPAR-1 neutralising antibody at concentrations of 50, 5 and 0.5 μg/ml and then stimulated with 10nM thrombin. Following a 6-hour incubation, cell supernatants were collected and CCL2 levels measured by ELISA; the results are presented as means ± SEM of n=3 replicate wells.

A1.3.4 mPAR neutralising antibody in LPS model of acute lung injury

BALB/c mice were injected intraperitoneally with 0.5 mg/kg of the mPAR-1 neutralising antibody or IgG isotype control 30 minutes prior to LPS injury. LPS (125 µg/kg) or saline were administered intranasally and the injury was allowed to develop for 3 hours. After this time, mice were sacrificed and the BALF collected. As shown in **Figure A1.3.5A**, administration of LPS into the lung leads to an influx of inflammatory cells into the lung. The differential counts showed a significant neutrophilia (**Figure A1.3.5B**) while the proportion of monocytes and macrophages seen in the BALF was significantly reduced in comparison to saline treated animal (**Figure A1.3.5C**). There was no difference in inflammation between the mPAR-1 and IgG isotype treated animals.

LPS administration into the lung also leads to increased vascular permeability and oedema formation in the lung. However, in this study no difference in the total BALF protein levels between saline control and LPS-injured groups was observed (**Figure A1.3.6).** Furthermore, the baseline levels in the saline-treated animals were increased when compared to historical baseline, as indicated by the dotted line, recorded in previous experiments performed in our laboratory. This potentially suggests that the administration of the isotype control and mPAR-1 antibody alone leads to increased vascular leak and increased protein concentration in the lung.

PAR-1 neutralising antibody has been proven *in vitro* to fully block the intracellular calcium flux (**Figure A1.3.3A**) but the *in vivo* results did not show attenuation of neutrophilia following LPS challenge. It is possible that the antibody concentration used in this experiment was not sufficient to affect the outcome of the lung injury. This may have been also caused by the limited bioavailability of the antibody in the lung due to systemic administration and potential off-target effects. The potential delay between antibody administration and the time it reaches the lung was addressed in the second experiment where the mPAR-1 neutralising antibody or isotype control were administered 24 hours prior to the LPS challenge.

As shown in **Figure A1.3.7**, LPS evoked a significant inflammatory response with an increase of total cell, neutrophils influx into the lung and the decrease in fraction of monocytes and macrophages in the BALF. However, again there was no difference between animals treated with mPAR-1 neutralising antibody and the isotype control.

The vascular leak has been assessed as previously by measuring the total BALF protein levels showing a trend toward increase in LPS-challenged groups (**Figure A1.3.8**), which is more consistent with our historical data. The levels of protein in the saline groups were still increased and there was no difference between the treatment groups.

Despite our confidence in the mPAR-1 neutralising antibody ability to block the receptor and considering several strategies to optimise it further *in vivo*, which will be described in detail in the discussion, we were concerned with the elevated protein levels in BALFs of saline + mPAR-1 IgG-treated animals. We worried that the residual level of endotoxin present in the antibody preparation may be responsible for this effect and therefore, before proceeding with next experiments, we opted for further endotoxin removal treatments.

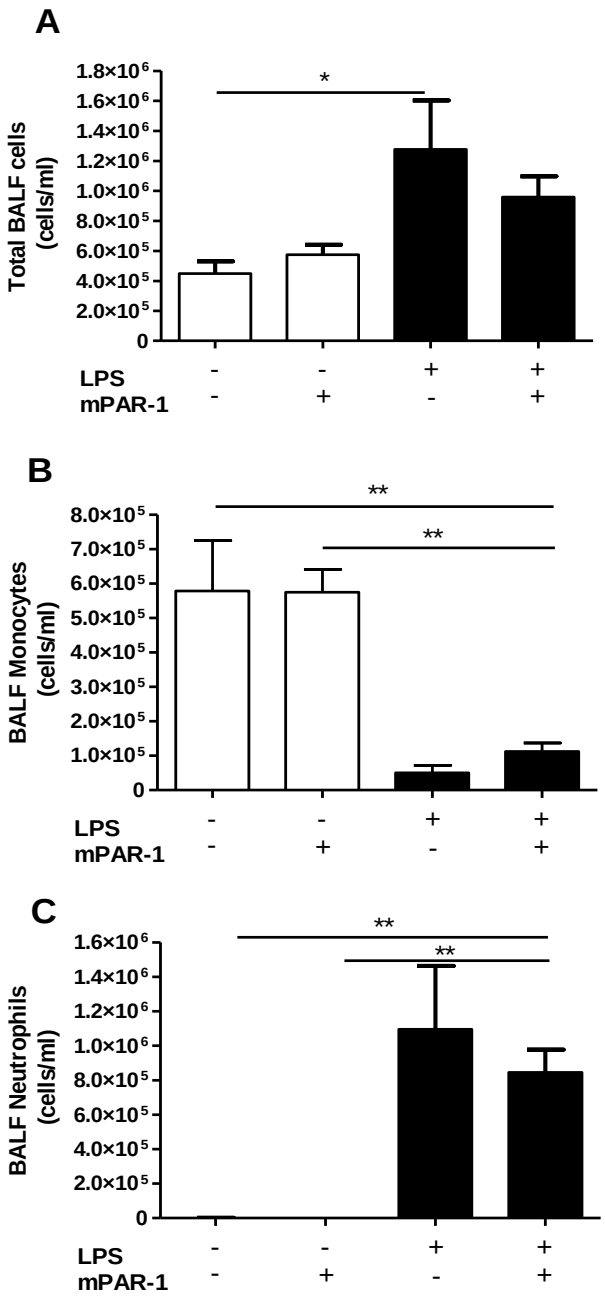

Figure A1.3.5. Assessment of inflammation in the model of LPS-induced acute lung injury (ALI).

BALB/c mice were administered 0.5 mg/kg of mPAR-1 neutralising antibody or isotype control 30 minutes prior to the intranasal challenge with 125 μg/kg LPS. Control animals were administered saline. After 3 hours, animals were sacrificed and BAL fluid collected. Inflammation was assessed by A- total cell counts in BALF; B- differential neutrophil counts; C- differential monocyte counts; Data show means ± SEM of n= 4-5 animals per group; One way Anova was performed for statistical analysis; *p<0.05; **p<0.01.

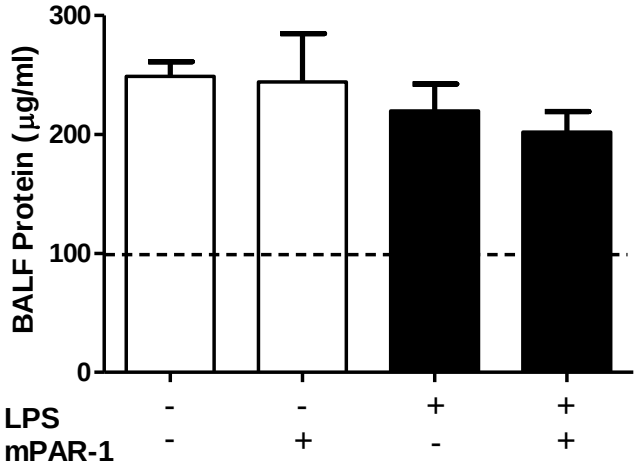

Figure A1.3.6. Assessment of vascular leak in the LPS model of acute lung injury (ALI).

BALB/c mice were administered 0.5 mg/kg of mPAR-1 neutralising antibody or isotype control 30 minutes prior to the intranasal challenge with 125 µg/kg LPS. Control animals were administered saline. After 3 hours, animals were sacrificed and BAL fluid collected and total protein measured. Data present mean ± SEM of n= 3-5 animals. The dotted line shows historical baseline for protein and albumin levels in the 3- hour LPS model of ALI.

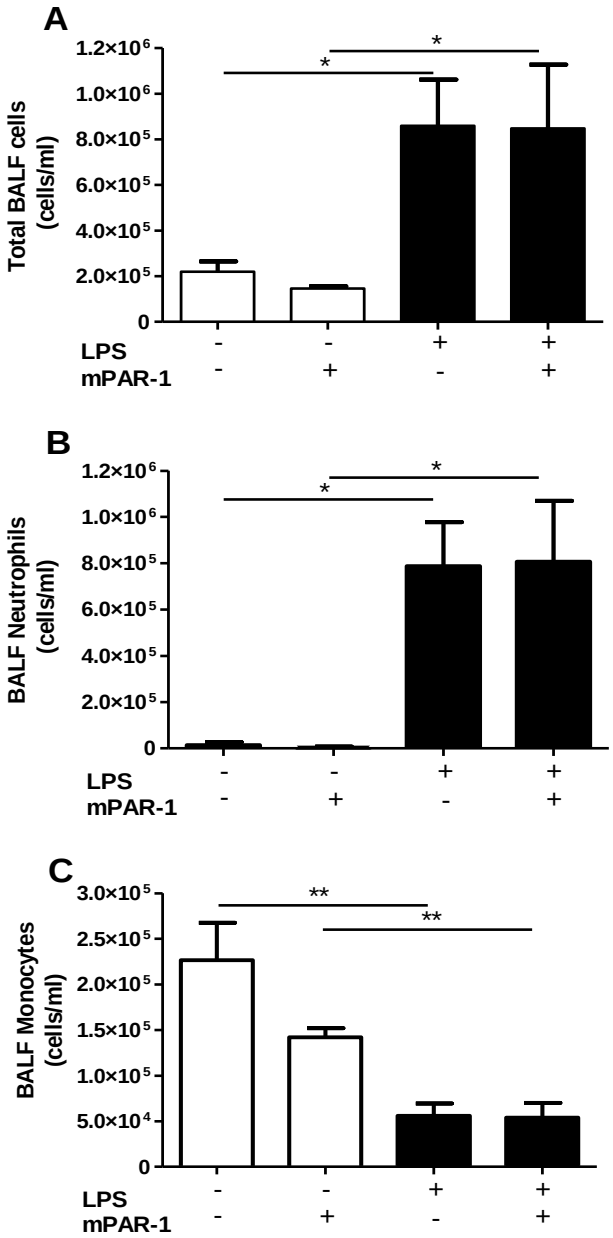

Figure A1.3.7. Assessment of inflammation in murine model of LPS- induced acute lung injury.

BALB/c mice were administered 0.5 mg/kg of mPAR-1 antagonist antibody or isotype control 24 hours prior to intranasal challenge with 50 µl LPS. Control animals were administered saline. After 3 hours the animals were sacrificed and BAL fluid collected. Inflammation was assessed by A- total cell counts in BALF; B- differential neutrophil counts; C- differential monocyte counts; Data show means ± SEM of n= 4-5 animals per group; *p<0.05, **p<0.01;

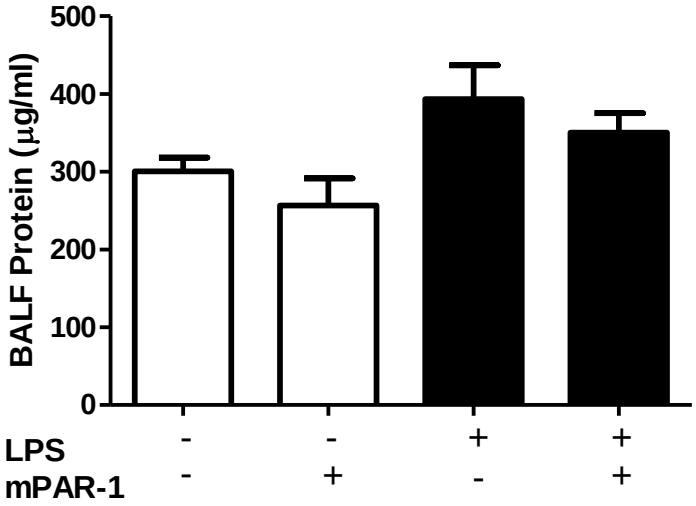

Figure A1.3.8. Assessment of vascular leak in the LPS model of acute lung injury (ALI)

BALB/c mice were administered 0.5 mg/kg of mPAR-1 antagonist antibody or IgG control 24 hours prior to intranasal LPS challenge. Control animals were administered 50 µl of saline. After 3 hours mice were sacrificed and BAL fluid collected. BCA assay was used to assess total protein level in the BALF. Data represent mean ± SEM of n= 4-5 animals.

A1.3.5 Summary

- The Armenian hamster antibody was purified from hybridoma cell supernatant and its purity and specificity confirmed by Commassie staining and Western blotting.
- The antibody was subsequently shown to inhibit intracellular calcium release in thrombin-stimulated murine lung fibroblasts.
- The antibody did not affect the intracellular calcium response to PAR-1-specific activating peptide, TFLLR.
- The mPAR-1 neutralising antibody appeared to induce the CCL2 release from the murine lung fibroblast rather than inhibit it.
- The antibody preparation was tested and found to be heavily contaminated with endotoxin. Following the decontamination treatment, the endotoxin level was reduced to 10 EU/ml (1 ng/ml).
- The mPAR-1 neutralising antibody had no effect on neutrophilia and monocytes numbers in the LPS model of acute lung injury.
- The saline-treated control animals administered the mPAR-1 blocking antibody and the isotype IgG showed increased BALF total protein levels.

A1.4 Discussion

Over-exuberant activation of the coagulation cascade in combination with the decreased activity of fibrinolytic pathways is strongly implicated in the pathogenesis of lung injury and fibrosis. However, recent clinical trial of warfarin in IPF patients showed increased mortality in the treatment arm (Noth et al., 2012), which suggests that global inhibition of coagulation cascade may be detrimental to the disease process. Furthermore, anticoagulants have extensive systemic effects that can lead to spontaneous and life-threatening haemorrhage. PAR-1 antagonists may provide attractive therapeutic solution through disrupting the local thrombin signalling pathways without affecting the systemic coagulation. There are already several clinical trials for PAR-1 antagonists ongoing in the setting of cardiovascular disease as described in Introduction section of this thesis.

Thrombin-induced PAR-1 signalling exerts major pro-fibrotic effects in the lung, including fibroblast proliferation and differentiation to myofibroblasts (Bogatkevich et al. 2009; Bogatkevich et al. 2003), collagen deposition (Chambers et al., 1998), release of chemokines, such as CCL2 (Deng et al., 2008; Mercer et al., 2009) and growth factors such as connective tissue growth factor (CTGF) from fibroblasts (Chambers et al. 2000). As previously discussed, PAR-1 signalling also mediates activation of latent TGFβ (Jenkins et al., 2006; Scotton et al., 2009). Furthermore PAR-1 knockout mice are protected from bleomycin-induced lung fibrosis (Howell et al. 2005), fMLP-induced chronic obstructive pulmonary disease (COPD) (Atzori et al., 2009), liver fibrosis (Rullier et al., 2008) and renal ischemia reperfusion injury (Sevastos et al., 2007).

In this study a hybridoma cell line producing a novel murine PAR-1 neutralising antibody was obtained through collaboration with Novartis Research Centre (Horsham, UK). The antibody displays high affinity for the mPAR-1 tethered ligand, irrespectively of thrombin cleavage, as demonstrated by Novartis in the immunoprecipitation studies. In the physiological system the antibody blocks PAR-1 by steric hindrance where the antibody binds to the tethered ligand and prevents thrombin binding and cleaving of the receptor. The mPAR-1 neutralising antibody

was purified from the hybridoma cell supernatants, characterised and its effect on thrombin-mediated signalling in murine lung fibroblasts assessed in *in vitro* assays.

In human plasma, the zymogen, prothrombin, is present at concentrations around 1.4 µM and the maximum concentration of active thrombin generated during blood clotting *in vivo* is estimated to be 130 nM (Walz et al., 1985). Thrombin levels in the extravascular compartments are expected to be much lower than in blood and *in vitro* experiments in our laboratory have shown that concentrations as low as 1 nM cause significant increases in CCL2 release from murine lung fibroblasts while intracellular calcium flux is detected from 0.3 nM thrombin. At a concentration of 10 nM thrombin induces robust intracellular flux and CCL2 release from murine lung fibroblasts and therefore this concentration was used to evaluate the blocking potential of mPAR-1 neutralising antibody in this set of experiments. The results show that mPAR-1 neutralising antibody efficiently inhibited thrombin-induced intracellular calcium release in a concentration-dependent manner. Cells were also stimulated with the PAR-1 specific agonist peptide TFLLR. The activating peptide binds to the second extracellular loop (ECL2) of the receptor and activates the receptor independently of proteolytic cleavage. It was therefore used to demonstrate the specificity of the intracellular calcium release downstream of PAR-1 signalling.

In the second functional assay the effect of mPAR-1 neutralising antibody on CCL2 release from murine lung fibroblasts was assessed. CCL2 is a potent chemoattractant for mononuclear cells, T lymphocytes and immature dendritic cells and this effect is largely mediated by PAR-1 (Chen et al. 2008). In the lungs of IPF patients, CCL2 immunoreactivity is associated with epithelial cells, monocytes, vascular endothelial cells, fibroblasts and fibrocytes (Mercer et al., 2009). CCL2 expression is also upregulated in the bleomycin model of lung injury and fibrosis and *in vitro* studies demonstrate that CCL2 can stimulate fibroblast collagen synthesis via the induction of TGF-β (Gharaee-Kermani et al. 1996). The thrombin-PAR-1- $G\alpha_q$ signalling axis leads to upregulation of CCL2 expression in lung fibroblasts both at the gene and protein levels as demonstrated in previous studies

in our laboratory (Deng et al., 2008). In the present experiments murine lung fibroblasts were stimulated with thrombin following pre-treatment with mPAR-1 neutralising antibody and the CCL2 levels measured in the cell supernatants. However, the results of this experiment were opposite to the predicted outcome and the antibody appeared to have induced a concentration-dependent increase in CCL2 release. The most plausible explanation was that the antibody is contaminated with endotoxin, which was subsequently confirmed by the standard endotoxin detection LAL assay. CCL2 release can be triggered by bacterial endotoxin, which is also the most common contaminant of biological preparations. Endotoxin binds to the Toll-like receptor- 4 (TLR-4) expressed on fibroblasts and triggers signalling via the NFκB pathway to release inflammatory mediators, including CCL2. The concentration of endotoxin matched to the level detected in the antibody preparation was shown to elicit CCL2 release of similar magnitude as observed in this experiment.

Endotoxins are components of Gram-negative bacteria's cell walls and are structurally lipopolysaccharides (LPS), composed of a polysaccharide chain that is highly variable among bacterial species, and lipid moiety lipid A, which is a constant part of the molecule. A commercially available polymyxin B-based treatment was used to decontaminate the antibody stock. Polymyxin B is an antibiotic that binds the preserved lipid A and is therefore able to neutralize endotoxin from a wide range of bacterial species. Furthermore, the polymyxin B is immobilised in a chromatography column that allows removal of the bound endotoxin from the antibody stock. This technique allowed for a significant reduction of the contamination to the levels, which were deemed acceptable for an *in vivo* use.

Research in our laboratory has shown that blocking PAR-1 with small-molecule antagonist, RWJ58259, in an LPS model of acute lung injury attenuates inflammatory cell recruitment and reduces microvascular leak (Mercer et al., 2013). Therefore, the initial *in vivo* experiments to assess the efficacy of the mPAR-1 antibody were undertaken in the LPS-model of acute lung injury, with a view to

progress into the more severe model of bleomycin-induced lung injury and pulmonary fibrosis.

There are many advantages of using a monoclonal neutralising antibody over a synthetic antagonist. Antibodies have a high affinity and avidity for the target epitope and show relatively low toxicity and side effects. The antigenic responses observed with the first murine therapeutic antibodies administered to humans have been greatly attenuated by producing chimeric and humanised antibodies. Furthermore, the large cost of producing engineered human antibodies has been reduced since the generation of transgenic mice encoding the human IgG constant region (reviewed in Gura 2002). Unlike RWJ58259, which is rapidly metabolised, antibodies have a prolonged half-life of approximately 21 days, which greatly reduces the need for frequent dosing.

To the best of our knowledge the mPAR-1 neutralising antibody was not previously used *in vivo* and hence there were no pharmacokinetic data available. Based on the *in vitro* functional assays, a range of antibody concentrations between 10 and 90 µg/ml inhibited thrombin-mediated intracellular calcium release and a cautious approach was adopted due to the residual endotoxin level still present in the antibody preparation. Generic endotoxin limit for humans is 5 endotoxin units (EU) per kilogram body weight and levels below that do not induce pyrogenic responses in living organisms. This value was also used as the basis to calculate the dose of antibody containing acceptable endotoxin level for an *in vivo* administration in mice (Malyala and Singh, 2008). The dose of 10 µg/ml was chosen on the basis that it blocked thrombin signalling *in vitro* and contained endotoxin levels below the threshold of triggering inflammatory responses.

The mPAR-1 neutralising antibody was administered intraperitoneally 30 minutes and 24 hours prior to the intranasal LPS challenge in two consecutive experiments. LPS-induced lung injury is characterised by neutrophillic inflammation and a reduction in monocyte and macrophage numbers and hence the inflammatory cell influx into the lung was assessed. Another prominent feature of this model is increased microvascular leak which was investigated by measuring total protein

levels in the BALF. Data obtained in these experiments are consistent with the previous results and show significant neutrophil recruitment into the lung and reduced numbers of monocytes and macrophages. However, in both experiments there was no difference in neutrophilia and monocytes numbers between the control isotype- and mPAR neutralising antibody-treated mice. Furthermore, all experimental groups had increased total protein levels suggesting that both saline controls and LPS-treated animals experienced increased microvascular leak. This is potential explanation for the fact that although the levels of total inflammatory cells were increased in LPS-treated mice compared to saline control, the differences were not statistically significant.

Several potential mechanisms were proposed to explain the lack of protective effect with the mPAR-1 neutralising antibody. Antibodies are large molecules and injected intraperitoneally reach the lung via the lymphatics and blood stream. It was postulated that the lack of protective effect was due to a delay between the onset of the injury and the antibody reaching the injured site. This issue was addressed in the second experiment where the antibody was administered 24 hours prior to LPS challenge. However, the level of neutrophil recruitment was comparable between the isotype control- and mPAR-1 neutralising antibody treated groups.

However, the assumption that antibodies have a long half-life may not be accurate in this experimental setting. Antibody half-life *in vivo* is regulated by the neonatal Fc receptor (FcRn), which in early stages of life transports the IgG through the placenta and across epithelial surfaces and in the adults protects the IgG from proteolytic degradation, extending its half-life for up to 21 days. Human FcRn discriminates between antibodies coming from different species and the lack of protection offered by this receptor can dramatically reduce the half-life of an antibody (Keizer et al., 2010; Kontermann, 2009). Although the mouse FcRn is promiscuous in binding IgGs from different species, its affinity for Armenian hamster IgG is uknown.

Second, the constant Fc fragment of the IgG can potentially cross-react with the Fc receptors expressed on the murine cells and elicit an antibody-mediated cytotoxic

reaction. In this instance, the antibody would trigger an inflammatory response that would mask any potential protective effect.

Also as previously discussed, PAR-1 is widely expressed on many cell types, including endothelial cells and circulating monocytes. It is plausible that the en route target-related clearance of the antibody prevents it from reaching the injured site in the lung at the sufficient concentrations to have a therapeutic effect. An increased dose of the antibody and intranasal route of administration are being considered to achieve higher local concentration at the site of injury.

Also, the protein data obtained in these experiments showing high levels of the total BALF protein across all experimental groups do not agree with the previous results obtained in our laboratory. This raises a potential technical issue which may relate to the sample collection technique or the BCA assay used to measure the total BALF protein. The collection of BALF is a disruptive procedure and if not performed carefully can dislodge a number of surface proteins or disrupt the lung vasculature and cause serum protein contamination. This protein will be then detected by BCA assay and obstruct the true magnitude of microvascular leak into the lung.

In conclusion, the aim of this study was to purify mPAR-1 neutralising antibody and validate it in the model of acute lung injury before assessing its therapeutic effect in bleomycin-induced lung injury and fibrosis. The antibody inhibited thrombin-mediated signalling *in vitro* but did not show a therapeutic effect *in vivo*. Apart from potential explanations discussed above, there is a concern that the remaining level of endotoxin present in the antibody preparation interferes with the inflammatory measurements evaluated in the model of acute lung injury. Therefore, future work will involve obtaining an endotoxin-free antibody preparation and further optimising of the antibody for *in vivo* use.

Appendix 2: PAR-1-dependent and PAR-1-independent pro-inflammatory signalling in human lung fibroblasts exposed to thrombin

J Cell Physiol. 2012 Nov;227(11):3575-84. doi: 10.1002/jcp.24061.

PAR-1-dependent and PAR-independent pro-inflammatory signaling in human lung fibroblasts exposed to thrombin.

Ortiz-Stern A[1], Deng X, Smoktunowicz N, Mercer PF, Chambers RC.

Abstract

Proteinase-activated receptors (PARs) are crucial in orchestrating cellular responses to coagulation proteinases, such as thrombin and FXa. Four PARs have been characterized and have been shown to be differentially expressed in mice and humans and between tissues. We have previously shown that in murine lung fibroblasts, PAR-1 is solely responsible for all cellular responses to thrombin and FXa. In contrast, we report here that in primary human lung fibroblasts (pHLFs), known PARs fail to account for all of the cellular responses to thrombin, in particular in the presence of high, but physiologically achievable concentrations of thrombin. We report that pHLFs secrete CCL2 in a PAR-1-dependent manner at low thrombin concentration (~0.3 nM). At or above 10 nM thrombin, pharmacological antagonism (RWJ-58259) fails to block thrombin-induced CCL2 release; whereas PAR-1 cleavage-blocking monoclonal antibodies (ATAP2 and WEDE15) only partially inhibit thrombin-induced CCL2 secretion. In addition, activation of PAR-3, PAR-4, and transactivation of either PAR-2 or EGFR were ruled out as being responsible for thrombin-mediated CCL2 secretion at high yet standard concentrations of the proteinase. We further provide evidence that PAR-1-dependent and PAR-independent signaling involves the rapid phosphorylation of ERK, which in turn is absolutely required for thrombin-induced CCL2 secretion at both low and standard concentration of the proteinase. Our findings suggest the existence of a PAR-independent signaling mechanism in human lung fibroblasts and have important implications for the design of therapeutic strategies aimed at blocking pro-inflammatory signaling responses associated with excessive thrombin generation.